AURORA KINASE B INHIBITION IN NON-SMALL CELL LUNG AND HEAD & NECK CANCER

By:

Timothy Ainsworth Mitchell

A thesis submitted in partial fulfilment of the requirements for the degree of

Doctor of Philosophy

The University of Sheffield

Faculty of Medicine, Dentistry and Health

Department of Oncology and Metabolism

November 2023

Declaration

I, the author, confirm that the Thesis is my own work. I am aware of the University's. Guidance on the Use of Unfair Means (www.sheffield.ac.uk/ssid/unfair-means). This work has not been previously presented for an award at this, or any other, university.

Acknowledgements

First and foremost, I want to express my heartfelt gratitude to Dr Helen Bryant, whose unwavering support was readily available throughout my journey. Coming from a purely clinical background, pursuing a PhD amid a pandemic was daunting, but her advice and patience kept me going, and I am immensely grateful for that. I could have easily given up many times, but her encouragement helped me maintain my confidence.

I also thank Professor Sarah Danson and Professor Mathew Hatton for their invaluable guidance and clinical expertise while I worked alongside them in their clinics. Our monthly meetings provided a platform for constructive questions and inspiring ideas that helped me focus my research and generate new insights.

To my family, thank you for understanding and supporting me during this challenging three-year journey. I know I was mostly buried in work, but your patience and understanding meant the world to me. I look forward to being more present in the near future.

I am also profoundly grateful to the Yorkshire Cancer Trust and Sheffield Teaching Hospital Trust for funding my PhD. Your support *mad*e this work possible, and I will always be thankful for the opportunity you provided me. I eagerly anticipate seeing the projects you fund in the future, as I know they will contribute to essential advancements in cancer research.

My time in Sheffield was *mad*e brighter by the presence of good friends like Francessca, Leona, Dan, Kathryn, Racheal, Aurelie, F*atm*a, Callum, Conner, Libby, and James. Your camaraderie and shared knowledge brought smiles to my face almost every day. I wish each of you the best and do not doubt that I will be reading about new and exciting discoveries from your respective labs in future journals.

At Weston Park, I thank Lori, Helen, Theingi, Muneeb, and Jess. I am confident that all of you will become outstanding consultants wherever you choose to work. Special thanks go to Maggie, who provided invaluable assistance with gathering essential immunohistochemistry and live-cell work during my final years. Her patience and expertise were essential in working with me.

Lastly, I want to acknowledge Hanna for helping me learn more about Immunohistochemistry techniques, which proved crucial toward the end of the project. It was refreshing to connect with someone clinical who understood the challenges. I wish you the best of luck in all your endeavours.

To everyone mentioned here, you have played a significant role in my academic and personal growth, and I am sincerely grateful for all your support and encouragement.

Publications and Presentations from this project

1. Investigation of Aurora Kinase A as a Potential Biomarker of radiation in Non-Small Cell lung cancer (NSCLC)

   Timothy Mitchell[1,2], Thomas Jones[1], Sarah Danson[2], Maggie Glover[1], Emma Hill[3], Emily Harrison[3], Jonathan Bury, Janet Horsman[2], Laura Christian[3], Gill Brown[2], Matthew Hatton[2,3], Helen Bryant[1]

2. Using an artificial neural network to predict tumour recurrence in Non-Small Cell Lung Cancer

   Timothy Mitchell, Joshua Astley, Matthew Hatton, Sarah Danson, Helen Bryant, Bilal Tahir

Abstract

Non-small cell lung cancer (NCSLC) and Head and Neck Squamous Cell cancer (HNSCC) are two of the most common tumour sites treated in oncology practices in the United Kingdom (UK). The survival for NSCLC and HNSCC is poor, with 10% and 19-59 % over ten years ("Lung cancer statistics, Cancer Research UK," 2023). Poor survival has been linked with early local recurrence and invariable metastatic disease. Aurora Kinase A (*AURKA*) and Aurora Kinase B (*AURKB*) are both overexpressed in these cancers and are linked with poor survival rates.

We have hypothesised that increased *AURKA* and *AURKB* expression is linked with radioresistance in NSCLC and HNSCC; inhibitors of both proteins can sensitise cell lines in these cancer groups to irradiation (IR).

We demonstrate that *AURKA* inhibition radiosensitises NSCLC cells in vitro in a *p53* dependent manner. We demonstrate that *AURKB* inhibition using Barasertib reduces cell survival in vitro in both NSCLC and HNSCC, which is not dependent on *p53* expression. We demonstrate that Barasertib leads to radiosensitisation of NSCLC cells in vitro in a non-*p53* dependent manner, but we could not demonstrate radiosensitisation in any HNSCC cell line.

We showed that combining different chemotherapy drugs with Barasertib led to radiosensitisation of H460 cells; this was possibly dependent on the mechanism of action of the chemotherapy agent.

We showed that adding Barasertib leads to increased levels of slippage in NSCLC (A549, H520) and HNSCC cell lines (UPCI-SCC72, SCC89). We found no direct effects on the cell cycle when NSCLC and HNSCC cell lines were exposed to

Barasertib. We then showed that *AURKB* inhibition increased polyploidy when UPCI-SCC72 and SCC89 cells were exposed to Barasertib over 24 hours.

We demonstrated that *AURKB* and *AURKA* show promise as prognostic biomarkers in NSCLC, whereas *AURKA* alone is a promising biomarker in the HNSCC oropharyngeal subtype. The results of our Prospective Study (looking at NSCLC patients who underwent radical radiotherapy at the Weston Park Cancer Centre) did not show a correlation between *AURKA* expression and patient Overall survival (OS) and progression-free survival (PFS). *AURKB* immunohistochemistry (IHC) optimisation was done after to assess for correlation between expression and survival. Differential staining can be demonstrated in H460 cell pellets but requires more optimisation to demonstrate staining in lung tissue confidently.

Finally, we wrote a phase one trial protocol looking at the combination of Barasertib and IR, which we hope to use in the future if the results of the preclinical work are promising.

Acronyms

i.	ADC	Adenocarcinoma
ii.	ANOVA	Analysis of Variance
iii.	APC	Anaphase Promoting Complex/Cyclosome
iv.	*ASPM*	Abnormal Spindle-Like Micro*cep*haly Associated
v.	ATP	Adenosine Triphosphate
vi.	*AURKA*	Aurora Kinase A
vii.	*AURKB*	Aurora Kinase B
viii.	*AURKC*	Aurora Kinase C
ix.	AZD	AstraZeneca
x.	BAEM	Black and ethnic minority
xi.	BICR	Baculoviral Inhibitor of Apoptosis Repeat
xii.	CCL	Chemokine (C-C motif) Ligand
xiii.	*CCNA*	Cyclin A
xiv.	*CCNB*	Cyclin B
xv.	CD	Cluster of Differentiation
xvi.	CDC	Cell Division Cycle
xvii.	*CDCA*	Cell Division Cycle-Associated Protein
xviii.	*CDK*	Cyclin-dependent kinases
xix.	*CDKN*	Cyclin-Dependent Kinase Inhibitor
xx.	*CENPF*	Centromere protein F
xxi.	*CEP*	Centrosomal Protein
xxii.	*CHEK*	Checkpoint Kinase
xxiii.	COL	Collagen

xxiv.	CSS	Cancer-specific survival
xxv.	CSV	Comma-separated values
xxvi.	CTLA	Cytotoxic T-Lymphocyte-Associated Protein
xxvii.	CXCL	Chemokine (C-X-C motif) Ligand
xxviii.	DAB	3, 3'- diaminobenzidine
xxix.	DEG	Differentially Expressed Gene
xxx.	DER	Dose enhancement ratio
xxxi.	DFS	Disease-free survival
xxxii.	*DLGAP*	Discs Large Homolog-Associated Protein -
xxxiii.	DMSO	Dimethylsulfoxide
xxxiv.	DNA	Deoxyribonucleic acid
xxxv.	EGA	European Genome-Phenome Archive
xxxvi.	*EGFR*	Epidermal growth factor Receptor
xxxvii.	*ENTPD*	Ectonucleoside triphosphate diphosphohydrolase
xxxviii.	ETS	E26 Transformation-Specific
xxxix.	FACS	Fluorescence-activated cell sorting
xl.	FC	Fold Change
xli.	*FN*	Fibronectin
xlii.	FU	5-Fluorouracil
xliii.	*GEB*	Glucose-Ethanolamine Phosphotransferase
xliv.	GEO	Gene expression omnibus
xlv.	GEPIA	Gene Expression Profiling Interactive Analysis
xlvi.	GPL	General Public License
xlvii.	GSE	Gene Expression Omnibus Series
xlviii.	GY	Gray

xlix.	HB	Helen Bryant
l.	HG	Human Genome
li.	HMMR	Hyaluronan-Mediated Motility Re*cep*tor
lii.	HNSCC	Head and Neck Squamous Cell Cancer
liii.	HQPA	Hydroxyquinoline Pivaloxy Methane sulfonate
liv.	HR	Hazard Ratio
lv.	IFCI	Interferon-Inducible CXC Chemokine
lvi.	IHC	immunohistochemistry
lvii.	IL	Interleukin
lviii.	IR	Irradiation
lix.	ISG	Interferon-Stimulated Gene
lx.	*ITGA*	Integrin Alpha
lxi.	*KIF*	Kinesin Family Protein
lxii.	KM	Kaplan-Meier
lxiii.	LD50	lethal dose
lxiv.	LUM	Lumican
lxv.	*MAD*	Mitotic Arrest-Deficient
lxvi.	MCM	Mini-Chromosome Maintenance
lxvii.	MCODE	Molecular Complex Detection
lxviii.	MELK	Maternal Embryonic Leucine Zipper Kinase
lxix.	*MMP*	M*atr*ix Metalloproteinase
lxx.	*NCAPG*	Non-SMC Condensin I Complex Subunit G
lxxi.	NCBI	National Centre for Biotechnology Information
lxxii.	NPC	Nasopharyngeal Carcinoma
lxxiii.	NSCLC	Non-Small Cell lung cancer

lxxiv.	*NUF*	Nuclear Protein Localization Protein
lxxv.	OS	Overall survival
lxxvi.	OSCC	Oral Squamous Cell Carcinoma
lxxvii.	PBK	PDZ-Binding Kinase
lxxviii.	PCA	Principal Component Analysis
lxxix.	PCR	Polymerase Chain Reaction
lxxx.	PD	Progressive Disease
lxxxi.	PFS	Progression-Free Survival
lxxxii.	*PH3*	Phospho-Histone H3
lxxxiii.	PI	Propidium iodide
lxxxiv.	*POSTN*	Periostin
lxxxv.	PPI	Protein-Protein Interaction
lxxxvi.	PPS	Progression-Free Survival
lxxxvii.	PTGS	Prostaglandin-Endoperoxide Synthase
lxxxviii.	RNA	Ribonucleic Acid
lxxxix.	RRM	RNA Recognition Motif
xc.	RT	Reverse Transcription
xci.	SAC	Spindle assembly checkpoint
xcii.	SCC	Squamous Cell Cancer
xciii.	SD	Stable Disease
xciv.	*SERPINE*	Serpin Family of Protease Inhibitors
xcv.	*SPP*	Signal Peptide Peptidase
xcvi.	STAT	Signal Transducer and Activator of Transcription
xcvii.	STRING	Search Tool for the Retrieval of Interacting Genes/Proteins
xcviii.	TCGA	The Cancer Genome Atlas

xcix. TGFB Transforming Growth Factor Beta

c. *THBS* Thrombospondin

ci. TNM Tumour Node and Metastasis

cii. *TOP* *Top*oisomerase

ciii. TPX Taxus brevifolia Plan

civ. TSCC Thyroid Squamous Cell Carcinoma

cv. *TTK* Targeting protein for Xenopus kinesin-like protein 2.

cvi. *UBE* Ubiquitin-Conjugating Enzyme

cvii. UPCI University of Pittsburgh Cancer Institute

cviii. USA United States of America

cix. WPCC Weston Park Cancer Centre

Table of Contents

1 Introduction 57

1.1 Non-small cell lung cancer (NSCLC) 57

1.1.1 Demographics (Incidence and environmental/socio-economic risk factors). 57

1.1.2 Staging and pathological subtypes. 58

1.1.3 Management of NSCLC. 61

1.2 Head and Neck Squamous Cell Cancer (HNSCC). 63

1.2.1 Demographics (incidence and environmental/socio-economic risk factors). 63

1.2.2 Staging and pathological subtypes. 65

1.2.3 Management of HNSCC 68

1.3 Radiobiology of NSCLC and HNSCC. 71

1.3.1 The R's of radiobiology. 71

1.3.2 Radiobiology and radiation schedules in NSCLC. 73

1.3.3 Radiobiology and Radiation Schedules in HNSCC 77

1.4 Radiotherapy resistance in NSCLC and HNSCC. 80

1.4.1 The molecular response to radiation damage in NSCLC. 80

1.4.2 Radioresistance in NSCLC 82

1.4.3 Therapeutic Approaches to Overcome Radioresistance in NSCLC 85

1.4.4 The molecular response to radiation damage in HNSCC. 87

1.4.5 Radioresistance in HNSCC 89

1.4.6 Therapeutic Approaches to Overcome Radioresistance in HNSCC 92
1.5 Genetics and cellular consequences of NSCLC and HNSCC. 95
1.5.1 Genetics and cellular consequences of NSCLC 95
1.5.2 Genetics and cellular consequences of HNSCC 99
1.5.3 *AURKA*. 104
1.5.4 *AURKC*. 109
1.5.5 *AURKB*. 111
1.5.6 AURK inhibitors. 136
1.6 Study context 139
2 Materials & Methods. 142
2.1 Materials..... 142
2.1.1 Laboratory Equipment. 142
2.1.2 Glassware, plastics, and disposables. 143
2.1.3 Purified Water. 144
2.1.4 Sterilisation. 144
2.1.5 Chemicals. 144
2.1.6 Cell lines. 146
2.1.7 Cell culture reagents. 148
2.1.8 Buffers. 149
2.1.9 Inhibitor Compounds. 152
2.1.10 Cytotoxic agents. 152

2.1.11 Irradiation. 153

2.1.12 Short interfering R.N.A. (siRNA) and transfection reagents. 153

2.1.13 Antibodies. 154

2.1.14 Immunohistochemistry detection kits. 156

2.2 Methods. 157

2.2.1 Mammalian cell culture. 157

2.2.2 Western blotting. 164

2.2.3 Fluorescence-activated cell sorting (FACS). 170

2.2.4 Immunohistochemistry (IHC). 174

2.2.5 Bioinformatics pathway. 182

2.2.6 Patients and primary tumour samples. 183

3 Evaluation of Barasertib, Alisertib and Ly3295668 as radiosensitising agents in NSCLC in vitro. 186

3.1 Introduction, Aims and Hypothesis. 186

3.2 Results. 190

3.2.1 Ly3295668 190

3.2.2 Barasertib 196

3.2.3 Examples of the cellular phenomenon seen in live cell assays. 220

3.2.4 Live cell analysis of NSCLC cell lines in response to Barasertib with or without radiation treatment. 226

3.2.5 Live cell analysis of NCSLC cell lines using Barasertib as monotherapy. 233

3.2.6 Live cell analysis using Barasertib over 72 hours. 242
3.2.7 Western blot analysis of genes in the SAC. 246
3.2.8 Cell cycle profiling using FACS. 249
3.3 Discussion 255
3.3.1 Radiosensitisation potential of Ly3295668 and Barasertib in HNSLC cell lines 255
3.3.2 There is a need to identify a better target to demonstrate Barasertib inhibition. 256
3.3.3 Chemotherapy combination work. 258
3.3.4 Combination radiosensitisation work. 259
3.3.5 Live cell imaging assays. 260
3.3.6 Western blot Assays. 262
3.3.7 FACS. 263
3.4 Future Work 264
3.4.1 Dose Refinement 264
3.4.2 Mechanistic Insights 264
3.4.3 Clinical Translation 264
3.4.4 Extended Radiosensitisation Studies 265
3.5 Conclusion 266
4 Evaluation of Barasertib, Alisertib and Ly3295668 as radiosensitising agents in HNSCC cell lines. 267
4.1 Introduction, Aims and Hypothesis. 267

4.2 Results. 272
4.2.1 Barasertib 272
4.2.2 Live cell analysis of HNSCC cell lines using Barasertib as monotherapy. 284
4.2.3 Live cell analysis using Barasertib over 72 hours. 297
4.2.4 Western blot analysis of genes in the SAC. 303
4.2.5 Cell cycle profiling using FACS. 305
4.3 Discussion 312
4.3.1 Radiosensitisation potential of Barasertib in HNSCC cell lines 312
4.3.2 Barasertib Monotherapy Displays Cytotoxicity in HNSCC Cell Lines: 313
4.3.3 Lack of Radiosensitisation by Barasertib in HNSCC Cell Lines: 314
4.3.4 Limited Efficacy of Barasertib Combined with Chemotherapy in HNSCC: 314
4.3.5 Increased Sensitivity of HNSCC Cells to Barasertib: 315
4.3.6 Slippage as a Central Mechanism of Barasertib Action: 315
4.3.7 Dose-Response Variability in Cellular Outcomes: 316
4.3.8 Polyploidy and Cell Cycle Perturbation: 316
4.3.9 No Observable Changes in Cyclin B1 and CDC20 Expression: 317
4.4 Future Work 318
4.5 Conclusion 321
5 Evaluation of *AURKA* and *AURKB* expression in published datasets and expression in NSCLC tissue 323

5.1 Introduction aims and hypothesis. 323

5.2 Results 327

5.2.1 Differential gene expression of *AURKA* and *AURKB* in NSCLC cancerous tissue. 327

5.2.2 Differential Gene expression of *AURKA* and *AURKB* between normal and cancerous HNSCC tissue 367

5.2.3 *AURKA* IHC in NSCLC patient cohort. 384

5.2.4 *AURKB* IHC in NSCLC patient cohort. 416

5.2.5 *AURKB* did not demonstrate visible staining in lung tissue using LC241m lung microarray cores. 425

5.2.6 Use of the I*MMP*RESS Excel Amplified Polymer Staining Kit, Anti-Rabbit IgG, increased stromal staining and generally did not improve *AURKB* staining on tissue samples. 432

5.3 Discussion 438

5.3.1 Pros and Cons of different data sources 439

5.3.2 Differential gene expression and Biomarker activity. 441

5.3.3 The difference between differential expression and a hub gene 442

5.3.4 Prospective Patient Study 445

5.4 Future Work 449

5.4.1 Strengthening the Case for *AURKA* and *AURKB* as Biomarkers 449

5.4.2 Exploring Other Key Genes 449

5.4.3 Personalized Biomarker Strategies for Different Cancers 449

5.4.4 Addressing Technical Hurdles and Improving Data Integration 450
5.4.5 Understanding the Functional Role of Key Genes 450
5.4.6 Finding Stronger Biomarkers 450
5.4.7 Overcoming Challenges in Immunohistochemistry (IHC) 451
5.4.8 Personalized Treatments for NSCLC Subtypes 451
5.4.9 Refining IHC Protocols 451
5.4.10 Targeting *AURKA* in Therapy 452
5.5 Conclusion 452
6 Discussion 454
6.1 Mitotic Slippage and Cellular Outcomes 455
6.2 Radiosensitisation Potential and Clinical Implications 456
6.3 Mechanisms of Resistance and Future Directions 457
6.4 Conclusion 458
7 Appendix 459
7.1 Source code for bioinformatics DGE pathway. 459
7.2 Volcano plots and DEG tables used in bioinformatics study. 484
7.2.1 NCSLC plots 484
7.2.2 Nasopharyngeal plots 488
7.2.3 Oropharyngeal plots 490
7.3 A SequeNtial Phase One stUdy of an Aurora Kinase inhibitor concurrent with radical fracTionated radiotherapy for Non-Small Cell Lung cancer. 493
7.3.1 Study Summary: 499

7.3.2 Summary Schedule of events: 531

7.3.3 Introduction 533

7.3.4 Investigational Medicinal Products (IMP) used in the study: 534

7.3.5 The rationale for the study: 536

7.3.6 The primary hypothesis of the trial: 538

7.3.7 Trial Design: 538

7.3.8 Projected Number of Subjects: 543

7.3.9 Replacement of Subjects: 543

7.3.10 Post-trial care and follow-up: 545

7.3.11 Objectives and Endpoints: 547

7.3.12 Inclusion Criteria: 549

7.3.13 Exclusion criteria: 551

7.3.14 Patient registration procedure: 556

7.3.15 Registration of patients: 557

7.3.16 Informed consent for the main study: 557

7.3.17 Contraceptive/ Pregnancy counselling: 558

7.3.18 Main screening: pre-dosing evaluations: 560

7.3.19 Early Patient Withdrawal: 568

7.3.20 Withdrawal of Consent: 569

7.3.21 Patient evaluability and replacement: 569

7.3.22 Treatment dose: 570

7.3.23 Duration of treatment: 571
7.3.24 Dose-limiting Toxicity (DLT): 572
7.3.25 Maximum Tolerated Dose (MTD) 575
7.3.26 Dose modification 577
7.3.27 Toxicities associated with Barasertib 580
7.3.28 Patient data acquisition 585
7.3.29 Treatment planning 585
7.3.30 Drug Management: 588
7.3.31 Evaluation of Response: 590
7.3.32 Assessment of Safety: 593
7.3.33 Death on study 596
7.3.34 Elective admissions and supportive care 597
7.3.35 Development Safety Update Reports (DUSRs) 597
7.3.36 Pregnancy and Breast Feeding: 598
7.3.37 Defining the End of Trial: 599
7.3.38 Statistical Considerations: 599
7.3.39 Trial Committees: 600
7.3.40 Data Management: 600
7.3.41 Study Site Management: 602
7.3.42 Regulatory and Ethical Considerations: 604
7.3.43 Protocol amendments 605

7.3.44 Expenses and Benefits: 609
7.3.45 Quality Assurance: 609
7.3.46 Study Funding: 612
7.4 Stacked Bar graphs of Live cell data. 614
7.4.1 0–16-hour time frame 614
7.4.2 24–36-hour time frame 624
7.4.3 36–48-hour time frame 657
7.5 Ly3295668 western phospho-blots 667
7.6 Barasertib western phospho-blots 668
7.7 IHC optimization work done by Prior PhD student 669
7.8 Live cell analysis plots over 72 hours in NSCLC cell lines 677
7.9 Live cell analysis plots over 72 hours in HNSCC cell lines 681
7.10 Western Blots CDC20, Cyclin B1 in HNSCC and NSCLC cell lines 690
8 References 693

Table of Figures

Figure 1-1: The TNM staging of NSCLC 8th edition. The TNM 8 staging system for non-small cell lung cancer (NSCLC), developed by the American Joint Committee on Cancer (AJCC) and the Union for International Cancer Control (UICC), categorizes cancer based on Tumor size and extent (T), lymph Node involvement (N), and presence of Metastasis (M). Tumor (T) classification ranges from Tis (carcinoma in situ) to T4, indicating increasing size and extent of invasion. Node (N) classification ranges from N0 (no regional lymph node metastasis) to N3 (contralateral mediastinal or supraclavicular lymph node involvement). Metastasis (M) is categorized as M0 (no distant metastasis) to M1c (multiple extrathoracic metastases). These categories combine to form overall stages from Stage 0 (Tis N0 M0) to Stage IVB (any T, any N, M1c), aiding in prognosis and treatment planning. 60

Figure 1-2: Genetic mutations in NSCLC and HNSCC Non-small cell lung cancer (NSCLC) is characterized by various genetic mutations that significantly influence its pathogenesis, prognosis, and treatment strategies. Among these, KRAS mutations are the most common, occurring in approximately 25% of NSCLC cases, predominantly in adenocarcinomas, and are associated with poor prognosis and resistance to certain therapies. The ALK-EML4 fusion gene, found in about 3-7% of NSCLC patients, particularly younger non-smokers, results from a chromosomal rearrangement that activates the ALK tyrosine kinase, leading to uncontrolled cell growth and survival. Epidermal growth factor receptor (EGFR) mutations, present in 10-15% of NSCLC patients in Western populations and up to 50% in Asian populations, often predict sensitivity to tyrosine kinase inhibitors (TKIs) like gefitinib and erlotinib. ROS1 rearrangements, occurring in about 1-2% of NSCLC cases, also drive oncogenic activity and respond well to ROS1 inhibitors such as Crizotinib. 101

Figure 1-3: Different phases of mitosis where Activity of Aurora Kinases are said to act most frequently and the chromosomal passenger complex (CPC). Mitosis, a fundamental process for cell division, is meticulously regulated by proteins such as Aurora kinases and the chromosomal passenger complex (CPC) (Carmena , 2012). Aurora kinases, comprising Aurora A, B, and C, play pivotal roles throughout mitosis. Aurora A is predominantly active during prophase at the centrosomes, facilitating centrosome maturation, separation, and the formation of the bipolar spindle apparatus through microtubule nucleation and organization. During prometaphase and metaphase, Aurora A stabilizes spindle

microtubules and ensures proper microtubule-kinetochore attachments. Aurora B, a core component of the CPC, exhibits critical activity from prometaphase to cytokinesis (Yan, 2009). It localizes to kinetochores in prometaphase, ensuring correct chromosome alignment and attachment, and later relocates to the central spindle in anaphase and the midbody in cytokinesis, regulating the spindle assembly checkpoint, chromosomal segregation, and cytokinesis (DeLuca , 2018). Aurora C, though less studied, is thought to function similarly to Aurora B, particularly in meiosis. The CPC, comprising Aurora B, INCENP, Survivin, and Borealin, orchestrates several mitotic processes, including chromosome condensation, alignment, segregation, and cytokinesis, through its dynamic localization and regulation of spindle assembly and checkpoint signaling (Becker , 2010; Carmena , 2012). 103

Figure 1-4: Interactions of AURKA in prophase Aurora kinase A (AURKA) plays a crucial role in the regulation of mitosis, particularly during the G2/M transition and prophase, through its interactions with several key proteins including Bora, Polo-like kinase 1 (Plk1), WEE1, and Cyclin B (Parrilla , 2016; Yan, 2009). During the G2 phase, AURKA is activated by its binding partner Bora, which enhances its kinase activity. This activation is critical for the initiation of mitotic entry. Bora facilitates the recruitment and activation of Plk1, another essential kinase in mitotic progression. Plk1, once activated by AURKA, phosphorylates various substrates that are necessary for centrosome maturation, separation, and spindle assembly, ensuring proper mitotic spindle formation. 105

Figure 1-5: Interactions of AURKA in prophase Aurora kinase A (AURKA) is a critical regulator of mitosis, particularly during the prophase stage, where it interacts with various proteins and structures to ensure proper mitotic progression. One of the key interactions of AURKA in prophase is with targeting protein for Xklp2 (TPX2) (Van Gijn , 2019). TPX2 is essential for AURKA activation and localization to the microtubule organizing centers (MTOCs), including the centrosomes. TPX2 binds to AURKA, protecting it from dephosphorylation and enhancing its kinase activity, which is crucial for spindle assembly (Van Gijn , 2019). Additionally, AURKA interacts with transforming acidic coiled-coil-containing protein (TACC) and its partner, microtubule-associated protein 215 (MAP215, also known as ch-TOG in humans). TACC/MAP215 is crucial for stabilizing microtubules and promoting their growth (Burgess , 2018). AURKA phosphorylates TACC, which enhances its ability to bind to microtubules and increases the stability and dynamics of the mitotic spindle. This interaction ensures that microtubules are properly organized and aligned, which is essential for accurate chromosome segregation (Ulisse , 2007). The combined actions

of AURKA at the microtubule organizing centers ensure the efficient formation and function of the mitotic spindle during prophase. By activating TPX2 and phosphorylating γ-tubulin and TACC/MAP215, AURKA orchestrates the assembly and stabilization of microtubules, facilitating the transition from G2 to M phase and the early stages of mitosis (Burgess , 2018). *107*

Figure 1-6: Some interactions of AURKB during Prophase Aurora kinase B (AURKB) is a crucial component of the chromosomal passenger complex (CPC) and plays an essential role in regulating various processes during mitosis, including chromosome condensation, kinetochore-microtubule attachments, and the spindle assembly checkpoint (Carmena , 2012; Gohard , 2014). During prophase, AURKB interacts with several key proteins and complexes to ensure proper mitotic progression. AURKB phosphorylates SSU72, modulating its activity and ensuring proper chromosome condensation and segregation. This regulation is vital for maintaining the structural integrity of chromosomes during the early stages of mitosis (Kim , 2013). *113*

Figure 1-7: Interactions of AURKB in Metaphase During metaphase, Aurora kinase B (AURKB) plays a critical role in ensuring proper chromosome alignment, tension across sister chromatids, and the activation of the spindle assembly checkpoint (SAC) through its interactions with mDia3, BUBR1, and Ajuba (Ditchfield , 2003b; Ferrand , 2009). AURKB phosphorylates mDia3, enhancing its ability to interact with microtubules and ensuring proper spindle formation and stabilization, which is essential for accurate chromosome alignment. By phosphorylating BUBR1, a key component of the SAC, AURKB activates and maintains this checkpoint, preventing anaphase onset until all chromosomes are correctly attached to the spindle microtubules with proper tension. *116*

Figure 1-8: Interactions with AURKB in Anaphase During anaphase, Aurora kinase B (AURKB) continues to play a pivotal role in coordinating chromosome segregation and cytokinesis through its interactions with various proteins such as CENP-E, KIF4A, LATS2, SDS22, and PP1. CENP-E (Centromere-associated protein E), a motor protein, is crucial for the stable attachment of microtubules to kinetochores and the movement of chromosomes toward the poles (Abe , 2006; Guo , 2012). AURKB phosphorylates CENP-E, regulating its motor activity and ensuring the correct alignment and movement of chromosomes, which is essential for accurate segregation. KIF4A (Kinesin family member 4A) is another motor protein that interacts with AURKB during anaphase (Bastos , 2014). *121*

Figure 1-9: Interactions of AURKB in cytokinesis During cytokinesis, Aurora kinase B (AURKB) orchestrates the final separation of daughter cells through interactions with various proteins, ensuring proper cell division and genomic stability. One of the key interactions is with RASSF1A (Ras association domain family member 1A), a tumor suppressor involved in microtubule stability and spindle organization. AURKB phosphorylates RASSF1A, modulating its function and contributing to the organization of the central spindle and the successful completion of cytokinesis. 128

Figure 1-10: Interaction between AURKB and P53 The interaction between Aurora kinase B (AURKB) and the tumor suppressor protein p53 is a critical aspect of cell cycle regulation and genomic stability. AURKB is a key mitotic kinase involved in various processes, including chromosome condensation, spindle assembly, and cytokinesis (C. P. Gully , 2012, p. 53; Wu , 2011a). 132

Figure 1-11: Aurora kinase B (AURKB) is primarily known for its critical role in mitosis, but emerging evidence suggests that it also interacts with the Wnt signaling pathway, which is crucial for regulating cell proliferation, differentiation, and migration (Bertran-Alamillo , 2019a; Shuda , 2009). The Wnt signaling pathway is divided into canonical (β-catenin dependent) and non-canonical (β-catenin independent) pathways, both of which play vital roles in development and tumorigenesis. AURKB has been shown to influence the canonical Wnt/β-catenin signaling pathway by modulating the stability and activity of β-catenin. β-catenin is a central player in the Wnt pathway, and its accumulation in the cytoplasm followed by translocation to the nucleus leads to the activation of Wnt target genes involved in cell proliferation and survival (Luo , 2019). 134

*Figure 3-1:**Ly3295668 monotherapy response in NSCLC cell lines** A: Survival fraction was calculated using clonogenic assay under continuous exposure to the AURKA inhibitor Ly3295668. Data points represent the mean survival fraction normalised to untreated control +/- SD (N= 3). B: Table showing the genetic type of each cell line. C: Representative western blot results for pan p-AURK, AURKA (total A) and GAPDH in protein extracts from H460, A549, H1299 and SW900 cells arrested overnight with 100 ng/ml Nocodazole (Noc) and released into increasing concentrations of Ly3295668 for 2 hours. 192*

*Figure 3-2: **Radiosensitisation of NSCLC cell lines by LY3295668.** The survival fraction was calculated using a clonogenic assay. Cells were pre-incubated with LY3295668 before irradiation and colony outgrowth under continuous exposure to the AURKA inhibitor Ly3295668. Data points represent the*

mean survival fraction normalised to unirradiated control +/- SD (N= ≥3). F-value and p-value derived from the extra sum of squares test. *194*

Figure 3-3: ***Barasertib monotherapy in NSCLC cell lines.*** *Survival fraction was calculated using clonogenic assay under continuous exposure to the AURKB inhibitor Barasertib. Data points represent the mean survival fraction normalised to untreated control +/- SD (N= 3). B: Table showing the genetic type of each cell line. C: Representative western blot quantification results for pan p-AURK, AURKA (total B) and GAPDH in protein extracts from H460, A549, H1299, H520 and H322 and SW900 cells arrested overnight with 100 ng/ml Nocodazole (Noc) and released into increasing concentrations of Barasertib. D: Representative western blot results for pan p53, GAPDH and PH3 in protein extracts from H460 cells arrested overnight with 100 ng/ml Nocodazole (Noc) and released into increasing concentrations of Barasertib* *199*

Figure 3-4 ***Barasertib and IR in NSCLC cell lines*** *the survival fraction was calculated using a clonogenic assay. Cells were pre-incubated with Barasertib before irradiation and colony outgrowth under continuous exposure to the AURKB inhibitor Barasertib. Data points represent the mean survival fraction normalised to unirradiated control +/- SD (N= ≥3). F-value and p-value derived from the extra sum of squares test.* *201*

Figure 3-5 ***Depletion of AURKB radiosensitises H460 cells.*** *H460 cells were depleted of AURKA using siRNA 24 h prior to plating for clonogenic assays with and without Barasertib +/- irradiation. All conditions were conducted in parallel, and data were re-represented in different combinations for clarity (A-C). Data points represent mean survival fraction normalised to untreated control +/- SD (N= 3). Lines connect points while dotted lines are fitted to the linear quadratic model of cell death. F-value and p-value derived from extra sum of squares test. (D) Western blot for AURKB for each biological repeat.*..... *204*

*Figure 3-6: Comparison of Alisertib plus Barasertib vs Alisertib in NSCLC cell lines (n=3/4). Cells were pre-incubated with either an AURKA or AURKB inhibitor (Alisertib or Barasertib), cells were left to form colonies for 10-14 days before colony outgrowth under continuous exposure to the AURKA and/or AURKB inhibitor Alisertib or Barasertib. Data points represent the mean survival fraction normalised to DMSO +/- SD (N= ≥3). F-value and p-value derived from the extra sum of squares test. NS (non-statistically significant) denotes p= >0.05, * denotes p= ≤0.05, ** denotes p= ≤0.01, *** denotes p= 0.001 (One-way ANOVA with Dunnett correction for multiple comparisons).* *207*

Figure 3-7: Survival curves of H460 exposed to four chemotherapy agents (n=5/6). *209*

*Figure 3-8: Comparison of Barasertib vs Barasertib and chemotherapy (Cisplatin and Vinorelbine) in H460 cell lines (n=3). Cells were pre-incubated with either Cisplatin, Vinorelbine or AURKB inhibitor Barasertib, cells were left to form colonies for 10-14 days before colony outgrowth under continuous exposure to the Cisplatin, Vinorelbine and/or AURKB inhibitor Barasertib. Data points represent the mean survival fraction normalised to DMSO +/- SD (N= ≥3). F-value and p-value derived from the extra sum of squares test. NS (non-statistically significant) denotes p= >0.05, * denotes p= ≤0.05, ** denotes p= ≤0.01, *** denotes p= 0.001 (One-way ANOVA with Dunnett correction for multiple comparisons).* *212*

*Figure 3-9: Comparison of Barasertib vs Barasertib and chemotherapy (5-FU and Etoposide) in H460 cell lines (n=3). Cells were pre-incubated with either 5FU, Etoposide or AURKB inhibitor Barasertib, cells were left to form colonies for 10-14 days before colony outgrowth under continuous exposure to the 5FU, Etoposide and/or AURKB inhibitor Barasertib. Data points represent the mean survival fraction normalised to DMSO +/- SD (N= ≥3). F-value and p-value derived from the extra sum of squares test. NS (non-statistically significant) denotes p= >0.05, * denotes p= ≤0.05, ** denotes p= ≤0.01, *** denotes p= 0.001 (One-way ANOVA with Dunnett correction for multiple comparisons).* *213*

*Figure 3-10: Comparison of Barasertib vs Barasertib and chemotherapy (Cisplatin and Vinorelbine) in H1299 cell lines (n=3). Cells were pre-incubated with either Cisplatin, Vinorelbine or AURKB inhibitor Barasertib, cells were left to form colonies for 10-14 days before colony outgrowth under continuous exposure to the Cisplatin, Vinorelbine and/or AURKB inhibitor Barasertib. Data points represent the mean survival fraction normalised to DMSO +/- SD (N= ≥3). F-value and p-value derived from the extra sum of squares test. NS (non-statistically significant) denotes p= >0.05, * denotes p= ≤0.05, ** denotes p= ≤0.01, *** denotes p= 0.001 (One-way ANOVA with Dunnett correction for multiple comparisons).* *215*

*Figure 3-11: Comparison of Barasertib vs Barasertib and chemotherapy (5-FU and Etoposide) in H1299 cell lines (n=3). Cells were pre-incubated with either 5FU, Etoposide or AURKB inhibitor Barasertib, cells were left to form colonies for 10-14 days before colony outgrowth under continuous exposure to the 5FU, Etoposide and/or AURKB inhibitor Barasertib. Data points represent the mean survival fraction normalised to DMSO +/- SD (N= ≥3). F-value and p-value derived from the extra sum of squares test. NS (non-statistically significant) denotes p= >0.05, * denotes p= ≤0.05, ** denotes p= ≤0.01, *** denotes p= 0.001 (One-way ANOVA with Dunnett correction for multiple comparisons).* *216*

Figure 3-12 ***Barasertib and Chemotherapy in H460 cell lines*** *Survival fraction of H460 cells after treatment with IR in combination with Barasertib and Chemotherapy, a combination which led to the lowest cell survival was seen in H460's treated with Barasertib and 5FU. Cells were pre-incubated with Cisplatin, 5FU, Vinorelbine and Barasertib before irradiation and colony outgrowth under continuous exposure to the AURKB inhibitor Barasertib. Data points represent the mean survival fraction normalised to unirradiated control +/- SD (N= ≥3). F-value and p-value derived from the extra sum of squares test. 218*

Figure 3-13: ***Normal Mitosis A-I*** *H1299 cell, undergoing mitosis, dividing into two daughter cells, the central spindle can be observed along with chromatin separation in anaphase. This was observed at 20X magnification using a Zeiss Cell Discoverer 7 HCS microscope; the cells were treated with Barasertib and viewed between successive time frames taken 120 seconds apart. 221*

Figure 3-14: ***Death in mitosis by apoptosis A-I*** *This SCC89 cell is undergoing apoptosis; the cell undergoes rounding as if it will go into the normal process of mitosis but instead undergoes cell blebbing and dies. The cell, over time, detaches from the plate and floats in the media. This was observed at 20X magnification using a Zeiss Cell Discoverer 7 HCS microscope; the cells were treated with Barasertib and viewed between successive time frames taken 120 seconds apart. 222*

Figure 3-15: ***Cell slippage A-I*** *An H1299 cell undergoing slippage where the cells round up but do not divide into two daughters; instead, it "escapes" rounding and becomes the mother cell again. We also observed this slippage occurring on two and three successive occasions. This was observed at 20X magnification using a Zeiss Cell Discoverer 7 HCS microscope; the cells were treated with Barasertib and viewed between successive time frames taken 120 seconds apart. 223*

Figure 3-16: ***Chromosome congression A-I*** *H1299 cells above demonstrate chromosomes "clumped in a ball," which could be possible chromosome congression heralding spindle assembly checkpoint, kinetochore-microtubule attachment, or centrosome function, and can lead to aneuploidy and genomic instability, in this case the cell ultimately underwent slippage, observed at 20X magnification using Zeiss Cell Discoverer 7 HCS microscope, the cells were treated with Barasertib and viewed between successive time frames taken 120 seconds apart. 224*

Figure 3-17: ***Multipolar spindle A-I*** *H1299 cells showing the multipolar spindle before undergoing slippage, multipolar spindle were seen before cells underwent aberrant mitosis observed at 20X*

magnification using Zeiss Cell Discoverer 7 HCS microscope, the cells were treated with Barasertib and viewed between successive time frames taken 120 seconds apart. 225

*Figure 3-18: **H460 live cell analysis 24-36 hours post-irradiation + 25nM Barasertib** showing time in mitosis, proportion of intra-mitotic death, aberrant mitosis resulting in >2 daughter cells and proportion of cells undergoing slippage—minimum 50 mitotic cells counted per repeat. Data points represent the mean proportion of mitotic cells with described outcome +/- SD (N= 3) NS (non-statistically significant) denotes p= >0.05, * denotes p= ≤0.05, ** denotes p= ≤0.01, *** denotes p= 0.001 (One-way ANOVA with Dunnett correction for multiple comparisons). 227*

*Figure 3-19: **H460 live cell analysis 24-36 hours post-irradiation + 50nM Barasertib** showing time in mitosis, proportion of intra-mitotic death, aberrant mitosis resulting in >2 daughter cells and proportion of cells undergoing slippage—minimum 50 mitotic cells counted per repeat. Data points represent the mean proportion of mitotic cells with described outcome +/- SD (N= 3) NS (non-statistically significant) denotes p= >0.05, * denotes p= ≤0.05, ** denotes p= ≤0.01, *** denotes p= ≤0.001 (One-way ANOVA with Dunnett correction for multiple comparisons). 228*

*Figure 3-20: **H1299 live cell analysis 24-36 hours post-irradiation + 25nM Barasertib A-D** showing proportion of intra-mitotic death and aberrant mitosis resulting in >2 daughter cells time in mitosis, and proportion of cells undergoing slippage —minimum 50 mitotic cells counted per repeat. Data points represent the mean proportion of mitotic cells with described outcome +/- SD (N= 3) NS (non-statistically significant) denotes p= >0.05, * denotes p= ≤0.05, ** denotes p= ≤0.01, *** denotes p= ≤0.001 (One-way ANOVA with Dunnett correction for multiple comparisons). 231*

*Figure 3-21: **H1299 live cell analysis 24-36 hours post-irradiation + 50nM A-D** showing proportion of intra-mitotic death and aberrant mitosis resulting in >2 daughter cells time in mitosis, and proportion of cells undergoing slippage —minimum 50 mitotic cells counted per repeat. Data points represent the mean proportion of mitotic cells with described outcome +/- SD (N= 3) NS (non-statistically significant) denotes p= >0.05, * denotes p= ≤0.05, ** denotes p= ≤0.01, *** denotes p= ≤0.001 (One-way ANOVA with Dunnett correction for multiple comparisons). 232*

*Figure 3-22: **A549 live cell analysis 24-36 hours Barasertib alone A-D** showing proportion of intra-mitotic death and aberrant mitosis resulting in >2 daughter cells time in mitosis, and proportion of cells undergoing slippage —minimum 50 mitotic cells counted per repeat. Data points represent the mean*

*proportion of mitotic cells with described outcome +/- SD (N= 3) NS (non-statistically significant) denotes p= >0.05, * denotes p= ≤0.05, ** denotes p= ≤0.01, *** denotes p= ≤0.001 (One-way ANOVA with Dunnett correction for multiple comparisons).* *234*

Figure 3-23: ***H520 live cell analysis 24-36 hours Barasertib alone A-D*** *showing proportion of intra-mitotic death and aberrant mitosis resulting in >2 daughter cells time in mitosis, and proportion of cells undergoing slippage —minimum 50 mitotic cells counted per repeat. Data points represent the mean proportion of mitotic cells with described outcome +/- SD (N= 3) NS (non-statistically significant) denotes p= >0.05, * denotes p= ≤0.05, ** denotes p= ≤0.01, *** denotes p= ≤0.001 (One-way ANOVA with Dunnett correction for multiple comparisons).* *236*

Figure 3-24: ***H460 live cell analysis 24-36 hours Barasertib alone A-D*** *showing proportion of intra-mitotic death and aberrant mitosis resulting in >2 daughter cells time in mitosis, and proportion of cells undergoing slippage —minimum 50 mitotic cells counted per repeat. Data points represent the mean proportion of mitotic cells with described outcome +/- SD (N= 3) NS (non-statistically significant) denotes p= >0.05, * denotes p= ≤0.05, ** denotes p= ≤0.01, *** denotes p= ≤0.001 (One-way ANOVA with Dunnett correction for multiple comparisons).* *237*

Figure 3-25: ***A549 live cell analysis 0-16 hours post-Barasertib A-D*** *showing proportion of intra-mitotic death and aberrant mitosis resulting in >2 daughter cells time in mitosis, and proportion of cells undergoing slippage —minimum 50 mitotic cells counted per repeat. Data points represent the mean proportion of mitotic cells with described outcome +/- SD (N= 3) NS (non-statistically significant) denotes p= >0.05, * denotes p= ≤0.05, ** denotes p= ≤0.01, *** denotes p= ≤0.001 (One-way ANOVA with Dunnett correction for multiple comparisons).* *240*

Figure 3-26: ***A549 live cell analysis 36-48 hours post-Barasertib A-D*** *showing proportion of intra-mitotic death and aberrant mitosis resulting in >2 daughter cells time in mitosis, and proportion of cells undergoing slippage —minimum 50 mitotic cells counted per repeat. Data points represent the mean proportion of mitotic cells with described outcome +/- SD (N= 3) NS (non-statistically significant) denotes p= >0.05, * denotes p= ≤0.05, ** denotes p= ≤0.01, *** denotes p= ≤0.001 (One-way ANOVA with Dunnett correction for multiple comparisons).* *241*

Figure 3-27: ***A549 live cell analysis 0-72 hours post-Barasertib*** *A. Time in mitosis resulting in cytokinesis. B. Proportion of intra-mitotic death C. Proportion of daughter cells dying after slippage D.*

*Proportion of cells dying after slippage. E. Proportion of cells undergoing slippage. F-H The proportion of cells undergoing slippage categorised by number of times the cells slipped in 72 hours regardless of outcome —minimum 50 mitotic cells counted per condition. Data points represent the mean proportion of mitotic cells with described outcome +/- SEM (N= 5). NS (non-statistically significant) denotes p= >0.05, * denotes p= ≤0.05, ** denotes p= ≤0.01, *** denotes p= ≤0.001 (One-way ANOVA with Dunnett correction for multiple comparisons).* *245*

*Figure 3-28: Quantification of CDC20 and Cyclin B1 expression normalised to GAPDH levels. A-B UPCI-SCC72 C-D SCC89 E-F BICR22 (N= ≥3). * Denotes p= ≤0.05, ** denotes p= ≤0.01, *** denotes p=≤0.001 (One-Way ANOVA).* *247*

*Figure 3-29: Quantification of CDC20 and Cyclin B1 expression normalised to GAPDH levels. A-B A549 C-D H460 (N= ≥3). * Denotes p= ≤0.05, ** denotes p= ≤0.01, *** denotes p=≤0.001 (One-Way ANOVA).* ... *248*

Figure 3-30: ***H520 cell cycle distribution 2-, 24- and 48-hours following treatment with 5 nM Barasertib.*** *NSCLC cells (1-2 x 10^5) were seeded per 90 mm^3 dish and harvested for FACS analysis at 24-, 48-, and 72-hours post-irradiation. Cells were washed, dislodged with trypsin, pooled, and centrifuged at 1200 RPM. After washing, they were resuspended in 100% methanol and stored at -20°C. For staining, cells were incubated with S10 p-Histone 3 primary antibody followed by Alexa 488 secondary antibody, then stained with propidium iodide (PI)/RNAse A solution. Flow cytometry analysis was conducted using FlowJo™ software, with cell populations gated based on PI intensity to identify G1, S, G2-M, mitotic, and polyploid populations. Doublets were excluded by plotting FL3-Area vs. FL3-Width. Data points represent mean cell cycle phase distribution +/- S SD (N= ≥3).* *250*

Figure 3-31: ***A549 cell cycle distribution 2-, 24- and 48-hours following treatment with 5 nM Barasertib.*** *NSCLC cells (1-2 x 10^5) were seeded per 90 mm^3 dish and harvested for FACS analysis at 24-, 48-, and 72-hours post-irradiation. Cells were washed, dislodged with trypsin, pooled, and centrifuged at 1200 RPM. After washing, they were resuspended in 100% methanol and stored at -20°C. For staining, cells were incubated with S10 p-Histone 3 primary antibody followed by Alexa 488 secondary antibody, then stained with propidium iodide (PI)/RNAse A solution. Flow cytometry analysis was conducted using FlowJo™ software, with cell populations gated based on PI intensity to identify G1, S, G2-M, mitotic, and polyploid populations. Doublets were excluded by plotting FL3-Area vs. FL3-Width. Data points represent mean cell cycle phase distribution +/- S SD (N= ≥3).* *251*

Figure 3-32: ***H520 and A549 cell cycle distribution 2-, 16- and 24-hours following treatment with 5 nM Barasertib.*** *NSCLC cells (1-2 x 10^5) were seeded per 90 mm^3 dish and harvested for FACS analysis at 24-, 48-, and 72-hours post-irradiation. Cells were washed, dislodged with trypsin, pooled, and centrifuged at 1200 RPM. After washing, they were resuspended in 100% methanol and stored at -20°C. For staining, cells were incubated with S10 p-Histone 3 primary antibody followed by Alexa 488 secondary antibody, then stained with propidium iodide (PI)/RNAse A solution. Flow cytometry analysis was conducted using FlowJo™ software, with cell populations gated based on PI intensity to identify G1, S, G2-M, mitotic, and polyploid populations. Doublets were excluded by plotting FL3-Area vs. FL3-Width. Data points represent mean cell cycle phase distribution +/- S SD (N= ≥3).Data points represent mean cell cycle phase distribution +/- SD (N= ≥3). Statistical testing: 2 tailed unpaired T.test where ns is non-significant, * p = <0.05 ** p = <0.001 *** p = <0.0001 and **** p = <0.00001..... 253*

Figure 3-33: ***H460 cell cycle distribution 2-, 16- and 24-hours following treatment with 5 nM Barasertib.*** *NSCLC cells (1-2 x 10^5) were seeded per 90 mm^3 dish and harvested for FACS analysis at 24-, 48-, and 72-hours post-irradiation. Cells were washed, dislodged with trypsin, pooled, and centrifuged at 1200 RPM. After washing, they were resuspended in 100% methanol and stored at -20°C. For staining, cells were incubated with S10 p-Histone 3 primary antibody followed by Alexa 488 secondary antibody, then stained with propidium iodide (PI)/RNAse A solution. Flow cytometry analysis was conducted using FlowJo™ software, with cell populations gated based on PI intensity to identify G1, S, G2-M, mitotic, and polyploid populations. Doublets were excluded by plotting FL3-Area vs. FL3-Width. Data points represent mean cell cycle phase distribution +/- S SD (N= ≥3).Data points represent mean cell cycle phase distribution +/- SD (N= ≥3). Statistical testing: 2 tailed unpaired T.test where ns is non-significant, * p = <0.05 ** p = <0.001 *** p = <0.0001 and **** p = <0.00001..... 254*

Figure 4-1: ***Barasertib monotherapy in HNSCC cell lines and Western Blots of Phospho H3 in HNSCC cell lines*** *Survival fraction was calculated using clonogenic assay under continuous exposure to the AURKB inhibitor Barasertib. Data points represent the mean survival fraction normalised to untreated control +/- SD (N= 3). B: Table showing the genetic type of each cell line. Representative western blot results for pan p-AURK, AURKA (total B) and GAPDH in protein extracts from OPSCC89, OPSCC72, FNB6, OPSCC2 and B22/BICR22 cells arrested overnight with 100 ng/ml Nocodazole (Noc) and released into*

increasing concentrations of Barasertib the OPSCC-89, OPSCC-72, FNB6 and OPSCC-2 assays were done with the help of Dr. Polly Greaves. 274

Figure 4-2 ***Barasertib and IR in HNSCC cell lines*** *Survival fraction of HNSCC cells after treatment with IR alone or IR in combination with Barasertib; no radiosensitisation was seen in any cell line tested. The survival fraction was calculated using a clonogenic assay. Cells were pre-incubated with Barasertib before irradiation and colony outgrowth under continuous exposure to the AURKB inhibitor Barasertib. Data points represent the mean survival fraction normalised to unirradiated control +/- SD (N= ≥3). F-value and p-value derived from the extra sum of squares test. 276*

*Figure 4-3: Comparison of Barasertib vs Barasertib and chemotherapy (Cisplatin and Vinorelbine) in BICR22 cell lines (n=3) Cells were pre-incubated with either Cisplatin, Vinorelbine or AURKB inhibitor Barasertib, cells were left to form colonies for 10-14 days before colony outgrowth under continuous exposure to the Cisplatin, Vinorelbine and/or AURKB inhibitor Barasertib. Data points represent the mean survival fraction normalised to DMSO +/- SD (N= ≥3). F-value and p-value derived from the extra sum of squares test. NS (non-statistically significant) denotes p= >0.05, * denotes p= ≤0.05, ** denotes p= ≤0.01, *** denotes p= 0.001 (One-way ANOVA with Dunnett correction for multiple comparisons). 279*

*Figure 4-4: Comparison of Barasertib vs Barasertib and chemotherapy (5-FU and Etoposide) in BICR22 cell lines (n=3). Cells were pre-incubated with either 5FU, Etoposide or AURKB inhibitor Barasertib, cells were left to form colonies for 10-14 days before colony outgrowth under continuous exposure to the 5FU, Etoposide and/or AURKB inhibitor Barasertib. Data points represent the mean survival fraction normalised to DMSO +/- SD (N= ≥3). F-value and p-value derived from the extra sum of squares test. NS (non-statistically significant) denotes p= >0.05, * denotes p= ≤0.05, ** denotes p= ≤0.01, *** denotes p= 0.001 (One-way ANOVA with Dunnett correction for multiple comparisons). 280*

*Figure 4-5: Comparison of Barasertib vs Barasertib and chemotherapy (Cisplatin and Vinorelbine) in FNB6 cell lines (n=3) Cells were pre-incubated with either Cisplatin, Vinorelbine or AURKB inhibitor Barasertib, cells were left to form colonies for 10-14 days before colony outgrowth under continuous exposure to the Cisplatin, Vinorelbine and/or AURKB inhibitor Barasertib. Data points represent the mean survival fraction normalised to DMSO +/- SD (N= ≥3). F-value and p-value derived from the extra sum of squares test. NS (non-statistically significant) denotes p= >0.05, * denotes p= ≤0.05, ** denotes p= ≤0.01, *** denotes p= 0.001 (One-way ANOVA with Dunnett correction for multiple comparisons). 282*

*Figure 4-6: Comparison of Barasertib vs Barasertib and chemotherapy (5-FU and Etoposide) in FNB6 cell lines (n=3) Cells were pre-incubated with either 5FU, Etoposide or AURKB inhibitor Barasertib, cells were left to form colonies for 10-14 days before colony outgrowth under continuous exposure to the 5FU, Etoposide and/or AURKB inhibitor Barasertib. Data points represent the mean survival fraction normalised to DMSO +/- SD (N= ≥3). F-value and p-value derived from the extra sum of squares test. NS (non-statistically significant) denotes p= >0.05, * denotes p= ≤0.05, ** denotes p= ≤0.01, *** denotes p= 0.001 (One-way ANOVA with Dunnett correction for multiple comparisons). 283*

*Figure 4-7: **UPCI-SCC72 live cell analysis 24-36 hours post-Barasertib A-D** showing proportion of intra-mitotic death and aberrant mitosis resulting in >2 daughter cells time in mitosis, and proportion of cells undergoing slippage —minimum 50 mitotic cells counted per repeat. Data points represent the mean proportion of mitotic cells with described outcome +/- SD (N= 3) NS (non-statistically significant) denotes p= >0.05, * denotes p= ≤0.05, ** denotes p= ≤0.01, *** denotes p= ≤0.001 (One-way ANOVA with Dunnett correction for multiple comparisons). 285*

*Figure 4-8: **SCC89 live cell analysis 24-36 hours post-Barasertib A-D** showing proportion of intra-mitotic death and aberrant mitosis resulting in >2 daughter cells time in mitosis, and proportion of cells undergoing slippage —minimum 50 mitotic cells counted per repeat. Data points represent the mean proportion of mitotic cells with described outcome +/- SD (N= 3) NS (non-statistically significant) denotes p= >0.05, * denotes p= ≤0.05, ** denotes p= ≤0.01, *** denotes p= ≤0.001 (One-way ANOVA with Dunnett correction for multiple comparisons). 287*

*Figure 4-9: **BICR22 live cell analysis 24-36 hours post-Barasertib A-D** showing proportion of intra-mitotic death and aberrant mitosis resulting in >2 daughter cells time in mitosis, and proportion of cells undergoing slippage —minimum 50 mitotic cells counted per repeat. Data points represent the mean proportion of mitotic cells with described outcome +/- SD (N= 3) NS (non-statistically significant) denotes p= >0.05, * denotes p= ≤0.05, ** denotes p= ≤0.01, *** denotes p= ≤0.001 (One-way ANOVA with Dunnett correction for multiple comparisons). 289*

*Figure 4-10: **FNB6 live cell analysis 24-36hours post Barasertib A-D** showing proportion of intra-mitotic death and aberrant mitosis resulting in >2 daughter cells time in mitosis, and proportion of cells undergoing slippage —minimum 50 mitotic cells counted per repeat. Data points represent the mean proportion of mitotic cells with described outcome +/- SD (N= 4) NS (non-statistically significant) denotes*

*p= >0.05, * denotes p= ≤0.05, ** denotes p= ≤0.01, *** denotes p= ≤0.001 (One-way ANOVA with Dunnett correction for multiple comparisons).* *290*

Figure 4-11: ***SCC89 live cell analysis 0-16 hours post-Barasertib A-D*** *showing proportion of intra-mitotic death and aberrant mitosis resulting in >2 daughter cells time in mitosis, and proportion of cells undergoing slippage —minimum 50 mitotic cells counted per repeat. Data points represent the mean proportion of mitotic cells with described outcome +/- SD (N= 3) NS (non-statistically significant) denotes p= >0.05, * denotes p= ≤0.05, ** denotes p= ≤0.01, *** denotes p= ≤0.001 (One-way ANOVA with Dunnett correction for multiple comparisons).* *292*

Figure 4-12: ***UPCI-SCC72 live cell analysis 0-16 hours post-Barasertib A-D*** *showing proportion of intra-mitotic death and aberrant mitosis resulting in >2 daughter cells time in mitosis, and proportion of cells undergoing slippage —minimum 50 mitotic cells counted per repeat. Data points represent the mean proportion of mitotic cells with described outcome +/- SD (N= 3) NS (non-statistically significant) denotes p= >0.05, * denotes p= ≤0.05, ** denotes p= ≤0.01, *** denotes p= ≤0.001 (One-way ANOVA with Dunnett correction for multiple comparisons).* *293*

Figure 4-13: ***UPCI-SCC72 live cell analysis 36-48 hours post-Barasertib A-D*** *showing proportion of intra-mitotic death and aberrant mitosis resulting in >2 daughter cells time in mitosis, and proportion of cells undergoing slippage —minimum 50 mitotic cells counted per repeat. Data points represent the mean proportion of mitotic cells with described outcome +/- SD (N= 3) NS (non-statistically significant) denotes p= >0.05, * denotes p= ≤0.05, ** denotes p= ≤0.01, *** denotes p= ≤0.001 (One-way ANOVA with Dunnett correction for multiple comparisons).* *295*

Figure 4-14: ***SCC89 live cell analysis 36-48 hours post-Barasertib A-D*** *showing proportion of intra-mitotic death and aberrant mitosis resulting in >2 daughter cells time in mitosis, and proportion of cells undergoing slippage —minimum 50 mitotic cells counted per repeat. Data points represent the mean proportion of mitotic cells with described outcome +/- SD (N= 3) NS (non-statistically significant) denotes p= >0.05, * denotes p= ≤0.05, ** denotes p= ≤0.01, *** denotes p= ≤0.001 (One-way ANOVA with Dunnett correction for multiple comparisons).* *296*

Figure 4-15: ***UPCI-SCC72 live cell analysis 0-72 hours post-Barasertib*** *A. Time in mitosis resulting in cytokinesis. B. Proportion of intra-mitotic death C. Proportion of daughter cells dying after slippage D. Proportion of cells dying after slippage. E. Proportion of cells undergoing slippage. F-H Proportion of cells*

*undergoing slippage categorised by number of times the cells slipped in 72 hours regardless of outcome —minimum 50 mitotic cells counted per condition. Data points represent the mean proportion of mitotic cells with described outcome +/- SEM (N= 5). NS (non-statistically significant) denotes p= >0.05, * denotes p= ≤0.05, ** denotes p= ≤0.01, *** denotes p= ≤0.001 (One-way ANOVA with Dunnett correction for multiple comparisons).* *299*

Figure 4-16: ***SCC89 live cell analysis 0-72 hours post-Barasertib*** *A. Time in mitosis resulting in cytokinesis. B. Proportion of intra-mitotic death C. Proportion of cells undergoing slippage. D. Proportion of cells dying after slippage. E. Proportion of daughter cells dying after slippage—minimum 50 mitotic cells counted per condition. Data points represent the mean proportion of mitotic cells with described outcome +/- SEM (N= 5). NS (non-statistically significant) denotes p= >0.05, * denotes p= ≤0.05, ** denotes p= ≤0.01, *** denotes p= ≤0.001 (One-way ANOVA with Dunnett correction for multiple comparisons).* *302*

*Figure 4-17: Quantification of CDC20 and Cyclin B1 expression normalised to GAPDH levels. A-B UPCI-SCC72 C-D SCC89 E-F BICR22 (N= ≥3). * Denotes p= ≤0.05, ** denotes p= ≤0.01, *** denotes p=≤0.001 (One-Way ANOVA).* *304*

Figure 4-18: ***SCC89 cell cycle distribution 2-, 24- and 48-hours following treatment with 1 nM Barasertib.*** *HNSCC cells (1-2 x 10^5) were seeded per 90 mm^3 dish and harvested for FACS analysis at 24-, 48-, and 72-hours post-irradiation. Cells were washed, dislodged with trypsin, pooled, and centrifuged at 1200 RPM. After washing, they were resuspended in 100% methanol and stored at -20°C. For staining, cells were incubated with S10 p-Histone 3 primary antibody followed by Alexa 488 secondary antibody, then stained with propidium iodide (PI)/RNAse A solution. Flow cytometry analysis was conducted using FlowJo™ software, with cell populations gated based on PI intensity to identify G1, S, G2-M, mitotic, and polyploid populations. Doublets were excluded by plotting FL3-Area vs. FL3-Width. Data points represent mean cell cycle phase distribution +/- S SD (N= ≥3).Data points represent mean cell cycle phase distribution +/- SD (N= ≥3). Statistical testing: 2 tailed unpaired T.test where ns is non-significant, * p = <0.05 ** p = <0.001 *** p = <0.0001 and **** p = <0.00001*..... *306*

Figure 4-19: ***UPCI-SCC72 cell cycle distribution 2-, 24- and 48-hours following treatment with 1 nM Barasertib.*** *HNSCC cells (1-2 x 10^5) were seeded per 90 mm^3 dish and harvested for FACS analysis at 24-, 48-, and 72-hours post-irradiation. Cells were washed, dislodged with trypsin, pooled, and centrifuged*

*at 1200 RPM. After washing, they were resuspended in 100% methanol and stored at -20°C. For staining, cells were incubated with S10 p-Histone 3 primary antibody followed by Alexa 488 secondary antibody, then stained with propidium iodide (PI)/RNAse A solution. Flow cytometry analysis was conducted using FlowJo™ software, with cell populations gated based on PI intensity to identify G1, S, G2-M, mitotic, and polyploid populations. Doublets were excluded by plotting FL3-Area vs. FL3-Width. Data points represent mean cell cycle phase distribution +/- S SD (N= ≥3).Data points represent mean cell cycle phase distribution +/- SD (N= ≥3). Statistical testing: 2 tailed unpaired T.test where ns is non-significant, * p = <0.05 ** p = <0.001 *** p = <0.0001 and **** p = <0.00001..... 307*

*Figure 4-20: **BICR22 cell cycle distribution 2-, 24- and 48-hours following treatment with 10 nM Barasertib.** HNSCC cells (1-2 x 10^5) were seeded per 90 mm^3 dish and harvested for FACS analysis at 24-, 48-, and 72-hours post-irradiation. Cells were washed, dislodged with trypsin, pooled, and centrifuged at 1200 RPM. After washing, they were resuspended in 100% methanol and stored at -20°C. For staining, cells were incubated with S10 p-Histone 3 primary antibody followed by Alexa 488 secondary antibody, then stained with propidium iodide (PI)/RNAse A solution. Flow cytometry analysis was conducted using FlowJo™ software, with cell populations gated based on PI intensity to identify G1, S, G2-M, mitotic, and polyploid populations. Doublets were excluded by plotting FL3-Area vs. FL3-Width. Data points represent mean cell cycle phase distribution +/- S SD (N= ≥3).Data points represent mean cell cycle phase distribution +/- SD (N= ≥3). Statistical testing: 2 tailed unpaired T.test where ns is non-significant, * p = <0.05 ** p = <0.001 *** p = <0.0001 and **** p = <0.00001..... 308*

*Figure 4-21: **SCC89 and UPCI-SCC72 cell cycle distribution 2-, 16- and 24-hours following treatment with 5 nM Barasertib.** Data points represent mean cell cycle phase distribution +/- SD (N= ≥3). Statistical testing: 2 tailed unpaired T.test where ns is non-significant, * p = <0.05 ** p = <0.001 *** p = <0.0001 and **** p = <0.00001 ..... 311*

*Figure 5-1: **The Bioinformatic Pathway outline on the NSCLC and HNSCC tissue data sets.** Five NSCLC samples were chosen alongside four oral cavity and two nasopharyngeal samples. 328*

*Figure 5-2: **A:** Using a Venn diagram demonstrating the common Hub genes between GSE30219, GSE33532 and GSE101929 (https://molbiotools.com/listcompare.php). **B-C** Using Cytoscape, the PPI network demonstrating a network comprising 277 nodes and 1825 edges is visualised. A close-up of AURKA and AURKB within the PPI network is shown. The Networks were plotted by inputting the 30 HUB*

*genes using the STRING app, part of the Cytoscape software **D** AURKA and AURKB were visualised using MCODE (Molecular Complex Detection) a plugin for Cytoscape a software tool for visualizing and analyzing biological networks using a Degree Cutoff of two a Node score cut off of 0.2 a K-score of 2 and a Max depth of 100. ..... 336*

Figure 5-3: Kaplein Mayer plots showed that overall survival was worse in all high-expressing patients using the identified hub genes and (labelled STK12 on https://kmplot.com/). NSCLC patients were chosen using the website https://kmplot.com/. Metastatic patients were excluded from the analysis; patients had to have surgery, chemotherapy, and radiotherapy, leaving 463 out of 2000 patients to be analysed. Multivariate analysis was done along with long-rank testing. 342

Figure 5-4: Kaplein Mayer plots showed that overall survival was worse in all high-expressing samples using the identified hub genes. Metastatic patients were excluded from the analysis; patients had to have surgery, chemotherapy, and radiotherapy, leaving 463 out of 2167. Multivariate analysis was done along with log-rank testing. 350

Figure 5-5: Kaplein Mayer plots showed that post-progression survival was no worse in all high-expressing patients using the identified hub genes and (labelled STK12 on https://kmplot.com/). NSCLC patients were chosen using the website https://kmplot.com/. Metastatic patients were excluded from the analysis; patients had to have surgery, chemotherapy, and radiotherapy, leaving 159 out of 477 available patients to be analysed. Multivariate analysis was done along with log-rank testing. 360

Figure 5-6 Expression Analysis using GEPIA demonstrated that all hub genes were overexpressed in adenocarcinoma and squamous cell cancer tissue compared to normal tissue samples (log2IFCI cut-off of 2 and p-value cut-off of 0.01). Expression box plots of the thirty hub genes in using the website (http://gepia2.cancer-pku.cn/#analysis). 366

*Figure 5-7 **A** Using a Venn diagram demonstrating the common Hub genes between GSE78060, and GSE74530 (https://molbiotools.com/listcompare.php). **B-C** Using Cytoscape, the PPI network demonstrating a network comprising 373 nodes and 1477 edges is visualised. A close-up of AURKA within the PPI network is shown. The Networks were plotted by inputting the 30 HUB genes using the STRING app, part of the Cytoscape software. 374*

Figure 5-8: AURKA was visualised using MCODE (Molecular Complex Detection), a plugin for Cytoscape, a software tool for visualizing and analyzing biological networks using a Degree Cutoff of two, a Node score cut off of 0.2, a K-score of 2, and a Max depth of 100. ..... *376*

Figure 5-9: Expression Analysis using GEPIA demonstrated that all hub genes were overexpressed in adenocarcinoma and squamous cell cancer tissue compared to normal tissue samples (log2IFCI cut-off of 2 and p-value cut-off of 0.01. Expression box plots of the select genes in the most significant module in the PPI network using the website (http://gepia2.cancer-pku.cn/#analysis). *377*

Figure 5-10: ***A*** *Using a Venn diagram demonstrating the common Hub genes between GSE12452 and GSE13597 (https://molbiotools.com/listcompare.php).* *382*

Figure 5-11 A-F: ***Representative images of staining in NSCLC tissue scored with increasing H-scores 0,4,30,65,120 and 240 A-F*** *respectively. Standard comparative protocol using labelled 1:200 used microwave retrieval with IMMPRESS® signal detection system and pH 6.1 citrate target retrieval solution. Antibody signal on stained cells was developed with DAB for 1 minute, and cells were counterstained with Gill's hematoxylin for 10 seconds (N=1). Scale bars represent 50 to 200µm. All slides were scanned using a panoramic 250 slide scanner using a 20x objective. H scores were calculated as a function of staining intensity and percentage of tumour cells positive.* *392*

Figure 5-12: ***Distribution of H-scores in patient diagnostic biopsies.*** *Points show individual samples, and the red line indicates the median value.* *393*

*Figure 5-13: H-scores in different subgroups of patients (A) Histological type. Note that large cell lung cancer and neuroendocrine were excluded from statistical analysis due to low sample size, (B) gender, (C) ethnicity, and (D) stage of disease. Dots represent individual samples; the red line represents the median value. Statistical significance was calculated using the Mann-Whitney U test where *=p<0.05 and ns = non-significant.* *395*

Figure 5-14: Overall survival (A) and Progression-free survival (B) comparing AURKA positive (+ve (H score 0 to 240)) to AURKA (-ve (H score 0 to 240) patients. Significance using the R programming software calculated by log-rank testing where ns = non-significant. *397*

Figure 5-15 Overall survival comparing positive (+ve) to (-ve) patients, within sub-populations (A) Male Gender, (B) Female Gender, (C) Non-Metastatic patients (D)Metastatic patients (E)SCC patients,

(F)Adenocarcinoma patients, (G) Current Smokers, (H) Former Smokers, (I) Patient is over 70 years old (J) Patients under 70 years old—significance calculated by log-rank testing where ns = non-significant... 401

Figure 5-16 Progression-free survival comparing positive (+ve) to (-ve) patients within sub-populations (A) Male Gender, (B) Female Gender, (C) Non-Metastatic patients (D)Metastatic patients (E)SCC patients, (F)Adenocarcinoma patients, (G) Current Smokers, (H) Former Smokers, (I) Patient is over 70 years old (J) Patients under 70 years old—significance calculated by log-rank testing where ns = non-significant. .. 405

Figure 5-17: ***Representative images of staining in NSCLC tissue with orange arrows pointing to increased tissue stroma and cellular cytoplasm staining****. Standard comparative protocol using labelled 1:200 used microwave retrieval with IMMPRESS® signal detection system and pH 6.1 citrate target retrieval solution. Antibody signal on stained cells was developed with DAB for 1 minute, and cells were counterstained with Gill's hematoxylin for 10 seconds (N=1). Scale bars represent 200µm. All slides were scanned using a panoramic 250 slide scanner using a 20x objective..... 407*

Figure 5-18 ***Results of the optimisation of antibody using the IMMPRESS® Excel Amplified Polymer Staining Kit demonstrating increased background staining and no improvement in nuclear staining in a slide with an H-score of 15 (A-B):*** *A Staining without the use of the IMMPRESS® Excel Amplified Polymer Staining Kit B Staining with use of the IMMPRESS® Excel Amplified Polymer Staining Kit black arrows show areas of heavy stromal staining****:*** *Standard comparative protocol using labelled 1:200 used microwave retrieval with IMMPRESS® Excel Amplified Polymer Staining Kit and pH 6.1 citrate target retrieval solution. Antibody signal on stained cells was developed with DAB for 1 minute, and cells were counterstained with Gill's hematoxylin for 10 seconds (N=1). Scale bars represent 50 µm. All slides were scanned using a panoramic 250 slide scanner using a 20x objective..... 410*

Figure 5-19 ***Results of the optimisation of antibody using the IMMPRESS® Excel Amplified Polymer Staining Kit demonstrating increased background staining and no improvement in nuclear staining in a slide with an H-score of 100 (A-B):*** *A Staining without the use of the IMMPRESS® Excel Amplified Polymer Staining Kit B Staining with use of the IMMPRESS® Excel Amplified Polymer Staining Kit black arrows show areas of "half stained" nuclei****:*** *Standard comparative protocol using labelled 1:200 used microwave retrieval with IMMPRESS® Excel Amplified Polymer Staining Kit and pH 6.1 citrate target retrieval solution. Antibody signal on stained cells was developed with DAB for 1 minute, and cells were*

counterstained with Gill's hematoxylin for 10 seconds (N=1). Scale bars represent 50µm. All slides were scanned using a panoramic 250 slide scanner using a 20x objective. *411*

Figure 5-20 ***Results of the optimisation of antibody using the IMMPRESS® Excel Amplified Polymer Staining Kit demonstrating increased background staining (A-B):*** *A Staining on low microwave settings B Staining on high microwave settings**:** Standard comparative protocol using labelled 1:200 used microwave retrieval with IMMPRESS® Excel Amplified Polymer Staining Kit and pH 6.1 citrate target retrieval solution. Antibody signal on stained cells was developed with DAB for 1 minute, and cells were counterstained with Gill's hematoxylin for 10 seconds (N=1). Scale bars represent 50µm. All slides were scanned using a panoramic 250 slide scanner using a 20x objective.* *412*

Figure 5-21 ***Results of the optimisation of antibody using the IMMPRESS® Excel Amplified Polymer Staining Kit demonstrating cells which look as if not all of the nuclei have been stained properly "half staining":*** *Standard comparative protocol using labelled 1:200 used microwave retrieval (low settings) with IMMPRESS® Excel Amplified Polymer Staining Kit and pH 6.1 citrate target retrieval solution. Antibody signal on stained cells was developed with DAB for 1 minute, and cells were counterstained with Gill's hematoxylin for 10 seconds (N=1). Scale bars represent 50 µm. All slides were scanned using a panoramic 250 slide scanner using a 20x objective.* *413*

Figure 5-22: ***Results of the optimisation of antibody using the IMMPRESS® Excel Amplified Polymer Staining Kit demonstrating no improvement in the slides which initially had no staining (H-Score 0):*** *A shows the original slide with an H score of 0 with no observable nuclear staining. In contrast, the slide shows increased stromal staining rather than some half-staining of cellular nuclei in B. C shows the original slide with an H score of 0 with no observable nuclear staining, while in D, the slide shows "dirty" and inconsistent nuclear staining "half staining" of cellular nuclei. Standard comparative protocol using labelled 1:200 used microwave retrieval (low settings) with IMMPRESS® Excel Amplified Polymer Staining Kit and pH 6.1 citrate target retrieval solution. Antibody signal on stained cells was developed with DAB for 1 minute, and cells were counterstained with Gill's hematoxylin for 10 seconds (N=1). Scale bars represent 50 µm. All slides were scanned using a panoramic 250 slide scanner using a 20x objective.* *415*

Figure 5-23 Western blot of total AURKB antibody using H460 cell pellets with GAPDH as the loading control. Cell extracts were made, and the western blot was done using the RIPA method. *417*

Figure 5-24 ***Representative images of (1:100) staining in Scrambled Control H460 Cell Pellets and a Negative Control A-C,*** *respectively. A. Negative control of the H460 cell pellet, B. staining using 1:100 concentration in the Scrambled control cell pellet, C staining using 1:100 concentration in the si611 cell pellet. Standard comparative protocol using labelled 1:100 used microwave retrieval (high settings) with IMMPRESS® signal detection system and pH 6.1 citrate target retrieval solution. Antibody signal on stained cells was developed with DAB for 1 minute, and cells were counterstained with Gill's hematoxylin for 10 seconds (N=1). Scale bars represent 50 to 200 µm. All slides were scanned using an Optika light microscope using a 20x objective. 418*

Figure 5-25 ***Representative images of (1:200) staining in Scrambled Control H460 Cell Pellets and a Negative control A-C,*** *respectively. A. Negative control of the H460 cell pellet, B-C staining using 1:200 concentration in the Scrambled control cell pellet D-E staining using 1:200 concentration in the si611 cell pellet. Standard comparative protocol using labelled 1:200 used microwave retrieval (high settings) with IMMPRESS® signal detection system and pH 6.1 citrate target retrieval solution. Antibody signal on stained cells was developed with DAB for 1 minute, and cells were counterstained with Gill's hematoxylin for 10 seconds (N=1). Scale bars represent 50 to 200µm. All slides were scanned using an Optika light microscope using a 20x objective. 419*

Figure 5-26 ***Representative images of (1:100) staining in Scrambled Control H460 Cell Pellets and a Negative control using Sodium Citrate instead of DAKO A-C,*** *respectively. A. Negative control of the H460 cell pellet, B staining using 1:100 concentration in the Scrambled control cell pellet, C staining using 1:100 concentration in the si611 cell pellet. Standard comparative protocol using labelled 1:100 used steam retrieval with IMMPRESS® signal detection system and sodium citrate target retrieval solution. Antibody signal on stained cells was developed with DAB for 1 minute, and cells were counterstained with Gill's hematoxylin for 10 seconds (N=1). Scale bars represent 50 to 200µm. All slides were scanned using a panoramic 250 slide scanner using a 20x objective. 421*

Figure 5-27 ***Representative images of (1:200) staining in Scrambled Control H460 Cell Pellets and a Negative control using Sodium Citrate instead of DAKO A-C,*** *respectively. A. Negative control of the H460 cell pellet, B staining using 1:200 concentration in the Scrambled control cell pellet, C staining using 1:200 concentration in the si611 cell pellet. Standard comparative protocol using labelled 1:200 used steam retrieval with IMMPRESS® signal detection system and sodium citrate target retrieval*

solution. Antibody signal on stained cells was developed with DAB for 1 minute, and cells were counterstained with Gill's hematoxylin for 10 seconds (N=1). Scale bars represent 50 to 200µm. All slides were scanned using a panoramic 250 slide scanner using a 20x objective. 422

Figure 5-28 ***Representative images of (1:100) staining in Scrambled Control H460 Cell Pellets and a Negative control using steam retrieval and DAKO A-C,*** *respectively. A. Negative control of the H460 cell pellet, B-C staining using 1:100 concentration in the Scrambled control cell pellet D-E staining using 1:100 concentration in the si611 cell pellet. Standard comparative protocol using labelled 1:100 used steam retrieval with IMMPRESS® signal detection system and pH 6.1 citrate target retrieval solution. Antibody signal on stained cells was developed with DAB for 1 minute, and cells were counterstained with Gill's hematoxylin for 10 seconds (N=1). Scale bars represent 50 to 200µm. All slides were scanned using a panoramic 250 slide scanner using a 20x objective. 423*

Figure 5-29 ***Representative images of (1:200) staining in Scrambled Control H460 Cell Pellets and a Negative control using steam retrieval and DAKO A-C,*** *respectively. A. Negative control of the H460 cell pellet, B-C staining using 1:200 concentration in the Scrambled control cell pellet D-E staining using 1:100 concentration in the si611 cell pellet. Standard comparative protocol using labelled 1:200 used steam retrieval with IMMPRESS® signal detection system and pH 6.1 citrate target retrieval solution. Antibody signal on stained cells was developed with DAB for 1 minute, and cells were counterstained with Gill's hematoxylin for 10 seconds (N=1). Scale bars represent 50 to 200µm. All slides were scanned using a panoramic 250 slide scanner using a 20x objective. 424*

Figure 5-30 ***Representative images of (1:200) staining in Lung cancer with matched lung tissue array (2015 WHO classification), including pathology grade, TNM and clinical stage (AJCC 7th edition), 6 cases/24 cores, replacing LC241l using steam retrieval and DAKO****. Standard comparative protocol using labelled 1:200 used steam retrieval with IMMPRESS® signal detection system and pH 6.1 citrate target retrieval solution. Antibody signal on stained cells was developed with DAB for 1 minute, and cells were counterstained with Gill's hematoxylin for 10 seconds (N=1). Scale bars represent 2000 µm. All slides were scanned using a panoramic 250 slide scanner using a 2000x objective. 426*

Figure 5-31 ***Representative images of (1:200) staining in selected cores (A-E) from the Lung cancer with matched lung tissue array (2015 WHO classification), including pathology grade, TNM and clinical stage (AJCC 7th edition), 6 cases/24 cores, replacing LC241l using steam retrieval and***

DAKO. *A represents normal lung tissue, B Keratinized Squamous Cell Cancer, C Basal Squamous Cell Cancer, D Acinar Adenocarcinoma E Slide of Squamous cell core showing early signs of stromal staining but non-specific nuclear cellular staining present in that slide. Standard comparative protocol using labelled 1:200 used steam retrieval with IMMPRESS® signal detection system and pH 6.1 citrate target retrieval solution. Antibody signal on stained cells was developed with DAB for 1 minute, and cells were counterstained with Gill's hematoxylin for 10 seconds (N=1). Scale bars represent 2000µm. All slides were scanned using a panoramic 250 slide scanner using a 2000x objective. 431*

Figure 5-32 ***Results of the optimisation of antibody using the IMMPRESS® Excel Amplified Polymer Staining Kit:*** *Standard comparative protocol using labelled 1:10, 1:25, 1:50, 1:100, 1:400 and 1:200 A. Weak staining of the nuclei with some stromal staining using antibody concentration of 1:200, B. Dirty staining of the stroma with no noticeable nuclear staining using antibody concentration of 1:10, C. Heavy stromal staining with dirty staining of the nuclei using antibody concentration of 1:10, D. Half stained nuclei with moderate to heavy stromal staining using antibody concentration of 1:25, E. Half stained nuclei, dirty nuclear staining and moderate stromal staining using antibody concentration of 1:50. used microwave retrieval with IMMPRESS® Excel Amplified Polymer Staining Kit and pH 6.1 citrate target retrieval solution. Antibody signal on stained cells was developed with DAB for 3 minutes 30 seconds, and cells were counterstained with Gill's hematoxylin for 10 seconds (N=1). 435*

Figure 5-33 Antibody signal on stained cells was developed with DAB for 1 minute, and cells were counterstained with Gill's hematoxylin for 10 seconds (N=1)...... 436

Figure 7-1: ***Stacked Bar charts showing the cellular outcomes of Barasertib*** *on live cell imaging using the conditions DMSO, 5nM and 10nM between 0-16 hours in A549 cells. Cells were treated with Barasertib for 2 hours before adding to IR and left for seven days. Dark blue indicates interphase before mitosis or slippage; Grey indicates mitosis; Pink indicates Interphase after slippage; Cyan indicates Interphase after mitosis; Green indicates Cell death in Mitosis; Sky blue indicates one cell died after division; Teal indicates both daughter cells died after division and orange indicates that the mother cell divided into more than two daughters. 616*

Figure 7-2: ***Stacked Bar charts showing the cellular outcomes of Barasertib*** *on live cell imaging using the conditions DMSO, 5nM and 10nM between 0-16 hours in SCC89 cells. Cells were treated with Barasertib for 2 hours before adding to IR and left for seven days. Dark blue indicates interphase before*

mitosis or slippage; Grey indicates mitosis; Pink indicates interphase after slippage; Cyan indicates interphase after mitosis; Green indicates Cell death in Mitosis; Sky blue indicates one cell died after division; Teal indicates both daughter cells died after division and orange indicates that the mother cell divided into more than two daughters. 619

*Figure 7-3: **Stacked Bar charts showing the cellular outcomes of Barasertib** on live cell imaging using the conditions DMSO, 5nM and 10nM between 0-16 hours in UPCI-SCC72 cells. Cells were treated with Barasertib for 2 hours before adding to IR and left for seven days. Dark blue indicates interphase before mitosis or slippage; Grey indicates mitosis; Pink indicates Interphase after slippage; Cyan indicates Interphase after mitosis; Green indicates Cell death in Mitosis; Sky blue indicates one cell died after division; Teal indicates both daughter cells died after division and orange indicates that the mother cell divided into more than two daughters. 622*

*Figure 7-4: **Stacked Bar charts showing the cellular outcomes of Barasertib +/-IR** on live cell imaging using the conditions DMSO, 2Gy, 4Gy, 25nM, 50nM, 25nM + 2Gy, 25 + 4Gy, 50nM + 2Gy, 50nM + 4Gy between 24-36 hours in H460 cells. Cells were treated with Barasertib for 2 hours before adding to IR and left for seven days. Dark blue indicates interphase before mitosis or slippage; Grey indicates mitosis; Pink indicates Interphase after slippage; Cyan indicates Interphase after mitosis; Green indicates Cell death in Mitosis; Sky blue indicates one cell died after division; Teal indicates both daughter cells died after division. Orange indicates that the mother cell is divided into more than two daughters. 629*

*Figure 7-5: **Stacked Bar charts showing the cellular outcomes of Barasertib +/-IR** on live cell imaging using the conditions DMSO, 2Gy, 4Gy, 25nM, 50nM, 25nM + 2Gy, 25 + 4Gy, 50nM + 2Gy, 50nM + 4Gy between 24-36 hours in H1299 cells. Cells were treated with Barasertib for 2 hours before adding to IR and left for seven days. Dark blue indicates interphase before mitosis or slippage; Grey indicates mitosis; Pink indicates Interphase after slippage; Cyan indicates Interphase after mitosis; Green indicates Cell death in Mitosis; Sky blue indicates one cell died after division, Teal indicates both daughter cells died after division, and orange indicates that the mother cell divided into more than two daughters. 635*

*Figure 7-6: **Stacked Bar charts showing the cellular outcomes of Barasertib** on live cell imaging using the conditions DMSO, 5nM and 10nM in 4Gy between 24-36 hours in A549 cells. Cells were treated with Barasertib for 2 hours before adding to IR and left for seven days. Dark blue indicates interphase before mitosis or slippage; Grey indicates mitosis; Pink indicates Interphase after slippage; Cyan indicates*

Interphase after mitosis; Green indicates Cell death in Mitosis; Sky blue indicates one cell died after division, Teal indicates both daughter cells died after division, and orange indicates that the mother cell divided into more than two daughters. 638

Figure 7-7: ***Stacked Bar charts showing the cellular outcomes of Barasertib*** *on live cell imaging using the conditions DMSO, 5nM and 10nM in 4Gy between 24-36 hours in H520 cells. Cells were treated with Barasertib for 2 hours before adding to IR and left for seven days. Dark blue indicates interphase before mitosis or slippage; Grey indicates mitosis; Pink indicates interphase after slippage; Cyan indicates interphase after mitosis; Green indicates Cell death in Mitosis; Sky blue indicates one cell died after division, Teal indicates both daughter cells died after division, and orange indicates that the mother cell divided into more than two daughters. 641*

Figure 7-8: ***Stacked Bar charts showing the cellular outcomes of Barasertib*** *on live cell imaging using the conditions DMSO, 5nM and 10nM between 24-36 hours in H460 cells. Cells were treated with Barasertib for 2 hours before adding to IR and left for seven days. Dark blue indicates interphase before mitosis or slippage; Grey indicates mitosis; Pink indicates Interphase after slippage; Cyan indicates Interphase after mitosis; Green indicates Cell death in Mitosis; Sky blue indicates one cell died after division, Teal indicates both daughter cells died after division, and orange indicates that the mother cell divided into more than two daughters. 644*

Figure 7-9: ***Stacked Bar charts showing the cellular outcomes of Barasertib*** *on live cell imaging using the conditions DMSO, 5nM and 10nM in 4Gy between 24-36 hours in UPCI-SCC72 cells. Cells were treated with Barasertib for 2 hours before adding to IR and left for seven days. Dark blue indicates interphase before mitosis or slippage; Grey indicates mitosis; Pink indicates Interphase after slippage; Cyan indicates Interphase after mitosis; Green indicates Cell death in Mitosis; Sky blue indicates one cell died after division, Teal indicates both daughter cells died after division, and orange indicates that the mother cell divided into more than two daughters. 647*

Figure 7-10: ***Stacked Bar charts showing the cellular outcomes of Barasertib*** *on live cell imaging using the conditions DMSO, 5nM and 10nM in 4Gy between 24-36 hours in SCC89 cells. Cells were treated with Barasertib for 2 hours before adding to IR and left for seven days. Dark blue indicates interphase before mitosis or slippage; Grey indicates mitosis; Pink indicates interphase after slippage; Cyan indicates interphase after mitosis; Green indicates Cell death in Mitosis; Sky blue indicates one cell died after*

division, Teal indicates both daughter cells died after division, and orange indicates that the mother cell divided into more than two daughters. 650

Figure 7-11: ***Stacked Bar charts showing the cellular outcomes of Barasertib*** *on live cell imaging using the conditions DMSO, 5nM and 10nM in 4Gy between 24-36 hours in FnB6 cells. Cells were treated with Barasertib for 2 hours before adding to IR and left for seven days. Dark blue indicates interphase before mitosis or slippage; Grey indicates mitosis; Pink indicates Interphase after slippage; Cyan indicates Interphase after mitosis; Green indicates Cell death in Mitosis; Sky blue indicates one cell died after division, Teal indicates both daughter cells died after division, and orange indicates that the mother cell divided into more than two daughters. 653*

Figure 7-12: ***Stacked Bar charts showing the cellular outcomes of Barasertib*** *on live cell imaging using the conditions DMSO, 5nM and 10nM in 4Gy between 24-36 hours in BICR22 cells. Cells were treated with Barasertib for 2 hours before adding to IR and left for seven days. Dark blue indicates interphase before mitosis or slippage; Grey indicates mitosis; Pink indicates interphase after slippage; Cyan indicates interphase after mitosis; Green indicates Cell death in Mitosis; Sky blue indicates one cell died after division, Teal indicates both daughter cells died after division, and orange indicates that the mother cell divided into more than two daughters. 656*

Figure 7-13: ***Stacked Bar charts showing the cellular outcomes of Barasertib*** *on live cell imaging using the conditions DMSO, 5nM and 10nM between 36-48 hours in A549 cells. Cells were treated with Barasertib for 2 hours before adding to IR and left for seven days. Dark blue indicates interphase before mitosis or slippage; Grey indicates mitosis; Pink indicates Interphase after slippage; Cyan indicates Interphase after mitosis; Green indicates Cell death in Mitosis; Sky blue indicates one cell died after division, Teal indicates both daughter cells died after division, and orange indicates that the mother cell divided into more than two daughters. 659*

Figure 7-14: ***Stacked Bar charts showing the cellular outcomes of Barasertib*** *on live cell imaging using the conditions DMSO, 5nM and 10nM between 36-48 hours in SCC89 cells. Cells were treated with Barasertib for 2 hours before adding to IR and left for seven days. Dark blue indicates interphase before mitosis or slippage; Grey indicates mitosis; Pink indicates interphase after slippage; Cyan indicates interphase after mitosis; Green indicates Cell death in Mitosis; Sky blue indicates one cell died after*

division, Teal indicates both daughter cells died after division, and orange indicates that the mother cell divided into more than two daughters. 662

*Figure 7-15: **Stacked Bar charts showing the cellular outcomes of Barasertib** on live cell imaging using the conditions DMSO, 5nM and 10nM between 36-48 hours in UPCI-SCC72 cells. Cells were treated with Barasertib for 2 hours before adding to IR and left for seven days. Dark blue indicates interphase before mitosis or slippage; Grey indicates mitosis; Pink indicates interphase after slippage; Cyan indicates interphase after mitosis; Green indicates Cell death in Mitosis; Sky blue indicates one cell died after division, Teal indicates both daughter cells died after division, and orange indicates that the mother cell divided into more than two daughters. 665*

*Figure 7-16: **AURKA IHC staining in H460 cell line pellets transfected with scrambled or AURKA siRNA after varying antigen retrieval method, antigen retrieval buffer and signal detection system.** Representative images of AURKA IHC staining in H460 cell line pellets after **A.** 1-hour primary antibody incubation and **B.** overnight primary antibody incubation. Standard comparative protocol using labelled 1:200 AURKA used pressure cooker retrieval, pH 6.1 citrate target retrieval solution and ABC detection system. Antibody signal on stained cells was developed with DAB for 3 minutes 30 seconds, and cells were counterstained with Gill's Haematoxylin (N=1). Scale bars represent 50 µm. All slides were scanned using a panoramic 250 slide scanner using a 20x objective. 671*

*Figure 7-17: **AURKA IHC staining in H460 cell line pellets transfected with scrambled or AURKA siRNA and patient biopsy samples after microwave retrieval method and ImmPRESS® detection system.** Representative images of AURKA IHC staining using H460 cell line pellets after **A.** microwave retrieval with ABC signal detection system and **B.** microwave retrieval with ImmPRESS® signal detection system. Tissues stained with 1:200 AURKA primary antibody +/- blocking peptide. Antibody signal on stained cells was developed with DAB for 3 minutes 30 seconds, and cells were counterstained with Gill's haematoxylin (N=1). Scale bars represent 50 µm **C.** AURKA staining in the diagnostic biopsy of an SCC NSCLC patient using 1:1000 primary antibody with overnight incubation, pressure cooker retrieval and ABC signal detection system re-represented for comparative purposes. DAB exposure was for 3 minutes. **D.** AURKA staining in a section from the same diagnostic biopsy in C, using 1:200 primary antibody with 1-hour incubation, microwave antigen retrieval and ImmPRESS® signal detection system. DAB exposure was for 15 minutes. Cells were counterstained with haematoxylin. Scale bars represent*

100 µm. The area within the small rectangle is re-represented in the image's bottom right corner, which is 5x larger. The black arrow indicates epithelial cancer cells with positive nuclear and cytoplasmic staining. All slides were scanned using a panoramic 250 slide scanner using a 20x objective..... 676

Figure 7-18: ***Stacked Bar charts showing the cellular outcomes of Barasertib (3 repeats A-B respectively)*** *on live cell imaging using the conditions DMSO, 5nM, 10nM and 25nM between 0-72 hours in A549 cells. Cells were treated with Barasertib for 72 hours and left for 7-10 days. Dark blue indicates interphase before mitosis or slippage; Dark Pink indicates slippage; dark violet indicates interphase after second slippage; Yellow-Green indicates second slippage; Sky blue indicates interphase prior to death in Mitosis; Light pink indicates mitosis, Turquoise indicates the final interphase, Light violet indicates death in the second daughter cell, Olympic blue indicates death in daughter one, Dark Cream indicates no observable event after slippage, Green indicates death in mitosis after slippage, Orange indicates cell death in mitosis, Black and white stripes indicates slippage in one daughter cells, Light cream indicates slippage in the second daughter cell, Cyan indicates division in daughter one of two, Grey indicates division in daughter two of two and Purple indicates slippage* ***and*** *death in both daughter cells..... 679*

Figure 7-19: ***Stacked Bar charts showing the cellular outcomes of Barasertib (3 repeats A-B respectively)*** *on live cell imaging using the conditions DMSO, 5nM, 10nM and 25nM between 0-72 hours in UPCI-SCC72 cells. Cells were treated with Barasertib for 72 hours and left for 7-10 days. Dark blue indicates interphase before mitosis or slippage; Dark Pink indicates slippage; dark violet indicates Interphase after second slippage; Yellow-Green indicates second slippage; Sky blue indicates interphase prior to death in Mitosis; Light pink indicates mitosis, Turquoise indicates the final interphase, Light violet indicates death in the second daughter cell, Olympic blue indicates death in daughter one, Dark Cream indicates no observable event after slippage, Green indicates death in mitosis after slippage, Orange indicates cell death in mitosis, Black and white stripes indicates slippage in one daughter cells, Light cream indicates slippage in the second daughter cell, Cyan indicates division in daughter one of two, Grey indicates division in daughter two of two and Purple indicates slippage* ***and*** *death in both daughter cells. 685*

Figure 7-20: ***Stacked Bar charts showing the cellular outcomes of Barasertib (3 repeats A-B respectively)*** *on live cell imaging using the conditions DMSO, 5nM, 10nM and 25nM between 0-72 hours in SCC89 cells. Cells were treated with Barasertib for 72 hours and left for 7-10 days. Dark blue indicates*

interphase before mitosis or slippage; Dark Pink indicates slippage; dark violet indicates Interphase after second slippage; Yellow-Green indicates second slippage; Sky blue indicates interphase prior to death in Mitosis; Light pink indicates mitosis, Turquoise indicates the final interphase, Light violet indicates death in the second daughter cell, Olympic blue indicates death in daughter one, Dark Cream indicates no observable event after slippage, Green indicates death in mitosis after slippage, Orange indicates cell death in mitosis, Black and white stripes indicates slippage in one daughter cells, Light cream indicates slippage in the second daughter cell, Cyan indicates division in daughter one of two, Grey indicates division in daughter two of two and Purple indicates slippage ***and*** *death in both daughter cells.* *689*

Table of Tables

Table 2-1: "Laboratory Equipment and Their Suppliers" *142*

Table 2-2: "Laboratory Consumables and Their Suppliers" *143*

Table 2-3: Chemical Reagents used and Their Suppliers *145*

Table 2-4: NCSLC and H&N cancer cell lines used throughout the project. *147*

Table 2-5: Summary of Compounds Used in the Study, Their Mechanisms, Diluent, Storage Conditions, and Suppliers *152*

Table 2-6: Cytotoxic Agents Used, Their Mechanisms, Diluent, Storage Conditions, and Suppliers *152*

Table 2-7: Antibodies Used in the Study, Their Applications in Western Blot (WB), Immunohistochemistry (IHC), and Fluorescence-Activated Cell Sorting (FACS) *154*

Table 2-8: Secondary Antibodies Used in the Study, Their Applications in Western Blot (WB), Immunohistochemistry (IHC), and Fluorescence-Activated Cell Sorting (FACS) *155*

Table 2-9: Detection Kits Used in the Study, Their Applications in Western Blot (WB), Immunohistochemistry (IHC), and Fluorescence-Activated Cell Sorting (FACS) *156*

Table 2-10: Specific Plating Densities and Radiation Therapy Dose per Cell Line *162*

Table 2-11: Production of a BSA protein standard curve *166*

Table 2-12: ***SDS-PAGE resolving gel and stacking gel recipes.*** *168*

Table 3-1: Ly3295688 Dose Enhancement Ratio (DER) and statistical significance indicated by two-tailed t-test values. *195*

Table 3-2 ***Barasertib DER ratios and t.test values*** *Barasertib Dose Enhancement Ratio (DER) and statistical significance indicated by two-tailed t-test values. Cells were pre-incubated with Barasertib before irradiation and colony outgrowth under continuous exposure to the AURKB inhibitor Barasertib. Data points represent the mean survival fraction normalised to unirradiated control +/- SD (N= ≥3). F-value and p-value derived from the extra sum of squares test.* *202*

Table 3-3 ***Barasertib DER ratios and t.test*** *values in H460s with depleted ARUKB The DER and t.test values demonstrate significant radiosensitisation with depleted AURKB and the addition of Barasertib and IR.* *205*

Table 3-4: Mean Barasertib LD_{50} values in NSCLC cell lines (n=5/6). *210*

Table 3-5 ***Barasertib and chemotherapy DER ratios and t.test*** *values in H460s demonstrating the highest DER ratios, F scores and P values of the separate combinations are listed, the P values represent the combination treatment compared to DMSO. Cells were pre-incubated with Cisplatin, 5FU, Vinorelbine and Barasertib before irradiation and colony outgrowth under continuous exposure to the AURKB inhibitor Barasertib. Data points represent the mean survival fraction normalised to unirradiated control +/- SD (N= ≥3). F-value and p-value derived from the extra sum of squares test. 219*

Table 4-1: ***Barasertib DER ratios and t.test values*** *The DER and t.test values demonstrate the lack of radiosensitisation in any HNSCC line. The survival fraction was calculated using a clonogenic assay. Cells were pre-incubated with Barasertib before irradiation and colony outgrowth under continuous exposure to the AURKB inhibitor Barasertib. Data points represent the mean survival fraction normalised to unirradiated control +/- SD (N= ≥3). F-value and p-value derived from the extra sum of squares test. 277*

Table 5-1 ***A-B: Accession numbers and patient characteristics of the NCSLC GEO samples. A:*** *Five GEO accession samples were chosen for the bioinformatic analysis.* ***B:*** *Each accession number has different ratios of normal vs cancer tissue and male's vs females demonstrating the heterogeneity of the samples in the analysis. 331*

Table 5-2: ***Table of log fold changes along with the significance values****: The and log fold changes and adj.P values are shown for GSE33532, GSE30219, and GSE30219, where both genes demonstrate significant differential gene expression.* ***LogFC (Log Fold Change):*** *Log Fold Change represents the logarithm of the ratio of gene expression levels between two conditions or groups. It quantifies how much a gene's expression has changed between two experimental conditions. A positive logFC indicates upregulation (increased expression) in one condition compared to the other, while a negative logFC indicates downregulation (decreased expression).* ***AveExpr (Average Expression):*** *AveExpr or Average Expression is the average gene expression level across all experiment samples. It provides a measure of the overall expression level of a gene, which can help filter out genes with very low expression levels that may not be biologically relevant or identify highly expressed genes****. P-value (t-test p-value):*** *The T p-value is a statistical measure that assesses whether the difference in gene expression between two groups (e.g., treatment vs. control) is statistically significant. It helps determine if the observed difference in gene expression is likely due to a natural biological effect or if it could have occurred by chance. A small p-value (typically less than 0.05) suggests the difference is significant.* ***Adj.P. Val (Adjusted P-***

Value): *The Adj.P. Val is a p-value adjusted for multiple testing to control the false discovery rate (FDR). One standard method for adjustment is the Benjamini-Hochberg procedure. Multiple hypothesis testing can increase the likelihood of false positives (Type I errors). Adjusted p-values help correct this by providing a more stringent criterion for significance. Genes with a low Adj.P. Val (typically less than 0.05) are considered statistically significant after adjusting for multiple comparisons. 333*

Table 5-3: List of genes generated from the common Hub genes between GSE30219, GSE33532 and GSE101929 (https://molbiotools.com/listcompare.php). The score indicates values representing the degree of connectivity of a node (gene) within a network. Genes with scores of greater than ten were chosen as potential hub genes. 339

*Table 5-4****: Accession numbers and Patient characteristics of the HNSCC GEO samples. A:*** *Six GEO accession samples were chosen for the bioinformatic analysis of four oral cavity and two nasopharyngeal tumours. 368*

Table 5-5: ***Accession numbers and patient characteristics of the HNSCC GEO samples. A:*** *Four GEO accession samples were chosen for the bioinformatic analysis. Each accession number has different ratios of normal vs cancer tissue and male's vs females demonstrating the heterogeneity of the samples in the analysis. 369*

Table 5-6: ***Table of log fold changes along with the significance values****: The log fold changes and adj.P values are shown for GSE74530, GSE78060, and GSE138206 and GSE30784 where the gene demonstrates significant differential gene expression.* ***LogFC (Log Fold Change):*** *Log Fold Change represents the logarithm of the ratio of gene expression levels between two conditions or groups. It quantifies how much a gene's expression has changed between two experimental conditions. A positive logFC indicates upregulation (increased expression) in one condition compared to the other, while a negative logFC indicates downregulation (decreased expression).* ***AveExpr (Average Expression):*** *AveExpr or Average Expression is the average gene expression level across all experiment samples. It provides a measure of the overall expression level of a gene, which can help filter out genes with very low expression levels that may not be biologically relevant or identify highly expressed genes****. P-value (t-test p-value):*** *The T p-value is a statistical measure that assesses whether the difference in gene expression between two groups (e.g., treatment vs. control) is statistically significant. It helps determine if the observed difference in gene expression is likely due to a natural biological effect or if it could have*

occurred by chance. A small p-value (typically less than 0.05) suggests the difference is significant. ***Adj. P. Val (Adjusted P-Value):*** *The Adj.P. Val is a p-value adjusted for multiple testing to control the false discovery rate (FDR). One standard method for adjustment is the Benjamini-Hochberg procedure. Multiple hypothesis testing can increase the likelihood of false positives (Type I errors). Adjusted p-values help correct this by providing a more stringent criterion for significance. Genes with a low Adj.P. Val (typically less than 0.05) are considered statistically significant after adjusting for multiple comparisons.* *370*

Table 5-7: List of genes generated from the common Hub genes between GSE78060 and GSE75430 (https://molbiotools.com/listcompare.php). The score indicates values representing the degree of connectivity of a node (gene) within a network. Genes with scores of greater than ten were chosen as potential hub genes. *379*

Table 5-8: ***Accession numbers and Patient characteristics of the HNSCC GEO samples. A:*** *Six GEO accession samples were chosen for the bioinformatic analysis of four oral cavity and two nasopharyngeal tumours.* *381*

Table 5-9: Table of log fold changes along with the significance values: The AURKA log fold changes and adj.P values are shown for GSE12452 and GSE13597 where neither AURKA nor AURKB demonstrates significant differential gene expression. LogFC (Log Fold Change): Log Fold Change represents the logarithm of the ratio of gene expression levels between two conditions or groups. It quantifies how much a gene's expression has changed between two experimental conditions. A positive logFC indicates upregulation (increased expression) in one condition compared to the other, while a negative logFC indicates downregulation (decreased expression). AveExpr (Average Expression): AveExpr or Average Expression is the average gene expression level across all experiment samples. It provides a measure of the overall expression level of a gene, which can help filter out genes with very low expression levels that may not be biologically relevant or identify highly expressed genes. P-value (t-test p-value): The T p-value is a statistical measure that assesses whether the difference in gene expression between two groups (e.g., treatment vs. control) is statistically significant. It helps determine if the observed difference in gene expression is likely due to a natural biological effect or if it could have occurred by chance. A small p-value (typically less than 0.05) suggests the difference is significant. Adj. P. Val (Adjusted P-Value): The Adj.P. Val is a p-value adjusted for multiple testing to control the false discovery rate (FDR). One standard

method for adjustment is the Benjamini-Hochberg procedure. Multiple hypothesis testing can increase the likelihood of false positives (Type I errors). Adjusted p-values help correct this by providing a more stringent criterion for significance. Genes with a low Adj.P. Val (typically less than 0.05) are considered statistically significant after adjusting for multiple comparisons. 383

Table 5-10 ***outlines the demographics of the prospective study*** *containing 101 patients treated over three years at the Weston Park Cancer Centre. 385*

Table 5-11 ***Results of the optimisation of antibody using the IMMPRESS® Excel Amplified Polymer Staining Kit:*** *Standard comparative protocol using labelled 1:10, 1:25, 1:50, 1:100, 1:400 and 1:200 used microwave retrieval with IMMPRESS® Excel Amplified Polymer Staining Kit and pH 6.1 citrate target retrieval solution. Antibody signal on stained cells was developed with DAB for 3 minutes 30 seconds, and cells were counterstained with Gill's hematoxylin (N=1). 409*

Table 5-12 ***Table of Lung cancer with matched lung tissue array (2015 WHO classification)****, including pathology grade, TNM and clinical stage (AJCC 7th edition), 6 cases/24 cores, replacing LC241l using steam retrieval and DAKO as shown in Figure 6-21. ..... 428*

Table 5-13 ***Results of the optimisation of antibody using the IMMPRESS® Excel Amplified Polymer Staining Kit:*** *Standard comparative protocol using labelled 1:10, 1:25, 1:50, 1:100, 1:400 and 1:200 used microwave retrieval with IMMPRESS® Excel Amplified Polymer Staining Kit and pH 6.1 citrate target retrieval solution. Antibody signal on stained cells was developed with DAB for 3 minutes 30 seconds, and cells were counterstained with Gill's hematoxylin for 10 seconds (N=1). 433*

Table 7-1: Schedule demonstrating the timing of Barasertib use in the dose escalation phase between day 1 to day 28. 531

Table 7-2: The dose expansion phase 532

1 Introduction

1.1 Non-small cell lung cancer (NSCLC)

1.1.1 Demographics (Incidence and environmental/socio-economic risk factors).

NSCLC is the third most common cancer in the UK, with approximately 50,000 new cases diagnosed yearly. It kills over 35,300 people, more than breast, bowel, bladder, and cervical cancer combined. The disease accounts for around a fifth of all UK cancer deaths (21%) and one in seven (13 %) new UK cancer cases. The incidence of lung cancer, which varies across the UK in the respective countries, is decreasing with the rates in men decreasing by a third; paradoxically, the rates in women have been increasing by a third. The incidence of lung cancer is projected to continue falling by 2% in 2040 ("Lung cancer statistics, Cancer Research UK," 2023). Lung cancer incidence tends to increase with age and is more common in older adults. Additionally, lung cancer rates have historically been higher in males than females, although this gender gap has been narrowing in recent years due to changing smoking patterns.

Smoking is the leading cause of lung cancer in the UK. It accounts for around 85% of all cases. Active smoking (smoking cigarettes) and passive smoking (exposure to second-hand smoke) are significant risk factors. Specific occupational exposures can increase the risk of developing lung cancer. For example, exposure to asbestos, arsenic, diesel exhaust, radon, and certain chemicals like nickel, chromium, and formaldehyde have been linked to lung cancer incidence (Hubaux et al., 2012). Long-term exposure to air pollution, including particulate matter, nitrogen dioxide

(NO2), and sulphur dioxide (SO2), has been associated with an increased risk of developing lung cancer (Hubaux et al., 2012; Manisalidis et al., 2020). This includes exposure to outdoor and indoor pollution from cooking and heating fuels. Radon is a naturally occurring radioactive gas that can seep into buildings from the ground. Prolonged exposure to high levels of radon gas indoors is a known risk factor for lung cancer. Individuals from lower socio-economic backgrounds may have a higher prevalence of smoking and increased exposure to occupational hazards, leading to an elevated risk of lung cancer (Krewski et al., 2005).

1.1.2 Staging and pathological subtypes.

Staging

Non-small cell lung cancer has several subtypes stratified into adenocarcinomas, squamous cell cancers, mucinous tumours, neuroendocrine tumours, papilloma's, adenomas, carcinoid tumours and unclassified carcinomas (Nicholson et al., 2022). Medical reporting pathologists categorise lung cancer into adenocarcinoma and squamous cell cancer due to the targetable driver genetic alterations identified in metastatic lung adenocarcinoma, namely *EGFR*, ALK-ELM4 fusion mutations, ROS-1, PD-1/PDL-1 and MET mutations (Gendarme et al., 2022; Reck et al., 2016; Shaw et al., 2014).

The staging of lung cancer is a critical process that assesses the extent and spread of the disease, guiding treatment decisions and providing prognostic information.

Typically, lung cancer staging involves the evaluation of tumour size, its local invasion into surrounding tissues, lymph node involvement, and distant metastases. The most used system for staging is the TNM (Tumour, Node, Metastasis) system (Figure 1-1). Regular advancements in diagnostic techniques and imaging technology contribute to more accurate staging (Hattori et al., 2019; Neppl et al., 2019).

T (primary tumour)	
T0	No primary tumour
Tis	Carcinoma in situ (squamous or adenocarcinoma)
T1	Tumour ≤3 cm
T1mi	Minimally invasive adenocarcinoma
T1a	Superficial spreading tumour in central airways
T1a	Tumour ≤1 cm
T1b	Tumour >1 but ≤ 2 cm
T1c	Tumour>2 but ≤ 3 cm
T2	Tumour >3 but ≤5 cm or tumour involving visceral pleura main bronchus (not carina), atelectasis to hilum
T2a	Tumour >3 but ?4 cm
T2b	Tumour >4 but ?5 cm
T3	Tumour >5 but ≤7 cm or invading chest wall, pericardium, phrenic nerve; or separate tumour nodule(s) in the same lobe
T4	Tumour>7 cm or tumour invading: mediastinum, diaphragm, heart, great vessels, recurrent laryngeal nerve, carina, trachea, oesophagus, spine; or tumour nodule(s) in a different ipsilateral lobe
N (regional lymph nodes)	
N0	No regional node metastasis
N1	Metastasis in ipsilateral pulmonary or hilar nodes
N2	Metastasis in ipsilateral mediastinal or subcarinal nodes
N3	Metastasis in contralateral mediastinal, hilar, or supraclavicular nodes
M (distant metastasis)	
M0	No distant metastasis
M1a	Malignant pleural or pericardial effusions or pleural or pericardial nodules or separate tumour nodule(s) in a contralateral lobe
M1b	Single extra thoracic metastasis
M1c	Multiple extra thoracic metastases (1 or>1 organ)

Figure 1-1: The TNM staging of NSCLC 8th edition. The TNM 8 staging system for non-small cell lung cancer (NSCLC), developed by the American Joint Committee on Cancer (AJCC) and the Union for International Cancer Control (UICC), categorizes cancer based on Tumor size and extent (T), lymph Node involvement (N), and presence of Metastasis (M). Tumor (T) classification ranges from Tis (carcinoma in situ) to T4, indicating increasing size and extent of invasion. Node (N) classification ranges from N0 (no regional lymph node metastasis) to N3 (contralateral mediastinal or supraclavicular lymph node involvement). Metastasis (M) is categorized as M0 (no distant metastasis) to M1c (multiple extrathoracic metastases). These categories combine to form overall stages from Stage 0 (Tis N0 M0) to Stage IVB (any T, any N, M1c), aiding in prognosis and treatment planning.

1.1.3 Management of NSCLC.

1.1.3.1 Chemotherapy.

Chemotherapy in NSCLC is given to patients in the early stage and metastatic setting. For fit patients with inoperable stage III NSCLC, cisplatin-based chemotherapy given concurrently to radiation therapy is recommended. Based on adjuvant chemotherapy in stage II and stage III disease, four cycles of cisplatin-based combination chemotherapy are defined as the standard of care (Aupérin et al., 2010; Fischer et al., 2011; Pignon et al., 2008).

For fit patients with inoperable stage III NSCLC, cisplatin-based chemotherapy given concurrently with radiation therapy is recommended. This is typically cisplatin + vinorelbine (Eberhardt et al., 2015).

The use of chemotherapy in the metastatic setting has become complex, and a summary of the main themes will be highlighted here.

1.1.3.2 Targeted Agents.

Epidermal growth factor Re*cep*tor (*EGFR*) inhibitors are specifically tailored to target NSCLC cells bearing *EGFR* gene mutations. Drugs in this class include Erlotinib, Afatinib, Gefitinib, Osimertinib, and Dacomitinib. Osimertinib holds particular efficacy against NSCLC cells bearing the T790M mutation, frequently serving as a therapeutic option following the failure of other *EGFR* inhibitors (Hendriks et al., 2023).

Angiogenesis inhibitors are therapeutic agents designed to impede neovascularisation in tumour growth. Some examples include Bevacizumab and

Ramucirumab. Their use in the UK is not routine ("Bevacizumab for the treatment of non-small-cell lung cancer " 2018.).

KRAS G12C inhibitors, such as Sotorasib and Adagrasib, are used to manage advanced NSCLC once other treatment modalities have been exhausted, specifically in cases where cancer cells harbour the KRAS G12C mutation (Adderley et al., 2019; Hong et al., 2020; Solomon et al., 2014).

Approximately 5% of NSCLC cases exhibit ALK gene rearrangements (Arbour and Riely, 2017). Several drugs in this class, including Crizotinib, Ceritinib, Alectinib, Brigatinib, and Lorlatinib, have been developed and are used in the first line setting over chemotherapy if the patient has the fusion mutation.

In cases featuring ROS1 gene rearrangements, Crizotinib, Ceritinib, Lorlatinib, and Entrectinib serve as therapeutic agents, with some constituting first-line treatments in the metastatic setting (Gendarme et al., 2022, p. 1).

Alterations in the MET gene are observed in certain NSCLC cases, producing an anomalous MET protein that fuels cancer cell growth. In response, MET inhibitors, namely Capmatinib and Tepotinib, are administered to manage metastatic NSCLC with specific MET gene changes (Paik et al., 2020; Wolf et al., 2020).

1.2 Head and Neck Squamous Cell Cancer (HNSCC).

1.2.1 Demographics (incidence and environmental/socio-economic risk factors).

According to the most recent available data from the UK, in 2018, there were approximately 12,600 new cases of head and neck cancer diagnosed in the country (“Head and Neck cancer statistics, Cancer Research UK,” 2023). The most common sites for head and neck cancer include the oral cavity, pharynx (including the oropharynx and nasopharynx), and larynx. The incidence rate of head and neck cancer has been gradually increasing over the past few decades, primarily due to the rise in cases related to HPV infection, particularly in the oropharynx (Pinkiewicz et al., 2022). It is estimated that there are currently over 65,000 people living with a diagnosis of head and neck cancer in the UK (“ Head and Neck cancer statistics, Cancer Research UK,” 2023). This includes individuals undergoing treatment, in remission, or living with the long-term effects of the disease.

Tobacco use, including smoking cigarettes and using smokeless tobacco products like chewing tobacco, is a significant risk factor for head and neck cancer. Heavy alcohol consumption, particularly when combined with smoking, further increases the risk. The risk is higher in individuals who both smoke and drink heavily compared to those who only smoke or drink (Hashibe, 2010; Lewin et al., 1998).

In recent years, there has been an increasing recognition of the role of HPV infection in head and neck cancer, particularly in the oropharynx (the back of the throat). Certain strains of HPV, such as HPV-16, are strongly associated with the development of these cancers. Some occupational exposures have been linked to an increased risk of head and neck cancer. These include exposure to chemicals

and substances like asbestos, formaldehyde, wood dust, and nickel dust. Chewing betel quid, a mixture of areca nut and other ingredients wrapped in a betel leaf, is a cultural practice common in specific populations (Song et al., 2015). Regular and long-term use of betel quid has been associated with an increased risk of the oral cavity and other head and neck cancers. Inadequate oral hygiene, chronic irritation, and poor dental health, such as missing teeth, gum disease, and oral infections, have been linked to an increased risk of certain types of head and neck cancers (Lewin et al., 1998). Socio-economic factors can play a role in head and neck cancer risk. Factors such as lower education level, lower income, and limited access to healthcare may contribute to a higher incidence of head and neck cancer due to disparities in tobacco and alcohol use, as well as delayed diagnosis and treatment.

1.2.2 Staging and pathological subtypes.

Staging

Staging in head and neck cancer involves the assessment of the extent of the disease determining its spread within the affected region and to distant sites. The complexity of staging arises from the intricate anatomy of the head and neck, encompassing multiple subsites with diverse structures and functions. The American Joint Committee on Cancer (AJCC) and the Union for International Cancer Control (UICC) have established a widely used staging system, the TNM system, which considers tumour size, lymph node involvement, and distant metastasis (Zanoni et al., 2019). Combining the T, N, and M classifications results in an overall stage grouping. The stage grouping comprehensively assesses the disease's extent and helps guide treatment decisions. Stages range from I (early-stage) to IV (advanced-stage), with subgroups within each stage reflecting increasing disease severity .

The diverse subsites, intricate anatomy, and the potential for multifocal involvement amplify the complexity of head and neck cancer staging. Additionally, the impact of factors like human papillomavirus (HPV) status in oropharyngeal cancers adds an extra layer of complexity, as HPV-positive tumours often exhibit distinct clinical behaviours and treatment responses.

Pathological Subtypes

Head and neck cancer represents a heterogeneous group of malignancies in various anatomical regions, including the oral cavity, pharynx, larynx, paranasal sinuses, and salivary glands (Zanoni et al., 2019). The complexity of these cancers is underscored by their diverse pathological subtypes, each characterised by distinct histological features, molecular signatures, and clinical behaviours. Understanding the pathological subtypes is crucial for accurate diagnosis, prognosis, and personalised treatment strategies.

The pathological classification of head and neck cancer is multifaceted, reflecting the diverse cellular origins within the intricate anatomy of the head and neck region. Squamous cell carcinoma (SCC), originating from the squamous epithelial cells lining the mucosal surfaces, represents a predominant subtype, accounting for most cases. However, beyond SCC, a spectrum of less common but equally significant subtypes exists, including adenocarcinomas, salivary gland tumours, and mesenchymal tumours (Skálová et al., 2024).

Squamous cell carcinoma is the most prevalent subtype of head and neck cancer, often originating from the squamous epithelial cells lining the mucosal surfaces of the oral cavity, pharynx, and larynx. Histologically, SCC is characterised by atypical squamous cells with keratinisation. Smoking and alcohol consumption are major risk factors for SCC, but the rise in human papillomavirus (HPV) infection has led to an increasing incidence of HPV-associated SCC, particularly in the oropharynx (Glastonbury, 2020; Skálová et al., 2024).

Adenocarcinomas, though more commonly associated with glandular tissues, can also occur in the head and neck region. These tumours arise from the glandular cells

of the salivary glands and can exhibit diverse histological patterns. The subtypes include mucoepidermoid carcinoma, adenoid cystic carcinoma, and acinic cell carcinoma. Adenocarcinomas often present unique challenges in diagnosis and treatment due to their varied clinical behaviour and response to therapies(Glastonbury, 2020; Skálová et al., 2024).

Mesenchymal tumours in the head and neck region are relatively rare but encompass a range of entities, such as sarcomas and neurogenic tumours. Examples include rhabdomyosarcoma and schwannoma. These tumours arise from connective tissues, nerves, or muscles, and their diagnosis requires careful examination of tissue morphology and, in some cases, immunohistochemical studies (Glastonbury, 2020; Skálová et al., 2024).. Treatment strategies often involve a multidisciplinary approach, considering surgery, radiation, and chemotherapy.

1.2.3 Management of HNSCC

The management of head and neck cancer in the UK is characterized by a comprehensive, multidisciplinary approach that integrates various treatment modalities and supportive care measures.

Multidisciplinary Team (MDT) Approach

A fundamental aspect of managing head and neck cancer is the involvement of a multidisciplinary team (MDT). This team typically comprises surgeons, radiologists, pathologists, medical oncologists, radiation oncologists, dieticians, and speech therapists. The collaborative effort of these specialists ensures that every aspect of the patient's condition is considered, from diagnosis to treatment and follow-up. The MDT approach is essential for developing an individualized treatment plan that optimizes outcomes and minimizes complications (Bradley, 2012).

Diagnostic and Staging Workup

Accurate diagnosis and staging are critical components of head and neck cancer management. The initial workup includes a thorough clinical examination, imaging studies such as CT, MRI, and PET scans, and a biopsy to confirm the His*top*athological diagnosis. The staging process follows the TNM classification system, which assesses the tumour size (T), lymph node involvement (N), and the presence of metastasis (M) (Head and Neck Cancer Study Group (HNCSG) et al., 2019). This precise staging is crucial for guiding treatment decisions and predicting prognosis.

Surgical Treatment

Surgery remains a primary treatment modality for resectable head and neck tumours. The goal is to remove the tumour completely while preserving as much function as possible. Techniques vary from traditional open surgeries to minimally invasive approaches like transoral robotic surgery (TORS), which is particularly useful for oropharyngeal cancers (Vidhyadharan et al., 2019). When lymph node involvement is suspected, a neck dissection is performed. Additionally, reconstructive surgery may be necessary to restore appearance and function after tumour removal (Vidhyadharan et al., 2019).

Chemotherapy and Targeted Therapy

Chemotherapy is used for advanced-stage head and neck cancers, either as part of concurrent chemoradiation or as a standalone treatment in metastatic settings. Common chemotherapeutic agents include cisplatin and fluorouracil. Targeted therapies have become increasingly significant, focusing on specific molecular targets. For instance, cetuximab, an *EGFR* inhibitor, is used in combination with radiotherapy, while immunotherapy agents like pembrolizumab and nivolumab are employed for recurrent or metastatic cancers, leveraging the body's immune system to combat the disease (Ali and Abdelraheem, 2011).

Nutritional and Supportive Care

Nutritional status is a critical factor in patient outcomes, as malnutrition is prevalent due to the cancer itself and the side effects of treatment. Malnutrition can significantly impact recovery and overall prognosis. A comprehensive nutritional assessment is conducted before treatment begins, and interventions are tailored to maintain or improve nutritional status. This may include enteral nutrition through feeding t*ube*s or parenteral nutrition in severe cases. Speech therapists and dieticians play vital roles in managing dysphagia and other nutritional challenges, providing strategies and therapies to help patients maintain adequate nutrition throughout their treatment.

1.3 Radiobiology of NSCLC and HNSCC.

1.3.1 The R's of radiobiology.

Radiobiology is the study of the effects of ionising radiation on living organisms, and it is guided by the principles of the 4 Rs: Repair, Repopulation, Redistribution, and Reoxygenation (Pajonk et al., 2010).

Repair

Repair refers to the ability of cells to mend radiation-induced damage to their DNA during and after exposure, ensuring their survival. The repair capacity of cells is a crucial factor in radiotherapy response. Cells with efficient DNA repair mechanisms may recover from radiation-induced damage, reducing the effectiveness of treatment. Tumours with impaired repair mechanisms may be more sensitive to radiation. Resistance can occur when tumour cells have enhanced DNA repair capabilities. This enables them to repair radiation-induced DNA damage quickly, reducing the effectiveness of radiation therapy (“Horst, K.C., Giaccia, A.J. (2010). Basic Principles of Radiobiology. In: Dirbas, F., Scott-Conner, C. (eds) Breast Surgical Techniques and Interdisciplinary Management. Springer, New York, NY. https://doi.org/10.1007/978-1-4419-6076-4_66,” n.d.; Qiu et al., 2020).

Redistribution

Redistribution refers to the movement of cells within the tumour population into different phases of the cell cycle between radiation treatments. Tumour cells are most sensitive to ionizing radiation during the G2 and M phases and least sensitive during the S phase. By fractionating the radiation dose over several sessions, it allows more tumour cells to cycle into these more sensitive phases, increasing the overall effectiveness of the treatment. This process helps to maximize the damage to cancer cells while sparing normal tissues (Qiu et al., 2020; Rakotomalala et al., 2021).

Repopulation

Repopulation of tumour cells during radiotherapy can impact treatment outcomes. Slower-replicating tumours may respond better to radiation because they have less repopulation. Accelerated repopulation can lead to resistance by allowing tumour cells to repopulate after radiation, rapidly offsetting the treatment's effects. This highlights the importance of fractionated radiation therapy, which delivers treatment in multiple sessions to mitigate repopulation effects (Qiu et al., 2020).

Re-Oxygenation

Oxygenation is another critical factor. Well-oxygenated tissues tend to be more radiosensitive due to the oxygen effect, which enhances the formation of reactive oxygen species and DNA damage. Conversely, hypoxic regions within tumours or tissues may exhibit resistance to radiation. The DNA repair capacity of cells is also

essential (Qiu et al., 2020; Rakotomalala et al., 2021). Cells have mechanisms to repair DNA damage caused by radiation. Differences in DNA repair efficiency can influence the response to radiation, with cells possessing more robust repair systems being more resistant to radiation-induced damage. The cell cycle phase during radiation exposure is a determinant of radiosensitivity. Cells in different phases of the cell cycle exhibit varying degrees of sensitivity. Cells in the G2 and M phases are more radiosensitive, while those in the S phase (DNA synthesis) and G0 (resting) phase may exhibit more excellent resistance (Rakotomalala et al., 2021).

1.3.2 Radiobiology and radiation schedules in NSCLC.

There is some variation in the UK's dose and fractionation schedules used for NSCLC. Most tumours are inoperable at the time of diagnosis, and as such, there has been a push to look for increased doses for local control tempered against increased normal tissue toxicity. Radiotherapeutic strategies to improve local control (LC) include dose escalation with conventional fractionation or shortening the overall treatment time (OTT) and increasing the biologically effective dose (BED) with altered fractionation (acceleration, hyperfractionation, or hypofractionation).

The radiobiology of normal lung tissue

Lung and bronchial tissue classically are considered non-regenerating and thus defined as a parallel organ. The tolerance of lung to radiotherapy ranges between 18 to 20Gy with an alpha/beta ratio of 3Gy, therefore exhibiting higher sensitivity to increased fraction sizes due to the dominant quadratic component in their response to radiation (Roy et al., 2021; Wrona and Mornex, 2021).

Radiation Therapy Oncology Group (RTOG) investigators defined the traditional dose and fractionation schedule as 60Gy in 30 fractions after comparison with 40Gy in 20 fractions and 50 Gy in 25 fractions . At this stage, it was noted that higher doses of IR lead to improved survival and increased toxicity rates (Bradley et al., 2015).

Hypofractionation

Hypofractionation schedules range from the standard dose of 55Gy in 20 fractions used in the UK to stereotactic body radiotherapy (SABR), which uses 54 to 60 Gray doses in 3 -8 fractions, respectively (Cheung et al., 2014; Lindblom et al., 2014). Cox et al. raised concerns that using large doses per fraction may adversely affect tumour control because it allows the repopulation of tumour cells between fractions (Cox et al., 1990). This work was done before more current schedules with increased fraction sizes and reduced fractionation were used.

Accelerated hypofractionation (55Gy in 20 fractions)

The use of 55Gy in 20 fractions is standard in the UK, and it is essential to note that this regime has never been investigated in a randomised phase 3 trial against 60Gy in 30 fractions. It is hypothesised that this regimen shortens the overall treatment time, which is believed to be beneficial regarding tumour repopulation (Din et al., 2013). Maguire et al investigated the use of chemotherapy concurrently with this schedule against a sequential chemotherapy and radiation regime. There were similar rates of treatment-related mortality and toxicity between the two groups,

leading to the addition of chemotherapy as a standard of care in the appropriate patients (Maguire et al., 2014).

Stereotactic body radiotherapy (SABR)

There has been uncertainty around using the standard linear quadratic (LQ) model when investigating the radiobiology of doses greater than 5Gy per fraction used in SABR (Li and Shen, 2020).

Shen et al. argue that the LQ model is an appropriate model for SABR as it can represent tissue control probability TCP and it performs better, but Qui argues that when you have a fractional dose higher than 8–10 Gy, the LQ model is inappropriate to predict the effects induced by radiation (Qiu et al., 2020). It is felt that a modified LD model is the most suitable to predict the effects of SABR, but the "4Rs" of radiobiology do not explain the killing effects of this approach (see figure)

Toxicity profiles have varied, with studies demonstrating similar grade three oesophagitis and pneumonitis levels at around 3-5 % ref. Indeed, SABR is now offered to patients with small tumours, with several trials attempting to investigate this modality against primary surgery trial numbers or references, but frustratingly, most have failed to recruit enough patients to derive a conclusion.

Hyperfractionation

Hyperfractionation is a radiation therapy technique used in the treatment of non-small cell lung cancer (NSCLC) that involves delivering smaller doses of radiation multiple times per day. This approach aims to increase the overall dose of radiation

to the tumour while minimizing damage to surrounding healthy tissues. The treatment is typically administered twice a day with at least six hours between sessions, over the same total number of treatment days as conventional fractionation (Cox et al., 1990; Fu et al., 2000).

In NSCLC, hyperfractionation is being explored as a way to enhance the effectiveness of radiation therapy, particularly for patients with locally advanced disease. This method can potentially improve local control of the tumour and overall survival rates compared to conventional fractionation, which involves fewer, larger doses given once a day. The rationale behind hyperfractionation is based on radiobiological principles that suggest dividing the radiation dose into smaller, more frequent treatments allows for better repair of normal tissue between sessions and enhances the radiosensitivity of the tumour cells (Bradley et al., 2015).

Clinical studies have indicated that hyperfractionated radiotherapy can be beneficial for certain subsets of NSCLC patients, particularly when combined with other treatments like chemotherapy. For example, continuous hyperfractionated accelerated radiotherapy (CHART) has been shown to significantly improve survival rates in NSCLC by shortening the overall treatment time while maintaining or increasing the total radiation dose (Dische and Saunders, n.d.; Martel, 1999).

However, hyperfractionation also comes with increased logistical demands and potential side effects, such as higher rates of acute radiation toxicity. Therefore, patient selection and careful planning are crucial to maximize the benefits and minimize the risks. Ongoing research and clinical trials continue to refine the protocols and identify which patients are most likely to benefit from hyperfractionated approaches in the treatment of NSCLC (Curran et al., 2011).

1.3.3 Radiobiology and Radiation Schedules in HNSCC

Conventional Fractionation

Conventional fractionation in radiotherapy involves delivering daily doses of 1.8 to 2.0 Gy, five days a week, over six to seven weeks, totalling approximately 70 Gy. This regimen is the standard for definitive treatment in head and neck cancer, as it balances effective tumour control with manageable toxicity levels. The prolonged treatment duration allows normal tissues to repair between sessions, reducing the risk of severe side effects (Lindblom et al., 2014) .

Hyperfractionation

Hyperfractionation involves administering smaller doses per fraction (typically 1.1-1.2 Gy) multiple times a day, leading to a higher total radiation dose. The goal of this approach is to take advantage of the repair mechanisms in normal tissues while delivering a higher cumulative dose to the tumour, thereby improving local control and survival. The Radiation Therapy Oncology Group (RTOG) 9003 trial demonstrated that hyperfractionation could result in better outcomes in terms of local-regional control and survival when compared to conventional fractionation (Fu et al., 2000).

Accelerated Fractionation

Accelerated fractionation shortens the overall treatment time by increasing the number of fractions per week without increasing the total radiation dose. This

approach aims to reduce tumour repopulation during therapy, which is particularly important for rapidly dividing tumour cells. The DAHANCA 6 and 7 trials have shown that accelerated fractionation can lead to improved treatment outcomes, with higher local control rates and better overall survival (Overgaard et al., 2003).

Concomitant Boost

The concomitant boost technique combines conventional fractionation with an additional daily dose or "boost" during the final weeks of treatment. This strategy intensifies the treatment without extending its overall duration, thereby enhancing local-regional control. The RTOG 9003 trial supported this approach, showing that it significantly improved outcomes in head and neck cancer patients (Fu et al., 2000).

Chemoradiation

Chemoradiation, which combines chemotherapy with radiation therapy, has become a standard treatment for locally advanced head and neck cancer. Chemotherapy serves as a radiosensitizer, making cancer cells more sus*cep*tible to radiation damage. This combined approach has been shown to provide superior survival rates compared to radiation alone, as evidenced by studies such as those conducted by Pignon et al. (2009) .

Intensity-Modulated Radiation Therapy (IMRT)

Intensity-Modulated Radiation Therapy (IMRT) allows for the precise targeting of tumours while minimizing exposure to surrounding normal tissues. This technique

significantly reduces the toxicity associated with treatment, particularly xerostomia (dry mouth), and improves patients' quality of life. Gupta et al. (2012) demonstrated that IMRT leads to better preservation of salivary gland function and overall treatment outcomes compared to conventional radiotherapy techniques .

1.4 Radiotherapy resistance in NSCLC and HNSCC.

1.4.1 The molecular response to radiation damage in NSCLC.

The DNA damage response (DDR) is activated in response to IR to promote survival and reduce cellular damage. Two significant pathways repair DSBs: homologous recombination (HR) and non-homologous end joining (NHEJ), while SSBs are fixed by single-strand break repair (SSBR). Cell death can occur through apoptosis, mitotic catastrophe, senescence, necrosis, or Au*top*hagy if any repair mechanism fails.

Regarding NSCLC, numerous genes lead to radioresistance, including *ATM*, *ATR*, *BCRA1*, *Chk1*, *WEE1* and *PARP1* through their respective DNA repair pathway activity (Zhou et al., 2023). Research into the inhibition of these genes and the potential for radiosensitisation is ongoing.

The DNA damage response (DDR) is a critical cellular mechanism activated in response to ionizing radiation (IR) to promote survival and minimize cellular damage. This response involves detecting and repairing DNA damage, particularly double-strand breaks (DSBs) and single-strand breaks (SSBs). The two primary pathways for DSB repair are homologous recombination (HR) and non-homologous end joining (NHEJ), while SSBs are typically repaired by single-strand break repair (SSBR). If these repair mechanisms fail, cell death can occur through apoptosis, mitotic catastrophe, senescence, necrosis, or Au*top*hagy (Hoeijmakers, 2001).

In non-small cell lung cancer (NSCLC), various genes contribute to radioresistance through their roles in DDR pathways. Key genes include *ATM*, *ATR*, BRCA1, *Chk1*, *WEE1*, and *PARP1*. *ATM* and *ATR* are essential for detecting DNA damage and initiating repair processes (Blackford and Jackson, 2017; Shiloh and Ziv, 2013). *ATM* responds primarily to DSBs, phosphorylating several substrates, including *p53*, *Chk2*, and H2AX, to coordinate DNA repair, cell cycle arrest, or apoptosis (Blackford and Jackson, 2017). *ATR*, on the other hand, is activated by replication stress and single-stranded DNA, playing a crucial role in stabilizing replication forks and coordinating DNA repair through the phosphorylation of *Chk1* and other targets (Mackay and Ullman, 2015).

BRCA1 and *BRCA2* are pivotal in the HR pathway, facilitating the accurate repair of DSBs by promoting the formation of *Rad51* nucleoprotein filaments, which are essential for strand invasion and homologous pairing (Ryser et al., 2009). Mutations in these genes compromise HR, leading to genomic instability and increased sensitivity to DNA-damaging agents, including IR. This vulnerability is exploited therapeutically using PARP inhibitors, which induce synthetic lethality in HR-deficient cells by blocking SSBR and trapping PARP-DNA complexes, resulting in the accumulation of unrepaired DNA damage and cell death (Deng et al., 2022).

WEE1 is another significant player in the DDR, regulating the G2/M checkpoint by inhibiting cyclin-dependent kinases (*CDK*s) and preventing cells with damaged DNA from entering mitosis prematurely (Bukhari et al., 2019; Deng et al., 2022). Inhibiting *WEE1* can enhance the effects of radiotherapy by forcing cells to undergo mitosis

with unrepaired DNA, leading to mitotic catastrophe and cell death (Bukhari et al., 2019). Similarly, *Chk1* inhibitors can sensitize cancer cells to radiotherapy by abrogating cell cycle checkpoints, thereby preventing DNA repair and promoting apoptosis in response to IR.

1.4.2 Radioresistance in NSCLC

Tumour hypoxia correlates with poor prognosis and poorer treatment outcomes in non-small cell lung cancer (NSCLC). Tumour hypoxia can be defined as a low oxygen tension (pO2) in the tumour compared to the surrounding tissue of pO2 ≤ 2.5 mmHg but is most commonly defined as a pO2 ≤ 10 mmHg. The presence of hypoxia has been shown to influence tumour responsiveness to radiotherapy and chemotherapy.

Hypoxia may be responsible for treatment failure through 2 primary mechanisms: (1) a treatment-related effect owing to reduced DNA damage and (2) an at least partially treatment-independent effect through upregulating several factors, leading to more aggressive tumour biology. Despite its small study sample size, Li et al. found that hypoxia measured through PET using 18F-FETNIM imaging has the potential to predict overall survival in NSCLC patients (Brustugun, 2015).

Takahashi et al. performed PET with 62Cu-ATSM in six patients with lung cancer and demonstrated high tumour uptake of the tracer in all patients; however, they did

not correlate tumour uptake of 62Cu-ATSM with response to therapy (Takahashi et al., 2000). Dehdashti et al. evaluated 14 patients' responses to treatment therapy by using the tumour SUV. There was no significant difference in mean tumour SUV for FDG of nonresponders (10.9±4.1) and responders (12.7±10.4) (P=0.7). In addition, there was no significant correlation between tumour uptake of 60Cu-ATSM and FDG (r=0.04; P=0.9) (Dehdashti et al., 2003).

Cancer stem cells (CSCs) are becoming increasingly attractive as a target for drug treatment and predicting survival. NSCLC cells may contain CSCs, contributing to tumour maintenance, metastasis and resistance to chemotherapy and radiotherapy(Gomez-Casal et al., 2013; Zakaria et al., 2015). Several CSCs are under investigation in vitro regarding their role in NSCLC radioresistance. Concerning the "Rs" of radiobiology CSCs are hypothesised to enrich cells with stem-like properties, CSC levels are increased by hypoxia, have increased levels of repair, and have a more prolonged G0 phase in the cell cycle (Nguyen et al., 2011). There are numerous examples where CSCs have demonstrated potential as biomarkers, at least in vitro. Tsolou et al. demonstrated that radioresistant A549-IR3 cells significantly increased stem cell markers, namely CD44, CD133, OCT4, SOX2 and NANOG (Nguyen et al., 2011). Surprisingly, they also found overexpression of ALDHA1 in populations of cells with low stem cell numbers. Casal et al. demonstrated increased expression of CD44 and CD166 in radioresistant A549 cell lines.

The epithelial-mesenchymal transition (EMT) is a complex biological process implicated in cancer characteristics. EMT process, regulated by a network of signalling pathways containing transforming growth factor-β(TGF-β), *Wnt*, Notch, *EGFR*, phosphatidylinositol 3-kinase (PI3K)/ protein kinase B (Akt), nuclear factor-kappa B (NF-κB) and extracellular signal-regulating kinase (ERK), contributes to radioresistance in several tumour types including NSCLC (Zhou et al., 2020). CSC enriched with CD44, CD29, and CD90 markers exhibit molecular characteristics of EMT and promote radioresistance.

Interestingly, *EGFR* and its downstream signalling pathway are essential in controlling cell proliferation, survival, epithelial-to-mesenchymal transition (EMT), migration and differentiation in various human cancers. *EGFR* pathway mediates the regulation of multiple CSC-related genes, including Sox2, CD44, CD133, Oct4, and ALDH1, but the underlying molecular mechanisms are unclear (Shi et al., 2018; Zhou et al., 2020).

1.4.3 Therapeutic Approaches to Overcome Radioresistance in NSCLC

Dose Escalation

Different radiotherapy schedules are used in the NHS to tackle radioresistance with doses ranging from 55 Gy in 20 fractions, CHART in 60 Gy in 30 fractions, and SBAR radiotherapy. Evidence shows that using doses above 66 Gy in patients only increases toxicity and ultimately reduces survival. Vera et al. attempted to boost patients with a PET-proven hypoxic centre with doses of up to 86 Gy using modern radiotherapy techniques, but neither progression-free nor Overall survival was improved.

Concomitant Immunotherapy

Preclinical studies have revealed that radiation improves the ability of the immune system to recognise solid tumours by uncovering or releasing previously hidden tumour-associated antigens (TAAs) and immunostimulatory molecules from within the tumour that can activate and prime an antitumor immune response.

Many active phase I and II trials are looking at combination immunotherapy and IR, but no clear answers exist on the superiority of OS and PFS.

Further preclinical work needs to be done to develop in-vitro models, the role of the appropriate fraction size and timing from immunotherapy to radiotherapy delivery.

New Irradiation Techniques using heavy ions such as proton and hadron ions.

Heavier ions can escalate doses to the tumour while sparing normal tissue due to the radiobiological con*cep*t of the "Bragg peak." This is the ability of particles to deposit their energy at the target's exact location based on its initial energy and atomic weight (Jin et al., 2021). Several phase I and II trials have evaluated the safety of using heavier ions, and so far, they have not yet demonstrated the superiority of the heavier ions over photons. OS and PFS data have not shown statistical improvement as yet. There are also questions about the cost and practicality of using these particles due to the large size of the gantries and the relatively new technologies used to produce these ions (Li et al., 2024).

1.4.4 The molecular response to radiation damage in HNSCC.

Radiation primarily induces DNA double-strand breaks (DSBs) in cancer cells. The recognition and repair of these breaks are crucial for cell survival. One key player in the repair of DSBs is the DNA-dependent protein kinase (DNA-PK), which is involved in non-homologous end joining (NHEJ), a major pathway for DSB repair. Inhibitors of DNA-PK, such as AZD7648, have shown promise in enhancing the radiosensitivity of HNSCC cells by preventing efficient DNA repair, thereby increasing radiation-induced cell death.

Another important aspect of the molecular response to radiation in HNSCC involves the role of poly (ADP-ribose) polymerase (PARP) in DNA repair. PARP is essential for the repair of single-strand breaks, which, if left unrepaired, can lead to DSBs during DNA replication (Jonuscheit et al., 2021). PARP inhibitors, like talazoparib and niraparib, have been found to radiosensitise HNSCC cells, particularly in HPV-positive cell lines, by increasing the accumulation of unrepaired DNA damage (Mentzel et al., 2024).

<u>Hypoxia and the tumour Microenvironment</u>

Hypoxia, or low oxygen levels within the tumour microenvironment, significantly impacts the response of HNSCC to radiation therapy (Rakotomalala et al., 2021). Hypoxic tumour cells are more resistant to radiation due to the reduced generation of reactive oxygen species (ROS) that mediate DNA damage under normoxic conditions. Research indicates that hypoxia-inducible factors (HIFs) contribute to this

resistance by upregulating genes involved in angiogenesis, metabolism, and survival pathways (Brustugun, 2015; Rakotomalala et al., 2021).

DNA Damage Response (DDR) Pathways

The DDR pathways are crucial in modulating the response of HNSCC to radiation. Key proteins involved in DDR, such as *ATM*, *ATR*, and *CHK1*, are activated upon DNA damage and facilitate cell cycle arrest, allowing time for repair or triggering apoptosis if the damage is irreparable (Blackford and Jackson, 2017). Targeting these pathways with specific inhibitors can enhance the radiosensitivity of HNSCC cells. For instance, *ATM* and *ATR* inhibitors have been shown to increase the efficacy of radiation therapy by preventing the repair of radiation-induced DNA damage (Bukhari et al., 2019; Shiloh and Ziv, 2013).

Immune Response and Inflammation

Radiation therapy also induces an immune response that can influence the treatment outcome. The release of damage-associated molecular patterns (DAMPs) from irradiated tumour cells can stimulate an anti-tumour immune response. However, radiation can also induce immunosuppressive factors within the tumour microenvironment (Adderley et al., 2019). Combining radiation with immunotherapy, such as immune checkpoint inhibitors targeting PD-1/PD-L1 or CTLA-4, has shown potential in overcoming this immunosuppressive barrier and enhancing anti-tumour immunity (S. Liu et al., 2022).

Molecular Targeted Therapies

Combining radiation therapy with molecular targeted therapies has shown promising results in improving treatment outcomes for HNSCC. Targeting the epidermal growth factor re*cep*tor (*EGFR*), which is often overexpressed in HNSCC, with agents like Cetuximab can enhance the radiosensitivity of tumour cells (Nair et al., 2022; Rehmani and Issaeva, 2020).

Role of Epigenetics

Epigenetic modifications, including DNA methylation and histone modification, play a significant role in the radiation response of HNSCC (Shi et al., 2024). Aberrant epigenetic regulation can lead to the silencing of tumour suppressor genes and the activation of oncogenes. Epigenetic therapies, such as histone deacetylase inhibitors (HDACI) and DNA methyltransferase inhibitors (DNMTI), are being explored to modulate the tumour response to radiation and improve therapeutic outcomes (Hu et al., 2021; Mazzone et al., 2017).

1.4.5 Radioresistance in HNSCC

DNA Damage Repair Mechanisms

One of the primary mechanisms of radioresistance is the enhanced capability of HNSCC cells to repair radiation-induced DNA damage. Radiation therapy exerts its effects primarily through the induction of DNA double-strand breaks (DSBs). The efficiency of DNA repair pathways such as non-homologous end joining (NHEJ) and homologous recombination (HR) is critical in determining the sensitivity of cancer cells to radiation (Rassamegevanon et al., 2021).

Tumour Microenvironment and Hypoxia

The tumour microenvironment plays a crucial role in the radioresistance of HNSCC. Hypoxia, a common feature in solid tumours, contributes significantly to radioresistance. Hypoxic tumour cells are less sus*cept*ible to radiation due to the reduced production of reactive oxygen species (ROS), which are necessary for mediating DNA damage (Rakotomalala et al., 2021). Hypoxia-inducible factors (HIFs) regulate the expression of genes involved in survival, angiogenesis, and metabolic adaptation, thereby promoting a resistant phenotype. Therapeutic strategies aimed at modifying the tumour microenvironment, such as the use of hypoxia-activated prodrugs or agents that normalize tumour vasculature, are being explored to overcome hypoxia-induced radioresistance (Brustugun, 2015).

Signalling Pathways and Oncogenes

Aberrant activation of various signalling pathways, including the *EGFR*, PI3K/AKT/mTOR, and *MAPK* pathways, has been implicated in the development of radioresistance. These pathways promote cell survival, proliferation, and repair mechanisms that counteract the effects of radiation. For instance, overexpression of *EGFR* in HNSCC is associated with increased radioresistance (Nair et al., 2022; Rehmani and Issaeva, 2020). Targeted therapies that inhibit *EGFR* and downstream signalling components have shown promise in sensitizing HNSCC cells to radiation.

Immune Evasion and Inflammation

The immune response and inflammation also influence radioresistance in HNSCC. Radiation therapy can modulate the immune microenvironment by inducing the release of damage-associated molecular patterns (DAMPs) that stimulate anti-tumour immunity (Mazzone et al., 2017). However, radiation can also upregulate immunosuppressive factors, such as PD-L1, contributing to immune evasion. Combining radiation therapy with immune checkpoint inhibitors, such as anti-PD-1/PD-L1 antibodies, is being investigated to enhance the immune response and overcome radioresistance (Hu et al., 2021).

Epigenetic Modifications

Epigenetic changes, including DNA methylation, histone modifications, and non-coding RNA expression, play a significant role in the regulation of genes involved in radioresistance. Epigenetic alterations can lead to the silencing of tumour

suppressor genes and the activation of oncogenes, thereby promoting resistance (Hu et al., 2021; Shi et al., 2024).

Au*top*hagy and Cell Death Mechanisms

Au*top*hagy, a cellular process that degrades and recycles cellular components, has been implicated in radioresistance (Shi et al., 2024). Under stress conditions, such as radiation, au*top*hagy can provide an adaptive survival mechanism by removing damaged organelles and proteins, thereby enhancing cell survival. However, excessive au*top*hagy can also lead to cell death. Modulating au*top*hagy through inhibitors or enhancers is being explored as a strategy to influence the response of HNSCC to radiation (Shi et al., 2024; Xu et al., 2024).

1.4.6 Therapeutic Approaches to Overcome Radioresistance in HNSCC

Targeting DNA Damage Repair Pathways

Radiation therapy primarily induces DNA double-strand breaks (DSBs) in cancer cells, and the efficiency of DNA repair mechanisms significantly impacts the sensitivity of HNSCC to radiation. Targeting DNA repair pathways is a promising approach to enhance radiosensitivity (Jonuscheit et al., 2021).

PARP Inhibitors: Poly (ADP-ribose) polymerase (PARP) inhibitors, such as talazoparib and niraparib, have been shown to increase the accumulation of

unrepaired DNA damage, particularly in HPV-positive HNSCC cell lines (Jonuscheit et al., 2021). These inhibitors work by blocking the repair of single-strand breaks, which can escalate to DSBs during replication, thereby enhancing the effectiveness of radiation therapy .

DNA-PK Inhibitors: DNA-dependent protein kinase (DNA-PK) is crucial for the non-homologous end joining (NHEJ) repair pathway. Inhibitors like AZD7648 can prevent the efficient repair of DSBs, increasing the cytotoxicity of radiation in HNSCC cells (Blackford and Jackson, 2017). These inhibitors have shown promise in preclinical studies by enhancing radiosensitivity without significantly affecting normal tissues .

Modifying the tumour Microenvironment

The tumour microenvironment, particularly hypoxia, plays a significant role in radioresistance. Hypoxic tumour cells are less responsive to radiation due to reduced reactive oxygen species (ROS) production (Brustugun, 2015; Rakotomalala et al., 2021).

Combining Radiation with Molecular Targeted Therapies

The epidermal growth factor re*cep*tor (*EGFR*) is often overexpressed in HNSCC and is associated with poor prognosis and radioresistance. Cetuximab, an *EGFR* inhibitor, can enhance the effects of radiation by inhibiting cell proliferation and survival pathways (Bonner et al., 2006; Nair et al., 2022). Combining cetuximab with radiation has shown improved outcomes in clinical trials .

The PI3K/AKT/mTOR pathway is involved in cell survival, growth, and metabolism. Inhibitors targeting PI3K, AKT, or mTOR can enhance radiosensitivity by disrupting these survival signals (Wang et al., 2016).

Enhancing Immune Response

Immune checkpoint inhibitors targeting PD-1/PD-L1 or CTLA-4 can enhance anti-tumour immunity. Radiation-induced immunogenic cell death can release tumour antigens and enhance the effectiveness of these immunotherapies . Combining radiation with checkpoint inhibitors has shown promising results in preclinical and clinical studies (Marabelle et al., 2022; Reck et al., 2016).

Epigenetic Modulation

Epigenetic changes play a significant role in the response to radiation. Targeting these changes can enhance radiosensitivity.

HDAC and DNMT Inhibitors: Histone deacetylase (HDAC) inhibitors and DNA methyltransferase (DNMT) inhibitors can reverse epigenetic modifications that contribute to radioresistance (Wang et al., 2016).

1.5 Genetics and cellular consequences of NSCLC and HNSCC.

1.5.1 Genetics and cellular consequences of NSCLC

Understanding the molecular biology of NSCLC is complex but essential as an increased understanding of targetable mutations has led to treatments being developed for metastatic disease with the potential for developing novel drugs plus IR combination trials.

Activating mutations in the KRAS oncogene are the most common oncogenic alteration in lung adenocarcinomas (ADC), occurring in about 25-40% of cases (Adderley et al., 2019), while HRAS and NRAS mutations are rare (Mathiot et al., 2022). Mutations in KRAS have been observed at differing rates in never- and ever-smokers. Compared to ever smokers, never smokers had decreased odds of KRAS mutations among those of Caucasian/Mixed ethnicity (OR = 0.22, 95% CI: 0.17–0.29) and those of Asian ethnicity (OR = 0.39, 95% CI: 0.30–0.50) (Chapman et al.,

2016). ADC in non-smokers has been reported to harbour KRAS mutations in 0-15% of cases (Adderley et al., 2019). KRAS mutations currently do not lead to any actionable drug target in the curative or radical setting (Cooper et al., 2013).

Although some studies have found a slightly lower prevalence, ALK rearrangements have been identified in approximately 4-5% of unselected NSCLCs (Arbour and Riely, 2017)). They are more commonly found in ADC than squamous cell cancers (SCCs) in younger patients who are never smokers or light smokers. ALK rearrangements are usually mutually exclusive with *EGFR* and KRAS mutations (Arbour and Riely, 2017); cases of coexistent *EGFR* mutations have been reported and provide a mechanism for TKI resistance (Cooper et al., 2013).

ROS1 fusion mutations in lung cancer, the ROS1 gene usually fuses with other genes, such as CD74, SLC34A2, or EZR. The fusion gene produces a novel protein, which is often a constitutively active re*cep*tor tyrosine kinase. The hybrid protein is always "turned on" and continuously sends signals within the cell, promoting cell growth and division. This leads to signalling through the PI3K/AKT/mTOR, STAT3 and RAS/*MAPK*/ERK pathways. ROS1 fusions are more common in never-smokers than current smokers and tend to be found in younger patients. There may be a female predominance of ROS1 fusions compared to male patients, but there seems to be a similar prevalence in East Asian and Caucasian populations. ROS1 fusion is an addictive oncogenic driver associated with adenocarcinogenesis in the peripheral lung epithelium (the terminal respiratory unit) unrelated to tobacco-driven carcinogenesis(Gendarme et al., 2022).

RET gain-of-function alterations can be found in multiple solid tumours, including thyroid carcinoma and non-small-cell lung cancer (NSCLC) (NCI Staff, 2020). RET rearrangements occur in about 1–2% of patients with NSCLC, usually in young, light/never smokers with adenocarcinoma histology, and are associated with a high rate of brain metastases at diagnosis(Cooper et al., 2013; NCI Staff, 2020).

NTRK gene fusion mutations are rare in NSCLC, with figures of roughly 1%. The first-generation TRK inhibitors (Larotrectinib and Entrectinib) are recommended as the first-line treatment for locally advanced or metastatic NSCLC patients with positive NTRK fusion (Haratake and Seto, 2021; F. Liu et al., 2022).

There is work on developing novel ways of detecting the gene and creating new drugs to target this mutation. Mutations of MET and their aberrant activation can promote tumour development and cancer progression by dysregulating downstream signalling pathways. MET signalling was believed to be the mechanism of resistance acquired by NSCLC tumour cells against certain therapeutics (Wolf et al., 2020). MET alterations in sustained MET pathway dysregulation led to oncogenesis. Clinically, NSCLCs with MET alterations are associated with poor prognosis and are recognised as an essential therapeutic target in various cancers, including NSCLC (Paik et al., 2020; Wolf et al., 2020).

The presence of *EGFR* mutations has important treatment implications. NSCLC patients with *EGFR* mutations are often sensitive to targeted therapies known as *EGFR* tyrosine kinase inhibitors (TKIs), such as gefitinib, erlotinib, afatinib, and

Osimertinib. These drugs can effectively inhibit the activity of the mutated *EGFR* protein, leading to tumour shrinkage and improved survival rates.

The tumour suppressor gene *p53* is frequently mutated in human cancers. The abnormality of the *p53* gene is one of the most significant events in lung cancers and plays an essential role in the tumorigenesis of lung epithelial cells (Mogi and Kuwano, 2011). The frequent detection of loss of heterozygosity (LOH) in lung cancer cell lines and tumour samples at the location of the *p53* gene on chromosome 17p13 suggested that this gene was likely to be involved in the pathogenesis of lung cancer, and genetic abnormality of the *p53* in lung cancers is associated with a poorer survival prognosis and increased cellular resistance to therapy (Baumann et al., 2009). The frequency of *p53* mutations is the highest in squamous cell carcinomas and lower in adenocarcinomas among NSCLC tumour samples (Tammemagi et al., n.d.).

BRAF mutations commonly occur in never-smokers, women, and aggressive histological types and account for 1%–2% of adenocarcinoma. Traditional chemotherapy presents limited efficacy in BRAF-mutated NSCLC patients. Specific BRAF mutations can coexist with KRAS mutations (9). However, routine platinum-based chemotherapy presents lower efficacy and is associated with poorer survival (Yan et al., 2022).

1.5.2 Genetics and cellular consequences of HNSCC

The c-Myc proto-oncogene at 8q24 plays a pivotal role in governing cell growth, differentiation, and apoptosis. In head and neck squamous cell carcinoma (HNSCC), the frequent and significant genetic event of c-Myc overactivation is well-documented. Particularly in laryngeal squamous cell carcinoma (LSCC), a predominant his*top*athological subtype within HNSCC, c-Myc gene amplification is implicated in the pathogenesis (Zhao et al., 2022). This overactivation of c-Myc is likely mediated through various oncogenic signalling pathways, including *WNT*, RAS, and PI3K/AKT (S. Liu et al., 2022). Notably, c-Myc amplification is observed prominently in HNSC patients with neck node metastases, suggesting its potential involvement in the metastatic spread of the disease (Haughey et al., 1992).

*CDKN*2A, the gene that encodes p16, is frequently inactivated via copy number loss among HPV-negative head and neck cancer patients, indicating poor clinical prognosis in terms of disease progression and OS (Chen et al., 2018). *CDKN*2A promoter hypermethylation might correlate with carcinogenesis of HNSCC and a significantly elevated frequency of *CDKN*2A promoter methylation in patients with lymph node metastasis (C. Zhou et al., 2018).

EGFR is overexpressed in over 90% of head and neck tumours and is a member of the erb-b2 re*cep*tor tyrosine kinase (ERBB) family of re*cep*tor tyrosine kinases (RTKs) that includes ERBB2-4 (Nair et al., 2022; Rehmani and Issaeva, 2020), furthermore, the association translates to shorter survival for patients. *EGFR* status

is increasingly recognised as a predictor of survival and chemoradiation response in HNSCC.

The *p53* gene is the most commonly mutated in HNC45, and loss of *p53* function is found in more than 90% of HNC cases. *p53* mutations in HNSCC are correlated with poor clinical outcomes, and *p53* protein also plays a significant role in acquired resistance to *EGFR* inhibitors based on the identification of a robust loss of *p53* in HNC cells that are resistant to cetuximab or erlotinib (Zhou et al., 2016).

HER2 mutations and amplifications of the HER2 gene are infrequent occurrences in HNSCC. *EGFR* can heterodimerise with HER2, and preclinical findings indicate that concurrently targeting *EGFR* and HER2 could enhance responses to cetuximab and potentially alleviate therapeutic resistance. However, the utilisation of targeted anti-ERBB2 therapies in HNSCC has not been conclusively established (Pollock and Grandis, 2015; Saddawi-Konefka et al., 2022).

Amplifications of chromosomal regions 11q13 and 11q22 are notable in HNSCC. The 11q13 amplification involves genes such as CCND1 (cyclin D1), promoting cell cycle progression. The 11q22 amplification often includes genes like BIRC2 and BIRC3, which inhibit apoptosis and contribute to chemoresistance (Jin et al., 2006).Mutations in the HRAS gene, part of the Ras family of oncogenes, occur in a subset of HNSCC cases. These mutations result in the constitutive activation of downstream signalling pathways such as *MAPK* and PI3K-AKT, promoting oncogenic growth and survival (Jung et al., 2018).

A figure summarising the above gene list is seen below in Figure 1-2.

Some important genetic mutations in NSCLC	Some important genetic mutations in HNSCC
KRAS mutation	Amplification and overexpression of *myc*
ALK-ELM4 rearrangement	CDKN2A inactivation
EGFR mutation	Amplifications of 11q13 and 11q22
ROS-1 mutation	Amplification and overexpression of *erbB-2*
RET gain of function	Amplification and overexpression of epidermal growth factor receptor (*EGFR*)
NTRK gene fusion	Ha-Ras mutaion
MET mutation	Tp53 mutation
Tp53 mutation	
BRAF mutation	

Figure 1-2: The genetic mutations in non-small cell lung cancer (NSCLC) and head and neck squamous cell carcinoma (HNSCC) significantly impact disease progression, prognosis, and treatment options. For NSCLC, common mutations include KRAS (25% of cases), which leads to poor prognosis and treatment resistance, and *EGFR* mutations (10-15% in Western populations, up to 50% in Asian populations), often making tumors sensitive to tyrosine kinase inhibitors. Other notable mutations include the ALK-EML4 fusion (3-7%), ROS1 rearrangements (1-2%), RET gain-of-function mutations, NTRK gene fusions, MET exon 14 skipping mutations, *p53* mutations (50% of cases, linked to aggressive disease), and BRAF mutations (1-3%, particularly the V600E variant). Each mutation highlights opportunities for targeted therapy. In HNSCC, key genetic alterations include amplification of MYC, CDKN2A inactivation, and amplifications of CCND1, BIRC2, BIRC3, and *EGFR*. Mutations in HRAS and *p53* are also common, contributing to unchecked cell growth, survival, and treatment resistance. These genetic insights provide potential targets for personalized treatments in both cancers.

The Aurora Kinase family consists of three members: Aurora Kinase A (*AURKA*), Aurora Kinase B (*AURKB*) a component of the chromosomal passenger complex (CPC), and Aurora Kinase C (*AURKC*). These serine/threonine kinases are essential for regulating mitosis in mammalian cells. *AURKA* is involved in the formation of the mitotic spindle, centrosome maturation and separation, and the assembly of the bipolar spindle (Figure 1-4). is critical for chromosomal congregation and cytokinesis. The exact function of *AURKC* remains unknown, but its expression in early embryos and germ cells and its presence in the chromosomal passenger complex suggests a role in meiosis and early development. Furthermore, *AURKA* and have also been shown to have non-mitotic functions.

I will briefly review *AURKA* and *AURKC*'s functions and then focus on *AURKB*.

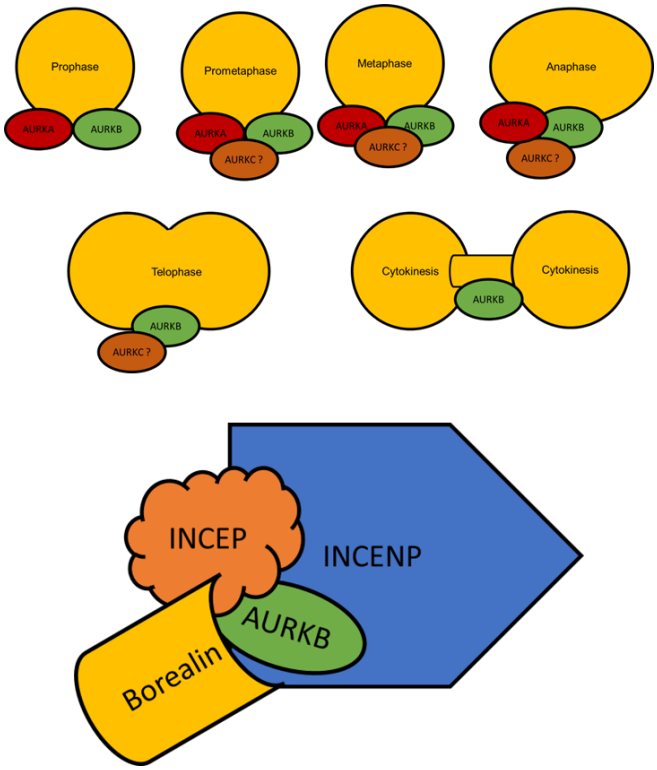


Figure 1-3: Different phases of mitosis where Activity of Aurora Kinases are said to act most frequently and the chromosomal passenger complex (CPC). Mitosis, a fundamental process for cell division, is meticulously regulated by proteins such as Aurora kinases and the chromosomal passenger complex (CPC) (Carmena et al., 2012). Aurora kinases, comprising Aurora A, B, and C, play pivotal roles throughout mitosis. Aurora A is predominantly active during prophase at the centrosomes, facilitating centrosome maturation, separation, and the formation of the bipolar spindle apparatus through microtubule nucleation and organization. During prometaphase and metaphase, Aurora A stabilizes spindle microtubules and ensures proper microtubule-kinetochore attachments. Aurora B, a core component of the CPC, exhibits critical activity from prometaphase to cytokinesis (Yan, 2009). It localizes to kinetochores in prometaphase, ensuring correct chromosome alignment and attachment, and later relocates to the central spindle in anaphase and the midbody in cytokinesis, regulating the spindle assembly checkpoint, chromosomal segregation, and cytokinesis (DeLuca et al., 2018). Aurora C, though less studied, is thought to function similarly to Aurora B, particularly in meiosis. The CPC, comprising Aurora B, INCENP, Survivin, and Borealin, orchestrates several mitotic processes, including chromosome condensation, alignment, segregation, and cytokinesis, through its dynamic localization and regulation of spindle assembly and checkpoint signaling (Becker et al., 2010; Carmena et al., 2012).

1.5.3 *AURKA*.

1.5.3.1 The role of *AURKA* in Mitosis.

1.5.3.1.1 Prophase

AURKA initiates mitosis by combining with Bora, leading to phosphorylation and Polo-like kinase 1 (PLK1) activation. PLK1 activates cyclin B by degrading *WEE1*; PLK1 also activates CDC25C and CDC25B *CDK*-promoting phosphatase to activate *CDK*1(Asteriti et al., 2015; Parrilla et al., 2016). This leads to the transition from the G2 to the M phase (Figure 1-5).

There is some uncertainty around whether is wholly required for complete entry into mitosis. Earlier studies showed the ability of cells to form monopolar spindle structures despite *AURKA* suppression, which ultimately delays but does not block mitotic entry (Girdler et al., 2006; Yang et al., 2005).

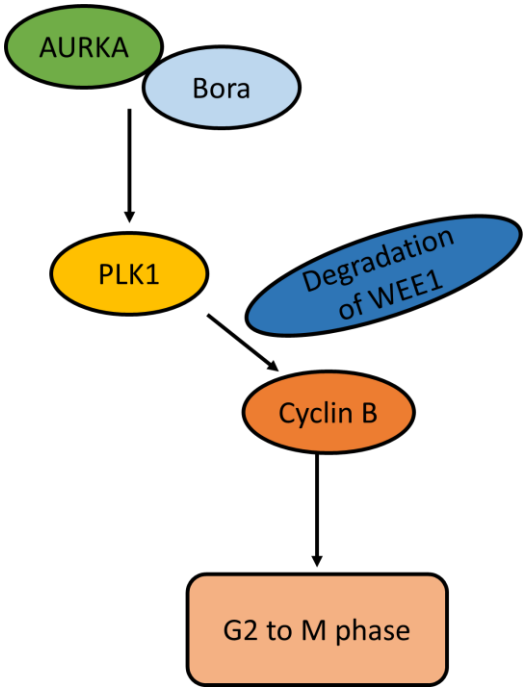


Figure 1-4: Interactions of *AURKA* in prophase Aurora kinase A (*AURKA*) plays a crucial role in the regulation of mitosis, particularly during the G2/M transition and prophase, through its interactions with several key proteins including Bora, Polo-like kinase 1 (Plk1), *WEE1*, and Cyclin B (Parrilla et al., 2016; Yan, 2009). During the G2 phase, *AURKA* is activated by its binding partner Bora, which enhances its kinase activity. This activation is critical for the initiation of mitotic entry. Bora facilitates the recruitment and activation of Plk1, another essential kinase in mitotic progression. Plk1, once activated by *AURKA*, phosphorylates various substrates that are necessary for centrosome maturation, separation, and spindle assembly, ensuring proper mitotic spindle formation.

WEE1 is a kinase that negatively regulates the cell cycle by phosphorylating and inhibiting Cyclin-dependent kinase 1 (*CDK*1), thereby preventing premature entry into mitosis. *AURKA* indirectly influences *WEE1* activity (Asteriti et al., 2015; Bukhari et al., 2019). As cells prepare for mitosis, *AURKA* activity leads to the activation of Plk1, which in turn phosphorylates *WEE1*, targeting it for degradation. This degradation of *WEE1* is crucial for the activation of the Cyclin B-*CDK*1 complex, a major driver of the G2/M transition (Bukhari et al., 2019). The activation of Cyclin B-*CDK*1 promotes various mitotic events, including chromatin condensation and nuclear envelope breakdown, which are hallmarks of prophase (Parrilla et al., 2016).

1.5.3.1.2 Prometaphase

In prometaphase (Figure 1-6), *AURKA* regulates centrosome amplification and maturation, microtubule remodelling and bipolar spindle formation. *AURKA* activates Lats2 (in a complex with Ajuga), leading to downstream activation of gamma-tubulin and subsequent centrosome maturation (Abe et al., 2006). Gamma-tubulin amount is linearly associated with increased centrosome formation (Abe et al., 2006; Khodjakov and Rieder, 1999).

Activated *AURKA* recruits γ-tubulin and TACC/MA*P215* to the microtubule organising centre (MTOCs), facilitating centrosome maturation and microtubule formation (Figure 1-6). After the nuclear membrane breaks down in prometaphase, *AURKA* is activated, then targeted to the microtubule by TPX2 and required for spindle assembly and the conformation of the bipolar spindle microtubule (Tang et al., 2017).

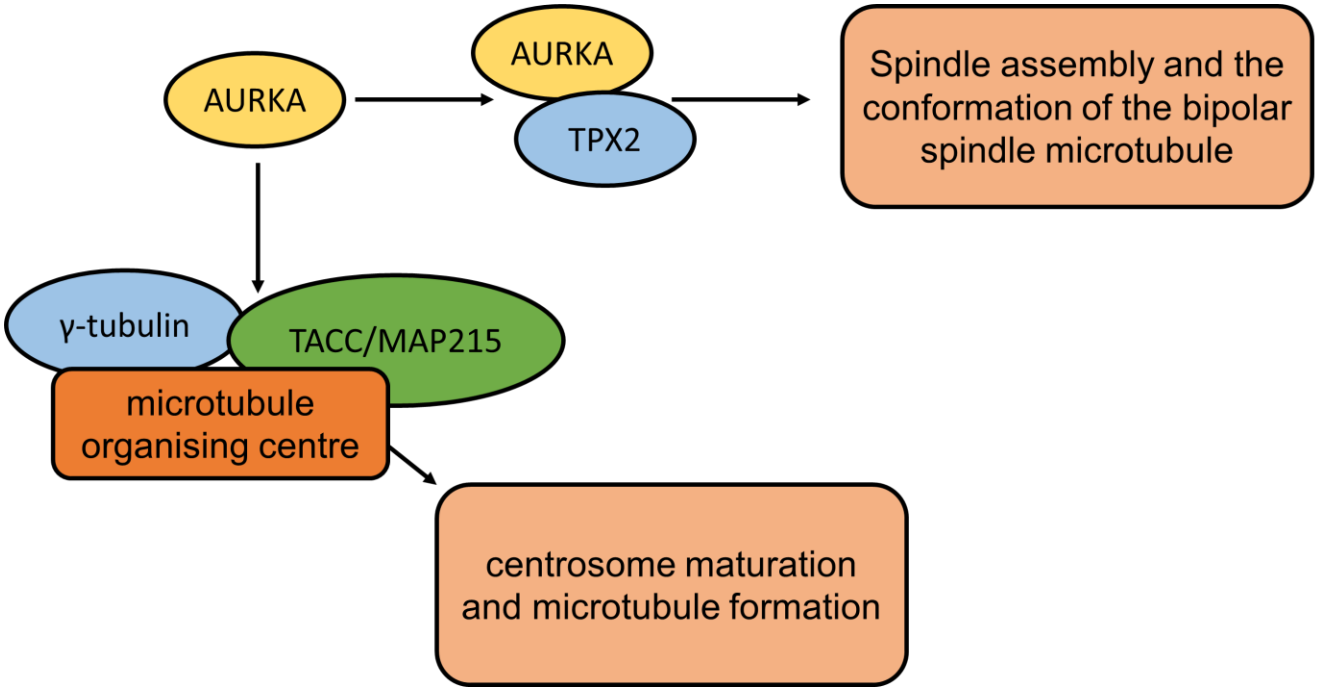


Figure 1-5: Interactions of *AURKA* in prophase Aurora kinase A (*AURKA*) is a critical regulator of mitosis, particularly during the prophase stage, where it interacts with various proteins and structures to ensure proper mitotic progression. One of the key interactions of *AURKA* in prophase is with targeting protein for Xklp2 (TPX2) (Van Gijn et al., 2019). TPX2 is essential for *AURKA* activation and localization to the microtubule organizing centers (MTOCs), including the centrosomes. TPX2 binds to *AURKA*, protecting it from dephosphorylation and enhancing its kinase activity, which is crucial for spindle assembly (Van Gijn et al., 2019). Additionally, *AURKA* interacts with transforming acidic coiled-coil-containing protein (TACC) and its partner, microtubule-associated protein 215 (MA*P215*, also known as ch-TOG in humans). TACC/MA*P215* is crucial for stabilizing microtubules and promoting their growth (Burgess et al., 2018). *AURKA* phosphorylates TACC, which enhances its ability to bind to microtubules and increases the stability and dynamics of the mitotic spindle. This interaction ensures that microtubules are properly organized and aligned, which is essential for accurate chromosome segregation (Ulisse et al., 2007). The combined actions of *AURKA* at the microtubule organizing centers ensure the efficient formation and function of the mitotic spindle during prophase. By activating TPX2 and phosphorylating γ-tubulin and TACC/MA*P215*, *AURKA* orchestrates the assembly and stabilization of microtubules, facilitating the transition from G2 to M phase and the early stages of mitosis (Burgess et al., 2018).

1.5.3.1.3 Metaphase

From metaphase onwards, it is felt that *AURKB* plays a more significant role in mitosis. Still, *AURKA* does have some activity through the phosphorylation of HEC-1. (DeLuca et al., 2018) HEC-1, an essential mitotic protein, is intricately involved in establishing appropriate microtubule attachments and chromosome alignment (Mo et al., 2013)

1.5.3.1.4 Anaphase

AURKA and *AURKB* work together to regulate this phase of mitosis; they do so through the phosphorylation of CENP-E (Hochegger et al., 2013). CENP-E associates with kinetochores in prometaphase and captures and stabilises kinetochore-microtubule (KT–MT) interactions (Maia et al., 2010a). The mechanism by which *AURKA* interacts with CENP-E is unclear and needs further investigation. It is felt that phosphorylation of CENP-E leads to its eventual migration to the chromosomes and subsequent chromosomal movement to opposite cellular poles.

1.5.3.2 Non-Mitotic roles of *AURKA*.

AURKA has been found to promote cell-cycle progression by repealing suppressors or enhancing cell-cycle promoters (Yan, 2009). *AURKA* activity helps to promote cell cycle transitions through processes such as evading the G2/M DNA damage

checkpoint or promotion of G2/M transition. The G2/M DNA damage checkpoint is avoided by activating *CDK*1 in cancer cells; *AURKA* promotes G2/M transition by phosphorylating *BRCA1* at Ser308.46.

AURKA promotes tumour cell migration and invasion through activating several oncogenic signalling proteins, including AKT-70, *MAPK*, Coffilin-F-actin, SRC, mitotic centromere- associated kinesin (MCAK) and focal adhesion kinase (FAK) pathways. (Mahankali et al., 2015). *AURKA* also interacts with oncogenes and tumour suppressors; for example, *AURKA* suppresses *p53* function by inducing its ubiquitination by activating HDM2.

1.5.4 *AURKC*.

Aurora Kinase C *AURKC* is the third kinase family member; it has not yet been studied as extensively as *AURKA* or *AURKB*. Earlier studies have shown it is mainly seen in meiotically dividing cells and located primarily in the testes of mammals (Libertini et al., 2010). It was expressed at higher levels than Aurora-B other tissues in healthy human placenta, colon, oocytes and mammary gland tissue, lung cancer, hepatocellular carcinoma and thyroid cancer cell lines. (Slattery et al., 2009)

The expression of *AURKC* levels is highest at the G2/M phase and localises mainly on the centrosome from anaphase to cytokinesis. Its gene is located on chromosome 19q13.43, and its expression is noted to be implicated with gliomas and colorectal cancer.

The relationship between *AURKC* and *AURKB* remains unclear, with conflicting mechanisms proposed. It has been argued that *AURKC* performs the same functions as *AURKB* in mitosis; *AURKC* performs nonoverlapping but cooperative roles with *AURKB* in mitosis. Alternatively, *AURKC* performs competitive tasks that interfere with *AURKB* function in mitosis, and *AURKC* performs only non-mitotic tissue-specific functions. (Slattery et al., 2009)

AURKC can fulfil the roles of Aurora-B in centromere assembly, kinetochore-microtubule attachment, the SAC, and cytokinesis. *AURKC* binds to CPC proteins; it co-localises with INCENP and Survivin and competes with the *AURKB* for binding. The CPC formed localises first to the inner centromere, then to the central spindle, and, ultimately, to the midbody of mitotic cells. INCENP is required to target *AURKC* to the centromere appropriately, and *AURKC* directly interacts with INCENP through the same binding domain involved in binding with Aurora-B.

Like *AURKB*, the kinase activity of *AURKC* contributes to its proper localisation of the centrosome. *AURKC* is involved in additional functions to ensure the correction of kinetochore-microtubule attachment errors and bipolar spindle stability to complement *AURKB* function during the later stages of mitosis. (Sasai et al., 2004)

1.5.5 *AURKB*.

Aurora B, part of the chromosomal passenger complex(CPC), localises to centromeres/inner kinetochores, the spindle midzone/central spindle and finally the midbody during telophase and cytokinesis, reflecting crucial roles in the regulation of chromosome condensation, correct chromosome-microtubule attachment, mitotic spindle stability and cytokinesis (Becker et al., 2010). Accordingly, *AURKB* expression peaks in the late G2/M phase during the cell cycle, but notably, it is expressed through the cell cycle at a basal level (Wu et al., 2011b), and recent findings suggest non-mitotic functions.

Upstream activation of *AURKB* requires its interaction with INCENP and TD-60, an inner centromere protein TD-60 (Guo et al., 2011). Protein phosphatase activity inhibits *AURKB* activation and increases inactive *AURKB* during interphase (Posch et al., 2010, p. 22). Aurora B recruits several proteins to the kinetochore (Ditchfield et al., 2003; Vigneron et al., 2004) and plays a direct role in a pathway that senses and corrects syntelic microtubule/kinetochore attachments, in which both sister kinetochores are attached to microtubules from the same spindle pole. Aurora B phosphorylates histone H3 on Ser10, essential for chromosome condensation (Tao et al., 2008a). It is also required to define the cleavage furrow and cytokinesis by phosphorylating MgcRacGAP, vimentin, desmin, myosin II regulatory light chain, and glial fibrillary acidic proteins.

1.5.5.1 Role of *AURKB* in mitosis.

1.5.5.1.1 Prophase

During prophase *AURKB* acts alongside *CDK*1 to directly phosphorylate Condensin I (Figure 1-7), which leads to its association with chromosomes. This association lasts throughout later phases until anaphase (Lipp et al., 2007). CENP-A's phosphorylation leads to *AURKB* targeting the inner centromere region (Kunitoku et al., 2003; Slattery et al). The phosphorylation of CENP-A is a stepwise process that begins with *AURKA* phosphorylation at the Ser-7 residue. Zeitlin et al. demonstrated the interaction between *AURKB* and CENP-A by using CENP-A-GST proteins, where the Ser-7 residue was changed to two different amino acid residues (Alanine and Glutamic Acid).

AUKRB also promotes MPS1 localisation to kinetochores (Saurin et al., 2011) to correct any errors during chromosomal alignment. It has been shown that Mps1, a mitotic checkpoint kinase, directly phosphorylates Borealin/DasraB, and this phosphorylation has been proposed to be crucial for total Aurora B kinase activity in chromosome alignment (Guo et al., 2011).

Prior to sister chromatid separation PLK1 phosphorylates Survivin at the SER20 residue, enhancing *AURKB* activity in the centromere and proper chromosome segregation (Chu et al., 2011). Ssu72 is phosphorylated by *AURKB* (Figure 1-6), which inhibits Cohesin binding from the chromosome arms in prophase (Kim et al., 2013).

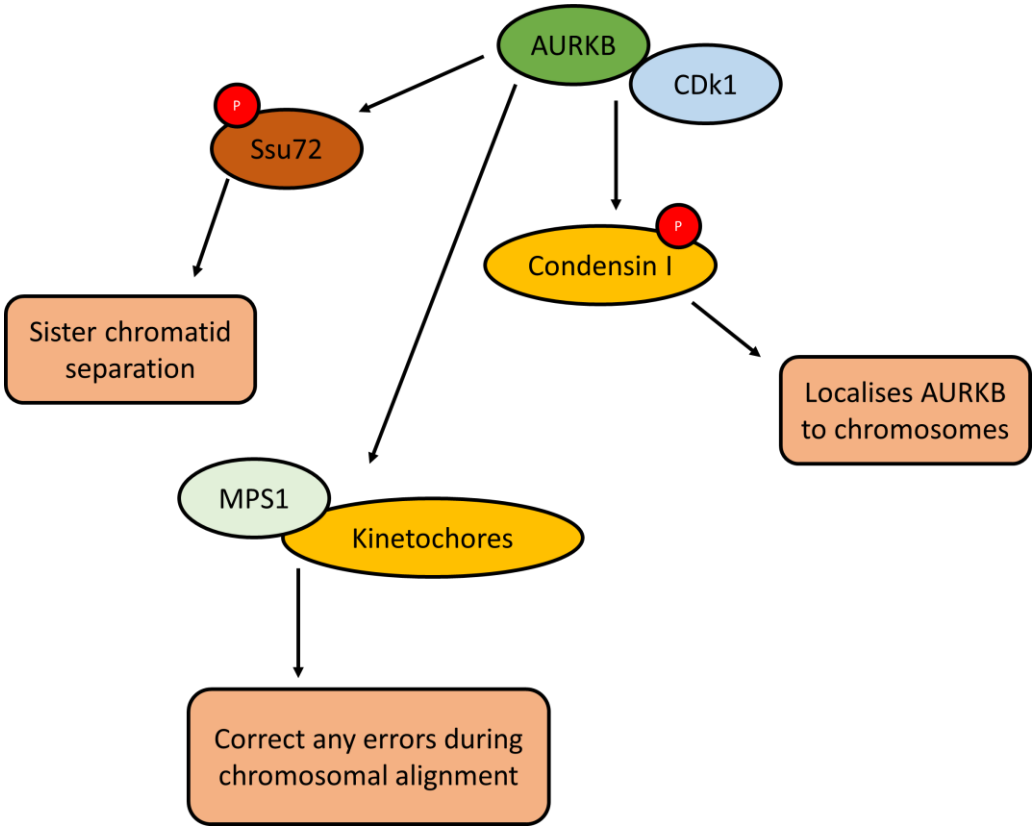


Figure 1-6: Some interactions of *AURKB* during Prophase Aurora kinase B (*AURKB*) is a crucial component of the chromosomal passenger complex (CPC) and plays an essential role in regulating various processes during mitosis, including chromosome condensation, kinetochore-microtubule attachments, and the spindle assembly checkpoint (Carmena et al., 2012; Gohard et al., 2014). During prophase, *AURKB* interacts with several key proteins and complexes to ensure proper mitotic progression. *AURKB* phosphorylates SSU72, modulating its activity and ensuring proper chromosome condensation and segregation. This regulation is vital for maintaining the structural integrity of chromosomes during the early stages of mitosis (Kim et al., 2013).

AURKB further modulates the activity of *CDK*1 through feedback loops, ensuring timely progression through prophase. This interplay between *AURKB* and *CDK*1 is crucial for the proper coordination of mitotic events (Jang et al., 2016; Parrilla et al., 2016). *AURKB* also interacts with Condensin I, a protein complex essential for chromosome condensation. During prophase, *AURKB* phosphorylates components of Condensin I, enhancing its ability to bind to DNA and promoting the compaction of chromosomes (Lipp et al., 2007).

1.5.5.1.2 Prometaphase

EB1 enhances the activity of *AURKB* by blocking the activity of PP2A, preventing its inactivation, and allowing it to phosphorylate EB2 and EB3 (Banerjee et al., 2014; Nehlig et al., 2017). EB1 is also crucial for recruiting the CPC towards the inner centromeres in prophase (Banerjee et al., 2014).

Small ubiquitin-related modifiers are essential in many cellular processes, and SUMOylation is essential for mitotic progression, including kinetochore and centromere function regulation. SUMOylation can affect substrates in at least two ways: an allosteric effect that induces substrate conformational change and an effect that involves the creation/inhibition of a binding interface (Ban et al., 2011). *AURKB* undergoes SUMOylation at Lys207, which leads to the proper localisation and activity of the CPC during chromosome alignment (Fernandez-Miranda et al., 2010). It remains unclear how the SUMOylation of *AURKB* leads to its subsequent activation.

1.5.5.1.3 Metaphase

The interaction with *AURKB* in the late G2 phase of the cell cycle is an essential step for entering mitosis (Hirota et al., 2003). Ajuba interacts with *AURKB* and BUBR1 at the kinetochore during metaphase, forming a complex. This complex's function is unclear; experimenting with cells deficient in Ajuba leads to a lack of progression throughout the G2/M phase (Ferrand et al., 2009). *AURKB* phosphorylates mDia3 (Figure 1-8), reducing microtubule binding to the kinetochore and destabilising

microtubules at colder temperatures (Cheng et al., 2011, p. 3). *AURKB* phosphorylation of mDia3 is also essential for chromosomal alignment in metaphase. Downstream inhibition of BUBR1 leads to abnormal chromosomal alignment defects. *AURKB* is critical for localising BUBR1 to the kinetochore during the spindle checkpoint (Figure 1-8). *AURKB* also aids the binding of BUBR1 to the kinetochore during metaphase (Ditchfield et al., 2003a).

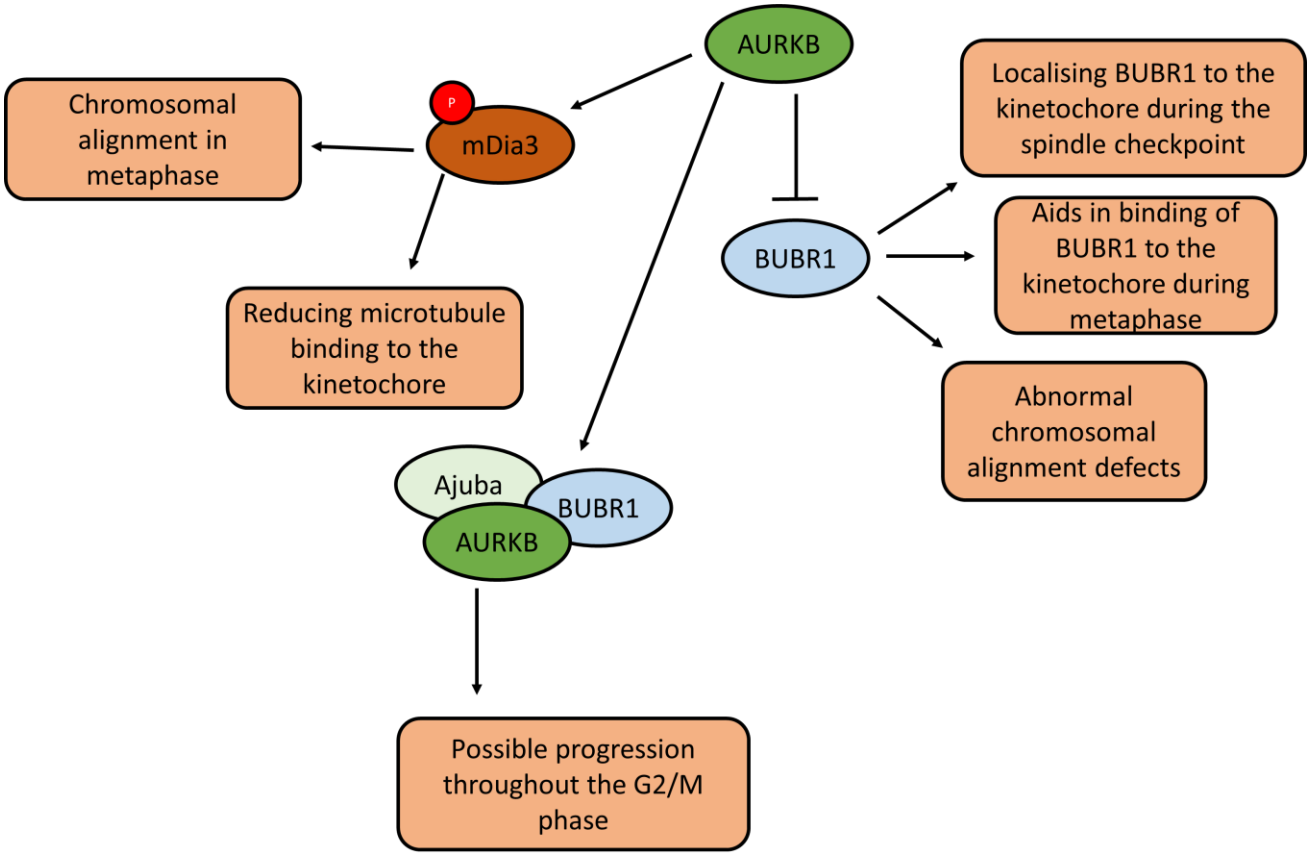


Figure 1-7: Interactions of *AURKB* in Metaphase During metaphase, Aurora kinase B (*AURKB*) plays a critical role in ensuring proper chromosome alignment, tension across sister chromatids, and the activation of the spindle assembly checkpoint (SAC) through its interactions with mDia3, BUBR1, and Ajuba (Ditchfield et al., 2003b; Ferrand et al., 2009). *AURKB* phosphorylates mDia3, enhancing its ability to interact with microtubules and ensuring proper spindle formation and stabilization, which is essential for accurate chromosome alignment. By phosphorylating BUBR1, a key component of the SAC, *AURKB* activates and maintains this checkpoint, preventing anaphase onset until all chromosomes are correctly attached to the spindle microtubules with proper tension.

1.5.5.1.4 Metaphase to anaphase transition (Spindle checkpoint)

Both *AURKB* and *CDK*2 are involved in the phosphorylation of EB2, governing the regulation of microtubule-binding affinity (Iimori et al., 2016, p. 2). Lack of phosphorylated EB2 leads to lagging chromosomes and aneuploidy. Mitotic kinesin-like protein-2 (MKlp-2), a member of the kinesis-6 family, is essential for transitions through metaphase, anaphase, telophase and cytokinesis (Tcherniuk et al., 2010). Concerning the CPC, it guides the relocation of this complex from the centromeres to the spindle midzone during the metaphase-to-anaphase transition.

AURKB and *MAD2L2* are frequently elevated in human tumours, leading to spindle assembly checkpoint (SAC) disruptions and subsequent chromosomal missegregation and centrosome amplification. *AURKB* plays a crucial role in SAC by recruiting SAC components like *MAD2L2* to kinetochores during error correction, generating unattached kinetochores. Rapid silencing of SAC is necessary after the proper and stable attachment of all chromosomes to permit entry into anaphase and exit from mitosis (Marima et al., 2021).

In the presence of an MKlp-2 inhibitor, as well as using RNAi depletion in a separate assay, *AURKB* and Survivin relocation to the midzone during anaphase is disrupted (Tcherniuk et al., 2010). The mechanism by which Mklp-2 controls localisation is due to the dual binding to both *AURKB* and Cdc14A, which dephosphorylates INCENP, regulating its localisation.

There are two Pds5 proteins (Pds5A and Pds5B) involved in telomere and arm cohesion; specifically, Pds5B is required for centromeric cohesion and *AURKB* recruitment centromeres (Carretero et al., 2013). Auto-cleavage of separase is an

essential marker for anaphase onset in mitosis. It cleaves centromeric Cohesin and removes it from chromosome arms, separating sister chromatin (Kim et al., 2013). *AURKB* regulates the recruitment of seperatase to chromosomes, aiding in its function (Yuan et al., 2009a).

The exact mechanism of how it regulates recruitment is unclear, whether it is the phosphorylation of seperatase leading to the binding with the chromosome or the chromosome's phosphorylation leading to increased seperatase binding. Ubiquitin-specific peptidase 39 (USP39) is a human protein necessary for gene expression due to splicing protein substrates (Ban et al., 2011; Gan et al., 2017). Usp39 controls the deubiquitination and splicing of aurora B. Studies show that the downregulation of Usp39 reduces mitotic activity (van Leuken et al., 2008).

1.5.5.1.5 Anaphase

Aurora B is required for the localisation at kinetochores and the phosphorylation of BUBR1 in cells entering mitosis. *AURKB* targets BUBR1 towards kinetochores, ultimately regulating the spindle checkpoint (Ditchfield et al., 2003a). Repression of BUBR1 leads to abnormal spindle checkpoint function with lagging chromosomes. CENP-E mediates the lateral sliding of sister chromatids along K-fibres, leading to proper chromosomal segregation. (Maia et al., 2010b). A lack of CENP-E leads to *AURKB* remaining at the centromere, activating the spindle assembly checkpoint due to detachment of the microtubules from polar chromosomes. *AURKB* is also required to target CENP-E towards the kinetochore (Guo et al., 2012; Yu et al., 2019). *AURKB*, in conjunction with CENP-E, regulates the congression of mono-

oriented chromosomes by destabilising their kinetochore-microtubule attachments (Figure 1-9). The cullin-RING family of ubiquitin ligases regulates diverse cellular functions, such as cell cycle control, via ubiquitylation (Moghe et al., 2012, p. 3). CUL3-KLHL21 E3 regulates chromosomal passenger complex (CPC) translocation from chromosomes to the spindle midzone in anaphase (Maerki et al., 2009). The activity of CUL3-KLHL21 E3 promotes translocation of the CPC to the spindle midzone through ubiquitination of *AURKB* (Maerki et al., 2009). The mechanism by which ubiquitination leads to translocation is unclear.

In anaphase, Aurora B phosphorylates *KIF*4A on T799 and increases its microtubule-stimulated ATPase activity as part of the mechanism controlling central spindle length (Figure 1-9). Mammalian Large tumour suppressor 2 (Lats2) and Mammalian Large tumour suppressor 1 (Lats1) are both members of the Dbf2 kinase family. *AURKA* phosphorylates Lats2 via the Ser280 residue (Figure 1-8). There is subsequent localisation with *AURKB* at the central spindle (Yabuta et al., 2011).

Although Lats2 localises to *AURKB* at the central spindle, it does not lead to its phosphorylation; instead, it binds to Lats1, forming a complex in which Lats1 phosphorylates *AURKB* aiding chromosome segregation and cytokinesis. In the absence of MKlp2, both the Aurora B–INCENP complex and Plk1 fail to localise correctly during anaphase and telophase, and cleavage furrow ingression and cytokine Sis fail (Neef et al., 2003). It is proposed that MKlp2 promotes the microtubule-dependent localisation of Plk1, Aurora B, and Cdc14A to the central spindle during anaphase.

PP1 is a crucial regulator of *AURKB* activity through phosphorylation, leading to its inactivation. Sds22 phosphorylates PP1 and leads to localisation at the kinetochore

(Figure 1-9). The depletion of Sds22 leads to an increase in *AURKB* at the kinetochore due to the downregulation of PP1(Posch et al., 2010, p. 22). The activity of Sds22 also regulates the phosphorylation of substrates downstream of *AURKB*.

Like Sds22, Repo-Man is a targeting subunit that recruits PP1 to chromatin, leading to *AURKB* de-phosphorylation (Wurzenberger et al., 2012). Repo-Man and Sds22 counteract Aurora B's sustained activity on anaphase chromatin and kinetochores after translocating the chromosomal passenger complex to the central spindle.

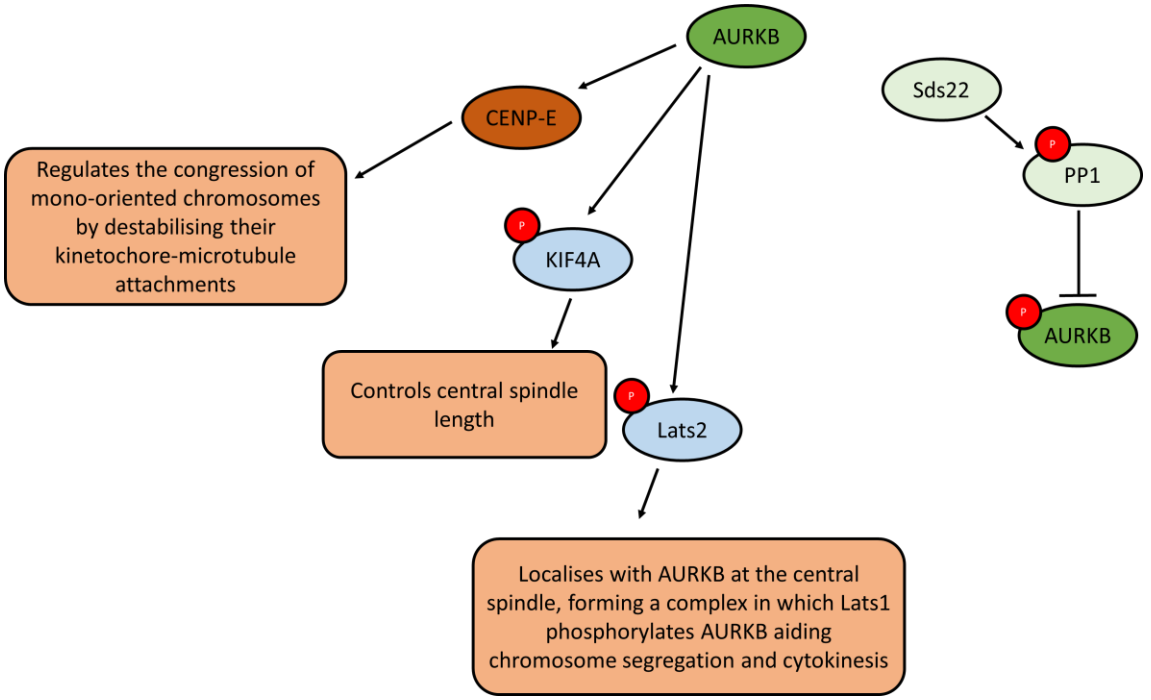


Figure 1-8: Interactions with *AURKB* in Anaphase During anaphase, Aurora kinase B (*AURKB*) continues to play a pivotal role in coordinating chromosome segregation and cytokinesis through its interactions with various proteins such as CENP-E, *KIF*4A, LATS2, SDS22, and PP1. CENP-E (Centromere-associated protein E), a motor protein, is crucial for the stable attachment of microtubules to kinetochores and the movement of chromosomes toward the poles (Abe et al., 2006; Guo et al., 2012). *AURKB* phosphorylates CENP-E, regulating its motor activity and ensuring the correct alignment and movement of chromosomes, which is essential for accurate segregation. *KIF*4A (Kinesin family member 4A) is another motor protein that interacts with *AURKB* during anaphase (Bastos et al., 2014).

LATS2 (Large tumor suppressor kinase 2) is a component of the Hippo signaling pathway that also interacts with *AURKB* in anaphase. *AURKB* phosphorylates LATS2, influencing its activity in regulating the cell cycle and maintaining genomic stability (Abe et al., 2006; Yabuta et al., 2011). This interaction ensures that the mitotic spindle is correctly positioned and that the cell cycle progresses smoothly from anaphase to telophase. SDS22 (Suppressor of Dis2) and PP1 (Protein Phosphatase 1) are regulatory proteins involved in the dephosphorylation of mitotic substrates. *AURKB* modulates the activity of PP1 through its interaction with SDS22, ensuring precise control over the dephosphorylation of key proteins required for the completion of mitosis (Bastos et al., 2014; Posch et al., 2010).

1.5.5.1.6 Anaphase to telophase transition

The separation of the chromosomes during anaphase is monitored by an *AURKB* phosphorylation gradient created at the spindle midzone (O. Afonso et al., 2014; Olga Afonso et al., 2014). *AURKB* prevents chromosomal decondensation before their long and short arms are separated, delaying the NER's completion (Afonso et al., 2017). The activity of *AURKB* is opposed by PP1 and PP2A, which is initially targeted to the kinetochores by the activity of Repo-Man and Sds22(Maiato et al., 2015). The activity of PP1 and PP2A leads to chromosome decondensation and NER (Afonso et al., 2017; Maiato et al., 2015).

1.5.5.1.7 Telophase and Cytokinesis

CaM co-localises with *AURKB* at the midbody and disrupts subsequent SCF^{FBXL2}-mediated ubiquitination and degradation (Chen et al., 2013; Mallampalli et al., 2013; Teng et al., 2012a). The interaction between CaM, FBXL2 and *AURKB* stabilises the ingressed furrow for delayed abscission.

Aurora-B acts at different steps throughout cytokinesis. Aurora-B promotes the formation of the cleavage furrow, central spindle, and midbody by phosphorylation and recruitment of motors and microtubule-associated proteins, including the centralspindlin components MKLP1 and MgcRacGAP, the Rho GTPase activator ECT2, and the microtubule-bundling protein PRC1. Finally, when lagging chromatin is present in the midbody, Aurora-B prevents abscission by activating the abscission checkpoint (Monteonofrio et al., 2018). Aurora B phosphorylates several other

substrates during anaphases, such as RACGAP1, vimentin, SHCBP1 (SHC binding and spindle associated1), and possibly myosin light chain and the myosin-binding subunit of myosin phosphatase, which all contribute to furrow ingression and cytokinesis in human cells (Figure 1-10) (Adriaans et al., 2019, p. 1). *AURKB* phosphorylates Ataxin-10 at its S12 residue, leading to localisation to the midbody. Depletion of Axatin-10 in Hela cells has been shown to result in multinucleated cells due to a failure of cytokinesis (Tian et al., 2015). The ongoing phosphorylation leads to increased affinity to binding with PLK1. How this interaction leads to cytokinesis needs further investigation.

Two known isoforms of BARD1 interact with *AURKB*, FL BARD1 and BARD1β. BARD1β co-localises with *AURKB* and TACC1 at the midbody, leading to the cleavage furrow and abscission (Ryser et al., 2009). FL BARD1 acts to regulate the activity of *AURKB* by ubiquitination, leading to its reduced expression. Brd4 is a tumour suppressor, a member of the BET family of proteins containing bromodomains, playing a vital role in G_1/S and G_2/M cell cycle progression. It remains unclear how Brd4 regulates cellular proliferation and tumour suppression. Downregulation of Brd4 is associated with reduced *AURKB* levels, leading to abnormal chromosome segregation and failed cytokinesis (You et al., 2009).

The phosphorylation of CENP-A is responsible for regulating the targeting of *AURKB*, INCENP and PPγ1 (Zeitlin et al., 2001). Cells with mutations of CENP-A show delayed separation during cytokinesis, with differences in the intercellular bridge's length and morphology. Mutations in CENP-A lead *AURKB* and INCENP to preferentially localise at the chromosomes instead of the midzone at anaphase, although they appear to localise normally during cytokinesis (Zeitlin et al., 2001). *AURKB* phosphorylates CHMP4C via S10, which leads to localisation to the

Flemming body and delayed abscission through activation of the NoCut checkpoint (Carlton et al., 2012). The NoCut checkpoint delays abscission, which prevents damage to lagging chromosomes trapped in the midbody. The lack of CHMP4C leads to accelerated abscission and cytokinesis.

EB3 is essential for stabilising the midbody microtubules during cytokinesis. *AURKB* creates a phosphorylation gradient by migrating from the chromosomes to the spindle midzone (Figure 1-10). The *AURKB* gradient phosphorylates EB3 on S176 (Figure 1-9), promoting midbody stability (Iimori et al., 2016).

EVI5 is an 810 amino acid-long ubiquitously expressed protein interacting with INCENP, *AURKB* and Survivin. The fundamental role of EV15 is unclear and requires further investigation (Faitar et al., 2006, p. 15). The resulting complex of EV15 and *AURKB*/INCENP leads to the localisation of EV15 to the midbody. Whether *AURKB* phosphorylates EV15 and its specific activity in conducting cytokinesis remains unclear.

Centralspindlin is a crucial target of PLK1 and activates RhoA GEF ECT2, leading to furrow ingression. PLK1 also acts to limit the activity of PRC1, which leads to AUKRB-dependent activity on centralspindlin (Adriaans et al., 2019). It remains unclear how PLK1 acts to limit the activity of PRC1, as mutations in PRC1 sites which bind to PLK1 lead to a lack of recruitment of PLK1 to the spindle midzone.

HIPK2 and H2B are localised to the midbody through the actions of *AURKB* (Monteonofrio et al., 2018). *AURKB* binds to and phosphorylates H2B at Ser32. It is thought that *AURKB* recruits MgcRacGAP and PRC1, which binds HIPK2, recruiting it to the midbody. HIPk2 is a Tyr-regulated Ser/Thr kinase in the DNA damage

response pathway. During cytokinesis, HIPK2 and H2B both localise at the midbody, where H2B is phosphorylated, leading to abscission.

MKlp2 is localised to the cell cortex, which recruits *AURKB* and INCENP, promoting the progression of the furrow in monopolar cytokinesis (Kitagawa et al., 2013). Nlp is recruited to the midbody and phosphorylated by AURBK during cytokinesis. Nlp organises the midbody and maintains the cell to complete cytokinesis (Yan et al., 2010).

AURKB phosphorylates RASSF1A on Ser203 (Figure 1-10), leading to the recruitment of Syntaxin16 to the midzone and midbody, leading to normal cytokinesis(Song et al., 2009). *AURKB* may also lead to the recruitment of RASSF1A to the midzone, although the result of this action is unclear.

AURKB also regulates MKLP1 localisation to the spindle midzone in anaphase. MKLP1 is responsible for assembling the midzone/midbody and preventing cleavage furrow regression(Soeda et al., 2013). *AURKB* phosphorylates ZEN-4 and MKLP1 on S680 and S708 residues, which aid in completing cytokinesis by forming the contractile ring (Guse et al., 2005, p. 4).

Centralspindlin is a crucial target of PLK1 and is involved in RhoA GEF activation, ECT2 leading to furrow ingression. PLK1 also acts to limit the activity of PRC1, which leads to AUKRB-dependent activity on centralspindlin (Adriaans et al., 2019, p. 1). It remains unclear how PLK1 acts to limit the activity of PRC1, as mutations in PRC1 sites which bind to PLK1 lead to a lack of recruitment of PLK1 to the spindle midzone.

AURKB phosphorylates RASSF1A on Ser203, leading to the recruitment of Syntaxin16 to the midzone and midbody, leading to normal cytokinesis (Song et al.,

2009). *AURKB* may also lead to the recruitment of RASSF1A to the midzone, although the result of this action is unclear (Figure 1-10).

The Rho-kinase/ROCK pathway is crucial for reorganising cleavage activities during cell division. Rho-kinase/ROCK acts downstream of Rho, regulating stress fibres and focal adhesion complexes. The phosphorylation of several proteins is required to carry out the cleavage activities. Rho-kinase/ROCK and *AURKB* synergistically phosphorylate multiple intermediate filaments (IF) protein bridge protein sites, such as Vimentin and Desmin (Yokoyama et al., 2005). The phosphorylation of the IF proteins aids in separating into two daughter cells. There is no clear evidence that *AURKB* and Rho-kinase/ROCK have a direct interaction with each other to perform this role. Rho is a GTPase involved in many normal cellular functions, including cytokinesis. To ensure proper cytokinesis, RhoA, for example, localises in the cleavage furrow (Minoshima et al., 2003), leading to the contractile ring assembly. MgcRacGAP is phosphorylated at Ser387 by *AURKB* in the midbody, leading to increased GAP activity toward RhoA with subsequent enhanced activity and development of the contractile ring (Figure 1-10).

They localise to the leading edge of cleavage furrows and eventually reside at the midbody. Septins belong to a conserved family of GTPase proteins known to regulate cytokinesis. *AURKB* phosphorylates Septin 1 *in vivo* at Ser248, Ser307 and Ser315 and co-localise to the midbody during cytokinesis (Figure 1-10) (Qi et al., 2005).

AURKB forms a complex with TACC1 via binding to its C-terminal fragment. The complex of TACC1 and *AURKB* localises to the midzone spindle and the midbody,

resulting in spindle formation (Delaval et al., 2004, p. 1). More work needs to be done, looking at the exact role TACC1 plays in cytokinesis.

EVI5 is an 810 amino acid-long ubiquitously expressed protein that interacts with INCENP, aurora B kinase (*AURKB*) and Survivin. The fundamental role of EV15 is unclear and requires further investigation (Faitar et al., 2006, p. 15). The resulting complex of EV15 and *AURKB*/INCENP leads to the localisation of EV15 to the midbody. Whether *AURKB* phosphorylates EV15 and its specific activity in conducting cytokinesis remains unclear.

NPM1 is a highly dynamic nucleolar protein that plays a vital role in diverse cellular processes, namely centrosome duplication and cytokinesis (Figure 1-10). *AURKB* phosphorylates NPM1 at Ser125, regulating proper centrosome numbers and cytokinesis (Shandilya et al., 2014, p. 1).

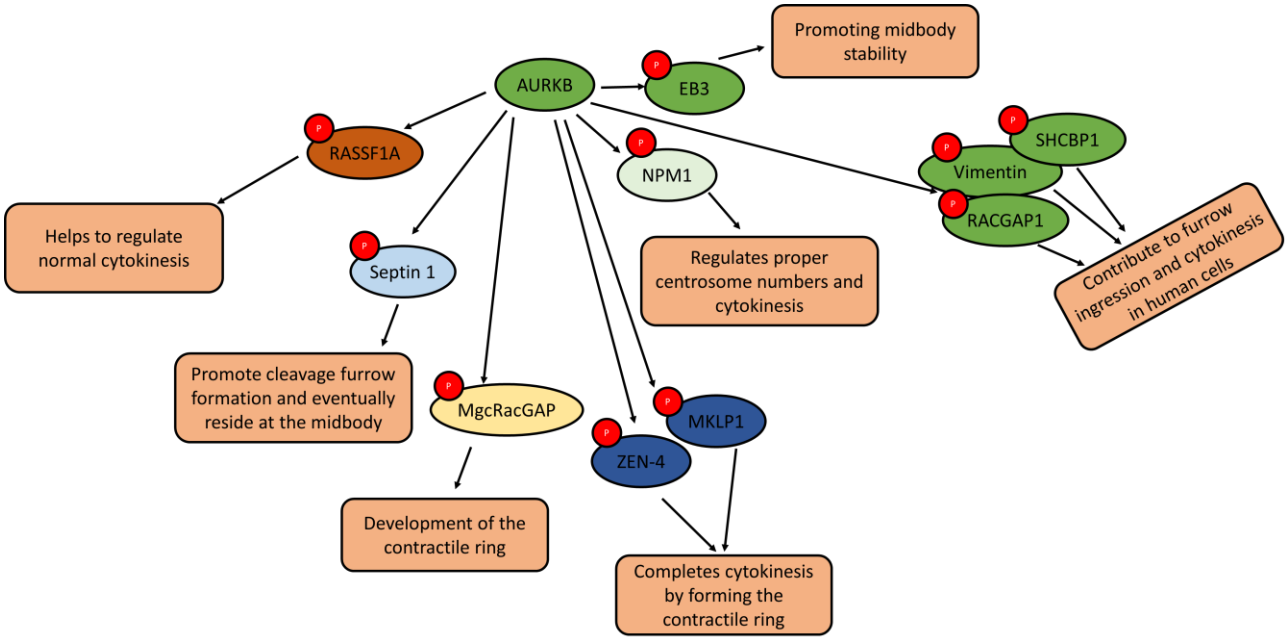


Figure 1-9: Interactions of *AURKB* in cytokinesis During cytokinesis, Aurora kinase B (*AURKB*) orchestrates the final separation of daughter cells through interactions with various proteins, ensuring proper cell division and genomic stability. One of the key interactions is with RASSF1A (Ras association domain family member 1A), a tumor suppressor involved in microtubule stability and spindle organization. *AURKB* phosphorylates RASSF1A, modulating its function and contributing to the organization of the central spindle and the successful completion of cytokinesis.

AURKB phosphorylates Septin 1, facilitating its proper assembly and function in the contractile ring, thereby ensuring efficient cleavage furrow ingression (Ditchfield et al., 2003b; Minoshima et al., 2003; Qi et al., 2005; Shandilya et al., 2014). NPM1 (Nucleophosmin 1) is involved in centrosome duplication and acts as a molecular chaperone. *AURKB*-mediated phosphorylation of NPM1 is crucial for the regulation of centrosome dynamics and ensuring accurate cytokinesis (Minoshima et al., 2003).

AURKB phosphorylates EB3, stabilizing microtubules at the midbody and aiding in the final separation of the daughter cells (Qi et al., 2005). MgcRacGAP (male germ cell RacGAP), a key regulator of the Rho family GTPases, interacts with *AURKB* to control the contractile machinery necessary for cytokinesis (Shandilya et al., 2014). *AURKB* phosphorylation of MgcRacGAP ensures proper localization and activation of the contractile apparatus at the cleavage furrow (Minoshima et al., 2003).

1.5.5.2 Role of *AURKB* outside of mitosis.

1.5.5.2.1 *p21* and *p38 MAPK*

AURKB inhibition leads to the activation of *p38 MAPK*, resulting in downstream activation of *p53* and *p21*. The mechanism of how inhibition of *AURKB* leads to the activation of *p38* remains unclear (Kumari et al., 2014). Increased expression of *p38 MAPK* leads to inhibition of S-phase entry; it is felt that inhibition of *p38 MAPK* leads to increased cell proliferation and sensitisation of tumour cells to anticancer therapy with *AURKB* inhibitors (Jin et al., 2016; Kumari et al., 2013).

AURKB inhibition stabilises *p53*, which transcribes *p21*, leading to its upregulation. The other way it leads to increased *p21* activity is ROS activation, leading to *p38*-mediated transcription elongation of *p21* (Kumari et al., 2014).

1.5.5.2.2 *AURKB* and *p53* function

p53 interacts directly with *AURKB*, a substrate during mitosis that is negatively regulated (Chris P. Gully et al., 2012). *p53* comprises an N-terminal transactivation domain, a central specific DNA-binding domain (DBD), and a C-terminal tetramerisation domain followed by a regulatory domain (Wu et al., 2011c). Novel INHAT repressor (NIR) mediates the interaction between *AURKB* and *p53* on multiple regions in the DBD, reducing its transcriptional activity (Chris P. Gully et al., 2012; Wu et al., 2011c). *AURKB* also acts independently of NIR to interact directly with *p53* through binding at the C terminus (amino acids 160-393). Apart from the

late M phase, when *AURKB* is degraded, *p53* and *AURKB* interact during most of the cell cycle. Aurora-B phosphorylates *p53* on several residues (Ser183, Thr211, and Ser215) to accelerate the degradation of *p53* through the polyubiquitination-proteasome pathway (Chris P. Gully et al., 2012). Decreasing *p53* transcriptional activity results in cell cycle progression and reduced apoptosis. This is done by reducing the expression of *p21*(Adams et al., 2001), which aids in driving the G1/s phase and enhancing the suppression of Cyclin B/Cdc2 (C. P. Gully et al., 2012). *AURKB* inhibition stabilises *p53*, which transcribes *p21*, leading to its upregulation. The other way it leads to increased *p21* activity is ROS activation, leading to *p38*-mediated transcription elongation of *p21* (Kumari et al., 2014).

Aurora B is a new *FBXW7*-associating protein; *FBXW7* regulates *AURKB* during mitosis, *FBXW7* regulates Aurora B post transcriptionally by enhancing Aurora B ubiquitination. *p53* deficiency causes the downregulation of *FBXW7*α. Additionally, Aurora B can phosphorylate *p53* and subsequently enhance MDM2-mediated *p53* degradation, *FBXW7*-mediated Aurora B degradation indicates that a feedback loop exists to maintain the equilibrium between Aurora B, *p53* and *FBXW7* (Teng et al., 2012b).

MAD2L2 is a potential link between *AURKB*, *p53*, and the DNA damage response (DDR) pathway. The involvement of *AURKB* and *MAD2L2* in the *p53* pathway remains unclear. The aberrant expression of *MAD2L2* during DNA repair at uncapped telomeres and double-strand breaks (DSBs) is speculated to contribute to genomic instability. In-silico analysis indicates a robust interaction between *AURKB* and *p53*. Although not depicted here, among the two isoforms, *AURKA* and *AURKB*, the latter exhibits a mild interaction with *MAD2L2*, in contrast to the absence of an

AURKA-MAD2L2 interaction. Notably, *p53* weakly interacts with *MAD2L2* (Marima et al., 2021).

AURKB inhibition leads to the activation of *p38 MAPK*, resulting in downstream activation of *p53* and *p21*. The mechanism of how inhibition of *AURKB* leads to the activation of *p38* remains unclear (Kumari et al., 2014). Increased expression of *p38 MAPK* leads to inhibition of S-phase entry; it is felt that inhibition of *p38 MAPK* leads to increased cell proliferation and sensitisation of tumour cells to anticancer therapy with *AURKB* inhibitors (Jin et al., 2016; Kumari et al., 2013).

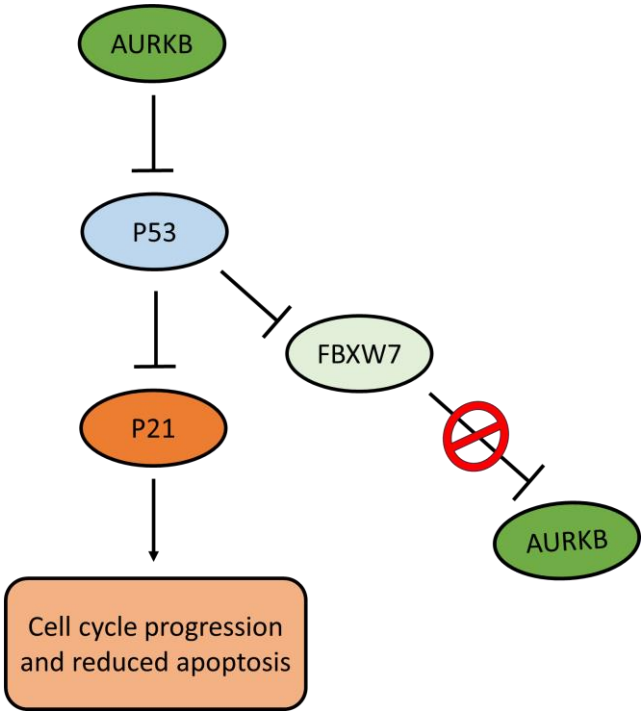


Figure 1-10: Interaction between *AURKB* and *P53* The interaction between Aurora kinase B (*AURKB*) and the tumor suppressor protein *p53* is a critical aspect of cell cycle regulation and genomic stability. *AURKB* is a key mitotic kinase involved in various processes, including chromosome condensation, spindle assembly, and cytokinesis (C. P. Gully et al., 2012, p. 53; Wu et al., 2011a).

During mitosis, *AURKB* and *p53* interaction plays a significant role in maintaining the integrity of cell division. *AURKB* can phosphorylate *p53*, which influences its stability and activity(C. P. Gully et al., 2012, p. 53; Wu et al., 2011a). This phosphorylation event can lead to the modulation of *p53*'s transcriptional activity, impacting its ability to induce cell cycle arrest and apoptosis. Specifically, *AURKB*-mediated phosphorylation of *p53* can inhibit *p53*'s transcriptional activity, thereby reducing its ability to trigger apoptosis in response to mitotic errors (Wu et al., 2011a).

1.5.5.2.3 *Wnt* signaling interaction with *AURKB*.

WNT signalling induces cell motility through multiple mechanisms. One of these is regulated by *AURKB* activity (Luo et al., 2019). Following *WNT* signalling, the effector DVL2 was shown to recruit the *CEP*192-PLK4-*AURKB* complex to cell protrusions; here, *AURKB* promoted the switching of formin *DAMM*1 to *DAMM*2 causing actin re-organisation and cell migration. Thus, inhibition of *AURKB* led to reduced migration in bladder cancer cells via retention of *DAMM*1 (Luo et al., 2019).

Moreover, the interaction between *AURKB* and *Wnt* is further established from the study (Luo et al., 2019), demonstrating how *Wnt* signalling stimulated cancer cells are highly dependent on *AURKB*. When *AURKB* switches the *Wnt* formins *DAMM*1 to *DAMM*2 within the cell protrusions, it causes an immediate cell migration. The *DAAM*s level was monitored upon AZD treatment. The result showed that inhibiting *AURKB* on the cell line allows the *DAAM*1 to sustain. When *DAAM*1 remains in the cell cortex, it prevents the forming of *DAAM*2. The outcome of this inhibition leads to the prevention of cell migration. In the clinical aspect, reducing the expression of *DAAM*1 and high levels of *DAAM*2 leads to high-grade bladder cancer in male patients. Therefore, inhibiting *AURKB* and preventing *DAAM*2 formation could be a potential treatment for bladder cancer.

Inhibition of *AURKB* also reduced migration of gastric cancer cells. Although the mechanism was not elucidated, the same study showed that gene expression changes co-incident with *AURKB* depletion suggest alterations in the VEGFA/Akt/mTOR and *Wnt*/β-catenin/Myc pathways.

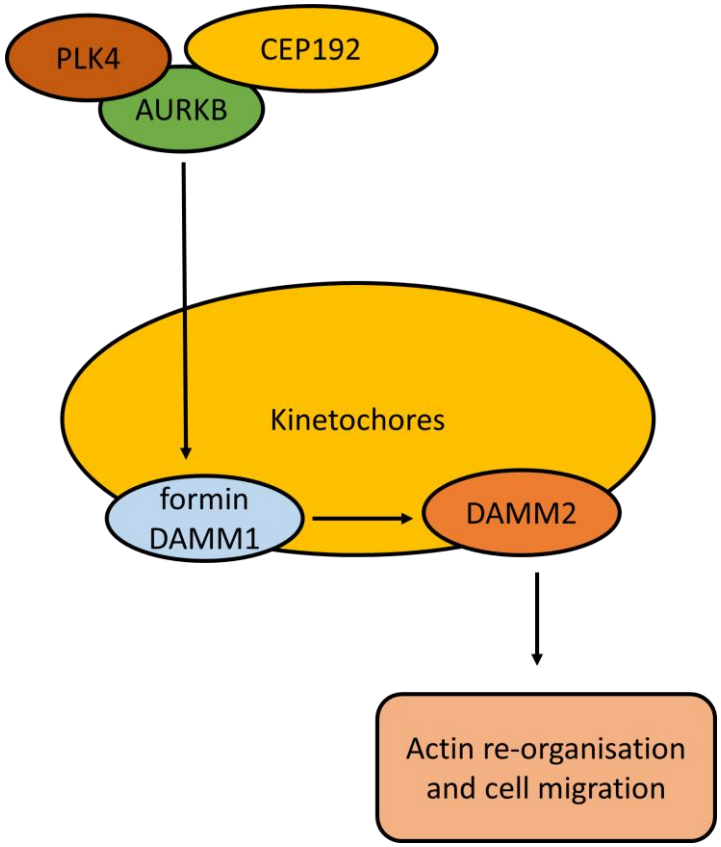


Figure 1-11: Aurora kinase B (*AURKB*) is primarily known for its critical role in mitosis, but emerging evidence suggests that it also interacts with the *Wnt* signaling pathway, which is crucial for regulating cell proliferation, differentiation, and migration (Bertran-Alamillo et al., 2019a; Shuda et al., 2009). The *Wnt* signaling pathway is divided into canonical (β-catenin dependent) and non-canonical (β-catenin independent) pathways, both of which play vital roles in development and tumorigenesis. *AURKB* has been shown to influence the canonical *Wnt*/β-catenin signaling pathway by modulating the stability and activity of β-catenin. β-catenin is a central player in the *Wnt* pathway, and its accumulation in the cyt*op*lasm followed by translocation to the nucleus leads to the activation of *Wnt* target genes involved in cell proliferation and survival (Luo et al., 2019).

1.5.5.3 The Oncogenic Role of *AURKB* overexpression.

1.5.5.3.1 Role of *AURKB* in NSCLC

AURKB overexpression is associated with aneuploidy and non-small cell lung cancer (NSCLC) development. Also, it has been linked to squamous cell pathology, increased lymph node metastasis, increased prevalence in males and poorly differentiated tumours (Vischioni et al., 2006). The expression of *AURKB* has also been associated with chemo- and radioresistance and a poor prognosis in NSCLC (Yu et al., 2018). Further, increased expression of *AURKB* has been correlated with *EGFR* Tyrosine Kinase resistance in cell lines and patients with NSCLC pathology (Bertran-Alamillo et al., 2019b). Increased *AURKB* expression also leads to aneuploidy, which may be a marker of tumour development and poorer prognosis in NSCLC tumours (Takeshita et al., 2013). *CDCA*8 is a putative oncogene aberrantly expressed in lung cancer cells along with *AURKB*, leading to NSCLC (Hayama et al., 2007). *CDCA*8 is a regulator of mitotic events responsible for correcting the error of bipolar attachments.

1.5.5.3.2 Role of *AURKB* in HNSCC

A study examining the expression of *AURKB* in nasopharyngeal tumours showed no statistically significant association with age, gender, tumour or nodal staging (Huang et al., 2015; Q. Zhang et al., 2019). The disease-free survival was higher in the *AURKB*

negative cohort than the positive one, but there was no difference in the overall or local recurrence-free survival between tumours that were either negative or positive expression for *AURKB*.

The expression of *AURKB* in thyroid cancer was associated with the more aggressive anaplastic carcinoma, with only moderate increases in expression seen in papillary and follicular carcinomas and very low (or absent) expression seen in benign adenomas, non-neoplastic thyroid lesions such as Hashimoto disease, and normal thyroid tissue. *AURKB* overexpression leads to multinucleation and polyploidy in thyroid tumours and may be linked to thyroid tumour progression (Hu et al., 2018). Encouragingly, depletion of *AURKB* using siRNA or inhibition with a small molecule inhibitor significantly reduced the proliferation of anaplastic thyroid carcinoma cells in vitro and in vivo. (Sorrentino et al., 2005).

1.5.6 AURK inhibitors.

Aurora Kinase inhibitors are under investigation in several clinical trials after promising preclinical data. (Table 2) *AURKA* inhibition temporarily induces a mitotic arrest; cells exit from mitosis with multipolar and monopolar spindle formation, leading to apoptosis, while Aurora-B inhibition induces endoreduplication, chromosome misalignments, and polyploidy. (Bavetsias and Linardopoulos, 2015)

The list of drugs used in current trials includes Barasertib (AZD1152), Alisertib (MLN8237), Danusertib (PHA-739358), AT9283, PF-03814735, AMG 900. The main

side effects of these inhibitors are febrile neutropenia, stomatitis, gastrointestinal toxicity, hypertension, and fatigue. (Bavetsias and Linardopoulos, 2015)

These drugs are being investigated both in haematological malignancies and solid tumours for their carcinogenic potential. Currently, in solid tumours, the results have been disappointing; it has been linked to the slower rate of growth of the tumours compared to haematological malignancies.

They have also been used with increasing interest due to preclinical studies showing increased radiosensitivity through the interaction of *AURKA* with other genes in the DNA damage repair response pathway (Wang , 2014). More specifically, it reduces the expression of *BCRA1*/2, *ATR*/*CHK1*, *P53* and RAD-51. Radio resistance has also been demonstrated in hepatocellular and prostate cancer cell line experiments. (Niermann , 2012; Shen , 2019)

AURKB inhibition in combination with irradiation (IR)

Studies have investigated the effect of *AURKB* and radiation, looking at a combination of AZD1152 and IR. The effect of *AURKB* inhibition in tumour cells is particularly more pronounced in subtypes that are *p53* deficient. This is attributed to the lack of a proper spindle checkpoint system that prevents cells from passing abnormal genomes to their daughter cells. *AURKB* inhibition reduces cellular repopulation and enhances effects during fractionated radiotherapy (Sak et al., 2012).

Inhibition of *AURKB* in combination with IR displays evidence of mitotic catastrophe *in vivo* and . AZD1152 alone leads to the development of multinucleate cells and micronuclei; this effect is further enhanced when combined with IR (Tao et al., 2009).

Studies have demonstrated that *AURKB* inhibitors, such as AZD1152, enhance the radiosensitivity of various cancer cell lines, including androgen-resistant prostate cancer cells (PC3 and DU145) (Chieffi et al., 2006). The combination of *AURKB* inhibition and irradiation leads to increased DNA damage, as evidenced by enhanced γ-H2AX foci formation, which is a marker of DNA double-strand breaks. Additionally, this combination results in a higher rate of mitotic catastrophe, a form of cell death occurring during mitosis, due to improper chromosome segregation and cytokinesis failure (Niermann et al., 2011; Schecher et al., 2017)

Mechanistically, *AURKB* inhibition disrupts the repair of radiation-induced DNA damage by affecting the cell cycle checkpoint control, particularly the G2/M checkpoint. This checkpoint ensures that cells do not enter mitosis with damaged DNA. By inhibiting *AURKB*, cells prematurely enter mitosis with unresolved DNA damage, leading to mitotic failure and subsequent cell death. This synergistic effect of *AURKB* inhibitors with irradiation highlights their potential in overcoming radioresistance in tumours (Shaalan et al., 2021).

1.6 Study context

The research focuses on understanding the role of Aurora Kinases, particularly *AURKA* and *AURKB*, in the development of radioresistance in non-small cell lung cancer (NSCLC) and head and neck squamous cell carcinoma (HNSCC). Despite advances in radiotherapy, radioresistance remains a significant barrier to effective treatment in these cancers, contributing to poor survival rates. Aurora Kinases, which are overexpressed in these cancer types, are implicated in mitotic processes and have emerged as potential therapeutic targets to enhance radiosensitivity.

While previous studies have identified the overexpression of Aurora Kinases in various cancers, the specific mechanisms by which *AURKA* and *AURKB* contribute to radioresistance in NSCLC and HNSCC are not fully understood. Additionally, there is a lack of comprehensive studies evaluating the effectiveness of Aurora Kinase inhibitors, like Barasertib which we used, in combination with radiation therapy. This gap limits the development of targeted therapies that could improve the efficacy of radiotherapy in these cancers.

The central hypothesis of this thesis is that the inhibition of *AURKA* and *AURKB* will enhance the radiosensitivity of NSCLC and HNSCC cells, leading to improved therapeutic outcomes. This effect is hypothesized to occur through mechanisms that involve both *p53*-dependent and independent pathways.

Aims and Objectives in the Thesis

Chapters Three and Four

Aim 1: To investigate the role of *AURKA* and *AURKB* in radioresistance in NSCLC and HNSCC.

Objective 1.1: Evaluate the expression levels of *AURKA* and *AURKB* in NSCLC and HNSCC tissues and cell lines.

Objective 1.2: Assess the correlation between *AURKA*/*AURKB* expression and patient outcomes, such as overall survival (OS) and progression-free survival (PFS). (Mapped to Chapter 6)

Chapters Five and Six

Aim 2: To determine the radiosensitisation potential of *AURKA* and *AURKB* inhibitors in vitro.

Objective 2.1: Test the effects of *AURKA* inhibitor (e.g., LY3295668) and *AURKB* inhibitor (e.g., Barasertib) on NSCLC and HNSCC cell survival post-radiation.

Objective 2.2: Explore the role of *p53* in mediating the effects of *AURKA*/*AURKB* inhibition on radiosensitivity. (Mapped to Chapter 3 and Chapter 4)

Chapter Seven

Aim 3: To elucidate the molecular mechanisms underlying the radiosensitisation effect of *AURKB* inhibition.

Objective 3.1: Investigate cell cycle alterations, mitotic processes, and DNA damage response pathways following *AURKB* inhibition in combination with radiation.

Objective 3.2: Analyse the potential synergistic effects of combining *AURKB* inhibition with different chemotherapeutic agents. (Mapped to Chapter 4)

Chapter Eight

Aim 4: To translate preclinical findings into potential clinical applications.

Objective 4.1: Develop a phase one trial protocol to test the combination of *AURKB* inhibitors and radiation in NSCLC patients. (See Appendix: Phase One Trial Protocol)

2 Materials & Methods.

2.1 Materials.

2.1.1 Laboratory Equipment.

Equipment	Supplier
Autoclave	Scientific Laboratory Supplies
BD LSR II Flow Cytometer	B.D. Biosciences
Bench*top* Centrifuge – accruSpin Micro	Fischer Scientific
Film Processor	Konica
Film Scanner	EPSON
Heamocytometer	Neubauer
Heat/Magnetic stirrer	Stuart
Heating Block DB-2A	Techne
Irradiator	C.I.S. Bio International
Laboratory fume cupboard	Fumex Ltd
Light microscope	Optika
Leica AF6000 Time-Lapse Microscope	Eppendorf
Mid bench centrifuge – Heraeus MegaFuge 16	Thermo Scientific
Microcentrifuge	Eppendorf
Microwave	-
Mr Frosty^{TM} freezing container	Thermo Fisher Scientific
pH meter	Jenway
Pipette boy	Drummond
Pipettes	Gibson
Power pack	Bio-Rad
Pannoramic slide scanner	3D HISTECH
Rice Steamer	-
Tissue Culture incubator	Thermo Fisher Scientific
Water bath	Gallenkamp
Western Tanks	Bio-Rad
7HCS microscope	Zeiss Celldiscover
Vortex	Scientific Industries

Table 2-1: "Laboratory Equipment and Their Suppliers"

2.1.2 Glassware, plastics, and disposables.

Item Name	Supplier
Centrifuge t*ube*s – 15 mL	SARSTDEDT
Centrifuge t*ube*s – 50 mL	Fischer Scientific
Coverslip – Rectangular 22 x 50 mm	Thermo Fischer Scientific
Coverslip – Circular 13 mm	V.W.R.
Coverslip – Circular 25 mm	Scientific Laboratory Supplies
Cryovials	SARSTDEDT
Culture plates – 6 well	STARLAB
Culture plates – 24 well	Corning Incorporated
Eppendorfs – 0.5 mL, 1.5 mL, and 2 mL	SARSTDEDT
Glass bottles	Fischer Scientific
Microlance needles	Becton Dickinson (B.D.)
Microscope slides - 76 x 26 mm	Thermo Fischer Scientific
Pipette tips	SARSTDEDT
Plastic pipettes –10 mL	Fischer Scientific
Plastic pipettes – 5 mL and 25 mL	SARSTDEDT
Sterile syringes	BD
Tissue culture dish – 90mm	CELLSTAR
Tissue culture flask – T25 and T75	SARSTDEDT
Universal vials	SARSTDEDT

Table 2-2: "Laboratory Consumables and Their Suppliers"

2.1.3 Purified Water.

A Triple Red System produced Type 1 Ultra-pure deionised water (ddH2O).

2.1.4 Sterilisation.

Glassware and solutions were sterilised by autoclaving at 15 p.s.i and 120 °C for 15 minutes.

2.1.5 Chemicals.

Chemical	Supplied by
Acetone	Fisher Scientific
Adenine	Sigma Aldrich
Agarose	Sigma Aldrich
Amersham enhanced chemiluminescence (ECL) western blotting reagent.	G.E. Life Sciences
Alcohol (95%)	Fisher Bioreagents
Ammonium persulphate (APS)	Fisher Scientific
Bovine serum albumin (BSA)	Sigma Aldrich
Bovine Pituitary Extract	Gibco
Bromophenol blue	Sigma Aldrich
4′,6-Diamidine-2′-phenylindole dihydrochloride	Vector Laboratories
Diaminobenzidine	Vector Laboratories
Dimethyl sulphoxide (DMSO)	Fisher Scientific
Dithiothreitol (DTT)	Fisher Scientific
Dharmafect 1	G.E. Life Sciences
Dharmafect 4	G.E. Life Sciences
EGF Human Recombinant	Gibco
Ethanol	Fisher Scientific
Glycerol	Fisher Scientific
Glycine	Fisher Scientific
Hydrochloric acid	Sigma Aldrich
Hydrocortisone, Bioreagent	Sigma Aldrich
Hydrocortisone, H0888-1G	Sigma Aldrich

Industrial methylated spirit (IMS)	Fisher Scientific
Insulin	Sigma Aldrich
L-Glutamine (200mM)	Fisher Scientific
Methanol	Fisher Scientific
Methylene Blue	Sigma Aldrich
Nutrient Mixture F12 Ham	Sigma Aldrich
4% paraformaldehyde	Boster
Phenylmethanesulfonyl fluoride (PMSF)	Sigma Aldrich
Phosphatase inhibitor cocktails I & II	Sigma Aldrich
Phosphate buffered saline	Thermo Fisher
Propidium iodide (PI)	Sigma Aldrich
Protease inhibitor	Sigma Aldrich
RPMI-1640 Medium power	Sigma Aldrich
7.5% Sodium bicarbonate ($NaHCO_3$)	Sigma Aldrich
Sodium dodecyl sulphate (SDS)	Sigma Aldrich
Sodium deoxycholate	Sigma Aldrich
Sodium hydroxide	Fisher Scientific
Target Retrieval Solution (10x), Citrate pH 6.1	Dako
Target Retrieval Solution (10x), Citrate pH 9.0	Dako
Tetramethylethylenediamine (TEMED)	V.W.R.
Tris Base	Fisher Scientific
Triton X-100	Sigma Aldrich
Tween 20	Acros Organics
Universal x-ray developer	Champion Protochemistry
Universal x-ray fixer	Champion Protochemistry
Xylene	Fisher Scientific

Table 2-3: Chemical Reagents used and Their Suppliers

2.1.6 Cell lines.

NSCLC Cell Line	**Supplied by**	**Genotype**	***p53* Status**	**HPV status**	***EGFR* status**
A549	PHE	Human lung adenocarcinoma	Wildtype	N/A	Wildtype
H520	ATCC	Human lung squamous cell carcinoma	Wildtype	N/A	Null
H460	P. Woll (Zhu et al. 2008)	Human lung large cell carcinoma	Wildtype	N/A	Wildtype
H322	PHE	Human lung adenocarcinoma	Mutant	N/A	Wildtype
H1299	ATCC	Human lung large cell carcinoma	Null	N/A	Wildtype
SW900	ATCC	Human lung squamous cell carcinoma	Mutant	N/A	Wildtype

HNSCC Cell Line	Supplied by	Genotype	*p53* Status	HPV status
BICR22 (B22)	Edington (1995) Mol Carcinog 13(4): 254-65	Neck Lymph nodes	Mutant	HPV -ve
SCC89	Lin (2007) Head Neck. 29(2):163-88	Tonsil	Mutant	HPV -ve
OKF6/TERT-1(OKFB)/*FN*B6	Dickson (2000) Mol Cell Biol 20 (4): 1436-47	Floor of Mouth	Wildtype	N/A
UD-SCC2	Lin (2007) Head Neck. 29(2):163-88	Hypopharynx	Positive	HPV +ve
UPCI-SCC72	Lin (2007) Head Neck. 29(2):163-88	Tonsil	Wildtype	HPV -ve

Table 2-4: NCSLC and H&N cancer cell lines used throughout the project.

P.H.E.: Public Health England, ATCC: American Type Culture Collection

2.1.7 Cell culture reagents.

2.1.7.1 Foetal calf serum (FCS).

Virus, endotoxin, and mycoplasma-free FCS were supplied by Seralab, aliquoted and stored at -20 ^{o}C until used.

2.1.7.2 Cell culture medium.

A549, UD-SCC2, UPCI-SCC72, and SCC89 cell lines were cultured in Dulbecco's modified eagles' medium (DMEM) containing 4.5 g/L glucose with L-glutamine supplied by Sigma Aldrich.

BICR22 (B22) and OKF6/TERT-1(OKFB)/*FN*B6 were cultured in Dulbecco's modified eagles' medium (DMEM) containing 4.5 g/L glucose with L-glutamine supplemented with adenine, hydrocortisone, insulin, foetal calf serum, EGF and Hams media (supplied by Sigma Aldrich)

H520, H460, H322 and H1299 were cultured in Roswell Park Memorial Institute (RPMI)-1640 medium with L-glutamine supplemented with Foetal calf serum.

SW900 was cultured in Dulbecco's modified eagles' medium (DMEM) containing 4.5 g/L glucose with L-glutamine supplied by Sigma Aldrich. The media for this cell line was supplemented with 10% foetal calf serum and, 1x non-essential amino acids (NEAA) supplied by Lonza, and additional L-glutamine.

2.1.7.3 Trypsin and versene/EDTA.

Trypsin EDTA with 0.5 g/L Trypsin and 0.2 g/L versene (EDTA) was supplied by Lonza.

2.1.8 Buffers.

2.1.8.1 Phosphate-buffered saline (PBS)

PBS was produced by dissolving 1 Oxoid PBS tablet per every 100 ml of ddH_2O. PBS was sterilised by autoclaving and stored at room temperature.

2.1.8.2 Tris-buffered saline (TBS)

10x TBS solution was produced by dissolving 24.2 g Tris Base (200 mM) and 80 g NaCl (1.4 M) in 900 ml ddH_2O. 5 M HCl was then used to adjust the solution pH to 7.6 before the final volume was adjusted to 1 L with ddH_2O. 10x solution was kept at room temperature. 1x solution was achieved by diluting 10x solution with ddH_2O.

2.1.8.3 1 M Tris pH 6.8 and 8.0

1 M Tris solution was produced by dissolving 121.1 g of Tris Base in 900 ml ddH_2O. 5 M HCl was then used to adjust the solution pH to 6.8 or 8.0 before the final volume was adjusted to 1 L with ddH_2O. 1 M Tris pH 6.8 and pH 8.0 were stored at room temperature.

2.1.8.4 1.5 M Tris pH 8.8

1.5 M Tris solution was produced by dissolving 181.7 g of Tris Base in 700 ml ddH_2O. 5 M HCl was then used to adjust the solution pH to 8.8 before the final

volume was adjusted to 1 L with ddH_2O. 1.5 M Tris pH 8.8 was stored at room temperature.

2.1.8.5 10 mM Tris 1 mM EDTA solution pH 9.0

Ten mM Tris 1 mM EDTA solution was produced by dissolving 1.21 g of Tris Base and 0.37 g EDTA in 900 ml ddH_2O. 5 M HCl was then used to adjust the solution pH to 9.0. 0.5 ml Tween 20 (0.05%) was added to the solution before increasing the volume to 1 L with ddH_2O.Ten mM Tris 1 mM EDTA pH 9.0 was stored at 4^oC.

100 mM PMSF

1 M DTT

2.1.8.6 5 x RIPA lysis buffer

100 ml 5 x RIPA lysis buffer was produced by adding 25 ml 1 M Tris pH 8.0 (250mM), 15 ml 5 M NaCl (750mM), 5 ml 10% SDS (0.5%), 5 ml NP-40 (5%), 2.5 g Sodium deoxycholate (2.5%) and ddH_2O to bring volume to 100 ml. 5 x RIPA lysis buffer was stored at room temperature.

2.1.8.7 SDS boiling mix.

SDS boiling mix was *mad*e by adding 62.5 mM Tris-HCl (pH 6.8) to

2% SDS (sodium dodecyl sulphate),10% glycerol, 0.1% bromophenol blue (as a tracking dye), 5% beta-mercaptoethanol or 100 mM DTT (dithiothreitol) as a reducing agent

2.1.8.8 5 x Sodium Dodecyl Sulphate - Polyacrylamide Gel Electrophoresis (SDS-PAGE) sample buffer

100 ml 5 X SDS-PAGE sample buffer was produced by adding 25 ml 1 M Tris pH 6.8 (250mM), 10 g SDS (10%), 50 ml glycerol (50%), 5 ml β-mercaptoethanol (5%), 20 mg bromophenol blue (0.02%) and ddH_2O to bring volume to 100 ml. 5 x SDS-PAGE sample buffer was stored at room temperature.

2.1.8.9 10 x SDS-polyacrylamide gel electrophoresis (SDS-PAGE) running buffer.

10 x SDS-PAGE running buffer was produced by dissolving 30 g Tris Base (250 mM) and 144 g Glycine (1.9 M) in 900 ml ddH_2O. Then 100 ml of 10% SDS (1%) was added to bring the volume up to 1 L.10 x SDS-PAGE running buffer was stored at room temperature.

2.1.8.10 1 x SDS-PAGE running buffer.

1 x SDS-PAGE running buffer was produced by diluting 100 ml 10 x SDS-PAGE running buffer with 900 ml ddH_2O.

2.1.8.11 10 x Towbin transfer buffer

10 x Towbin transfer buffer was produced by dissolving 30.3 g Tris Base (250 mM) and 144 g Glycine (1.9 M) in ddH_2O, bringing volume to 1 L.

2.1.8.12 1 x Towbin transfer buffer

1 x Towbin transfer buffer was produced by mixing 100 ml 10 x Towbin buffer, 700 ml of ddH_2O and 200 ml methanol in that order; 1 x Towbin transfer buffer was stored at 4 ^oC on the day of use.

2.1.9 Inhibitor Compounds.

Compound	Mechanism	Diluent	Storage	Company
MLN8237 (Alisertib) 10mM (1mL in DMSO)	Inhibits T288 auto-phosphorylation of *AURKA*	DMSO	-20ºC	Selleckchem
Barasertib 10mM (1mL in DMSO)	Inhibits Aurora Kinase B (*AURKB*)	DMSO	-20ºC	Selleckchem
Nocodazole	Inhibits microtubule polymerisation	DMSO	-20ºC	Sigma Aldrich

Table 2-5: Summary of Compounds Used in the Study, Their Mechanisms, Diluent, Storage Conditions, and Suppliers

2.1.10 Cytotoxic agents.

Compound	Mechanism	Diluent	Storage	Company
E*top*oside (1mM stock)	*Top*oisomerase II poison	DMSO	-20ºC	Sigma Aldrich
5-Fluorouracil (500nM stock)	It is an analogue of the pyrimidine uracil and thus acts as a pyrimidine antagonist.	DMSO	-20ºC	Sigma Aldrich
Vinorelbine (1mM) 10mg in 12.84 of DMSO	Disrupts the assembly of DNA microtubules	DMSO	-20ºC	Adooq BioScience
Cisplatin (1mM stock)	Inhibits DNA crosslinks	DMSO	-20ºC	Sigma Aldrich

Table 2-6: Cytotoxic Agents Used, Their Mechanisms, Diluent, Storage Conditions, and Suppliers

2.1.11 Irradiation.

Irradiation of cells was performed using a CIB/IBL 437 CS-137 irradiator. Irradiations were performed in a 3.8 L irradiation canister and were delivered to cells directly in 100 mm^3 dishes (when cells were plated four h prior to irradiation) or to cells in 15 ml falcon t*ube*s (when cells were to be plated immediately following irradiation).

2.1.12 Short interfering R.N.A. (siRNA) and transfection reagents.

All siRNAs were *mad*e to a stock concentration of 20 µM with the ma*nuf*acturer-supplied buffer, aliquoted and stored at -20 ºC.

SR30004 Universal scrambled negative control siRNA duplex (Origene)

AURKA B duplexes (Origene):

AURKB-siRNA s17612: 5’ UCGUCAAGGUGGACCUAAAtt 3’

AURKB-siRNA s17611: 5’ CCUGCGUCUCUACAACUAUtt 3’

2.1.13 Antibodies.

2.1.13.1 Primary antibodies.

Antibody	Host Animal	Ma*nuf*acturer (Cat number)	Application WB (Dilution)	Application IHC (Dilution)	Application FACS (Dilution)
AURKA	Mouse	Sigma Aldrich (A1231)	1:1000	1:200	-
AURKB	Rabbit	Abcam(ab2254)	1:1000	1:100, 1:200	-
Phospho-Aurora A (Thr288)/Aurora B (Thr232)/Aurora C (Thr198)	Rabbit	Cell Signalling Technology ()	1:200	-	-
β-tubulin	Mouse	Sigma-Aldrich (T8328)	1:10000	-	-
pSer10 Histone 3	Rabbit	Cell Signalling Technology (9701)	1:20000	-	-
pSer10 Histone 3	Rabbit	Abcam (Ab47297)		-	1:500
CDC20	Rabbit	Cell Signalling Technology (4823)	1:1000	-	-
Cyclin B1	Mouse	Cell Signalling Technology (V152)	1:2000	-	-
GAPDH	Mouse	Proteintech	1:20000	-	-
Total H3	Rabbit	Cell Signalling Technology (9715)	1:1000	-	-

Table 2-7: Antibodies Used in the Study, Their Applications in Western Blot (WB), Immunohistochemistry (IHC), and Fluorescence-Activated Cell Sorting (FACS)

WB: Western blot, IHC: Immunohistochemistry, IF: Immunofluorescence, FACS: Fluorescence-activated cell sorting

2.1.13.2 Secondary antibodies

Antibody	Host Animal	Ma*nuf*acturer (Cat number)	Application WB (Dilution)	Application IHC (Dilution)	Application FACS (Dilution)
Anti-mouse IgG horse radish peroxidase (H.R.P.)	Horse	Cell Signalling Technology (7076)	1:2000	-	-
Anti-rabbit IgG H.R.P.	Goat	Cell Signalling Technology (7074)	1:2000	-	-
Anti-rabbit Alexa 488	Mouse	Life Technologies (A11008)	-	-	1:200
Anti-mouse IgG Biotinylated	Goat	Vector Labs (BA-9200)	-	1:200	-
Anti-rabbit IgG Biotinylated	Goat	Vector Labs (BA-1100)	-	1:200	-
Anti-rat IgG Biotinylated (mouse adsorbed)	Rabbit	Vector Labs (BA-4001)	-	1:200	-

Table 2-8: Secondary Antibodies Used in the Study, Their Applications in Western Blot (WB), Immunohistochemistry (IHC), and Fluorescence-Activated Cell Sorting (FACS)

WB: Western blot, IHC: Immunohistochemistry, IF: Immunofluorescence,

FACS: Fluorescence-activated cell sorting

2.1.14 Immunohistochemistry detection kits.

Detection Kit	Host Animal	Ma*nuf*acturer (Cat number)	Application WB (Dilution)	Application IHC (Dilution)	Application FACS (Dilution)
I*MMP*RESS® H.R.P. Horse Anti-Mouse IgG Polymer Detection Kit, Peroxidase	Mouse	Vector Laboratories MP-7402	-	1:200	-
I*MMP*RESS® H.R.P. Horse Anti-Rabbit IgG PLUS Polymer Kit, Peroxidase	Rabbit	Vector Laboratories MP-7801	-	1:00, 1:200, 1:400	-
I*MMP*RESS® Excel Amplified Polymer Staining Kit, Anti-Mouse IgG, Peroxidase	Mouse	Vector Laboratories MP-7602	-	1:00, 1:200 1:400	-
I*MMP*RESS® Excel Amplified Polymer Staining Kit, Anti-Rabbit IgG, Peroxidase	Rabbit	Vector Laboratories MP-7601	-	1:00, 1:200 1:400	-

Table 2-9: Detection Kits Used in the Study, Their Applications in Western Blot (WB), Immunohistochemistry (IHC), and Fluorescence-Activated Cell Sorting (FACS)

2.2 Methods.

2.2.1 Mammalian cell culture.

2.2.1.1 Passaging cells

NSCLC and H&N cell lines were maintained at 37 ^{o}C with 5% CO_2 in T25 or T75 flasks. Culture media was removed from passaged cells, and cells were washed twice in 5 ml PBS. Following washing, cells were dislodged from the bottom of the flask by adding 1 ml Trypsin EDTA and returning cells to 37 ^{o}C. Once cells were fully dislodged in trypsin EDTA, 9 ml of warm (37 ^{o}C) culture media was used to neutralise trypsin. Freshly resuspended cells were then used to seed new flasks. All experiments were performed when cells were 60-80% confluent to ensure cells were in the logarithmic growth phase.

2.2.1.2 Freezing cells

After cells had been suspended in fresh media following trypsin EDTA exposure, they were centrifuged in 15 ml falcon t*ube*s using Mid bench centrifuge – Heraeus MegaFuge 16 at 1200 revolutions per minute (R.P.M.) for 3 minutes. Cell pellets were resuspended in culture media with 10% DMSO at a density of $1x10^6$ cells per ml. Cells for freezing were distributed into 1 ml cryovials and stored overnight at -80 ^{o}C in a Mr Frosty™ Freezing Container supplied by Thermo Fisher Scientific. Following this, cells were kept at -80 ^{o}C for short-term storage (< 1 year) and in liquid nitrogen for long-term storage (> 1 year).

2.2.1.3 Thawing cells

Frozen cells were rescued by rapidly thawing cells at 37 ^{o}C in a water bath. Following this, cells were transferred from the cryovial to a 15 ml falcon t*ube* before 9 ml of warm culture media was gently added dropwise. Cells were centrifuged at 1200 RPM for 3 minutes before resuspending in 10 ml media and transferred to a T25 culture flask.

2.2.1.4 Clonogenic survival assays

The plating density of NSCLC cells varied between 500-5000 cells per condition plated in 90 mm^3 dishes. After appropriate treatment, cells were left to form colonies for 10-14 days; following this, media was removed, and colonies were stained with methylene blue in methanol (4 g/L). Colonies were defined using a threshold of 50 viable cells and counted. Plating efficiency was calculated as the number of colonies/the number of cells plated, and survival fraction was determined as the plating efficiency of condition/plating efficiency of unirradiated control. Unirradiated controls were sham irradiated by rotation in an irradiation canister without irradiation exposure. A minimum of three independent biological repeats were achieved, with averages and standard deviations calculated. To determine the LD50 (the dose at which 50% of the cells are unable to form colonies) we use the data from the dose-response curve. This is done by finding the concentration or dose of radiation corresponding to a survival fraction of 0.5.

2.2.1.5 Irradiation/inhibitor alone experiments

Cells were plated and allowed approximately 4 hours to adhere to the plate; following this, cells were treated as appropriate.

2.2.1.6 Irradiation inhibitor combination experiments

When plating, pre-treatment cells were allowed approximately 4 hours to adhere to the plate; following this, cells were treated with *AURKA* or *AURKB* inhibitor for 2 hours before irradiation as appropriate. When plating, post-treatment cells were treated with *AURKA* or *AURKB* inhibitor for 2 hours in a flask before being dislodged with trypsin EDTA. Cells were then irradiated in 15ml falcon t*ube*s before being plated. Plated cells were provided with fresh media complemented with/without fresh *AURKA* inhibitor where appropriate.

2.2.1.7 Drug-Drug combination assays

The plating density of NSCLC cells varied between 500-5000 cells per condition plated in 90 mm^3 dishes. After appropriate treatment with *AURKB* inhibitor and either Alisertib, E*top*oside, Vinorelbine, 5-Flourouracil and Cisplatin, cells were left to form colonies for 10-14 days; following this, media was removed, and colonies were stained with methylene blue in methanol (4 g/L). Colonies were defined using a threshold of 50 viable cells and counted.

2.2.1.8 Summary of specific plating densities for each cell line and radiation therapy (RT)

2.2.1.8.1 Irradiation/Inhibitor Alone Experiments

Day 0: Cell plating in 90mm dishes, incubation for 4 hours.

Day 0 (Post 4 hours): Cells treated with inhibitor or control.

Day 0 (2 hours post-inhibitor): Irradiation applied (if applicable).

Day 1-10: Colony formation.

Day 10-14: Colony staining with methylene blue, counting.

2.2.1.8.2 Irradiation/Inhibitor Combination Experiments

Day 0: Cell plating, incubation for 4 hours.

Day 0 (Pre-treatment): Cells treated with *AURKA*/*AURKB* inhibitor for 2 hours.

Day 0: Irradiation applied (pre or post plating).

Day 1-10: Colony formation.

Day 10-14: Colony staining with methylene blue, counting.

2.2.1.8.3 Drug-Drug Combination Assays

Day 0: Cell plating in 90mm dishes, incubation for 4 hours.

Day 0: Cells treated with *AURKB* inhibitor and cytotoxic agents (e.g., Etoposide, Cisplatin, Vinorelbine, etc.).

Day 1-10: Colony formation.

Day 10-14: Colony staining with methylene blue, counting.

Cell Line	Plating Density (Cells/Condition)	RT Dose (Gy)
A549	500 - 5000	2 - 10
H520	500 - 5000	2 - 10
H460	500 - 5000	2 - 10
H322	500 - 5000	2 - 10
H1299	500 - 5000	2 - 10
SW900	500 - 5000	2 - 10
BICR22 (B22)	500 - 5000	2 - 10
SCC89	500 - 5000	2 - 10
OKF6/TERT-1	500 - 5000	2 - 10
UD-SCC2	500 - 5000	2 - 10
UPCI-SCC72	500 - 5000	2 - 10
H1299	500 - 5000	2 - 10

Table 2-10: Specific Plating Densities and Radiation Therapy Dose per Cell Line

2.2.1.9 siRNA transfection

2.25×10^5 H460 cells were seeded per well in 2 ml culture media in 6 well plates 24 hours before transfection for approximately 50% confluency at the time of transfection. Per well, 2.5 μl of 20 μm siRNA was diluted with 197.5 μl FCS-free RPMI-1640 and left for 5 minutes to incubate at room temperature. Simultaneously, five μl of Dharmafect 1 was diluted with 195 μl FCS-free RPMI-1640 and left for 5 minutes to incubate at room temperature. After this, siRNA/media was mixed 1:1 with Dharmafect 1/media gently with a pipette and incubated for 20 minutes at room temperature. During 20-minute incubation, media was removed from the cells and replaced with 1.6 ml normal serum-containing RPMI-1640. Then 400 μl of siRNA-Dharmafect one complex was added dropwise to the media for a final concentration of 25nM siRNA and 0.0025% Dharmafect 1 per well. Non-transfected controls were achieved by adding 400 μl of serum-free RPMI-1640 to cells in place of the siRNA-Dharmafect one complex. Vehicle controls were achieved by mixing Dharmafect 1 in serum-free RPMI-1640 1:1 with serum-free RPMI alone and adding dropwise to cells as above. Scrambled siRNA controls were achieved using Trilencer 27 Universal scrambled negative control siRNA duplex supplied by Origene.

2.2.2 Western blotting.

2.2.2.1 Lysate preparation for western blot

To analyse pThr288 *AURKA* and pThr232 *AURKB*, 1-3 x 10^6 NSCLC cells were plated 48 hours before lysate production in 90 mm dishes. After 24 hours, cells were arrested in mitosis by treating cells overnight with 100 ng/ml Nocodazole. Nocodazole untreated plates were employed for comparison. The following morning, all plates were gently removed from the media and washed twice with warm culture media to remove Nocodazole before re-complementing plates with 10 ml culture media, where appropriate cells were treated with *AURKA* and *AURKB* inhibitor for 2 hours prior to lysate production.

2.2.2.2 Lysate production (2xSDS sample buffer method)

Media was removed, and cells were gently washed with 1ml ice-cold PBS. Cells were then lysed on ice directly in 200µl 2 x SDS boiling mix with 100 mM DTT (800 µl 5 x SDS sample buffer, 1000 µl ddH2O, 200 µl 1 M DTT per 1 ml). Cell scrapers were then used to collect all cells in lysis buffer on ice before lysate was passed through a 25G needle 20 times with a 1 ml syringe and collected in ice-chilled 1.5 ml Eppendorf t*ube*s. Lysates were then boiled at 90 ^oC for 10 minutes before being quickly pulse centrifuged and stored at -20 ^oC until required.

2.2.2.3 RIPA lysis buffer method

Cells plated at 2.25 x 10^5 per well in a 6-well plate 24, 48, 72 and 96 hours earlier were washed twice with 500 µl PBS and dislodged using 500 µl trypsin EDTA. Trypsin was then diluted with 2 ml warm culture media, and cells were collected in 15 ml falcon t*ube*s. Cells were pelleted at 1200 RPM before being resuspended in 1 ml ice-cold PBS and transferred to ice-chilled 1.5 ml Eppendorf t*ube*s. Cells were pelleted at 1200RPM and were lysed in 100 µl 1x RIPA lysis buffer (200 µl 5 x RIPA lysis buffer, ten µl 100mM PMSF, ten µl 100 x SIGMAFAST protease inhibitor, ten µl each of phosphatase inhibitor cocktail I & II and 770 µl ddH_2O per 1 ml). The pellet was mixed with RIPA lysis buffer by vortexing every 10 minutes for 30 minutes before being passed through a 25G needle 20 times. The Lysis mix was centrifuged for 10 minutes using Mid bench centrifuge – Heraeus MegaFuge 16at 13400 RPM, of which the supernatant was retained and stored at -20 ^oC prior to quantification and analysis via western blot.

2.2.2.4 Protein quantification

Total protein concentration in lysates achieved with 1x RIPA buffer was quantified via the Bradford assay in 1.5ml Eppendorf t*ube*s. Protein standard curves were *mad*e using BSA of known concentration (see Table 2.1).

Total Protein (µg)	0.1mg/ml BSA (µl)	ddH_2O (µl)	Bio-Rad Protein Assay Dye Reagent Concentrate (µl)
0	0	800	200
1	10	790	200
5	50	750	200
10	100	700	200
15	150	650	200
20	200	600	200

Table 2-11: Production of a BSA protein standard curve

2 µl of each lysate was added to 798 µl of ddH_2O. 200 µl of Bio-Rad Protein Assay Dye Reagent Concentrate was added to the lysates and BSA standards after the proteins were diluted in ddH_2O. Diluted lysates and standards were then incubated at room temperature for 15 minutes before optical density (O.D.) at 595 nm wavelength was measured using the Thermo Scientific Multiskan FC. BSA standards O.D.s were used to plot protein concentration against O.D. The standard curve line from this allowed the calculation of total protein in lysates from their O.D. values. This allowed the amount of protein loaded per lane for western blot to be calculated.

Lysates achieved via lysis directly in the SDS sample buffer could not be quantified. Relative protein concentrations in these samples were approximated by western blotting for β-tubulin.

2.2.2.5 SDS-PAGE

8-12% polyacrylamide resolving gels were produced using ddH_2O, Protogel 30% w/v acrylamide 0.8% w/v bis-acrylamide stock solution (Gene Flow), 1.5 M Tris pH 8.8, 10% SDS, 10 % APS and TEMED. 5% stacking gels were produced using 1 M Tris pH 6.8 instead of 1.5 M Tris pH 8.8 (see Table 2.2).

Resolving gel (10 ml)				Stacking gel (ml)	
	8%	**10%**	**12%**		**5%**
ddH_2O (ml)	4.6	4.0	3.3	ddH_2O (ml)	3.4
30% Acrylamide 0.8% bis acrylamide (ml)	2.7	3.3	4.0	30% Acrylamide 0.8% bis acrylamide (ml)	0.83
1.5 M Tris pH 8.8 (ml)	2.5	2.5	2.5	1 M Tris pH 6.8 (ml)	0.63
10% SDS	0.1	0.1	0.1	10% SDS	0.05
10% APS (ml)	0.1	0.1	0.1	10% APS (ml)	0.05
TEMED (ml)	0.006	0.004	0.004	TEMED (ml)	0.005

Table 2-12: **SDS-PAGE resolving gel and stacking gel recipes.**

For lysates achieved via the 2 x SDS sample buffer method, 5-25 μl of the sample was loaded per lane. For lysates achieved via the RIPA lysis buffer method, 5-30 μg of protein was loaded per lane. Five μl of Precision Plus Protein Standards (Bio-Rad) was run parallel to samples. Proteins were separated by size for 1 to 1 hour 30 minutes at 180 V in 1 x SDS-PAGE running buffer.

2.2.2.6 Protein transfer

Proteins were transferred out of the gels onto Protran Nitrocellulose Transfer Membrane. This was achieved in a Criterion Blotter (Bio-Rad) running at 80-100 V for 2 hours in pre-chilled (4 ^{o}C) 1 x Towbin Buffer on ice.

2.2.2.7 Membrane blocking and probing.

All membrane incubations and washings were performed on a rocker. Membranes were blocked with 5% milk (Marvel) TBS for 1 hour at room temperature. Membranes were incubated with primary antibody diluted in blocking solution at 4 ^{o}C overnight. Following the primary antibody incubation, membranes were washed thrice with TBS-Tween 20 (0.05%), changing the wash every 10 minutes. Then, membranes were incubated with HRP-labelled secondary antibody diluted in blocking solution for 1 hour at room temperature. Following the secondary antibody, incubation membranes were washed three times with TBS-Tween 20 (0.05%), changing the wash every 10 minutes before proceeding to enhanced chemiluminescence.

2.2.2.8 Enhanced chemiluminescence (ECL)

Two ml each of detection reagents 1 and 2 from the Amersham ECL Western Blotting Detection Reagent kit were mixed in a 15 ml falcon t*ube* and then applied to the membrane for 1 minute at room temperature. Membranes were then exposed to X-ray film in a dark room, and the chemiluminescent signal was developed and fixed using R.G. Universal X-ray Developer and R.G. Universal X-ray Fixer.

2.2.2.9 Western blot quantification

Films were scanned into JPEG format, and ImageJ software (Schneider et al 2012) performed band densitometry. Relative protein expression levels were determined by normalising the target protein band density to β-tubulin band density for the same sample. Higher exposures were excluded from densitometry to ensure signal saturation did not occur.

2.2.3 Fluorescence-activated cell sorting (FACS).

2.2.3.1 Cell harvesting

1-2 x 10^5 NSCLC cells were seeded per 90 mm^3 dish and treated as appropriate. Cells were harvested for FACS analysis 24-, 48- and 72-hours post-irradiation by washing plates twice with PBS and dislodging cells with 1 ml trypsin EDTA. Cells were collected in 5 ml ice-cold PBS and pooled with media and PBS wash-offs on ice in 50 ml falcon t*ube*s. Cells were pelleted using a Mid bench centrifuge – Heraeus MegaFuge-16at 1200 RPM for three minutes, washed once in ice-cold PBS

whilst transferring to 15 ml falcon t*ube*s and resuspended in 1 ml ice-cold 100% methanol with vortexing. Cells were stored in 100% methanol for at least 1 hour and a maximum of 2 weeks at -20 ^{o}C.

2.2.3.2 Propidium iodide (PI) and S10 p-Histone 3 co-staining

Cells were retrieved from -20 ^{o}C and pelleted using a Mid bench centrifuge – Heraeus MegaFuge 16 at 1200 RPM for 3 minutes before methanol was poured off, and cells were washed twice in PBS. Following this, cells were resuspended in PBS with 0.5% BSA and 0.25% Triton-X100 and incubated on ice for 15 minutes. Cells were then pelleted using a Mid bench centrifuge – Heraeus MegaFuge at 1200 RPM, the supernatant removed and resuspended in 100 μl of PBS 0.5% BSA (Sigma Aldrich) 0.25% Triton-X100 containing 1:500 dilution of S10 p-Histone 3 (#47297 Abcam) primary antibodies. Cells were incubated with primary antibodies for 1 hour at room temperature. Cells were washed of unbound primary antibody twice with PBS 0.25% Triton-X100. Cells were then resuspended in 100 μl PBS 1% BSA containing 1:200 dilution of Anti-rabbit Alexa 488 antibody. Cells were incubated for 30 minutes with the secondary antibody in the dark at room temperature. Cells were then washed of unbound secondary antibody once with PBS before resuspending in 200 μl PI/RNAse A solution (18 μg/ml PI, 8 μg/ml RNAse A). Cells were incubated in PI/RNAse A solution in the dark at 4 ^{o}C for a minimum of 1 hour 30 minutes before being analysed with a B.D. Biosciences FACSCalibur. No primary antibody controls were employed to investigate the extent of non-specific secondary antibody staining.

2.2.3.3 Analysis

Using FlowJo™ Software version 10.10 Cell doublets were excluded by plotting FL3 (PI)-Area against FL3-Width and gating FL3-Width low cells (see Figure 2.1). Ten thousand events were collected in this gating region per sample, and an FL3-height (FL3-H) histogram was produced. G1 proportion of cells was defined by gating across the base of the first peak in the FL3-H plot (~200 FL3-H), G2-M proportion of cells was defined by gating across the base of the second peak in the FL3-H plot (~400 FL3-H). Sub G1 population was defined as all signals to the left of the first peak, and the S phase population was defined as all signals between the first and second peaks. The mitotic population was discriminated by plotting G2-M population FSC-H against FL1-H for S10 p-Histone 3 staining. The mitotic population was discriminated with the least 0.5 log separation in FL1-H intensity versus the G2 population. The polyploid population was defined as all signals on the right of the G2-M population.

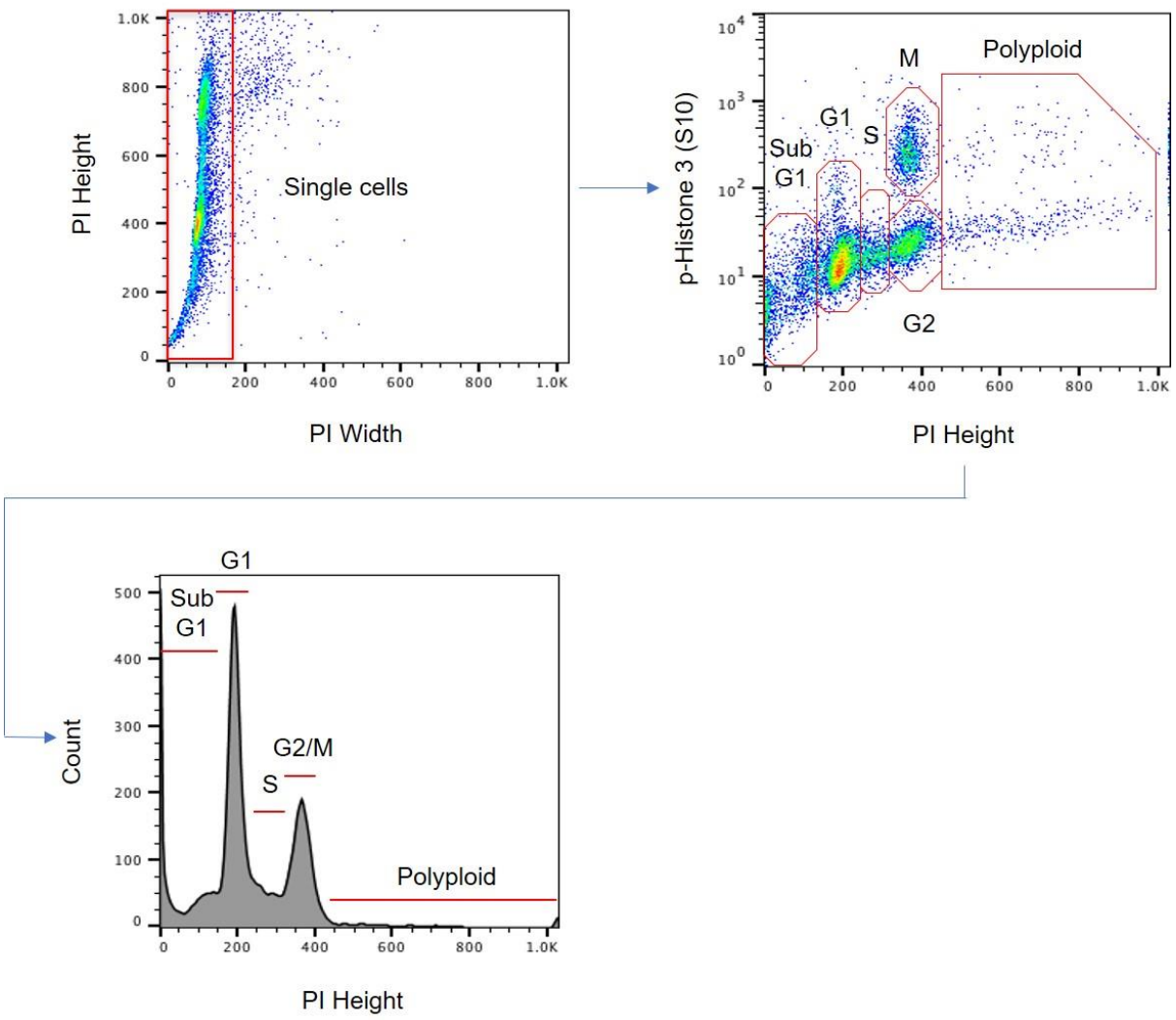


Figure 2.1. **FACS gating strategy outline**. Cell doublets were excluded in the plot of the top left with gate in red. Doublets are visible as a population that stained with greater PI width. Single cell population was taken forward for cell cycle analysis. The plot of the top right illustrates cell cycle profile produced when PI height was plotted against S10 p-Histone 3 positivity allowing discrimination of

2.2.4 Immunohistochemistry (IHC).

2.2.4.1 Sample preparation

2.2.4.1.1 Cell line pellet preparation

To prepare a cell line pellet for IHC, at least two T75 flasks of cells were washed with PBS, dislodged with trypsin EDTA, resuspended in media, and pelleted at pelleted using a Mid bench centrifuge – Heraeus MegaFuge 16 1200 RPM for 5 minutes in a 50 ml falcon t*ube*. Cells were washed once with 5 ml PBS and transferred to a 15 ml falcon t*ube* before being pelleted again. One ml of 4% paraformaldehyde was then slowly dripped down the side of the falcon t*ube* to fix but not disturb the cell pellet. Cells were fixed overnight at 4 ^{o}C before paraformaldehyde was pipetted off, carefully replaced with 1 ml ice-cold 70% ethanol, and stored at -20 oC for a maximum of 2 weeks.

To embed cell pellets in wax, 70% ethanol was removed from the cell pellet, and the pellet was then encased in molten 2% agarose with 4% paraformaldehyde. After the agarose had cooled and set, the agarose-encased pellet was placed in a cassette and stored in 70% ethanol at room temperature until processing. Cell pellets were processed using a Leica TP 1020. Processed cell pellets were embedded in wax the following day using a Leica EG1150 wax embedder. Five µm sections of wax-embedded tissue were produced using a Leica RM2125 RTS microtome. Sections were then floated on warm water (approximately 47 ^{o}C) in a floatation bath and manoeuvred onto Menzel-Glaser Superfrost Plus Adhesion microscope slides (Thermo Fisher). The tissue slice was dried and fixed to the microscope slide

surface through baking in an oven at 37 ^{o}C for 48 hours. Sections were then ready to be stained and stored out of light at room temperature.

2.2.4.1.2 NSCLC patient diagnostic biopsy samples

Wax-embedded NSCLC patient diagnostic biopsy samples were sectioned and fixed onto microscope slides as performed for cell line pellets above. Five sections were retrieved per sample in line with the clinical study protocol.

2.2.4.2 Staining procedure

2.2.4.2.1 Dewaxing and hydration of tissue (cell line pellets and diagnostic biopsies)

Slides were dewaxed in xylene for 20 minutes, spending 10 minutes each in separate xylene baths. Slides were then gradually hydrated for 3 minutes each in baths of 100% IMS, 100% IMS, 95% IMS, 90% IMS and 70% IMS.

2.2.4.2.2 Fixation and hydration of tissue (O.C.T. frozen tissues only)

Slides were retrieved from -20 ^{o}C and allowed to air dry for 30 minutes before tissues were fixed in an ice-cold 1:1 mix of methanol and acetone for 20 minutes at -20 ^{o}C. Following fixation, tissues were gently washed twice with PBS to rehydrate, each for 5 minutes, at room temperature.

2.2.4.2.3 Blocking endogenous peroxidase activity

Following tissue hydration, slides were incubated in 10% H_2O_2 in methanol for 30 minutes at room temperature to block endogenous peroxidase activity. Following this, slides were washed in tap water for 5 minutes.

2.2.4.3 Antigen retrieval

2.2.4.3.1 Pressure cooker method

Antigen retrieval was achieved by immersing slides in 1x pH 6.1 citrate Target Retrieval Solution (Dako) diluted in ddH_2O or ten mM Tris 1 mM EDTA pH 9.0 buffer. These slides were then heated in buffer for 20 minutes in a retriever 2100 pressure cooker (Aptum Biologics) according to the ma*nuf*acturer's instructions. Slides remained in buffer for 2 hours to cool after antigen retrieval. Slides were rinsed once in PBS-Tween 20 (0.1%) before being washed twice for three minutes each in PBS-Tween 20 (0.1%).

2.2.4.3.2 Microwave method

1 x Target Retrieval Solution (Dako) diluted in ddH_2O was heated on a high setting until boiling in a microwave before slides were heated in buffer for four minutes in a 700W microwave on a high setting. After antigen retrieval, slides remained in buffer for a further 10 minutes to cool before being rinsed once in PBS Tween 20 (0.1%) before being washed twice for three minutes each in PBS-Tween 20 (0.1%).

An extended microwave antigen retrieval protocol was used as above but involved retrieval for 10 minutes on high followed by 5 minutes on medium microwave setting.

2.2.4.3.3 Rice steamer method

1 x Target Retrieval Solution (Dako) diluted in ddH_2O was heated over 20 mins in a rice steamer on a high setting. The rice steamer was turned on for around 5 mins before inserting the DAKO after antigen retrieval, and slides remained in buffer for a further 10 minutes to cool before being rinsed once in PBS Tween 20 (0.1%) before being washed twice for three minutes each in PBS-Tween 20 (0.1%).

2.2.4.3.4 Antigenic blocking

Secondary antibody host serum (goat/rabbit) (Vector Laboratories) was diluted 1:10 in PBS 1% BSA 0.1% Tween 20. After antigen retrieval, a hydrophobic barrier was drawn around the tissue on the slide using an ImmEdge™ pen (Vector Laboratories). Approximately 250 µl of 10% secondary antibody host serum in PBS 1% BSA 0.1% Tween 20 was dropped onto the tissue section and allowed 1 hour to incubate at room temperature in a humidifying chamber.

2.2.4.3.5 Antibody Incubation

The blocking solution was tapped off slides and was replaced with 250 µl of PBS 1% BSA, 0.1% Tween 20, 2% secondary antibody host serum containing appropriate dilution of primary antibody. Tissue sections were incubated with primary antibody for 1 hour at room temperature or overnight at 4 ^{o}C in a humidified chamber. Controls lacking primary antibodies were used to investigate non-specific signals.

Following primary antibody incubation, the primary antibody was tapped off the slides. Slides were then rinsed once in PBS-Tween 20 (0.1%) before being washed twice for three minutes each in PBS-Tween 20 (0.1%). Biotinylated secondary antibody (Vector Laboratories) was diluted 1:200 in PBS 1% BSA 0.1% Tween 20 2 % secondary antibody host serum, and 250 µl of this was dropped onto tissue sections. Secondary antibody incubation was for 1 hour at room temperature in a humidified chamber.

2.2.4.3.6 Avidin-biotin complex (A.B.C.) signal amplification

A.B.C. solution (Vector Laboratories) was prepared 30 minutes prior to its use. A.B.C. solution was *mad*e by adding two drops of reagent A and two drops of reagent B to every 5 ml of PBS-Tween 20 (0.1%) diluent with vortexing after each addition. After secondary antibody incubation, slides were rinsed once in PBS-Tween 20 (0.1%) before being washed twice for five minutes each in PBS-Tween 20 (0.1%). 250 µl A.B.C. solution was added to tissue sections and incubated for 30 minutes at room temperature in a humidified chamber.

2.2.4.3.7 I*MMP*RESS® signal detection kit

The I*MMP*RESS Horse anti-mouse H.R.P. Polymer detection kit (Vector Laboratories) was used according to the ma*nuf*acturer's instructions as an alternative to A.B.C. signal amplification. Sections were blocked for 1 hour in 2.5% ready-to-use horse serum before primary antibody incubation in PBS 1% BSA 0.1% Tween 20. After primary antibody incubation, slides were then rinsed once in PBS-Tween 20 (0.1%) before being washed twice for five minutes each in PBS-Tween 20 (0.1%) before being incubated with I*MMP*RESS Peroxidase Anti-Mouse IgG reagent for 30 minutes before signal development.

2.2.4.3.8 Diaminobenzidine (DAB) signal development

After A.B.C./I*MMP*RESS Peroxidase Anti-Mouse IgG reagent incubation, slides were rinsed once in PBS-Tween 20 (0.1%) before being washed twice for five minutes each in PBS-Tween 20 (0.1%). DAB solution (Vector Laboratories) was prepared by adding two drops of buffer, four drops of DAB and two drops of H_2O_2 per 5 ml H_2O diluent with vortexing after each addition. 250 µl of DAB solution was dropped over tissue sections, and signal development in a brown precipitate was allowed to occur between 30 seconds and 15 minutes. After significant signal development, this process was halted by washing away DAB from the slides using ddH_2O.

2.2.4.3.9 Haematoxylin counterstain

Slides were counterstained in a bath of Gills haematoxylin for 1 minute. Excess stain was removed by washing slides with running tap water for 5 minutes.

2.2.4.3.10 Dehydration and mounting of slides.

Slides were then gradually dehydrated for 3 minutes each in baths of 70% IMS, 90% IMS, 95% IMS, 100% IMS and 100% IMS. Slides were then bathed in mounting xylene for 10 minutes, 5 minutes each, in separate baths before being mounted using D.P.X. Slides were left to dry overnight before being imaged.

2.2.4.3.11 Imaging

Slides were scanned using a Pannoramic 250 Flash III slide scanner using a 20x brightfield objective. Slide scans were analysed using Qu Path software (v0.1.2) (Bankhead 2017).

2.2.5 Bioinformatics pathway.

To investigate the potential correlation between the expression of *AURKA* and *AURKB* and head and neck cancers, mRNA expression data from the Gene Expression Omnibus (GEO) database, https://www.ncbi.nlm.nih.gov/geo/ was downloaded for bioinformatic analysis. Only [HG-U133_Plus_2] Affymetrix Human Genome U133 Plus 2.0 arrays were used to ensure the consistency of the pathway. To analyse the data, we used the GSE accession numbers and the "R" programming language to identify differentially expressed genes (the code for this analysis can be found in Appendix 7-1).

Protein-protein interaction (PPI) networks were constructed using the STRING database and visualised by Cytoscape software. Molecular Complex Detection (MCODE) was used to identify the significant networks in the PPI network. Hub genes were filtered using CytoHubba software (The *TOP* 30 genes in terms of rank **and** having a degree score >10), and correlation against overall and post-progression-free survival was done using the Kaplan-Meier plotter. Hub gene expression of NSCL adenocarcinoma and squamous cell cancers vs normal tissue were investigated using GeneExpression Profiling Interactive Analysis (GEPIA).

Hub genes were analysed using the KM plotter online database https://kmplot.com/. Sources for the databases include GEO, The European Genome-phenome Archive (EGA), and the Cancer Genome Atlas (TCGA). The correlation between the target gene mRNA expression levels, overall survival (OS) rate and post-progression survival (PPS) in NSCLC groups were calculated by the Kaplan‑Meier curve and

log-rank test (Győrffy et al., 2013). Post-progression survival (PPS) is the survival time following progressive disease (PD) during treatment with any drug.

2.2.6 Patients and primary tumour samples.

2.2.6.1 Patient population

Yorkshire ethically approved the clinical study and the Humber Sheffield Research Ethics Committee, sponsored by Sheffield Teaching Hospitals and the portfolio adopted by the NIHR (IRAS 174043). To be eligible for this study, participants must meet several specific criteria, including having confirmed non-small cell lung cancer (NSCLC) through cytological or histological testing. Additionally, eligible individuals should receive radical or high-dose palliative radiotherapy, with doses equal to or greater than 36 Gy delivered in 12 fractions. The study is open to patients aged 16 years or older without an upper age limit, and they must have archived tissue available for analysis. Furthermore, participants are required to provide written informed consent. Notably, no exclusion criteria exist, meaning no specific conditions or factors would disqualify potential participants from participating in the study.

2.2.6.2 Study endpoints

Overall survival was defined following the start date of radiotherapy treatment. Radiotherapy response was assessed via C.T. scan by a radiologist at approximately 2-3 months post-radiotherapy. Tumour radiotherapy response within

the irradiated volume was defined according to the RECIST criteria (Eisenhauer 2009) into complete response (C.R.), partial response (P.R.), stable disease (SBD) and progressive disease (P.D.). Time to tumour progression was defined as the time from the start date of radiotherapy treatment to the date of confirmed progression.

2.2.6.3 Statistical Analysis

Data were expressed as means +/- standard deviation (S.D.) when data points were derived from each experiment. Data were expressed as means +/- standard error of the mean (S.E.M.) when multiple data points were expressed as a mean from each experiment, resulting in a mean of means after several experiments. Statistical difference between the two means was performed using an unpaired two-tailed t-test.

When more than two means were to be compared statistically with each other, a one-way ANOVA with Dunnett correction for multiple comparisons was performed. Radiation dose-response data were fitted to the linear quadratic model of cell death in GraphPad Prism v7. Dose enhancement ratios at 10% survival fraction were calculated using these data: radiation dose (Gy) for 10% survival fraction of I.R. alone control/radiation dose for 10% survival of an irradiated condition. The extra sum of squares F test was used statistically to compare the survival curves of I.R. alone control compared to other irradiated conditions.

All statistical calculations were performed using GraphPad Prism v7, assuming a cut-off for statistical significance of p= <0.05. Univariate Cox regression was used to calculate a p-value and hazard ratio associated with high and low *AURKA* mRNA expression and a given clinical outcome using a K.M. plotter.

3 Evaluation of Barasertib, Alisertib and Ly3295668 as radiosensitising agents in NSCLC in vitro.

3.1 Introduction, Aims and Hypothesis.

AURKA is primarily associated with the early stages of mitosis. It promotes the assembly and stabilization of microtubules, essential components of the cell's cytoskeleton and the mitotic spindle (Nikonova et al., 2013). helps ensure the proper alignment/attachment of chromosomes on the spindle during cell division. is also essential for centrosome maturation and separation, which are crucial for proper spindle assembly (Willems et al., 2018). Dysregulation of can lead to abnormal cell division and is associated with various forms of cancer, including breast, non-small cell lung, and colorectal cancers (Lo Iacono et al., 2011; Mou et al., 2021).

 functions during the later stages of mitosis, particularly in segregating sister chromatids (Yuan et al., 2009b). It is a vital component of the chromosomal passenger complex (CPC), which helps regulate chromosome condensation, attachment to the spindle, and proper chromosome segregation (Shuda et al., 2009). then re-localises to the spindle midzone and midbody from anaphase to cytokinesis (Shaalan et al., 2021). Overexpression of in tumours triggers aneuploidy and genomic instability, leading to tumour development, invasion and metastasis (Borah and Reddy, 2021). The integrity of these processes can regulate how cells respond to radiotherapy and chemotherapy (Hendry and West, 1997).

Previously, in the lab, inhibition of *AURKA* by Alisertib has been shown to radiosensitise NSCLC both and *in vivo*. The plan at the end of that study was to translate it into a clinical trial, but the drug company did not want to proceed. In order to develop an alternative, two drugs were identified: an alternative *AURKA* inhibitor, Ly3295668 and the *AURKB* inhibitor, Barasertib. Both have been used in clinical trials previously. Barasertib has been tested in Phase 1 and 2 settings in both AML and solid tumours (Kantarjian et al., 2013; Schwartz et al., 2013), while Ly3295668 has been tested in refractory neuroblastoma in a Phase one clinical trial (Chu et al., 2021), meaning they are safe to use in humans and thus increase the chance of translation if we can show effectivity in vitro.

The first chapter of this thesis will first test Ly3295668 as an alternative *AURKA* inhibitor and radiosensitising agent and then test whether *AURKB* with Barasertib can enhance IR or chemotherapy response in NSCLC and H&N cancer.

The hypotheses of this chapter are:

1. Barasertib and Ly3295668 will enhance the IR killing of NSCLC *cell lines* .
2. Barasertib will enhance the IR killing of HNSCC *cell lines* .
3. Barasertib disrupts cell cycle progression, leading to increased cell death in sensitive NSCLC and HNSCC cell lines.
4. Barasertib increases the incidence of abnormal mitotic events in NSCLC and HNSCC cells, leading to increased cell death in sensitive cell lines.
5. Following irradiation, Barasertib treatment will increase mitotic aberrance in NSCLC cells, leading to increased cell death.

This chapter aims to assess the following:

1. Establish an inhibitory dose of Ly3295668 that is *AURKA* specific and minimally toxic in NSCLC cell lines, then test the ability of Ly3295668 to radiosensitise.

2. Establish an inhibitory dose of Barasertib that is *AURKB* specific and minimally toxic in NSCLC and HNSCC cell lines, then test whether Barasertib can radiosensitive or chemo-sensitise NSCLC and HNSCC cancer cell lines .

3. Gain preliminary data which can be used in writing a phase one clinical trial protocol looking a combination Barasertib and IR (Appendix 7.3)

4. To assess the effect of Barasertib alone and IR on cell cycle progression, including mitotic transit, in NSCLC and HNSCC cell lines.
5. To assess mitotic aberrance following Barasertib alone and in combination with IR in NSCLC and HNSCC cell lines.

3.2 Results.

3.2.1 Ly3295668

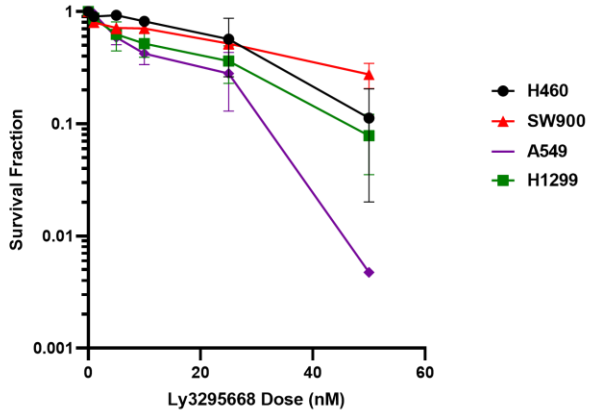
3.2.1.1 Determining an effective minimally toxic dose of Ly3295668 in NSCLC cell lines.

Ly3295668 Is a potent *AURKA* inhibitor explicitly targeting the p-Thr288 region with activity seen both in vitro and in vivo (Du et al., 2019). Before radio or chemotherapy-sensitising activity can be determined, a suitable dose of Ly3295668 is needed for each cell line. Ideally, the dose used should be minimally toxic when used alone and should be *AURKA*-specific. Four NSCLC cell lines were exposed to increasing doses of Ly3295668, and the survival fraction was determined by clonogenic assay (Figure 3-1 A) to investigate toxicity. The responses varied; A549 was the most sensitive, with an LD_{50} of 17.4nM. The SW900 cell line was the least sensitive, with an LD_{50} of 29.1nM.

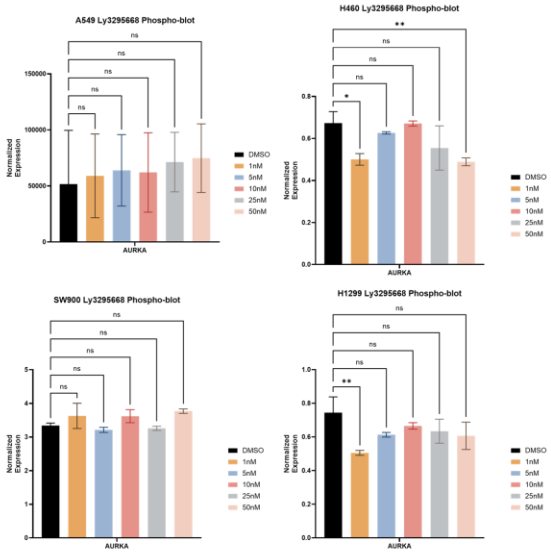
Using western blotting, the ability of Ly3295668 to inhibit *AURKA*, *AURKB* and *AURKC* was investigated in each cell line (Figure 3-1 C). Following 2 hours of treatment with Ly3295668, 25nM was seen as partially and 50nM as fully inhibiting *AURKA* in H460, SW900 and H1299 cells. While in A549, 5nM was an effective inhibitory dose. In each case, an effect on *AURKA* was seen with little/no effect on *AURKB* or C, demonstrating the specificity of the inhibitor; a significant limitation is that blots were done only twice, limiting confidence.

For H460, H1299 and SW900 cells, the partially inhibitory dose of 25nM resulted in greater than 60% survival, while the fully inhibitory dose of 50nM left between 10 and 30 % of cells surviving. Therefore, 25nM was taken forward to the radiosensitising assays. Interestingly, A549 cells showed approximately—60% survival at just 5nM, at which dose *AURKA* was inhibited in these cells. Thus, in A549 cells, 5nM was used in radiosensitising assays below.

A



C



B

Cell line	SW900	H460	H1299	A549
Ly3295668 LD50 (nM)	29.10	28.10	19.85	17.40
Tp53 status	Mutant	Wildtype	Null	Wildtype
EGFR status	Wildtype	Wildtype	Wildtype	Wildtype
KRAS status	K-ras (G12V)	K-ras (Q61H)	Wildtype	K-ras (G12S)
NRAS status	Wildtype	Wildtype	N-ras (Q61K)	Wildtype
PIK3CA status	Wildtype	Mutant	Wildtype	Wildtype
ALK translocation status	*	Wildtype	Wildtype	Wildtype
ROS-1 status	*	*	*	*
STK11/LKB1 status	*	Mutant	Wildtype	Mutant
MET status	*	C-MET low expressor	*	C-MET low expressor
BRAF status	Wildtype	Wildtype	Wildtype	Wildtype

Figure 3-1:**Ly3295668 monotherapy response in NSCLC cell lines** A: Survival fraction was calculated using clonogenic assay under continuous exposure to the *AURKA* inhibitor Ly3295668. Data points represent the mean survival fraction normalised to untreated control +/- SD (N= 3). B: Table showing the genetic type of each cell line. C: Representative western blot results for pan p-AURK, *AURKA* (total A) and GAPDH in protein extracts from H460, A549, H1299 and SW900 cells arrested overnight with 100 ng/ml Nocodazole (Noc) and released into increasing concentrations of Ly3295668 for 2 hours.

3.2.1.2 Ly3295668 can radiosensitise *p53* wildtype NSCLC cell lines

To test whether Ly3295668 can radiosensitise, the doses determined above were added to cells 2 hours prior to irradiation and were present continuously throughout colony survival assays. Consistent with the results found previously with alisertib, Ly3295668 was seen to radiosensitise the *p53* wild-type cell lines, H460 and A549 (Figure 3-2), but not the *p53* null or negative cell lines, SW900 or H1299 (Figure 3-2). The dose enhancement ratio (DER) was used to assess the radiosensitivity of the combination with increasing doses of radiation, the formula being:

DER at (x) Gy = Average survival in DMSO (x) Gy ***/*** The average survival in target Barasertib dose (x) Gy

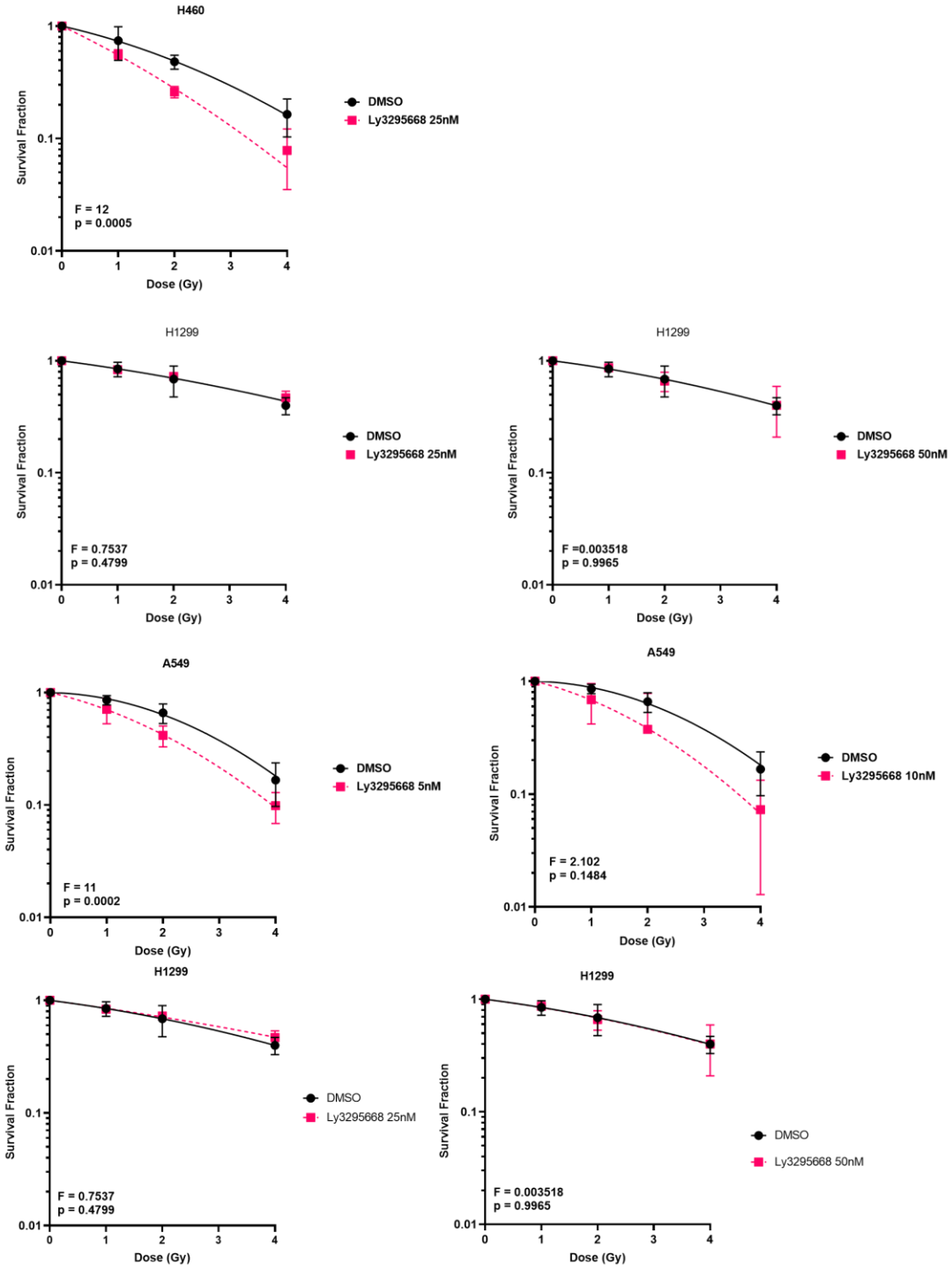


Figure 3-2: **Radiosensitisation of NSCLC cell lines by LY3295668.** The survival fraction was calculated using a clonogenic assay. Cells were pre-incubated with LY3295668 before irradiation and colony outgrowth under continuous exposure to the *AURKA* inhibitor Ly3295668. Data points represent the mean survival fraction normalised to unirradiated control +/- SD (N= ≥3). F-value and p-value derived from the extra sum of squares test.

Cell line	NSCLC Subtype	P53 status	DER using 25nM (0Gy)	DER using 25nM (1Gy)	DER using 25nM (2Gy)	DER using 25nM (4Gy)
H460	LCC	Wildtype	1	1.315	1.853	2.093
H1299	LCC	Null	1	1.012	0.947	0.852
SW900	SCC	Mutant	1	1.197	1.155	1.265

Cell line	NSCLC Subtype	P53 status	DER using 25nM (0Gy)	DER using 25nM (1Gy)	DER using 25nM (2Gy)	DER using 25nM (4Gy)
H1299	LCC	Null	1	0.975	1.039	0.995
SW900	SCC	Mutant	1	1.047	1.031	1.521

Cell line	NSCLC Subtype	P53 status	DER 5nM (0Gy)	DER 5nM (1Gy)	DER 5nM (2Gy)	DER 5nM (4Gy)
A549	ADC	Wildype	1	1.244	1.706	1.660
Cell line	**NSCLC Subtype**	**P53 status**	**DER 10nM (0Gy)**	**DER 10nM (1Gy)**	**DER 10nM (2Gy)**	**DER 10nM (4Gy)**
A549	ADC	Wildype	1	1.285	1.893	2.245

A549		
	t.test values at 5nM	t.test values at 10nM
2 Gy	0.021	0.271
4 Gy	0.123	0.154

	H460	
	t.Test values at 25nM	t.Test values at 50nM
2 Gy	0.006	N/A
4 Gy	0.189	N/A
	SW900	
2 Gy	0.116	0.118
4 Gy	0.219	0.232
	H1299	
2 Gy	0.733	0.987
4 Gy	0.204	0.534

Table 3-1: Ly3295688 Dose Enhancement Ratio (DER) and statistical significance indicated by two-tailed t-test values.

The DER ratios are shown in Table 3-1 along with the significance values; the increase in the DER was significant using 2Gy + 5nM and 2GY + 25nM in the A549 and H460s, respectively, the H1299 and SW900 showed either non-significant increases or decreases in the DER at 2Gy confirming the lack of sensitization.

3.2.2 Barasertib

3.2.2.1 Determining an effective minimally toxic effective dose of Barasertib in NSCLC cell lines

Six NSCLC cell lines were exposed to increasing doses of Barasertib, and the survival fraction was determined by clonogenic assay (Figure 3.4) to investigate toxicity. The responses varied; The A549 and H520 cell lines were the most sensitive to Barasertib monotherapy LD50 of 15.2 and 13.9 nM, respectively. The H460 cell line was the least sensitive to Barasertib monotherapy, with a mean LD_{50} of 40.9 nM (Figure 3-3).

Apart from the H460 cell lines, which demonstrated an approximately 70% survival for the H520 and A549 lines, the partially inhibitory dose of 25 nM resulted in less than 5% survival, while the fully inhibitory dose of 50 nM left 0 % of cells surviving in the H520 and A549 lines while in the H460 lines, there was 30% survival. In the H1299 and SW900 cell lines at 25 nM, there was 40 and 25% survival, although, in the H322 lines, there was less than 5% survival; the fully inhibitory dose of 50 nM led

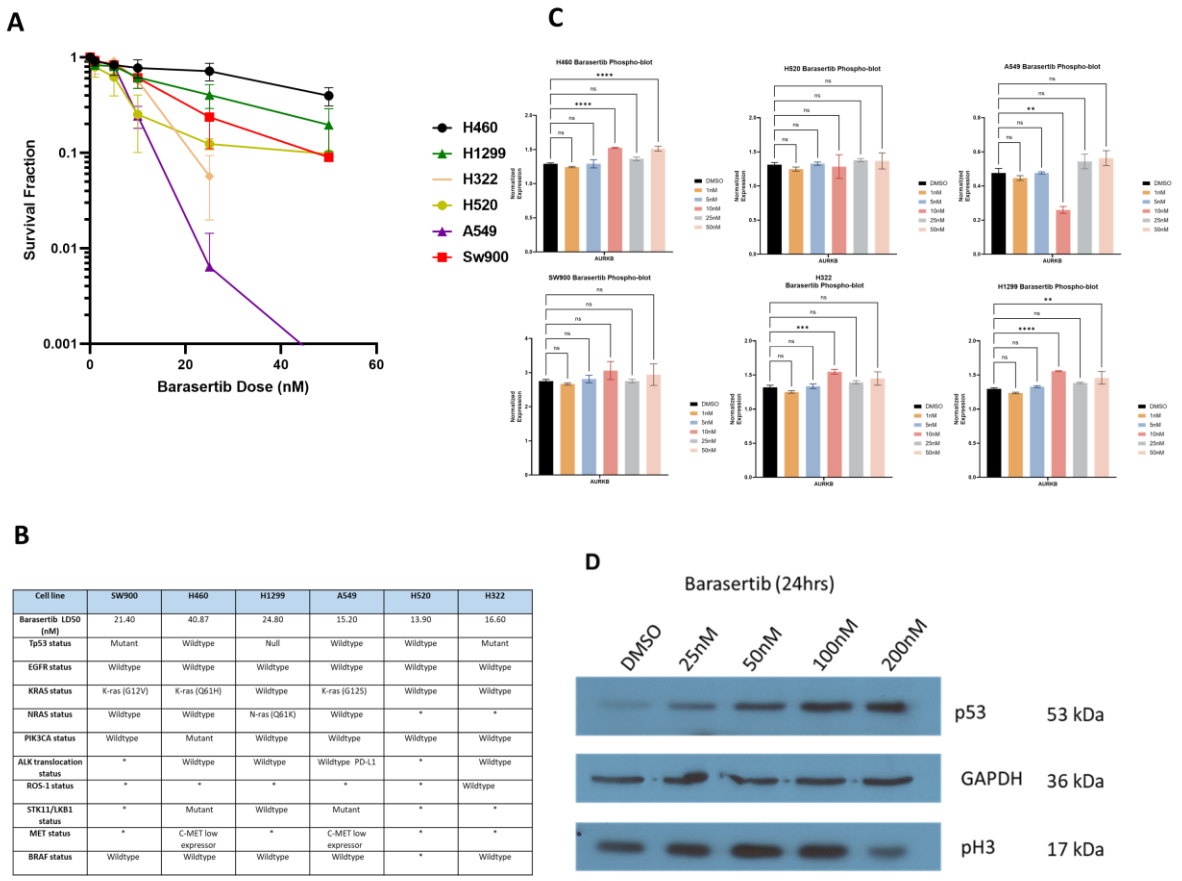
to a less than 20% survival in all three lines. We used 25 nM in the radiosensitising assays, as using 50 nM would be too toxic to get any meaningful results.

Using western blotting, the ability of Barasertib to inhibit *AURKA*, *AURKB* and *AURKC* was investigated in each cell line (Figure 3-5). Inhibition was also not seen in H520 or H322 cells. In A549 cells, *AURKA* and *AURKB* au*top*hosphorylation was inhibited at 25 and 50 nM In SW900 and H1299 cells, some specific inhibition of *AURKB* over *AURKA* was seen at 25 nM and 50 nM Given the variability in results, phosphorylated histone H3 (Phospho-H3) inhibition was used as a surrogate marker of *AURKB* inhibition. *AURKB*-mediated phosphorylation of histone H3 is essential for chromosomal condensation and the start of mitosis (Hirota et al., 2005; Li et al., 2017). Following 2 hours of treatment with Barasertib, a moderate reduction in *PH3* levels was seen in H460, H520 and SW900 cells, with no reduction in A549, H1299, and H1332 cells. Again, this result was inconsistent, and we considered it an unreliable way to determine the dose of Barasertib that was effective in inhibiting *AURKB*.

Finally, we investigated the *p53* level as a marker of *AURKB* inhibition, as *p53* interacts directly with *AURKB*, is an *AURKB* substrate during mitosis and is negatively regulated (C. P. Gully et al., 2012). We demonstrated that *p53* is upregulated by 25 nM Barasertib, indicating at least in H460 that Barasertib has a functional effect.

In the absence of reliable, effective *AURKB* inhibitor dose data, we decided to test two doses in each cell line. Considering the monotherapy toxicity data, we used 25 nM and 50 nM in the relatively Barasertib -resistant cell lines H460, H1299 and Sw900, as we thought using doses near the LD50 values would allow us to observe

radiosensitisation. We then used 1 nM and 5 nM in A549 cells to see if we could observe radiosensitisation.



Cell line	SW900	H460	H1299	A549	H520	H322
Barasertib LD50 (nM)	21.40	40.87	24.80	15.20	13.90	16.60
Tp53 status	Mutant	Wildtype	Null	Wildtype	Wildtype	Mutant
EGFR status	Wildtype	Wildtype	Wildtype	Wildtype	Wildtype	Wildtype
KRAS status	K-ras (G12V)	K-ras (Q61H)	Wildtype	K-ras (G12S)	Wildtype	Wildtype
NRAS status	Wildtype	Wildtype	N-ras (Q61K)	Wildtype	*	*
PIK3CA status	Wildtype	Mutant	Wildtype	Wildtype	Wildtype	Wildtype
ALK translocation status	*	Wildtype	Wildtype	Wildtype PD-L1	*	Wildtype
ROS-1 status	*	*	*	*	*	Wildtype
STK11/LKB1 status	*	Mutant	Wildtype	Mutant	*	*
MET status	*	C-MET low expressor	*	C-MET low expressor	*	*
BRAF status	Wildtype	Wildtype	Wildtype	Wildtype	*	Wildtype

Figure 3-3: **Barasertib monotherapy in NSCLC cell lines.** Survival fraction was calculated using clonogenic assay under continuous exposure to the *AURKB* inhibitor Barasertib. Data points represent the mean survival fraction normalised to untreated control +/- SD (N= 3). B: Table showing the genetic type of each cell line. C: Representative western blot quantification results for pan p-AURK, *AURKA* (total B) and GAPDH in protein extracts from H460, A549, H1299, H520 and H322 and SW900 cells arrested overnight with 100 ng/ml Nocodazole (Noc) and released into increasing concentrations of Barasertib. D: Representative western blot results for pan *p53*, GAPDH and *PH3* in protein extracts from H460 cells arrested overnight with 100 ng/ml Nocodazole (Noc) and released into increasing concentrations of Barasertib

3.2.2.2 Barasertib can radiosensitise NSCLC cell lines

To test whether Barasertib can radiosensitise, the doses determined above were added to cells 2 hours prior to irradiation and were present continuously throughout colony survival assays. Barasertib did not demonstrate any difference in radiosensitivity between the *p53* wild type vs. the null or mutant lines. When combining different doses of Barasertib with IR, the mean dose enhancement ratio indicated that the H460's (*p53* wild-type cell line) was radiosensitised at 25nM of Barasertib with a DEF of 2.37 with modest radiosensitisation in the *p53* null and negative cell lines H1299 and SW900 respectively. Using the higher dose of 50nM in the H460 and SW900 led to no discernible radiosensitisation. The A549 cell lines were more sensitive to Barasertib monotherapy; therefore, we used 1nM and 5nM doses. No radiosensitisation was seen using these concentrations, possibly because the doses were too low to lead to any activity (Figures 3-5 and Table 3-2).

The dose enhancement ratio (DER) was used to assess the radiosensitivity of the combination with increasing doses of radiation, the formula being:

The DER ratios are shown in Table 3-2 along with the significance values; the increase in the DER was significant using 2Gy + 25nM in the H460s, the increase in the DER was just significant using 4Gy + 25nM in the SW900 but non-significant in the H1299's possibly demonstrating a weaker effect in the *p53* mutant and null lines.

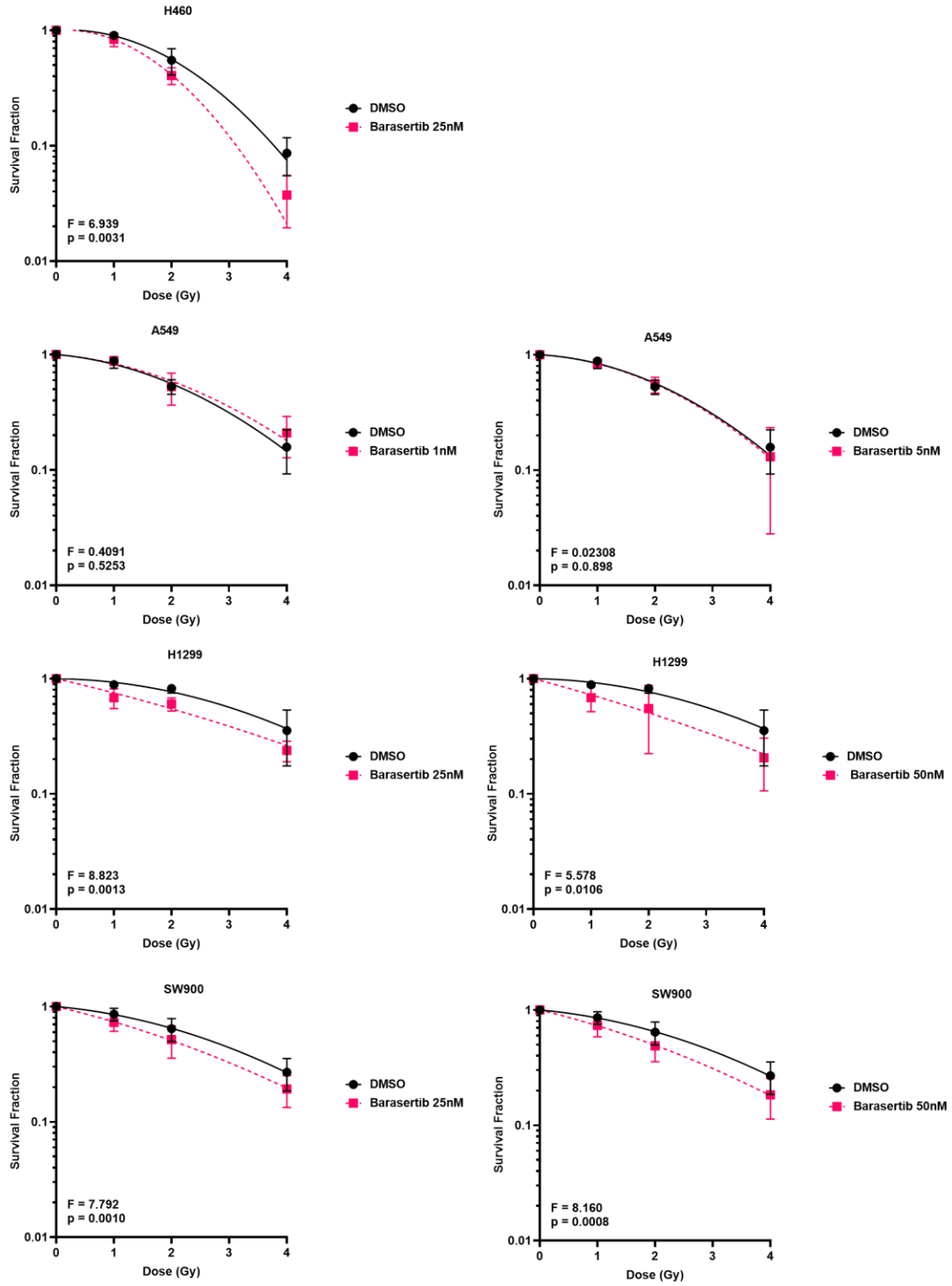


Figure 3-4 **Barasertib and IR in NSCLC cell lines** the survival fraction was calculated using a clonogenic assay. Cells were pre-incubated with Barasertib before irradiation and colony outgrowth under continuous exposure to the *AURKB* inhibitor Barasertib. Data points represent the mean survival fraction normalised to unirradiated control +/- SD (N= ≥3). F-value and p-value derived from the extra sum of squares test.

Cell line	NSCLC Subtype	P53 status	DER using 25nM (0Gy)	DER using 25nM (1Gy)	DER using 25nM (2Gy)	DER using 25nM (4Gy)
H460	LCC	Wildtype	1	1.119	1.451	2.307
H1299	LCC	Null	1	1.241	1.366	1.256
SW900	SCC	Mutant	1	1.175	1.240	1.398

Cell line	NSCLC Subtype	P53 status	DER using 50nM (0Gy)	DER using 50nM (1Gy)	DER using 50nM (2Gy)	DER using 50nM (4Gy)
H460	LCC	Wildtype	1	1.313	1.323	1.344
H1299	LCC	Null	1	1.294	1.496	1.724
SW900	SCC	Mutant	1	1.213	1.040	1.028

Cell line	NSCLC Subtype	P53 status	DER 1nM (0Gy)	DER 1nM (1Gy)	DER 1nM (2Gy)	DER 1nM (4Gy)
A549	ADC	Wildype	1	0.996	1.002	0.753
Cell line	**NSCLC Subtype**	**P53 status**	**DER 5nM (0Gy)**	**DER 5nM (1Gy)**	**DER 5nM (2Gy)**	**DER 5nM (4Gy)**
A549	ADC	Wildype	1	1.042	0.980	0.812

A549		
	t.test values at 1nM	t.test values at 5nM
2 Gy	0.984	0.612
4 Gy	0.184	0.015
	H460	
	t.Test values at 25nM	t.Test values at 50nM
2 Gy	0.047	0.369
4 Gy	0.011	0.008
	SW900	
2 Gy	0.154	0.885
4 Gy	0.053	0.159
	H1299	
2 Gy	0.012	0.257
4 Gy	0.504	0.062

Table 3-2 **Barasertib DER ratios and t.test values** Barasertib Dose Enhancement Ratio (DER) and statistical significance indicated by two-tailed t-test values. Cells were pre-incubated with Barasertib before irradiation and colony outgrowth under continuous exposure to the *AURKB* inhibitor Barasertib. Data points represent the mean survival fraction normalised to unirradiated control +/- SD (N= ≥3). F-value and p-value derived from the extra sum of squares test.

3.2.2.3 *AURKB* depletion enhances H460's response to IR.

To test whether depletion of *AURKB* could also radiosensitise and whether the effect seen with Barasertib was due to inhibition of *AURKB*. H460 cells were plated at low density 24 hours post-transfection with scrambled siRNA or a siRNA against *AURKB*, with or irradiated, then left for colonies to form in a clonogenic survival assay (Figure 3-9 A-C). Depletion of *AURKB* was also checked for each repeat using western blotting (Figure 3-9 D). Four conditions were prepared and assessed in parallel on each repeat: scrambled siRNA control, Barasertib (25nM), *AURKB* siRNA alone and *AURKB* siRNA and Barasertib (25nM). Data are represented in different combinations to aid the discussion of results.

As expected, adding Barasertib to scrambled siRNA caused radiosensitisation compared to scrambled siRNA alone (Figure 3-9 A). In addition, cells were more radiosensitive when *AURKB* was depleted (*AURKB* siRNA treated cells) than when *AURKB* was present (scrambled siRNA treated cells) (Figure 3-9 B). These data support the role of *AURKB* in promoting survival following radiation. However, when Barasertib was added to *AURKB*-depleted cells, they were more sensitive to radiation than the *AURKB*-depleted alone cells (Figure 3-9 C). This could be because *AURKB* is not entirely depleted by the siRNA (indeed, longer exposure of the x-ray film during western blotting does show residual protein (Figure 3-9 E) or because Barasertib has other targets. It should also be noted that for all other conditions, the line that joins the data points overlies the fitted line, which represents the linear quadratic model of cell death, but for the *AURKB* siRNA + Barasertib condition, this was not true. This casts some doubt over the robustness of the data for this condition.

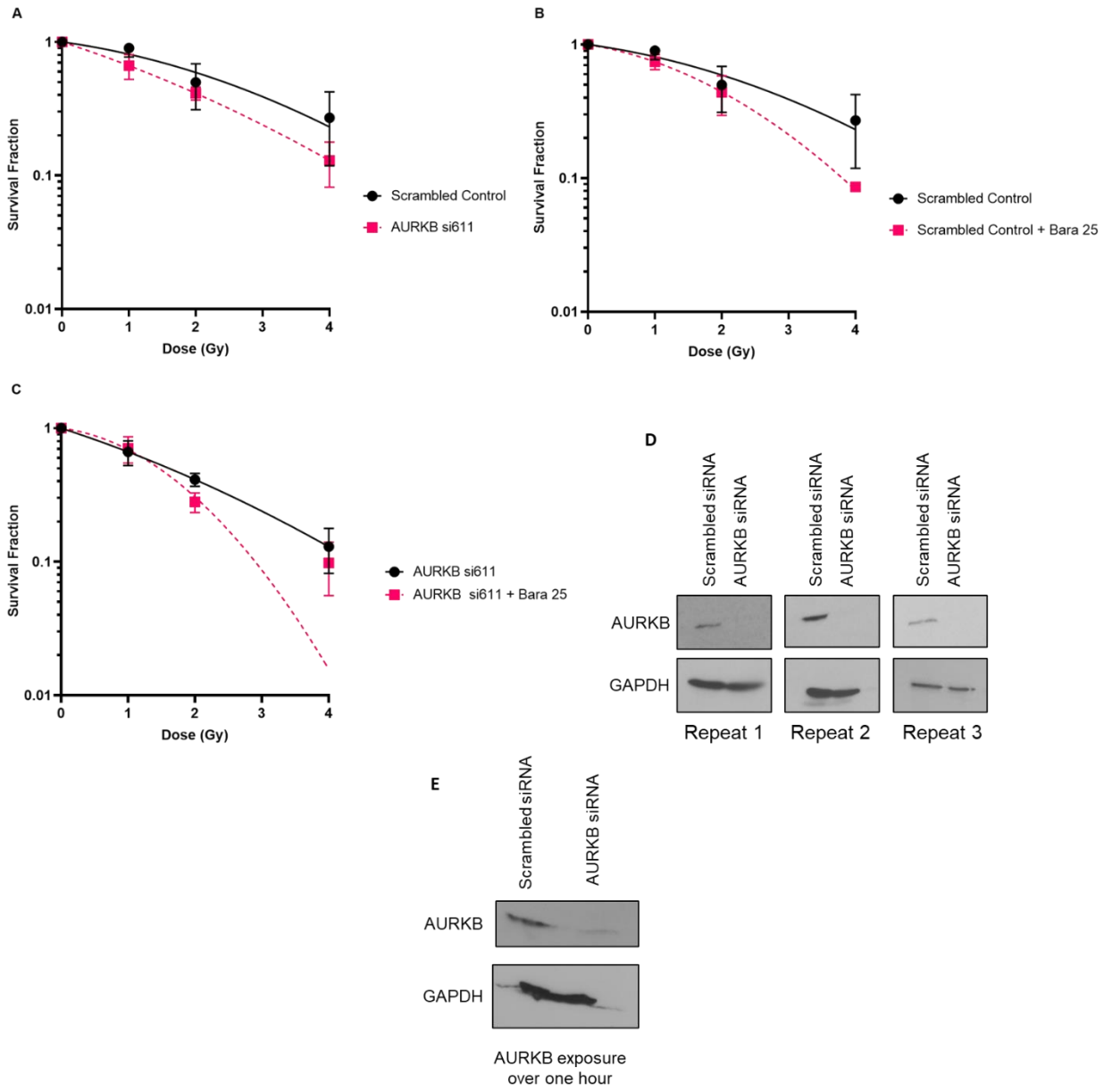


Figure 3-5 **Depletion of *AURKB* radiosensitises H460 cells.** H460 cells were depleted of *AURKA* using siRNA 24 h prior to plating for clonogenic assays with and without Barasertib +/- irradiation. All conditions were conducted in parallel, and data were re-represented in different combinations for clarity (A-C). Data points represent mean survival fraction normalised to untreated control +/- SD (N= 3). Lines connect points while dotted lines are fitted to the linear quadratic model of cell death. F-value and p-value derived from extra sum of squares test. (D) Western blot for *AURKB* for each biological repeat.

	DEF 0 Gy	DEF 1 Gy	DEF 2 Gy	DEF 4 Gy
SC and 25nM	1	1.208	1.197	3.101
Si611	1	1.355	1.164	1.186
Si611 and 25nM	1	1.274	1.735	3.128

t.test SC + 25nM	
2 Gy	0.510
4 Gy	0.393
t.test si611	
2 Gy	0.670
4 Gy	0.842
t.test si611 + 25nM	
2 Gy	0.175
4 Gy	0.270

Table 3-3 **Barasertib DER ratios and t.test** values in H460s with depleted ARUKB The DER and t.test values demonstrate significant radiosensitisation with depleted *AURKB* and the addition of Barasertib and IR.

3.2.2.4 Barasertib and Alisertib are probably non-additives in NCSLC cell lines.

In clinical practice, drug combinations are commonly used to counteract the varied resistance mechanisms present in tumours. *AURKA* and *AURKB* are highly related genes with differing roles in the regulation of mitosis. We hypothesised that adding Barasertib to Alisertib would be additive. Alternatively, a different result may be seen if there may be unknown overlapping or compensatory functions of *AURKA* and *AURKB*.

Three NSCLC cell lines, H460, H1299 and SW900, were co-treated with the *AURKA* inhibitor Alisertib and the *AURKB* inhibitor Barasertib (Figure 3-9). In H460 cells, compared to DMSO control, Alisertib reduced survival by 42 % ($p=0.0019$), while Barasertib did not significantly alter survival ($p=0.3147$), and co-treatment reduced survival by 32 % ($p=0.01$). As Barasertib did not alter survival, it is not possible to make a comment about additivity in these cell lines. In H1299 cells, compared to DMSO control, Alisertib reduced survival by 42 % ($p<0.0391$), while Barasertib reduced survival by 26 % ($p=0.2756$) and co-treatment reduced survival by 63 % ($p<0.0041$). The combination treatment was not significantly different to the alisertib treatment alone ($p=0.7008$). This means that in these cells, the effect of combination treatment is less than additive. In SW900 cells, compared to DMSO control, Alisertib did not significantly reduce survival ($p=0.2351$), while Barasertib reduced survival by 57% ($p=0.0004$), and co-treatment reduced survival by 66 % ($p=0.0001$). As Alisertib did not reduce survival in this cell line, no conclusion can be reached about additivity.

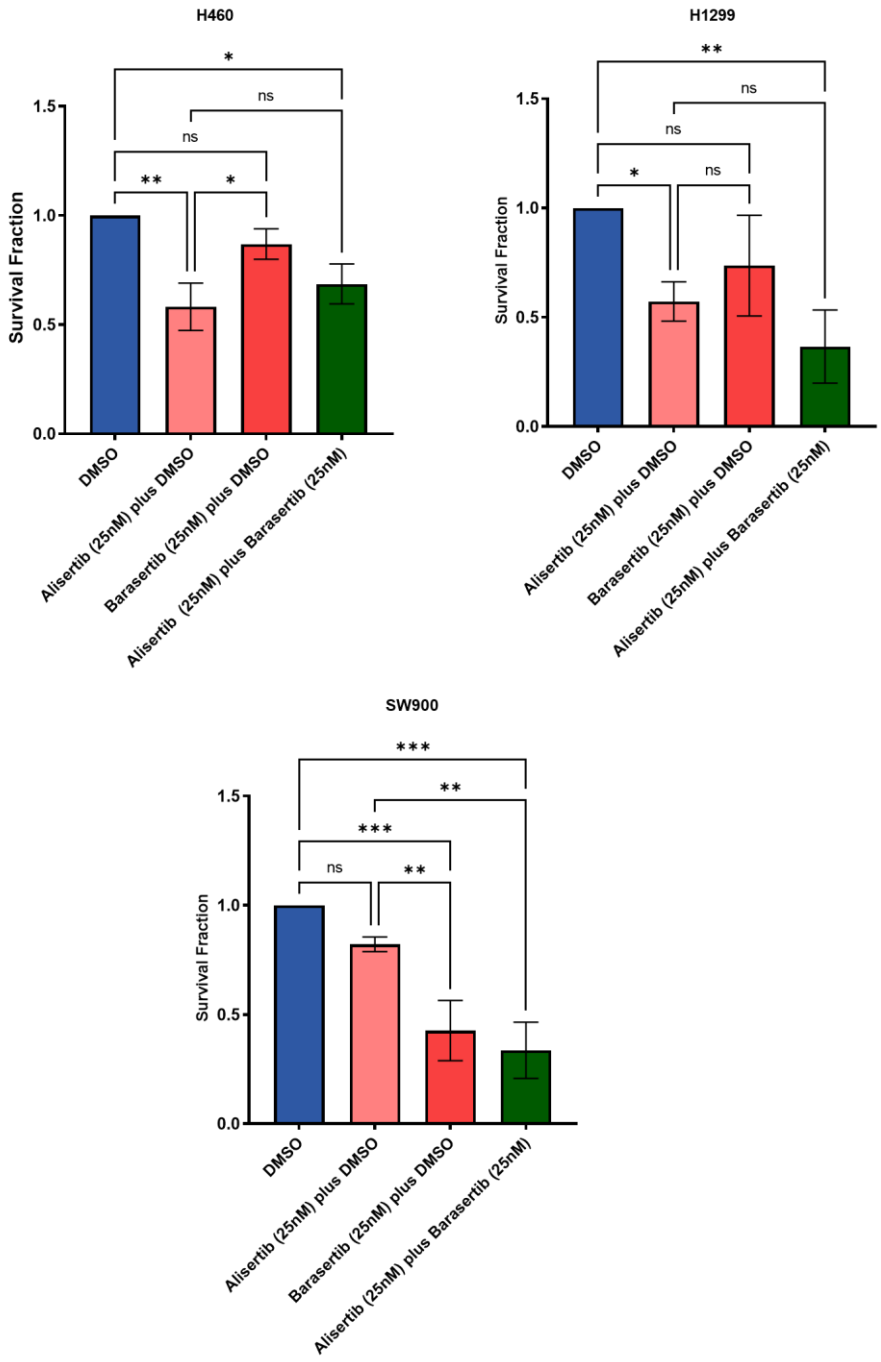


Figure 3-6: Comparison of Alisertib plus Barasertib vs Alisertib in NSCLC cell lines (n=3/4). Cells were pre-incubated with either an *AURKA* or *AURKB* inhibitor (Alisertib or Barasertib), cells were left to form colonies for 10-14 days before colony outgrowth under continuous exposure to the *AURKA* and/or *AURKB* inhibitor Alisertib or Barasertib. Data points represent the mean survival fraction normalised to DMSO +/- SD (N= ≥3). F-value and p-value derived from the extra sum of squares test. NS (non-statistically significant) denotes p= >0.05, * denotes p= ≤0.05, ** denotes p= ≤0.01, *** denotes p= 0.001 (One-way ANOVA with Dunnett correction for multiple comparisons).

3.2.2.5 Chemotherapy dose optimisation in H460's

After examining Alisertib activity, we were interested in examining the effect of combining Barasertib with standard chemotherapy agents used in clinical practice for HNSLC and HNSCC patients. Initial optimisation of four chemotherapy agents, Vinorelbine, e*topo*side, 5-fluorouracil, and Cisplatin, was done using H460 cell lines in order to establish baseline sensitivity. Cells were plated with increasing doses of each agent, and the survival fraction was calculated from clonogenic assays (Figure 3-11). The LD_{50} was then calculated and used to determine the dose of chemotherapy, which would be combined with Barasertib (25nM). The doses were adjusted slightly to the nearest round number to help in setting up subsequent experiments. (Table 3-5).

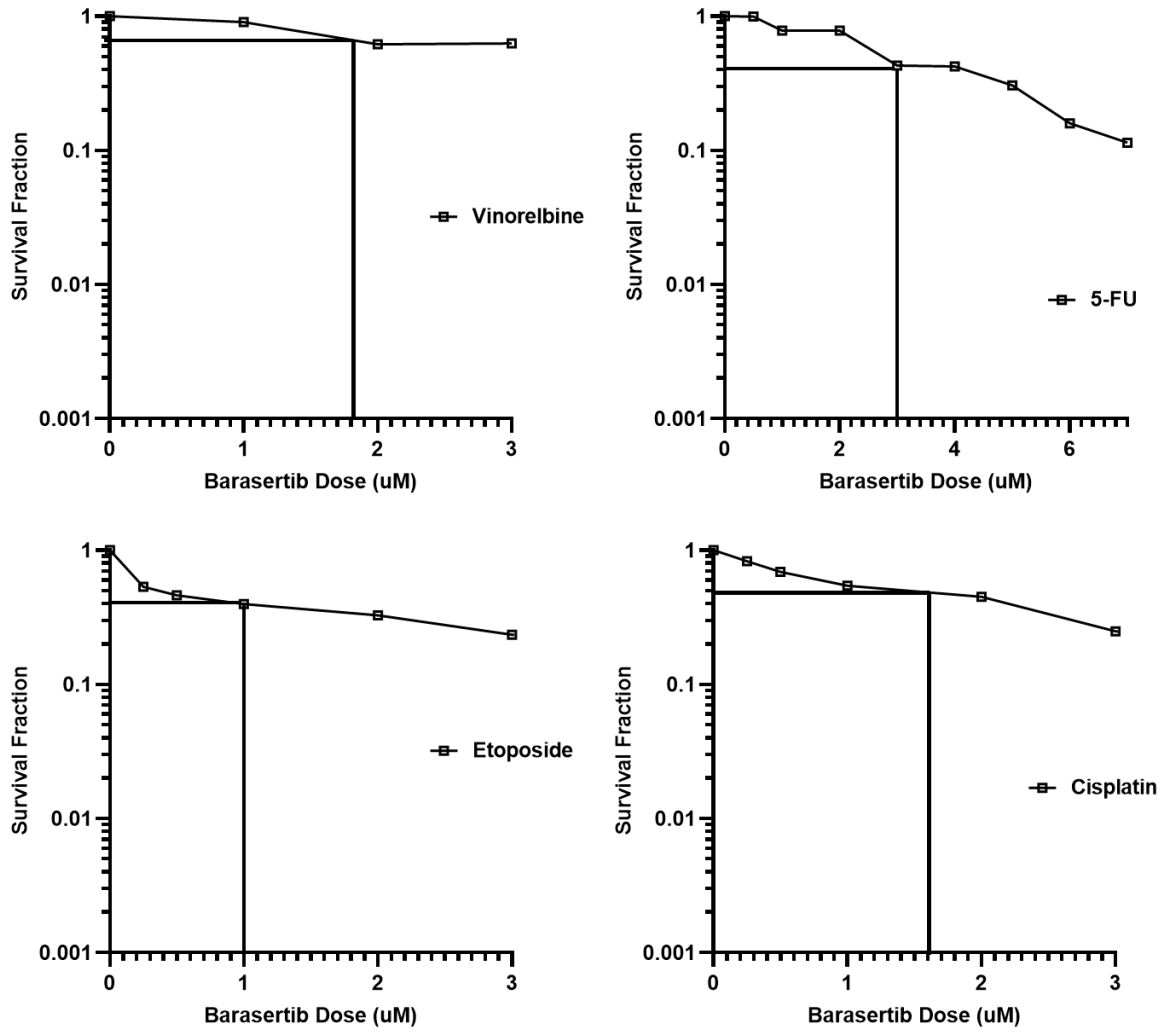


Figure 3-7: Survival curves of H460 exposed to four chemotherapy agents (n=5/6).

Chemotherapy Drug	LD_{50} of chemotherapy in H460 cells	Dose used in combination with Barasertib
Cisplatin	1.6uM	1.5uM
Etoposide	1.082uM	1uM
5-FU	3.36uM	3uM
Vinorelbine	1.89uM	1.5uM

Table 3-4: Mean Barasertib LD_{50} values in NSCLC cell lines (n=5/6).

3.2.2.6 Barasertib does not sensitise to other chemotherapies in the H460 and H1299 cell lines.

We wanted to examine whether Barasertib could increase the tumoricidal activity of standard chemotherapies in NSCLC and HNSCC cell lines. Cisplatin, Vinorelbine, e*top*oside and 5-FU were compared to four conditions: Barasertib+Cisplatin, Barasertib+Vinorelbine, Barasertib+E*top*oside, and Barasertib+5-FU. Drugs were added together, and survival was assessed using clonogenic survival assays. All conditions were carried out in parallel for each cell line, but the data are represented as separate graphs for clarity (i.e., the same Barasertib data is presented on four graphs).

There was no significant reduction in cell survival when Barasertib alone was added to H460 cells (Figure 3-11 and 3-12). For cisplatin and Vinorelbine, in contrast to the optimization experiments, no decrease in survival was seen when the LD50- dose was used (Figure 3-11). Therefore, it is not possible to conclude whether Barasertib sensitizes to cisplatin/ Vinorelbine or whether the drugs have gone off. For e*top*oside and 5-FU, there was no sensitisation when Barasertib was added (Figure 3-12).

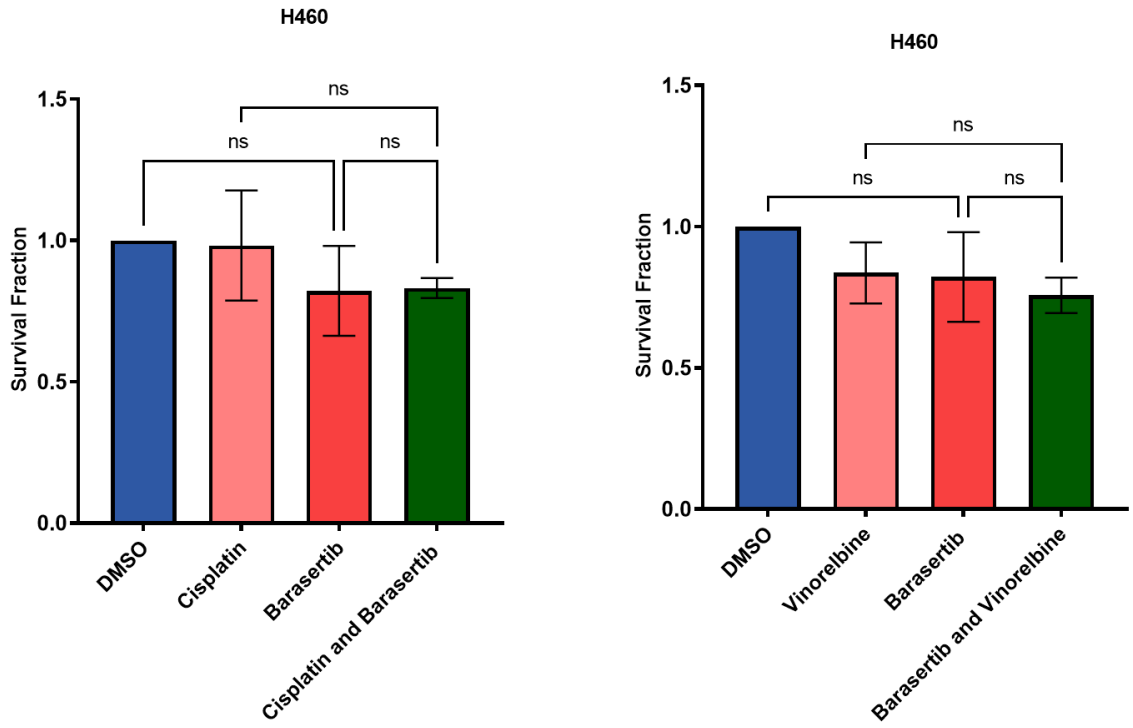


Figure 3-8: Comparison of Barasertib vs Barasertib and chemotherapy (Cisplatin and Vinorelbine) in H460 cell lines (n=3). Cells were pre-incubated with either Cisplatin, Vinorelbine or *AURKB* inhibitor Barasertib, cells were left to form colonies for 10-14 days before colony outgrowth under continuous exposure to the Cisplatin, Vinorelbine and/or *AURKB* inhibitor Barasertib. Data points represent the mean survival fraction normalised to DMSO +/- SD (N= ≥3). F-value and p-value derived from the extra sum of squares test. NS (non-statistically significant) denotes p= >0.05, * denotes p= ≤0.05, ** denotes p= ≤0.01, *** denotes p= 0.001 (One-way ANOVA with Dunnett correction for multiple comparisons).

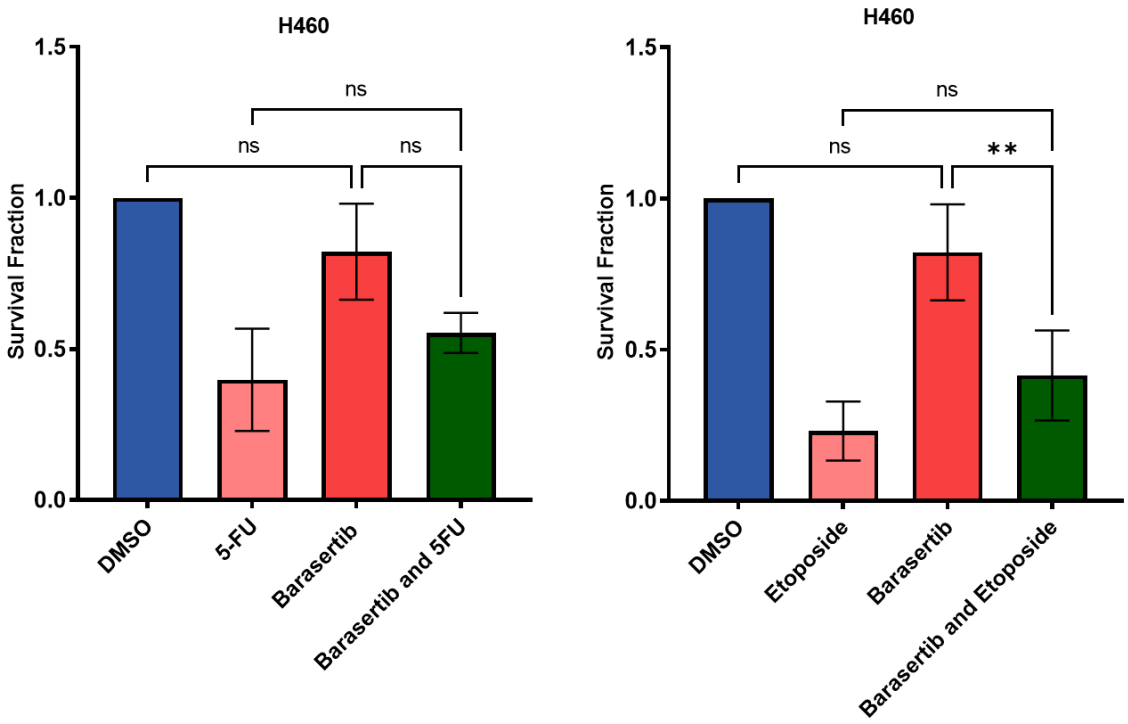


Figure 3-9: Comparison of Barasertib vs Barasertib and chemotherapy (5-FU and E*topo*side) in H460 cell lines (n=3). Cells were pre-incubated with either 5FU, Etoposide or *AURKB* inhibitor Barasertib, cells were left to form colonies for 10-14 days before colony outgrowth under continuous exposure to the 5FU, Etoposide and/or *AURKB* inhibitor Barasertib. Data points represent the mean survival fraction normalised to DMSO +/- SD (N= ≥3). F-value and p-value derived from the extra sum of squares test. NS (non-statistically significant) denotes p= >0.05, * denotes p= ≤0.05, ** denotes p= ≤0.01, *** denotes p= 0.001 (One-way ANOVA with Dunnett correction for multiple comparisons).

In H1299 cells, Barasertib did induce a significant decrease in survival in all four assays ($p = 0.0001$). Cisplatin alone did not induce a significant decrease in survival, again suggesting a difference in its activity in the optimisation experiments. There was no further decrease in survival comparing Barasertib to Barasertib + Cisplatin, so there is either no sensitisation or, as above, the Cisplatin had done off. Vinorelbine did not affect survival alone; interestingly, adding Vinorelbine with Barasertib protected from Barasertib alone induced cell killing ($p=0.0011$) (Figure 3-13). For e*topo*side there was sensitisation when Barasertib was added but in the case of the 5FU there was no sensitisation when Barasertib was added.

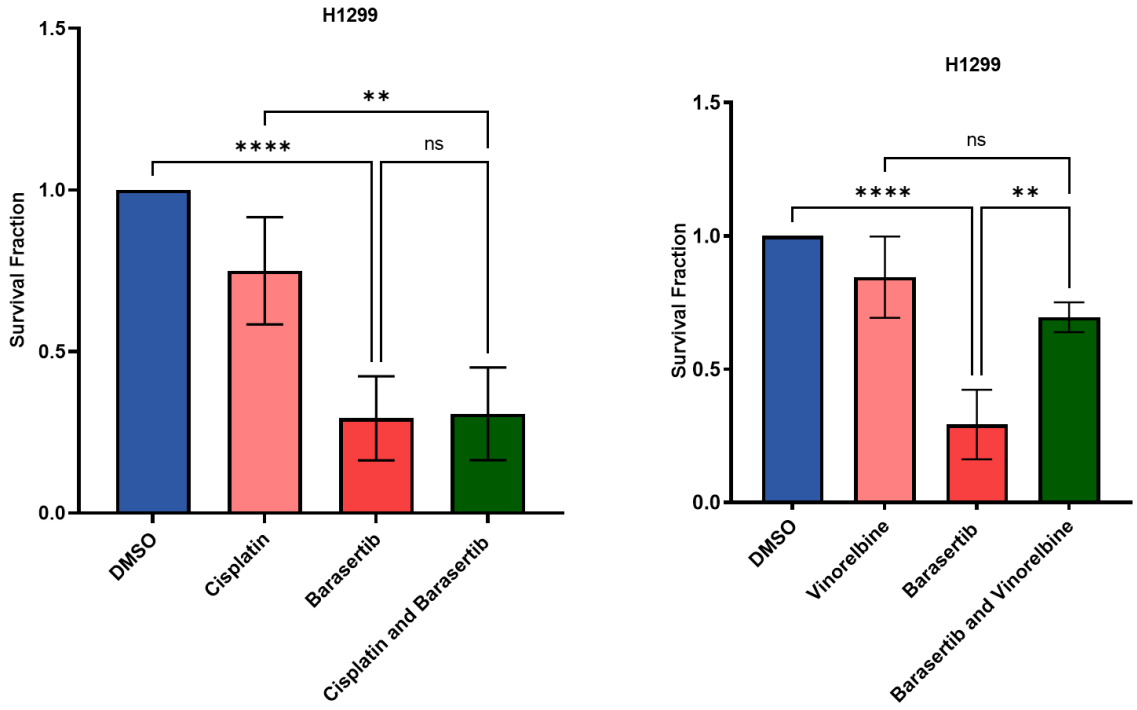


Figure 3-10: Comparison of Barasertib vs Barasertib and chemotherapy (Cisplatin and Vinorelbine) in H1299 cell lines (n=3). Cells were pre-incubated with either Cisplatin, Vinorelbine or *AURKB* inhibitor Barasertib, cells were left to form colonies for 10-14 days before colony outgrowth under continuous exposure to the Cisplatin, Vinorelbine and/or *AURKB* inhibitor Barasertib. Data points represent the mean survival fraction normalised to DMSO +/- SD (N= ≥3). F-value and p-value derived from the extra sum of squares test. NS (non-statistically significant) denotes p= >0.05, * denotes p= ≤0.05, ** denotes p= ≤0.01, *** denotes p= 0.001 (One-way ANOVA with Dunnett correction for multiple comparisons).

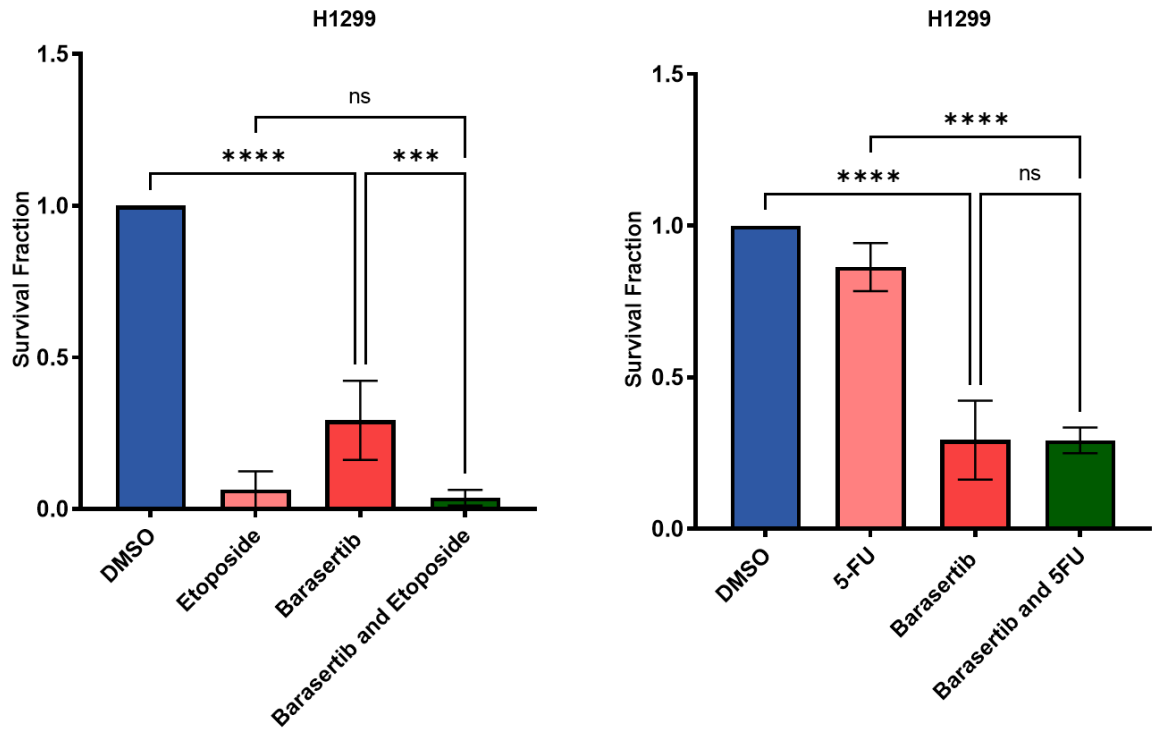


Figure 3-11: Comparison of Barasertib vs Barasertib and chemotherapy (5-FU and E*topo*side) in H1299 cell lines (n=3). Cells were pre-incubated with either 5FU, Etoposide or *AURKB* inhibitor Barasertib, cells were left to form colonies for 10-14 days before colony outgrowth under continuous exposure to the 5FU, Etoposide and/or *AURKB* inhibitor Barasertib. Data points represent the mean survival fraction normalised to DMSO +/- SD (N= ≥3). F-value and p-value derived from the extra sum of squares test. NS (non-statistically significant) denotes p= >0.05, * denotes p= ≤0.05, ** denotes p= ≤0.01, *** denotes p= 0.001 (One-way ANOVA with Dunnett correction for multiple comparisons).

3.2.2.7 Comparison of Barasertib and Vinorelbine, Cisplatin and Barasertib and Cisplatin plus 5FU demonstrate radiosensitisation in all combinations ex*cep*t the combination of Barasertib and Vinorelbine in the H460s.

The ability of Barasertib combined with standard chemotherapy to radiosensitise was tested using Vinorelbine, Cisplatin and 5-FU in colony survival assays. Barasertib plus chemotherapy was given 2 hours before irradiation and was present continuously throughout the colony survival assay. Dose enhancement ratios for 2 Gy and 4Gy were calculated compared to DMSO control. Consistent with previous data, Barasertib alone radiosensitised ($p<0.05$) and induced DERs of around 1.4 and 1.8-2 at 2Gy and 4Gy, respectively. Likewise, Cisplatin and 5FU (at 2 Gy) radiosensitised ($p=0.03$ and 0.01 respectively) with DERs of a magnitude similar to Barasertib (DER 2 Gy around 1.4). Adding Barasertib and Cisplatin (at 4 Gy) or Barasertib and 5FU (both at 2 and 4 Gy) increased the radiosensitising effect seen with each agent alone (DERs: 5.78 and 14.81; $p=0.03$ and 0.004, respectively). (Figure 3-19 and Table 3-6). In contrast, vinorelbine did not radiosensitise either at 2 nor 4 Gy ($p=0.42$ and 0.23), and its addition negated the Barasertib-induced radiosensitisation.

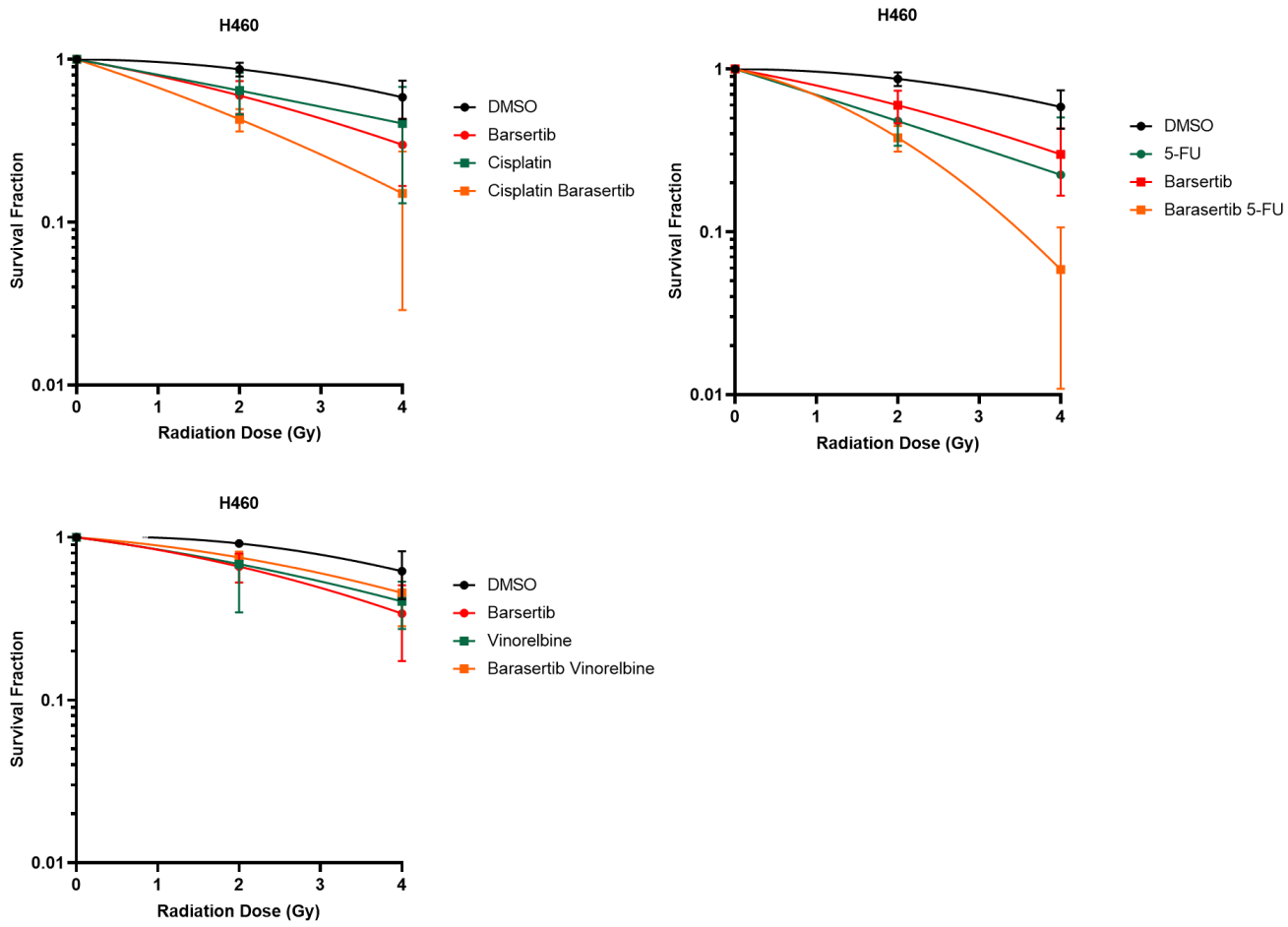


Figure 3-12 **Barasertib and Chemotherapy in H460 cell lines** Survival fraction of H460 cells after treatment with IR in combination with Barasertib and Chemotherapy, a combination which led to the lowest cell survival was seen in H460's treated with Barasertib and 5FU. Cells were pre-incubated with Cisplatin, 5FU, Vinorelbine and Barasertib before irradiation and colony outgrowth under continuous exposure to the *AURKB* inhibitor Barasertib. Data points represent the mean survival fraction normalised to unirradiated control +/- SD (N= ≥3). F-value and p-value derived from the extra sum of squares test.

	DMSO	2Gy	4Gy
Barasertib	1	1.387	1.819
Vinorelbine	1	1.339	1.533
Barasertib and Vinorelbine	1	1.219	1.358

	DMSO	2Gy	4Gy
Barasertib	1	1.451	1.957
Cisplatin	1	1.352	1.448
Barasertib and Cisplatin	1	2.030	5.786

	DMSO	2Gy	4Gy
Barasertib	1	1.451	1.957
5-FU	1	1.816	2.611
Barasertib and 5-FU	1	2.298	14.815

Chemotherapy combination	F-score	p value
Barasertib/Cisplatin	40.17	<0.0001
Barasertib/Vinorelbine	0.8590	0.4526
Barasertib/5FU	71.87	<0.0001

t.Test Barasertib		t.Test Vinorelbine		t.Test Barasertib and Vinorelbine	
2 Gy	0.084	2 Gy	0.426	2 Gy	0.045
4 Gy	0.187	4 Gy	0.232	4 Gy	0.475
t.Test Barasertib		t.Test Cisplatin		t.Test Barasertib and Cisplatin	
2 Gy	0.022	2 Gy	0.030	2 Gy	0.832
4 Gy	0.031	4 Gy	0.031	4 Gy	0.031
t.Test Barasertib		t.Test 5-FU		t.Test Barasertib and 5-FU	
2 Gy	0.022	2 Gy	0.014	2 Gy	0.001
4 Gy	0.031	4 Gy	0.122	4 Gy	0.004

Table 3-5 **Barasertib and chemotherapy DER ratios and t.test** values in H460s demonstrating the highest DER ratios, F scores and P values of the separate combinations are listed, the P values represent the combination treatment compared to DMSO. Cells were pre-incubated with Cisplatin, 5FU, Vinorelbine and Barasertib before irradiation and colony outgrowth under continuous exposure to the *AURKB* inhibitor Barasertib. Data points represent the mean survival fraction normalised to unirradiated control +/- SD (N= ≥3). F-value and p-value derived from the extra sum of squares test.

3.2.3 Examples of the cellular phenomenon seen in live cell assays.

Before quantifying the different phenotypes, the following figures give examples of the phenotypes observed.

3.2.3.1 Normal Mitosis

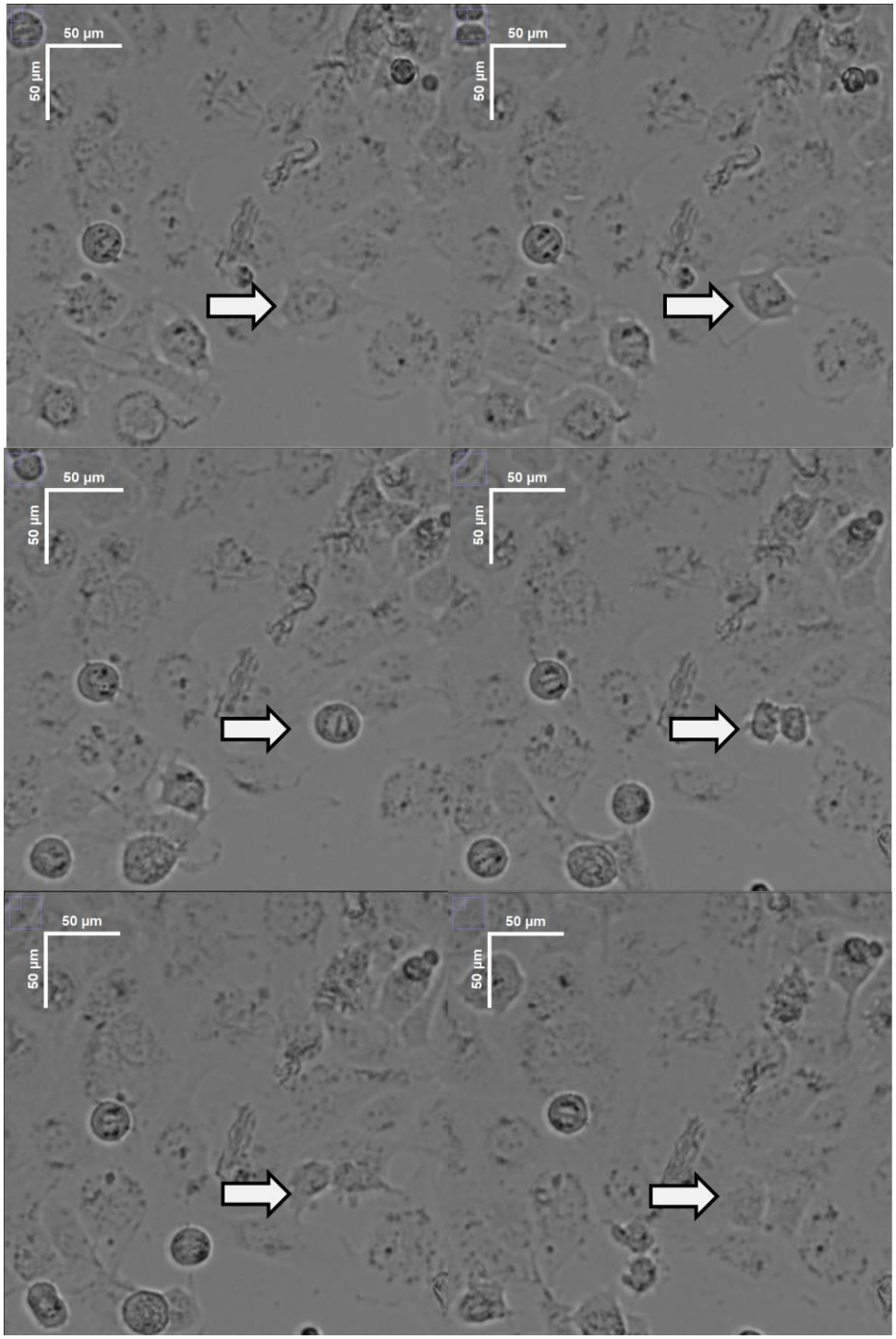


Figure 3-13: **Normal Mitosis A-I** H1299 cell, undergoing mitosis, dividing into two daughter cells, the central spindle can be observed along with chromatin separation in anaphase. This was observed at 20X magnification using a Zeiss Cell Discoverer 7 HCS microscope; the cells were treated with Barasertib and viewed between successive time frames taken 120 seconds apart.

3.2.3.2 Death in mitosis by apoptosis

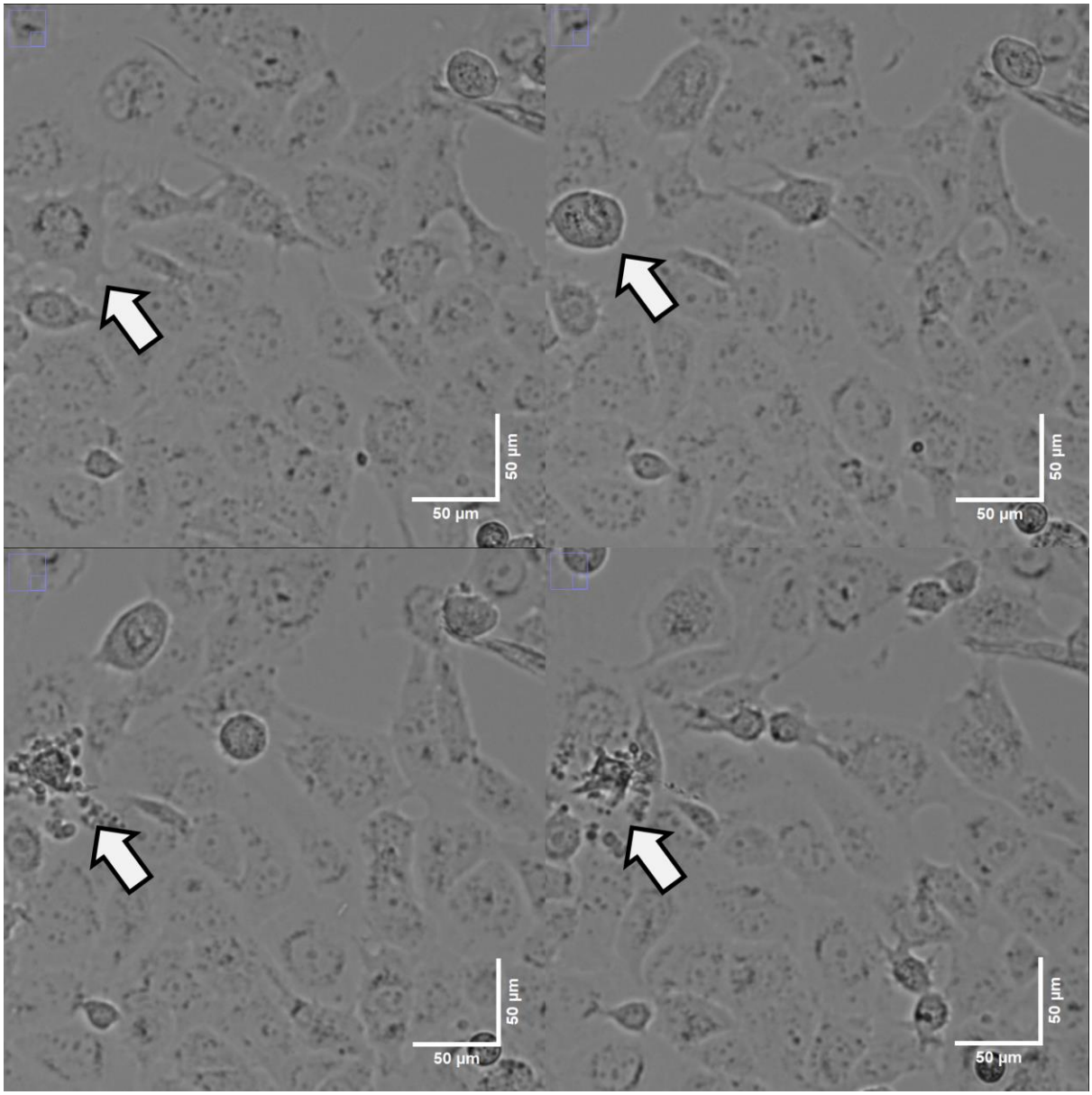


Figure 3-14: **Death in mitosis by apoptosis A-I** This SCC89 cell is undergoing apoptosis; the cell undergoes rounding as if it will go into the normal process of mitosis but instead undergoes cell blebbing and dies. The cell, over time, detaches from the plate and floats in the media. This was observed at 20X magnification using a Zeiss Cell Discoverer 7 HCS microscope; the cells were treated with Barasertib and viewed between successive time frames taken 120 seconds apart.

3.2.3.3 Cell slippage

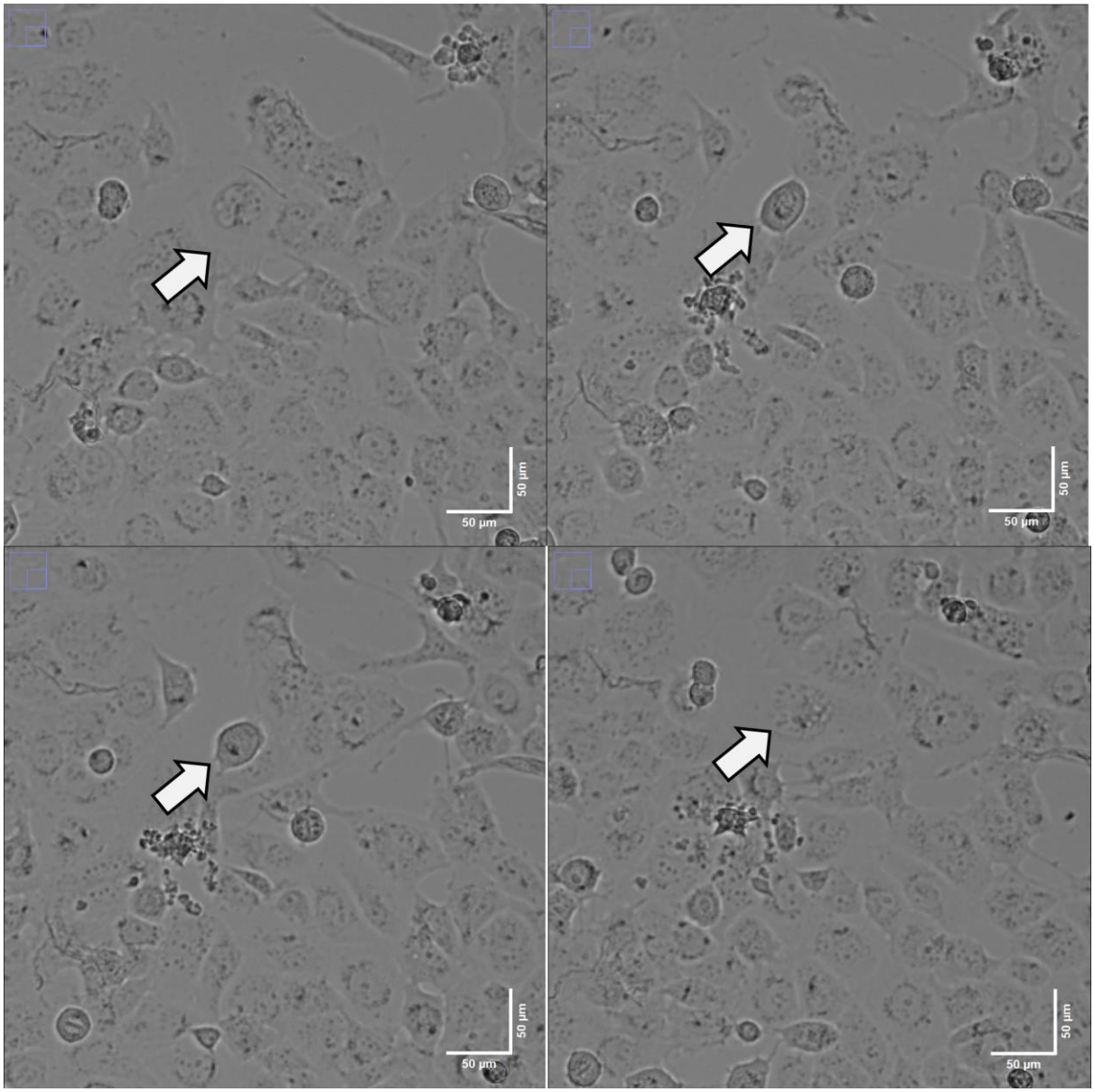


Figure 3-15: **Cell slippage A-I** An H1299 cell undergoing slippage where the cells round up but do not divide into two daughters; instead, it “escapes” rounding and becomes the mother cell again. We also observed this slippage occurring on two and three successive occasions. This was observed at 20X magnification using a Zeiss Cell Discoverer 7 HCS microscope; the cells were treated with Barasertib and viewed between successive time frames taken 120 seconds apart.

3.2.3.4 Chromosome congression

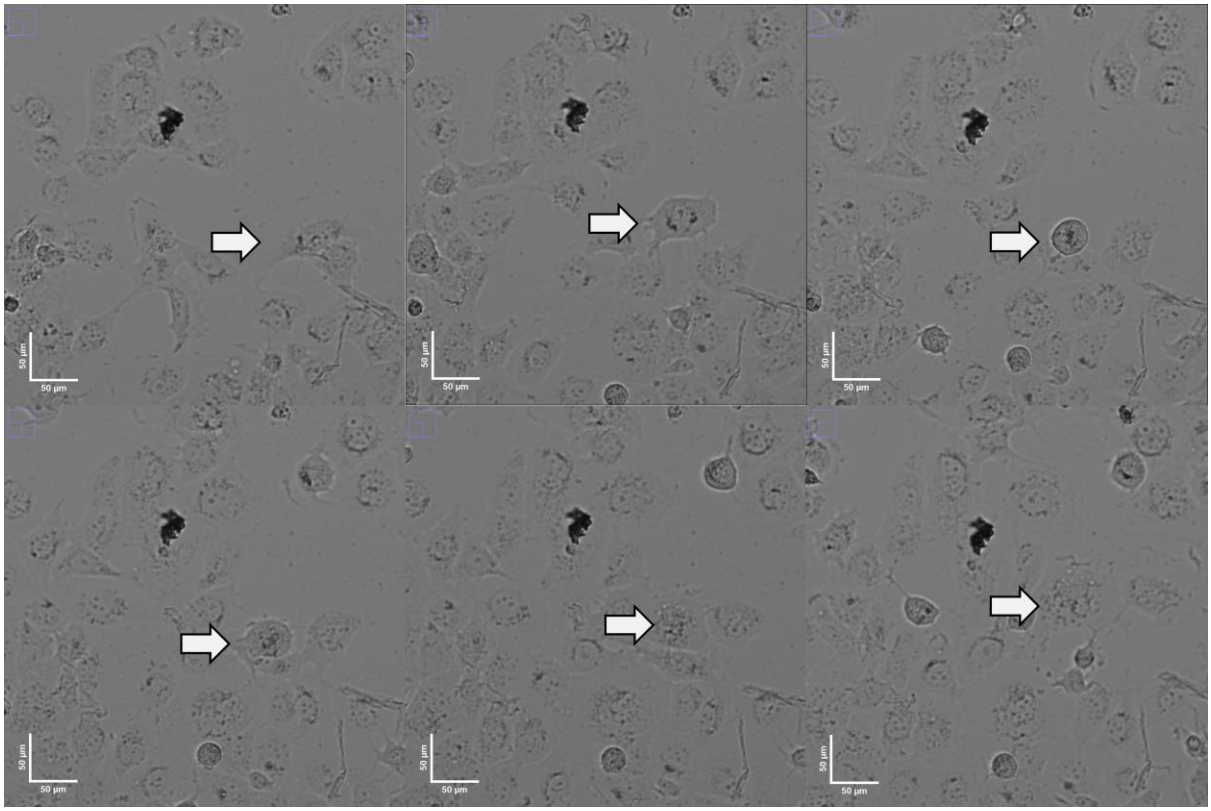


Figure 3-16: **Chromosome congression A-I** H1299 cells above demonstrate chromosomes "clumped in a ball," which could be possible chromosome congression heralding spindle assembly checkpoint, kinetochore-microtubule attachment, or centrosome function, and can lead to aneuploidy and genomic instability, in this case the cell ultimately underwent slippage, observed at 20X magnification using Zeiss Cell Discoverer 7 HCS microscope, the cells were treated with Barasertib and viewed between successive time frames taken 120 seconds apart.

3.2.3.5 Multipolar spindle prior to slippage

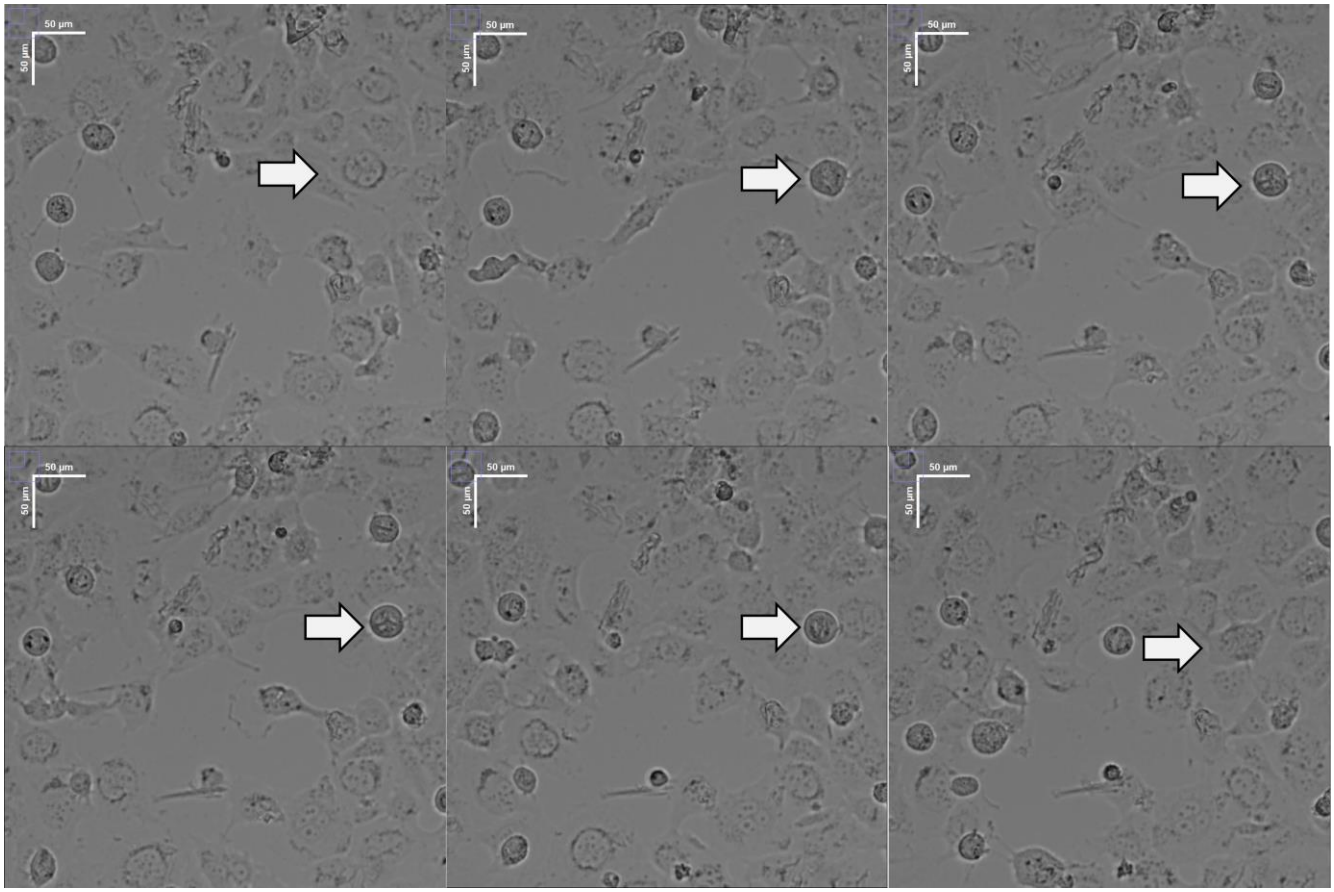


Figure 3-17: **Multipolar spindle A-I** H1299 cells showing the multipolar spindle before undergoing slippage, multipolar spindle were seen before cells underwent aberrant mitosis observed at 20X magnification using Zeiss Cell Discoverer 7 HCS microscope, the cells were treated with Barasertib and viewed between successive time frames taken 120 seconds apart.

3.2.4 Live cell analysis of NSCLC cell lines in response to Barasertib with or without radiation treatment.

We have seen in the previous chapter that NSCLC cell lines have a range of responses to Barasertib monotherapy, with A549, H520 being sensitive, and H460 being resistant. In addition, we saw that NSCLC cell lines could be sensitised to radiation using Barasertib. We first examined the radiosensitising effects of 25nM and 50nM Barasertib in cells resistant to monotherapy.

3.2.4.1 The NSCLC H460 cell line does not demonstrate significantly increased levels of slippage nor mitotic death when exposed to Barasertib alone or Barasertib (25nM) plus IR at 24 – 36 hours but demonstrates significant increases in slippage using Barasertib 50nM and IR.

H460 was insensitive to Barasertib alone and was radiosensitised. We examined the cellular response of H460 by live cell imaging 24 to 36 hours after DMSO, Barasertib alone, IR alone or combination treatment.

Average time in mitosis, percentage of cell death in mitosis, percentage of aberrant mitosis and percentage of mitotic cells with mitotic slippage were examined (Figures 4-9 A-D and 4-10 A-D). Stacked bar graphs are shown in the appendix, and summarised data from 3 independent repeats are shown in Figures 7-4.

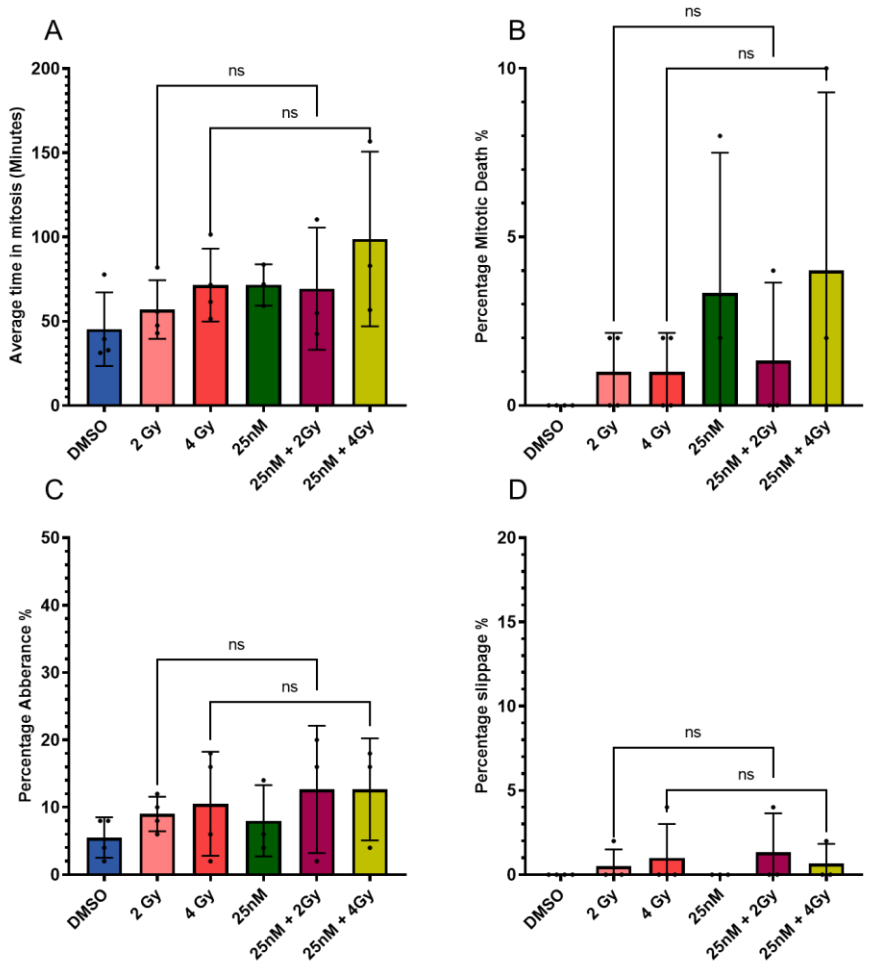


Figure 3-18: ***H460 live cell analysis 24-36 hours post-irradiation + 25nM Barasertib*** showing time in mitosis, proportion of intra-mitotic death, aberrant mitosis resulting in >2 daughter cells and proportion of cells undergoing slippage—minimum 50 mitotic cells counted per repeat. Data points represent the mean proportion of mitotic cells with described outcome +/- SD (N= 3) NS (non-statistically significant) denotes p= >0.05, * denotes p= ≤0.05, ** denotes p= ≤0.01, *** denotes p= 0.001 (One-way ANOVA with Dunnett correction for multiple comparisons).

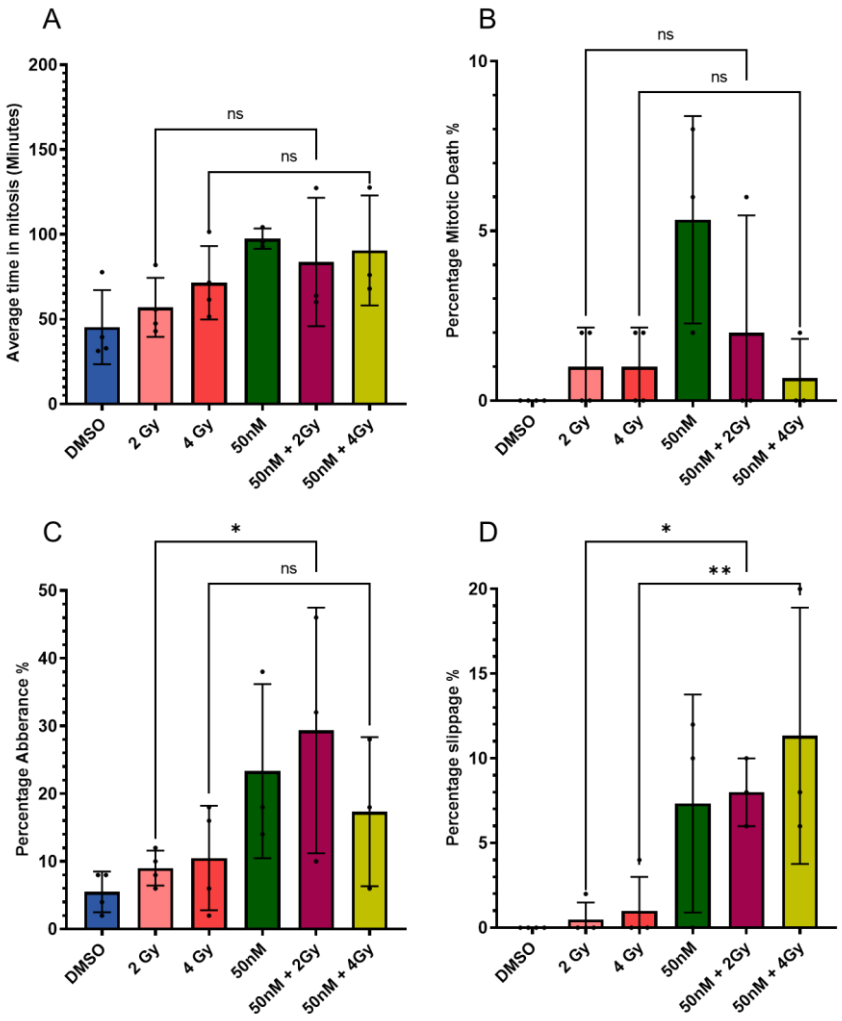


Figure 3-19: ***H460 live cell analysis 24-36 hours post-irradiation + 50nM Barasertib*** showing time in mitosis, proportion of intra-mitotic death, aberrant mitosis resulting in >2 daughter cells and proportion of cells undergoing slippage—minimum 50 mitotic cells counted per repeat. Data points represent the mean proportion of mitotic cells with described outcome +/- SD (N= 3) NS (non-statistically significant) denotes p= >0.05, * denotes p= ≤0.05, ** denotes p= ≤0.01, *** denotes p= ≤0.001 (One-way ANOVA with Dunnett correction for multiple comparisons).

The addition of Barasertib alone at concentrations of 25nM or 50nM or in combination with either 2Gy or 4Gy radiation did not result in a significant increase in the duration of mitosis, the percentage of cell death during mitosis. There was a significant increase in slippage over the 24-36-hour period at the 50nM concentration in H460 cells comparing 2Gy or 4Gy IR alone to respective IR plus bara conditions (Figure 4-10 D). There was also an increase in mitotic aberrance at 2Gy + 50nM Barasertib compared to 2Gy alone (Figure 4-10 C).

The findings are consistent with the finding that Barasertib is not particularly toxic alone (Figure 3-3) and suggest that there may be a role for altered mitosis following IR in the presence of Barasertib. Experiments with Barasertib alone presented later in this chapter suggest that the cellular effects of exposure to Barasertib are seen up to 72 hours after its addition, so possibly more time is needed to observe the effects in combination with IR.

3.2.4.2 H1299 cell lines do not demonstrate significantly increased levels of slippage nor mitotic death when exposed to Barasertib plus IR at 24 – 36 hours.

Like H460 cells, H1299 cells were relatively insensitive to monotherapy with Barasertib and could be radiosensitised (Figure 3-4). However, unlike H460, which contains wild type *p53*, H1299 cells are defective in *p53*. As *p53* is known to influence cell cycle progression and fate, we next analysed the effects of Barasertib alone and in combination with IR in H1299 cell lines, specifically at the 24 to 36-hour interval after treatment (Figures 4-11 A-D and 4-12 A-D).

At 25nM, either alone or with IR, Barasertib did not change mitosis duration, percentage of cell death occurring during mitosis or aberrant mitosis percentage. On 2 out of 3 repeats, slippage was increased when 25nM Barasertib was added to 2Gy or 4Gy radiation. At 50nM, mitotic transit time was significantly increased following 4Gy radiation (4Gy vs 50nM + 4Gy, p=0.0360), and there was a trend for increased mitotic slippage (2 out of 3 repeats) when 50nM Barasertib was combined with 2Gy or 4Gy radiation.

As with H460, it is therefore seen that there may be a function for *AURKB* in preventing slippage following radiation; however, it is essential to remember that 24-36 hours may not be the right time to see maximal effects.

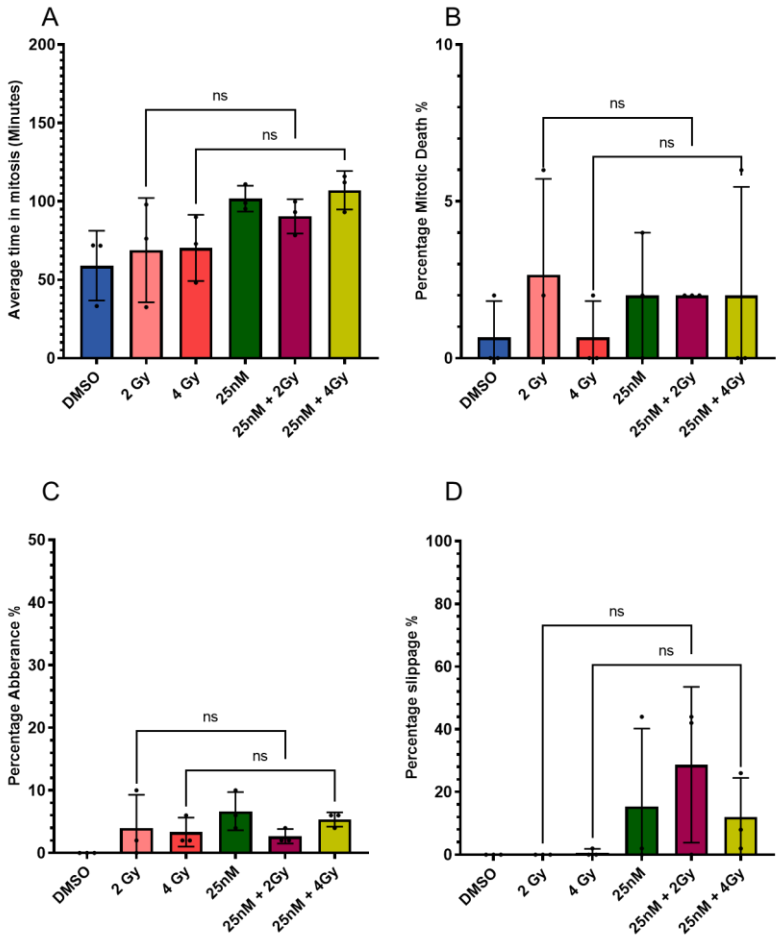


Figure 3-20: ***H1299 live cell analysis 24-36 hours post-irradiation + 25nM Barasertib A-D*** showing proportion of intra-mitotic death and aberrant mitosis resulting in >2 daughter cells time in mitosis, and proportion of cells undergoing slippage —minimum 50 mitotic cells counted per repeat. Data points represent the mean proportion of mitotic cells with described outcome +/- SD (N= 3) NS (non-statistically significant) denotes p= >0.05, * denotes p= ≤0.05, ** denotes p= ≤0.01, *** denotes p= ≤0.001 (One-way ANOVA with Dunnett correction for multiple comparisons).

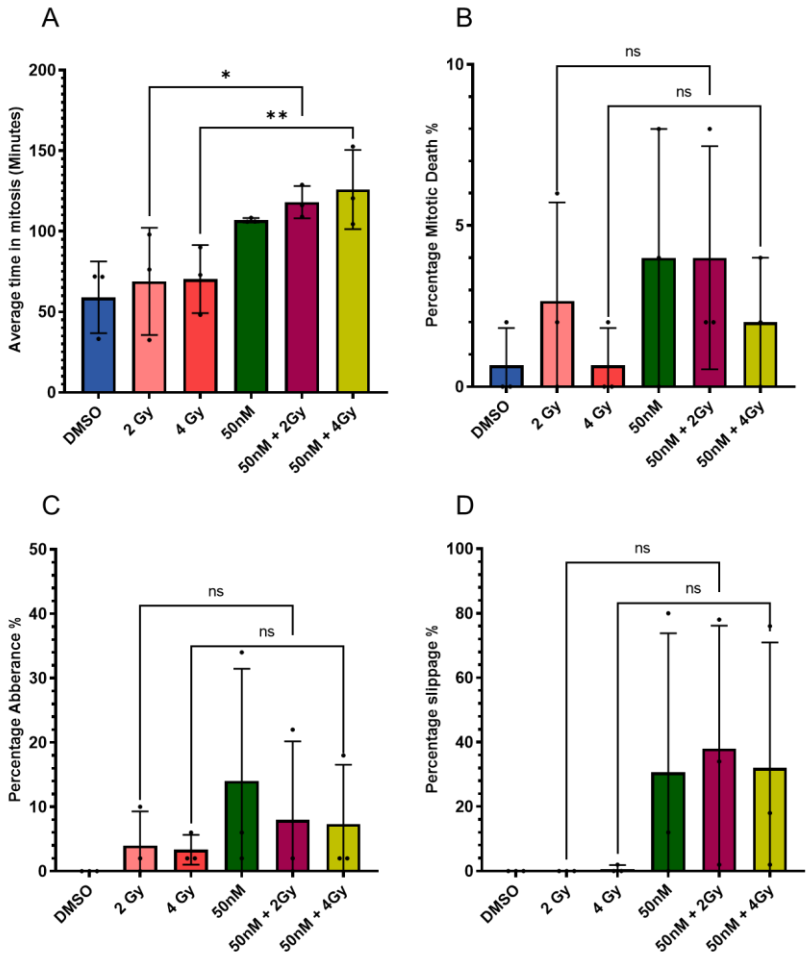


Figure 3-21: ***H1299 live cell analysis 24-36 hours post-irradiation + 50nM A-D*** *showing proportion* of intra-mitotic death and aberrant mitosis resulting in >2 daughter cells time in mitosis, and proportion of cells undergoing slippage —minimum 50 mitotic cells counted per repeat. Data points represent the mean proportion of mitotic cells with described outcome +/- SD (N= 3) NS (non-statistically significant) denotes p= >0.05, * denotes p= ≤0.05, ** denotes p= ≤0.01, *** denotes p= ≤0.001 (One-way ANOVA with Dunnett correction for multiple comparisons).

3.2.5 Live cell analysis of NCSLC cell lines using Barasertib as monotherapy.

Having looked at the cellular response of relatively Barasertib-resistant cell lines at 25nM and 50nM, we next examined the responses of cells sensitive to Barasertib (A549 and H520) at lower doses – 5nM and 10nM for comparison; we also exposed the resistant H460 cell line to the same low doses of Barasertib. As before, stacked bar graphs are in the appendix and data of 3 independent repeats is summarised in Figures 7.4.2.3 and 7.4.2.4.

3.2.5.1 A549 and H520 cell lines demonstrate increased mitotic slippage at increasing doses of Barasertib compared to H460 cells at 24 – 36 hours.

In the A549 cell line, we observed no increase in mitotic duration, cell death during mitosis, nor any significant levels of mitotic aberrance during the 24 to 36 hours following the addition of 5nM or 10nM Barasertib (Figures 4-13). However, mitotic slippage was significantly increased with 10nM Barasertib (DMSO vs 10nM, p-value = 0.0062) (Figure 4-13). This observation provides preliminary insights into the potential mechanism underlying the sensitivity of A549 cells to Barasertib. The lack of cellular mitotic death at the observed time-point could be because it is too early to see cell death. Alternatively, there may have been many cell deaths earlier, and the remaining cells represent a resistant sub-population.

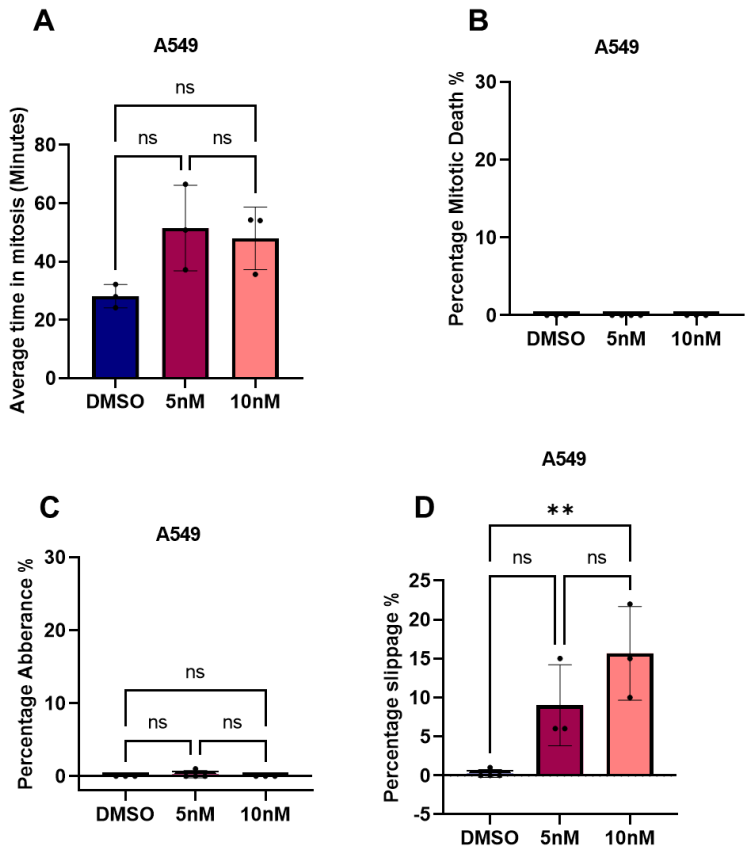


Figure 3-22: ***A549 live cell analysis 24-36 hours Barasertib alone A-D*** *showing proportion of intra-*mitotic death and aberrant mitosis resulting in >2 daughter cells time in mitosis, and proportion of cells undergoing slippage —minimum 50 mitotic cells counted per repeat. Data points represent the mean proportion of mitotic cells with described outcome +/- SD (N= 3) NS (non-statistically significant) denotes p= >0.05, * denotes p= ≤0.05, ** denotes p= ≤0.01, *** denotes p= ≤0.001 (One-way ANOVA with Dunnett correction for multiple comparisons).

In the H520 cell line, 10nM Barasertib increased the percentage of mitotic cell death (DMSO vs 10nM, p = 0.0309). Furthermore, Barasertib increased mitotic aberrance (DMSO vs 5nM and DMSO vs 10nM, p = 0.0309 and 0.0154, respectively). The analysis also revealed a significant increase in the percentage of cells undergoing mitotic slippage with 10nM Barasertib (DMSO vs 10nM, p = 0.0075). Lastly, Barasertib increased the time spent in mitosis (DMSO vs 5nM and 10nM, p = 0.0114 and 0.0007, respectively) (Figure 4-14). As expected, 5nM and 10nM Barasertib did not affect any cellular phenotypes analysed in H460 cells (Figure 4-15).

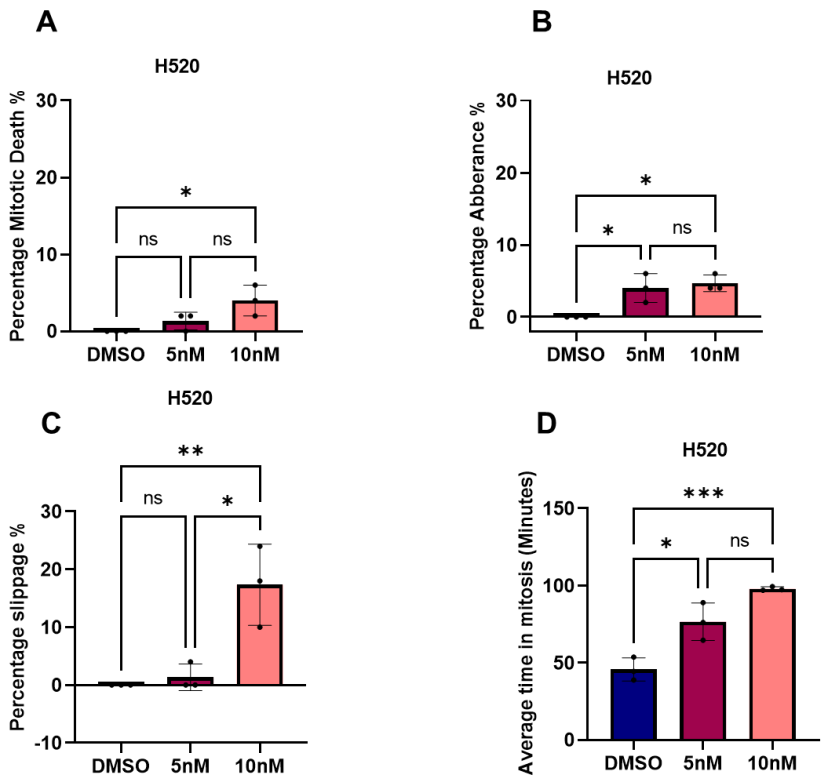


Figure 3-23: ***H520 live cell analysis 24-36 hours Barasertib alone A-D*** showing proportion of intra-mitotic death and aberrant mitosis resulting in >2 daughter cells time in mitosis, and proportion of cells undergoing slippage —minimum 50 mitotic cells counted per repeat. Data points represent the mean proportion of mitotic cells with described outcome +/- SD (N= 3) NS (non-statistically significant) denotes p= >0.05, * denotes p= ≤0.05, ** denotes p= ≤0.01, *** denotes p= ≤0.001 (One-way ANOVA with Dunnett correction for multiple comparisons).

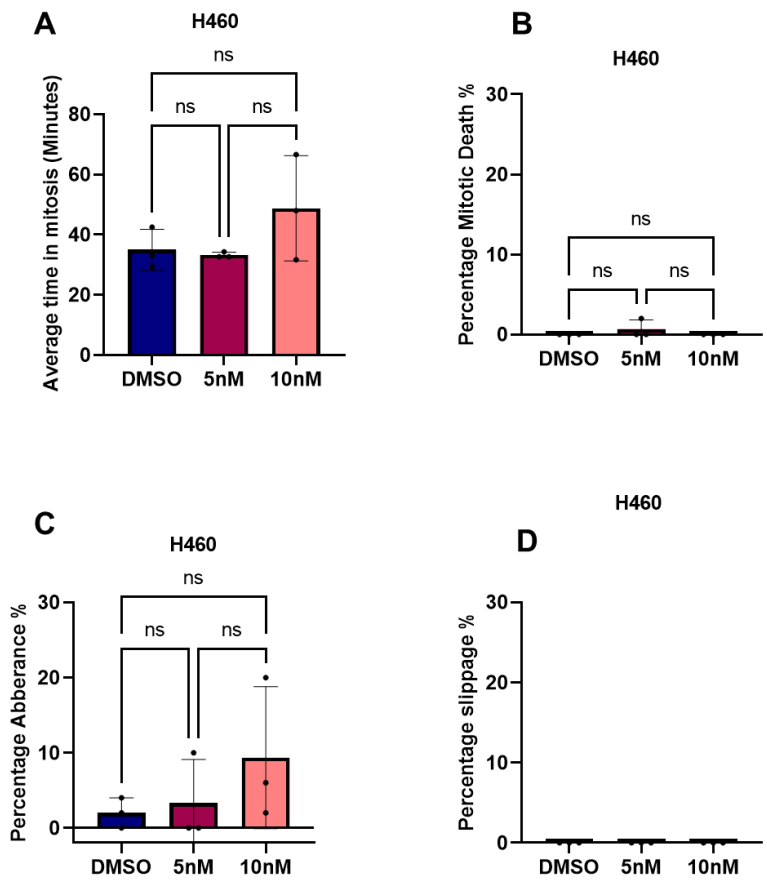


Figure 3-24: ***H460 live cell analysis 24-36 hours Barasertib alone A-D*** showing proportion of intra-mitotic death and aberrant mitosis resulting in >2 daughter cells time in mitosis, and proportion of cells undergoing slippage —minimum 50 mitotic cells counted per repeat. Data points represent the mean proportion of mitotic cells with described outcome +/- SD (N= 3) NS (non-statistically significant) denotes p= >0.05, * denotes p= ≤0.05, ** denotes p= ≤0.01, *** denotes p= ≤0.001 (One-way ANOVA with Dunnett correction for multiple comparisons).

3.2.5.2 A549 cell lines demonstrate increased levels of slippage at 10nM Barasertib alone at 0 – 16 hours and 36-48 hours, but no cellular outcomes preceding or occurring after slippage were seen.

The live cell imaging data from 24-36 hours of low dose (5nM and 10nM) Barasertib suggest effects on mitosis, especially slippage in cells sensitive to Barasertib as monotherapy. We were concerned we could miss additional cellular effects by looking only at this 12-hour window. To overcome the potential effects of time, we tried looking at 0-16- and 36-48 hours post-addition of Barasertib.

Regarding NSCLC cells, only the A549's was examined as the question was only to look at the outcomes occurring before and after slippage, **not** whether slippage had a greater tendency to occur in the cells more sensitive to Barasertib.

There was still no induction of death nor mitotic aberrance at these time points. Similar to 24-36 hours, mitotic slippage was seen at earlier and later times following the addition of 10nM Barasertib (DMSO vs 10nM, p= 0.0221 (0-16 hours) and 0.0228 (36-48 hours, respectively). In addition, Barasertib increased mitosis time at earlier times (p=0.0327, DMSO vs 10nM).

Unfortunately, a later time point assay with H520 cells could not be conducted because the clumping behaviour of H520 cells hindered the ability to track and assess their responses over a longer duration. Nonetheless, conducting such a long-term assay would have been valuable for obtaining a comprehensive understanding of the cellular effects of Barasertib on H520 cells.

Although we did not see any pattern to events post or pre-slippage, we did postulate that as slippage could occur early and late after the administration of Barasertib,

perhaps slippage could occur more than once (we did see this occurring in the HNSCC cells between 0-72 hours), (Figure 4-24 and 4-25).

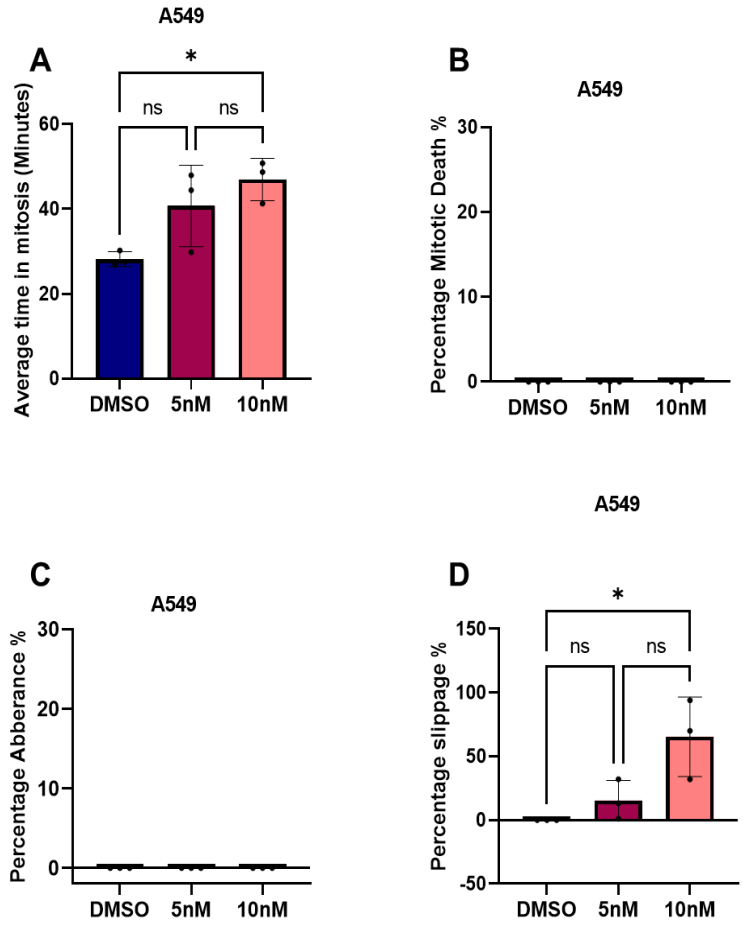


Figure 3-25: ***A549 live cell analysis 0-16 hours post-Barasertib A-D*** showing proportion of intra-mitotic death and aberrant mitosis resulting in >2 daughter cells time in mitosis, and proportion of cells undergoing slippage —minimum 50 mitotic cells counted per repeat. Data points represent the mean proportion of mitotic cells with described outcome +/- SD (N= 3) NS (non-statistically significant) denotes p= >0.05, * denotes p= ≤0.05, ** denotes p= ≤0.01, *** denotes p= ≤0.001 (One-way ANOVA with Dunnett correction for multiple comparisons).

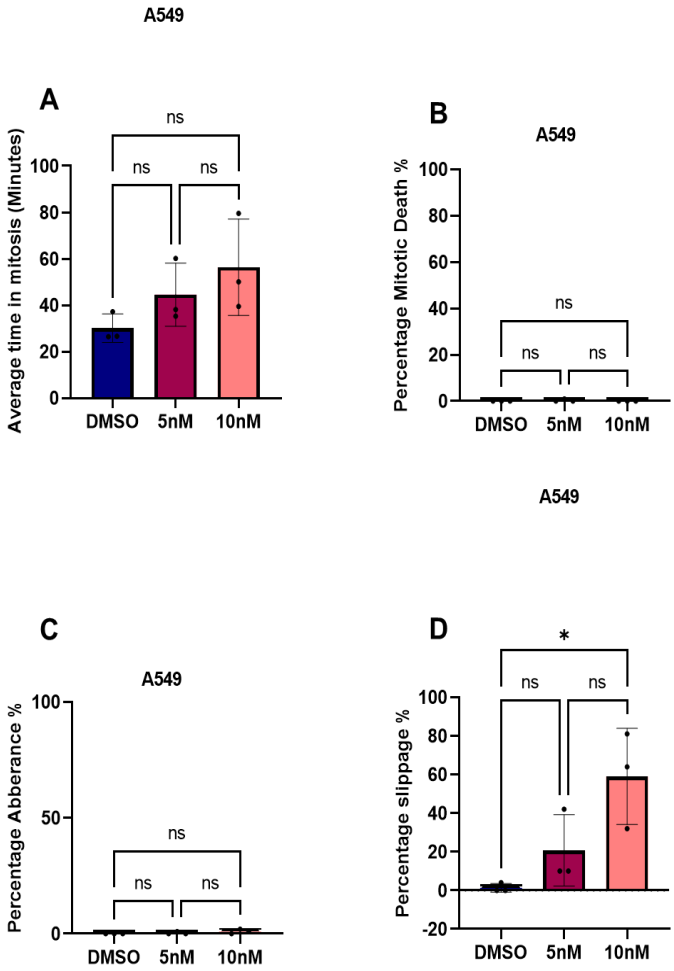


Figure 3-26: ***A549 live cell analysis 36-48 hours post-Barasertib A-D*** showing proportion of intra-mitotic death and aberrant mitosis resulting in >2 daughter cells time in mitosis, and proportion of cells undergoing slippage —minimum 50 mitotic cells counted per repeat. Data points represent the mean proportion of mitotic cells with described outcome +/- SD (N= 3) NS (non-statistically significant) denotes p= >0.05, * denotes p= ≤0.05, ** denotes p= ≤0.01, *** denotes p= ≤0.001 (One-way ANOVA with Dunnett correction for multiple comparisons).

In general, increased time in mitosis and mitotic slippage correlated with sensitivity to Barasertib, suggesting this may be the mechanism of toxicity – however, the molecular players and their link to *AURKB* are yet to be established. In addition, carrying out different assays of 12-hour windows has failed to allow us to really understand the fate of cells pre- and post-slippage.

3.2.6 Live cell analysis using Barasertib over 72 hours.

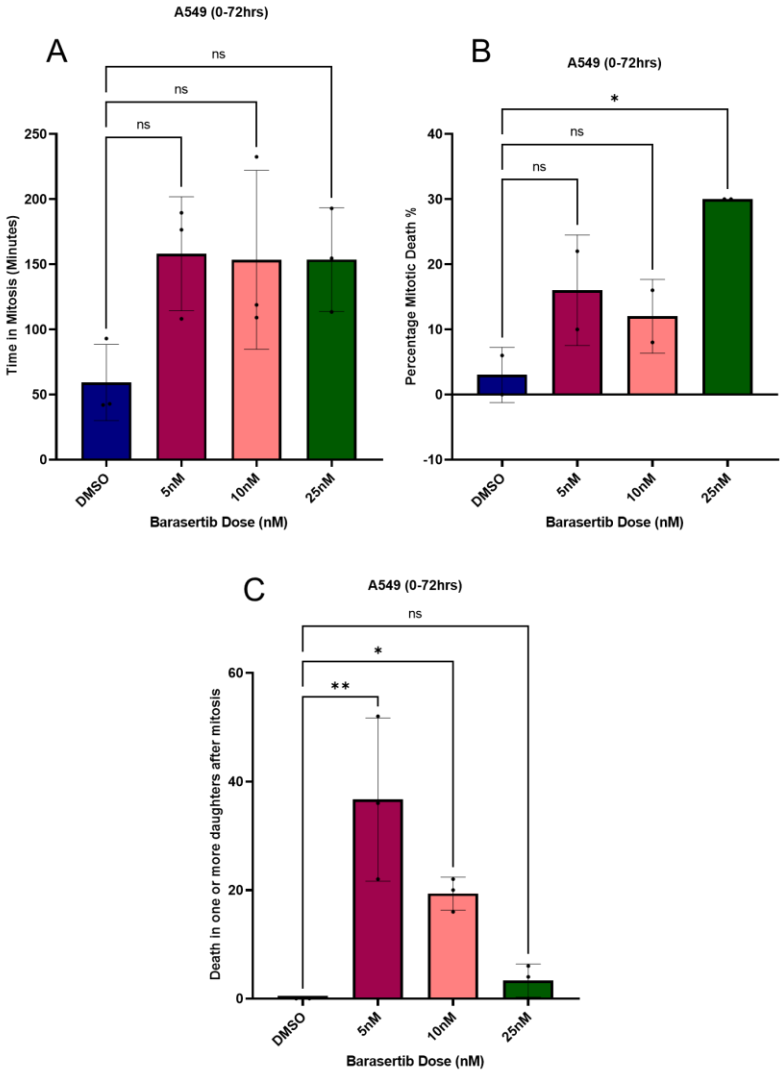
3.2.6.1 Live cell imaging between 0 -72 hours reveals that A549 cells eventually slip and die in mitosis.

The results of different 12-hour live cell assays at various time points have been presented to this point. While we saw significant levels of slippage in cells more sensitive to Barasertib, we could not determine the outcomes of this phenomenon. To address this query, we designed a 72-hour assay encompassing three distinct cell lines - A549, UPCI-SCC072, and SCC089, to investigate cellular outcomes before and after slippage. The stacked bar graphs and summary graphs are shown in the main thesis for these data.

Examining time in mitosis in the A549 cell line revealed no statistically significant increase (Figures 4-26 and 4-27). Consistent with the shorter time window studies, slippage was increased, with a dose dependency observed (DMSO vs 10nM and 25nM). Interestingly, 2.3 % of cells had two slippage events (Figure 4-26A Barasertib concentrations 10nM and 25nM). In addition, the longer observation window allowed us to see cell death after slippage induced by Barasertib (DMSO vs 10nM). Cell death in mitosis without observed slippage was also seen in Barasertib (DMSO vs

25nM p= 0.0241). Suggesting both slippage and no slippage-related mechanisms of Barasertib-induced cell death.

A549 cells were amongst the most sensitive NSCLC cells when exposed to Barasertib; when exposed to 5nM Barasertib (but not 10nM or 25nM), the A549 cells were able to divide into two daughters before both ended up dying in mitosis. In contrast, when the A549 cells were exposed to concentrations of 25nM, the mother cells ended up dying without division, possibly due to increased defects in the mitotic spindle during metaphase compared to cells exposed to lower doses or because only at these low doses' cells were not slipping and so only in these could post-mitotic death was seen.


A549 (0-72hrs)
A
ns
ns
ns
Time in Mitosis (Minutes)
250
200
150
100
50
0
DMSO
5nM
10nM
25nM
Barasertib Dose (nM)
B
A549 (0-72hrs)
*
ns
ns
Percentage Mitotic Death %
40
30
20
10
0
-10
DMSO
5nM
10nM
25nM
Barasertib Dose (nM)
C
A549 (0-72hrs)
ns
*
**
Death in one or more daughters after mitosis
60
40
20
0
DMSO
5nM
10nM
25nM
Barasertib Dose (nM)

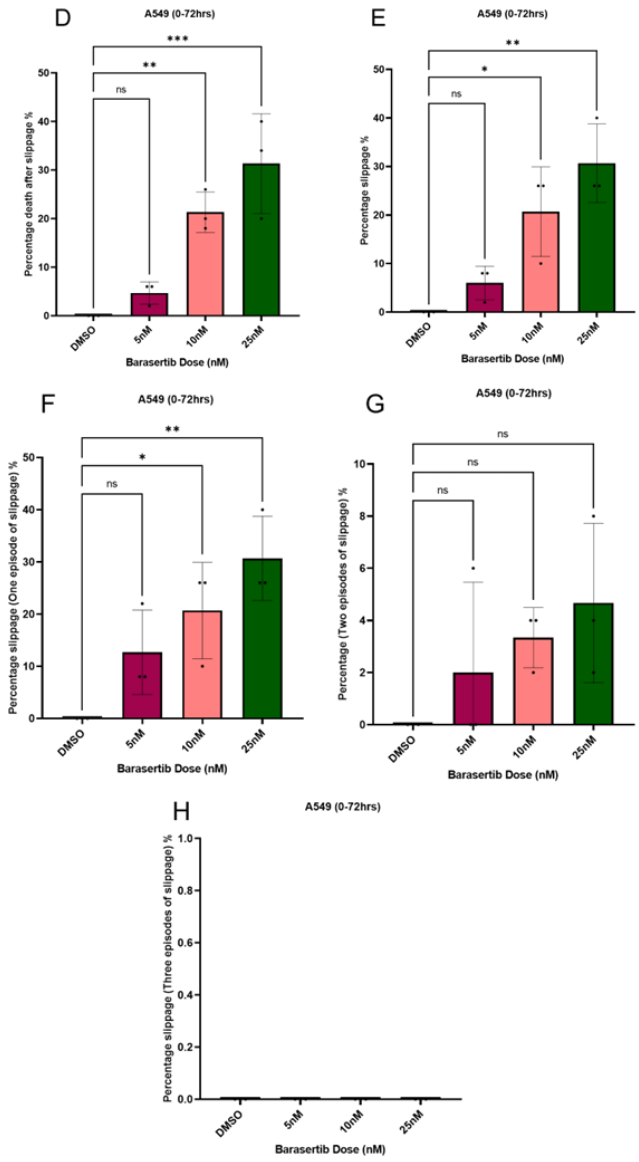


Figure 3-27: ***A549 live cell analysis 0-72 hours post-Barasertib*** *A.* Time in mitosis resulting in cytokinesis. B. Proportion of intra-mitotic death C. Proportion of daughter cells dying after slippage D. Proportion of cells dying after slippage. E. Proportion of cells undergoing slippage. F-H The proportion of cells undergoing slippage categorised by number of times the cells slipped in 72 hours regardless of outcome —minimum 50 mitotic cells counted per condition. Data points represent the mean proportion of mitotic cells with described outcome +/- SEM (N= 5). NS (non-statistically significant) denotes p= >0.05, * denotes p= ≤0.05, ** denotes p= ≤0.01, *** denotes p= ≤0.001 (One-way ANOVA with Dunnett correction for multiple comparisons).

3.2.7 Western blot analysis of genes in the SAC.

3.2.7.1 Barasertib does not alter Cyclin B1 and CDC20 levels.

We hypothesised that inhibiting *AURKB* would lead to cells undergoing prolonged mitotic arrest in the presence of reduced levels of cyclin B1, explaining the high levels of slippage in cells more sensitive to Barasertib (Lok et al., 2020).

To test this, DMSO or Barasertib (10nM) were added to B22, SCC089, UPCI-SCC72 H460 and A549 cells and left for 4 and 24 hours prior to western blotting for CDC20 and CyclinB1 expression. B22 and H460 were chosen due to their relative radioresistance compared to SCC89, UPCI-SCC72 and A549 cells. However, Barasertib did not induce any change in expression in either protein at either point in any cell line (Fig 4-51) (Figure 4-52). The lack of effect on CDC20 and Cyclin B1 could be due to the lack of a direct interaction between Barasertib and Cyclin B1 and CDC20.

.

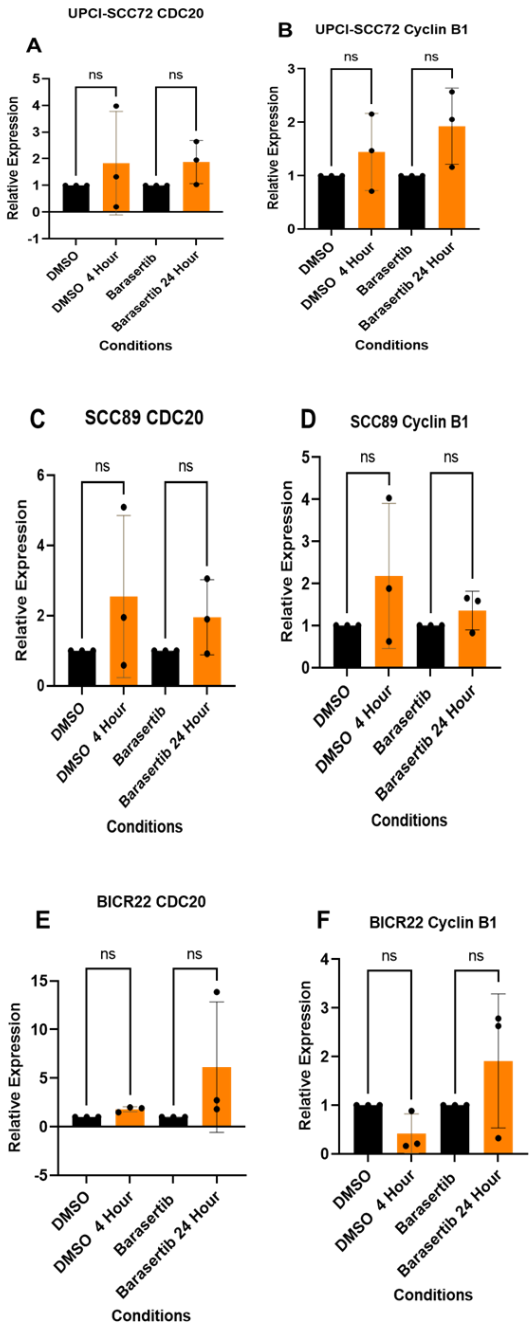


Figure 3-28: Quantification of CDC20 and Cyclin B1 expression normalised to GAPDH levels. A-B UPCI-SCC72 C-D SCC89 E-F BICR22 (N= ≥3). * Denotes p= ≤0.05, ** denotes p= ≤0.01, *** denotes p=≤0.001 (One-Way ANOVA).

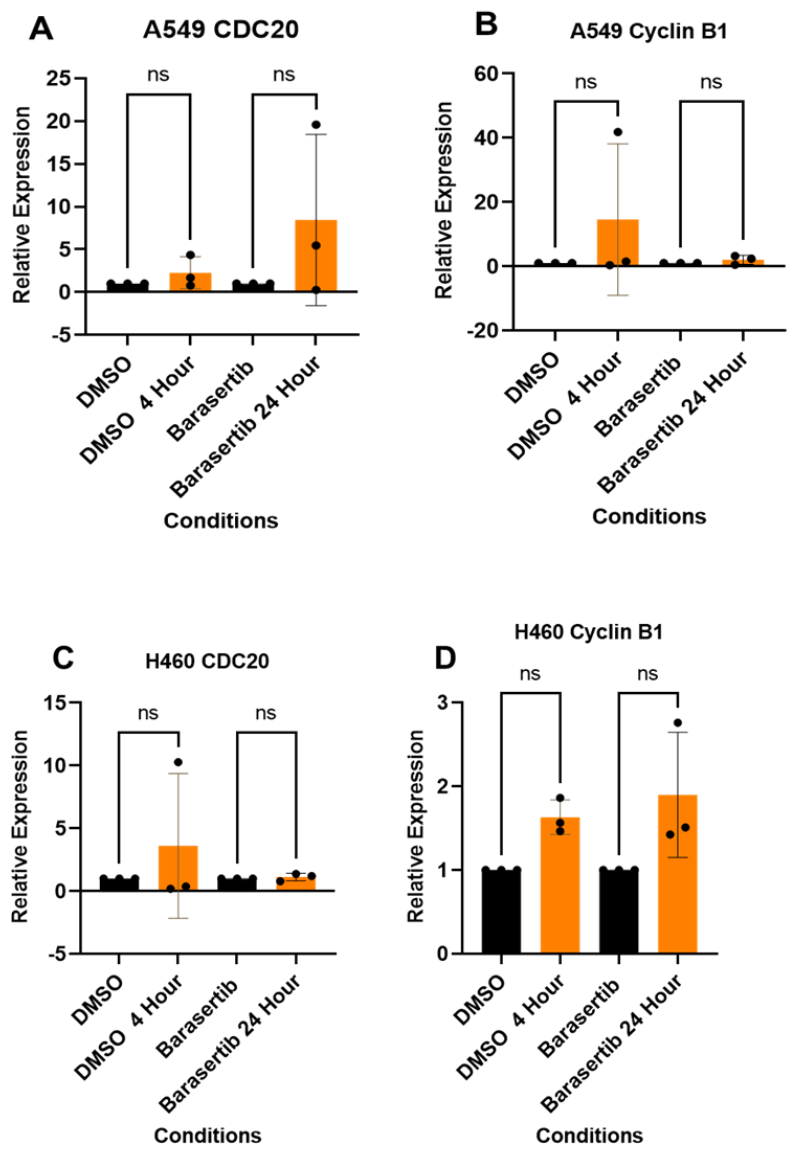


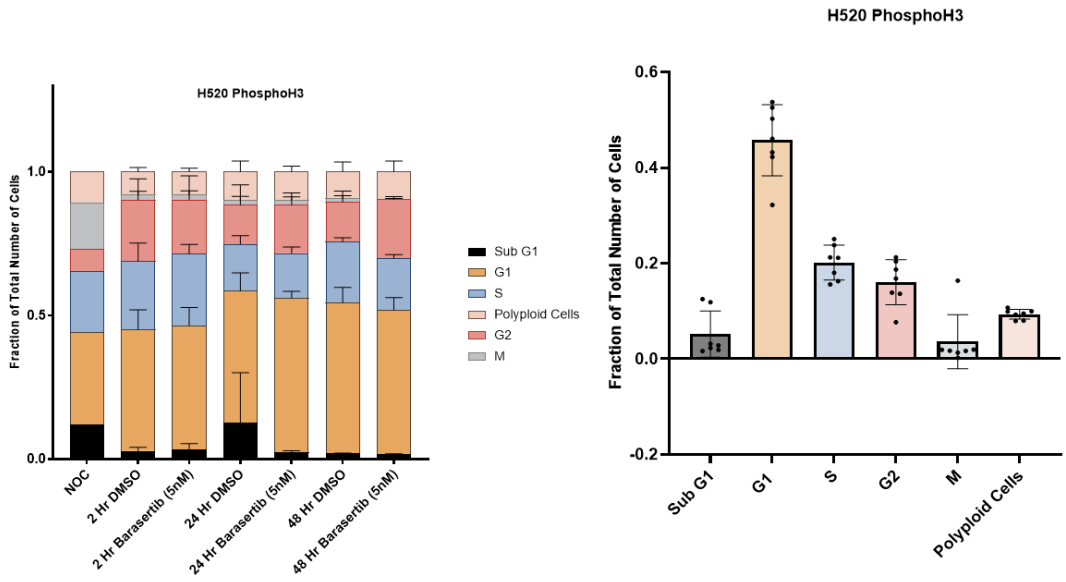
Figure 3-29: Quantification of CDC20 and Cyclin B1 expression normalised to GAPDH levels. A-B A549 C-D H460 (N= ≥3). * Denotes p= ≤0.05, ** denotes p= ≤0.01, *** denotes p=≤0.001 (One-Way ANOVA).

3.2.8 Cell cycle profiling using FACS.

3.2.8.1 Barasertib does not alter the cell cycle profile in A549 and H520 cells.

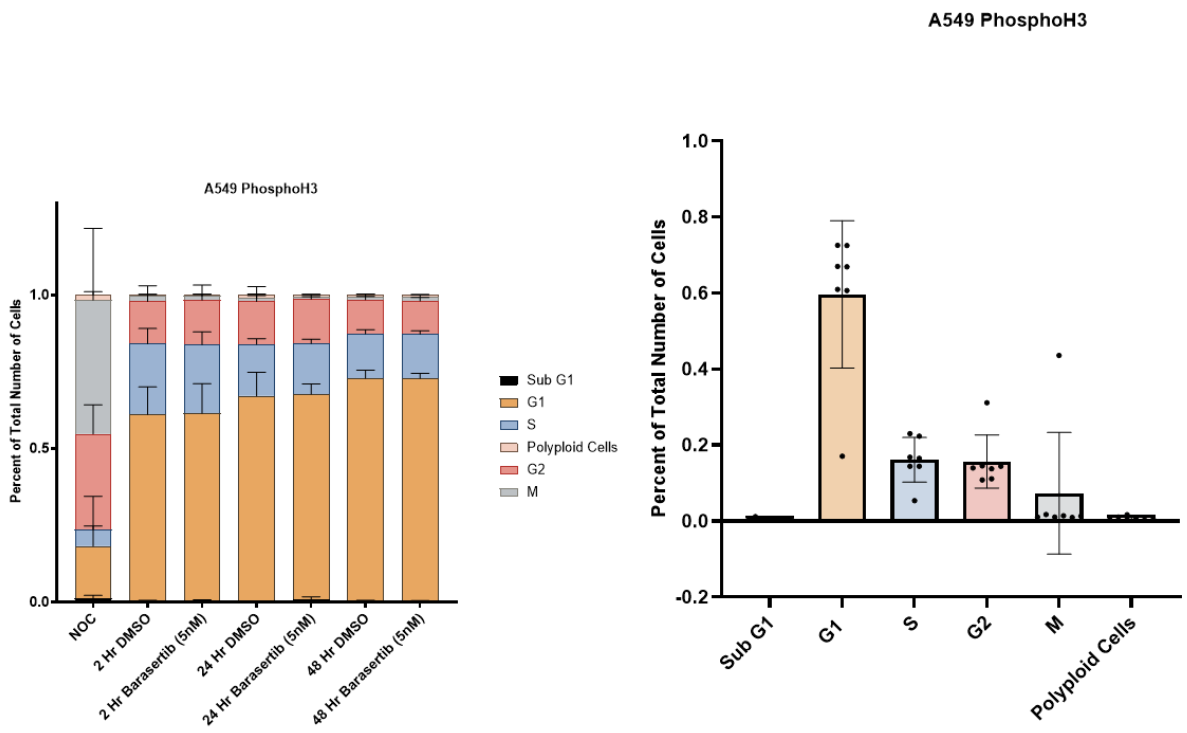
Cell cycle analysis was conducted to investigate the impact of Barasertib on the cell cycle distribution of various HNSCC and NSCLC cell lines. Following treatments, cells were stained for phospho-H3 as a marker of mitosis and propidium iodide to determine DNA content and thus indicate G0, G1, S, G2/M and polyploid cells; FACS then identified cell populations.

Initially, the A549 and H520 cell lines were treated with 5 nM Barasertib or DMSO controls over 2, 24, and 48 hours. No changes in the cell cycle profile could be detected at any time point in either cell line (Figure 4-53). At 5 nM, cell survival is 80 % in A549 and 60 % in H520, so it could be that this dose is too low to induce significant change or that 24 hours is too early to detect change. Nocodazole treatment was included as a positive control for cells synchronised in mitosis.



H520 PH3	T-statistic	p-value
2 Hr DMSO vs 2 Hr Barasertib (5nM)	0.0125	0.9901
2 Hr DMSO vs 24 Hr DMSO	-0.1033	0.9185
2 Hr DMSO vs 24 Hr Barasertib (5nM)	-0.0926	0.9269
2 Hr DMSO vs 48 Hr DMSO	-0.0752	0.9406
2 Hr DMSO vs 48 Hr Barasertib (5nM)	-0.0202	0.9841
2 Hr Barasertib (5nM) vs 24 Hr DMSO	-0.1146	0.9096
2 Hr Barasertib (5nM) vs 24 Hr Barasertib	-0.1032	0.9186
2 Hr Barasertib (5nM) vs 48 Hr DMSO	-0.0859	0.9322
2 Hr Barasertib (5nM) vs 48 Hr Barasertib	-0.0318	0.9748
24 Hr DMSO vs 24 Hr Barasertib (5nM)	0.0028	0.9978
24 Hr DMSO vs 48 Hr DMSO	0.0195	0.9846
24 Hr DMSO vs 48 Hr Barasertib (5nM)	0.0782	0.9383
24 Hr Barasertib (5nM) vs 48 Hr DMSO	0.0156	0.9876
24 Hr Barasertib (5nM) vs 48 Hr Barasertib	0.0701	0.9447
48 Hr DMSO vs 48 Hr Barasertib (5nM)	0.0535	0.9577

Figure 3-30: ***H520 cell cycle distribution 2-, 24- and 48-hours following* treatment *with 5 nM Barasertib.*** NSCLC cells (1-2 x 10^5) were seeded per 90 mm^3 dish and harvested for FACS analysis at 24-, 48-, and 72-hours post-irradiation. Cells were washed, dislodged with trypsin, pooled, and centrifuged at 1200 RPM. After washing, they were resuspended in 100% methanol and stored at -20°C. For staining, cells were incubated with S10 p-Histone 3 primary antibody followed by Alexa 488 secondary antibody, then stained with propidium iodide (PI)/RNAse A solution. Flow cytometry analysis was conducted using FlowJo™ software, with cell populations gated based on PI intensity to identify G1, S, G2-M, mitotic, and polyploid populations. Doublets were excluded by plotting FL3-Area vs. FL3-Width. Data points represent mean cell cycle phase distribution +/- S SD (N= ≥3).



A549 PH3	T-statistic	p-value
2 Hr DMSO vs 2 Hr Barasertib (5nM)	0.0226	0.9822
2 Hr DMSO vs 24 Hr DMSO	-0.0172	0.9864
2 Hr DMSO vs 24 Hr Barasertib (5nM)	-0.0156	0.9877
2 Hr DMSO vs 48 Hr DMSO	-0.0196	0.9845
2 Hr DMSO vs 48 Hr Barasertib (5nM)	-0.0241	0.9809
2 Hr Barasertib (5nM) vs 24 Hr DMSO	-0.0387	0.9694
2 Hr Barasertib (5nM) vs 24 Hr Barasertib	-0.0372	0.9706
2 Hr Barasertib (5nM) vs 48 Hr DMSO	-0.0401	0.9682
2 Hr Barasertib (5nM) vs 48 Hr Barasertib	-0.0447	0.9647
24 Hr DMSO vs 24 Hr Barasertib (5nM)	0.0016	0.9987
24 Hr DMSO vs 48 Hr DMSO	-0.0031	0.9976
24 Hr DMSO vs 48 Hr Barasertib (5nM)	-0.0074	0.9942
24 Hr Barasertib (5nM) vs 48 Hr DMSO	-0.0046	0.9964
24 Hr Barasertib (5nM) vs 48 Hr Barasertib	-0.0089	0.9929
48 Hr DMSO vs 48 Hr Barasertib (5nM)	-0.0041	0.9967

Figure 3-31: ***A549 cell cycle distribution 2-, 24- and 48-hours following* treatment *with 5 nM Barasertib.*** NSCLC cells (1-2 x 10^5) were seeded per 90 mm^3 dish and harvested for FACS analysis at 24-, 48-, and 72-hours post-irradiation. Cells were washed, dislodged with trypsin, pooled, and centrifuged at 1200 RPM. After washing, they were resuspended in 100% methanol and stored at -20°C. For staining, cells were incubated with S10 p-Histone 3 primary antibody followed by Alexa 488 secondary antibody, then stained with propidium iodide (PI)/RNAse A solution. Flow cytometry analysis was conducted using FlowJo™ software, with cell populations gated based on PI intensity to identify G1, S, G2-M, mitotic, and polyploid populations. Doublets were excluded by plotting FL3-Area vs. FL3-Width. Data points represent mean cell cycle phase distribution +/- S SD (N= ≥3).

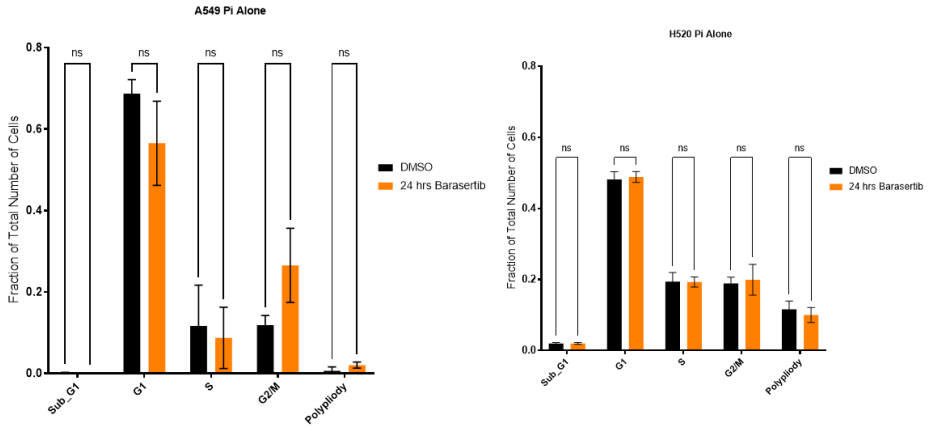
3.2.8.2 A549 and H520 do not exhibit polyploidy and an increased G2M fraction compared to H460 cell lines when treated with Barasertib using PI-alone staining.

The A549 cells exhibited non-significant reductions in the G1 fraction (p = 0.0.209) and S-phase fraction (p=0.0.835) and non-significant increases in the G2/M fraction (p=0.209) and polyploidy (p=0.209) when exposed to 10nM of Barasertib for 24 hours. (Figure 4-38). When analysing the H520 cell line, there was no significant increase in the G2/M fraction size and a decrease in polyploidy (Figure 4-38).

The H520 cell line's response to Barasertib, specifically its lack of increase in the G2/M fraction size and polyploidy, may be attributed to inherent differences in its cell cycle checkpoints, su*scep*tibility to the drug or its ability to undergo endoreduplication. However, it is essential to acknowledge that a 72-hour live cell imaging assay was not performed on the H520 cell line, which could have provided valuable information regarding its ability to slip over time upon exposure to Barasertib.

Analysing the H520 cells poses specific challenges due to their inherent tendency to stack on each other and form cell clumps over time. This clumping behaviour can impede the observation of cellular events and make accurate analysis more difficult. Consequently, obtaining precise and reliable data from the H520 cell line becomes challenging, potentially leading to limited insights into its response to Barasertib.

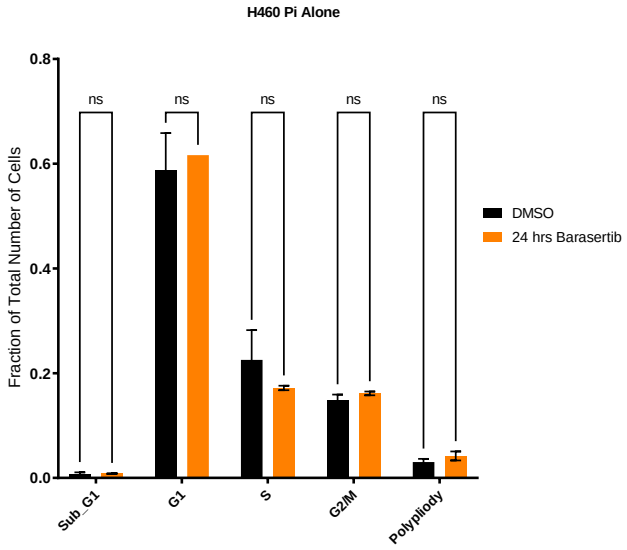
In H460, cells exhibited no reduction in G1 fraction, no increases in the G2/M fraction or polyploidy when exposed to 5 nM of Barasertib for 24 hours (Figure 4-39); this could be explained by the relative resistance of H460 to Barasertib (LD_{50} of 40)



A549	Mean of DMSO	Mean of 24 hrs Barasertib	Difference	P value	SE of difference
Sub_G1	0.001593	0.001445	0.0001479	0.827013	0.0006341
G1	0.6872	0.5651	0.1221	0.124251	0.06290
S	0.1165	0.08730	0.02919	0.707166	0.07234
G2/M	0.1186	0.2655	-0.1468	0.053870	0.05431
Polypliody	0.006452	0.02050	-0.01405	0.116316	0.007031

H520	Mean of DMSO	Mean of 24 hrs Barasertib	Difference	P value	SE of difference
Sub_G1	0.01990	0.01990	-7.000e-006	0.997553	0.002146
G1	0.4815	0.4882	-0.006690	0.686345	0.01540
S	0.1938	0.1927	0.001063	0.952751	0.01686
G2/M	0.1889	0.1991	-0.01026	0.724849	0.02717
Polypliody	0.1160	0.1001	0.01589	0.429791	0.01811

Figure 3-32: ***H520 and A549 cell cycle distribution 2 and 24-hours following* treatment *with 5 nM Barasertib.*** NSCLC cells (1-2 x 10^5) were seeded per 90 mm^3 dish and harvested for FACS analysis at 24-, 48-, and 72-hours post-irradiation. Cells were washed, dislodged with trypsin, pooled, and centrifuged at 1200 RPM. After washing, they were resuspended in 100% methanol and stored at -20°C. For staining, cells were stained with propidium iodide (PI)/RNAse A solution. Flow cytometry analysis was conducted using FlowJo™ software, with cell populations gated based on PI intensity to identify G1, S, G2-M, mitotic, and polyploid populations. Doublets were excluded by plotting FL3-Area vs. FL3-Width. Data points represent mean cell cycle phase distribution +/- S SD (N= ≥3).Data points represent mean cell cycle phase distribution +/- SD (N= ≥3). Statistical testing: 2 tailed unpaired T.test where ns is non-significant, * p = <0.05 ** p = <0.001 *** p = <0.0001 and **** p = <0.00001



H460	Mean of DMSO	Mean of 24 hrs Barasertib	Difference	P value	SE of difference
Sub_G1	0.007635	0.008178	-0.0005427	0.823952	0.002237
G1	0.5880	0.6164	-0.02843	0.625555	0.05246
S	0.2255	0.1718	0.05363	0.295458	0.04242
G2/M	0.1484	0.1615	-0.01304	0.213393	0.008284
Polypliody	0.03046	0.04207	-0.01161	0.165135	0.006355

Figure 3-33: ***H460 cell cycle distribution 2 and 24-hours following* treatment *with 5 nM Barasertib.*** NSCLC cells (1-2 x 10^5) were seeded per 90 mm^3 dish and harvested for FACS analysis at 24-, 48-, and 72-hours post-irradiation. Cells were washed, dislodged with trypsin, pooled, and centrifuged at 1200 RPM. After washing, they were resuspended in 100% methanol and stored at -20°C. For staining, cells were stained with propidium iodide (PI)/RNAse A solution. Flow cytometry analysis was conducted using FlowJo™ software, with cell populations gated based on PI intensity to identify G1, S, G2-M, mitotic, and polyploid populations. Doublets were excluded by plotting FL3-Area vs. FL3-Width. Data points represent mean cell cycle phase distribution +/- S SD (N= ≥3).Data points represent mean cell cycle phase distribution +/- SD (N= ≥3). Statistical testing: 2 tailed unpaired T.test where ns is non-significant, * p = <0.05 ** p = <0.001 *** p = <0.0001 and **** p = <0.00001

3.3 Discussion

3.3.1 Radiosensitisation potential of Ly3295668 and Barasertib in HNSLC cell lines

Barasertib, formerly AZD1152, is a potent and selective inhibitor of Aurora B kinase (Schwartz et al., 2013). Upon administration, Barasertib is converted into its active form, Barasertib-hydroxyquinazoline-pyrazole-aniline (Barasertib-HQPA), which acts as a reversible ATP-competitive inhibitor of Aurora B. By targeting Aurora B, Barasertib disrupts its enzymatic activity, leading to chromosome misalignment and the termination of cell division, resulting in the formation of polyploid cells. Consequently, the viability of cancer cells is significantly reduced, and apoptosis, a process of programmed cell death, is induced (Helfrich et al., 2016). Inhibition of *AURKB* also triggers mitotic slippage and tetraploidisation (Marxer et al., 2014).

We were able to demonstrate the potential of both agents as radiosensitisers as well as drugs that could be used as monotherapy. Although this thesis focuses mainly on Barasertib, we initially began with Ly3295668 (an *AURKA* inhibitor), which demonstrated a preference for increased radiosensitisation in the cell, which were *p53* wild type with similar results to alisertib in work shown previously by the Bryant lab.

Barasertib monotherapy did not preferentially increase toxicity in the *p53* NSCLC wild-type cells over *p53* mutant lines, with similar results in the HNSCC cell lines. This is in contrast to the findings of Marxer et al., where they found *P53* mutant lines

demonstrating increased sensitivity to Barasertib; in our work, the cell lines most sensitive to Barasertib were the A549 and H520 lines, which are both *P53* wild type. It must be noted that the H322 cell line was also quite sensitive and is a *p53* mutant. There were highly significant reductions in two HNSCC cell lines (SCC89 and UPCI-SCC72) where the *p53* status was different, leading to uncertainty around the relevance of *p53* status in determining the response to *AURKB* inhibition.

Radiosensitisation due to Barasertib was noted in both *p53* wild-type and null lines, with slightly greater DER values in the wild-type lines. This contradicts what has been seen in another study, where much more significant cell death was seen in *p53* null lines (A549 treated with cyclic pifithrin-α, a chemical *p53* inhibitor) than in the *p53* wild-type lines (Tao et al., 2008b). Notable differences in our work include that cells were only pretreated for two hours compared to a twenty-four-hour pretreatment in Tao's study, which led to enhanced cell killing at that time frame. Also, in Tao's work, a more comprehensive range of native *p53* null and mutant lines was not used compared to *p53* wild-type lines, which could have yielded less significant results. Barasertib did not radiosensitise cell any HNSCC cancer cell lines, regardless of which dose was used; we think this was due to the cells' low clonogenic survival when exposed to Barasertib alone.

3.3.2 There is a need to identify a better target to demonstrate Barasertib inhibition.

Despite the apparent effects on the HNSCC and NSCLC cell lines, we could not show Barasertib inhibiting the Thr232 region of *AURKB* at the doses where there was cell death, specifically in the NSCLC cell lines.

While We demonstrated that *p53* is upregulated by 25 nM Barasertib, indicating at least in H460 that Barasertib has a functional effect, we also used cells with null or mutant *p53* expression; we need to find a suitable target in those cell lines. The Phospho-H3 blots, were inconsistent, and we considered it an unreliable way to determine the dose of Barasertib that was effective in inhibiting *AURKB*.

Nocodazole is a microtubule-depolymerizing agent, microtubules are important components of the cytoskeleton and play a crucial role in various cellular processes, including cell division. Nocodazole is used to synchronize cells at a specific stage of the cell cycle, typically the G2/M phase. This synchronization allows for the analysis of phosphorylation events or changes in protein expression at specific points in the cell cycle.

We feel that using nocodazole release is possibly one of the main problems leading to the lack of inhibition. During the spindle assembly checkpoint, *AURKB* plays a critical role in monitoring the attachment of chromosomes to the mitotic spindle. If a chromosome is not attached correctly, the spindle assembly checkpoint prevents the cell from progressing further in the cell cycle until all chromosomes are correctly aligned and attached. *AURKB* helps to correct improper attachments and stabilise proper attachments through the phosphorylation of target proteins.

Several authors have noted that *AURKB* inhibition may not be seen during nocodazole mediated mitotic arrest (Biggins and Murray, 2001; Ditchfield et al., 2003b; Hauf et al., 2003). *AURKB* acts as a sensor for lack of tension at the microtubules, which may not be present using nocodazole treatment; tension is seen in cells treated with Taxol's, which act as microtubule stabilisers at varying levels, leading to *AURKB* activity. Loss of Aurora-B function fails to retain checkpoint

proteins at the kinetochore and an override of the Taxol-sensitive, tension-sensing spindle checkpoint (Tao et al., 2008b). Using Taxol-treated cells could lead to better results on the Western blots, but that would require optimisation.

3.3.3 Chemotherapy combination work.

We felt it was interesting to see the potential activity of Barasertib in combination with other chemotherapy agents, as this could be a potential strategy in the clinics. Barasertib did not demonstrate significant synergism with any of the agents tested, but combinations showed the potential for enhanced radiosensitisation compared to Barasertib alone, as shown in the IR studies with Barasertib and 5FU and Barasertib and Cisplatin.

One reason for the lack of cell killing could be the need to use higher doses of chemotherapy in the combination treatments, but the cell survival was very low when the H460s were exposed to Barasertib at 25nM and the chemotherapy original LD_{50} values, leading to the slight adjustments in the chemotherapy doses.

Another issue was not investigating any schedule dependency between Barasertib and the chemotherapy agents; for example, 5 Fluorouracil terminates the cell cycle at the S-phase and prevents tumour cells from entering the M-phase, which may then abrogate the cytotoxic effect of Barasertib a similar issue was noted by Takahiro et al. although they were using Cytarabine (Yamauchi et al., 2013).

The combination of Barasertib and chemotherapy does not significantly reduce cell survival in the NSCLC and HNSCC cancer cell lines. However, in most cases, with

one ex*cep*tion, it was no worse, which is an important finding showing that Barasertib has the potential to replace platinum agents in clinical trials, which are the cornerstone of combination therapy regimes in the chemoradiotherapy and metastatic setting.

This would be a significant change in the management of NSCLC and HNSCC; therefore, further work needs to be done with more confident optimisation of the chemotherapy dosing, timing, and testing in-vivo before this could be taken to a phase one clinical trial. Adding Barasertib to combination chemotherapy did not demonstrate significant survival in any cell line tested; this will spare any further unnecessary testing of triple therapy combination, which may provide no clinical benefit and only prove toxic to patients.

3.3.4 Combination radiosensitisation work.

Barasertib and 5FU demonstrated significant radiosensitisation compared to the other radiotherapy combinations. It should be noted that the survival of cells in the Barasertib and Fluorouracil combination was higher than in cells with fluorouracil alone.

Yamauchi et al. investigated the combination of Barasertib and Cytarabine (which acts similarly to 5FU) in HL-60 cells and found that the cytotoxicity of the combination was more significant than Cytarabine alone. While the lack of cell death compared to 5FU alone could be explained by the need to increase the 5FU dose or the need to synchronise the timing of drug administration to the cells, there was still significant radiosensitisation; this could be because the cells were being targeted in

multiple phases of the cell cycle. Another finding that would be interesting to explore was whether the DNA uptake of 5FU was affected by Barasertib. Yamauchi et al. showed that cytarabine uptake was unaffected by Barasertib-HQPA, which could explain the enhanced cell effects of the combination plus IR, another insult to DNA.

3.3.5 Live cell imaging assays.

Barasertib has activity against *AURKB* both in monotherapy and in addition to IR; therefore, we needed to conduct assays to assess the cellular outcomes in both scenarios. The initial assays conducted between 24 and 36 hours were not long enough to capture the effects of Barasertib, leading to early uncertainty around the effects of its activity both as monotherapy and in combination with IR. However, for monotherapy, extended analysis to 72 hours provided helpful insight.

Monotherapy

Barasertib use led to several cellular outcomes, but one of the most significant effects was its tendency to cause increased levels of slippage in those cells which were more sensitive to Barasertib (SCC89, UPCI-SCC72, A549 and H520) relative to the resistant cells (B22, *FN*B6 and H460).

Aurora kinase B is known to directly phosphorylate and activate cyclin B1, which activates the cyclin-dependent kinase 1 (*CDK*1), a vital cell cycle regulator (Trakala et al., 2013). The activation of *CDK*1 by cyclin B1 is required to transition the cell cycle from G2 to M phase and initiate mitosis (Jang et al., 2016). Thus, inhibition of

Aurora kinase B could lead to a decrease in the activation of *CDK*1 and the subsequent arrest of the cell cycle at the G2/M checkpoint (Van Horn et al., 2010).

In addition to its direct effects on Cyclin B1 and *CDK*1, Aurora kinase B also indirectly regulates the expression of cyclin B1 and CDC20 through several downstream signalling pathways. For example, Aurora kinase B is known to activate the Anaphase Promoting Complex/Cyclosome (APC/C), a multi-subunit E3 ubiquitin ligase critical in regulating the cell cycle (Willems et al., 2018). The APC/C complex targets cyclin B1 and CDC20 for degradation, which is required to transition from metaphase to anaphase during mitosis (Pesin and Orr-Weaver, 2008). Inhibition of Aurora kinase B can lead to decreased activation of APC/C, preventing the degradation of cyclin B1 and CDC20 and thus preventing metaphase anaphase transition (Musacchio and Salmon, 2007).

Degradation of cyclin B1 during prolonged mitotic arrest is believed to trigger mitotic slippage through an unclear and likely complex mechanism (Lok et al., 2020). We saw the increased levels of slippage on live cell imaging in cells more sensitive to Barasertib and felt there could be a link between *AURKB* inhibition, Cyclin B1 decreased activity and increased levels of slippage.

If cells slipped, they eventually died in mitosis regardless of how often they underwent slippage. Some cells slipped on three occasions, but we assumed they would also die in subsequent mitosis, although this was not demonstrated. Interestingly, at lower concentrations (5nM), the A549 cells showed a propensity to divide first before both daughters died in mitosis around the same time rather than the “mother” cells dying in mitosis; further work could be done to see if this was replicated in the SCC89 and UPCI-SCC72 cells at 1nM.

Barasertib plus IR

No other published data has looked at the combination of Barasertib and IR in NSCLC cell lines. We saw that in H460 cells (between 24-36 hr), cells with IR + 50 nM Bara had significantly higher levels of slippage than IR alone. This was not the case in other cell lines and at 25 nM Bara, but a trend was observed. In these cases, the time-point was likely too soon to assess the effects of combining Barasertib with radiotherapy. More extended assays would help investigate Barasertib activity with IR at lower doses and in other cell lines, as we know radiosensitisation occurs (Figure 3-4).

We would have liked to have done a 0–72-hour assay looking at the effect of Barasertib and IR in the H460 and H1299 cells, similar to when Barasertib was used as monotherapy.

3.3.6 Western blot Assays.

There is a relationship between Cyclin B1, CDC20 and *AURKB* in the SAC, which governs the entry of cells into later stages of mitosis. In addition, rapid degradation of Cyclin B1 without activation of separase (to ensure proper exit from mitosis) is thought to trigger mitotic slippage. We hypothesised that the slippage we observed could be due to Barasertib-induced degradation of Cyclin B. However, no difference in Cyclin B1 level was seen in any cell line up to 24 h post 10 nM Barasertib. We also looked at CDC20 levels as the APC/CDC20 complex promotes the degradation of Cyclin B1 during the mitotic slippage. No change in CDC20 levels was seen. Thus, the established route of mitotic slippage may not be how Barasertib works.

Alternatively, as seen in live cell imaging, we have examined at a time point which was too early.

3.3.7 FACS.

Barasertib increases polyploidy and the G2/M fraction in the sensitive HNSCC and NSCLC cell analysis. Polyploidy is consistent with mitotic slippage. The observation of G2/M arrest could be real or could be an artefact of slippage, as discussed above.

A functional assay we would have liked to perform would be a metaphase spread to assess the polyploidy levels in these cells. This would have shown increased chromosome numbers in the cells that underwent slippage, confirming our findings on FACS.

3.4 Future Work

3.4.1 Dose Refinement

The variability in how different cell lines respond to treatment highlights the need to refine dosing strategies. Future studies should focus on identifying and validating biomarkers that can predict how sensitive a tumour is to Ly3295668 and Barasertib. By doing so, we can move towards more personalized treatments, allowing doctors to tailor dosing regimens based on the unique molecular profile of each NSCLC tumour.

3.4.2 Mechanistic Insights

The lack of additive effects when inhibiting both AURKA and AURKB signals that we need a deeper understanding of the underlying pathways leading to their activation. We'd expect that targeting two key proteins involved in cell division would have an additive or even synergistic effect, especially if both play crucial roles in tumour growth. However, the absence of this effect implies that AURKA and AURKB might not be working independently. therapeutic targets, giving us better options for treatment.

3.4.3 Clinical Translation

The fact that Ly3295668 and Barasertib show potential to enhance the effects of radiotherapy in p53 wild-type NSCLC cell lines makes a strong case for clinical trials.

Future research should focus on bringing these preclinical findings to the clinic, evaluating how Aurora kinase inhibitors perform alongside radiation therapy. Particular attention should be given to tumour subtypes that are more sensitive to radiation, especially those with intact p53, to identify which patients might benefit most from these targeted treatments.

3.4.4 Extended Radiosensitisation Studies

There’s still much to learn about the long-term effects of combining radiation with kinase inhibitors, including whether these combinations lead to delayed tumour cell death or sustained anti-tumour effects. Future studies should look at the extended impact of radiosensitisation on cellular fate. A better grasp of this prolonged window could help refine treatment schedules.

3.5 Conclusion

This chapter demonstrates the efficacy of Ly3295668 and Barasertib as AURK inhibitors with potential radiosensitising effects in NSCLC. The relationship between *p53* status and radiosensitivity highlights the need for personalized approaches in targeting Aurora kinases. Although Barasertib showed limited success in combination with chemotherapeutic agents, it remains a viable candidate for further exploration in radiosensitisation. The use of siRNA knockdowns to probe the function of *AURKB* in radiation response offers valuable mechanistic insights, which could inform future therapeutic strategies. Crucial findings on the effects of Barasertib in NSCLC and HNSCC cell lines, with a focus on mitotic slippage, radiosensitisation, and resistance mechanisms were also investigated. The results emphasize Barasertib's potential as a therapeutic agent, particularly in combination with radiation, and underscore the need for further molecular studies to fully understand the mechanisms driving its cytotoxicity. While Barasertib shows promise in Barasertib-sensitive cells, overcoming resistance in refractory cell lines remains a significant challenge for future research.

4 Evaluation of Barasertib, Alisertib and Ly3295668 as radiosensitising agents in HNSCC cell lines.

4.1 Introduction, Aims and Hypothesis.

Aurora kinases, particularly *AURKA* and *AURKB*, play crucial roles in the regulation of mitosis and are pivotal in maintaining genomic stability during cell division. *AURKA*, primarily associated with the early stages of mitosis, facilitates the assembly and stabilization of microtubules, which are essential components of the cell's cytoskeleton and mitotic spindle (Nikonova et al., 2013). This kinase ensures the proper alignment and attachment of chromosomes on the spindle, which is vital for accurate chromosome segregation. Furthermore, *AURKA* is critical for centrosome maturation and separation, both of which are necessary for proper spindle assembly and function (Willems et al., 2018). Dysregulation of *AURKA* can result in abnormal cell division, contributing to tumorigenesis in various cancers, including head and neck cancer (HNC) (Lo Iacono et al., 2011; Mou et al., 2021).

AURKB, on the other hand, is primarily active during the later stages of mitosis, particularly in the segregation of sister chromatids (Yuan et al., 2009). A key component of the chromosomal passenger complex (CPC), *AURKB* regulates critical processes such as chromosome condensation, attachment to the spindle, and the proper segregation of chromosomes (Shuda et al., 2009). During anaphase to cytokinesis, *AURKB* relocates to the spindle midzone and midbody, where it plays a

crucial role in completing cell division (Shaalan et al., 2021). Overexpression of *AURKB* has been linked to aneuploidy and genomic instability, processes that drive tumour development, invasion, and metastasis in various cancers, including HNC (Borah and Reddy, 2021). The integrity of these mitotic processes is also known to influence the sensitivity of cancer cells to radiotherapy and chemotherapy, making *AURKB* a potential target for enhancing treatment efficacy (Hendry and West, 1997).

Aurora kinase B (*AURKB*) is a key mitotic regulator that plays a critical role in chromosome alignment, spindle assembly, and cytokinesis during cell division. In the context of head and neck squamous cell carcinoma (HNSCC), *AURKB* has garnered significant attention due to its overexpression in various cancers, including HNSCC, where it is associated with poor prognosis. *AURKB*'s overexpression in HNSCC is linked to increased cellular proliferation, aneuploidy, and resistance to apoptosis, contributing to the aggressive nature of this cancer. The kinase's role in ensuring proper chromosome segregation means that its dysregulation can lead to genomic instability, a hallmark of cancer progression.

In HNSCC, *AURKB* overexpression has been correlated with advanced tumour stage, increased lymph node metastasis, and decreased overall survival. Studies have shown that *AURKB* promotes the survival and proliferation of cancer cells through its involvement in the G2/M phase transition of the cell cycle, making it a critical player in the maintenance of malignant phenotypes in HNSCC. Additionally, *AURKB* is implicated in the development of therapeutic resistance, particularly in response to chemotherapeutic agents like cisplatin. The kinase's ability to regulate key cell cycle checkpoints allows cancer cells to evade the cytotoxic effects of these treatments, contributing to treatment failure and disease recurrence.

Given its crucial role in HNSCC pathogenesis, *AURKB* has emerged as a potential therapeutic target. Inhibitors of *AURKB*, such as Barasertib and AZD1152, have shown promise in preclinical models by inducing mitotic defects and apoptosis in HNSCC cells. These inhibitors work by disrupting the normal function of *AURKB*, leading to cell cycle arrest and cell death, especially in cells with high *AURKB* expression. The therapeutic targeting of *AURKB* offers a promising strategy for improving treatment outcomes in HNSCC, particularly for patients with advanced or recurrent disease who are less responsive to conventional therapies .

This chapter of this thesis will test whether *AURKB* with Barasertib can enhance IR or chemotherapy response in H&N cancer. We investigate whether it is disruption of the mitotic function of *AURKB* that leads to Barasertib effects either alone or in combination with IR, live cell imaging and cell cycle profiling using *PH3*/PI staining and FACS were used in HNSCC cell lines.

The hypotheses of this chapter are:

1. Barasertib disrupts cell cycle progression, leading to increased cell death in sensitive NSCLC and HNSCC cell lines.
2. Barasertib increases the incidence of abnormal mitotic events in NSCLC and HNSCC cells, leading to increased cell death in sensitive cell lines.
3. Following irradiation, Barasertib treatment will increase mitotic aberrance in NSCLC cells, leading to increased cell death.
4. Barasertib and Ly3295668 will enhance the IR killing of NSCLC *cell lines* .
5. Barasertib will enhance the IR killing of HNSCC *cell lines* .

The aims of this chapter are:

1. To assess the effect of Barasertib alone and IR on cell cycle progression, including mitotic transit, in NSCLC and HNSCC cell lines.

2. To assess mitotic aberrance following Barasertib alone and in combination with IR in NSCLC and HNSCC cell lines.

3. Establish an inhibitory dose of Ly3295668 that is *AURKA* specific and minimally toxic in NSCLC cell lines, then test the ability of Ly3295668 to radiosensitise.

4. Establish an inhibitory dose of Barasertib that is *AURKB* specific and minimally toxic in NSCLC and HNSCC cell lines, then test whether Barasertib can radiosensitive or chemo-sensitise NSCLC and HNSCC cancer cell lines .

5. Gain preliminary data which can be used in writing a phase one clinical trial protocol looking a combination Barasertib and IR (Appendix 7.3)

4.2 Results.

4.2.1 Barasertib

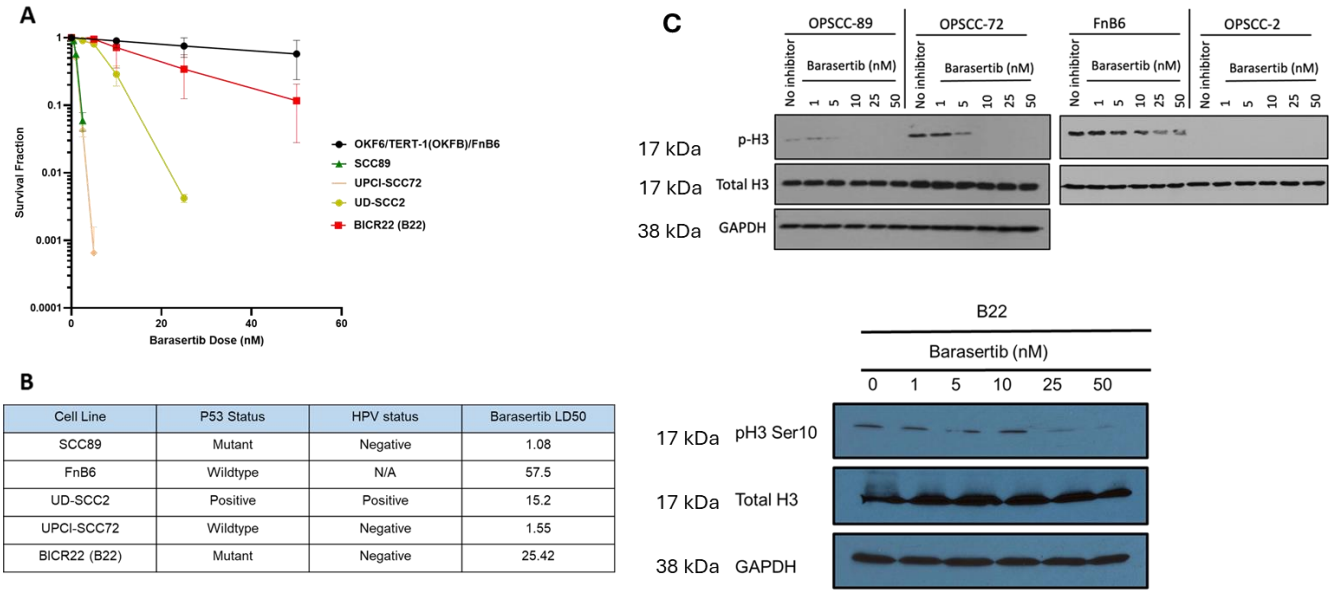
4.2.1.1 Barasertib therapy displays significant reductions in survival in HNSCC cell lines.

Six HNSCC cell lines were exposed to increasing doses of Barasertib, and the survival fraction was determined by clonogenic assay (Figure 3.5) to investigate toxicity. The responses to all the cell lines varied; UPSI-SCC072 and SCC089 were the most sensitive cell lines using low doses of Barasertib with LD_{50} doses of 1.55 and 1.08nM, respectively. The *FN*B6 cell line, an immortalised normal oral cell line (Cathie Garnis, 2015), was least sensitive with an LD_{50} of 57.5nM, followed by B22 and UD-SCC2. The survival in the HNSCC cell lines varied markedly; the UPCI-SCC72 and the SCC89 cell lines at 5nM of Barasertib demonstrated approximately a 5% survival, with no cells surviving at 25nM.

The ability of Barasertib to inhibit *AURKA*, *AURKB* and *AURKC* was not investigated in the HNSCC cell lines due to the difficulty of getting consistent results in the above NCSLC lines. Therefore, using western blotting, the ability of Barasertib to inhibit Phopho-H3 was investigated in each cell line (Figure 3.6). After two hours of treatment with Barasertib, partial inhibition was seen in the UPCI-SCc72 and SCC89 cell lines at 5nM, with full inhibition at 10nM. The BICR22 (B22) and *FN*B6 cell lines demonstrated partial inhibition at 25 and 50nM concentrations. The OPSCC2 cell

lines did not demonstrate *PH3* expression at any concentration, including the DMSO control.

Considering the monotherapy toxicity data, we used 25 nM in the relatively Barasertib-resistant cell lines *FN*B6 and BICR22 (B22), as we thought using doses near the LD50 values would allow us to observe radiosensitisation. We then used 1nM in UPCI-SCC72 and SCC89 cells to see if we could observe radiosensitisation.



B

Cell Line	P53 Status	HPV status	Barasertib LD50
SCC89	Mutant	Negative	1.08
FnB6	Wildtype	N/A	57.5
UD-SCC2	Positive	Positive	15.2
UPCI-SCC72	Wildtype	Negative	1.55
BICR22 (B22)	Mutant	Negative	25.42

Figure 4-1: **Barasertib monotherapy in HNSCC cell lines and Western Blots of Phospho H3 in HNSCC cell lines** Survival fraction was calculated using clonogenic assay under continuous exposure to the *AURKB* inhibitor Barasertib. Data points represent the mean survival fraction normalised to untreated control +/- SD (N= 3). B: Table showing the genetic type of each cell line. Representative western blot results for pan p-AURK, *AURKA* (total B) and GAPDH in protein extracts from OPSCC89, OPSCC72, *FN*B6, OPSCC2 and B22/BICR22 cells arrested overnight with 100 ng/ml Nocodazole (Noc) and released into increasing concentrations of Barasertib the OPSCC-89, OPSCC-72, *FN*B6 and OPSCC-2 assays were done with the help of Dr. Polly Greaves.

4.2.1.2 Barasertib plus IR does not display significant reductions in survival in HNSCC cell lines.

Like the NSCLC cell lines, Barasertib was added to IR, and the effect of the combination was investigated. Barasertib was given 2 hours before irradiation and was present continuously throughout the colony survival assay (Figure 3-8).

The analysis of mean dose enhancement ratios (DER) for different combinations of Barasertib with IR revealed no evidence of radiosensitisation in any of the HNSCC cell lines (Table 3-3).

The doses of Barasertib in UPCI-SCC72 and SCC89 were notably lower than those used in SCC2, BICR22, and *FN*6B cell lines. This was due to the low LD_{50} values observed when using Barasertib alone in UPCI-SCC72 and SCC89 cell lines.

*FN*B6 cell lines provided valuable insights into Barasertib's behaviour in "normal tissue" compared to cancer cells. It was hypothesised that the DER would not significantly increase even at higher doses of IR in these "normal tissue" cell lines. The results validated this hypothesis, as the DER remained relatively stable with values of 0.983, 0.882, and 0.856 at IR doses of 1, 2, and 4Gy, respectively.

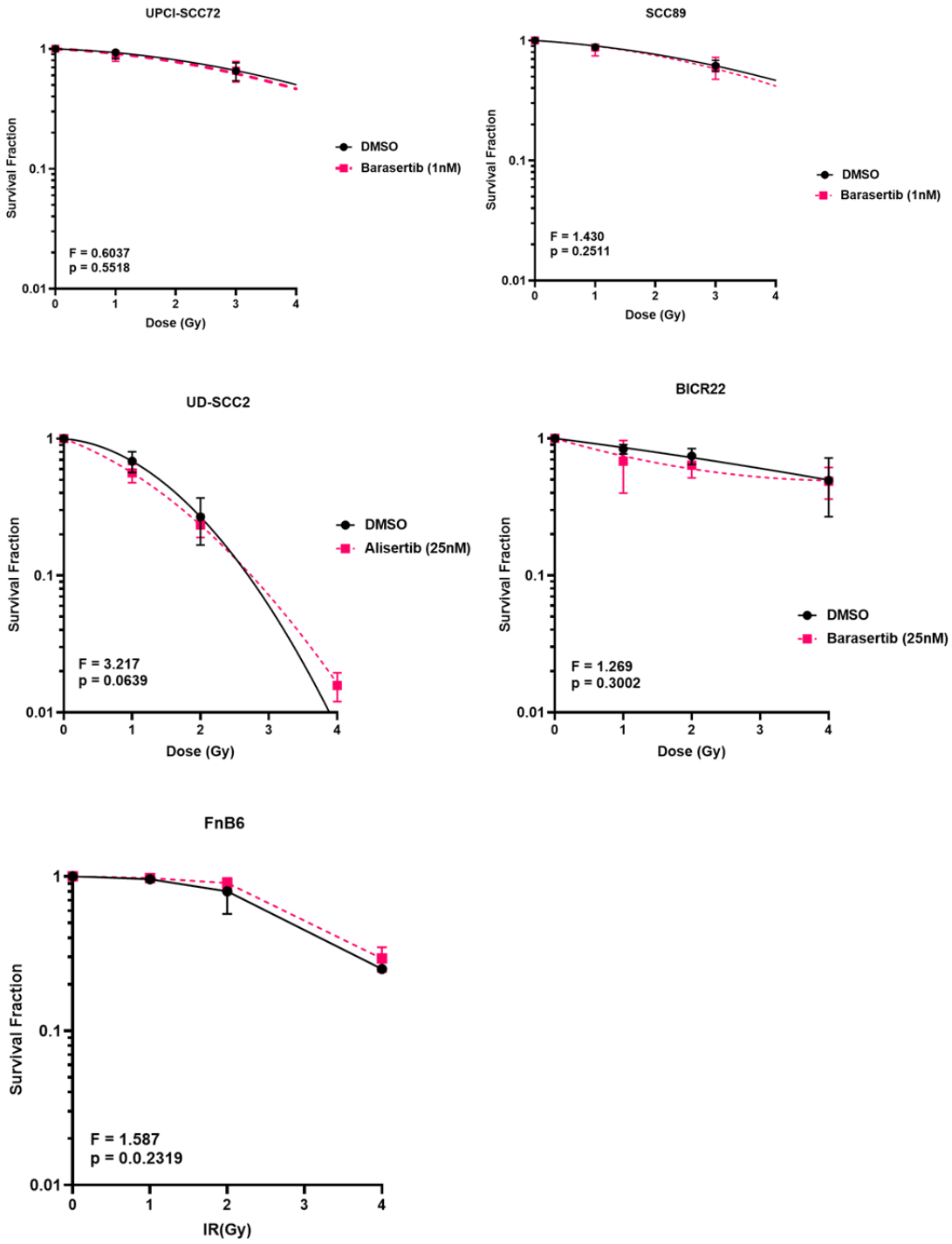


Figure 4-2 **Barasertib and IR in HNSCC cell lines** Survival fraction of HNSCC cells after treatment with IR alone or IR in combination with Barasertib; no radiosensitisation was seen in any cell line tested. The survival fraction was calculated using a clonogenic assay. Cells were pre-incubated with Barasertib before irradiation and colony outgrowth under continuous exposure to the *AURKB* inhibitor Barasertib. Data points represent the mean survival fraction normalised to unirradiated control +/- SD (N= ≥3). F-value and p-value derived from the extra sum of squares test.

Cell Line	HNSCC Subtype	DER using 1nM 0Gy	DER using 1nM 1Gy	DER using 1nM 3 Gy	DER using 1nM 5Gy
SCC89	SCC	1	1.006	1.030	1.276
UPCI-SCC72	SCC	1	1.080	1.009	1.133
Cell Line	HNSCC Subtype	DER using 25nM 0Gy	DER using 25nM 1Gy	DER using 25nM 2 Gy	DER using 25nM 4Gy
SCC2	SCC	1	1.216	1.144	0.387
FnB6	"Normal Tissue"	1	0.983	0.882	0.856
B22	SCC	1	1.813	1.305	1.051

SCC89	
	t.Test values at 1nM
3 Gy	0.7820
5 Gy	0.0924
UPCI-SCC72	
	t.Test values at 1nM
3 Gy	0.9329
5 Gy	0.4156
SCC2	
	t.Test values at 25nM
2 Gy	0.6230
4 Gy	0.3541
FnB6	
	t.Test values at 25nM
2 Gy	0.4756
4 Gy	0.3677
B22	
	t.Test values at 25nM
2 Gy	0.2210
4 Gy	0.7446

Table 4-1: **Barasertib DER ratios and t.test values** The DER and t.test values demonstrate the lack of radiosensitisation in any HNSCC line. The survival fraction was calculated using a clonogenic assay. Cells were pre-incubated with Barasertib before irradiation and colony outgrowth under continuous exposure to the *AURKB* inhibitor Barasertib. Data points represent the mean survival fraction normalised to unirradiated control +/- SD (N= ≥3). F-value and p-value derived from the extra sum of squares test.

4.2.1.3 Using Barasertib in combination with chemotherapy demonstrated mainly non-significant reductions in cellular survival in the BICR22 and *FN*B6 cell lines.

There was significant reduction in cell survival when Barasertib alone was added to BICR22 cells (Figure 3-15 and 3-16). For cisplatin and Vinorelbine, no decrease in survival was seen when the LD50- dose was used and there was no sensitisation when Barasertib was added (Figure 3-15). There was no sensitisation when Barasertib to 5FU but e*topo*side and Barasertib demonstrated sensitisation when compared to Barasertib alone (Figure 3-16).

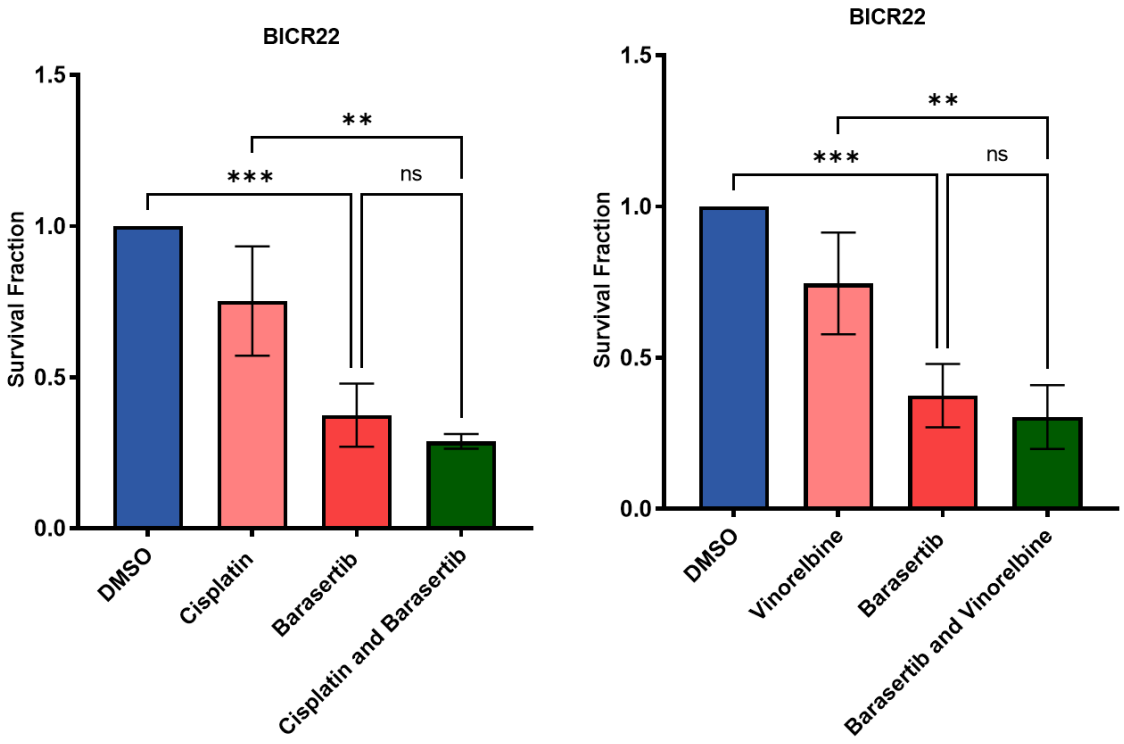


Figure 4-3: Comparison of Barasertib vs Barasertib and chemotherapy (Cisplatin and Vinorelbine) in BICR22 cell lines (n=3) Cells were pre-incubated with either Cisplatin, Vinorelbine or *AURKB* inhibitor Barasertib, cells were left to form colonies for 10-14 days before colony outgrowth under continuous exposure to the Cisplatin, Vinorelbine and/or *AURKB* inhibitor Barasertib. Data points represent the mean survival fraction normalised to DMSO +/- SD (N= ≥3). F-value and p-value derived from the extra sum of squares test. NS (non-statistically significant) denotes p= >0.05, * denotes p= ≤0.05, ** denotes p= ≤0.01, *** denotes p= 0.001 (One-way ANOVA with Dunnett correction for multiple comparisons).

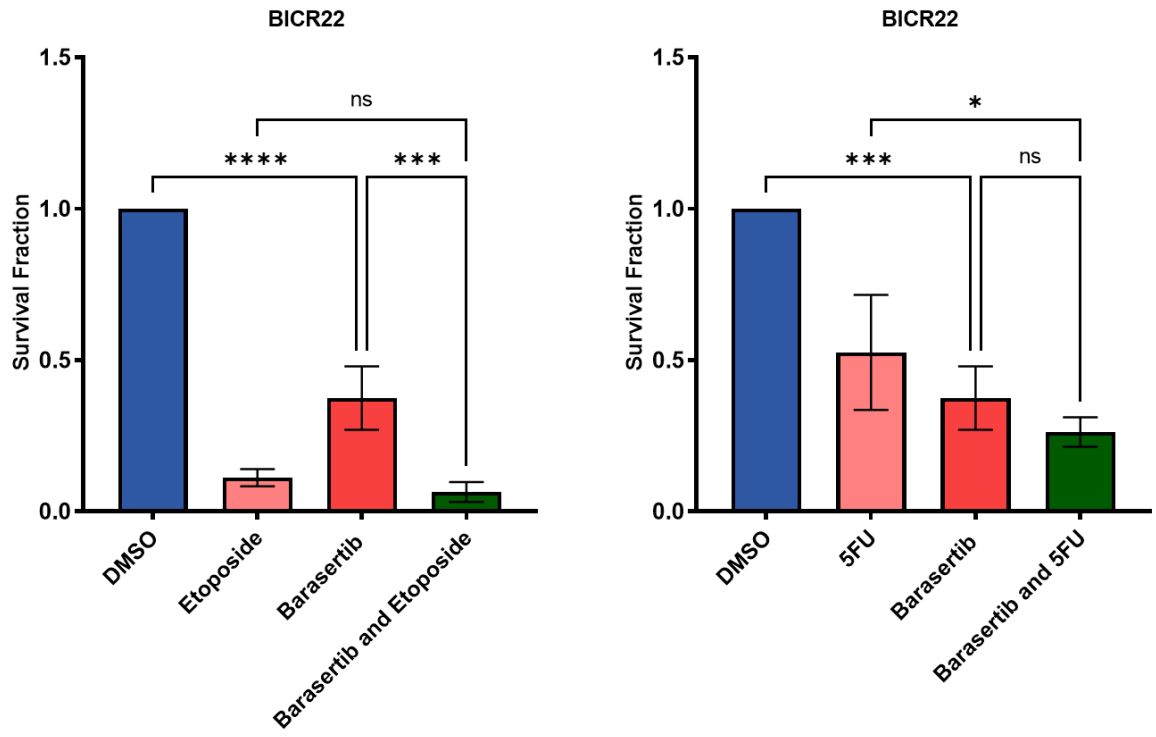


Figure 4-4: Comparison of Barasertib vs Barasertib and chemotherapy (5-FU and E*topo*side) in BICR22 cell lines (n=3). Cells were pre-incubated with either 5FU, Etoposide or *AURKB* inhibitor Barasertib, cells were left to form colonies for 10-14 days before colony outgrowth under continuous exposure to the 5FU, Etoposide and/or *AURKB* inhibitor Barasertib. Data points represent the mean survival fraction normalised to DMSO +/- SD (N= ≥3). F-value and p-value derived from the extra sum of squares test. NS (non-statistically significant) denotes p= >0.05, * denotes p= ≤0.05, ** denotes p= ≤0.01, *** denotes p= 0.001 (One-way ANOVA with Dunnett correction for multiple comparisons).

In *FN*B6 cells, Barasertib did induce a significant decrease in survival. Neither Cisplatin nor 5FU alone did not induce a significant decrease in survival. There was no further decrease in survival comparing Barasertib to Barasertib + cisplatin and Barasertib to Barasertib + Vinorelbine Barasertib alone induced cell killing. Lie the BICR22 cells there was no sensitisation when Barasertib to 5FU but e*top*oside and Barasertib demonstrated sensitisation when compared to Barasertib alone.

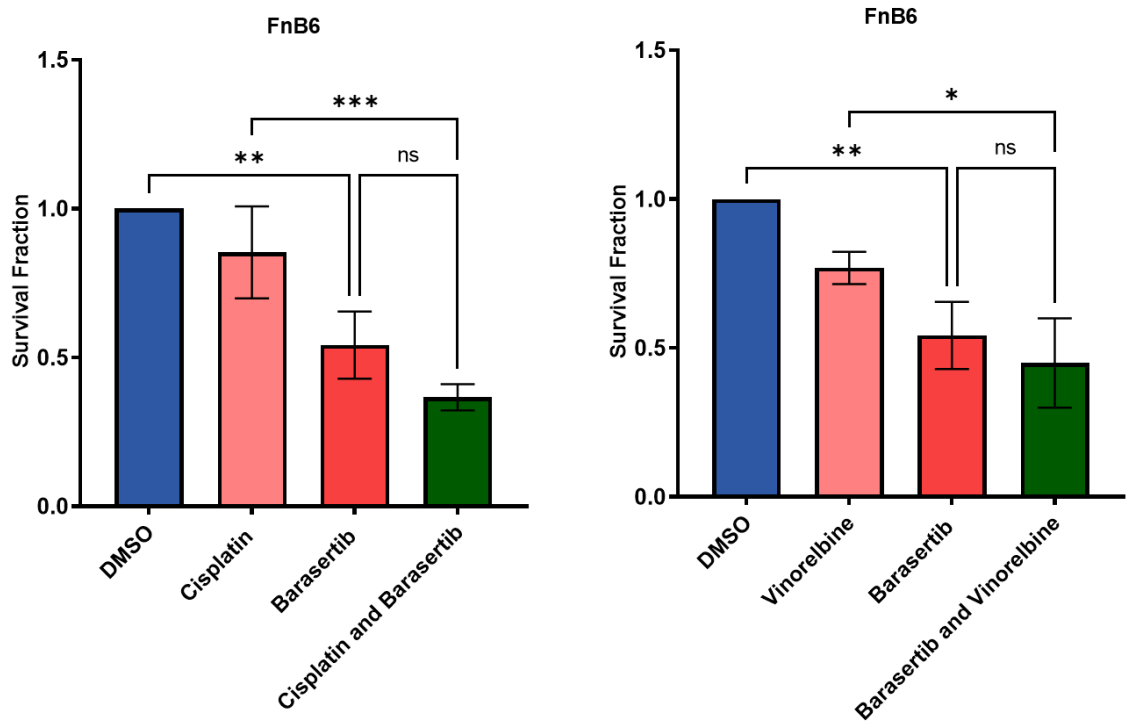


Figure 4-5: Comparison of Barasertib vs Barasertib and chemotherapy (Cisplatin and Vinorelbine) in *FN*B6 cell lines (n=3) Cells were pre-incubated with either Cisplatin, Vinorelbine or *AURKB* inhibitor Barasertib, cells were left to form colonies for 10-14 days before colony outgrowth under continuous exposure to the Cisplatin, Vinorelbine and/or *AURKB* inhibitor Barasertib. Data points represent the mean survival fraction normalised to DMSO +/- SD (N= ≥3). F-value and p-value derived from the extra sum of squares test. NS (non-statistically significant) denotes p= >0.05, * denotes p= ≤0.05, ** denotes p= ≤0.01, *** denotes p= 0.001 (One-way ANOVA with Dunnett correction for multiple comparisons).

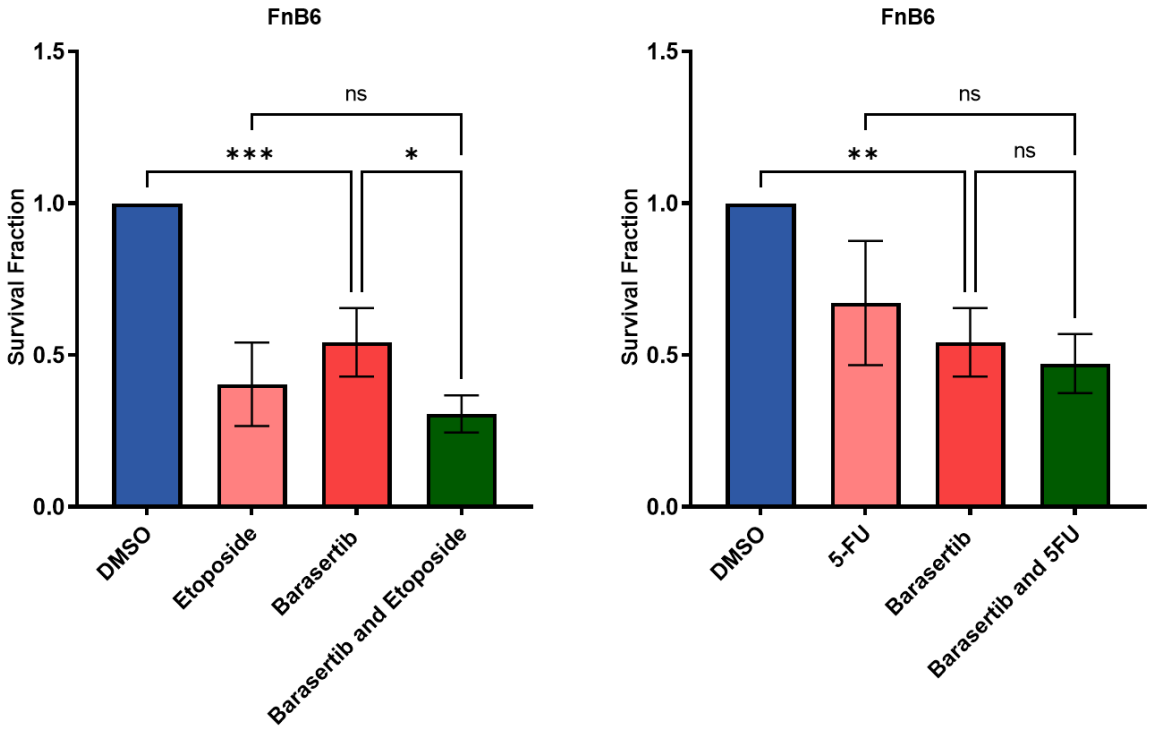


Figure 4-6: Comparison of Barasertib vs Barasertib and chemotherapy (5-FU and E*top*oside) in *FN*B6 cell lines (n=3) Cells were pre-incubated with either 5FU, Etoposide or *AURKB* inhibitor Barasertib, cells were left to form colonies for 10-14 days before colony outgrowth under continuous exposure to the 5FU, Etoposide and/or *AURKB* inhibitor Barasertib. Data points represent the mean survival fraction normalised to DMSO +/- SD (N= ≥3). F-value and p-value derived from the extra sum of squares test. NS (non-statistically significant) denotes p= >0.05, * denotes p= ≤0.05, ** denotes p= ≤0.01, *** denotes p= 0.001 (One-way ANOVA with Dunnett correction for multiple comparisons).

4.2.2 Live cell analysis of HNSCC cell lines using Barasertib as monotherapy.

4.2.2.1 UPCI-SCC72 and SCC89 cell lines demonstrate increased levels of slippage at increasing doses of Barasertib alone compared to B22 (BICR22) and *FN*B6 cells at 24 – 36 hours.

UPCI-SCC72 and SCC89 cells demonstrate a notable decrease in survival upon exposure to relatively low concentrations of Barasertib compared to BICR22 and *FN*B6 cell lines (Figure 3-5). Analogous to the earlier investigations on A549 and H520 cell lines, we investigated the mitotic consequences of Barasertib in HNSCC.

Upon examination of the UPCI-SCC72 cell lines (*p53* wild-type cell line), Barasertib was seen to cause a significant increase in the percentage of cells dying in mitosis (1nM vs 5nM and DMSO vs 5nM, p=0.0027 and p=0.0023 respectively), increased time in mitosis (DMSO vs 5nM and 1nM vs 5nM, p = 0.0185 and 0.0276 respectively) and mitotic slippage (DMSO vs 5nM Barasertib, p = <0.0001) (Figure 4-18).

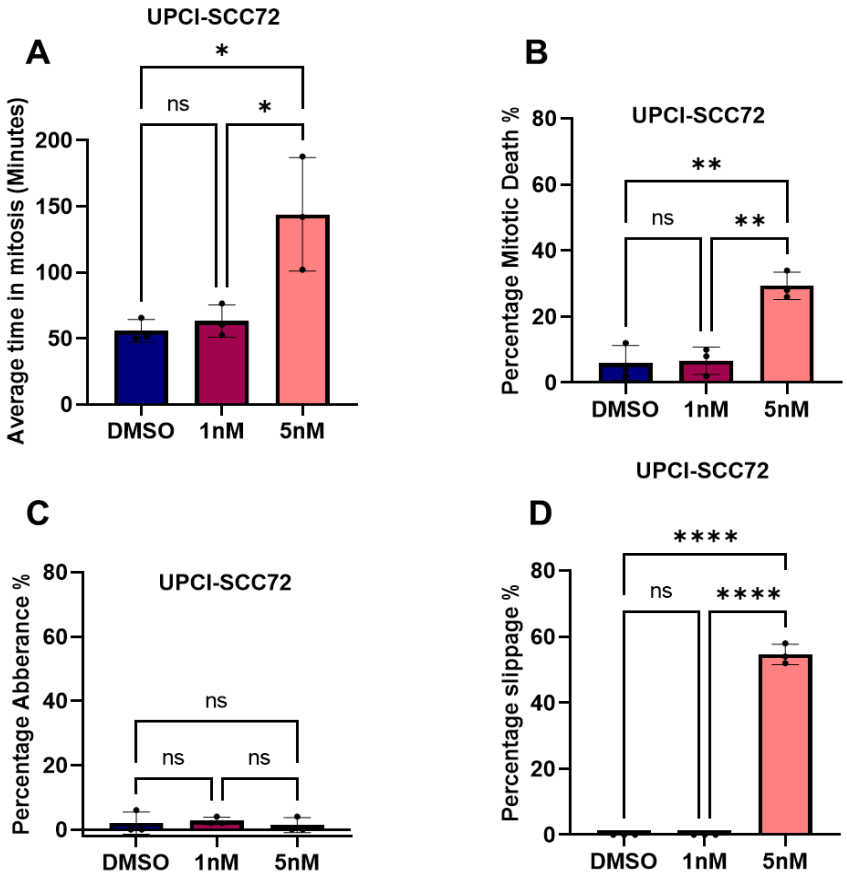


Figure 4-7: ***UPCI-SCC72 live cell analysis 24-36 hours post-Barasertib A-D*** *showing proportion of intra-mitotic death and aberrant mitosis resulting in >2 daughter cells time in mitosis, and proportion of cells undergoing slippage —minimum 50 mitotic cells counted per repeat. Data points represent the mean proportion of mitotic cells with described outcome +/- SD (N= 3) NS (non-statistically significant) denotes p= >0.05, * denotes p= ≤0.05, ** denotes p= ≤0.01, *** denotes p= ≤0.001 (One-way ANOVA with Dunnett correction for multiple comparisons).*

Regarding the SCC89 cell lines (*p53* mutant cell line) treated with Barasertib, our analysis revealed no aberrant cell division and no statistically significant increase in the percentage of cell death. However, on 2/3 repeats, Barasertib-induced mitotic cell death levels were seen following Barasertib. However, significant increases in slippage and increased time in mitosis were seen with 5nM Barasertib (DMSO vs 5nM p=0.0029 and 0.0019, respectively. (Figure 4-19).

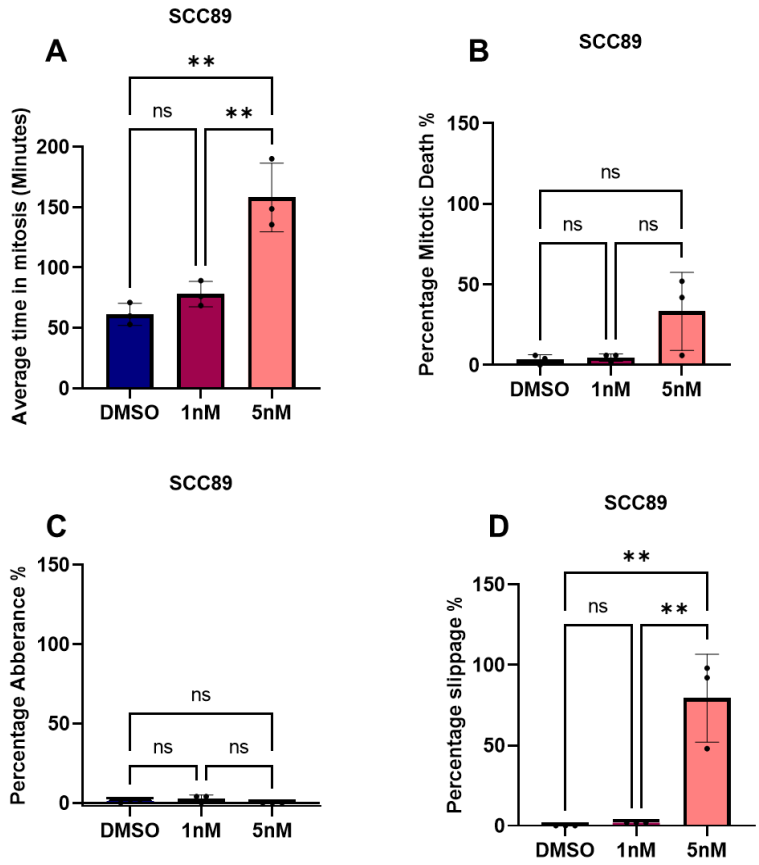


Figure 4-8: ***SCC89 live cell analysis 24-36 hours post-Barasertib A-D*** *showing proportion of intra-mitotic death and aberrant mitosis resulting in >2 daughter cells time in mitosis, and proportion of cells undergoing slippage —minimum 50 mitotic cells counted per repeat. Data points represent the mean proportion of mitotic cells with described outcome +/- SD (N= 3) NS (non-statistically significant) denotes p= >0.05, * denotes p= ≤0.05, ** denotes p= ≤0.01, *** denotes p= ≤0.001 (One-way ANOVA with Dunnett correction for multiple comparisons).*

Upon examining the B22 (BICR22) cell lines, no significant increase in the percentage of death during mitosis, percentage of aberrant mitosis, slippage or duration of mitosis was observed, which was expected due to the increased resistance to Barasertib relative to the SCC89 and UPCI-SCC72 cell lines (Figure 4-20). The *FN*B6 is an immortalised cell line which serves as a model for “normal HNSCC tissue,” similar to the results seen in the B22 line, with no significant increase in the percentage of death during mitosis, percentage of aberrant mitosis, slippage or duration of mitosis was seen (Figure 4-21). These results align with our expectations, as both cell lines (BICR22 and *FN*B6) exhibited relatively lower sensitivity to Barasertib’s effects than the UPCI-SCC72 and SCC89 cell lines.

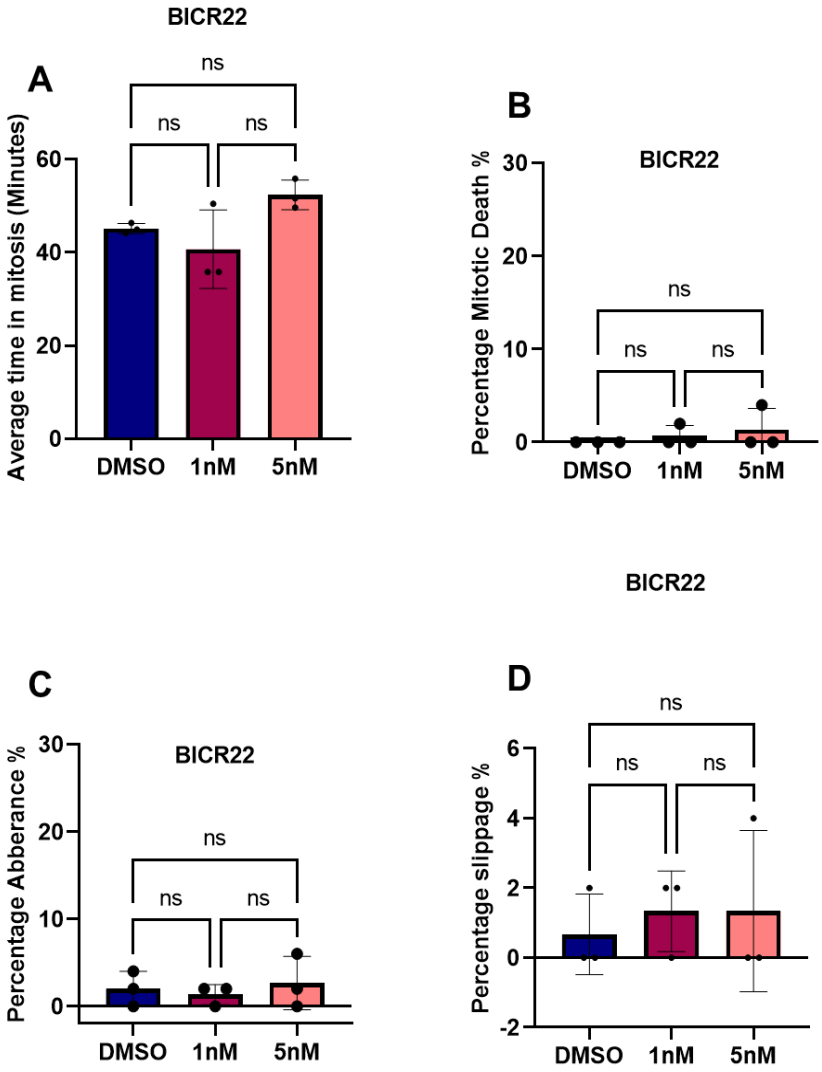


Figure 4-9: ***BICR22 live cell analysis 24-36 hours post-Barasertib A-D*** *showing proportion of intra-mitotic death and aberrant mitosis resulting in >2 daughter cells time in mitosis, and proportion of cells undergoing slippage —minimum 50 mitotic cells counted per repeat. Data points represent the mean proportion of mitotic cells with described outcome +/- SD (N= 3) NS (non-statistically significant) denotes p= >0.05, * denotes p= ≤0.05, ** denotes p= ≤0.01, *** denotes p= ≤0.001 (One-way ANOVA with Dunnett correction for multiple comparisons).*

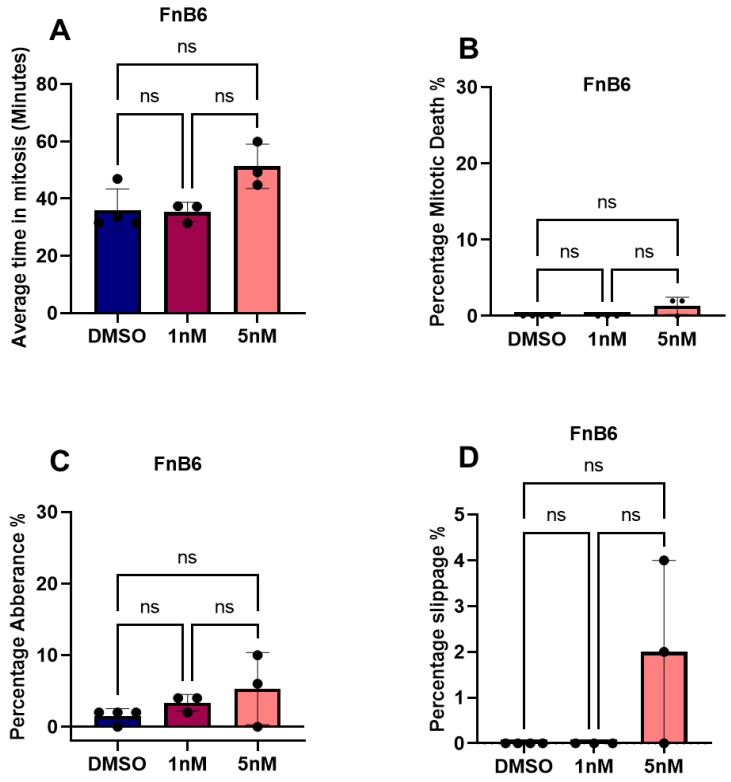


Figure 4-10: ***FNB6 live cell analysis 24-36hours post Barasertib A-D*** *showing proportion of intra-mitotic death and aberrant mitosis resulting in >2 daughter cells time in mitosis, and proportion of cells undergoing slippage —minimum 50 mitotic cells counted per repeat. Data points represent the mean proportion of mitotic cells with described outcome +/- SD (N= 4) NS (non-statistically significant) denotes p= >0.05, * denotes p= ≤0.05, ** denotes p= ≤0.01, *** denotes p= ≤0.001 (One-way ANOVA with Dunnett correction for multiple comparisons).*

4.2.2.2 UPCI-SCC72 and SCC89 cell lines demonstrate increased levels of slippage at increasing doses of Barasertib alone at 0 – 16 hours and 36-48 hours, but no cellular outcomes before or after slippage were seen.

SCC89 and UPCI-SCC72 both show increased sensitivity to Barasertib; the significant increase in slippage observed in both cell lines does not explain the significant reduction in cell survival observed in the clonogenic assays. This could be because the outcomes of slippage were not evident at the 24–36-hour time point, as seen in the NSCLC cell lines. We therefore examined the cellular outcomes at 0-16 hrs and 36-48hrs post addition of Barasertib.

For both the UPCI-SCC72 and SCC89 cell lines at 0-16 hours, we observed no significant increase in the percentage of death during mitosis nor the percentage of aberrant division. However, both slippage and the duration of mitosis were significantly prolonged with 5nM Barasertib DMSO vs 5nM p=0.0001 and p= 0.0004 in UPCI-SCC72 (DMSO vs 5nM p=0.0001 and p= 0.0005) and SCC89 (DMSO vs 5nM p=0.0001 and p= 0.0004) respectively (Figure 4-22, 4-23).

Furthermore, close examination of the stacked bar graphs (Appendix 7.4.1) for UPCI-SCC72 and SCC89 cell lines did not reveal any cellular events preceding or following slippage.

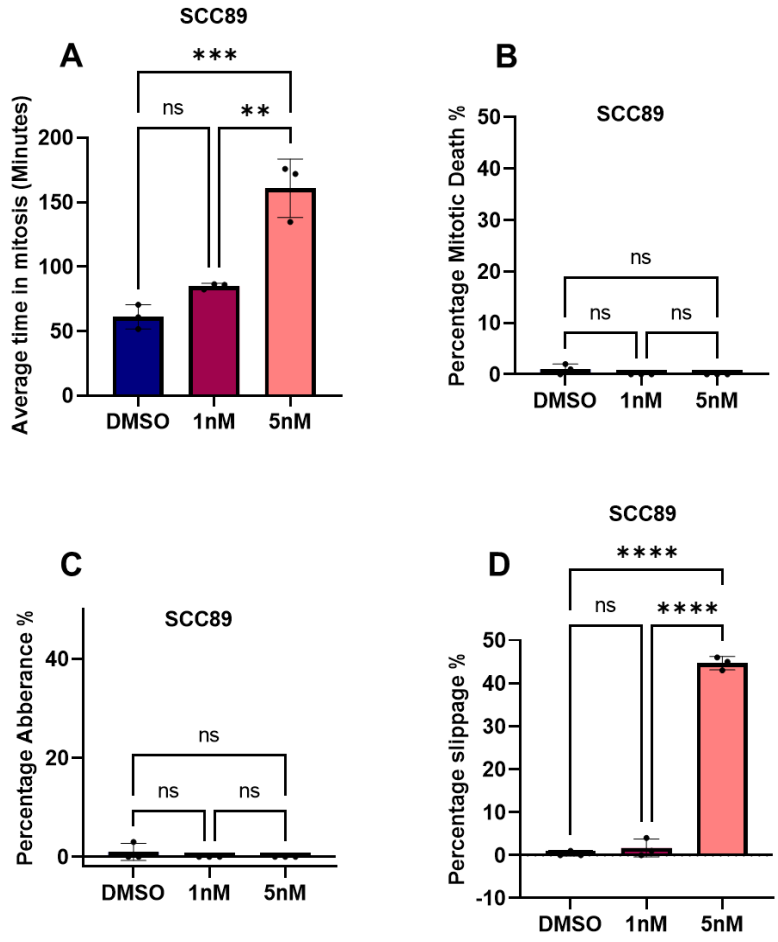


Figure 4-11: ***SCC89 live cell analysis 0-16 hours post-Barasertib A-D*** *showing proportion of intra-mitotic death and aberrant mitosis resulting in >2 daughter cells time in mitosis, and proportion of cells undergoing slippage —minimum 50 mitotic cells counted per repeat. Data points represent the mean proportion of mitotic cells with described outcome +/- SD (N= 3) NS (non-statistically significant) denotes p= >0.05, * denotes p= ≤0.05, ** denotes p= ≤0.01, *** denotes p= ≤0.001 (One-way ANOVA with Dunnett correction for multiple comparisons).*

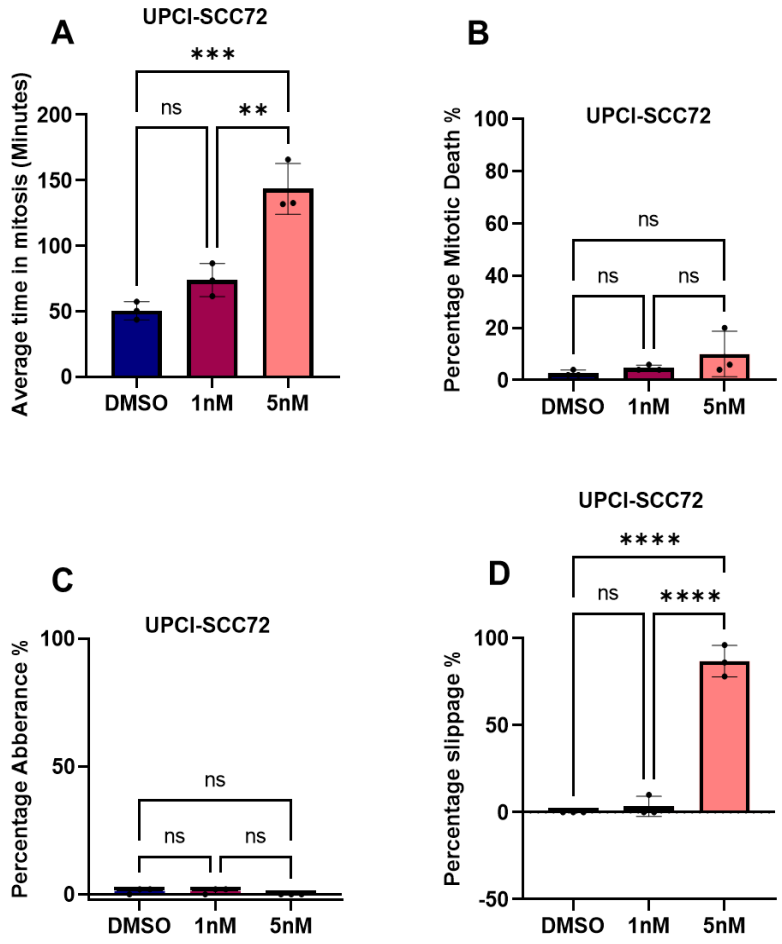


Figure 4-12: ***UPCI-SCC72 live cell analysis 0-16 hours post-Barasertib A-D*** *showing proportion of intra-mitotic death and aberrant mitosis resulting in >2 daughter cells time in mitosis, and proportion of cells undergoing slippage —minimum 50 mitotic cells counted per repeat. Data points represent the mean proportion of mitotic cells with described outcome +/- SD (N= 3) NS (non-statistically significant) denotes p= >0.05, * denotes p= ≤0.05, ** denotes p= ≤0.01, *** denotes p= ≤0.001 (One-way ANOVA with Dunnett correction for multiple comparisons).*

In UPCI-SCC072 and SCC089 during 36-48 hours of Barasertib, the addition of Barasertib failed to induce aberrant mitotic divisions. However, 5nM Barasertib caused an increase in average time in mitosis (DMSO vs 5nM p=0.0183 and p=0.0001 in UPCI-SCC072 and SCC089 respectively) and an increase in slippage (DMSO vs 5nM p=0.0001 and p=0.0004 in UPCI-SCC072 and SCC089 respectively) and an increase in mitotic cell death (DMSO vs 5nM p=0.0023 and p=0.0031 in UPCI-SCC072 and SCC089). (Figures 4-24 and 4-25). In summary for both cell lines there was increased time in mitosis, increased slippage, and increased cell death, especially at later time points.

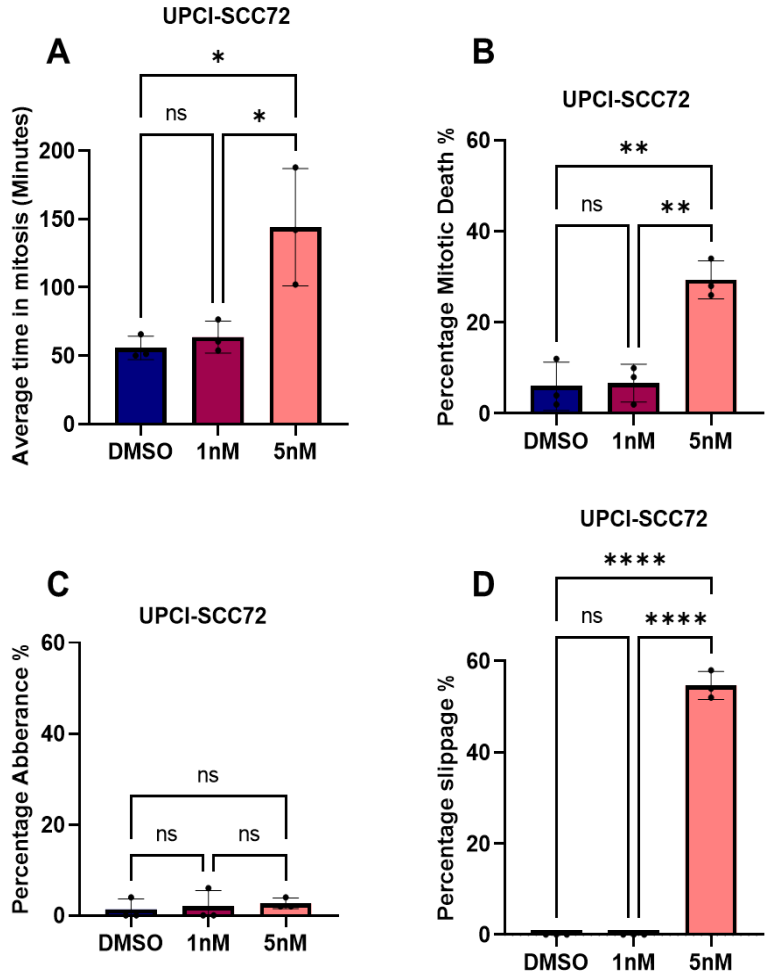


Figure 4-13: ***UPCI-SCC72 live cell analysis 36-48 hours post-Barasertib A-D*** *showing proportion of intra-mitotic death and aberrant mitosis resulting in >2 daughter cells time in mitosis, and proportion of cells undergoing slippage —minimum 50 mitotic cells counted per repeat. Data points represent the mean proportion of mitotic cells with described outcome +/- SD (N= 3) NS (non-statistically significant) denotes p= >0.05, * denotes p= ≤0.05, ** denotes p= ≤0.01, *** denotes p= ≤0.001 (One-way ANOVA with Dunnett correction for multiple comparisons).*

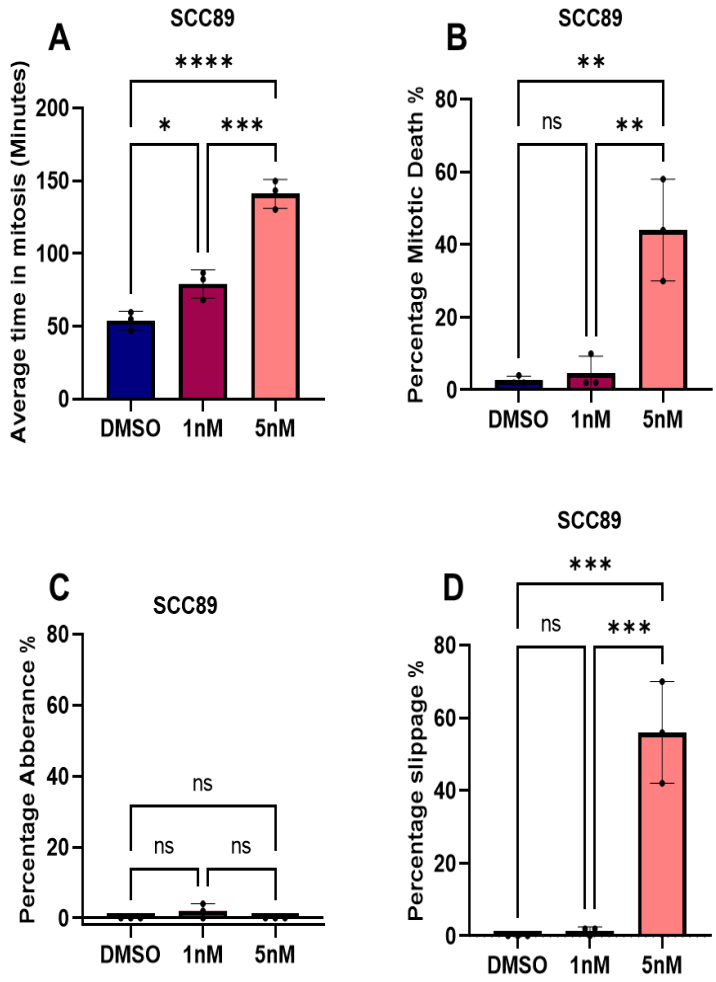


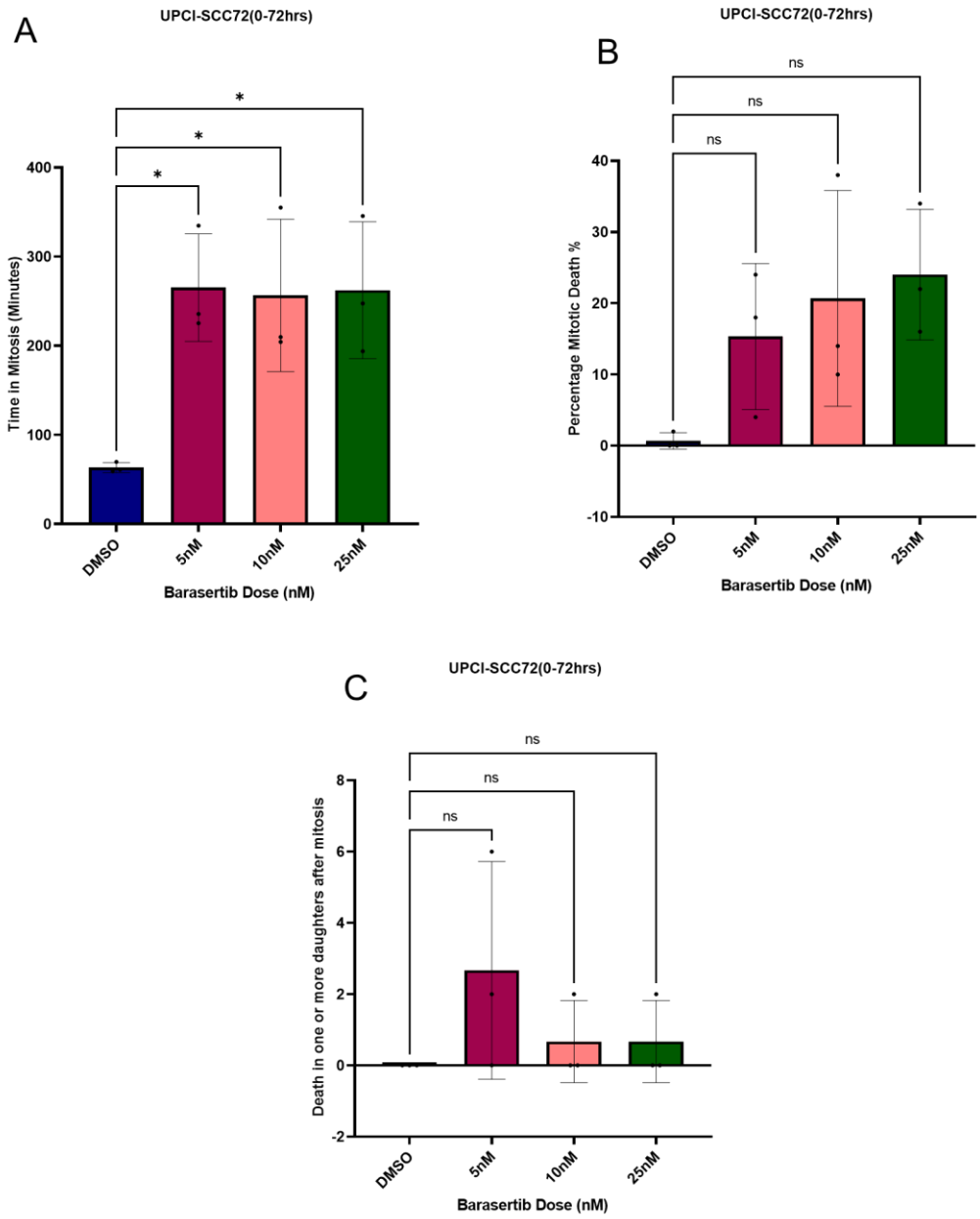
Figure 4-14: ***SCC89 live cell analysis 36-48 hours post-Barasertib A-D*** *showing proportion of intra-mitotic death and aberrant mitosis resulting in >2 daughter cells time in mitosis, and proportion of cells undergoing slippage —minimum 50 mitotic cells counted per repeat. Data points represent the mean proportion of mitotic cells with described outcome +/- SD (N= 3) NS (non-statistically significant) denotes p= >0.05, * denotes p= ≤0.05, ** denotes p= ≤0.01, *** denotes p= ≤0.001 (One-way ANOVA with Dunnett correction for multiple comparisons).*

4.2.3 Live cell analysis using Barasertib over 72 hours.

4.2.3.1 Live cell imaging between 0 -72 hours reveals that UPCI-SCC072, SCC089 cells eventually slip and die in mitosis.

The HNSCC UPCI-SCC72 cell line is more sensitive to Barasertib than any NSCLC cell line. Over 72 hours, there were significant increases in the time spent in mitosis (DMSO vs 5nM, DMSO vs 10nM and DMSO vs 25nM p = 0.0155, 0.0197 and0.0168 respectively), percentage of deaths after slippage (DMSO vs 5nM, DMSO vs 10nM and DMSO vs 25nM p = 0.0017, 0.0042 and 0.0012 respectively), and percentage of slippage overall (DMSO vs 10nm and DMSO vs 25nM p = 0.122 and 0.0303 respectively), with an increase in mitotic death occurring on all three repeats but not reaching statistical significance. Interestingly, in contrast to A549 cells, the death of one or more daughters after mitosis only occurred with very low frequency and was variable, not reaching statistical significance (Figures 4-49 and 4-50).

We also demonstrated in the UPCI-SCC72 cell lines that cells could undergo multiple rounds of slippage before dying (Figures 4-28C 5,10 and 25 nM); in some cases where there were three rounds of slippage, the cells were still alive at the end of the 72-hour time point, it is assumed that they eventually died in mitosis. Using Barasertib in the UPCI-SCC72 cell line increases cellular events using Barasertib compared to DMSO treatment. However, there is little difference in using higher doses of Barasertib (25nM) compared to 5nM as cells. This likely reflects that the cells are sensitive to Barasertib, with clonogenic assays showing 99.93 % cell death at 5nM.


A
UPCI-SCC72(0-72hrs)
Time in Mitosis (Minutes)
400
300
200
100
0
*
*
*
DMSO
5nM
10nM
25nM
Barasertib Dose (nM)
B
UPCI-SCC72(0-72hrs)
Percentage Mitotic Death %
40
30
20
10
0
-10
ns
ns
ns
DMSO
5nM
10nM
25nM
Barasertib Dose (nM)
C
UPCI-SCC72(0-72hrs)
Death in one or more daughters after mitosis
8
6
4
2
0
-2
ns
ns
ns
DMSO
5nM
10nM
25nM
Barasertib Dose (nM)

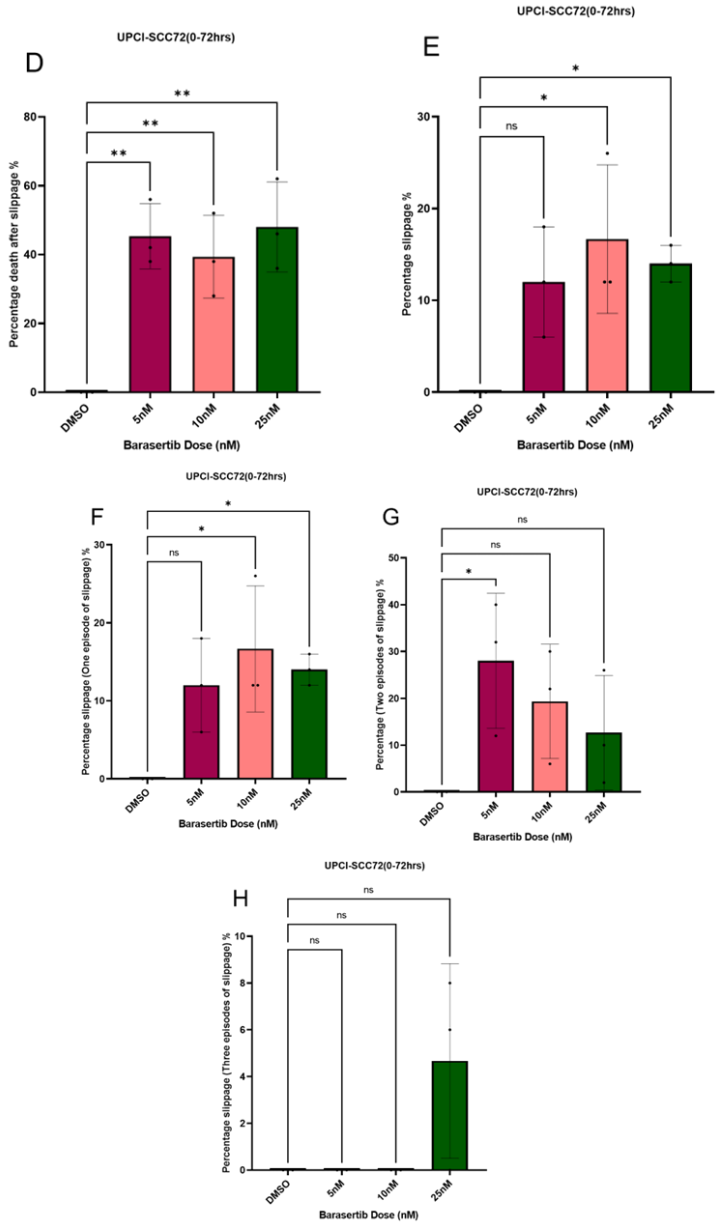
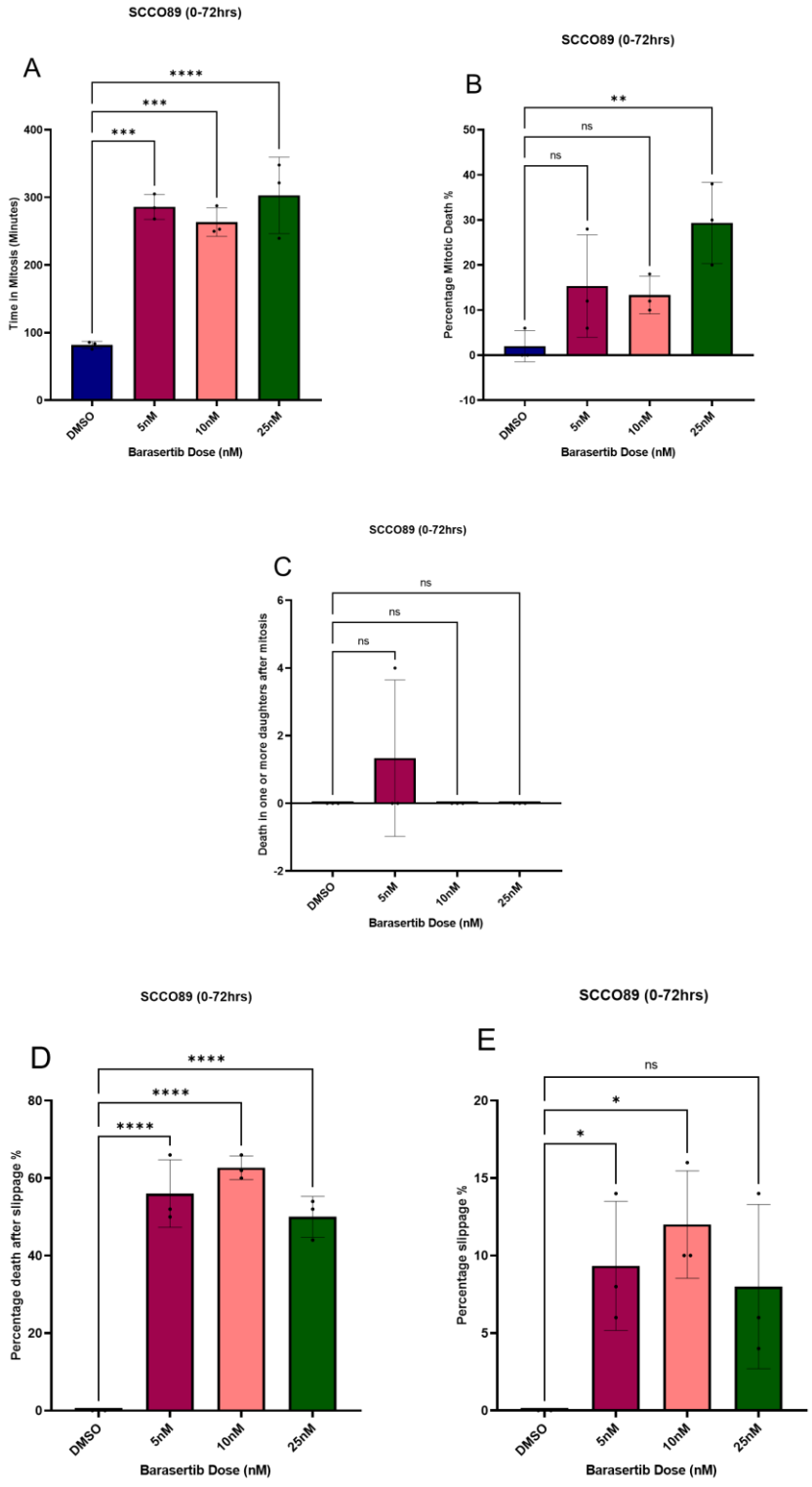


Figure 4-15: ***UPCI-SCC72 live cell analysis 0-72 hours post-Barasertib*** *A.* Time in mitosis resulting in cytokinesis. B. Proportion of intra-mitotic death C. Proportion of daughter cells dying after slippage D. Proportion of cells dying after slippage. E. Proportion of cells undergoing slippage. F-H Proportion of cells undergoing slippage categorised by number of times the cells slipped in 72 hours regardless of outcome —minimum 50 mitotic cells counted per condition. Data points represent the mean proportion of mitotic cells with described outcome +/- SEM (N= 5). NS (non-statistically significant) denotes p= >0.05, * denotes p= ≤0.05, ** denotes p= ≤0.01, *** denotes p= ≤0.001 (One-way ANOVA with Dunnett correction for multiple comparisons).

The SCC089 cell line has a similar sensitivity to UPCI-SCC72. In this cell line, low (5nM or 10nM) and high (25nM) doses of Barasertib induced significant increases in the duration of mitosis (DMSO vs 5nM, DMSO vs 10nM and DMSO vs 25nM p = 0.0001, 0.0003 and <0.0001 respectively), frequency of slippage (DMSO vs 5nM and DMSO vs 10nM p = 0.0489 and 0.0139 respectively), and the percentage of death after slippage (DMSO vs 5nM, DMSO vs 10nM and DMSO vs 25nM p = <0.0001 in all conditions). However, in contrast to UPCI-SCC72 and similar to A459, significant levels of death in mitosis were induced at the higher dose of 25 nM (with lower doses giving a consistent increase on every occasion). (Figures 4-28 and 4-29).

SCC089 dose response to Barasertib is similar to UPCI-SCC72, where using Barasertib increased the number of cellular events seen compared to DMSO, but there was no significant difference when using higher doses compared to the lower dose as there were a large number of cells already dying in mitosis at 5nM.

SCC089 cells underwent multiple rounds of slippage either before death or with no visible outcome (Figure 4-30A 5nM, 4-30C 5,10 and 25nM). Cells undergoing multiple rounds of slippage did not seem to die earlier than cells that slipped once. We, therefore, concluded that the number of times a cell slipped has no bearing on the mitotic outcome and that in the UPCI-SCC72 and SCC89 cells, Barasertib-induced changes were not dependent on the dose, likely because 5 nM is enough for a complete response. This is consistent with 99.93 % and 100 % cell death in clonogenic cell death in UPCI-SCC72 and SCC89 cells, respectively.


SCCO89 (0-72hrs)
A
Time in Mitosis (Minutes)
400
300
200
100
0
****
***
***
DMSO
5nM
10nM
25nM
Barasertib Dose (nM)
SCCO89 (0-72hrs)
B
Percentage Mitotic Death %
50
40
30
20
10
0
-10
**
ns
ns
DMSO
5nM
10nM
25nM
Barasertib Dose (nM)
SCCO89 (0-72hrs)
C
Death in one or more daughters after mitosis
6
4
2
0
-2
ns
ns
ns
DMSO
5nM
10nM
25nM
Barasertib Dose (nM)
SCCO89 (0-72hrs)
D
Percentage death after slippage %
80
60
40
20
0
****
****
****
DMSO
5nM
10nM
25nM
Barasertib Dose (nM)
SCCO89 (0-72hrs)
E
Percentage slippage %
20
15
10
5
0
ns
*
*
DMSO
5nM
10nM
25nM
Barasertib Dose (nM)

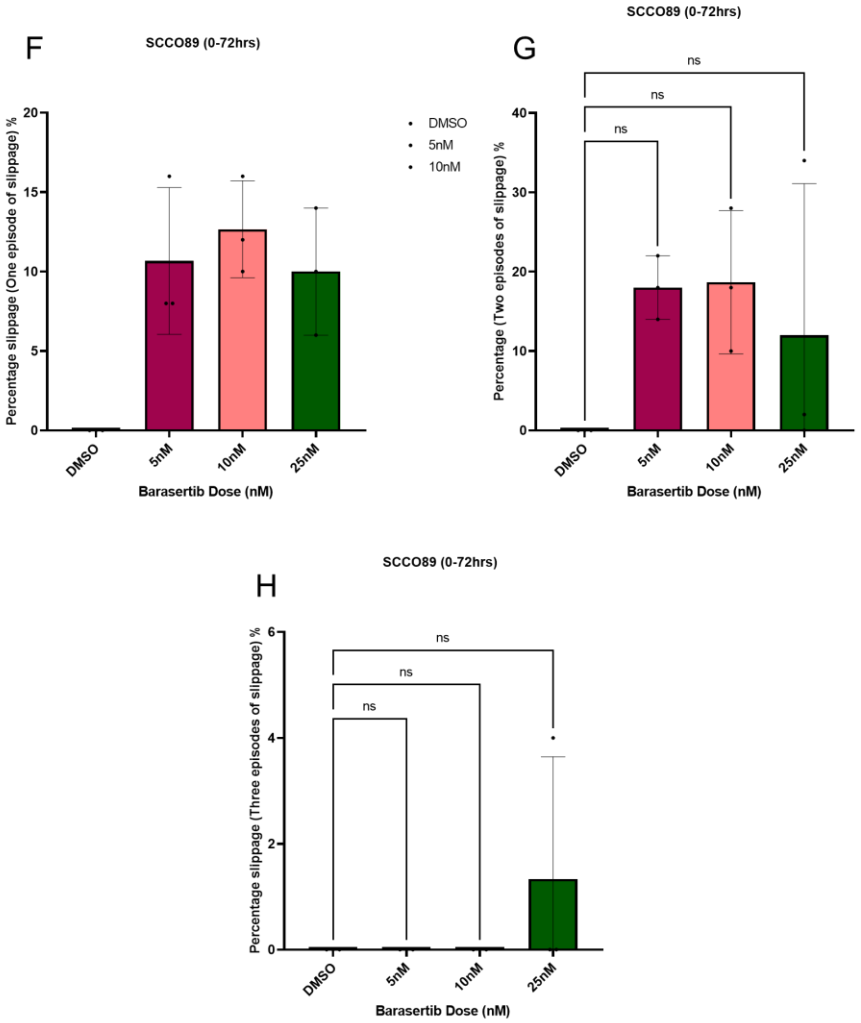


Figure 4-16: ***SCC89 live cell analysis 0-72 hours post-Barasertib*** A. Time in mitosis resulting in cytokinesis. B. Proportion of intra-mitotic death C. Proportion of cells undergoing slippage. D. Proportion of cells dying after slippage. E. Proportion of daughter cells dying after slippage—minimum 50 mitotic cells counted per condition. Data points represent the mean proportion of mitotic cells with described outcome +/- SEM (N= 5). NS (non-statistically significant) denotes p= >0.05, * denotes p= ≤0.05, ** denotes p= ≤0.01, *** denotes p= ≤0.001 (One-way ANOVA with Dunnett correction for multiple comparisons).

4.2.4 Western blot analysis of genes in the SAC.

4.2.4.1 Barasertib does not alter Cyclin B1 and CDC20 levels.

We hypothesised that inhibiting *AURKB* would lead to cells undergoing prolonged mitotic arrest in the presence of reduced levels of cyclin B1, explaining the high levels of slippage in cells more sensitive to Barasertib (Lok et al., 2020).

To test this, DMSO or Barasertib (10nM) were added to B22, SCC089, UPCI-SCC72 H460 and A549 cells and left for 4 and 24 hours prior to western blotting for CDC20 and CyclinB1 expression. B22 and H460 were chosen due to their relative radioresistance compared to SCC89, UPCI-SCC72 and A549 cells. However, Barasertib did not induce any change in expression in either protein at either point in any cell line (Fig 4-51) (Figure 4-52). The lack of effect on CDC20 and Cyclin B1 could be due to the lack of a direct interaction between Barasertib and Cyclin B1 and CDC20.

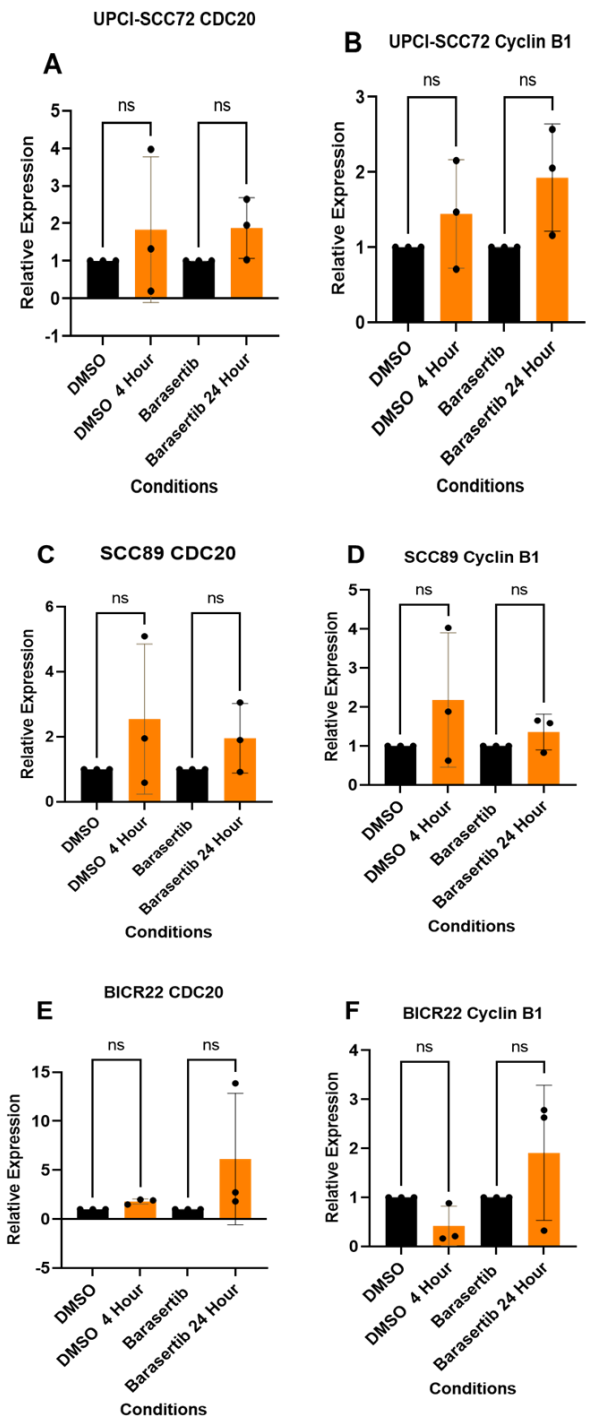
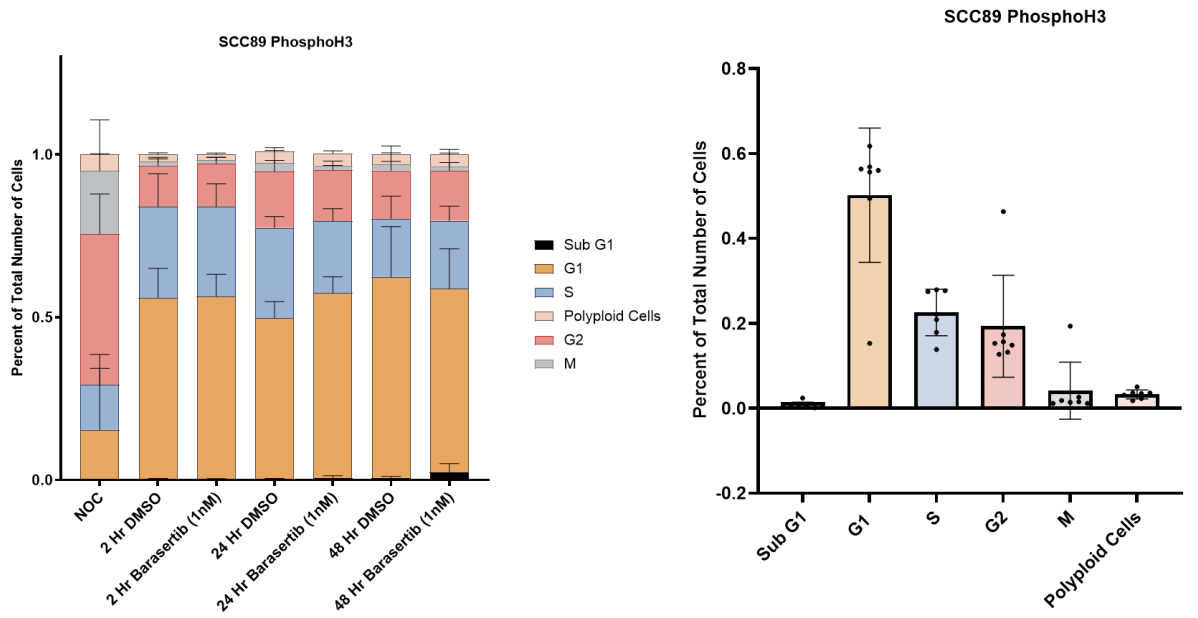


Figure 4-17: Quantification of CDC20 and Cyclin B1 expression normalised to GAPDH levels. A-B UPCI-SCC72 C-D SCC89 E-F BICR22 (N= ≥3). * Denotes p= ≤0.05, ** denotes p= ≤0.01, *** denotes p=≤0.001 (One-Way ANOVA).

4.2.5 Cell cycle profiling using FACS.

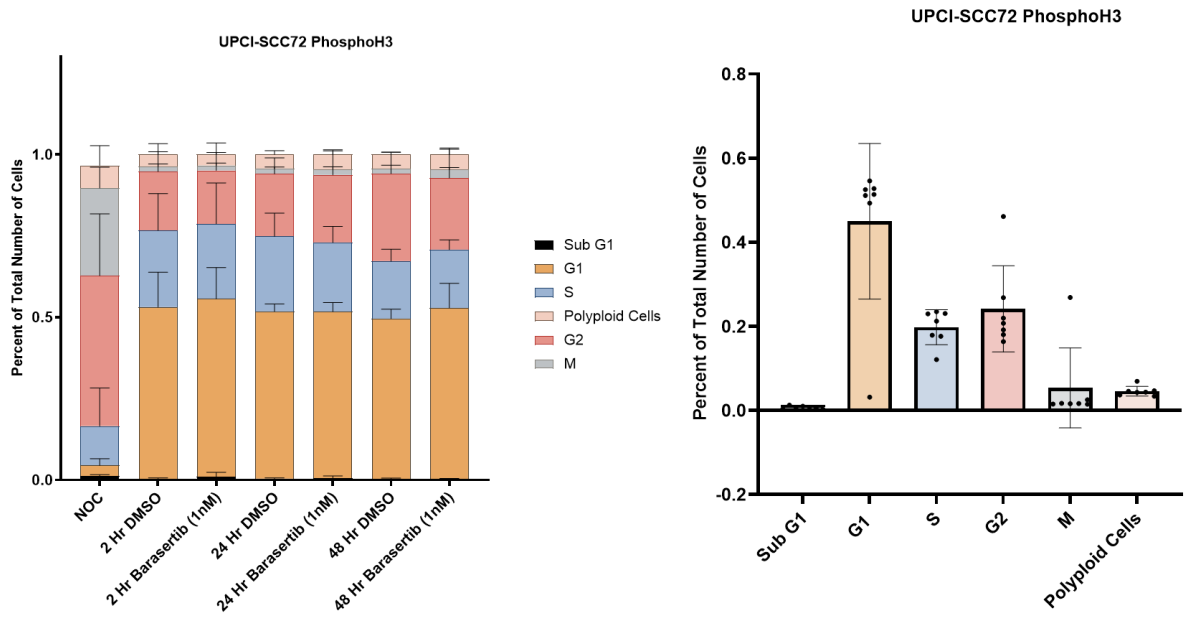
4.2.5.1 Cell cycle progression is not altered in 072, 089 and B22 cells treated with Barasertib using the *PH3* Marker alone.

In a separate analysis, Barasertib at a concentration of 1nM was employed in B22, SCC89 and UPCI-SCC72 cell lines. However, no significant differences were observed in cell cycle fractions when comparing Barasertib-treated cells with the DMSO control group at 2, 24, and 48 hours (Figure 4-54).



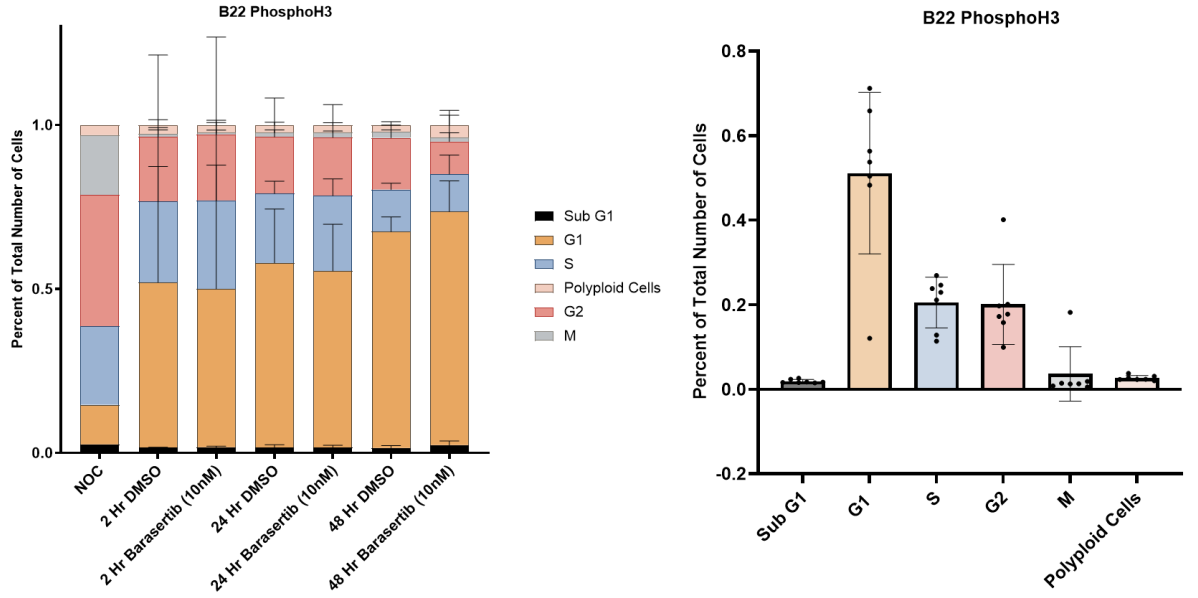
SCCO89 PH3	T-statistic	p-value
2 Hr DMSO vs 2 Hr Barasertib (5nM)	-0.0052	0.9959
2 Hr DMSO vs 24 Hr DMSO	-0.0002	0.9998
2 Hr DMSO vs 24 Hr Barasertib (5nM)	-0.0348	0.9724
2 Hr DMSO vs 48 Hr DMSO	0.0844	0.9332
2 Hr DMSO vs 48 Hr Barasertib (5nM)	0.0792	0.9373
2 Hr Barasertib (5nM) vs 24 Hr DMSO	0.0053	0.9958
2 Hr Barasertib (5nM) vs 24 Hr Barasertib	-0.0297	0.9765
2 Hr Barasertib (5nM) vs 48 Hr DMSO	0.0898	0.9289
2 Hr Barasertib (5nM) vs 48 Hr Barasertib	0.0849	0.9329
24 Hr DMSO vs 24 Hr Barasertib (5nM)	-0.037	0.9707
24 Hr DMSO vs 48 Hr DMSO	0.09	0.9288
24 Hr DMSO vs 48 Hr Barasertib (5nM)	0.085	0.9328
24 Hr Barasertib (5nM) vs 48 Hr DMSO	0.12	0.9052
24 Hr Barasertib (5nM) vs 48 Hr Barasertib	0.1162	0.9082
48 Hr DMSO vs 48 Hr Barasertib (5nM)	-0.0083	0.9934

Figure 4-18: ***SCC89 cell cycle distribution 2-, 24- and 48-hours following* treatment *with 1 nM Barasertib.*** HNSCC cells (1-2 x 10^5) were seeded per 90 mm^3 dish and harvested for FACS analysis at 24-, 48-, and 72-hours post-irradiation. Cells were washed, dislodged with trypsin, pooled, and centrifuged at 1200 RPM. After washing, they were resuspended in 100% methanol and stored at -20°C. For staining, cells were incubated with S10 p-Histone 3 primary antibody followed by Alexa 488 secondary antibody, then stained with propidium iodide (PI)/RNAse A solution. Flow cytometry analysis was conducted using FlowJo™ software, with cell populations gated based on PI intensity to identify G1, S, G2-M, mitotic, and polyploid populations. Doublets were excluded by plotting FL3-Area vs. FL3-Width. Data points represent mean cell cycle phase distribution +/- S SD (N= ≥3).Data points represent mean cell cycle phase distribution +/- SD (N= ≥3). Statistical testing: 2 tailed unpaired T.test where ns is non-significant, * p = <0.05 ** p = <0.001 *** p = <0.0001 and **** p = <0.00001



UPCI-SCCO72 PH3	T-statistic	p-value
2 Hr DMSO vs 2 Hr Barasertib (5nM)	-0.0131	0.9896
2 Hr DMSO vs 24 Hr DMSO	-0.2061	0.8378
2 Hr DMSO vs 24 Hr Barasertib (5nM)	-0.1837	0.8553
2 Hr DMSO vs 48 Hr DMSO	0.5544	0.5826
2 Hr DMSO vs 48 Hr Barasertib (5nM)	0.4943	0.6239
2 Hr Barasertib (5nM) vs 24 Hr DMSO	-0.1866	0.853
2 Hr Barasertib (5nM) vs 24 Hr Barasertib	-0.1648	0.87
2 Hr Barasertib (5nM) vs 48 Hr DMSO	0.5495	0.5859
2 Hr Barasertib (5nM) vs 48 Hr Barasertib	0.4921	0.6255
24 Hr DMSO vs 24 Hr Barasertib (5nM)	0.0226	0.9821
24 Hr DMSO vs 48 Hr DMSO	0.7669	0.4479
24 Hr DMSO vs 48 Hr Barasertib (5nM)	0.6986	0.4891
24 Hr Barasertib (5nM) vs 48 Hr DMSO	0.7442	0.4614
24 Hr Barasertib (5nM) vs 48 Hr Barasertib	0.6767	0.5027
48 Hr DMSO vs 48 Hr Barasertib (5nM)	-0.0399	0.9684

Figure 4-19: ***UPCI-SCC72 cell cycle distribution 2-, 24- and 48-hours following* treatment *with 1 nM Barasertib.*** HNSCC cells (1-2 x 10^5) were seeded per 90 mm^3 dish and harvested for FACS analysis at 24-, 48-, and 72-hours post-irradiation. Cells were washed, dislodged with trypsin, pooled, and centrifuged at 1200 RPM. After washing, they were resuspended in 100% methanol and stored at -20°C. For staining, cells were incubated with S10 p-Histone 3 primary antibody followed by Alexa 488 secondary antibody, then stained with propidium iodide (PI)/RNAse A solution. Flow cytometry analysis was conducted using FlowJo™ software, with cell populations gated based on PI intensity to identify G1, S, G2-M, mitotic, and polyploid populations. Doublets were excluded by plotting FL3-Area vs. FL3-Width. Data points represent mean cell cycle phase distribution +/- S SD (N= ≥3). Data points represent mean cell cycle phase distribution +/- SD (N= ≥3). Statistical testing: 2 tailed unpaired T.test where ns is non-significant, * p = <0.05 ** p = <0.001 *** p = <0.0001 and **** p = <0.00001



BICR22 PH3	T-statistic	p-value
2 Hr DMSO vs 2 Hr Barasertib (5nM)	-0.0364	0.9712
2 Hr DMSO vs 24 Hr DMSO	0.1216	0.9041
2 Hr DMSO vs 24 Hr Barasertib (5nM)	0.1065	0.916
2 Hr DMSO vs 48 Hr DMSO	0.167	0.8685
2 Hr DMSO vs 48 Hr Barasertib (5nM)	0.669	0.509
2 Hr Barasertib (5nM) vs 24 Hr DMSO	0.1582	0.8754
2 Hr Barasertib (5nM) vs 24 Hr Barasertib	0.1442	0.8864
2 Hr Barasertib (5nM) vs 48 Hr DMSO	0.201	0.8421
2 Hr Barasertib (5nM) vs 48 Hr Barasertib	0.6948	0.493
24 Hr DMSO vs 24 Hr Barasertib (5nM)	-0.0194	0.9847
24 Hr DMSO vs 48 Hr DMSO	0.0561	0.9557
24 Hr DMSO vs 48 Hr Barasertib (5nM)	0.5943	0.5571
24 Hr Barasertib (5nM) vs 48 Hr DMSO	0.0755	0.9404
24 Hr Barasertib (5nM) vs 48 Hr Barasertib	0.6275	0.5355
48 Hr DMSO vs 48 Hr Barasertib (5nM)	0.5043	0.618

Figure 4-20: ***BICR22 cell cycle distribution 2-, 24- and 48-hours following* treatment *with 10 nM Barasertib.*** HNSCC cells (1-2 x 10^5) were seeded per 90 mm^3 dish and harvested for FACS analysis at 24-, 48-, and 72-hours post-irradiation. Cells were washed, dislodged with trypsin, pooled, and centrifuged at 1200 RPM. After washing, they were resuspended in 100% methanol and stored at -20°C. For staining, cells were incubated with S10 p-Histone 3 primary antibody followed by Alexa 488 secondary antibody, then stained with propidium iodide (PI)/RNAse A solution. Flow cytometry analysis was conducted using FlowJo™ software, with cell populations gated based on PI intensity to identify G1, S, G2-M, mitotic, and polyploid populations. Doublets were excluded by plotting FL3-Area vs. FL3-Width. Data points represent mean cell cycle phase distribution +/- S SD (N= ≥3). Data points represent mean cell cycle phase distribution +/- SD (N= ≥3). Statistical testing: 2 tailed unpaired T.test where ns is non-significant, * p = <0.05 ** p = <0.001 *** p = <0.0001 and **** p = <0.00001

4.2.5.2 UPCI-SCC072 and SCC089 exhibit polyploidy and an increased G2M fraction compared to B22 cell lines when treated with Barasertib using Pi-alone staining.

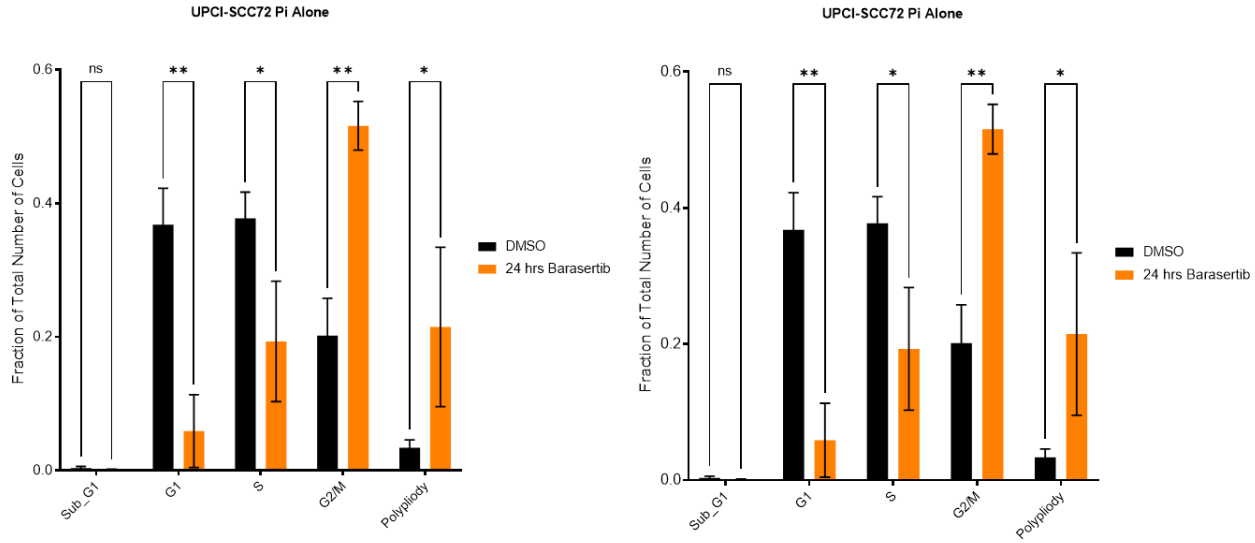
We considered whether too low a dose of Barasertib to see any effect on the cell cycle was being used, and so cell cycle profile analysis was repeated at higher doses but with PI staining alone.

B22, UPCI-SCC72 and SCC89 cells were treated with 5 nM of Barasertib and DMSO control. The UPCI-SCC72 cells exhibited reduced G1 fraction ($p = 0.0033$), reduced S-phase fraction ($p=0.031$), increased G2/M fraction ($p=0.0033$) and increased polyploidy ($p=0.044$) when exposed to 5 nM of Barasertib for 24 hours. In addition, in all three independent repeats, an increase in the polyploid fraction was seen – in 2 of these, the increase was very large (Figure 4-37).

In SCC89, cells exhibited reduced G1 fraction ($p = 0.000021$), reduced S-phase fraction ($p=0.000021$), increased G2/M fraction ($p=0.000024$) and increased polyploidy ($p=0.0000064$) when exposed to 5 nM of Barasertib for 24 hours. Like in the UPCI-SCC cell line in all three independent repeats, an increase in the polyploid fraction was seen (Figure 4-37).

These findings posed a challenge regarding explanation since the observed higher G2/M fraction in the sensitive cell lines did not align with earlier results, particularly considering that the cells did not spend more time in mitosis, as evidenced by the 72-hour assays. One explanation could be that the cells were actually stuck in the G2/M phase during this assay (Yu et al., 2017). Alternatively, we proposed that the observed increase in the G2/M fraction does not indicate cells spending more time in

the G2/M phases but rather a result of cells slipping and re-entering the G1 phase with increased cellular content and size due to endoreduplication. In the context of FACS analysis, cells undergoing slippage and endoreduplication may be mistakenly identified as cells in the G2 phase. This can occur because the FACS reader interprets the increased cellular content and size as characteristics of cells in the G2 phase rather than correctly identifying them as cells in the subsequent G1 phase. As a result, a false positive increase in the G2/M fraction is possibly observed during analysis (Figure 4-56). The observed increase in polyploid content, on the other hand, is consistent with the known activity of Barasertib, where inhibiting the activity of *AURKB* induces chromosome misalignment, terminating cell division with the introduction of polyploidy(Yamauchi et al., 2013). It also fits with the increased slippage seen on live cell imaging.



SCC89	Mean of DMSO	Mean of 24 hrs Barasertib	Difference	P value	SE of difference
Sub_G1	0.001102	0.004757	-0.003655	0.353037	0.003334
G1	0.4269	0.007792	0.4191	0.000041	0.01109
S	0.3611	0.04474	0.3163	0.000024	0.006998
G2/M	0.1869	0.5949	-0.4080	0.000071	0.01300
Polypliody	0.02408	0.3478	-0.3237	0.000254	0.01580

UPCI-SCC72	Mean of DMSO	Mean of 24 hrs Barasertib	Difference	P value	SE of difference
Sub_G1	0.003436	0.001211	0.002226	0.203663	0.001466
G1	0.3680	0.05872	0.3093	0.002227	0.04437
S	0.3775	0.1931	0.1844	0.031313	0.05671
G2/M	0.2016	0.5158	-0.3142	0.001250	0.03869
Polypliody	0.03385	0.2148	-0.1809	0.059283	0.06927

Figure 4-21: ***SCC89 and UPCI-SCC72 cell cycle distribution 2-, 16- and 24-hours following* treatment *with 5 nM Barasertib.*** HNSCC cells (1-2 x 10^5) were seeded per 90 mm^3 dish and harvested for FACS analysis at 24-, 48-, and 72-hours post-irradiation. Cells were washed, dislodged with trypsin, pooled, and centrifuged at 1200 RPM. After washing, they were resuspended in 100% methanol and stored at -20°C. For staining, stained with propidium iodide (PI)/RNAse A solution. Flow cytometry analysis was conducted using FlowJo™ software, with cell populations gated based on PI intensity to identify G1, S, G2-M, mitotic, and polyploid populations. Doublets were excluded by plotting FL3-Area vs. FL3-Width. *Data points represent mean cell cycle phase distribution +/- SD (N= ≥3). Statistical testing: 2 tailed unpaired T.test where ns is non-significant, * p = <0.05 ** p = <0.001 *** p = <0.0001 and **** p = <0.00001*

4.3 Discussion

4.3.1 Radiosensitisation potential of Barasertib in HNSCC cell lines

Barasertib is a potent inhibitor of Aurora B kinase (*AURKB*), which plays a crucial role in regulating mitosis and maintaining chromosomal stability during cell division. In head and neck squamous cell carcinoma (HNSCC), Barasertib has demonstrated significant potential as an anticancer agent, particularly in its ability to induce mitotic catastrophe and apoptosis (Tinhofer et al., 2020). Studies have shown that Barasertib effectively disrupts the cell cycle in cancer cells, leading to their death, regardless of their mutational status (Azzariti et al., 2014; Yamauchi et al., 2013). This makes it a promising candidate for targeting HNSCC tumours, which are often resistant to conventional therapies.

However, the ability of Barasertib to act as a radiosensitiser in HNSCC has shown limited success in preclinical models (Kantarjian et al., 2013). Radiosensitisation involves enhancing the effect of radiation therapy to increase the death of cancer cells. While Barasertib demonstrates strong cytotoxic effects as a monotherapy, studies combining it with ionizing radiation in HNSCC have not shown significant improvements in survival outcomes compared to radiation therapy alone (Tsuboi et al., 2011).

Moving forward, research is needed to explore the reasons behind Barasertib's limited radiosensitisation potential in HNSCC and to identify ways to improve its

efficacy when combined with radiation therapy. Investigations into combination therapies with other targeted agents or immune checkpoint inhibitors may provide insights into more effective therapeutic strategies. Furthermore, understanding the tumour microenvironment's role and developing biomarkers to predict responsiveness could enhance the utility of Barasertib in treating resistant HNSCC tumour

4.3.2 Barasertib Monotherapy Displays Cytotoxicity in HNSCC Cell Lines:

Barasertib demonstrated potent cytotoxicity in several HNSCC cell lines, with notably low LD50 values in UPCI-SCC72 (1.55 nM) and SCC89 (1.08 nM). These cell lines exhibited dramatic reductions in survival, with less than 5% of cells surviving at 5 nM and no survival at 25 nM in contrast, the immortalized normal oral cell line FNB6 was relatively resistant (LD50 = 57.5 nM), highlighting the differential sensitivity between cancerous and non-cancerous cells. Western blot analysis further confirmed that Barasertib effectively inhibited phosphorylation of histone H3 (Phopho-H3), a surrogate marker for *AURKB* inhibition, in sensitive HNSCC lines at concentrations as low as 5 nM

4.3.3 Lack of Radiosensitisation by Barasertib in HNSCC Cell Lines:

Despite its efficacy as a monotherapy, Barasertib failed to demonstrate radiosensitisation across all tested HNSCC cell lines. Dose enhancement ratios (DERs) were not significantly altered by the combination of Barasertib and ionizing radiation (IR), even when lower doses were used in the sensitive UPCI-SCC72 and SCC89 cell lines. The stability of the DER in FNB6 cells at various radiation doses suggests that normal cells do not undergo radiosensitisation with Barasertib, which may indicate that resistance mechanisms inherent in normal cells prevent radiosensitisation.

4.3.4 Limited Efficacy of Barasertib Combined with Chemotherapy in HNSCC:

Barasertib, when combined with chemotherapeutic agents, demonstrated inconsistent results. In BICR22 cells, Barasertib alone significantly reduced cell survival; however, no significant reduction in survival was observed when combined with cisplatin or vinorelbine. The combination of Barasertib with etoposide resulted in moderate sensitisation, but no synergistic effects were seen with 5-FU. Similarly, in FNB6 cells, Barasertib induced a significant decrease in survival, yet its combination with cisplatin or vinorelbine did not further enhance cell death. Etoposide showed some sensitisation when combined with Barasertib, but no significant effects were observed with 5-FU.

4.3.5 Increased Sensitivity of HNSCC Cells to Barasertib:

The UPCI-SCC72 and SCC89 cell lines demonstrated significantly increased sensitivity to Barasertib, as indicated by increased mitotic slippage and prolonged time in mitosis, particularly at higher doses. This contrasts with B22 and FNB6 cells, which exhibited a relative resistance to Barasertib, with no significant alterations in mitotic duration, cell death, or mitotic aberrations. This differential response reinforces the hypothesis that the cellular sensitivity to *AURKB* inhibition is not uniform across cancer types and reflects intrinsic cellular heterogeneity in mitotic regulation.

4.3.6 Slippage as a Central Mechanism of Barasertib Action:

A key finding in this chapter is the role of mitotic slippage as a response to Barasertib. In both UPCI-SCC72 and SCC89, significant slippage was observed across time points, with some cells undergoing multiple rounds of slippage before mitotic death. This suggests that slippage may not always be immediately lethal but can lead to eventual mitotic catastrophe. Interestingly, slippage did not always lead to mitotic death, particularly at lower doses of Barasertib, raising the possibility of a subpopulation of cells that may escape death following slippage and potentially contribute to tumour persistence.

4.3.7 Dose-Response Variability in Cellular Outcomes:

While the clonogenic assays demonstrated near-total cell death at low concentrations of Barasertib (e.g., 5nM), live-cell analysis revealed that cellular outcomes, including slippage and death, were not significantly dose-dependent beyond a threshold concentration. This plateau effect suggests that once *AURKB* is sufficiently inhibited, increasing the dose does not markedly enhance the cytotoxic effects in these sensitive cell lines. This observation could inform dosing strategies for Barasertib, where lower concentrations may achieve the same therapeutic effect as higher concentrations, thus minimizing potential toxicity in clinical applications.

4.3.8 Polyploidy and Cell Cycle Perturbation:

Cell cycle analysis via flow cytometry revealed increased polyploidy in both UPCI-SCC72 and SCC89 cell lines following Barasertib treatment, which aligns with the expected outcomes of *AURKB* inhibition leading to chromosome misalignment and failed cytokinesis. An increase in the G2/M fraction was observed, likely due to endoreduplication rather than an actual extension of the G2/M phase. These results further support the concept that Barasertib induces significant genomic instability through its effects on the spindle assembly checkpoint (SAC), leading to polyploidy and subsequent cell death. However, the lack of corresponding time in mitosis in 72-hour assays suggests that the increased G2/M fraction in flow cytometry could result from misidentification by the flow cytometer, where slippage cells re-entering the cell cycle are mistaken for G2/M phase cells due to their increased DNA content.

4.3.9 No Observable Changes in Cyclin B1 and CDC20 Expression:

Western blot analysis revealed that neither Cyclin B1 nor CDC20 protein levels were significantly altered following Barasertib treatment across all cell lines. This finding suggests that Barasertib's effects on mitotic progression and slippage are not mediated through direct modulation of these key mitotic regulators, which contrasts with some proposed mechanisms of *AURKB* inhibition. These results indicate that alternative pathways, independent of Cyclin B1 and CDC20, may be involved in Barasertib-induced slippage and polyploidy, necessitating further exploration into the molecular drivers of these phenomena.

4.4 Future Work

4.4.1.1 Optimizing Therapeutic Dosing and Delivery:

Given the significant variability in response among different cell lines, future studies should aim to refine dosing strategies for Barasertib, particularly in combination with other therapies. Additionally, exploring optimal drug delivery schedules, including varying time points for drug administration relative to radiation or chemotherapy, may help overcome the lack of radiosensitisation observed in these studies.

4.4.1.2 Mechanistic Exploration of Resistance to Radiosensitisation:

The lack of radiosensitisation observed in all tested HNSCC cell lines suggests that resistance mechanisms are preventing the synergistic effects of Barasertib and radiation. Further mechanistic studies are needed to elucidate the pathways involved in this resistance. Investigations into the role of the DNA damage response, cell cycle checkpoints, and apoptotic pathways in mediating resistance to combination treatments could uncover novel targets for sensitisation strategies.

4.4.1.3 Exploration of Combination Therapies Beyond Standard Chemotherapeutics:

The limited efficacy of Barasertib in combination with standard chemotherapeutic agents warrants the exploration of alternative combination strategies. Future studies should consider testing Barasertib with emerging targeted therapies, immune checkpoint inhibitors, or agents targeting specific survival pathways in HNSCC.

4.4.1.4 Translational Studies in Alternative Preclinical Models:

To further assess the therapeutic potential of Barasertib in HNSCC, it is essential to extend these findings to preclinical animal models. Evaluating the efficacy of Barasertib in xenograft or genetically engineered mouse models of HNSCC, both as a monotherapy and in combination with radiation or chemotherapy, will be critical to advancing this agent towards clinical trials. Additionally, investigating the pharmacokinetics and pharmacodynamics of Barasertib in vivo will help optimize dosing regimens for clinical application.

4.4.1.5 Exploration of Molecular Pathways Governing Slippage and Death:

While this chapter provides evidence that Barasertib induces mitotic slippage and polyploidy, the precise molecular mechanisms remain unclear. Future studies should focus on identifying additional proteins and pathways involved in these processes. Investigating the role of SAC components, kinetochores, and proteins associated

with spindle checkpoint regulation, such as BubR1 and *Mad*2, may yield insights into how Barasertib disrupts mitotic progression and induces slippage.

4.4.1.6 Mechanisms Underlying Differential Sensitivity:

The differential sensitivity of HNSCC cell lines to Barasertib, particularly between UPCI-SCC72 and SCC89 versus B22 and FNB6, warrants further investigation. Exploring the molecular signatures of resistant versus sensitive cells may uncover resistance mechanisms, such as compensatory activation of parallel pathways or differential expression of *AURKB* targets. Such knowledge could inform the development of combination therapies that overcome resistance to *AURKB* inhibition.

4.4.1.7 Studies of Post-Slippage Cellular Fate:

The observed lack of immediate cellular outcomes following slippage in some cell lines, particularly in earlier time points, suggests that the fate of cells post-slippage requires further elucidation. Studies that track cellular outcomes beyond the observed 72-hour window could reveal whether cells that undergo multiple rounds of slippage eventually succumb to death, enter senescence, or contribute to long-term tumour survival.

4.4.1.8 Translation into Preclinical Models:

Given the promising results of Barasertib in inducing cell death in sensitive HNSCC lines, future work should extend to in vivo models. Assessing Barasertib's efficacy in animal models of HNSCC, both as a monotherapy and in combination with radiation or chemotherapy, will be critical for determining its therapeutic potential in clinical settings. Such studies will also help identify optimal dosing strategies and further evaluate the relevance of observed in vitro effects in a more physiologically relevant context.

4.5 Conclusion

This chapter highlights the potent cytotoxicity of Barasertib in HNSCC cell lines, particularly in the more sensitive UPCI-SCC72 and SCC89 lines. However, the lack of radiosensitisation observed across all HNSCC lines indicates that Barasertib's therapeutic potential may be limited to monotherapy or select combination regimens. Further research into the mechanisms of resistance, as well as the exploration of novel therapeutic combinations, is warranted. Translational studies in preclinical models will be essential to determining the clinical utility of Barasertib in the treatment of HNSCC.

This chapter underscores the significant potential of Barasertib as a therapeutic agent in HNSCC, particularly in cell lines sensitive to *AURKB* inhibition. The key mechanisms of action include mitotic slippage, polyploidy induction, and subsequent cell death, though the molecular underpinnings of these processes remain to be fully elucidated. Despite Barasertib's pronounced effects on sensitive cell lines, its

differential activity across cell lines emphasizes the need for a deeper understanding of resistance mechanisms and alternative pathways. Future studies should focus on validating these findings in preclinical models, optimizing dosing strategies, and investigating combination therapies to enhance Barasertib's therapeutic efficacy. The insights gained from this chapter provide a solid foundation for further research into the clinical application of *AURKB* inhibitors in cancer therapy.

5 Evaluation of *AURKA* and *AURKB* expression in published datasets and expression in NSCLC tissue.

5.1 Introduction aims and hypothesis.

An alternative approach to collecting our material is using published data sets from online repositories. We chose to use Gene Expression Omnibus (GEO), a public repository of microarray and other high-throughput functional genomics data. It is maintained by the National Centre for Biotechnology Information (NCBI) and contains data from various organisms and experimental conditions. Non-small cell lung cancer (NSCLC) is characterised by poor patient survival rates, primarily attributed to delayed patient presentation and the inevitable occurrence of local recurrence following radiation therapy (Radiotherapy for lung cancer RCR consensus statements, 2019). In previous chapters, the therapeutic potential of *AURKA* and *AURKB* inhibitors, both as radiosensitisers and monotherapy agents, has been demonstrated in NSCLC and HNSCC using in vitro models.

Elevated expression of *AURKA* has been implicated in tumorigenesis across various cancer types, including NSCLC, thymoma, lower-grade glioma, and prostate adenocarcinoma (Du et al., 2021). Furthermore, several studies have provided evidence linking increased *AURKA* expression with clinical aggressiveness and tumour progression (Nadler et al., 2008; Tong et al., 2004). Notably, a systematic review conducted by Zhang et al. demonstrated a significant association between

AURKA expression and poorer prognosis, encompassing overall survival (OS), progression-free survival (PFS), and disease-free survival (DFS) across multiple solid tumours, even after adjustment for publication bias (Zhang et al., 2015).

Overexpression of *AURKB* has explicitly been associated with aneuploidy and the development of NSCLC, along with squamous cell pathology, increased lymph node metastasis, higher prevalence in males, and poorly differentiated tumours (Vischioni et al., 2006). Studies have also revealed a correlation between *AURKB* expression and chemo- and radio-resistance, leading to a poor prognosis in NSCLC (Yu et al., 2018). Moreover, increased *AURKB* expression has been linked to *EGFR* Tyrosine Kinase resistance in both NSCLC cell lines and patients (Bertran-Alamillo et al., 2019). The observed induction of aneuploidy by heightened *AURKB* expression further suggests its potential as a marker for tumour development and poorer prognosis in NSCLC tumours (Takeshita et al., 2013).

This chapter's primary objective is to assess the correlation between *AURKA* and *AURKB* expression levels and patient overall and progression-free survival in NSCLC. These findings hold significant promise for advancing our understanding of the role played by *AURKA* and *AURKB* in NSCLC progression, thereby aiding in the development of targeted therapeutic strategies and the identification of potential biomarkers for guiding clinical decision-making.

The work in this chapter will also aim to assess whether *AURKA* or *AURKB* can be identified as potential biomarkers in NSCLC and HNSCC, which could have practical diagnostic and prognostic implications in clinical practice.

The hypotheses of this chapter are:

1. *AURKA* and *AURKB* are significantly differentially expressed in both NSCLC and HNSCC at the mRNA level.

2. Hub genes identify genes associated with progression-free survival (PFS) and Overall survival (OS) in NSCLC and HNSCC.

3. High *AURKA* protein expression is correlated with poor overall and progression-free survival in NSCLC patients.

4. High *AURKB* protein expression is correlated with poor overall and progression-free survival in NSCLC patients.

Aims of this chapter is to assess the following:

1. The differential gene expression of each *AURKA* and *AURKB* mRNA in HNSCC versus normal tissue.

2. The differential gene expression of each *AURKA* and *AURKB* mRNA in NSCLC compared to normal tissue.

3. To assess whether *AURKA* and *AURKB* are potential hub genes/biomarkers in HNSCC and NSCLC.

4. Correlate protein expression of *AURKA* with patient overall and progression-free survival in NSCLC.

5. Determine the optimal staining conditions for *AURKB* in IHC.

6. Correlate protein expression of *AURKB* with patient overall and progression-free survival in NSCLC.

Previous work:

Previous work in the HB lab optimised IHC staining for *AURKA* in cell lines of NSCLC and tested NSCLC biopsy samples. (Figures in appendix 7.7).

5.2 Results

5.2.1 Differential gene expression of *AURKA* and *AURKB* in NSCLC cancerous tissue.

We started by loading several R packages that are commonly used for gene expression analysis, namely: library(affy), library(GEOquery), library(EnhancedVolcano), library(ggplot2), library(ggrepel), library(wesanderson), library(annotate), library(enrichplot), library(phe*atm*ap), library(dplyr), library(PCAtools), library(limma), library(ggpubr). Then, we downloaded and imported the dataset specified by the GEO accession number. The script performed several quality control steps, such as checking the distribution of gene expression levels and removing lowly expressed genes. Next, differential gene expression analysis was done between two sample groups (normal vs. cancer tissue) using linear regression, contrasts, and empirical Bayes methods. A table of significantly differentially expressed genes and their corresponding fold changes, p-values, and adjusted p-values were generated. Visualisation steps, such as a gene expression he*atm*ap and a PCA plot of sample clustering, were also generated. Finally, expression and feature data as CSV files were exported and used for network analysis.

Protein-protein interaction (PPI) networks were constructed using the STRING database and visualised by Cytoscape software using these gene lists from the expression data. Molecular Complex Detection (MCODE) was used to identify the significant networks in the PPI network. Hub genes were filtered using CytoHubba software (The *TOP* 30 genes in terms of rank AND having a degree score >10), and

correlation against overall and post-progression-free survival was done using the Kaplan-Meier plotter. Hub gene expression of NSCLC adenocarcinoma and squamous cell cancers vs. normal tissue were investigated using GeneExpression Profiling Interactive Analysis (GEPIA).

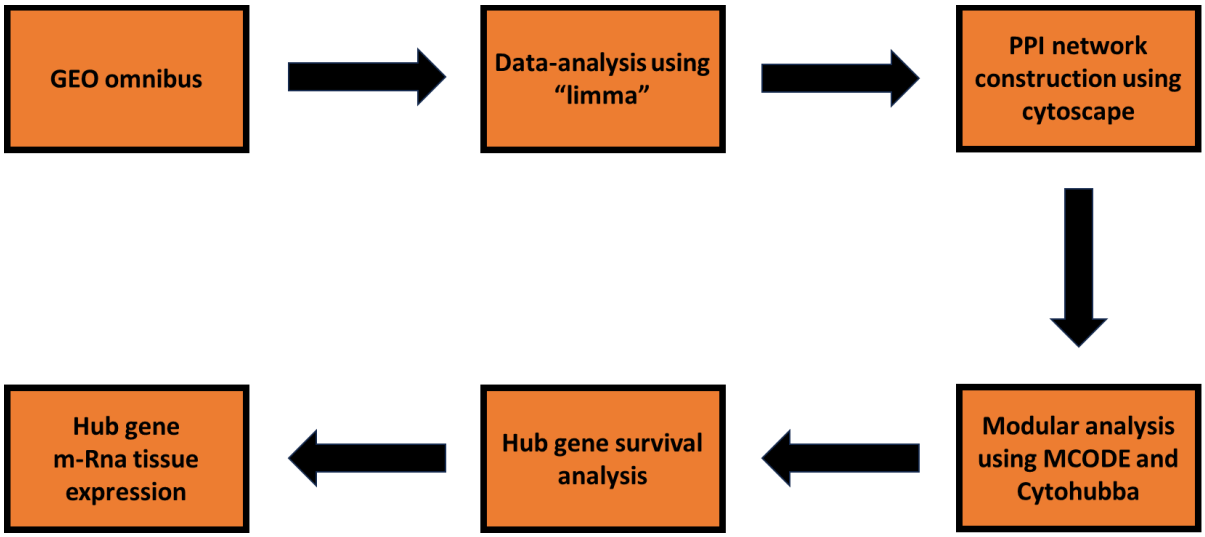


Figure 5-1: **The Bioinformatic Pathway outline on the NSCLC and HNSCC tissue data sets.** Five NSCLC samples were chosen alongside four oral cavity and two nasopharyngeal samples.

They were chosen using the GEO omnibus dataset https://www.ncbi.nlm.nih.gov/geo/. Data analysis was done using the R "limma package." The PPI network was constructed using Cytoscape, with the significant modules constructed and analysed using CytoHubba and MCODE. Survival analysis was done using the kmplotter website of the hub genes, and their m-RNA tissue expression was reviewed using GEPIA2.

We started by loading several R packages that are commonly used for gene expression analysis, namely: **library**(affy), **library**(GEOquery), **library**(EnhancedVolcano), **library**(ggplot2), **library**(ggrepel), **library**(wesanderson), **library**(annotate), **library**(enrichplot), **library**(phe*atm*ap), **library**(dplyr), **library**(PCAtools), **library**(limma), **library**(ggpubr). Then, we downloaded and imported the dataset specified by the GEO accession number. The script performed several quality control steps, such as checking the distribution of gene expression levels and removing lowly expressed genes. Next, differential gene expression analysis was done between two sample groups (normal vs. cancer tissue) using linear regression, contrasts, and empirical Bayes methods. A table of significantly differentially expressed genes and their corresponding fold changes, p-values, and adjusted p-values were generated. Visualisation steps, such as a gene expression ph*eat*map and a PCA plot of sample clustering, were also generated. Finally, expression and feature data as CSV files were exported and used for network analysis.

Protein-protein interaction (PPI) networks were constructed using the STRING database and visualised by Cytoscape software using these gene lists from the expression data. Molecular Complex Detection (MCODE) was used to identify the significant networks in the PPI network. Hub genes were filtered using CytoHubba software (**The *TOP* 30 genes in terms of rank AND having a degree score >10**), and correlation against overall and post-progression-free survival was done using the Kaplan-Meier plotter. Hub gene expression of NSCLC adenocarcinoma and squamous cell cancers vs. normal tissue were investigated using GeneExpression Profiling Interactive Analysis (GEPIA).

5.2.1.1 *AURKA* and *AURKB* were differentially expressed in three out of five NSCLC datasets analysed.

Five GEO microarray datasets downloaded from **GSE10072**, **GSE19804**, **GSE30219**, **GSE33532**, and **GSE101929** (Table 5-1 A-B) https://www.ncbi.nlm.nih.gov/geo/ were used to assess *AURKA* and *AURKB* differential gene expression. After pre-processing the data, the limma package performed the differential analysis with cut-off criteria of adjusted P-value (adj.P) <0.05 and |logFC|≥2.

A

Accession number	Tumour type
GSE10072	NSCLC
GSE19804	NSCLC
GSE101929	NSCLC
GSE30219	NSCLC
GSE33532	NSCLC

B

Lung					
GSE accession number	**Total number of samples**	**Normal tissue**	**Cancer Tissue**	**Males**	**Females**
GSE33532	100	20	80	80	20
GSE10072	107	49	58	69	38
GSE19804	120	60	60	0	120
GSE101929	66	34	32	28	38
GSE30219	307	14	293	264	43

Table 5-1 **A-B: Accession numbers and *patient characteristics of the NCSLC GEO samples.* A:** Five GEO accession samples were chosen for the bioinformatic analysis. **B:** Each accession number has different ratios of normal vs cancer tissue and male's vs females demonstrating the heterogeneity of the samples in the analysis.

AURKA was significantly differentially expressed in three datasets, **GSE30219** (LogFC of 2.5891, adj.P of 5.84E-30), **GSE33532** (LogFC of 2.57159, adj.P of 1.78E-28) and **GSE101929** (LogFC of -3.02834, adj.P of 1.37E-13). *AURKB* was also found to be differentially expressed in **GSE30219** (LogFC of 2.41239, adj.P of 5.68E-21), **GSE33532** (LogFC of 2.12364, adj.P of 6.33E-24) and **GSE101929** (LogFC of -2.50062, adj.P of 8.68E-13) (Table 5-2). Appendix Table 7.1.2.5 shows the full results of DEG analysis in each GEO data set.

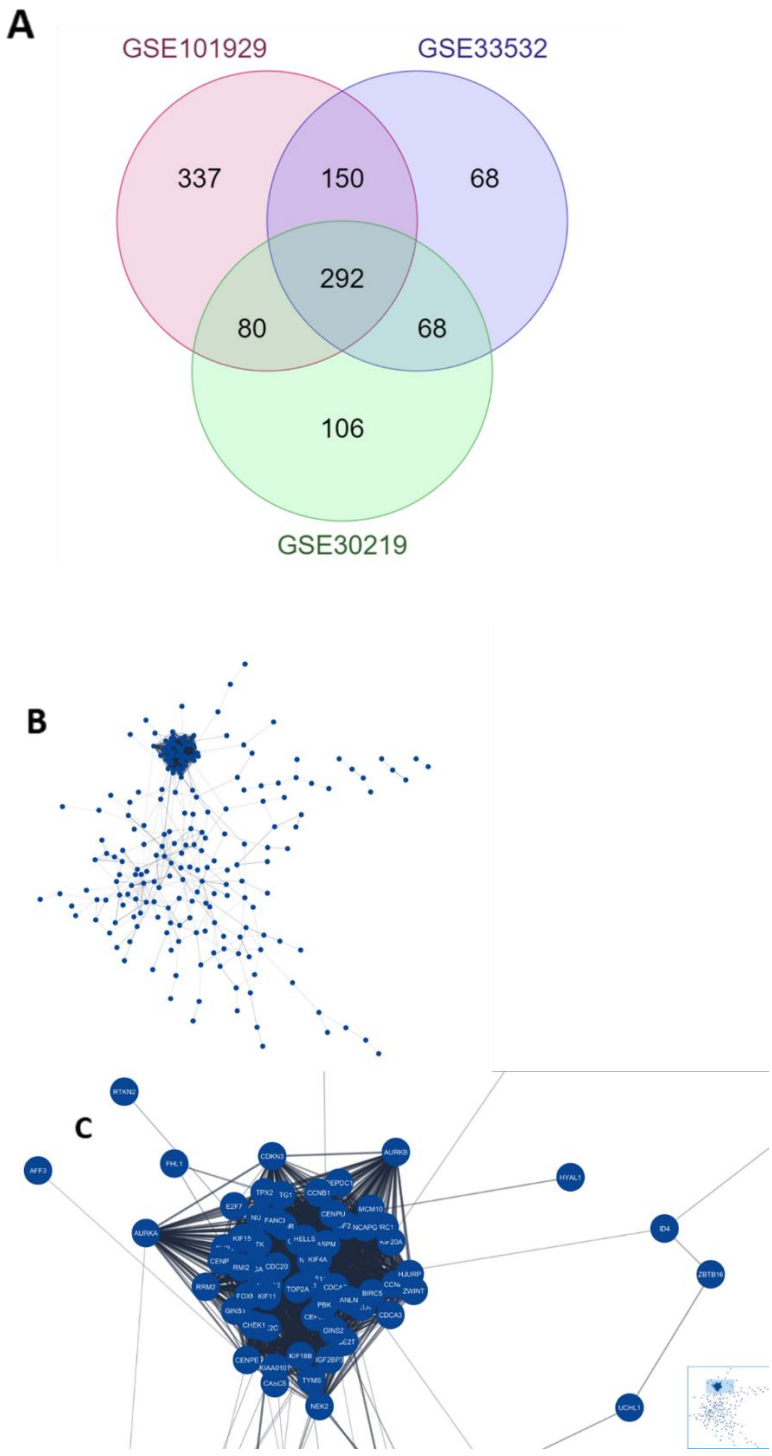
GSE accession number	Gene Symbol	logFC	AveExpr	p.Value	Adj.P.Val
GSE10072	AURKA	-0.098900526	7.013529	0.47971101	0.9937806
	AURKB	0.02922091	6.278096	0.726486	0.9989598
GSE19804	AURKA	1.27080423	6.623573	2.218498e-16	4.992764e-15
	AURKB	0.8407858	5.483904	2.279022e-13	3.088999e-1
GSE30219	AURKA	2.5891	7.709997	1.01E-31	5.84E-30
	AURKB	2.412394	6.419426	2.30E-22	5.68E-21
GSE33532	AURKA	2.571591	7.110377	8.30E-30	1.78E-28
	AURKB	2.123643	5.826907	5.48E-25	6.33E-24
GSE101929	AURKA	-3.02834	6.458477	3.06E-15	1.37E-13
	AURKB	-2.50062	3.874679	2.42E-14	8.68E-13

Table 5-2: **Table of log fold changes along with the significance values**: *The and log fold changes and adj.P values are shown for GSE33532, GSE30219, and GSE30219, where both genes demonstrate significant differential gene expression.* ***LogFC (Log Fold Change):*** *Log Fold Change represents the logarithm of the ratio of gene expression levels between two conditions or groups. It quantifies how much a gene's expression has changed between two experimental conditions. A positive logFC indicates upregulation (increased expression) in one condition compared to the other, while a negative logFC indicates downregulation (decreased expression).* ***AveExpr (Average Expression):*** *AveExpr or Average Expression is the average gene expression level across all experiment samples. It provides a measure of the overall expression level of a gene, which can help filter out genes with very low expression levels that may not be biologically relevant or identify highly expressed genes****. P-value (t-test p-value):*** *The T p-value is a statistical measure that assesses whether the difference in gene expression between two groups (e.g.,* treatment *vs. control) is statistically significant. It helps determine if the observed difference in gene expression is likely due to a natural biological effect or if it could have occurred by chance. A small p-value (typically less than 0.05) suggests the difference is significant.* ***Adj.P. Val (Adjusted P-Value):*** *The Adj.P. Val is a p-value adjusted for multiple testing to control the false discovery rate (FDR). One standard method for adjustment is the Benjamini-Hochberg procedure. Multiple hypothesis testing can increase the likelihood of false positives (Type I errors). Adjusted p-values help correct this by providing a more stringent criterion for significance. Genes with a low Adj.P. Val (typically less than 0.05) are considered statistically significant after adjusting for multiple comparisons.*

5.2.1.2 *AURKA* and *AURKB* were present in the PPI network, and both were found to be HUB genes.

The common significant (both up and downregulated together) DEGs in the three datasets were taken and submitted to STRING. The lists of DEG genes (Appendix 7.2.2) from each data set where *AURKA* and *AURKB* were significantly differentially expressed were combined, and the shared genes between all three were grouped using a multiple list comparator (https://molbiotools.com/listcompare.php).

The DEG PPI network comprised 277 nodes and 1825 edges, and 30 hub genes were identified using the CytoHubba software described above. *AURKA* and *AURKB* were located in the 1st module using MCODE (Figures 5-2: A, B and C) (Bader and Hogue, 2003).


A
GSE101929
GSE33532
337
150
68
292
80
68
106
GSE30219
B
C
RTKN2
AFF3
FHL1
CDKN3
AURKB
HYAL1
ID4
ZBTB16
AURKA
CENPF
NEK2
UCHL1

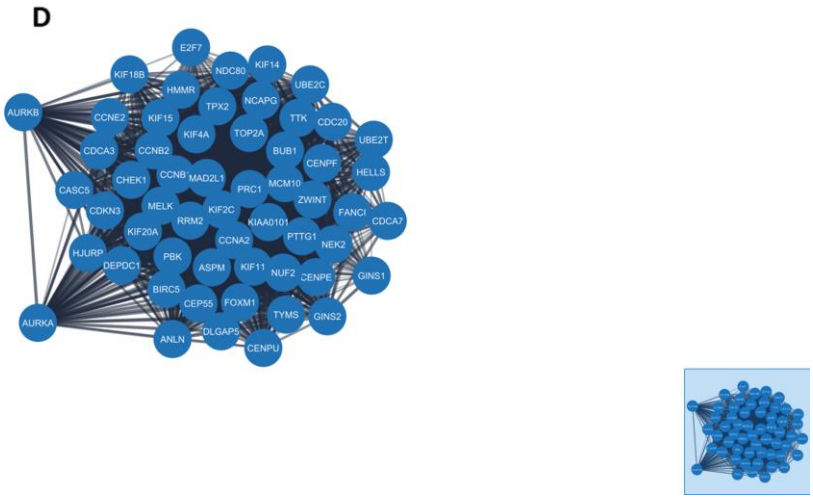


Figure 5-2: **A:** Using a Venn diagram demonstrating the common Hub genes between GSE30219, GSE33532 and GSE101929 (https://molbiotools.com/listcompare.php). **B-C** *Using Cytoscape, the PPI network demonstrating a network comprising 277 nodes and 1825 edges is visualised.* A close-up of *AURKA* and *AURKB* within the PPI network is shown. The Networks were plotted by inputting the 30 HUB genes using the STRING app, part of the Cytoscape software **D** *AURKA* and *AURKB* were visualised using MCODE (Molecular Complex Detection) a plugin for Cytoscape a software tool for visualizing and analyzing biological networks using a Degree Cutoff of two a Node score cut off of 0.2 a K-score of 2 and a Max depth of 100.

The top thirty nodes with a degree score >10 was classed as potential HUB genes. The potential hub genes identified were *ASPM*, *AURKA*, *AURKB*, BIRC5, BUB1, *CCNA*2, *CCNB*1, *CCNB*2, CDC20, *CENPF*, *CEP*55, *CHEK*1, *DLGAP*5, *HMMR*, KIAA0101, *KIF*11, *KIF*15, *KIF*20A, *KIF*2C, *MAD*2L1, MCM10, MELK, *NCAPG*, *NUF*2, PBK, RRM2, *TOP*2A, TPX2, *TTK* and *UBE*2C (Table 5-3)

Rank	Gene Name	Gene Number	Function	Score
1	ASPM	9606.ENSP00000356379	Regulates brain size and development during fetal growth.	60
2	TTK	9606.ENSP00000358813	Plays a role in cell division and ensures proper chromosome separation.	58
2	KIF20A	9606.ENSP00000378356	Involved in cell division and helps move cellular materials.	58
2	TOP2A	9606.ENSP00000411532	Manages DNA topology by facilitating DNA strand cutting and rejoining.	58
5	NCAPG	9606.ENSP00000251496	Part of the condensin complex, aiding in chromosome condensation.	57
5	CCNB1	9606.ENSP00000256442	Encodes a protein crucial for cell cycle progression.	57
5	CCNA2	9606.ENSP00000274026	Encodes a protein involved in regulating the cell cycle.	57
5	MAD2L1	9606.ENSP00000296509	Monitors chromosome alignment during cell division.	57
5	TPX2	9606.ENSP00000300403	Assists in microtubule organization during cell division.	57
5	CENPF	9606.ENSP00000355922	Contributes to the formation of the kinetochore during cell division.	57
5	HMMR	9606.ENSP00000377492	Participates in cell motility and cell division processes.	57
5	PBK	9606.ENSP00000428489	Regulates cell cycle progression and cell proliferation.	57
13	AURKA	9606.ENSP00000216911	Involved in controlling cell division and centrosome function.	56
13	DLGAP5	9606.ENSP00000247191	Facilitates microtubule bundling during cell division.	56
13	KIF11	9606.ENSP00000260731	Functions in cell division by moving and organizing microtubules.	56

Rank	Gene Name	Gene Number	Function	Score
13	NUF2	9606.ENSP00000271452	Part of the kinetochore complex, important for chromosome segregation.	56
13	CCNB2	9606.ENSP00000288207	Encodes a protein that regulates the cell cycle.	56
13	CCNB2	9606.ENSP00000288207	Encodes a protein that regulates the cell cycle.	56
13	MELK	9606.ENSP00000298048	Implicated in cell cycle regulation and stem cell maintenance.	56
13	KIAA0101	9606.ENSP00000300035	Plays a role in DNA replication and cell cycle control.	56
13	BUB1	9606.ENSP00000302530	Monitors proper attachment of chromosomes to spindle fibers.	56
13	AURKB	9606.ENSP00000313950	Regulates chromosome segregation and cytokinesis.	56
13	UBE2C	9606.ENSP00000348838	Participates in protein degradation and cell cycle control.	56
13	RRM2	9606.ENSP00000353770	Provides building blocks for DNA synthesis during cell division.	56
13	KIF2C	9606.ENSP00000361298	Involved in microtubule dynamics and chromosome alignment.	56
13	CDC20	9606.ENSP00000361540	Regulates progression through the cell cycle by controlling protein degradation.	56
13	CHEK1	9606.ENSP00000388648	Acts as a checkpoint kinase to ensure DNA integrity during replication.	56
27	CENPE	9606.ENSP00000265148	Facilitates chromosome movement during cell division.	55
27	BIRC5	9606.ENSP00000301633	Inhibits cell death and promotes cell survival.	55
27	NEK2	9606.ENSP00000355966	Regulates centrosome separation and spindle assembly.	55
27	MCM10	9606.ENSP00000418268	Involved in DNA replication initiation and cell cycle progression.	55

Table 5-3: List of genes generated from the common Hub genes between GSE30219, GSE33532 and GSE101929 (https://molbiotools.com/listcompare.php). The score indicates values representing the degree of connectivity of a node (gene) within a network. Genes with scores of greater than ten were chosen as potential hub genes.

5.2.1.3 Although *AURKA* and *AURKB* were revealed to be negative prognostic markers, they were no more specific than the other hub gene candidates.

Thirty hub genes were analysed using the KM plotter online database https://kmplot.com/. Sources for the database are GEO, The European Genome-phenome Archive (EGA), and the Cancer Genome Atlas (TCGA). The correlation between the target gene mRNA expression levels, overall survival (OS) rate and post-progression survival (PPS) in NSCLC groups were calculated by the Kaplan–Meier curve and log-rank test (Győrffy et al., 2013). Post-progression survival (PPS) is the survival time following progressive disease (PD) during treatment with any drug.

To assess survival, the analysis included all patients with curative surgery, chemotherapy, and radiotherapy (patients with metastatic disease were excluded). The datasets used included patients from GEO omnibus and the TCGA cohorts, leaving 463 patients from a possible 2167.

The results are shown using Kaplan–Meier survival plots. The hazard ratio (HR) and 95% confidence were calculated automatically and listed. The values of each group are shown as the mean +/- SD. P-value < 0.05 was regarded as statistically significant by using the Log-rank test and multivariate analysis.

Increased expression of *AURKA* and *AURKB* was associated with a reduction in overall survival in patients with NSCLC with log-rank p-values of 5.9e-0.6 and 3.4e-0.7, respectively (Figure 5-3). The other twenty-eight hub genes were also analysed, demonstrating that their increased expression was associated with poor overall survival (Figure 5-4). This result shows that while *AURKA* and *AURKB* could

potentially function as biomarkers in patients with chemotherapy and radiotherapy, we could not show that they have greater specificity than other HUB gene candidates identified using CytoHubba.

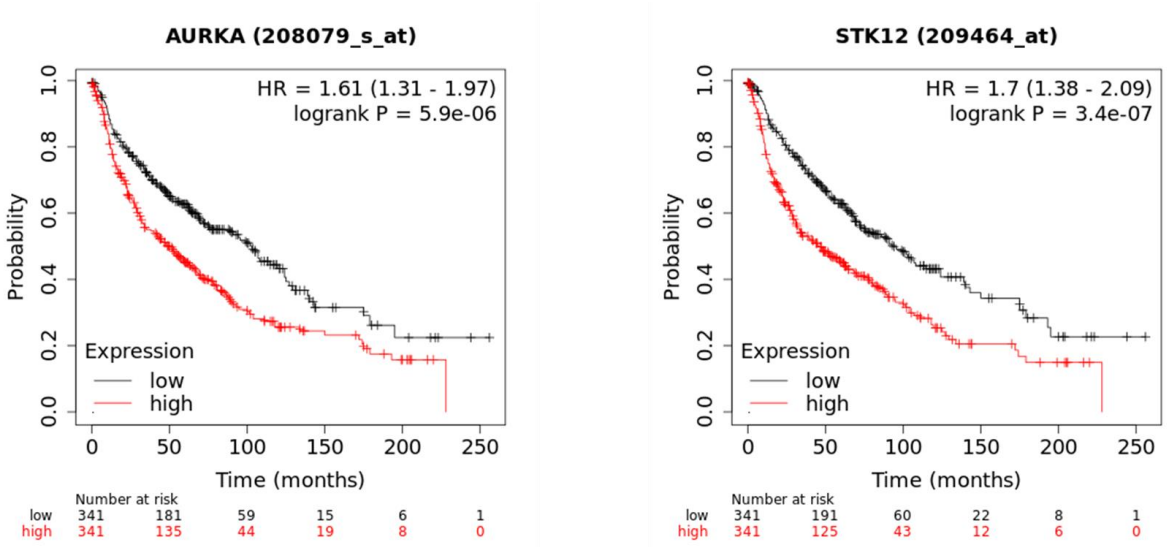
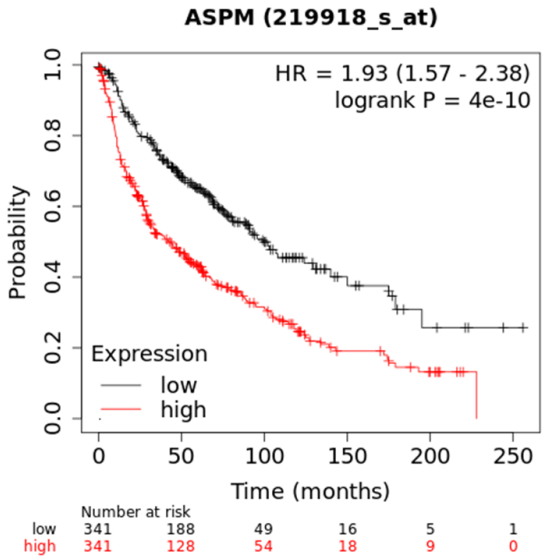
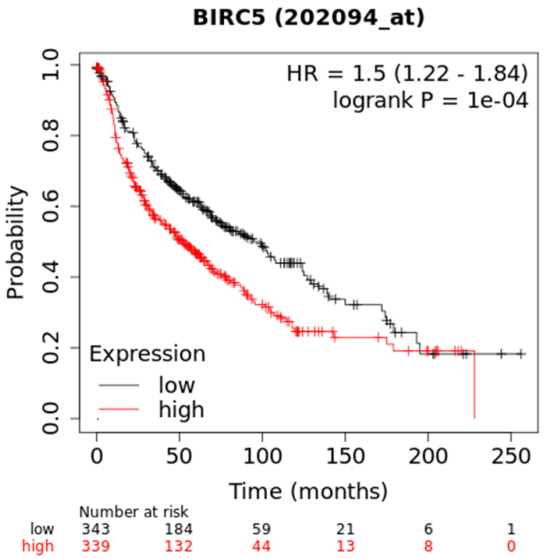
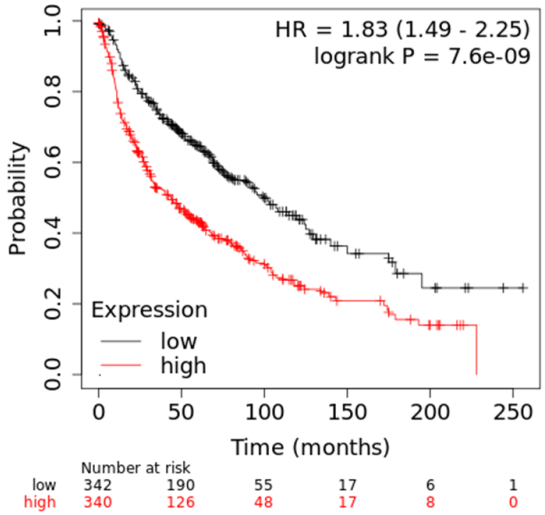
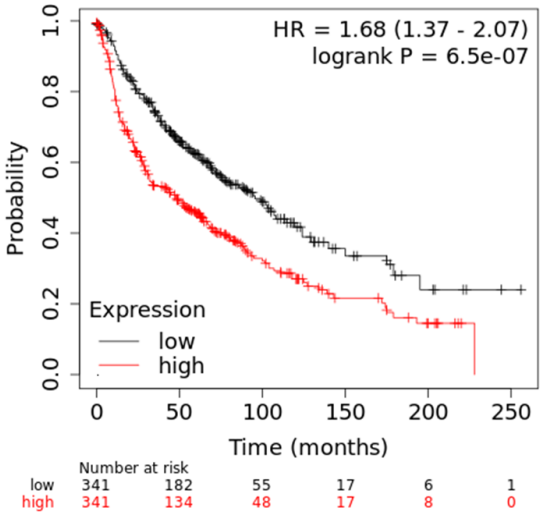


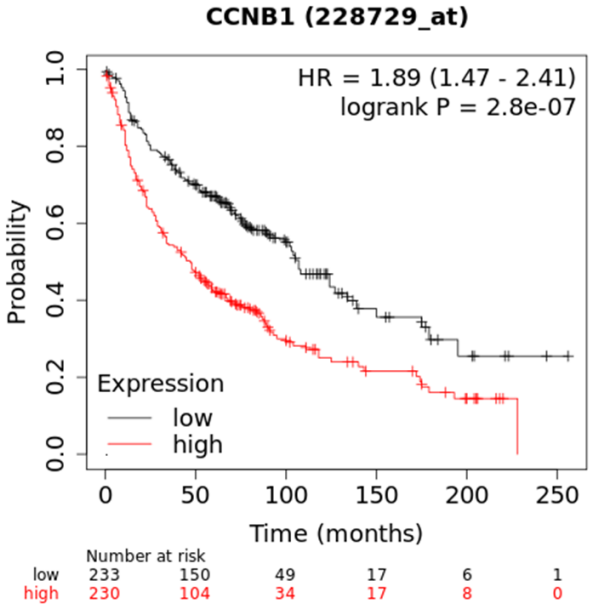
Figure 5-3: *Kaplein Mayer plots showed that overall survival was worse in all high-expressing patients using the identified hub genes and (labelled STK12 on* https://kmplot.com/*). NSCLC patients were chosen using the website* https://kmplot.com/*. Metastatic patients were excluded from the analysis; patients had to have surgery, chemotherapy, and radiotherapy, leaving 463 out of 2000 patients to be analysed. Multivariate analysis was done along with long-rank testing.*

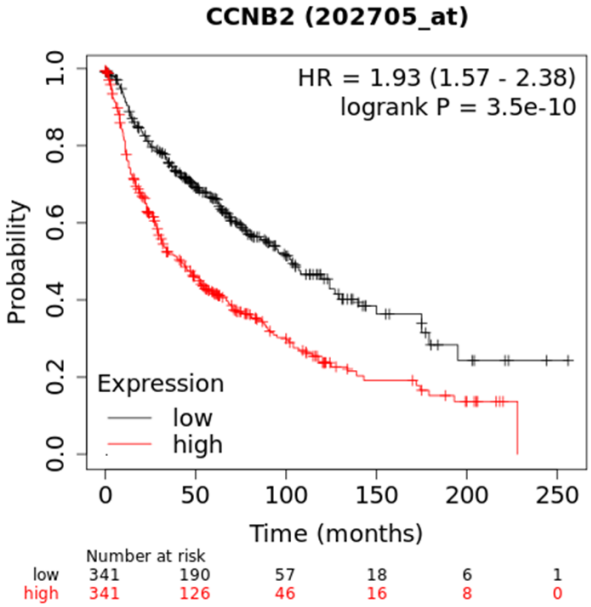

ASPM (219918_s_at)
HR = 1.93 (1.57 - 2.38)
logrank P = 4e-10
Probability
Expression
low
high
Time (months)
Number at risk
low 341 188 49 16 5 1
high 341 128 54 18 9 0

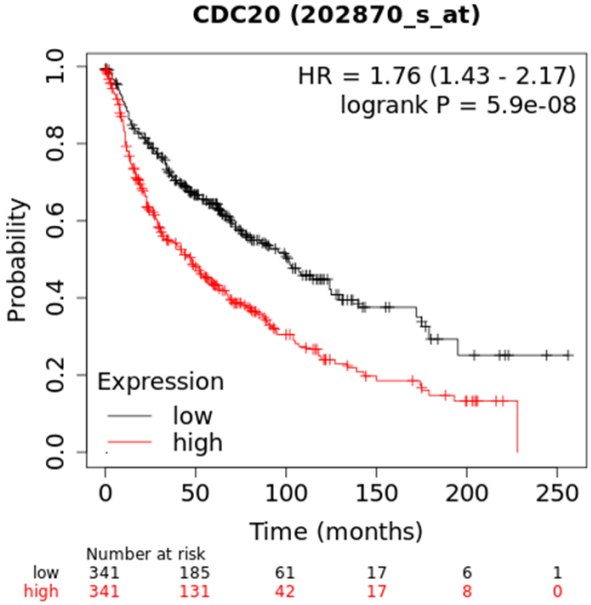

BIRC5 (202094_at)
HR = 1.5 (1.22 - 1.84)
logrank P = 1e-04
Probability
Expression
low
high
Time (months)
Number at risk
low 343 184 59 21 6 1
high 339 132 44 13 8 0

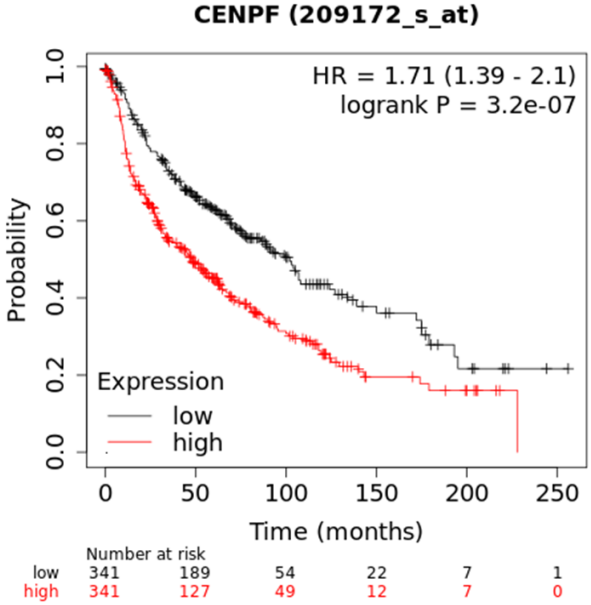

BUB1 (209642_at)
HR = 1.83 (1.49 - 2.25)
logrank P = 7.6e-09
Probability
Expression
low
high
Time (months)
Number at risk
low 342 190 55 17 6 1
high 340 126 48 17 8 0

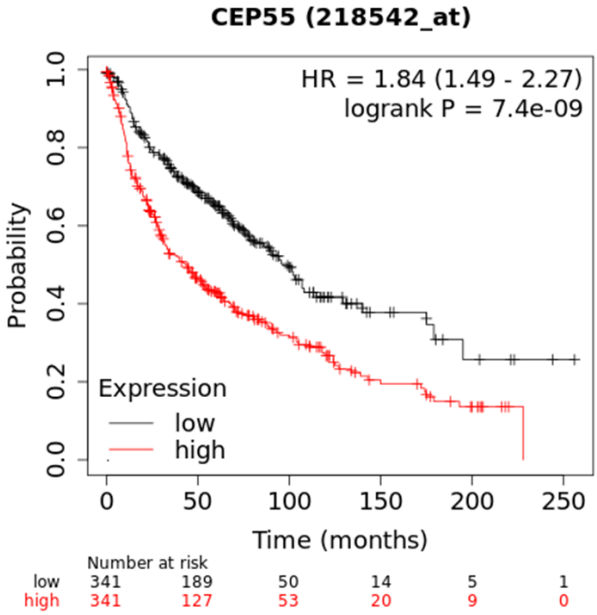

CCNA (213226_at)
HR = 1.68 (1.37 - 2.07)
logrank P = 6.5e-07
Probability
Expression
low
high
Time (months)
Number at risk
low 341 182 55 17 6 1
high 341 134 48 17 8 0

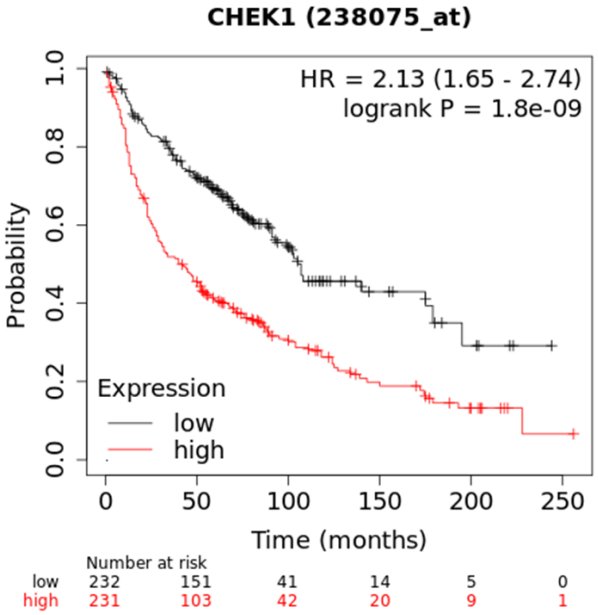

CCNB1 (228729_at)
HR = 1.89 (1.47 - 2.41)
logrank P = 2.8e-07
Probability
Expression
low
high
Time (months)
Number at risk
low 233 150 49 17 6 1
high 230 104 34 17 8 0

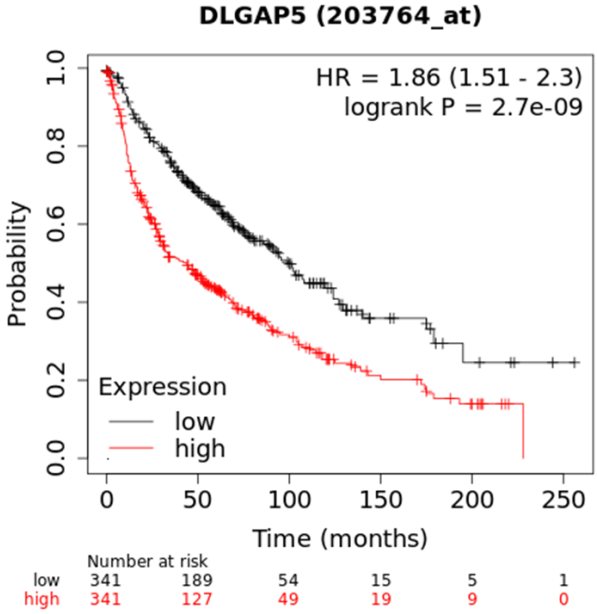

CCNB2 (202705_at)
HR = 1.93 (1.57 - 2.38)
logrank P = 3.5e-10
Probability
Expression
low
high
Time (months)
Number at risk
low 341 190 57 18 6 1
high 341 126 46 16 8 0

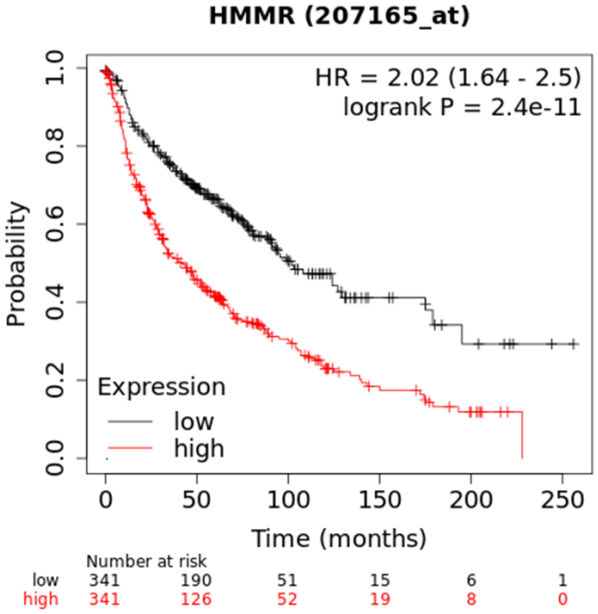

CDC20 (202870_s_at)
HR = 1.76 (1.43 - 2.17)
logrank P = 5.9e-08
Probability
Expression
low
high
Time (months)
Number at risk
low 341 185 61 17 6 1
high 341 131 42 17 8 0

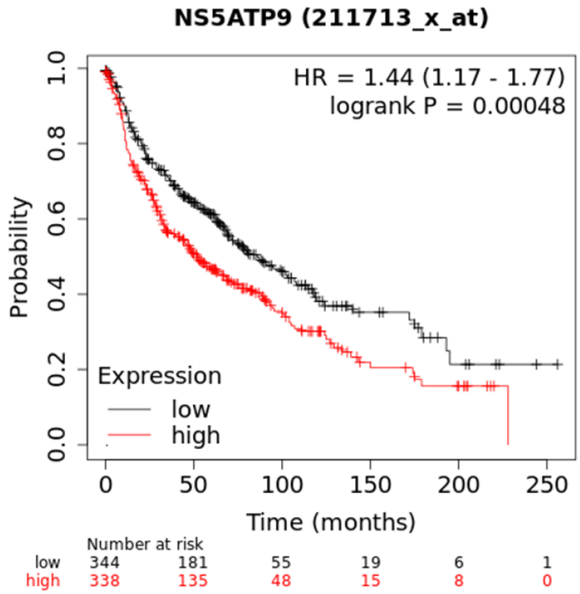

CENPF (209172_s_at)
HR = 1.71 (1.39 - 2.1)
logrank P = 3.2e-07
Probability
Expression
low
high
Time (months)
Number at risk
low 341 189 54 22 7 1
high 341 127 49 12 7 0

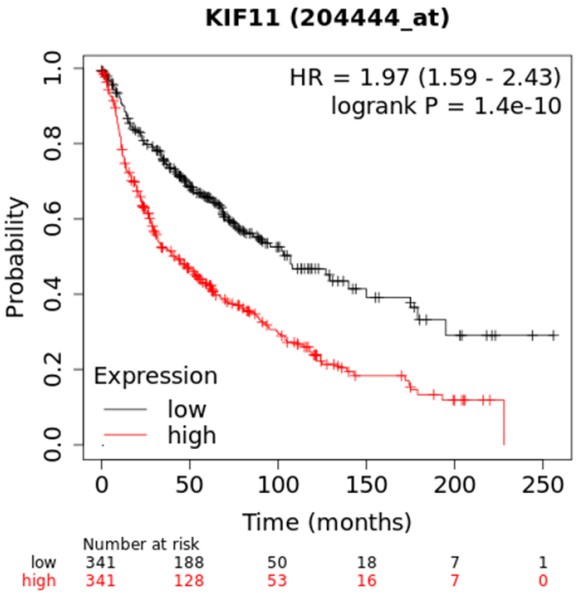

CEP55 (218542_at)
HR = 1.84 (1.49 - 2.27)
logrank P = 7.4e-09
Probability
Expression
low
high
Time (months)
Number at risk
low 341 189 50 14 5 1
high 341 127 53 20 9 0

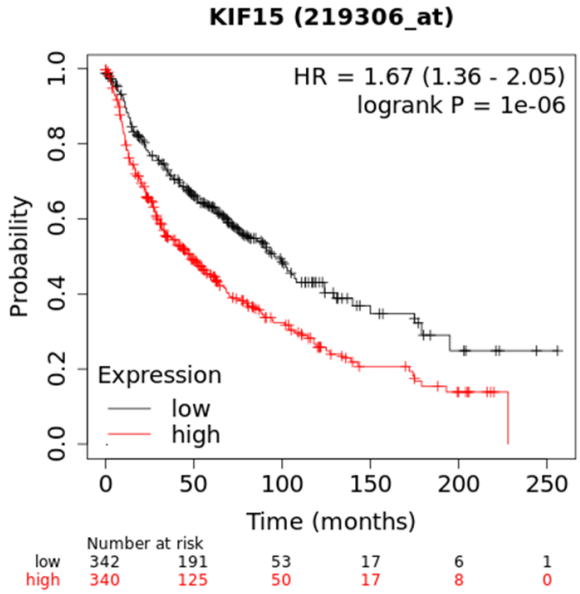

CHEK1 (238075_at)
HR = 2.13 (1.65 - 2.74)
logrank P = 1.8e-09
Probability
Expression
low
high
Time (months)
Number at risk
low 232 151 41 14 5 0
high 231 103 42 20 9 1

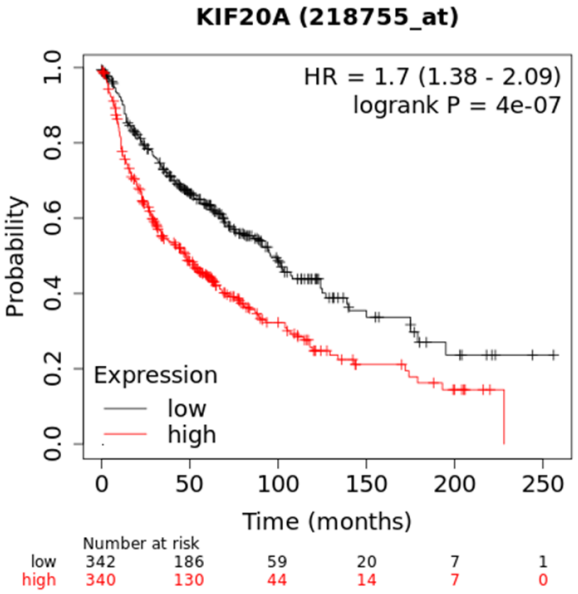

DLGAP5 (203764_at)
HR = 1.86 (1.51 - 2.3)
logrank P = 2.7e-09
Probability
Expression
low
high
Time (months)
Number at risk
low 341 189 54 15 5 1
high 341 127 49 19 9 0

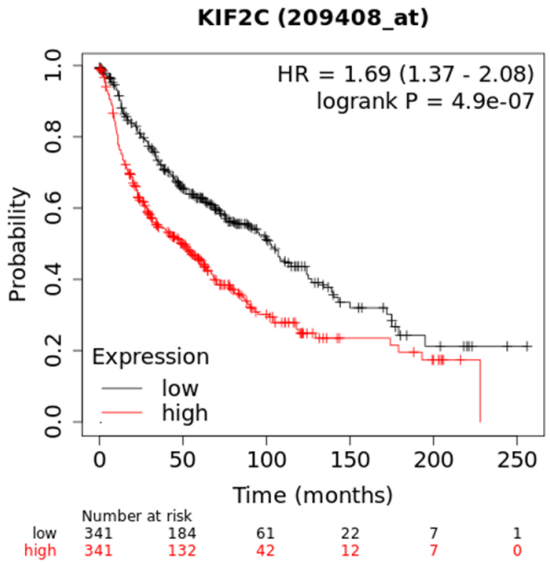

HMMR (207165_at)
HR = 2.02 (1.64 - 2.5)
logrank P = 2.4e-11
Probability
Expression
low
high
Time (months)
Number at risk
low 341 190 51 15 6 1
high 341 126 52 19 8 0

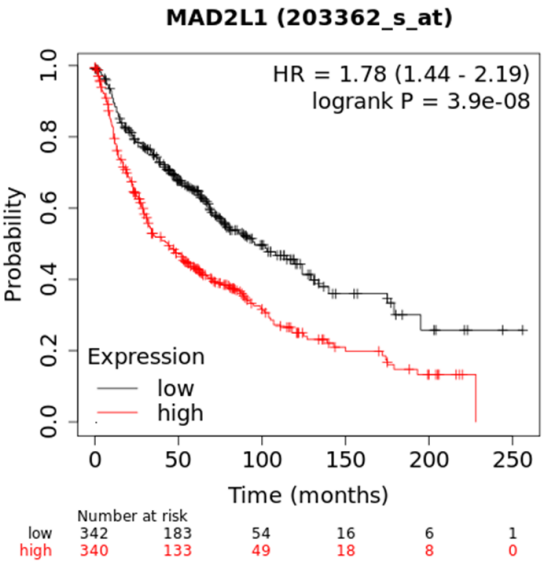

NS5ATP9 (211713_x_at)
HR = 1.44 (1.17 - 1.77)
logrank P = 0.00048
Probability
Expression
low
high
Time (months)
Number at risk
low 344 181 55 19 6 1
high 338 135 48 15 8 0

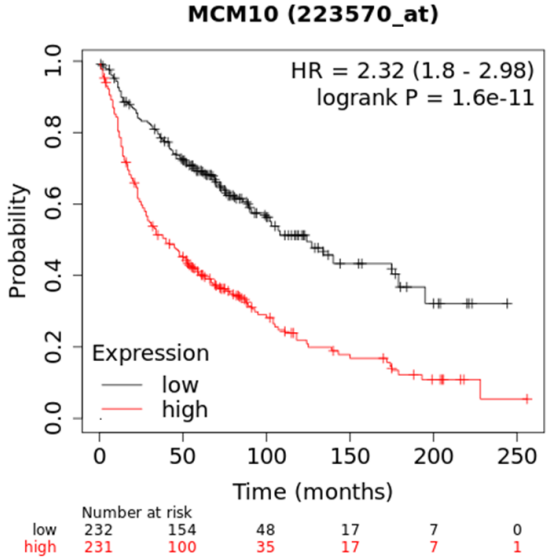

KIF11 (204444_at)
HR = 1.97 (1.59 - 2.43)
logrank P = 1.4e-10
Probability
Expression
low
high
Time (months)
Number at risk
low 341 188 50 18 7 1
high 341 128 53 16 7 0

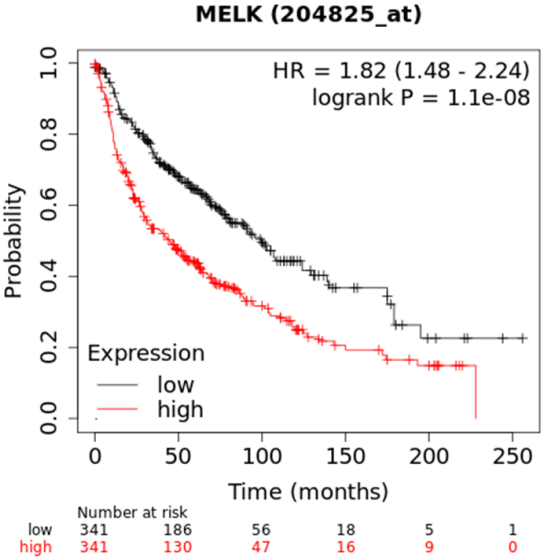

KIF15 (219306_at)
HR = 1.67 (1.36 - 2.05)
logrank P = 1e-06
Probability
Expression
low
high
Time (months)
Number at risk
low 342 191 53 17 6 1
high 340 125 50 17 8 0

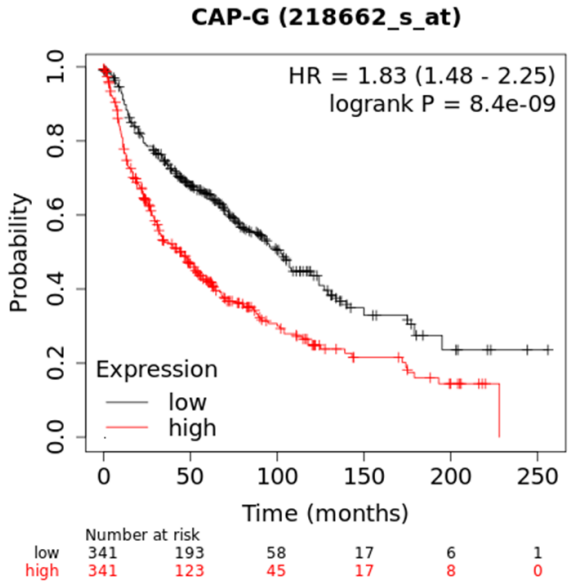

KIF20A (218755_at)
HR = 1.7 (1.38 - 2.09)
logrank P = 4e-07
Probability
Expression
low
high
Time (months)
Number at risk
low 342 186 59 20 7 1
high 340 130 44 14 7 0

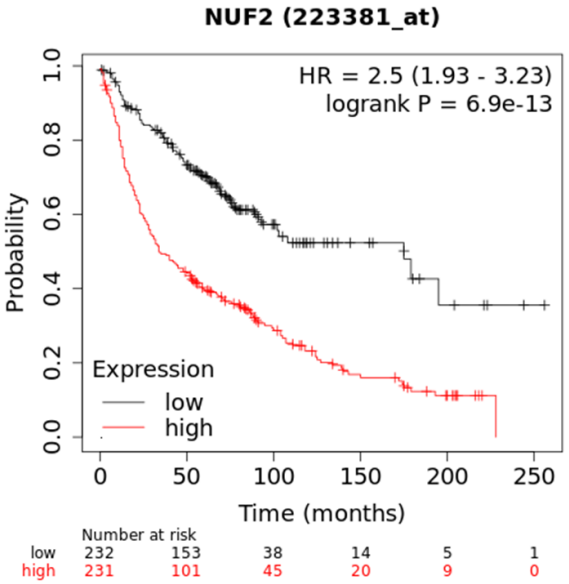

KIF2C (209408_at)
HR = 1.69 (1.37 - 2.08)
logrank P = 4.9e-07
Probability
Expression
low
high
Time (months)
Number at risk
low 341 184 61 22 7 1
high 341 132 42 12 7 0

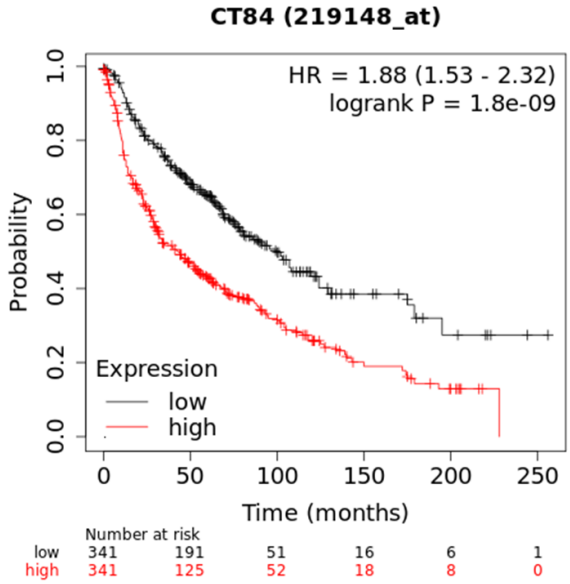

MAD2L1 (203362_s_at)
HR = 1.78 (1.44 - 2.19)
logrank P = 3.9e-08
Probability
Expression
low
high
Time (months)
Number at risk
low 342 183 54 16 6 1
high 340 133 49 18 8 0

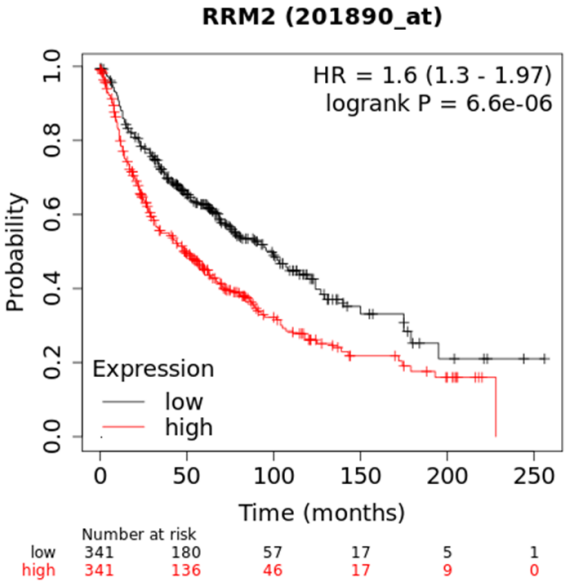

MCM10 (223570_at)
HR = 2.32 (1.8 - 2.98)
logrank P = 1.6e-11
Probability
Expression
low
high
Time (months)
Number at risk
low 232 154 48 17 7 0
high 231 100 35 17 7 1

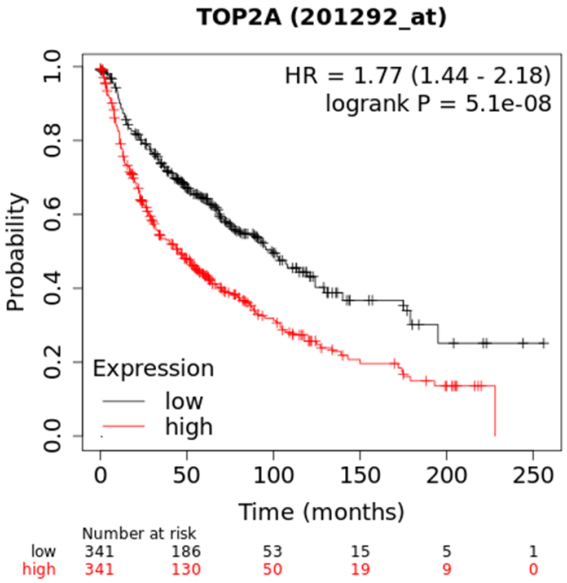

MELK (204825_at)
HR = 1.82 (1.48 - 2.24)
logrank P = 1.1e-08
Probability
Expression
low
high
Time (months)
Number at risk
low 341 186 56 18 5 1
high 341 130 47 16 9 0

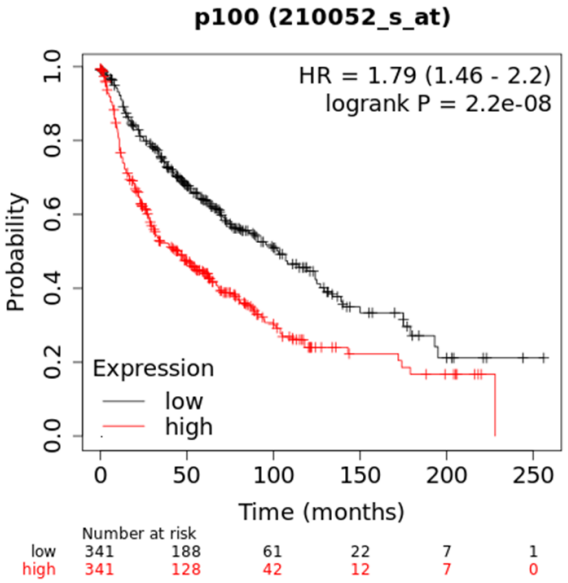

CAP-G (218662_s_at)
HR = 1.83 (1.48 - 2.25)
logrank P = 8.4e-09
Probability
Expression
low
high
Time (months)
Number at risk
low 341 193 58 17 6 1
high 341 123 45 17 8 0

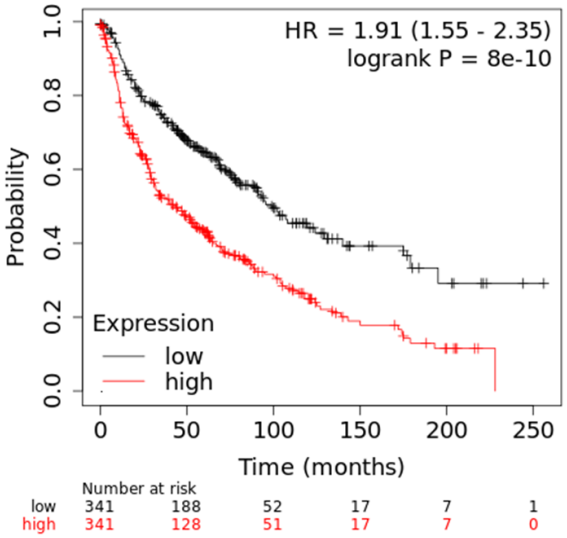

NUF2 (223381_at)
HR = 2.5 (1.93 - 3.23)
logrank P = 6.9e-13
Probability
Expression
low
high
Time (months)
Number at risk
low 232 153 38 14 5 1
high 231 101 45 20 9 0

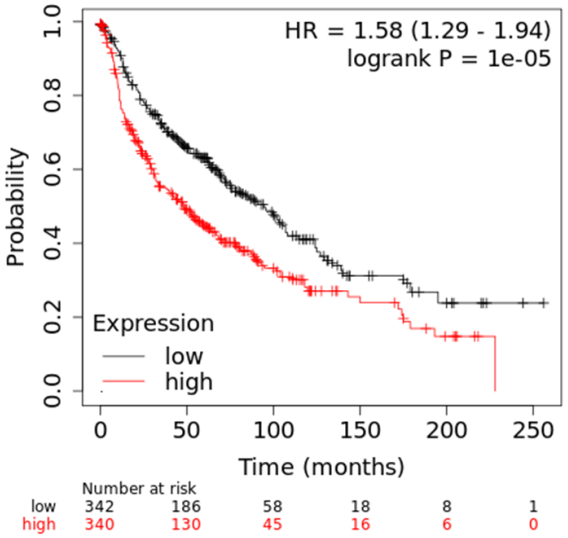

CT84 (219148_at)
HR = 1.88 (1.53 - 2.32)
logrank P = 1.8e-09
Probability
Expression
low
high
Time (months)
Number at risk
low 341 191 51 16 6 1
high 341 125 52 18 8 0


RRM2 (201890_at)
HR = 1.6 (1.3 - 1.97)
logrank P = 6.6e-06
Probability
Expression
low
high
Time (months)
Number at risk
low 341 180 57 17 5 1
high 341 136 46 17 9 0


TOP2A (201292_at)
HR = 1.77 (1.44 - 2.18)
logrank P = 5.1e-08
Probability
Expression
low
high
Time (months)
Number at risk
low 341 186 53 15 5 1
high 341 130 50 19 9 0


p100 (210052_s_at)
HR = 1.79 (1.46 - 2.2)
logrank P = 2.2e-08
Probability
Expression
low
high
Time (months)
Number at risk
low 341 188 61 22 7 1
high 341 128 42 12 7 0

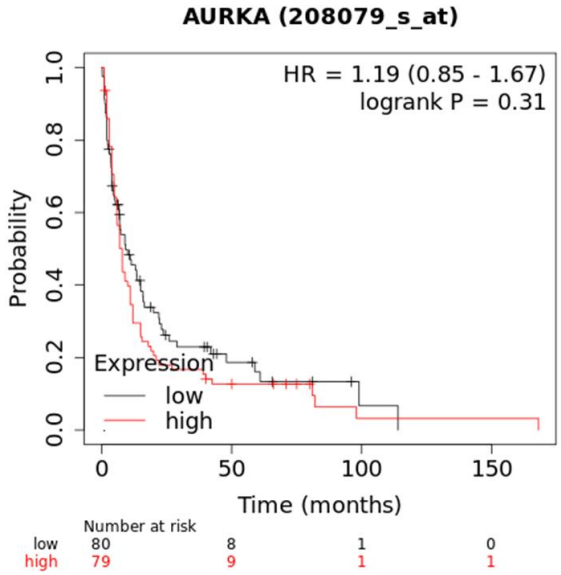

CT96 (204822_at)
HR = 1.91 (1.55 - 2.35)
logrank P = 8e-10
Probability
Expression
low
high
Time (months)
Number at risk
low 341 188 52 17 7 1
high 341 128 51 17 7 0

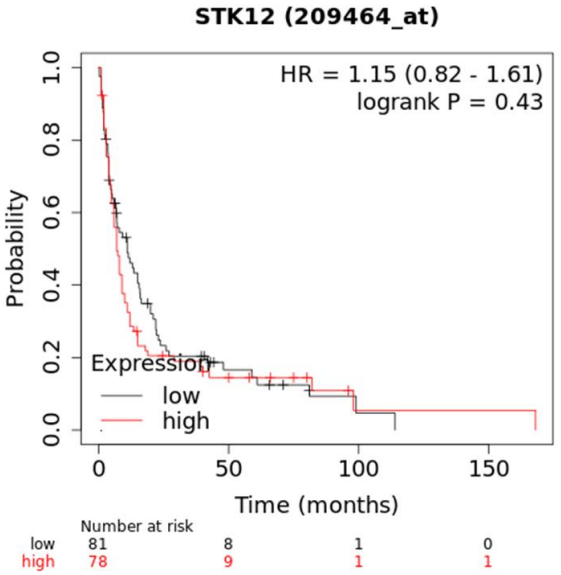

UBE2C (202954_at)
HR = 1.58 (1.29 - 1.94)
logrank P = 1e-05
Probability
Expression
low
high
Time (months)
Number at risk
low 342 186 58 18 8 1
high 340 130 45 16 6 0

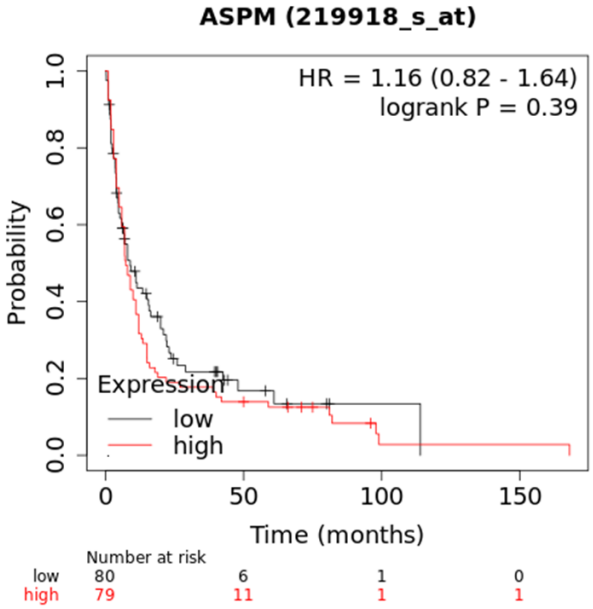
Gene Name	OS Hazard Ratio	OS P-value
ASPM	1.93	4 x 10-10
AURKA	1.61	5.9 x 10-6
AURKB	1.7	3.4 x 10-7
BIRC5	1.5	1.0 x 10-4
BUB1	1.83	7.6 x 10-9
CCNA	1.68	6.5 x 10-7
CCNB1	1.89	2.8 x 10-7
CCNB2	1.93	3.5 x 10-10
CDC20	1.76	5.9 x 10-8
CENPF	1.71	3.2 x 10-7
CEP55	1.84	7.4 x 10-9
CHEK1	2.13	1.8 x 10-9
DLGAP5	1.86	2.7 x 10-9
HMMR	2.02	2.4 x 10-11
KIAA0101	1.44	4.8 x 10-4
KIF11	1.97	1.4 x 10-10
KIF15	1.67	1 x 10-6
KIF20A	1.7	4 x 10-7
KIF2C	1.69	4.9x10-7
MAD2L1	1.78	3.9 x 10-8
MCM10	2.32	1.6 x 10-11
MELK	1.82	1.1 x 10-8
NCAPG	1.83	8.4 x 10-9
NUF2	2.5	6.9 x 10-13
PBK	1.88	1.8 x 10-9
RRM2	1.6	6.6 x 10-6
TOP2A	1.77	5.1 x 10-8
TPX2	1.79	2.2 x 10-8
TTK	1.91	8.0 x 10-10
UBE2C	1.58	10 x 10-5

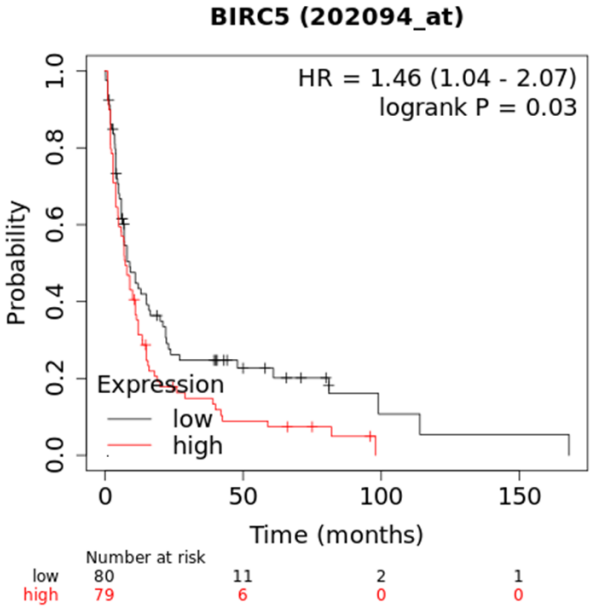
Figure 5-4: *Kaplein Mayer plots showed that overall survival was worse in all high-expressing samples using the identified hub genes. Metastatic patients were excluded from the analysis; patients had to have surgery, chemotherapy, and radiotherapy, leaving 463 out of 2167. Multivariate analysis was done along with log-rank testing.*

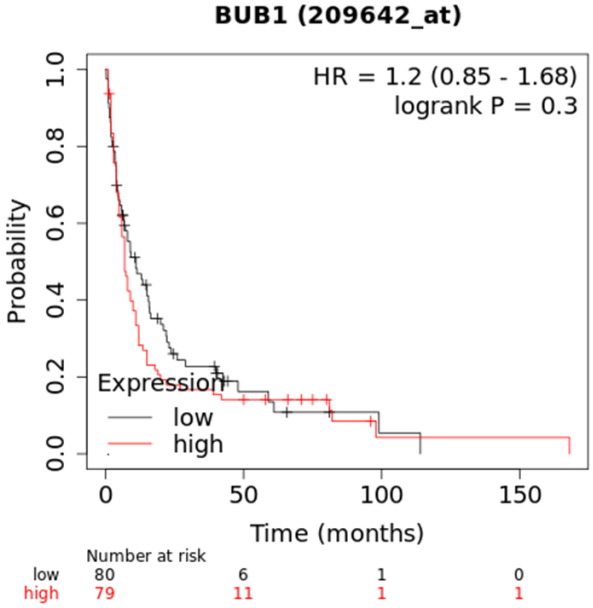
Neither *AURKA* nor *AURKB* shows potential as a biomarker for post-progression survival (PPS). To assess the post-progression survival of the hub genes, the analysis included all patients who had surgery, chemotherapy, and radiotherapy; patients with metastatic disease were excluded, leaving 159 patients (Figure 5-5).

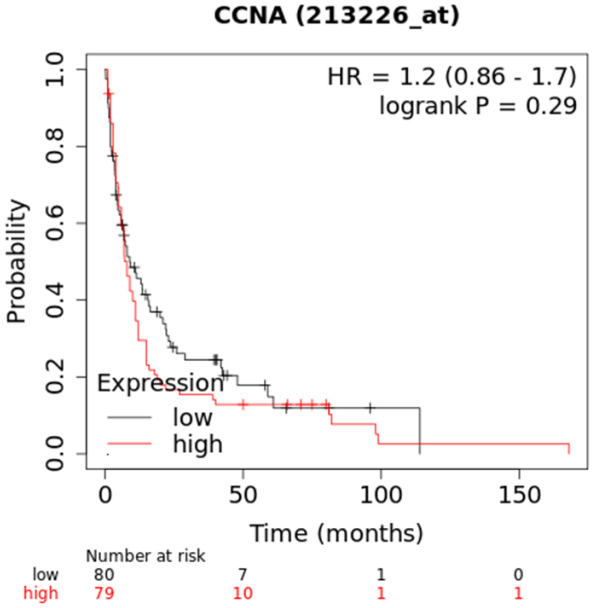

AURKA (208079_s_at)
HR = 1.19 (0.85 - 1.67)
logrank P = 0.31
Probability
Expression
low
high
Time (months)
Number at risk
low 80 8 1 0
high 79 9 1 1

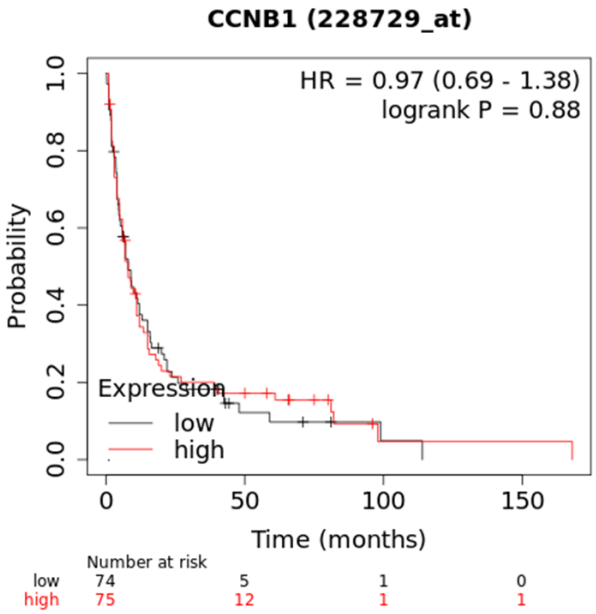

STK12 (209464_at)
HR = 1.15 (0.82 - 1.61)
logrank P = 0.43
Probability
Expression
low
high
Time (months)
Number at risk
low 81 8 1 0
high 78 9 1 1

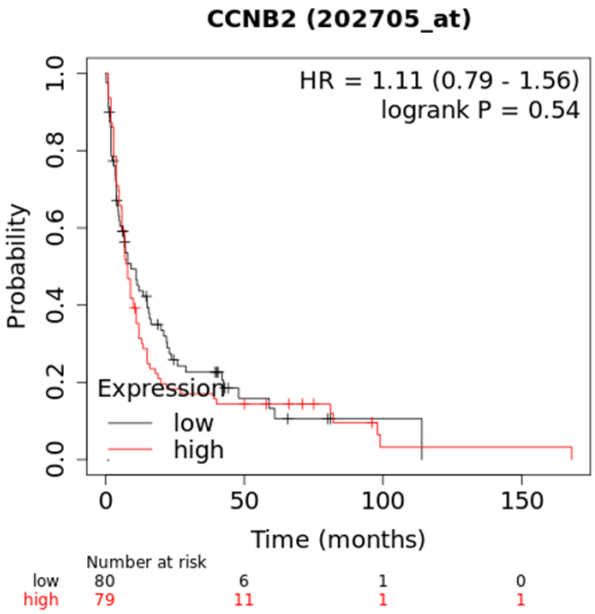

ASPM (219918_s_at)
HR = 1.16 (0.82 - 1.64)
logrank P = 0.39
Probability
Expression
low
high
Time (months)
Number at risk
low 80 6 1 0
high 79 11 1 1

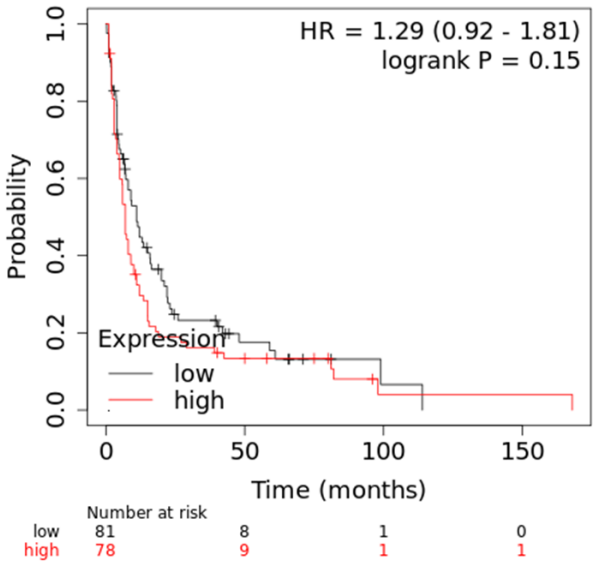

BIRC5 (202094_at)
HR = 1.46 (1.04 - 2.07)
logrank P = 0.03
Probability
Expression
low
high
Time (months)
Number at risk
low 80 11 2 1
high 79 6 0 0

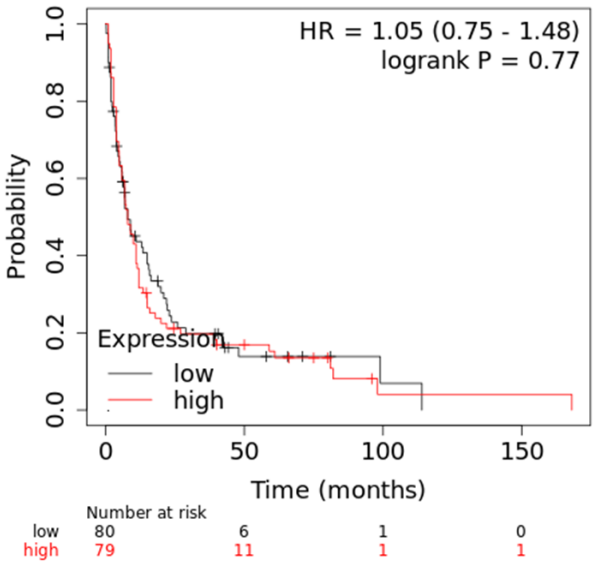

BUB1 (209642_at)
HR = 1.2 (0.85 - 1.68)
logrank P = 0.3
Probability
Expression
low
high
Time (months)
Number at risk
low 80 6 1 0
high 79 11 1 1

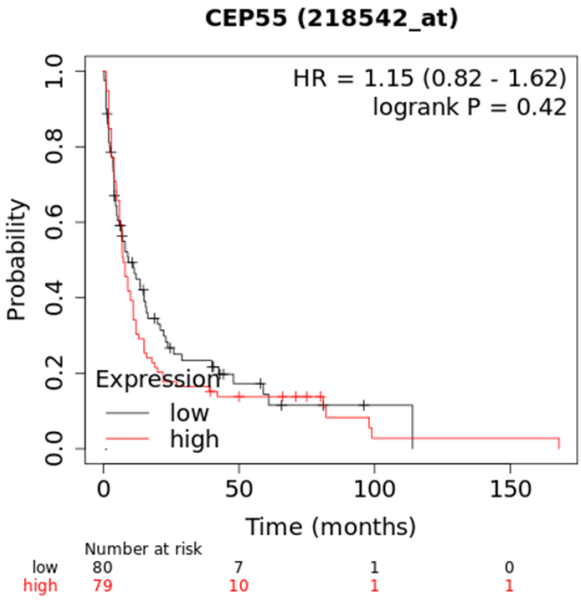

CCNA (213226_at)
HR = 1.2 (0.86 - 1.7)
logrank P = 0.29
Probability
Expression
low
high
Time (months)
Number at risk
low 80 7 1 0
high 79 10 1 1

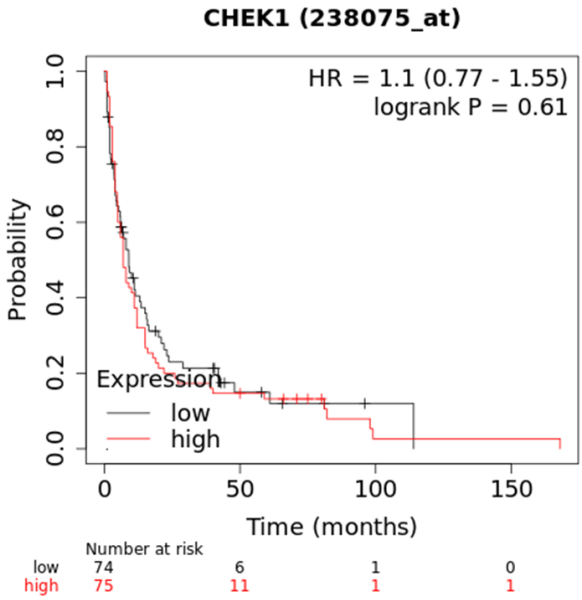

CCNB1 (228729_at)
HR = 0.97 (0.69 - 1.38)
logrank P = 0.88
Probability
Expression
low
high
Time (months)
Number at risk
low 74 5 1 0
high 75 12 1 1

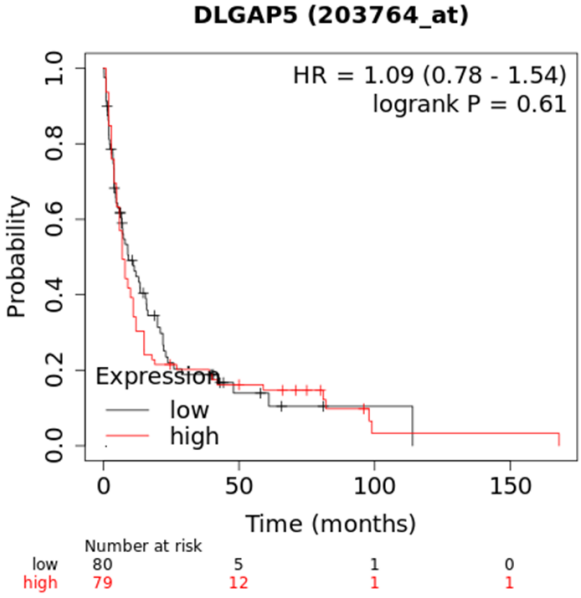

CCNB2 (202705_at)
HR = 1.11 (0.79 - 1.56)
logrank P = 0.54
Probability
Expression
low
high
Time (months)
Number at risk
low 80 6 1 0
high 79 11 1 1

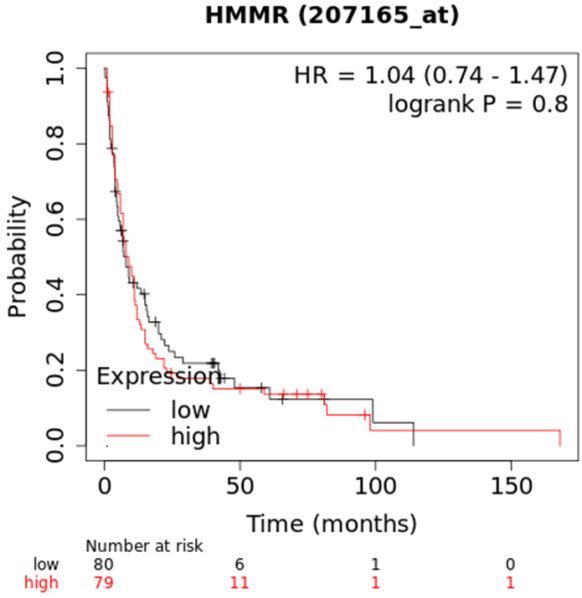

CDC20 (202870_s_at)
HR = 1.29 (0.92 - 1.81)
logrank P = 0.15
Probability
Expression
low
high
Time (months)
Number at risk
low 81 8 1 0
high 78 9 1 1

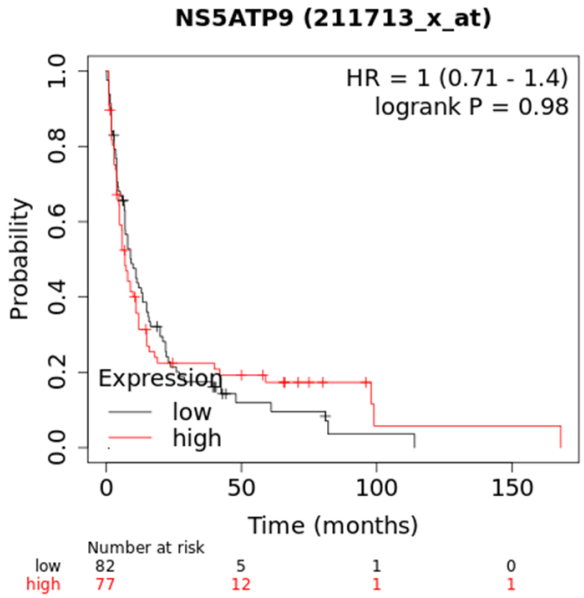

CENPF (209172_s_at)
HR = 1.05 (0.75 - 1.48)
logrank P = 0.77
Probability
Expression
low
high
Time (months)
Number at risk
low 80 6 1 0
high 79 11 1 1

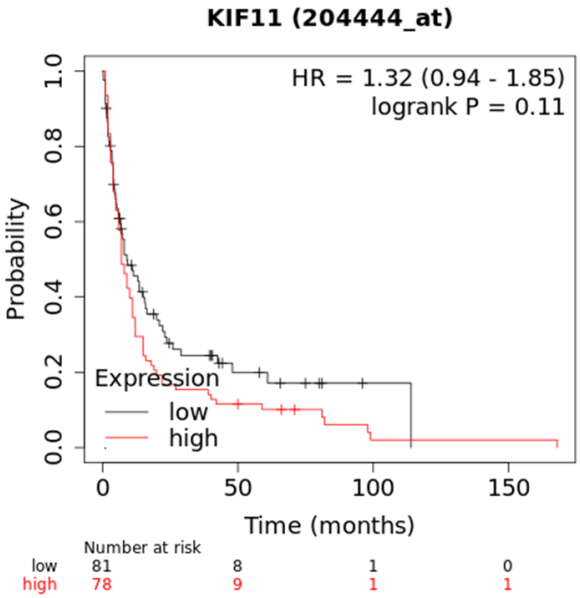

CEP55 (218542_at)
HR = 1.15 (0.82 - 1.62)
logrank P = 0.42
Probability
Expression
low
high
Time (months)
Number at risk
low 80 7 1 0
high 79 10 1 1

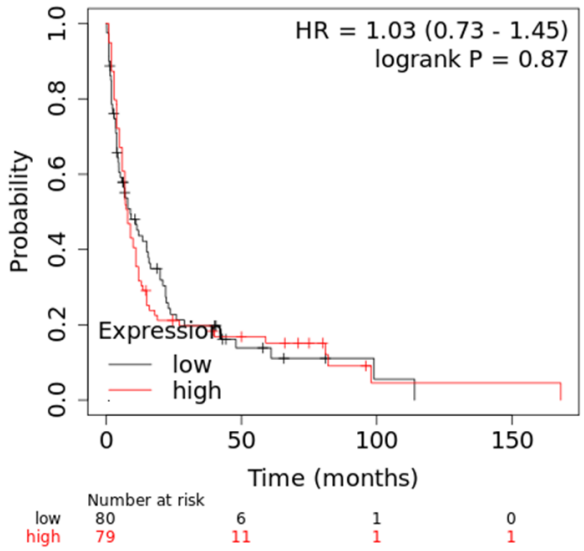

CHEK1 (238075_at)
HR = 1.1 (0.77 - 1.55)
logrank P = 0.61
Probability
Expression
low
high
Time (months)
Number at risk
low 74 6 1 0
high 75 11 1 1

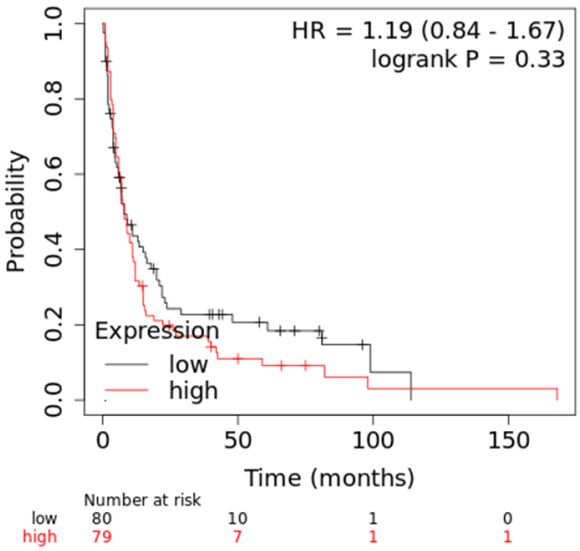

DLGAP5 (203764_at)
HR = 1.09 (0.78 - 1.54)
logrank P = 0.61
Probability
Expression
low
high
Time (months)
Number at risk
low 80 5 1 0
high 79 12 1 1

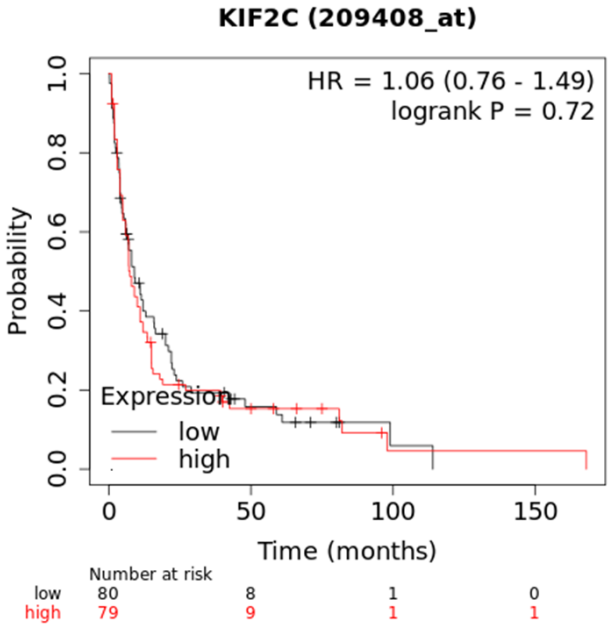

HMMR (207165_at)
HR = 1.04 (0.74 - 1.47)
logrank P = 0.8
Probability
Expression
low
high
Time (months)
Number at risk
low 80 6 1 0
high 79 11 1 1

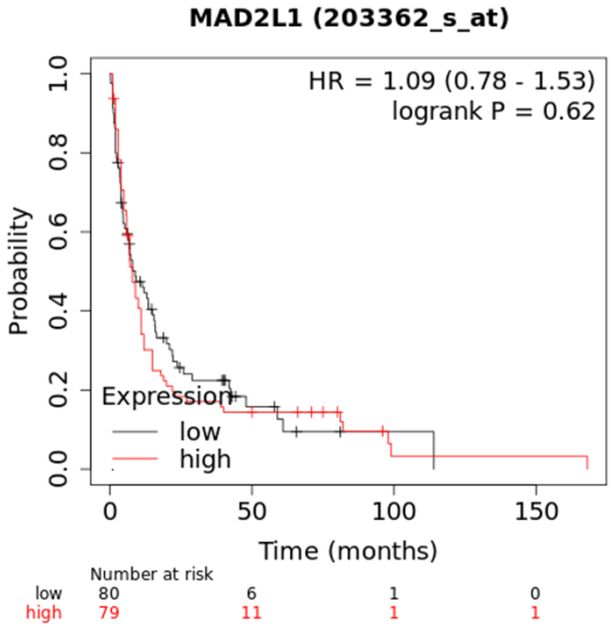

NS5ATP9 (211713_x_at)
HR = 1 (0.71 - 1.4)
logrank P = 0.98
Probability
Expression
low
high
Time (months)
Number at risk
low 82 5 1 0
high 77 12 1 1

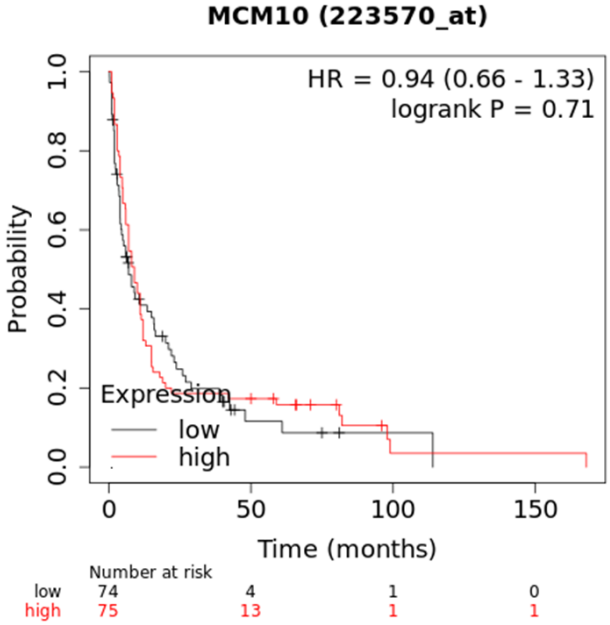

KIF11 (204444_at)
HR = 1.32 (0.94 - 1.85)
logrank P = 0.11
Probability
Expression
low
high
Time (months)
Number at risk
low 81 8 1 0
high 78 9 1 1

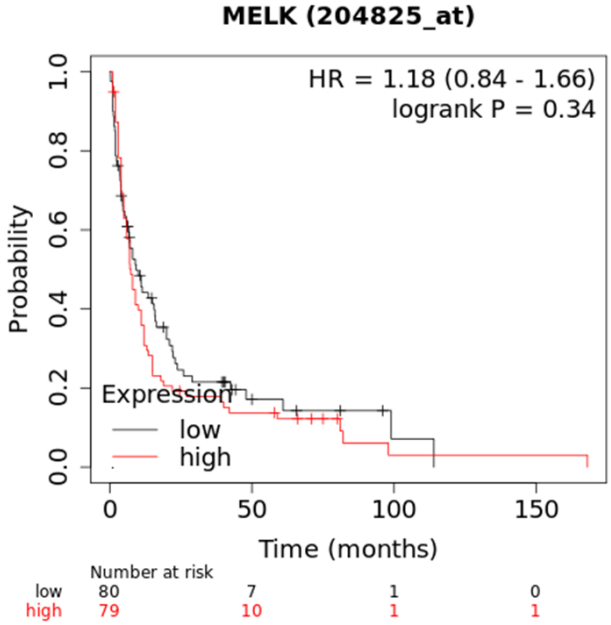

KIF15 (219306_at)
HR = 1.03 (0.73 - 1.45)
logrank P = 0.87
Probability
Expression
low
high
Time (months)
Number at risk
low 80 6 1 0
high 79 11 1 1

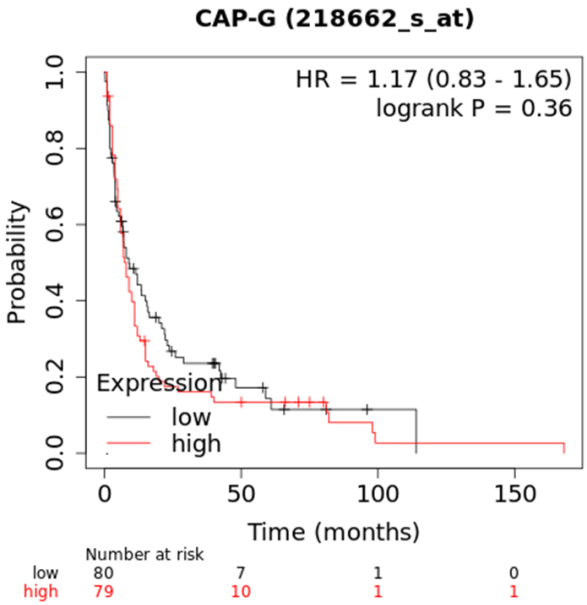

KIF20A (218755_at)
HR = 1.19 (0.84 - 1.67)
logrank P = 0.33
Probability
Expression
low
high
Time (months)
Number at risk
low 80 10 1 0
high 79 7 1 1

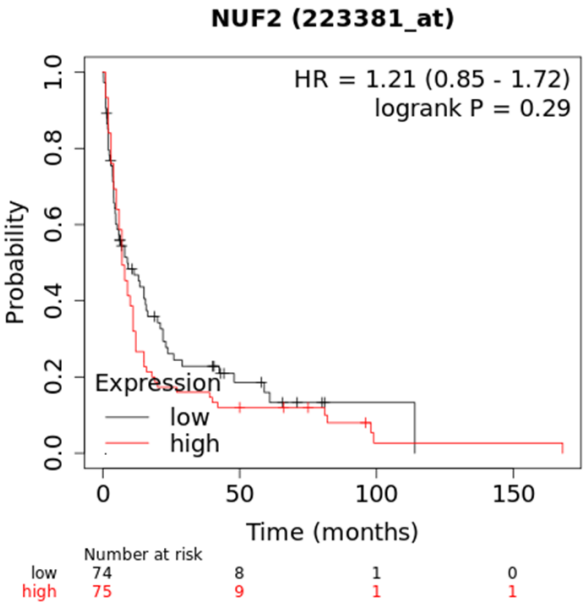

KIF2C (209408_at)
HR = 1.06 (0.76 - 1.49)
logrank P = 0.72
Probability
Expression
low
high
Time (months)
Number at risk
low 80 8 1 0
high 79 9 1 1

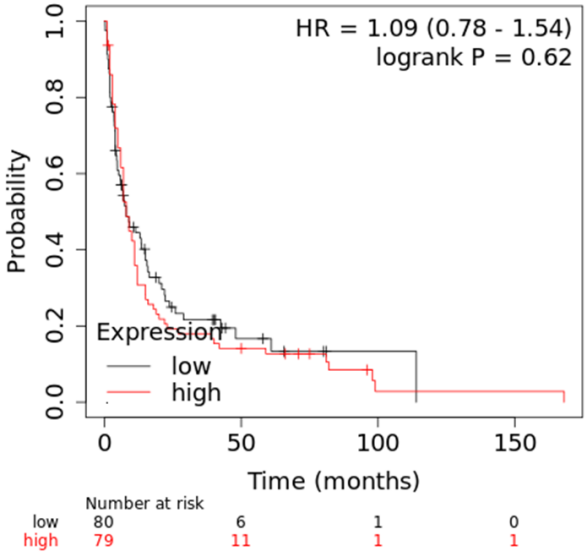

MAD2L1 (203362_s_at)
HR = 1.09 (0.78 - 1.53)
logrank P = 0.62
Probability
Expression
low
high
Time (months)
Number at risk
low 80 6 1 0
high 79 11 1 1

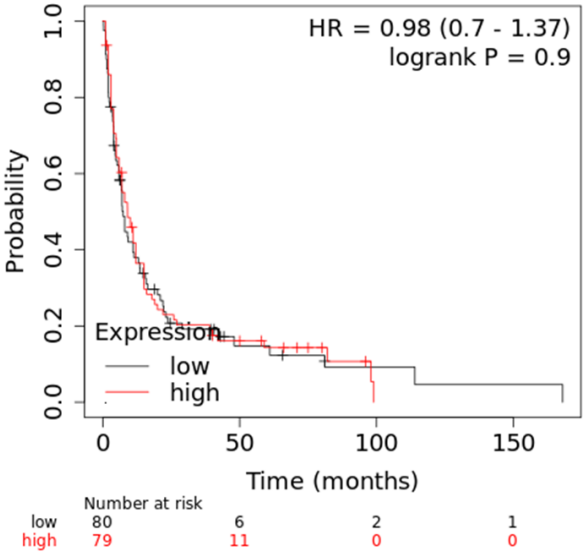

MCM10 (223570_at)
HR = 0.94 (0.66 - 1.33)
logrank P = 0.71
Probability
Expression
low
high
Time (months)
Number at risk
low 74 4 1 0
high 75 13 1 1

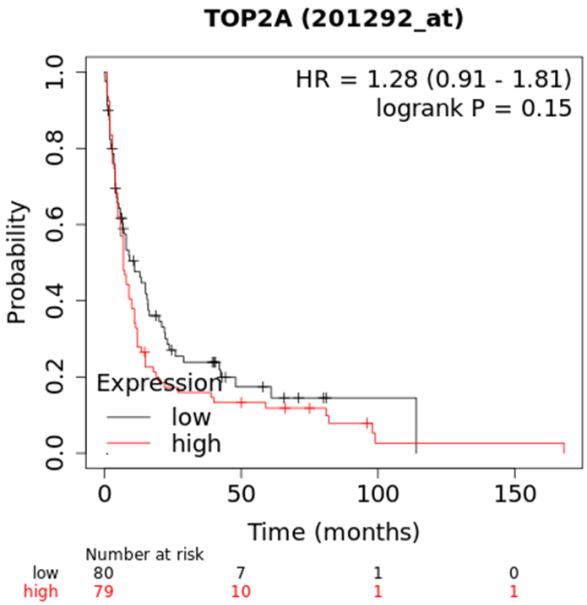

MELK (204825_at)
HR = 1.18 (0.84 - 1.66)
logrank P = 0.34
Probability
Expression
low
high
Time (months)
Number at risk
low 80 7 1 0
high 79 10 1 1

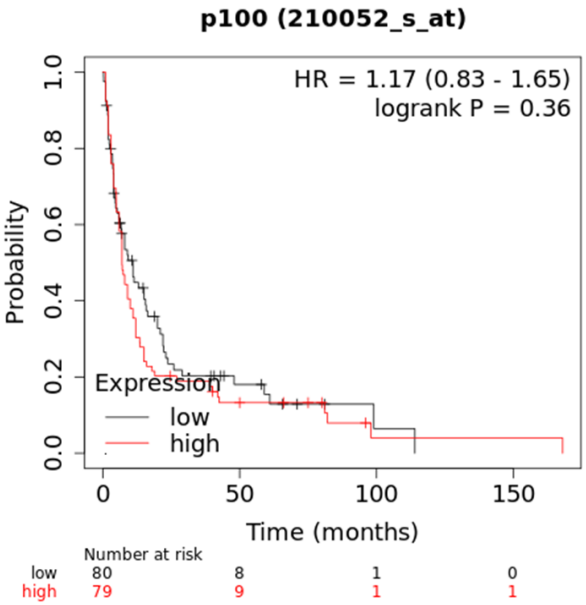

CAP-G (218662_s_at)
HR = 1.17 (0.83 - 1.65)
logrank P = 0.36
Probability
Expression
low
high
Time (months)
Number at risk
low 80 7 1 0
high 79 10 1 1

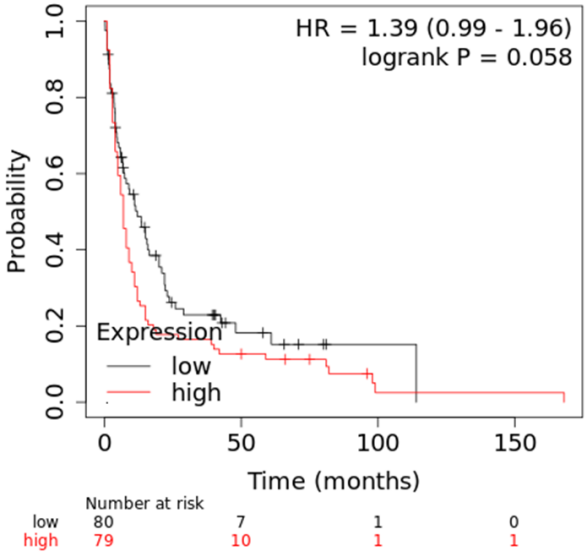

NUF2 (223381_at)
HR = 1.21 (0.85 - 1.72)
logrank P = 0.29
Probability
Expression
low
high
Time (months)
Number at risk
low 74 8 1 0
high 75 9 1 1

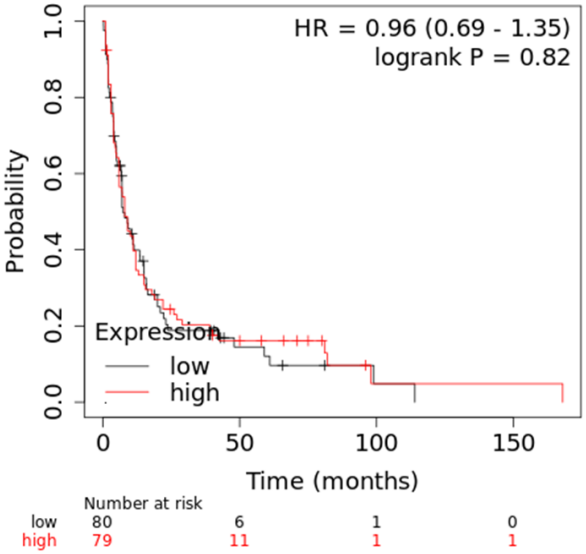

CT84 (219148_at)
HR = 1.09 (0.78 - 1.54)
logrank P = 0.62
Probability
Expression
low
high
Time (months)
Number at risk
low 80 6 1 0
high 79 11 1 1


RRM2 (201890_at)
HR = 0.98 (0.7 - 1.37)
logrank P = 0.9
Probability
Expression
low
high
Time (months)
Number at risk
low 80 6 2 1
high 79 11 0 0


TOP2A (201292_at)
HR = 1.28 (0.91 - 1.81)
logrank P = 0.15
Probability
Expression
low
high
Time (months)
Number at risk
low 80 7 1 0
high 79 10 1 1


p100 (210052_s_at)
HR = 1.17 (0.83 - 1.65)
logrank P = 0.36
Probability
Expression
low
high
Time (months)
Number at risk
low 80 8 1 0
high 79 9 1 1


CT96 (204822_at)
HR = 1.39 (0.99 - 1.96)
logrank P = 0.058
Probability
Expression
low
high
Time (months)
Number at risk
low 80 7 1 0
high 79 10 1 1

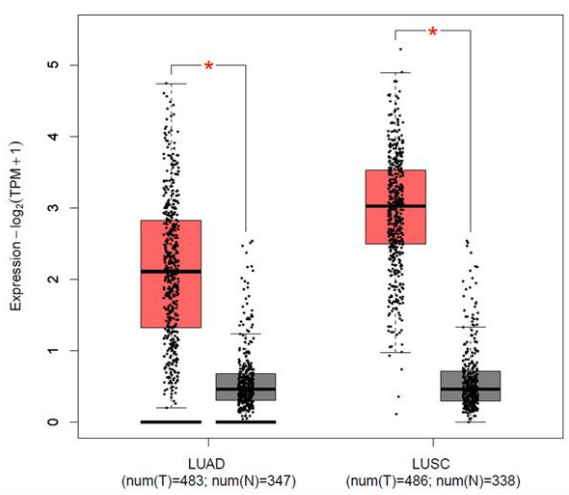

UBE2C (202954_at)
HR = 0.96 (0.69 - 1.35)
logrank P = 0.82
Probability
Expression
low
high
Time (months)
Number at risk
low 80 6 1 0
high 79 11 1 1

Gene Name	PPS Hazard Ratio	PPS P-value
ASPM	1.16	0.39
AURKA	1.19	0.31
AURKB	1.15	0.43
BIRC5	1.46	0.03
BUB1	1.20	0.30
CCNA	1.20	0.29
CCNB1	0.97	0.88
CCNB2	1.11	0.54
CDC20	1.29	0.15
CENPF	1.05	0.77
CEP55	1.15	0.42
CHEK1	1.10	0.61
DLGAP5	1.09	0.61
HMMR	1.04	0.80
KIAA0101	1.00	0.98
KIF11	1.32	0.11
KIF15	1.03	0.87
KIF20A	1.19	0.33
KIF2C	1.06	0.72
MAD2L1	1.09	0.62
MCM10	0.94	0.71
MELK	1.18	0.34
NCAPG	1.17	0.36
NUF2	1.21	0.29
PBK	1.09	0.62
RRM2	0.98	0.90
TOP2A	1.28	0.15
TPX2	1.17	0.36
TTK	1.39	0.058
UBE2C	0.96	0.82

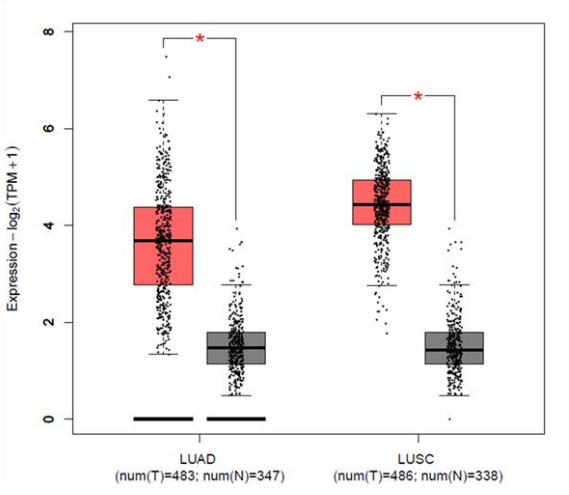
Figure 5-5: *Kaplein Mayer plots showed that post-progression survival was no worse in all high-expressing patients using the identified hub genes and (labelled STK12 on* https://kmplot.com/*). NSCLC patients were chosen using the website* https://kmplot.com/*. Metastatic patients were excluded from the analysis; patients had to have surgery, chemotherapy, and radiotherapy, leaving 159 out of 477 available patients to be analysed. Multivariate analysis was done along with log-rank testing.*

Previous reports on lung cancer have shown that an increase in PFS does not necessarily increase OS (Imai et al., 2017, 2016); however, PPS is strongly associated with OS after early-line treatment (Imai et al., 2020). Previous reports indicate that PPS is highly associated with OS after first and second-line chemotherapy in patients with advanced non-small and small-cell lung cancer. In contrast, PFS is only moderately associated with OS.

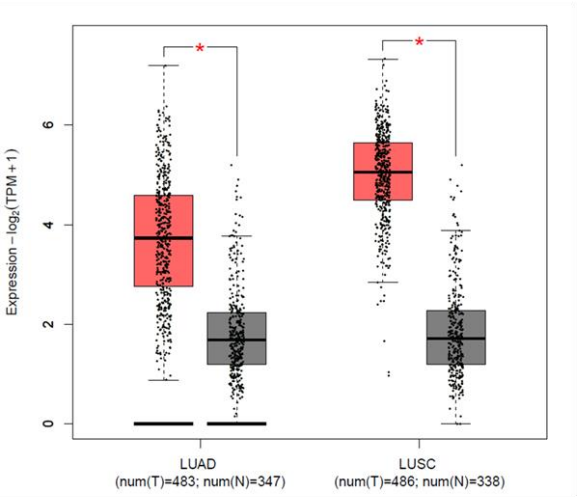
Despite the perceived superiority of PPS over PFS in specific clinical scenarios, PFS is used more widely in clinical trials. Ideally, we wanted to measure this as well, but PFS was not available to be assessed using Kmplotter. Increased expression of *AURKA* and *AURKB* did not demonstrate an improvement in PPS, with log-rank scores of 0.89 and 0.66, respectively. None of the other twenty-eight genes showed significant improvement in PPS when analysed. *AURKA* and *AURKB* do not indicate potential as a biomarker using this outcome measure, and the results were no worse when compared to the other hub genes identified using CytoHubba. GEPIA2 (http://gepia.cancer-pku.cn/index.html) showed increased expression of all hub genes in lung adenocarcinomas and lung squamous cell cancers compared to normal tissue (Figure 5-6).



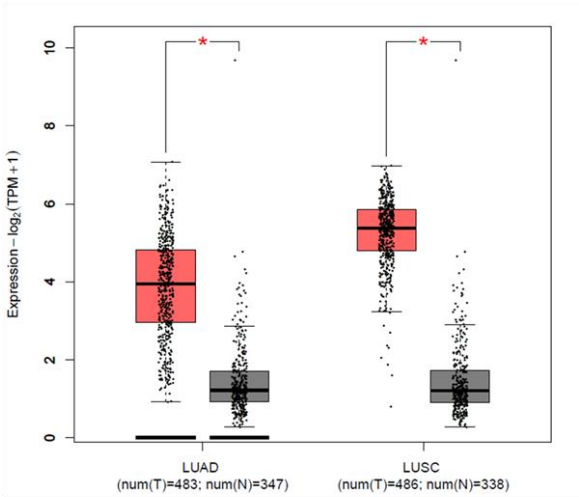
ASPM



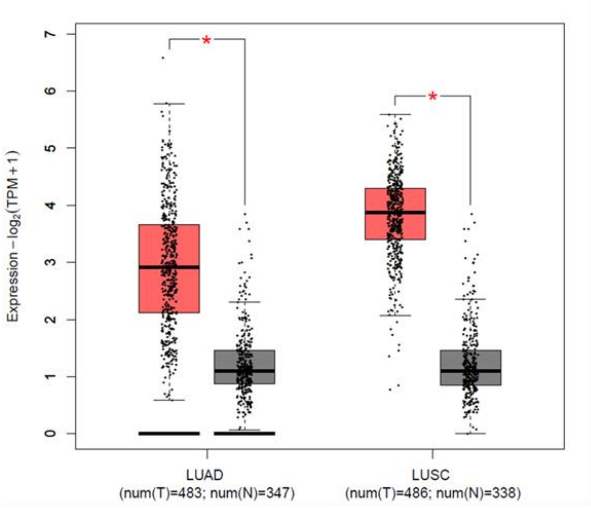
AURKA



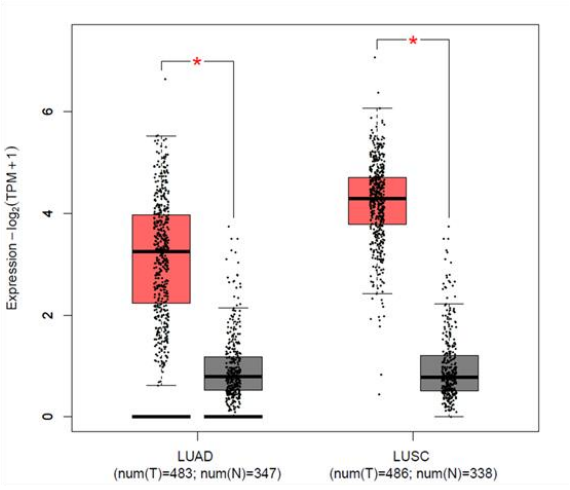
AURKB



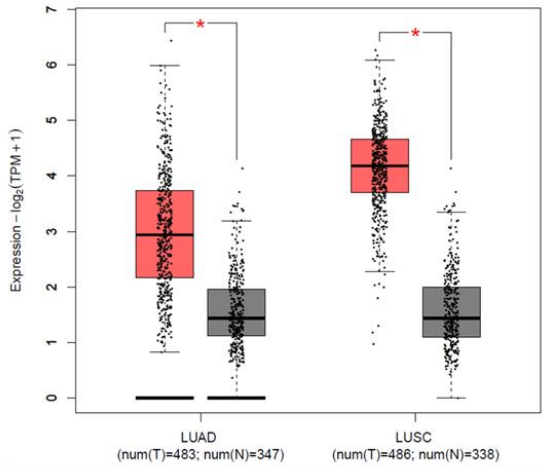
BIRC5



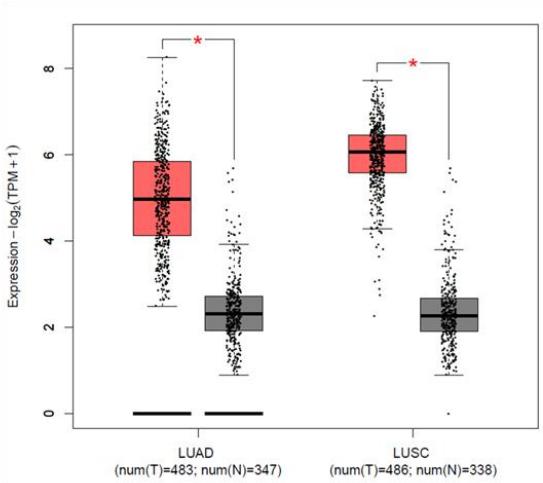
BUB1



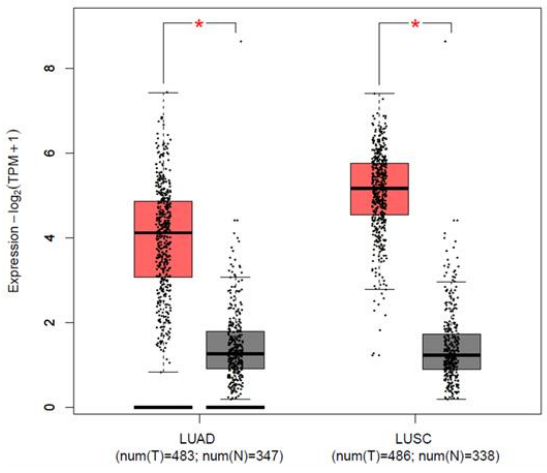
CEP55



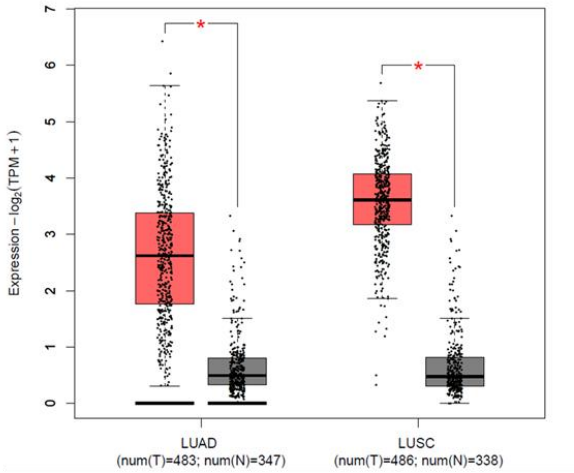
CCNA2



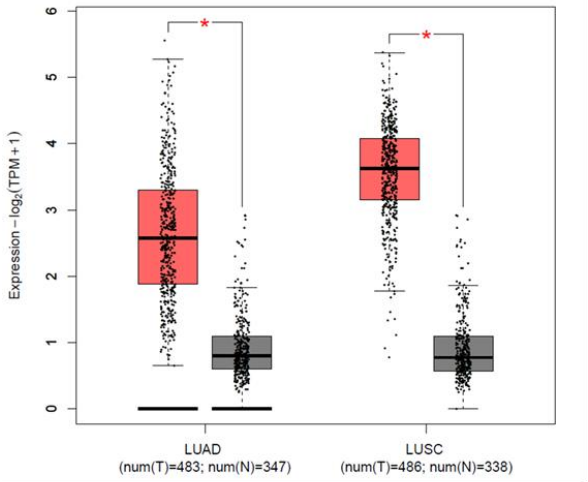
CCNB1



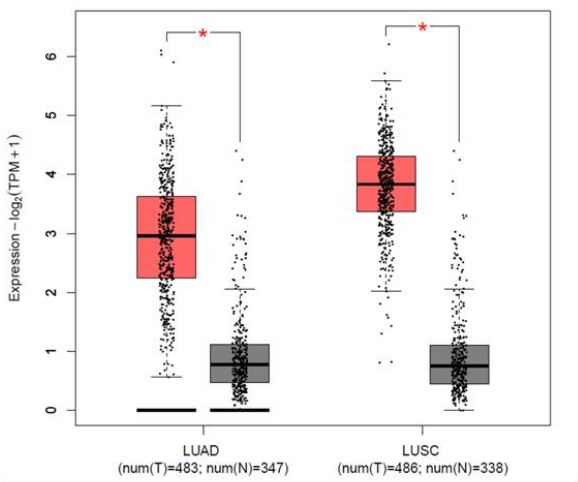
CENPF



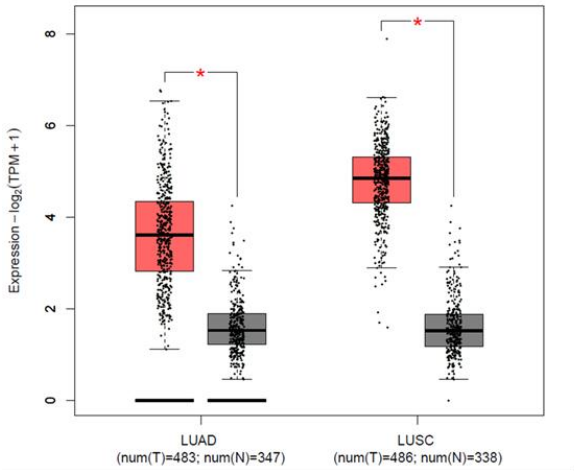
DLGAP5



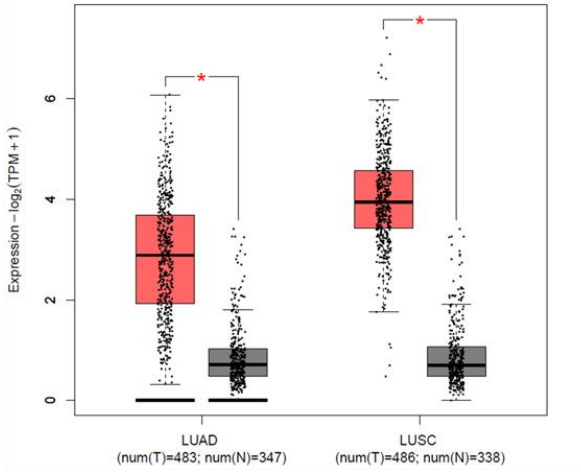
KIF11



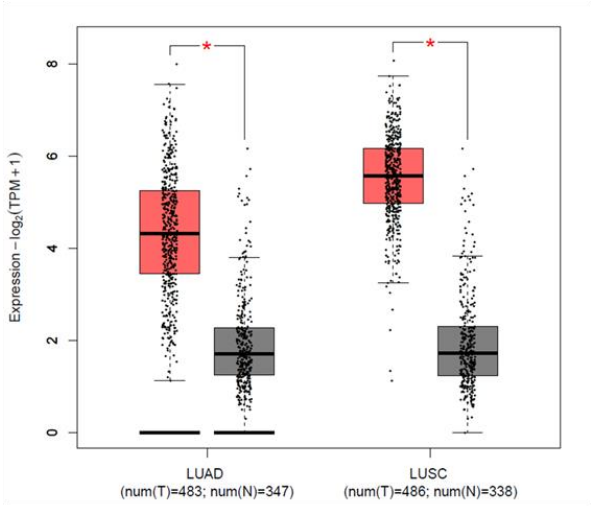
KIF20A



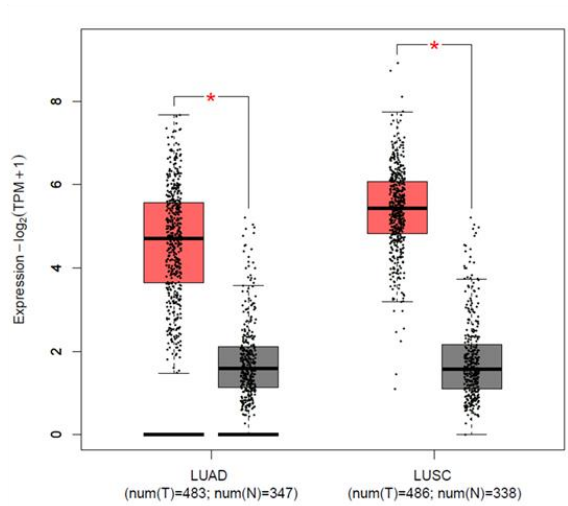
MAD2L1



MELK



RRM2



TOP2A

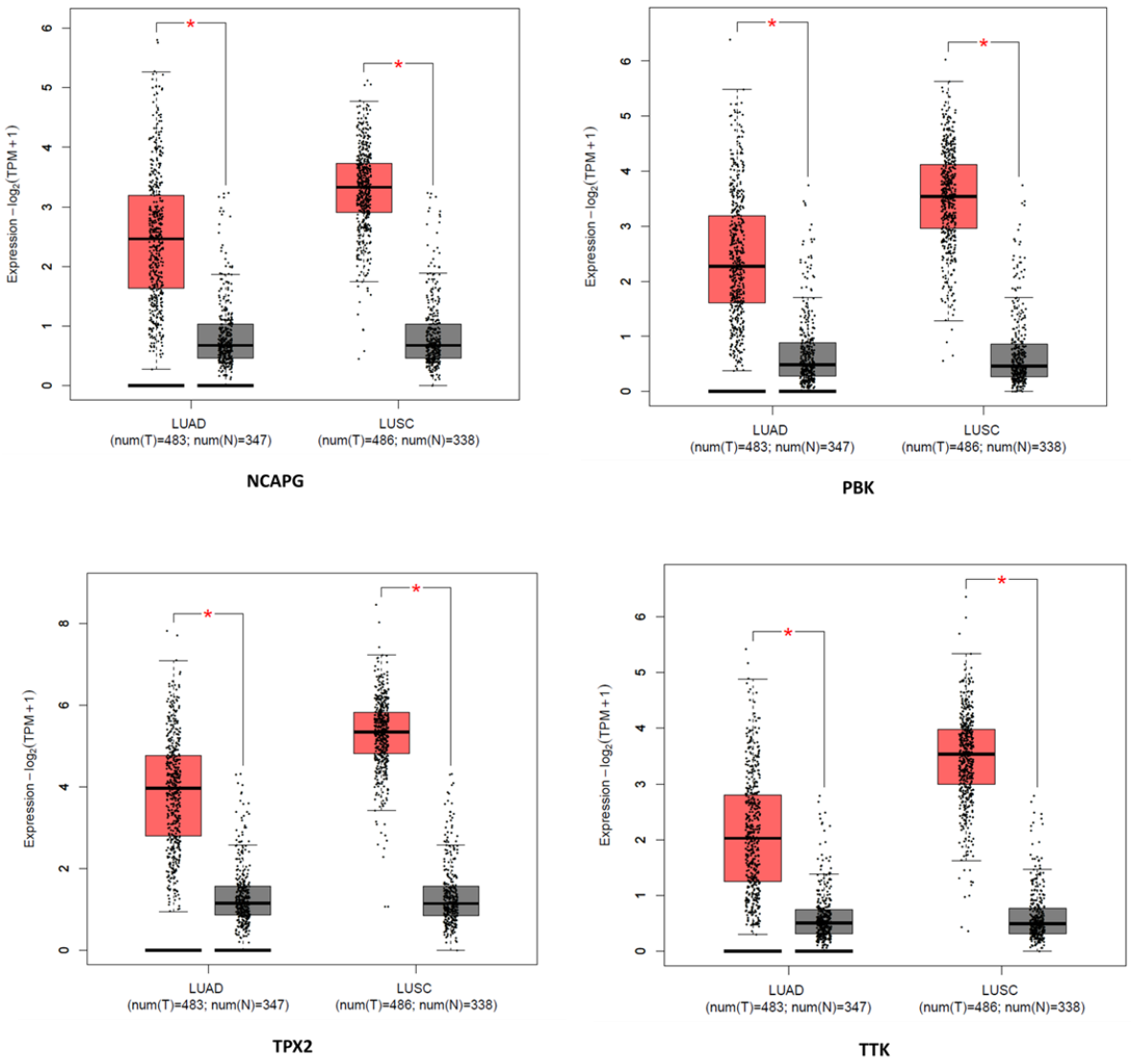


Figure 5-6 *Expression Analysis using GEPIA demonstrated that all hub genes were overexpressed in adenocarcinoma and squamous cell cancer tissue compared to normal tissue samples (log2IFCI cut-off of 2 and p-value cut-off of 0.01). Expression box plots of the thirty hub genes in using the website (http://gepia2.cancer-pku.cn/#analysis).*

5.2.2 Differential Gene expression of *AURKA* and *AURKB* between normal and cancerous HNSCC tissue.

To analyse the data, we used the GSE accession numbers listed in Table 5-4 and the “R” programming language to identify differentially expressed genes between cancer and normal tissue (the code for this analysis can be found in Appendix 11-1).

Our approach to bioinformatic analysis is broadly similar to bioinformatic published studies in HNSCC. In previous studies, cancerous tissue was taken from patients from the oral cavity and the tongue. While both tumour regions are subjected to the same clinical treatment strategies, there is evidence that their cellular biology is different. For example, higher levels of downregulation of p16 and *p21* are seen in tongue cancer cases compared to oral cavity tumours (Sathyan et al., 2006). For this reason, we considered data from oropharyngeal and nasopharyngeal cancers separately.

Accession number	Tumour type
GSE30784	Oral Cavity
GSE74530	Oral Cavity
GSE78060	Oral Cavity
GSE138206	Oral Cavity
GSE13597	Nasopharynx
GSE12452	Nasopharynx

Table 5-4**: Accession numbers and *Patient characteristics of the HNSCC GEO samples.* A:** Six GEO accession samples were chosen for the bioinformatic analysis of four oral cavity and two nasopharyngeal tumours.

5.2.2.1 *AURKA* but not *AURKB* was differentially expressed in oropharyngeal tumour gene expression sets compared to normal tissue.

Four GEO microarray datasets, **GSE30784**, **GSE138206**, **GSE78060** and **GSE74530** (Table 5-5), representing oropharyngeal tumours were downloaded from https://www.ncbi.nlm.nih.gov/geo/ and used to assess *AURKA* and *AURKB* differential gene expression. After pre-processing the data, the limma package performed the differential analysis with the cut-off criteria for a DEG an **adjusted P-value (adj.P) <0.05 and |logFC|≥2.**

Oropharynx						
GSE accession number	**Total number of samples**	**Normal tissue**	**Cancer Tissue**		**Males**	**Females**
GSE3074	229	45 +17 dysplasia tissue samples	167		162	67
GSE138206	18	12	6		15	3
GSE78060	30	4	26		21	9
GSE74530	12	6	6		Unknown	Unknown

Table 5-5: **Accession numbers and *patient characteristics of the HNSCC GEO samples.* A:** Four GEO accession samples were chosen for the bioinformatic analysis. Each accession number has different ratios of normal vs cancer tissue and male's vs females demonstrating the heterogeneity of the samples in the analysis.

GSE accession number	Gene Symbol	logFC	AveExpr	t	P.Value	adj.P.Val
GSE74530	AURKA	-2.5501	6.544833	-8.40277	3.75E-07	0.000117
GSE78060	AURKA	-393.169	815.2959	-3.37067	0.002146	0.005349
GSE138206	AURKA	162.0485	155.3289	5.865282	2.29E-05	0.000623
GSE30784	AURKA	1.074106066	6.403707	9.28538366	1.303760e-17	1.215987e-16

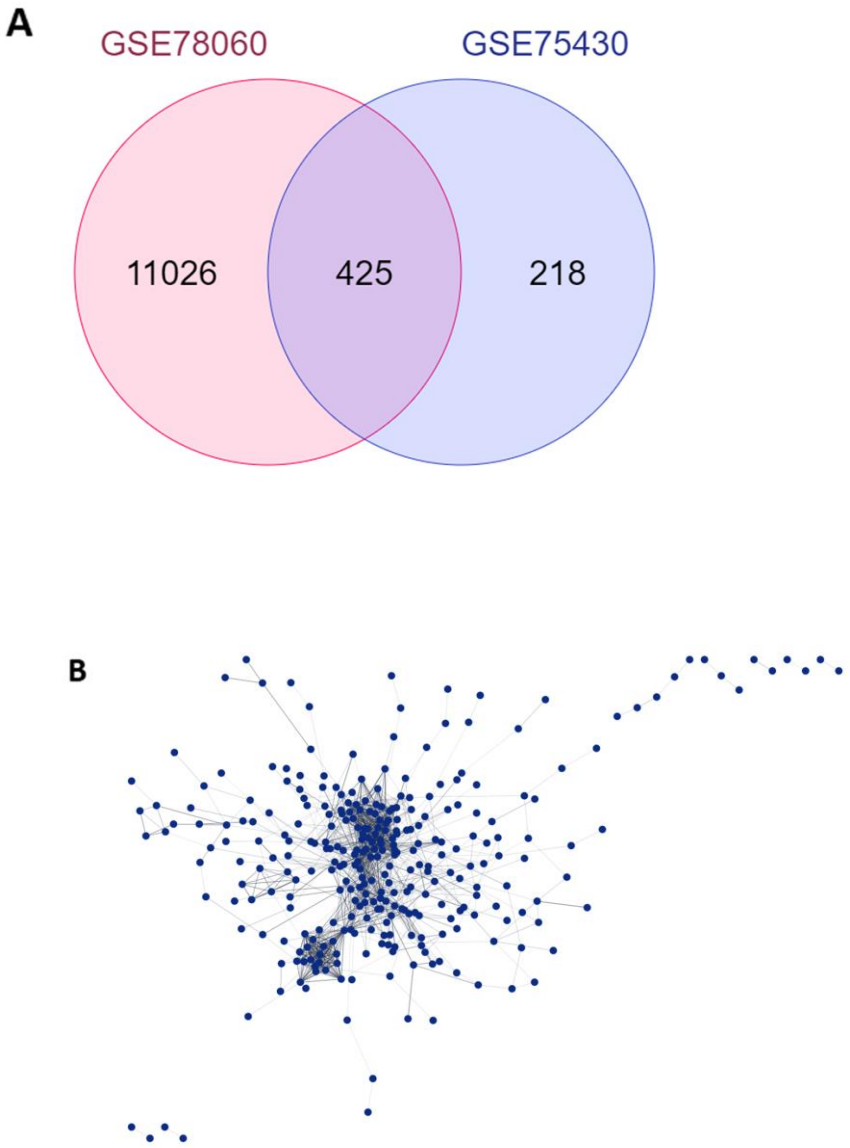
Table 5-6: **Table of log fold changes along with the significance values**: *The log fold changes and adj.P values are shown for GSE74530, GSE78060, and GSE138206 and GSE30784 where the gene demonstrates significant differential gene expression.* ***LogFC (Log Fold Change):*** *Log Fold Change represents the logarithm of the ratio of gene expression levels between two conditions or groups. It quantifies how much a gene's expression has changed between two experimental conditions. A positive logFC indicates upregulation (increased expression) in one condition compared to the other, while a negative logFC indicates downregulation (decreased expression).* ***AveExpr (Average Expression):*** *AveExpr or Average Expression is the average gene expression level across all experiment samples. It provides a measure of the overall expression level of a gene, which can help filter out genes with very low expression levels that may not be biologically relevant or identify highly expressed genes.* ***P-value (t-test p-value):*** *The T p-value is a statistical measure that assesses whether the difference in gene expression between two groups (e.g.,* treatment *vs. control) is statistically significant. It helps determine if the observed difference in gene expression is likely due to a natural biological effect or if it could have occurred by chance. A small p-value (typically less than 0.05) suggests the difference is significant.* ***Adj. P. Val (Adjusted P-Value):*** *The Adj.P. Val is a p-value adjusted for multiple testing to control the false discovery rate (FDR). One standard method for adjustment is the Benjamini-Hochberg procedure. Multiple hypothesis testing can increase the likelihood of false positives (Type I errors). Adjusted p-values help correct this by providing a more stringent criterion for significance. Genes with a low Adj.P. Val (typically less than 0.05) are considered statistically significant after adjusting for multiple comparisons.*

AURKA was significantly differentially expressed in three datasets, **GSE78060** (LogFC of 393.169, adj.P of 0.005349) and **GSE75430** (LogFC of 2.5501, adj.P of 0.000117) and **GSE138206** (LogFC of 162.0485, adj.P of 0.000623) but not in **GSE3074** (Table 5-6). *AURKB* was not found to be differentially expressed in any dataset using the cut-off criteria above (Figure 5-13). Appendix Table 7.2.2 shows the full results of DEG analysis in each GEO data set.

Interestingly, GSE3074 had the largest number of tumour samples and showed no differential expression of *AURKA* compared to the other three smaller datasets. This could mean that the expression of *AURKA* in oropharyngeal cancer tumours is possibly not significant either due to random noise in the dataset leading to inconsistent patterns of differential expression or in smaller datasets, specific characteristics or confounding factors of individual samples can have a more substantial influence on the overall gene expression patterns, overshadowing any true differential expression. With a larger dataset, the effects of individual samples or specific confounding factors can be diluted, allowing the true differential expression signals to emerge more prominently.

5.2.2.2 *AURKA* is present in the PPI network using Cytoscape analysis but was not identified as a Hub gene.

Having determined that *AURKA* is upregulated in three datasets we examined, we wanted to examine whether *AURKA* was a hub gene. Hub genes that are differentially expressed can serve as potential biomarkers with enhanced diagnostic, prognostic, or predictive value. Their dual characteristics as both hub and differentially expressed genes suggest their potential as powerful indicators of disease states or treatment responses. The combination of these attributes makes them attractive candidates for further validation as potential biomarkers in clinical settings. The lists of DEG genes (Appendix 7.2.2) from each data set where *AURKA* was significantly differentially expressed were combined, and the shared genes between all three were grouped using a multiple list comparator (Figure 5-7 A) (https://molbiotools.com/listcompare.php) with the resulting DEG PPI network found to comprise 373 nodes and 1477 edges (Figure 5-7 B). In addition, 30 hub genes (Figure 5-16) were identified using CytoHubba (Chin et al., 2014).


A
GSE78060
GSE75430
11026
425
218
B

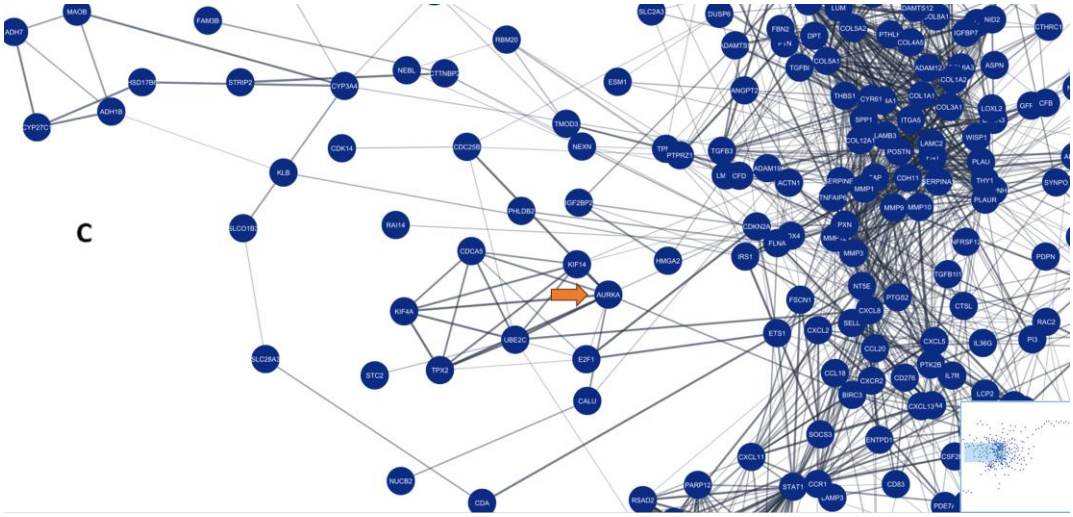


Figure 5-7 **A** Using a Venn diagram demonstrating the common Hub genes between GSE78060, and GSE74530 (https://molbiotools.com/listcompare.php). **B-C** *Using Cytoscape, the PPI network demonstrating a network comprising 373 nodes and 1477 edges is visualised.* A close-up of *AURKA* within the PPI network is shown. The Networks were plotted by inputting the 30 HUB genes using the STRING app, part of the Cytoscape software.

AURKA was found in the fifth *TOP* module using MCODE (Bader and Hogue, 2003). Ten other genes, CD276, *CDCA*5, *CDKN*2A, *ENTPD*1, ETS1, IL7R, *KIF*14, *KIF*4A, TPX2, and *UBE*2C, were also present in this module (Figure 5-8). Using GEPIA2 (http://gepia.cancer-pku.cn/index.html), increased expression of *AURKA*, CD276, *CDCA*5, *CDKN*2A, *KIF*14, *KIF*4A, TPX2, *UBE*2C was seen in lung adenocarcinomas and lung squamous cell cancers compared to normal tissue (Figure 5-9). Although *AURKA* has been demonstrated in several studies to be a promising biomarker in HNSCC (Lu et al., 2021; Wang et al., 2021), we could not demonstrate that this was a hub Gene in our work, but we wanted to examine whether the expression of any of the genes identified as HUB genes were associated with reduced survival in patients, indicating they might be potential biomarkers. Thirty genes were identified as hub genes *FN*1, COL1A1, CXCL8, *MMP*9, STAT1, COL3A1, *POSTN*, COL1A2, COL5A1, *THBS*1, COL4A1, *ITGA*5, COL4A2, *SERPINE*1, COL12A1, COL5A2, *SPP*1, *MMP*3, COL6A3, *MMP*1, THY1, LUM, CCL20, PTGS2, CTLA4, TGFB3, *MMP*12, CXCL11, ISG15, IL7R (Table 5-7).

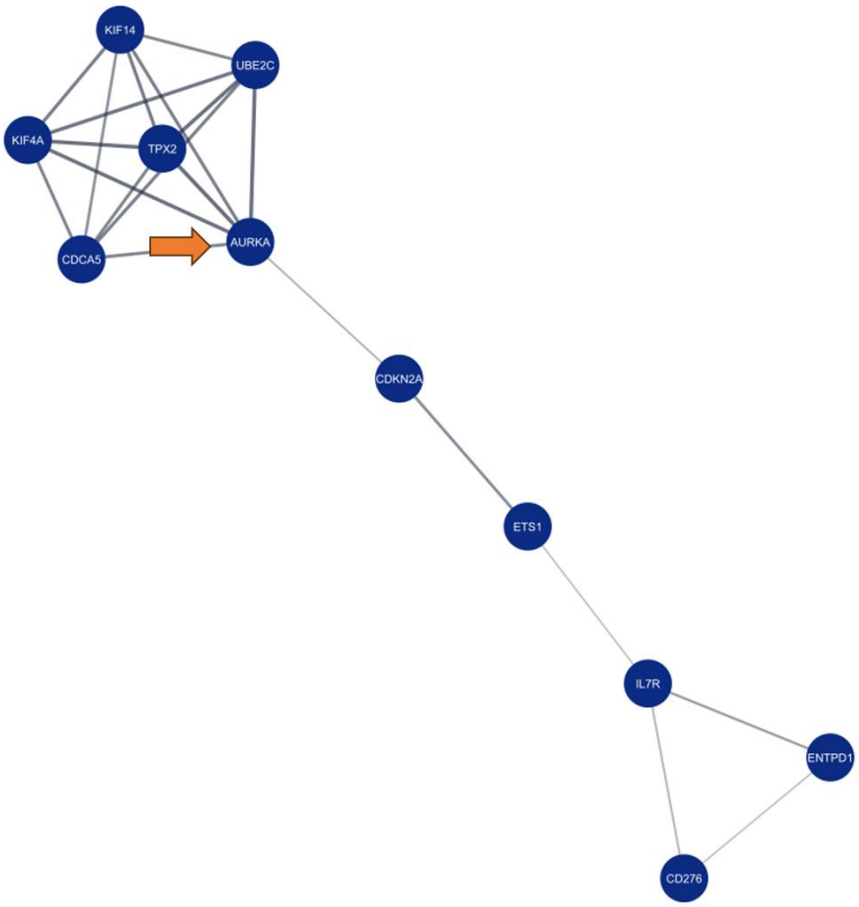


Figure 5-8: *AURKA* was visualised using MCODE (Molecular Complex Detection), a plugin for Cytoscape, a software tool for visualizing and analyzing biological networks using a Degree Cutoff of two, a Node score cut off of 0.2, a K-score of 2, and a Max depth of 100.

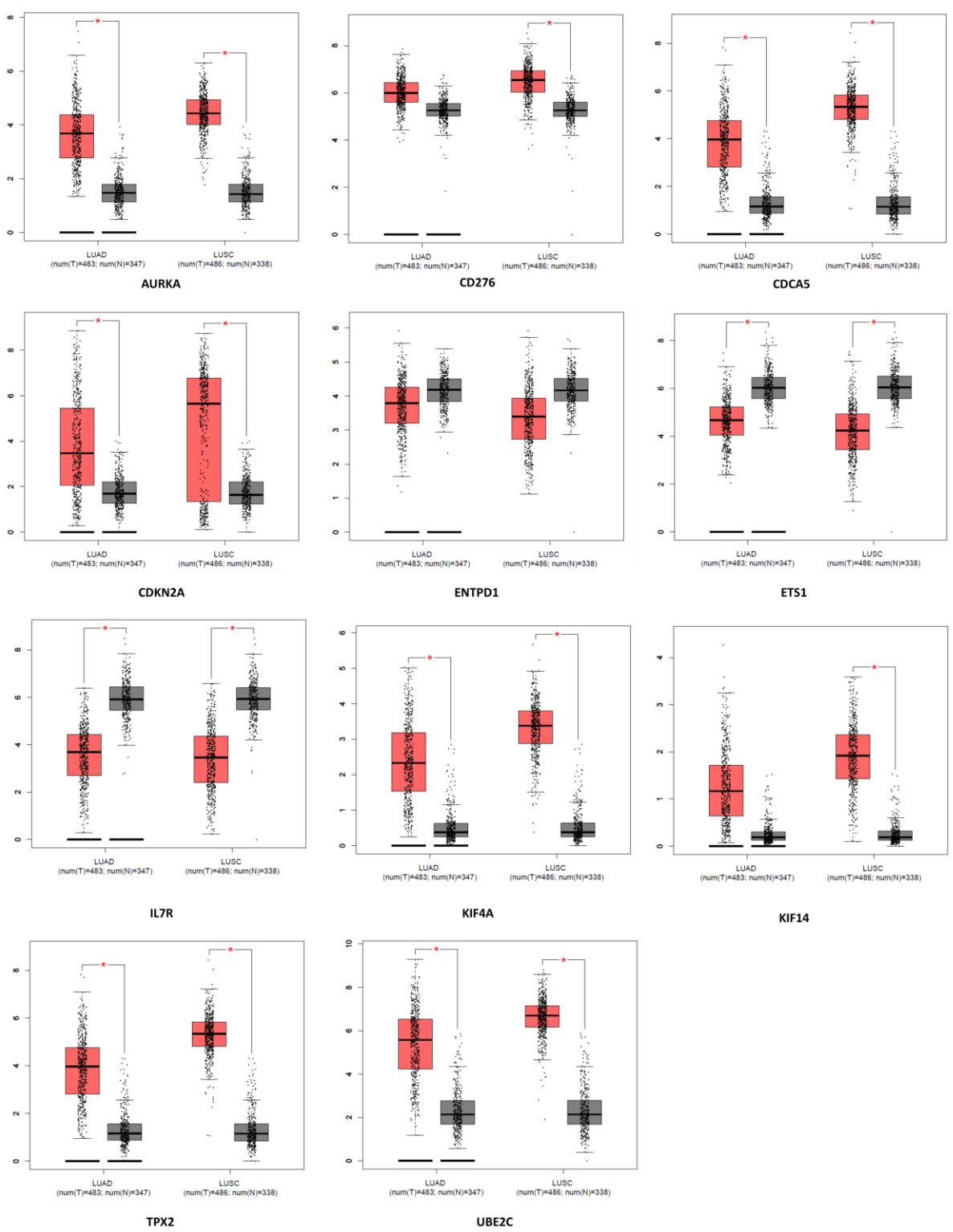


Figure 5-9: *Expression Analysis using GEPIA demonstrated that all hub genes were overexpressed in adenocarcinoma and squamous cell cancer tissue compared to normal tissue samples (log2IFCI cut-off of 2 and p-value cut-off of 0.01. Expression box plots of the select genes in the most significant module in the PPI network using the website (http://gepia2.cancer-pku.cn/#analysis).*

Rank	Gene name	Description	Function
14	SERPINE1	Serpin Family E Member 1	Encodes a protein that regulates the breakdown of blood clots and has roles in wound healing and tissue remodeling.
14	COL12A1	Collagen Type XII Alpha 1 Chain	Encodes collagen type XII, which plays a role in maintaining tissue structure.
16	COL5A2	Collagen Type V Alpha 2 Chain	Is another gene involved in collagen type V synthesis.
16	SPP1	Secreted Phosphoprotein 1	Is involved in bone mineralization and can also play a role in immune responses and inflammation.
16	MMP3	Matrix Metallopeptidase 3	Encodes an enzyme involved in ECM remodeling and tissue repair.
19	COL6A3	Collagen Type VI Alpha 3 Chain	Is a gene involved in collagen type VI synthesis, which is found in connective tissues.
19	MMP1	Matrix Metallopeptidase 1	Is another matrix metalloproteinase involved in ECM degradation and tissue remodeling.
21	THY1	Thy-1 Cell Surface Antigen	Plays a role in cell adhesion and signal transduction in various cell types.
22	LUM	Lumican	Encodes a proteoglycan involved in collagen fibril assembly and corneal transparency.
23	CCL20	C-C Motif Chemokine Ligand 20	Encodes a chemokine involved in immune cell recruitment and inflammation.
23	PTGS2	Prostaglandin-Endoperoxide Synthase 2	Is an enzyme that produces prostaglandins and is involved in inflammation and pain.
23	CTLA4	Cytotoxic T-Lymphocyte Associated Protein 4	Is involved in regulating the immune response by inhibiting T-cell activation.
26	TGFB3	Transforming Growth Factor Beta 3	Is a growth factor involved in tissue development, wound healing, and immune regulation.
26	MMP12	Matrix Metallopeptidase 12	Is another matrix metalloproteinase with a role in ECM remodeling and inflammation.
28	CXCL11	C-X-C Motif Chemokine Ligand 11	Is a chemokine that plays a role in immune cell recruitment and inflammation.
28	ISG15	ISG15 Ubiquitin Like Modifier	Is involved in the antiviral immune response and can also play a role in inflammation.

Rank	Gene name	Description	Function
14	SERPINE1	Serpin Family E Member 1	Encodes a protein that regulates the breakdown of blood clots and has roles in wound healing and tissue remodeling.
14	COL12A1	Collagen Type XII Alpha 1 Chain	Encodes collagen type XII, which plays a role in maintaining tissue structure.
16	COL5A2	Collagen Type V Alpha 2 Chain	Is another gene involved in collagen type V synthesis.
16	SPP1	Secreted Phosphoprotein 1	Is involved in bone mineralization and can also play a role in immune responses and inflammation.
16	MMP3	Matrix Metallopeptidase 3	Encodes an enzyme involved in ECM remodeling and tissue repair.
19	COL6A3	Collagen Type VI Alpha 3 Chain	Is a gene involved in collagen type VI synthesis, which is found in connective tissues.
19	MMP1	Matrix Metallopeptidase 1	Is another matrix metalloproteinase involved in ECM degradation and tissue remodeling.
21	THY1	Thy-1 Cell Surface Antigen	Plays a role in cell adhesion and signal transduction in various cell types.
22	LUM	Lumican	Encodes a proteoglycan involved in collagen fibril assembly and corneal transparency.
23	CCL20	C-C Motif Chemokine Ligand 20	Encodes a chemokine involved in immune cell recruitment and inflammation.
23	PTGS2	Prostaglandin-Endoperoxide Synthase 2	Is an enzyme that produces prostaglandins and is involved in inflammation and pain.
23	CTLA4	Cytotoxic T-Lymphocyte Associated Protein 4	Is involved in regulating the immune response by inhibiting T-cell activation.
26	TGFB3	Transforming Growth Factor Beta 3	Is a growth factor involved in tissue development, wound healing, and immune regulation.
26	MMP12	Matrix Metallopeptidase 12	Is another matrix metalloproteinase with a role in ECM remodeling and inflammation.
28	CXCL11	C-X-C Motif Chemokine Ligand 11	Is a chemokine that plays a role in immune cell recruitment and inflammation.
28	ISG15	ISG15 Ubiquitin Like Modifier	Is involved in the antiviral immune response and can also play a role in inflammation.

Table 5-7: List of genes generated from the common Hub genes between GSE78060 and GSE75430 (https://molbiotools.com/listcompare.php). The score indicates values representing the degree of connectivity of a node (gene) within a network. Genes with scores of greater than ten were chosen as potential hub genes.

5.2.2.3 Neither *AURKA* nor *AURKB* were found to be differentially expressed in nasopharyngeal datasets.

Two GEO microarray datasets, GSE12452 and GSE13597, were downloaded from https://www.ncbi.nlm.nih.gov/geo/ to assess *AURKA* and *AURKB* differential gene expression (Table 5-8). The data was again pre-processed using the limma package with the same cut-off criteria for the oropharyngeal patient samples. Neither *AURKA* nor *AURKB* was found to be differentially expressed in any dataset using the cut-offs **adjusted P-value (adj.P) <0.05 and |logFC|≥2**. (Figure 5-20 – GEO, *AURKA*, and *AURKB* gene expression and p.Value). Complete DEG analysis is shown in Appendix 7.2.2. The result presented here differs from published literature, likely due to the use of different microarray platforms (Illumina HiSeq 2000 [Homo sapiens; GPL11154] chip platform and [HG-U133_Plus_2] Affymetrix Human Genome U133 plus 2.0 Array) in their research and the small patient numbers in our chosen datasets.

Accession number	Tumour type
GSE30784	Oral Cavity
GSE74530	Oral Cavity
GSE78060	Oral Cavity
GSE138206	Oral Cavity
GSE13597	Nasopharynx
GSE12452	Nasopharynx

Nasopharynx			
GSE accession number	**Total number of samples**	**Normal tissue**	**Cancer Tissue**
GSE12452	41	10	31
GSE13597	28	3	25

Table 5-8: **Accession numbers and *Patient characteristics of the HNSCC GEO samples.* A:** Six GEO accession samples were chosen for the bioinformatic analysis of four oral cavity and two nasopharyngeal tumours.



Figure 5-10: **A** Using a Venn diagram demonstrating the common Hub genes between GSE12452 and GSE13597 (https://molbiotools.com/listcompare.php).

GSE accession number	Gene.Symbol	logFC	AveExpr	t	P.Value	adj.P.Val
GSE12452	AURKA	1.4313941	8.396393	6.3998818	1.089338e-07	4.294898e-06
	AURKB	0.6021202	6.292460	3.0612998	3.847656e-03	1.989452e-02
GSE13597	AURKA	24.5858092	81.49195	1.83867433	0.07692150	0.251880
	AURKB	27.2104197	73.94305	1.71075825	0.09852542	0.2896160

Table 5-9: Table of log fold changes along with the significance values: The *AURKA* log fold changes and adj.P values are shown for GSE12452 and GSE13597 where neither *AURKA* nor *AURKB* demonstrates significant differential gene expression. LogFC (Log Fold Change): Log Fold Change represents the logarithm of the ratio of gene expression levels between two conditions or groups. It quantifies how much a gene's expression has changed between two experimental conditions. A positive logFC indicates upregulation (increased expression) in one condition compared to the other, while a negative logFC indicates downregulation (decreased expression). AveExpr (Average Expression): AveExpr or Average Expression is the average gene expression level across all experiment samples. It provides a measure of the overall expression level of a gene, which can help filter out genes with very low expression levels that may not be biologically relevant or identify highly expressed genes. P-value (t-test p-value): The T p-value is a statistical measure that assesses whether the difference in gene expression between two groups (e.g., treatment vs. control) is statistically significant. It helps determine if the observed difference in gene expression is likely due to a natural biological effect or if it could have occurred by chance. A small p-value (typically less than 0.05) suggests the difference is significant. Adj. P. Val (Adjusted P-Value): The Adj.P. Val is a p-value adjusted for multiple testing to control the false discovery rate (FDR). One standard method for adjustment is the Benjamini-Hochberg procedure. Multiple hypothesis testing can increase the likelihood of false positives (Type I errors). Adjusted p-values help correct this by providing a more stringent criterion for significance. Genes with a low Adj.P. Val (typically less than 0.05) are considered statistically significant after adjusting for multiple comparisons.

5.2.3 *AURKA* IHC in NSCLC patient cohort.

5.2.3.1 A prospective study of 101 Patients at the Weston Park Cancer Centre.

To investigate the relationship between *AURKA* expression, OS and PFS in patients with non-small cell lung cancer (NSCLC), a study was conducted at the Weston Park Cancer Centre (WPCC). One hundred one (101) eligible patients with NSCLC were recruited for radical radiotherapy and chemotherapy over two years. The study population comprised forty-nine (49) males and fifty-two (52) females, forty-six (46) adenocarcinomas, fifty-two (52) squamous cell cancers, one (1) large cell cancer, and two (2) neuroendocrine tumours. Most lesions were stage T4, N2 and non-metastatic. A wide range of radiation doses was delivered to the patients, with the dose and fractionations delivered for both palliative and curative intent. After treatment, the patients were followed up to determine their overall and progression-free survival after two years (Table 6-1).

Demographics of prospective study	
Title:	Patient number:
Number of Patients:	101
Average age:	72.10
Gender:	
Male	49
Female	52
Smoking Status:	
Current	15
Former	65
Never	9
Not Known	12
Race:	
Black Caribbean	1
White	98
Unrecorded	2
T Stage:	
T1	10
T2	27
T3	21
T4	41
TX	2
N Stage:	
N0	40
N1	16
N2	35
N3	10
M Stage:	
M0	68
M1	17
MX	16

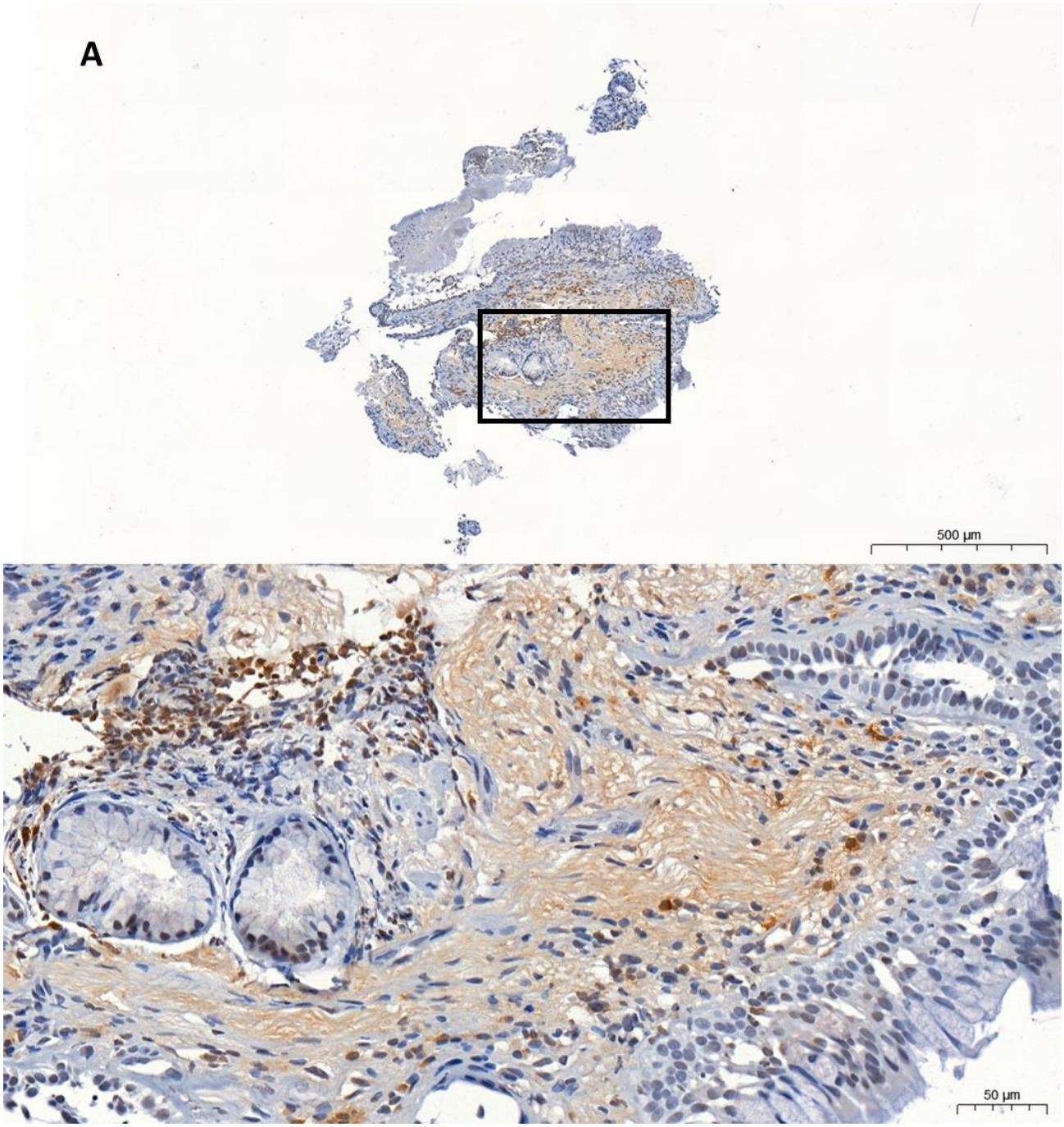
Demographics of prospective study	
Title:	Patient number:
Pathological Diagnosis:	
Adenocarcinoma	46
Squamous Cell Cancer	52
Large Cell Cancer	1
Neuroendocrine Cancer*	2
Radiotherapy Doses Delivered:	
36 Gy in 12 Fractions	29
45 Gy in 25 fractions	1
54 Gy in 36 Fractions	20
55 Gy in 20 Fractions	42
55 Gy in 5 Fractions	2
63 Gy in 30 Fractions	3
64 Gy in 5 Fractions (SABR)	1
64.8 Gy in 42 Fractions	1
72 Gy in 40 Fractions	1
77.4 Gy in 43 Fractions	1
Response to CT scan:	
Complete Response	7
Partial Response	36
Progressive Disease	30
Stable Disease	22
Unable To Determine	6

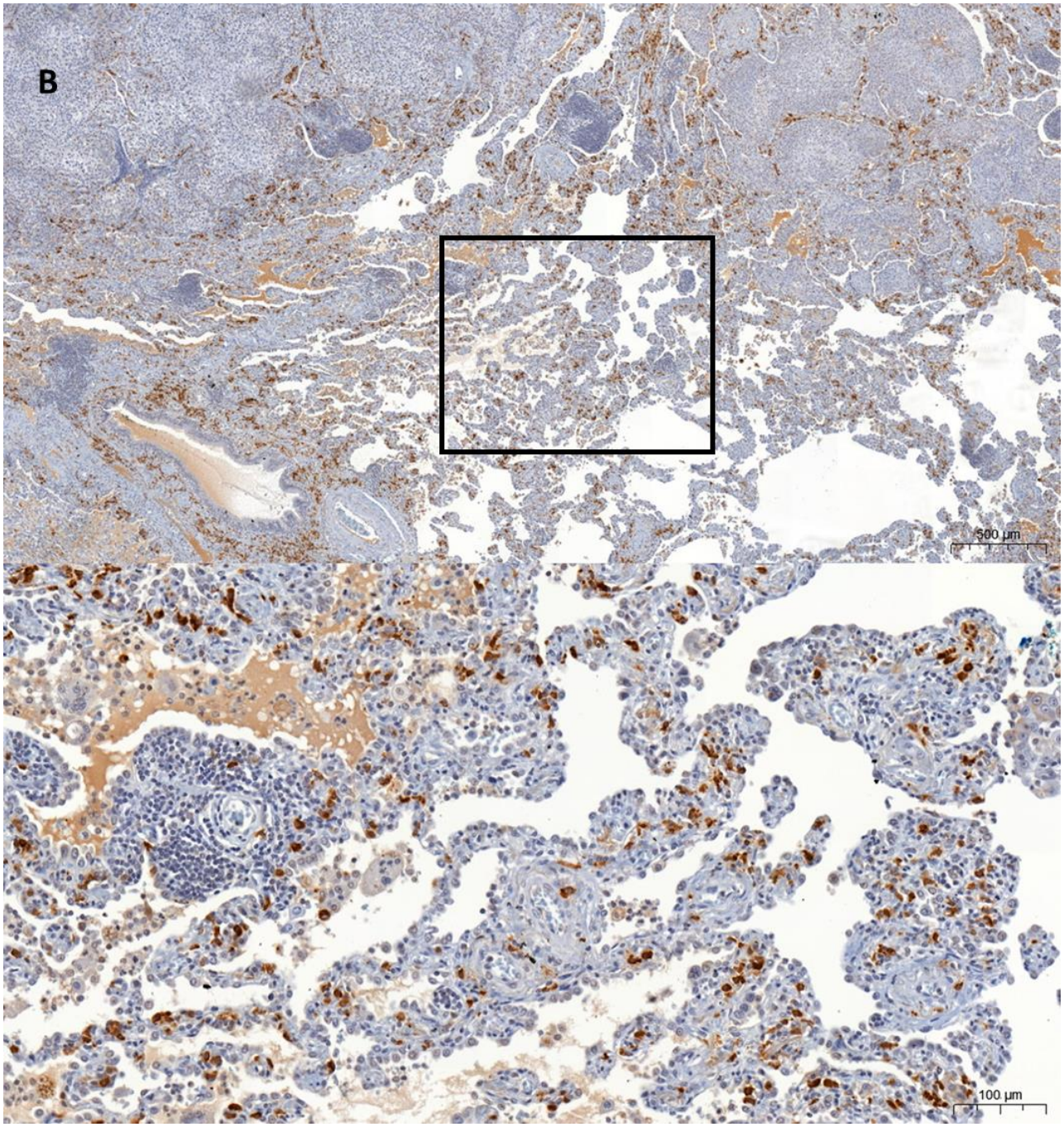
Table 5-10 **outlines the demographics of the prospective study** containing 101 patients treated over three years at the Weston Park Cancer Centre.

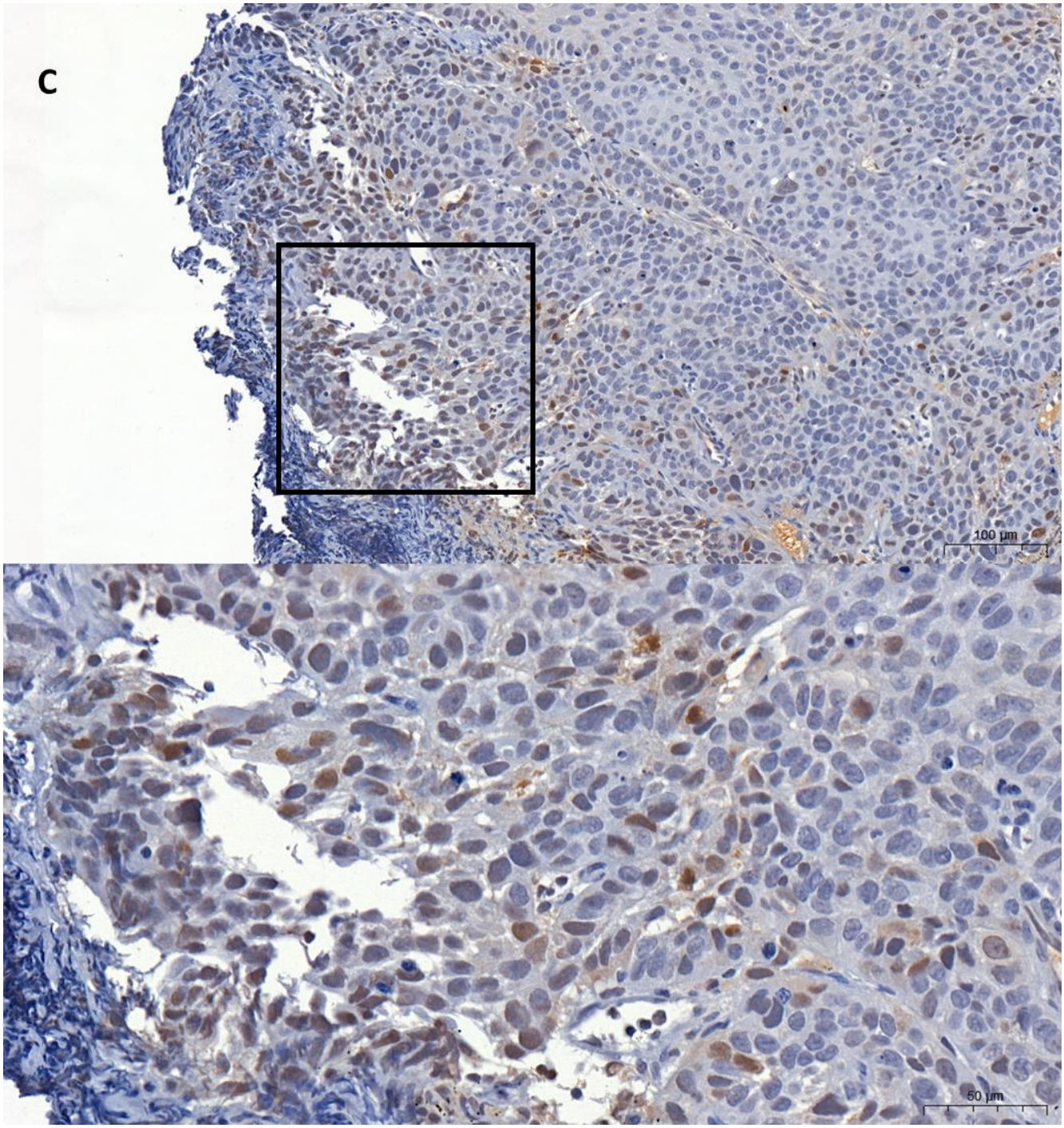
5.2.3.2 Patient *AURKA* H-Scores differed between patients diagnosed with adenocarcinomas and squamous cell cancer but did not correlate with the patient's overall or progression-free survival.

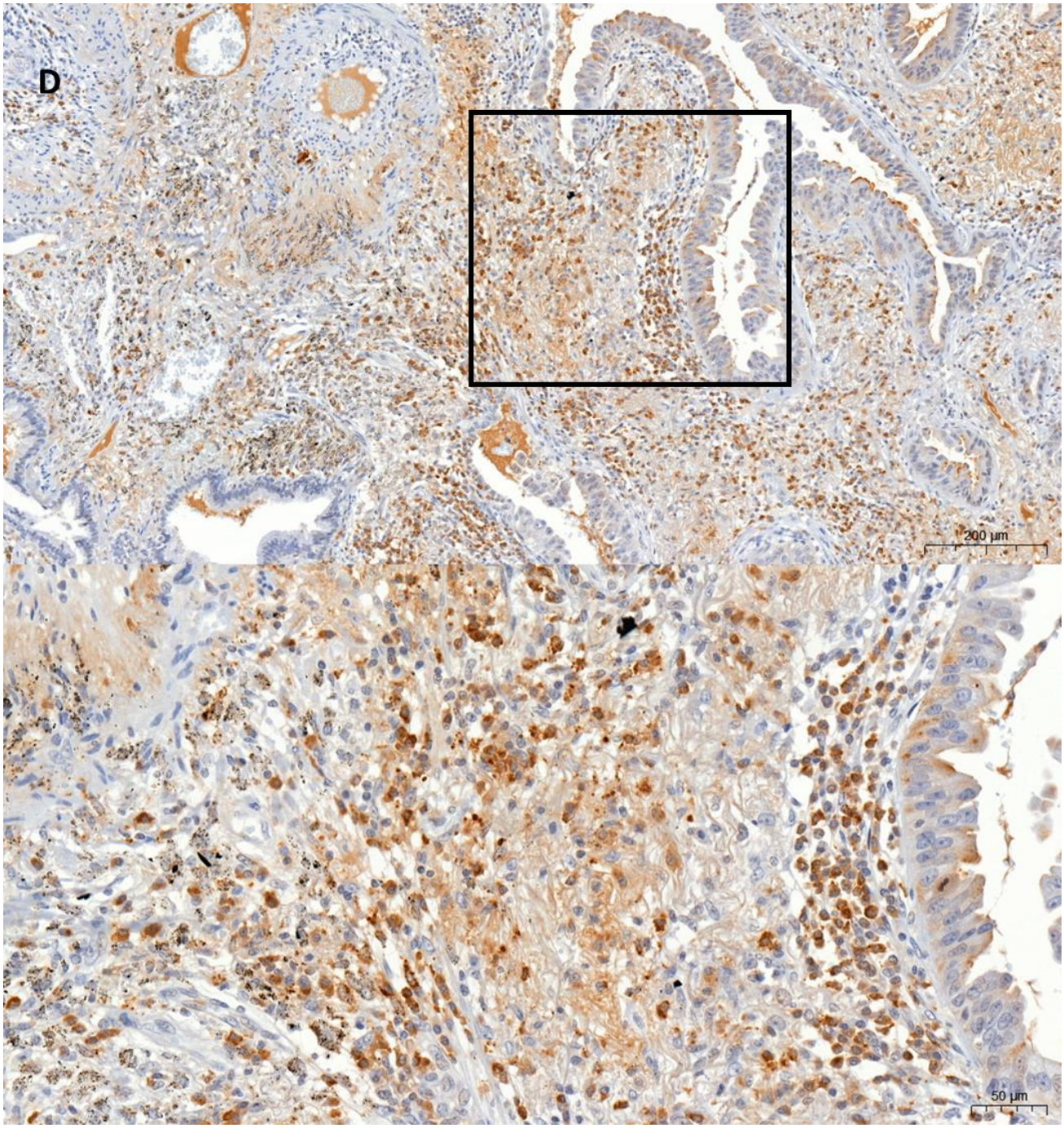
Here, biopsy slides from the patients were stained for Aurora Kinase A. Stained IHC specimens were viewed with a microscope and scored by a pathologist (Jon Bury), who assigned an H-score to each sample. This semi-quantitative scoring system calculates a score from 0 to 300 based on the intensity of tumour nuclear staining and the percentage of cells stained. Intensity is considered "0" for absent expression, "1+" for weak staining, "2+" for moderate staining, and "3+ for strong staining (Figure 4). The H-score is calculated as follows: H-Score = (0 x percentage of cells with absent cy*top*lasmic staining) + (1 x percentage of "1+" cells) + (2 x percentage of "2+" cells) + (3 x percentage of "3+ cells). A positive test was defined as a slide with an H-score greater than 1%, while a negative test was described as a slide for which an H-score could not be determined.

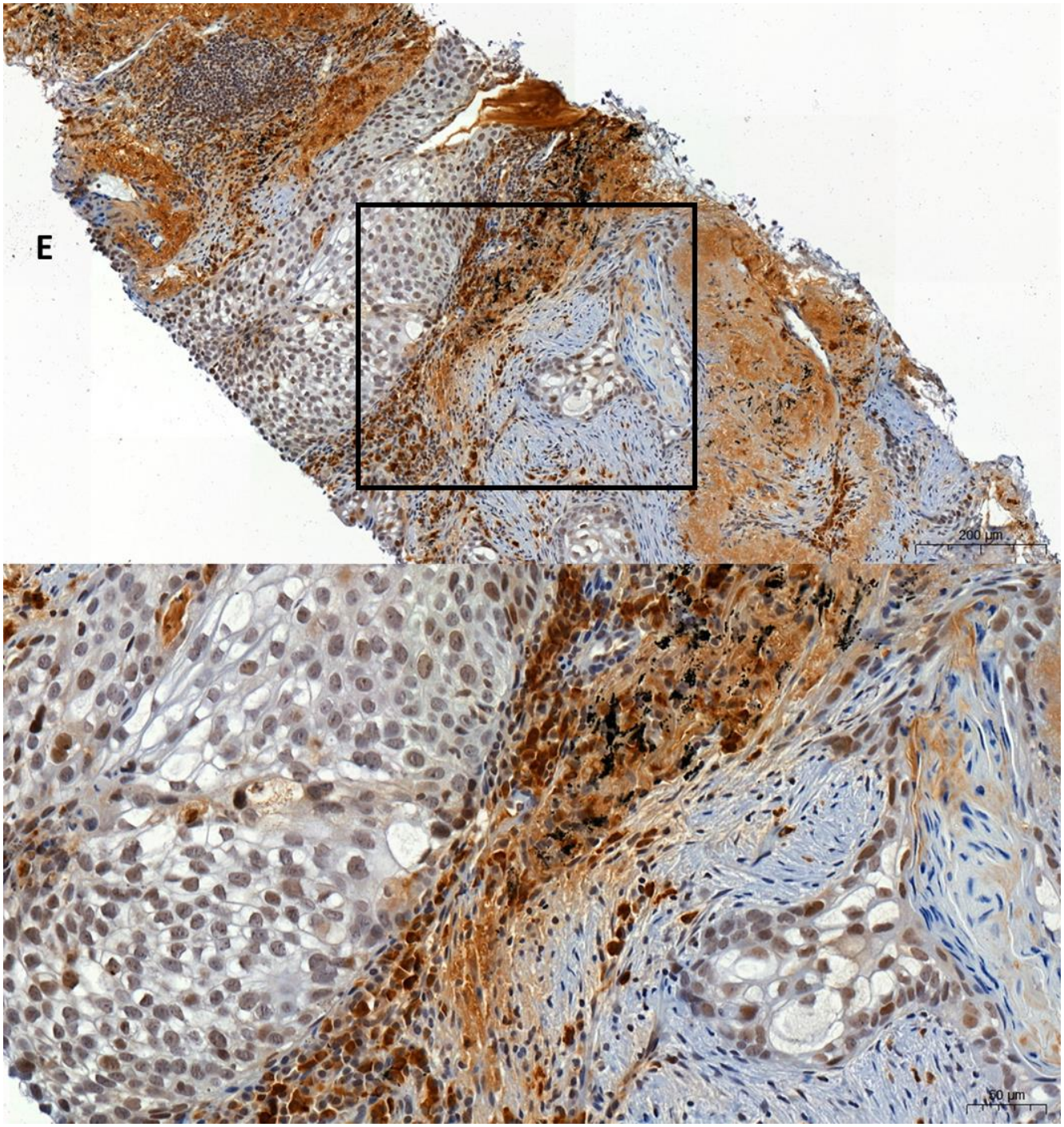
The H-scores ranged from two hundred and forty (240) to zero (0) (Figure 6-3 (A-F) and 6-4); thirty-three (33) slides did not generate a score, fifty-one (51) slides were classed as "weak to intermediate" staining with scores between four (4) and eighty (80), and eighteen (18) slides demonstrated "strong" staining with scores between one hundred (100) to two hundred and forty (240).


A
500 µm
50 µm


B
500 µm
100 µm


C
100 µm
50 µm


D
200 µm
50 µm


E
200 µm
50 µm

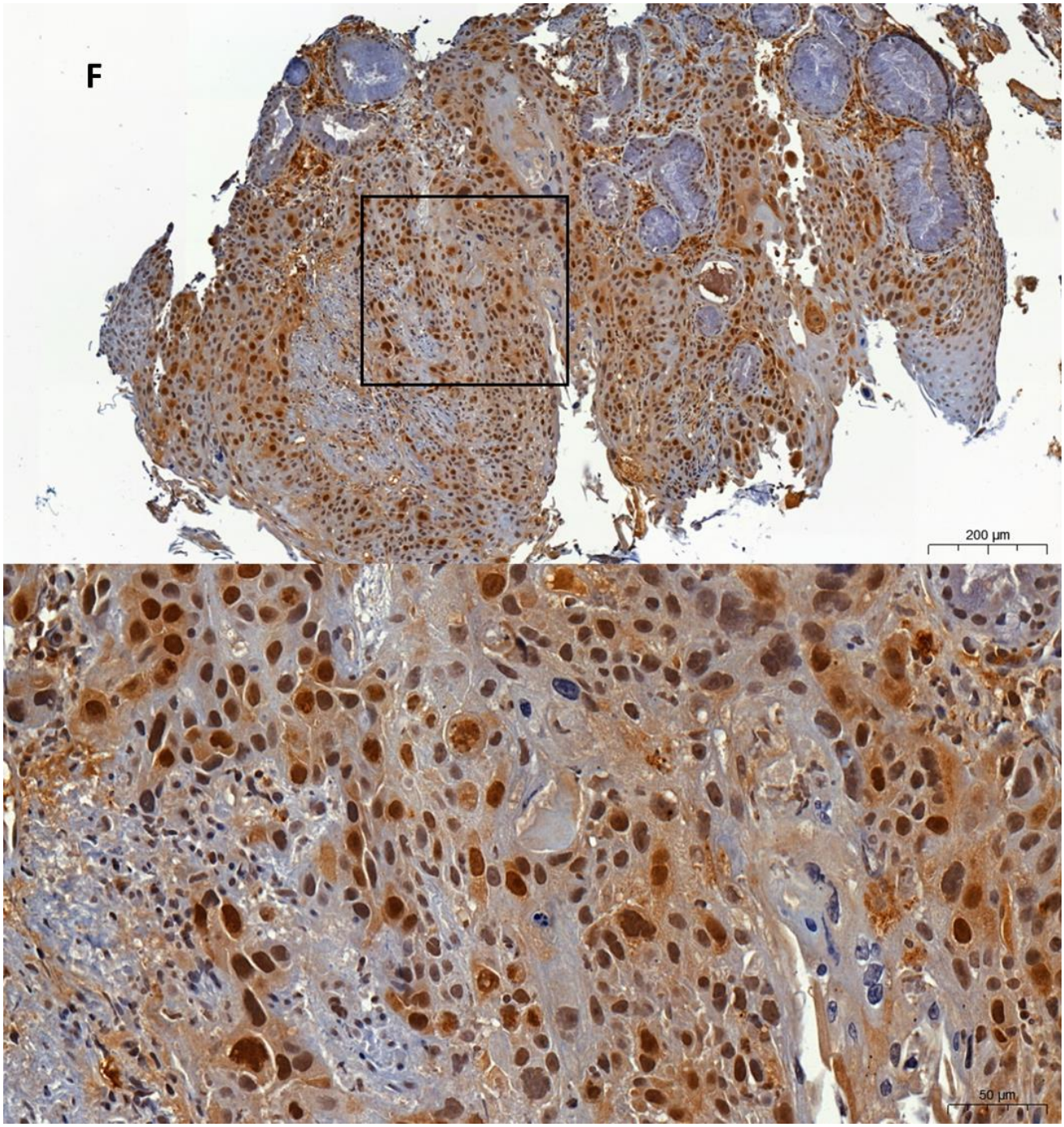


Figure 5-11 A-F: ***Representative images of staining in NSCLC tissue scored with increasing H-scores 0,4,30,65,120 and 240 A-F*** *respectively. Standard comparative protocol using labelled 1:200 used microwave retrieval with IMMPRESS® signal detection system and pH 6.1 citrate target retrieval solution. Antibody signal on stained cells was developed with DAB for 1 minute, and cells were counterstained with Gill's hematoxylin for 10 seconds (N=1). Scale bars represent 50 to 200µm. All slides were scanned using a panoramic 250 slide scanner using a 20x objective. H scores were calculated as a function of staining intensity and percentage of tumour cells positive.*

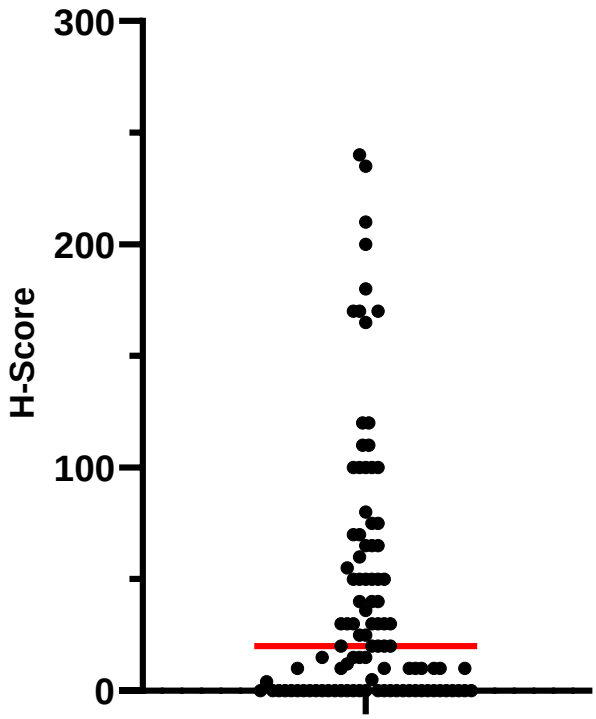


Figure 5-12: **Distribution of H-scores in patient diagnostic biopsies.** Points show individual samples, and the red line indicates the median value.

The H-scores, representing a quantitative measure of a specific parameter, were compared in different subgroups of patients diagnosed with adenocarcinomas and squamous cell cancers. The results showed a significant difference between the H-scores of these two histological types ($p=0.0461$, Mann-Whitney test). Specifically, the median H-score for adenocarcinomas was eleven, while the median for squamous cell cancers was thirty.

Furthermore, an analysis was conducted to investigate the potential influence of gender on H-scores. The comparison of H-scores between males and females revealed no statistically significant difference ($p=0.1898$, Mann-Whitney test). The median H-score for males was ten, whereas the median H-score for females was twenty-five.

Another subgroup analysis focused on comparing H-scores between patients of white ethnicity and those with BAEM (Black and Asian patients). The results indicated no significant difference in the H-scores between these two patient groups ($p=0.6646$, Mann-Whitney test). Both groups had a median H-score of twenty.

The comparison between patients with metastatic disease and those without metastatic disease showed no significant disparity in H-scores ($p=0.6646$, Mann-Whitney test). Both patient groups exhibited a median H-score of twenty-seven and a half and twenty, respectively (Figure 6-5).

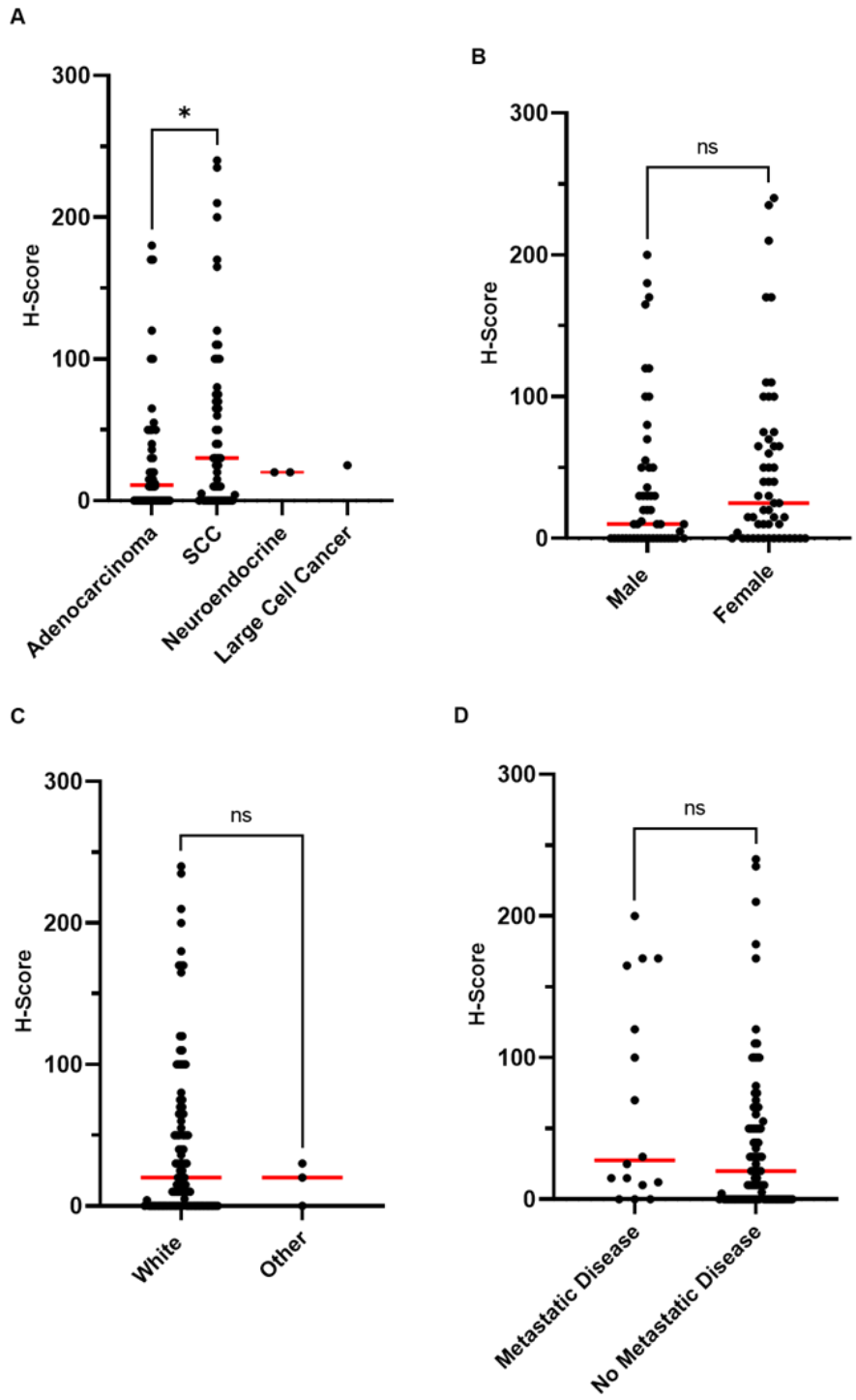


Figure 5-13: H-scores in different subgroups of patients (A) Histological type. Note that large cell lung cancer and neuroendocrine were excluded from statistical analysis due to low sample size, (B) gender, (C) ethnicity, and (D) stage of disease. Dots represent individual samples; the red line represents the median value. Statistical significance was calculated using the Mann-Whitney U test where *=$p<0.05$ and ns = non-significant.

Log-rank testing used the calculated H-Scores to assess the relationship between *AURKA* expression and overall patient progression-free survival with a chosen significance alpha level of 0.05 (5%) (Figure 6-6). This analysis showed that the H-Scores did not significantly correlate with overall survival ($X^2 = 2.637$, $p = 0.1044$). Similarly, no significant difference in progression-free survival was observed based on the H-Scores ($X^2 = 0.06739$, $p = 0.7952$).

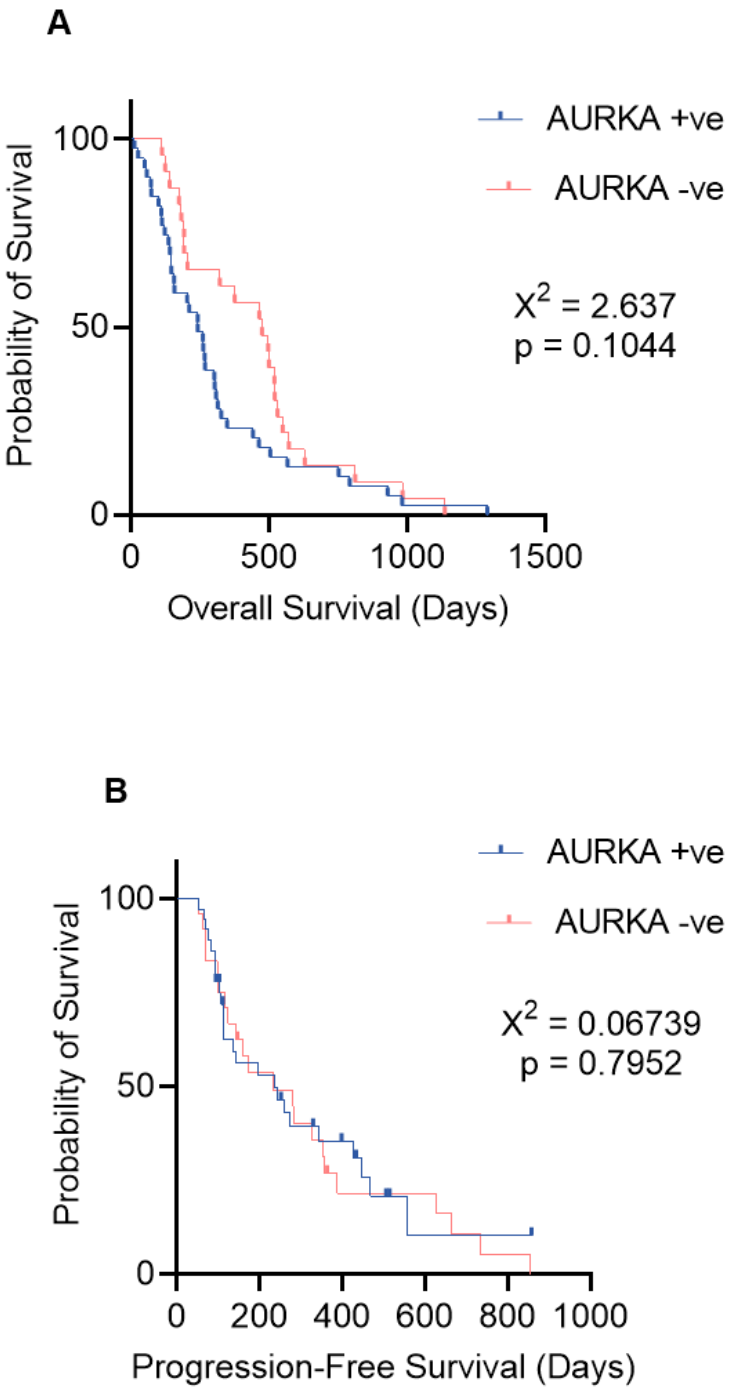
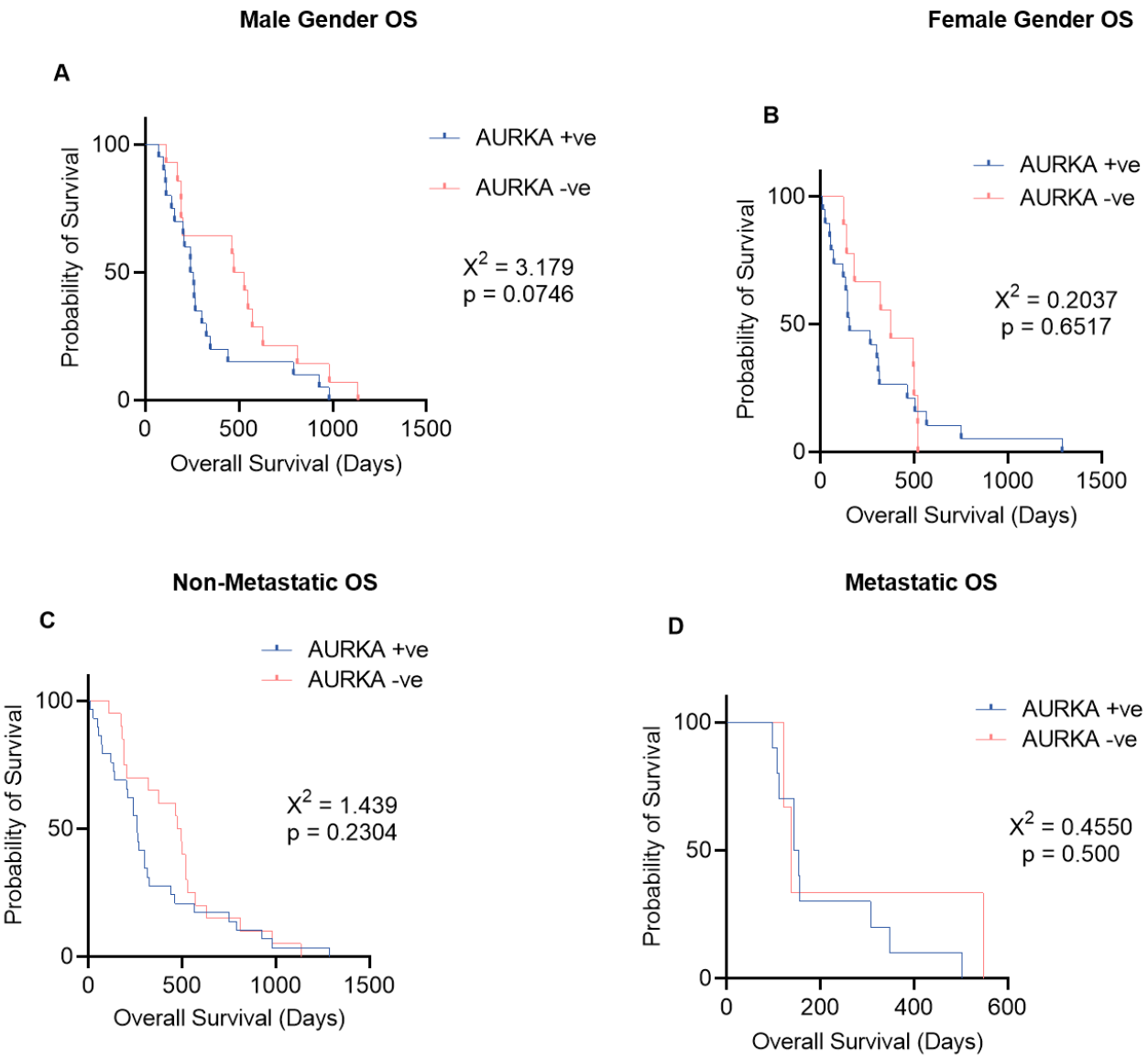


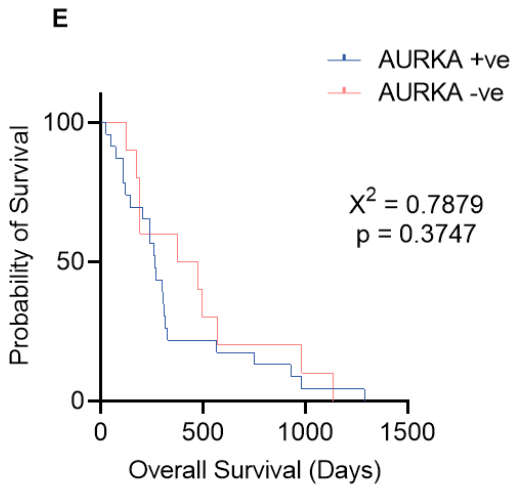
Figure 5-14: Overall survival (A) and Progression-free survival (B) comparing *AURKA* positive (+ve (H score 0 to 240)) to *AURKA* (-ve (H score 0 to 240) patients. Significance using the R programming software calculated by log-rank testing where ns = non-significant.

5.2.3.3 Patient *AURKA* H-Scores did not correlate with overall survival when patient gender or stage was considered but demonstrated significance when SCC pathology and smoking status subgroup analysis were done.

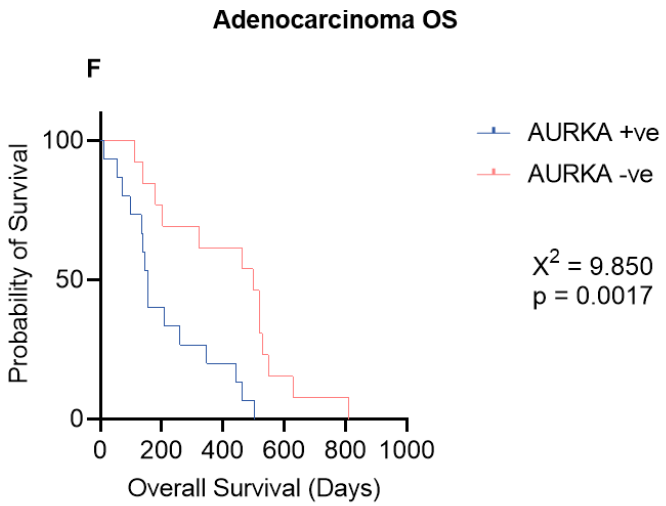
Overall survival subgroup analysis of patients with positive and negative *AURKA*-stained slides was done and assessed using log-rank testing (Figure 6-7). Subgroup analysis was done in Females, Males, Patients with and without Mets, Squamous cell cancers, and current and former smokers' patients over and under 70. There was a significant difference in *AURKA* staining in the adenocarcinomas with an H-score of 0.0017; the rest of the subgroups were non-significant.


Male Gender OS
A
Probability of Survival
100
50
0
0
500
1000
1500
Overall Survival (Days)
AURKA +ve
AURKA -ve
X2 = 3.179
p = 0.0746
Female Gender OS
B
Probability of Survival
100
50
0
0
500
1000
1500
Overall Survival (Days)
AURKA +ve
AURKA -ve
X2 = 0.2037
p = 0.6517
Non-Metastatic OS
C
Probability of Survival
100
50
0
0
500
1000
1500
Overall Survival (Days)
AURKA +ve
AURKA -ve
X2 = 1.439
p = 0.2304
Metastatic OS
D
Probability of Survival
100
50
0
0
200
400
600
Overall Survival (Days)
AURKA +ve
AURKA -ve
X2 = 0.4550
p = 0.500

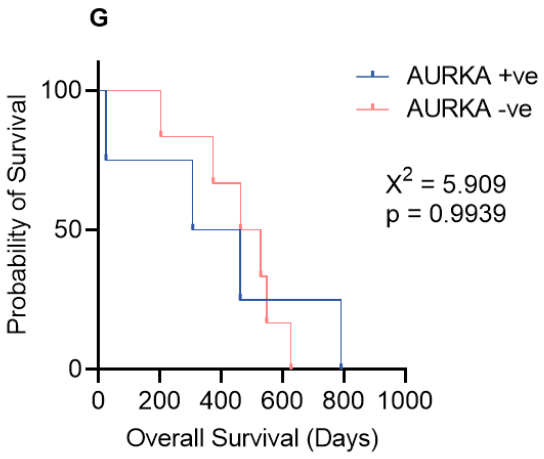
Sqaumous Cell cancer OS



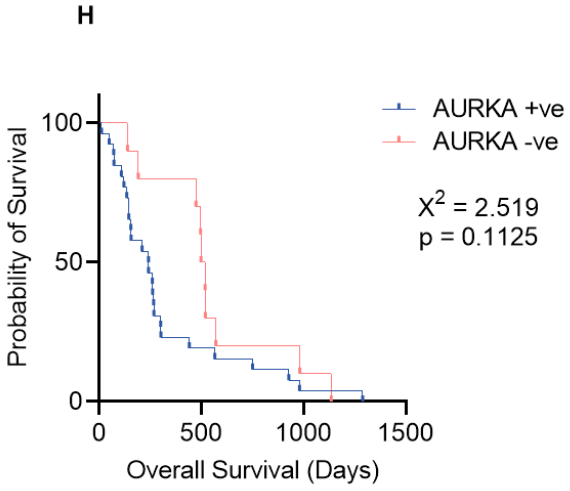
Adenocarcinoma OS



Current Smoker OS



Former Smoker OS



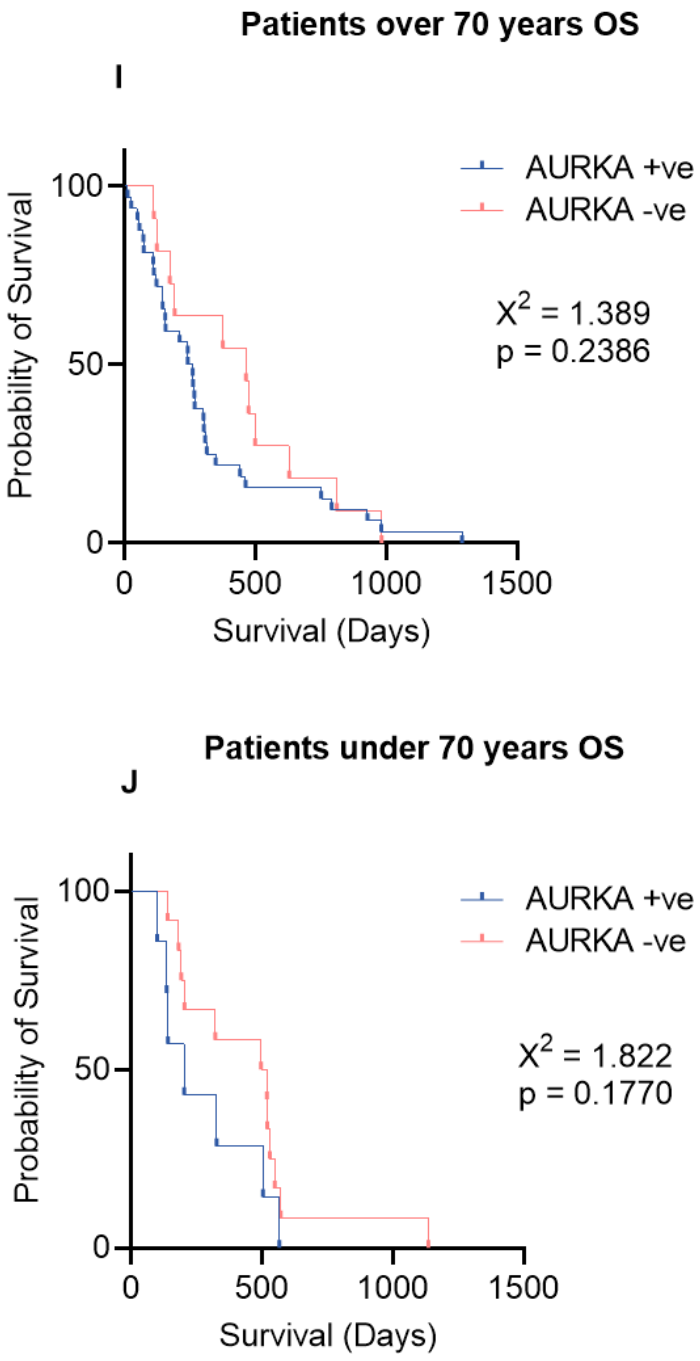
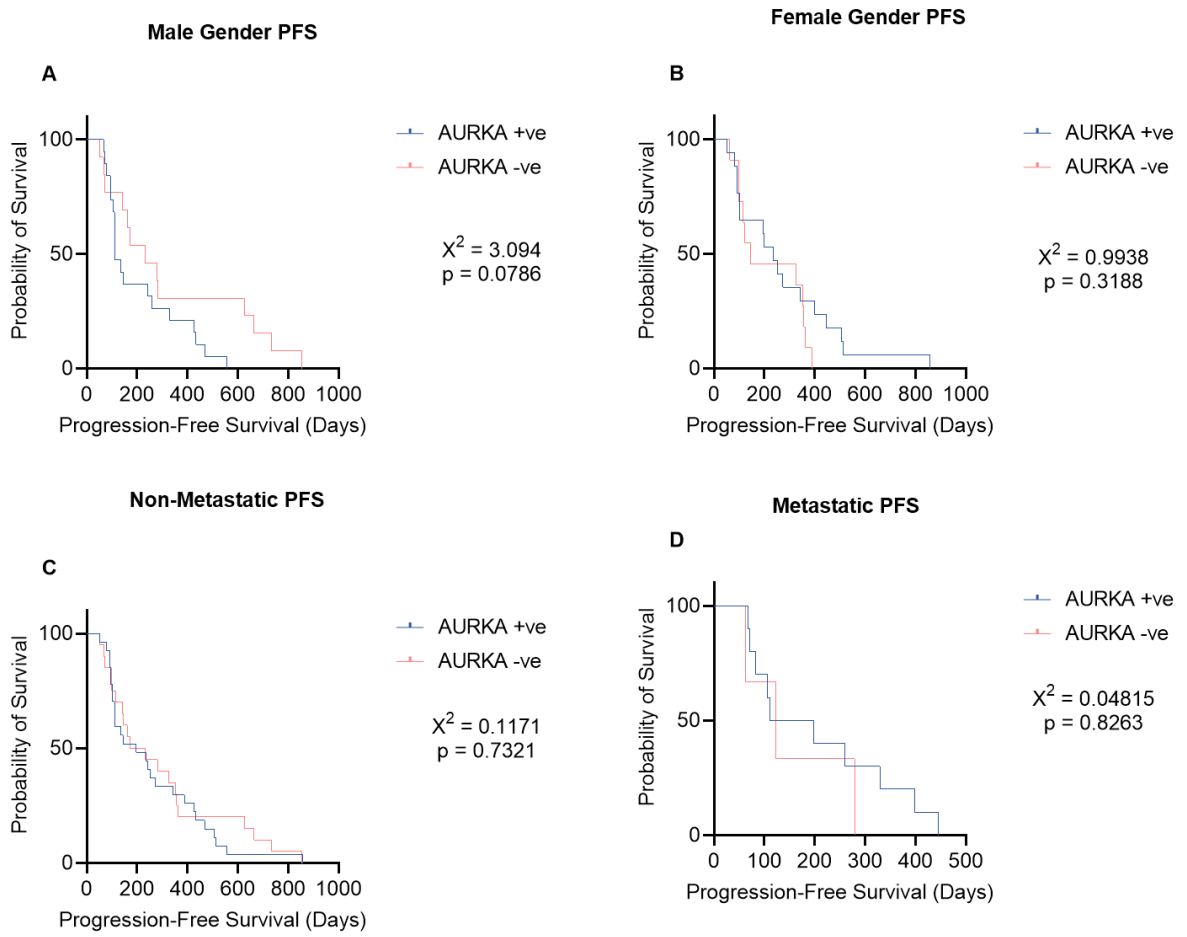
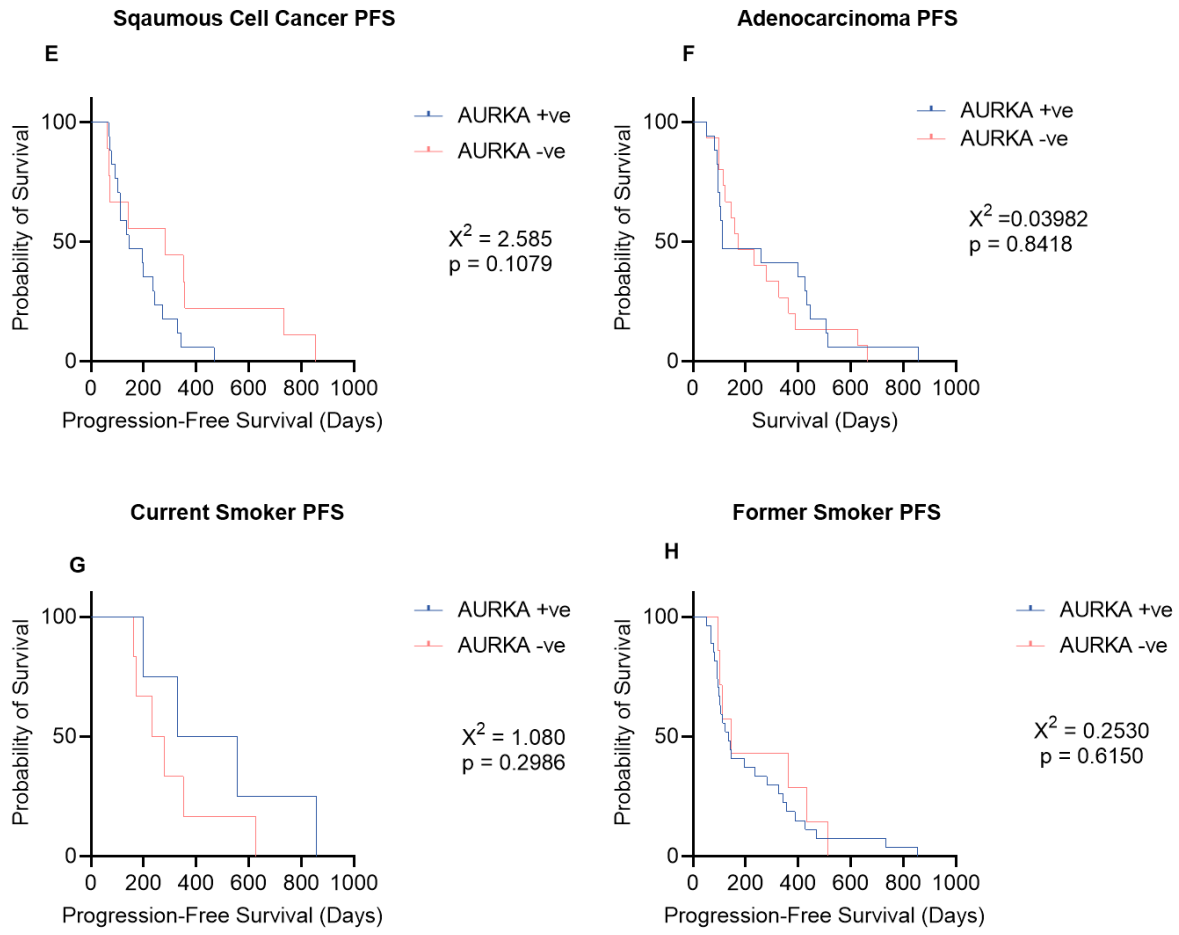


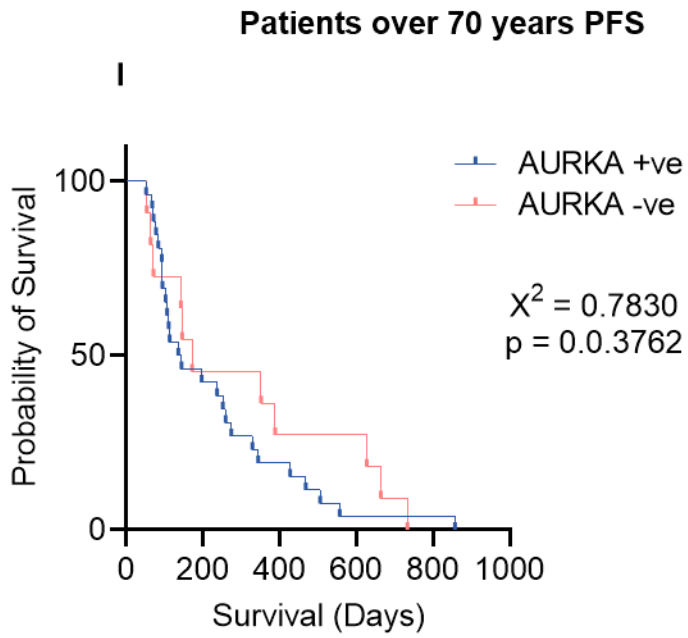
Figure 5-15 *Overall survival comparing positive (+ve) to (-ve) patients, within sub-populations (A) Male Gender, (B) Female Gender, (C) Non-Metastatic patients (D)Metastatic patients (E)SCC patients, (F)Adenocarcinoma patients, (G) Current Smokers, (H) Former Smokers, (I) Patient is over 70 years old (J) Patients under 70 years old—significance calculated by log-rank testing where ns = non-significant.*

5.2.3.4 Patient *AURKA* H-Scores did not correlate progression-free survival when patient gender, pathology, or stage subgroup analysis were considered.

Progression-free survival subgroup analysis of patients with positive and negative *AURKA*-stained slides was done and assessed using log-rank testing with the same subgroups for overall survival analysis. Log-rank testing showed that these differences did not significantly correlate in any subgroup tested. (Figure 6-8).


Male Gender PFS
A
Probability of Survival
100
50
0
0 200 400 600 800 1000
Progression-Free Survival (Days)
AURKA +ve
AURKA -ve
X2 = 3.094
p = 0.0786
Female Gender PFS
B
Probability of Survival
100
50
0
0 200 400 600 800 1000
Progression-Free Survival (Days)
AURKA +ve
AURKA -ve
X2 = 0.9938
p = 0.3188
Non-Metastatic PFS
C
Probability of Survival
100
50
0
0 200 400 600 800 1000
Progression-Free Survival (Days)
AURKA +ve
AURKA -ve
X2 = 0.1171
p = 0.7321
Metastatic PFS
D
Probability of Survival
100
50
0
0 100 200 300 400 500
Progression-Free Survival (Days)
AURKA +ve
AURKA -ve
X2 = 0.04815
p = 0.8263


Sqaumous Cell Cancer PFS
E
Probability of Survival
100
50
0
0 200 400 600 800 1000
Progression-Free Survival (Days)
AURKA +ve
AURKA -ve
X2 = 2.585
p = 0.1079
Adenocarcinoma PFS
F
Probability of Survival
100
50
0
0 200 400 600 800 1000
Survival (Days)
AURKA +ve
AURKA -ve
X2 =0.03982
p = 0.8418
Current Smoker PFS
G
Probability of Survival
100
50
0
0 200 400 600 800 1000
Progression-Free Survival (Days)
AURKA +ve
AURKA -ve
X2 = 1.080
p = 0.2986
Former Smoker PFS
H
Probability of Survival
100
50
0
0 200 400 600 800 1000
Progression-Free Survival (Days)
AURKA +ve
AURKA -ve
X2 = 0.2530
p = 0.6150



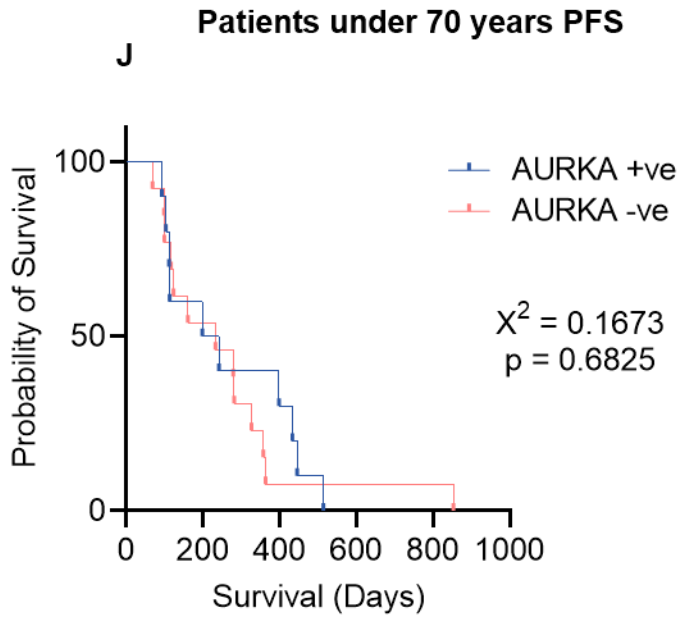


Figure 5-16 *Progression-free survival comparing positive (+ve) to (-ve) patients within sub-populations (A) Male Gender, (B) Female Gender, (C) Non-Metastatic patients (D)Metastatic patients (E)SCC patients, (F)Adenocarcinoma patients, (G) Current Smokers, (H) Former Smokers, (I) Patient is over 70 years old (J) Patients under 70 years old—significance calculated by log-rank testing where ns = non-significant.*

5.2.3.5 Reoptimisation of *AURKA* staining – antigen retrieval temperature.

Although a previous student had optimised *AURKA* staining, one problem we encountered was the increased staining of stromal tissue and cy*top*lasm (Figure 6-9). Some slides were too difficult to analyse as the increased stromal staining *mad*e it challenging to see the nuclei. This led to uncertainty in registering an H-score; we, therefore, set out to improve the staining protocol. We initially thought the increased levels of background staining might be due to exposing the tissue to higher temperatures during the antigen retrieval step. We, therefore, reduced the temperature settings in the microwave when testing the I*MMP*RESS® Excel Amplified Polymer Staining Kit, but little difference was seen (Figure 6-9)

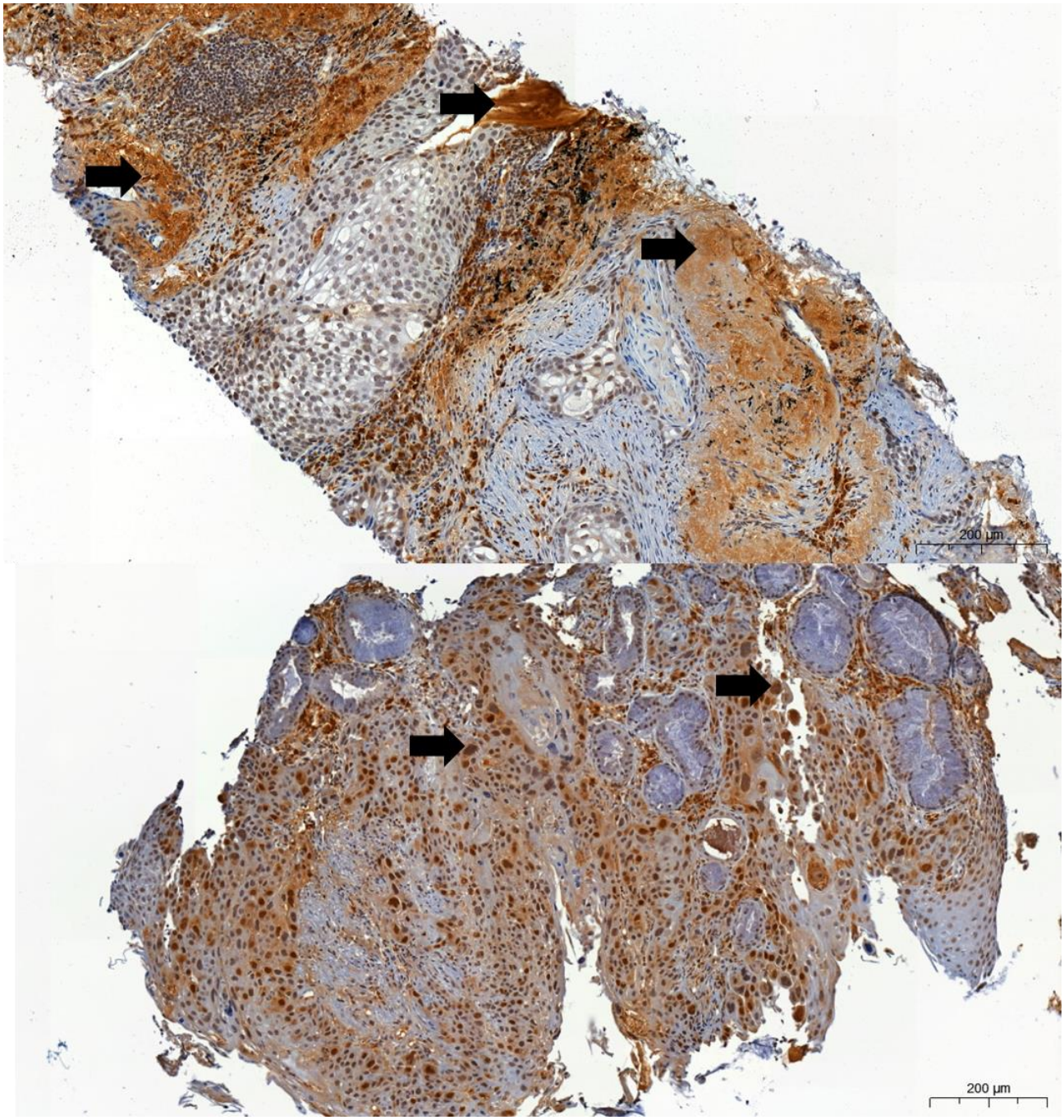


Figure 5-17: ***Representative images of staining in NSCLC tissue with orange arrows pointing to increased tissue stroma and cellular cytoplasm staining***. *Standard comparative protocol using labelled 1:200 used microwave retrieval with IMMPRESS® signal detection system and pH 6.1 citrate target retrieval solution. Antibody signal on stained cells was developed with DAB for 1 minute, and cells were counterstained with Gill's hematoxylin for 10 seconds (N=1). Scale bars represent 200µm. All slides were scanned using a panoramic 250 slide scanner using a 20x objective.*

5.2.3.6 Reoptimisation of *AURKA* staining - Use of the I*MMP*RESS Excel Amplified Polymer Staining Kit.

The high number of slides with H-scores of less than one raised concerns about the sensitivity of the antibody in patient tissue. In the previous protocol, the I*MMP*RESS HRP Polymer System was used. To try and increase the sensitivity of the antibody staining, an I*MMP*RESS® Excel Amplified Polymer Staining Kit was used at different concentrations (ranging from 1:10 to 1:400) on test slides with varying H-Scores, as shown in Table 6-2 and Figure 6-11 and 6-12. I*MMP*RESS® Excel Amplified Polymer Staining Kit uses an amplifier antibody, followed by an I*MMP*RESS Excel HRP Polymer Reagent to increase the DAB targeting. However, the I*MMP*RESS® kit was found to have several problems. First, it increased background staining on low and high microwave settings, making slide analysis more challenging (Figure 6-13). Second, it produced inconsistent nuclear staining, with some cells appearing “half-stained” and thus almost impossible to score (Figure 6-14). Finally, the kit did not improve *AURKA* slide staining with zero H-scores (Table 6-2 and Figure 6-15). These issues suggest that using the I*MMP*RESS® Excel Amplified Polymer Staining Kit may not be a suitable solution for improving the H-Scores in this study.

Antibody concentration	Previous H Score	Pathologist review
1 in 10	0	Dirty
1 in 10	40	Dirty
1 in 10	70	Dirty
1 in 25	0	Weak
1 in 25	75	Dirty
1 in 25	80	Weak
1 in 50	15	Dirty
1 in 50	36	Dirty
1 in 50	0	Nil
1 in 100	0	Weak
1 in 100	15	Dirty
1 in 100	110	Nil
1 in 200	0	Nil
1 in 200	50	Weak
1 in 200	120	Nil
1 in 400	0	Nil
1 in 400	15	Nil
1 in 400	100	Weak

Table 5-11 ***Results of the optimisation of antibody using the IMMPRESS® Excel Amplified Polymer Staining Kit:*** *Standard comparative protocol using labelled 1:10, 1:25, 1:50, 1:100, 1:400 and 1:200 used microwave retrieval with IMMPRESS® Excel Amplified Polymer Staining Kit and pH 6.1 citrate target retrieval solution. Antibody signal on stained cells was developed with DAB for 3 minutes 30 seconds, and cells were counterstained with Gill's hematoxylin (N=1).*

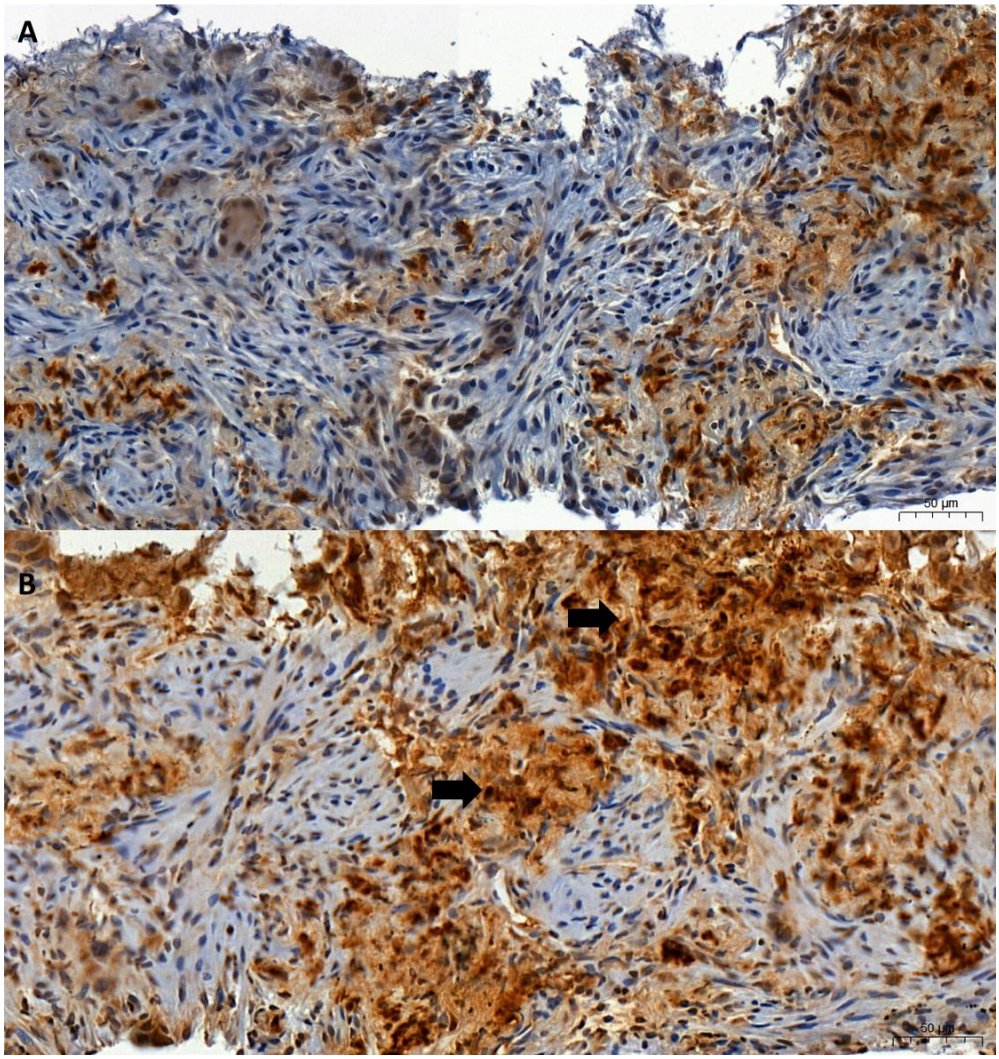


Figure 5-18 ***Results of the optimisation of antibody using the IMMPRESS® Excel Amplified Polymer Staining Kit demonstrating increased background staining and no improvement in nuclear staining in a slide with an H-score of 15 (A-B):*** *A Staining without the use of the IMMPRESS® Excel Amplified Polymer Staining Kit B Staining with use of the IMMPRESS® Excel Amplified Polymer Staining Kit black arrows show areas of heavy stromal staining**:** Standard comparative protocol using labelled 1:200 used microwave retrieval with IMMPRESS® Excel Amplified Polymer Staining Kit and pH 6.1 citrate target retrieval solution. Antibody signal on stained cells was developed with DAB for 1 minute, and cells were counterstained with Gill's hematoxylin for 10 seconds (N=1). Scale bars represent 50 µm. All slides were scanned using a panoramic 250 slide scanner using a 20x objective.*

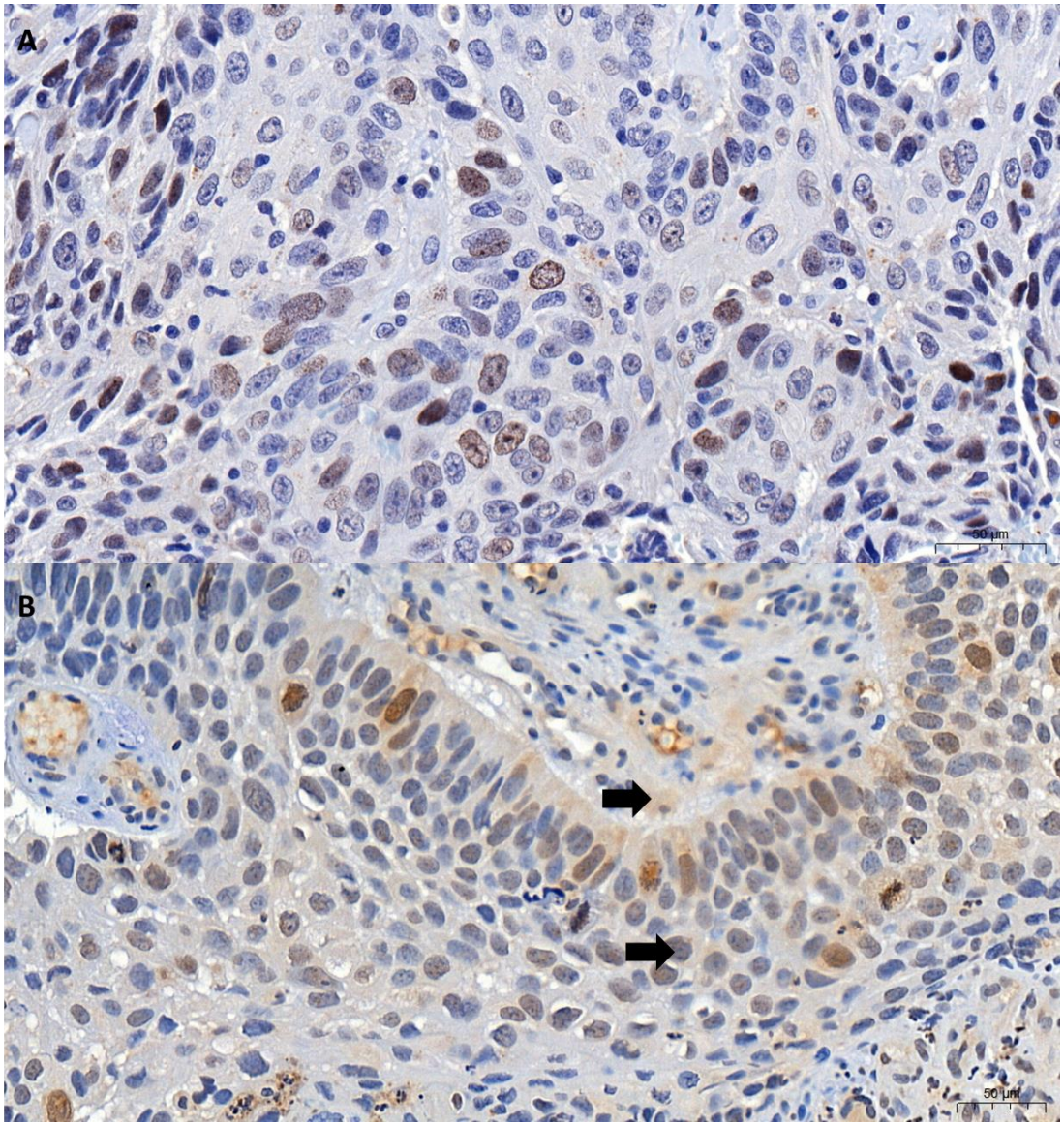


Figure 5-19 ***Results of the optimisation of antibody using the IMMPRESS® Excel Amplified Polymer Staining Kit demonstrating increased background staining and no improvement in nuclear staining in a slide with an H-score of 100 (A-B):*** *A Staining without the use of the IMMPRESS® Excel Amplified Polymer Staining Kit B Staining with use of the IMMPRESS® Excel Amplified Polymer Staining Kit black arrows show areas of "half stained" nuclei: Standard comparative protocol using labelled 1:200 used microwave retrieval with IMMPRESS® Excel Amplified Polymer Staining Kit and pH 6.1 citrate target retrieval solution. Antibody signal on stained cells was developed with DAB for 1 minute, and cells were counterstained with Gill's hematoxylin for 10 seconds (N=1). Scale bars represent 50µm. All slides were scanned using a panoramic 250 slide scanner using a 20x objective.*

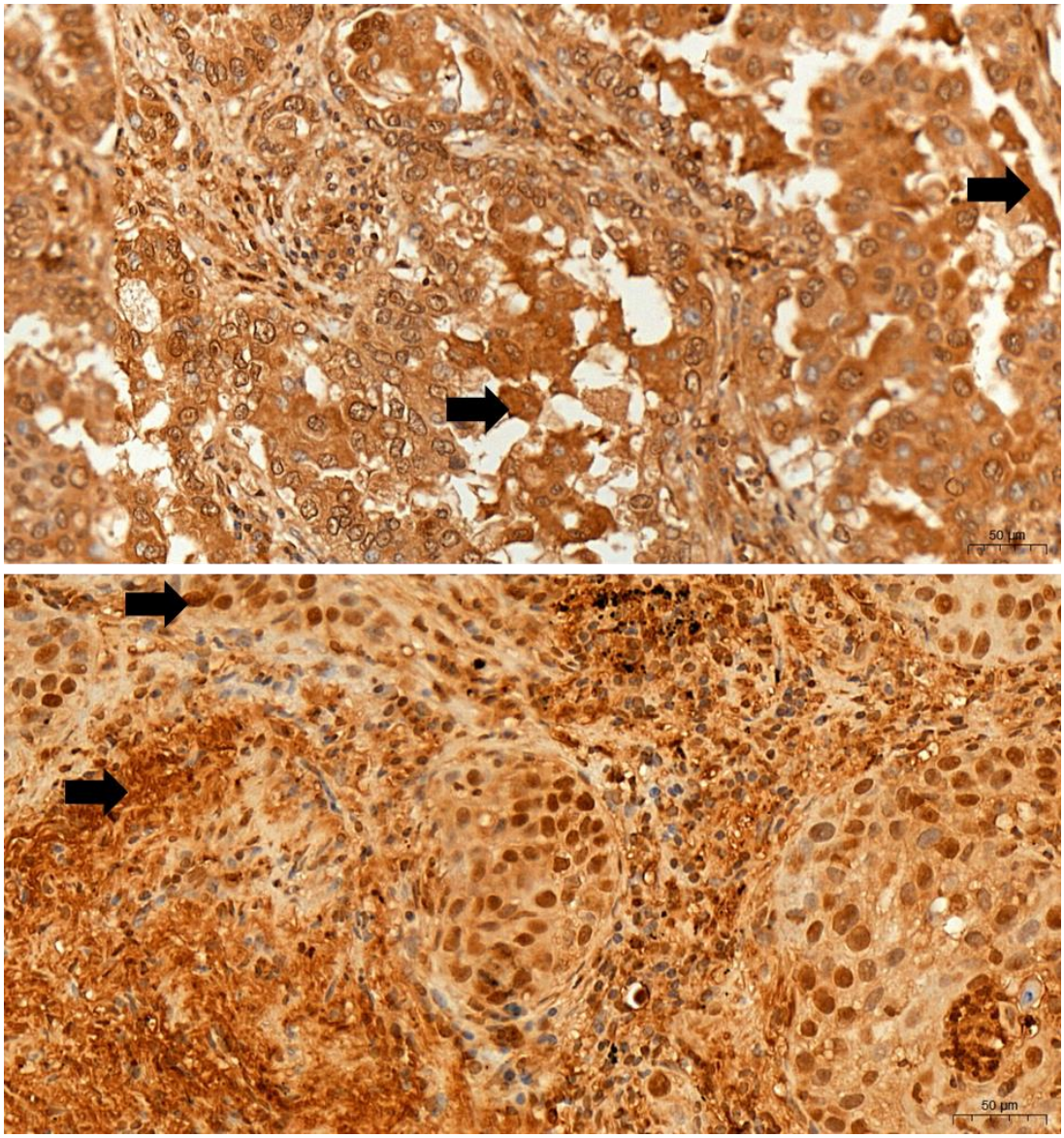


Figure 5-20 ***Results of the optimisation of antibody using the IMMPRESS® Excel Amplified Polymer Staining Kit demonstrating increased background staining (A-B):*** *A Staining on low microwave settings B Staining on high microwave settings: Standard comparative protocol using labelled 1:200 used microwave retrieval with IMMPRESS® Excel Amplified Polymer Staining Kit and pH 6.1 citrate target retrieval solution. Antibody signal on stained cells was developed with DAB for 1 minute, and cells were counterstained with Gill's hematoxylin for 10 seconds (N=1). Scale bars represent 50µm. All slides were scanned using a panoramic 250 slide scanner using a 20x objective.*

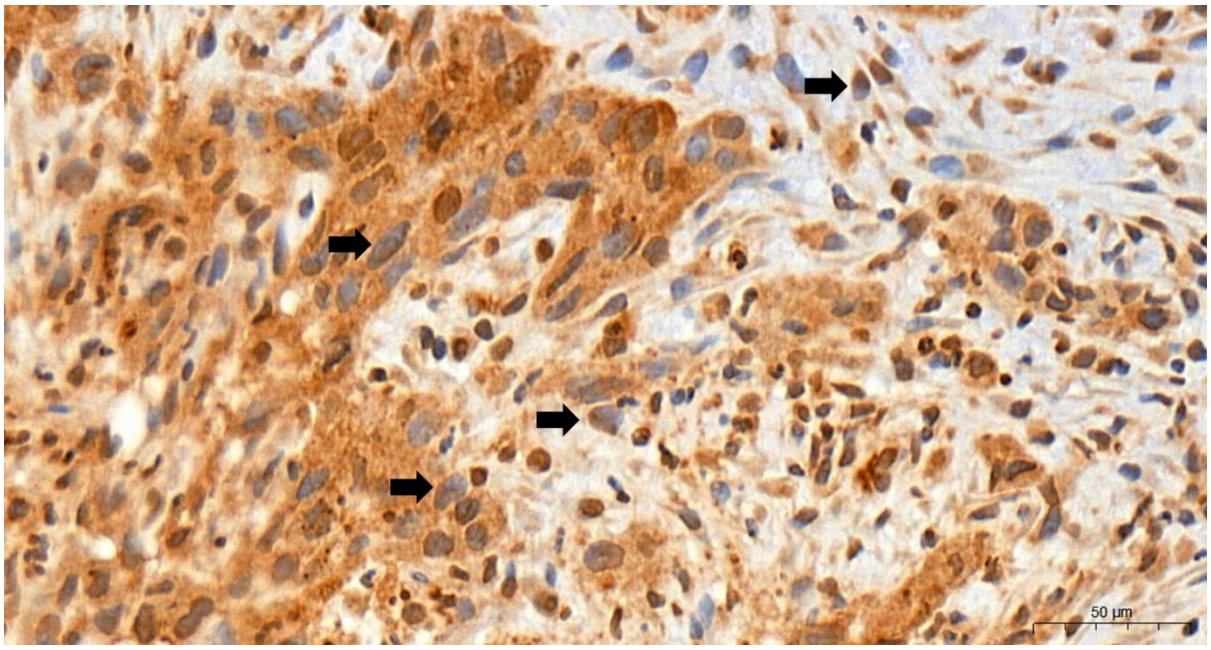
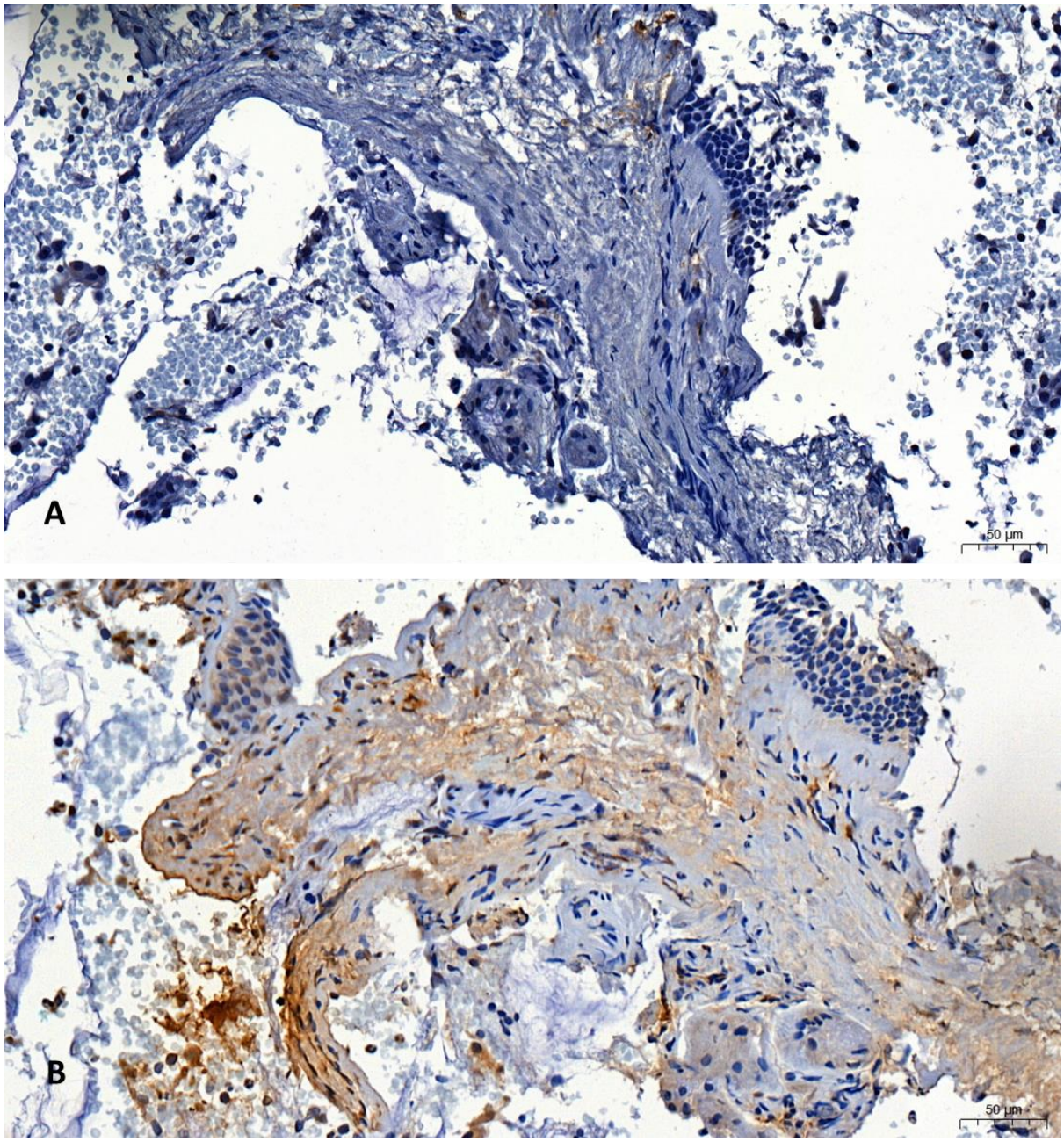


Figure 5-21 ***Results of the optimisation of antibody using the IMMPRESS® Excel Amplified Polymer Staining Kit demonstrating cells which look as if not all of the nuclei have been stained properly "half staining":*** *Standard comparative protocol using labelled 1:200 used microwave retrieval (low settings) with IMMPRESS® Excel Amplified Polymer Staining Kit and pH 6.1 citrate target retrieval solution. Antibody signal on stained cells was developed with DAB for 1 minute, and cells were counterstained with Gill's hematoxylin for 10 seconds (N=1). Scale bars represent 50 µm. All slides were scanned using a panoramic 250 slide scanner using a 20x objective.*


A
50 µm
B
50 µm

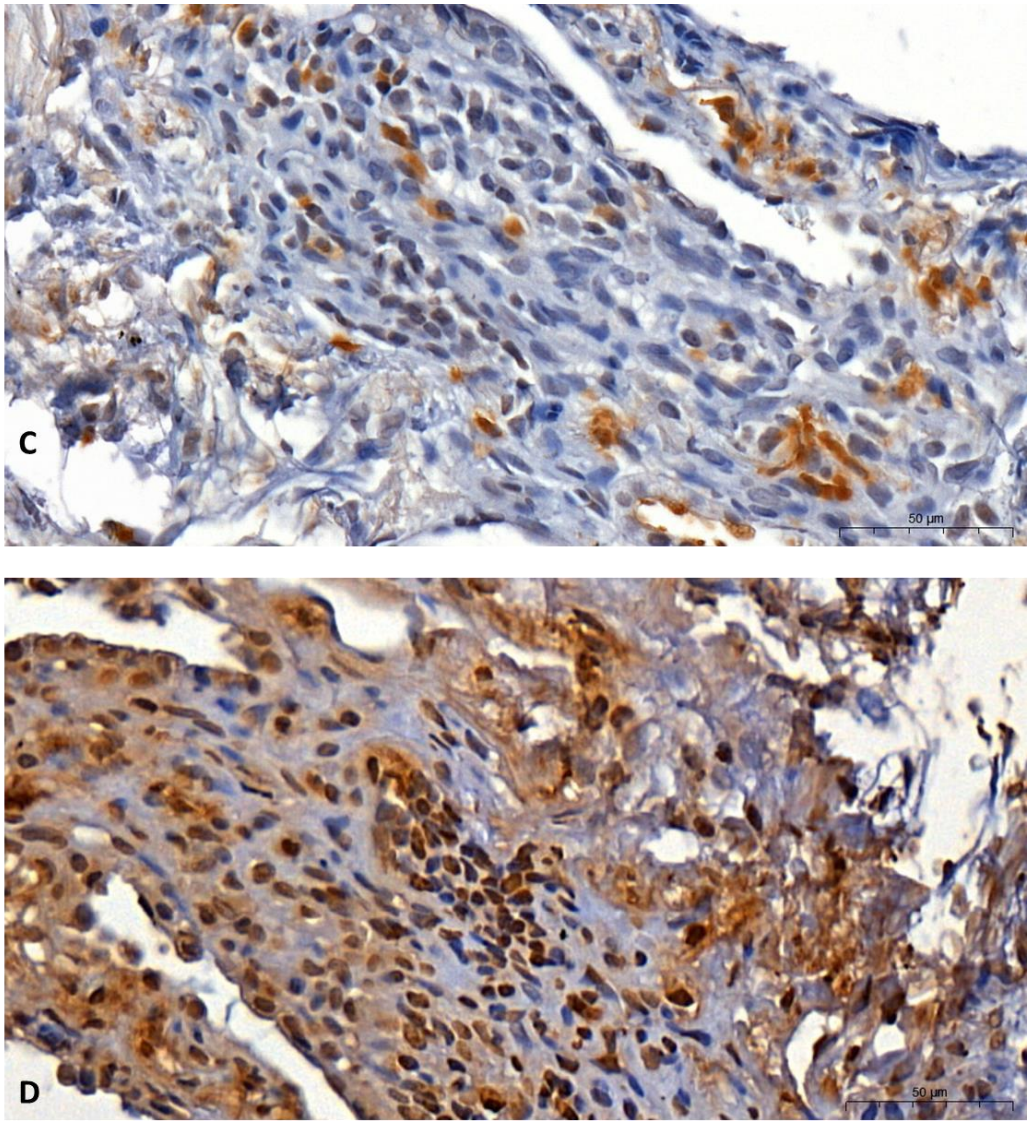


Figure 5-22: ***Results of the optimisation of antibody using the IMMPRESS® Excel Amplified Polymer Staining Kit demonstrating no improvement in the slides which initially had no staining (H-Score 0):*** *A shows the original slide with an H score of 0 with no observable nuclear staining. In contrast, the slide shows increased stromal staining rather than some half-staining of cellular nuclei in B. C shows the original slide with an H score of 0 with no observable nuclear staining, while in D, the slide shows "dirty" and inconsistent nuclear staining "half staining" of cellular nuclei. Standard comparative protocol using labelled 1:200 used microwave retrieval (low settings) with IMMPRESS® Excel Amplified Polymer Staining Kit and pH 6.1 citrate target retrieval solution. Antibody signal on stained cells was developed with DAB for 1 minute, and cells were counterstained with Gill's hematoxylin for 10 seconds (N=1). Scale bars represent 50 µm. All slides were scanned using a panoramic 250 slide scanner using a 20x objective.*

5.2.4 *AURKB* IHC in NSCLC patient cohort.

5.2.4.1 Optimising *AURKB* staining in NSCLC cell lines and confirming the specificity of *AURKB* antibody.

The *AURKB* staining protocol was optimised using an anti-*AURKB* (Abcam - ab2254) antibody. First, H460 cells were grown and treated with scrambled control siRNA or siRNA targeting *AURKB* (si611) for 48 hours. Cell pellets were harvested, and western blot analysis was performed to confirm that *AURKB* had been depleted from the cells (Figure 6-16). Duplicate pellets were fixed and processed for IHC staining. The slides prepared from these pellets were stained with antibody dilutions of 1:100 and 1:200; a negative antibody control was also included (Figures 6-17 and 6-18). Nuclear staining was seen in the scrambled siRNA-treated samples that were reduced in the *AURKB*-depleted samples at both dilutions and, therefore, assumed to be specific to *AURKB*. At 1:200 dilution, a more significant differential in staining was seen between the scrambled and *AURKB* siRNA-treated conditions, suggesting this was a more suitable dilution.

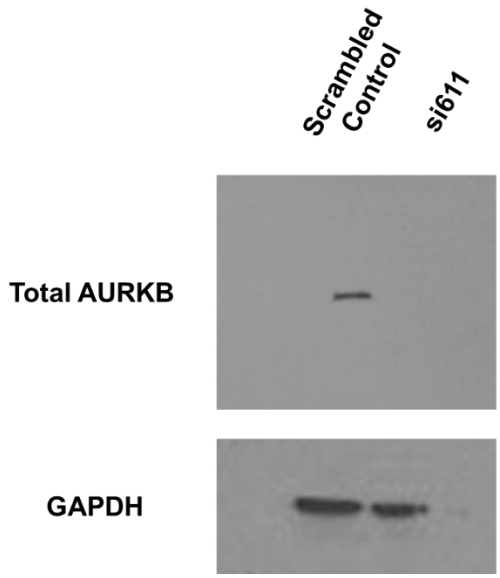


Figure 5-23 Western blot of total *AURKB* antibody using H460 cell pellets with GAPDH as the loading control. Cell extracts were *mad*e, and the western blot was done using the RIPA method.

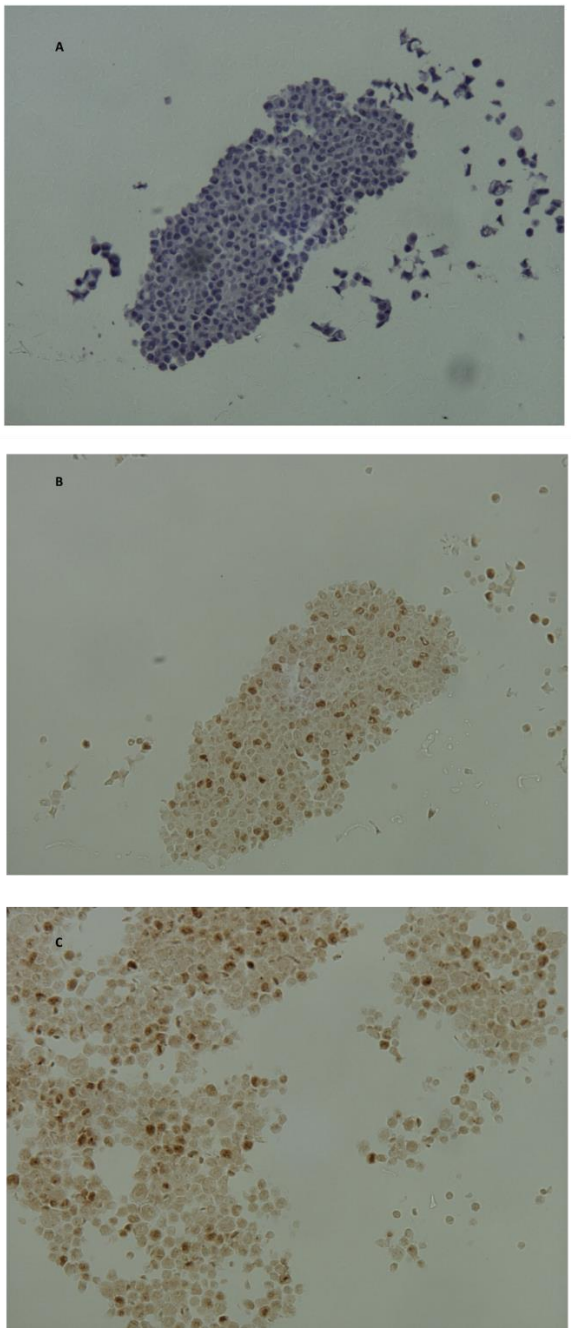


Figure 5-24 ***Representative images of (1:100) staining in Scrambled Control H460 Cell Pellets and a Negative Control A-C,*** *respectively. Negative control of the H460 cell pellet, B. staining using 1:100 concentration in the Scrambled control cell pellet, C staining using 1:100 concentration in the si611 cell pellet. Standard comparative protocol using labelled 1:100 used microwave retrieval (high settings) with IMMPRESS® signal detection system and pH 6.1 citrate target retrieval solution. Antibody signal on stained cells was developed with DAB for 1 minute, and cells were counterstained with Gill's hematoxylin for 10 seconds (N=1). Scale bars represent 50 to 200 µm. All slides were scanned using an Optika light microscope using a 20x objective.*

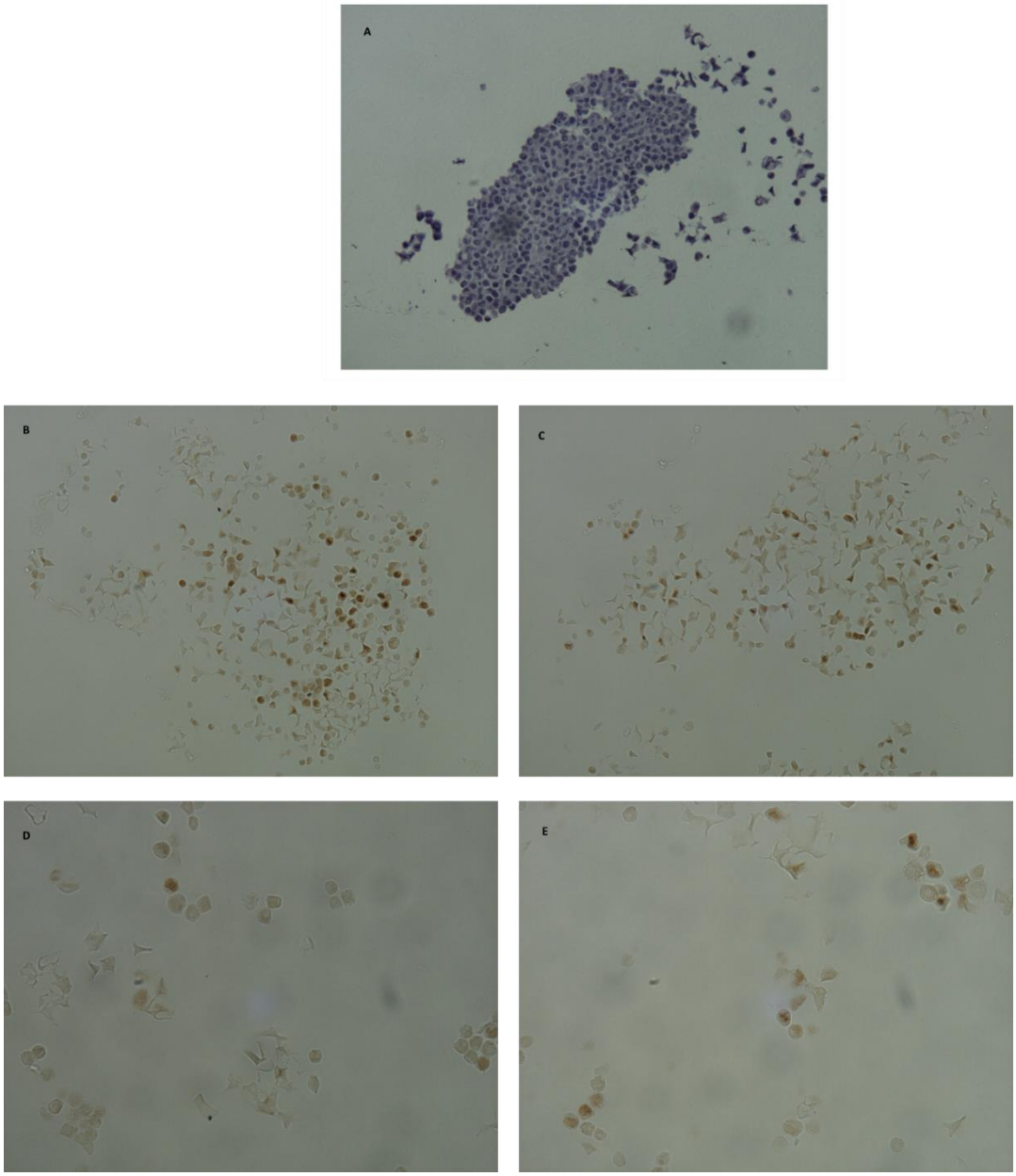


Figure 5-25 ***Representative images of (1:200) staining in Scrambled Control H460 Cell Pellets and a Negative control A-C,*** *respectively. A. Negative control of the H460 cell pellet, B-C staining using 1:200 concentration in the Scrambled control cell pellet D-E staining using 1:200 concentration in the si611 cell pellet. Standard comparative protocol using labelled 1:200 used microwave retrieval (high settings) with IMMPRESS® signal detection system and pH 6.1 citrate target retrieval solution. Antibody signal on stained cells was developed with DAB for 1 minute, and cells were counterstained with Gill's hematoxylin for 10 seconds (N=1). Scale bars represent 50 to 200µm. All slides were scanned using an Optika light microscope using a 20x objective.*

However, concerns over the potential for high background staining of the stroma in the NCSLC tissue prompted the investigation of alternate antigen retrieval methods. Using sodium citrate rather than DAKO buffer pH 6.1 resulted in the loss regardless of the condition scrambled control or *AURKA* siRNA si-611 (Figure 6-19 and 6-20). using steam compared to a microwave resulted in similar differential *AURKB* staining between control and *AURKB*-depleted cells with the added advantage of reducing background staining (Figures 6-21 and 6-22).

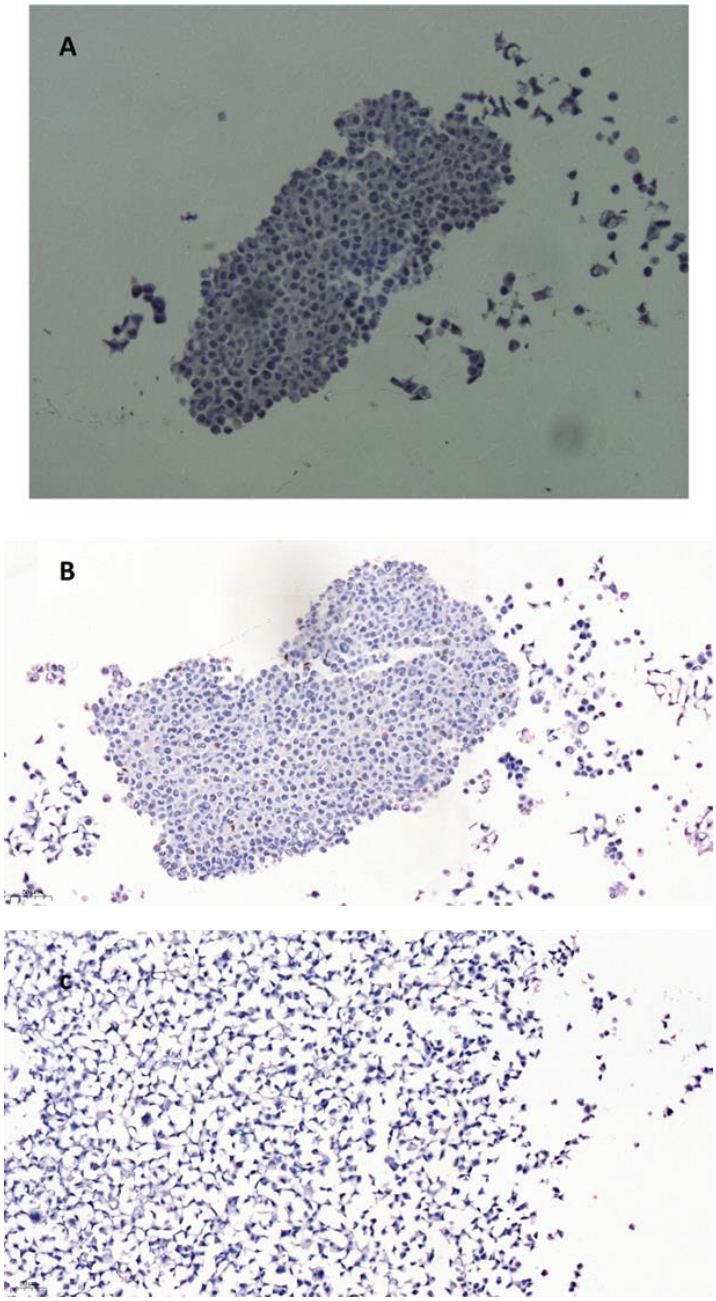


Figure 5-26 ***Representative images of (1:100) staining in Scrambled Control H460 Cell Pellets and a Negative control using Sodium Citrate instead of DAKO A-C,*** *respectively. A. Negative control of the H460 cell pellet, B staining using 1:100 concentration in the Scrambled control cell pellet, C staining using 1:100 concentration in the si611 cell pellet. Standard comparative protocol using labelled 1:100 used steam retrieval with IMMPRESS® signal detection system and sodium citrate target retrieval solution. Antibody signal on stained cells was developed with DAB for 1 minute, and cells were counterstained with Gill's hematoxylin for 10 seconds (N=1). Scale bars represent 50 to 200µm. All slides were scanned using a panoramic 250 slide scanner using a 20x objective.*

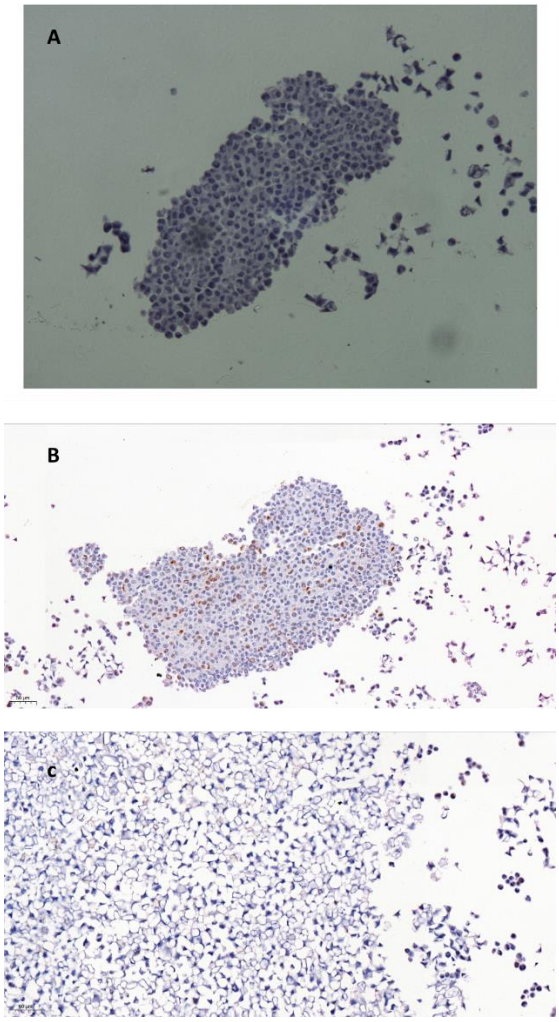


Figure 5-27 ***Representative images of (1:200) staining in Scrambled Control H460 Cell Pellets and a Negative control using Sodium Citrate instead of DAKO A-C,*** *respectively. A. Negative control of the H460 cell pellet, B staining using 1:200 concentration in the Scrambled control cell pellet, C staining using 1:200 concentration in the si611 cell pellet. Standard comparative protocol using labelled 1:200 used steam retrieval with IMMPRESS® signal detection system and sodium citrate target retrieval solution. Antibody signal on stained cells was developed with DAB for 1 minute, and cells were counterstained with Gill's hematoxylin for 10 seconds (N=1). Scale bars represent 50 to 200µm. All slides were scanned using a panoramic 250 slide scanner using a 20x objective.*

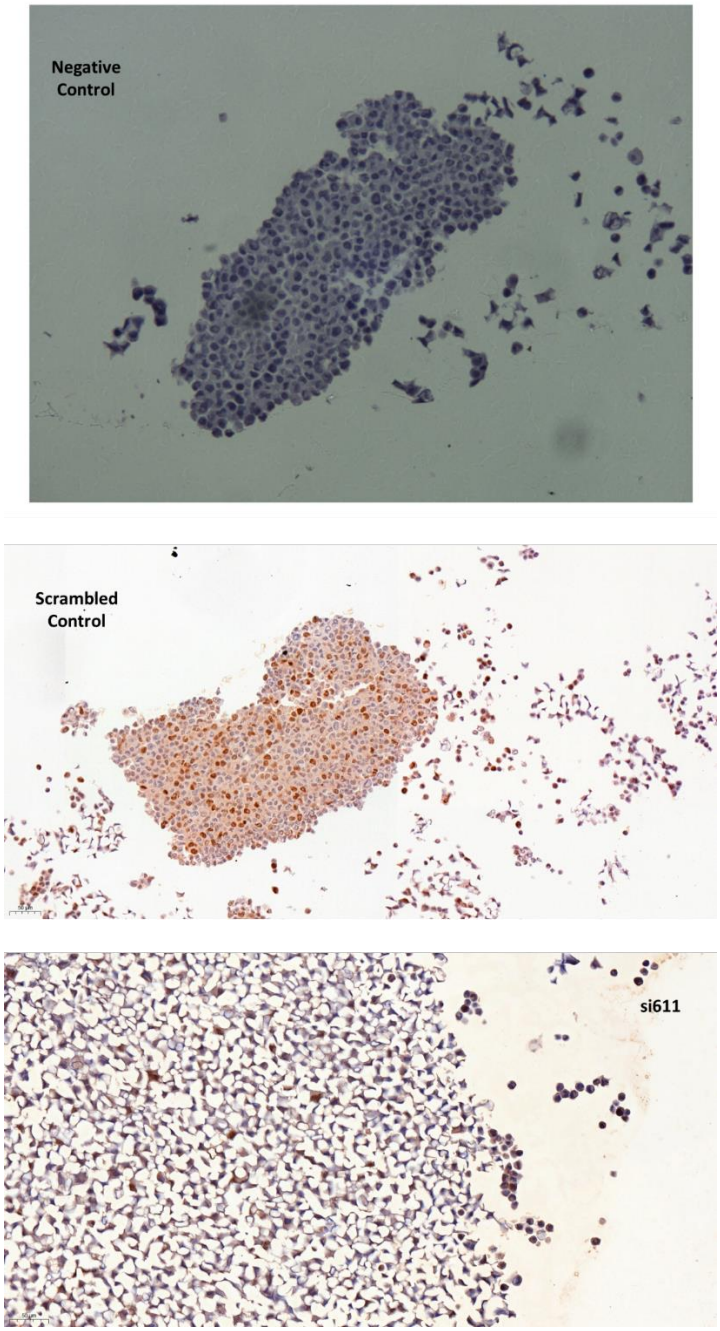


Figure 5-28 ***Representative images of (1:100) staining in Scrambled Control H460 Cell Pellets and a Negative control using steam retrieval and DAKO A-C,*** *respectively. A. Negative control of the H460 cell pellet, B-C staining using 1:100 concentration in the Scrambled control cell pellet D-E staining using 1:100 concentration in the si611 cell pellet. Standard comparative protocol using labelled 1:100 used steam retrieval with IMMPRESS® signal detection system and pH 6.1 citrate target retrieval solution. Antibody signal on stained cells was developed with DAB for 1 minute, and cells were counterstained with Gill's hematoxylin for 10 seconds (N=1). Scale bars represent 50 to 200µm. All slides were scanned using a panoramic 250 slide scanner using a 20x objective.*

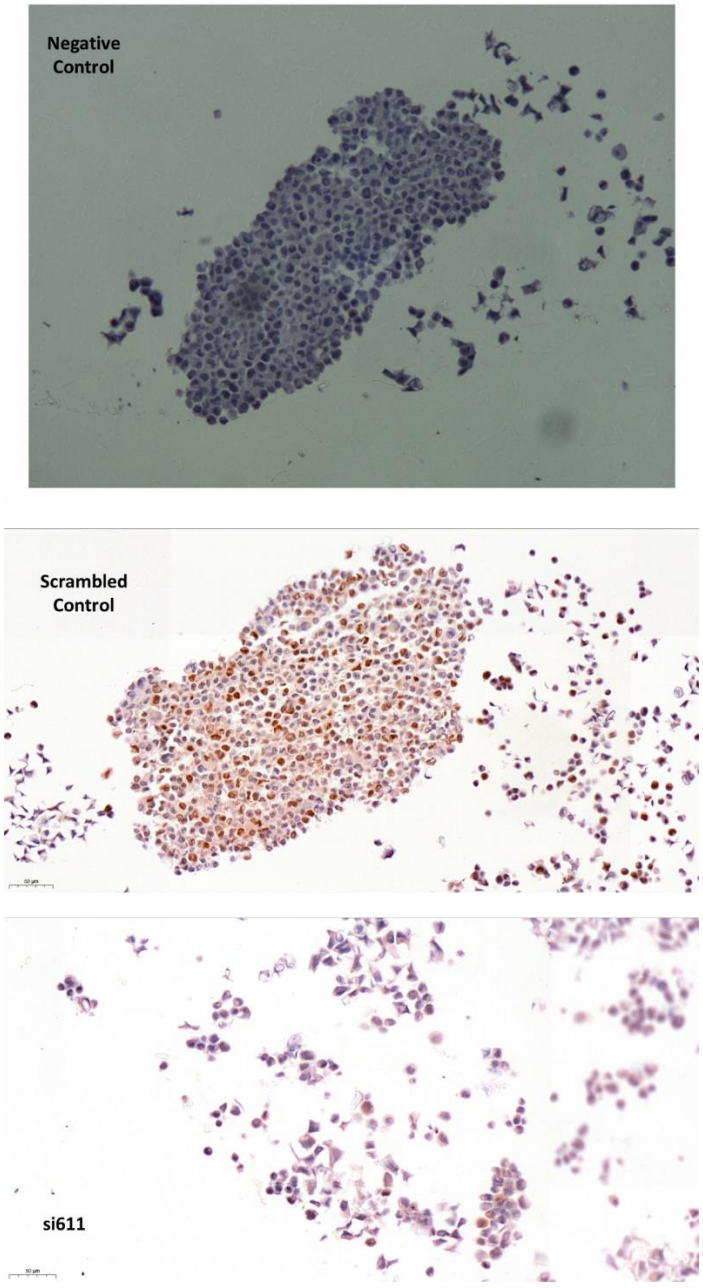


Figure 5-29 ***Representative images of (1:200) staining in Scrambled Control H460 Cell Pellets and a Negative control using steam retrieval and DAKO A-C,*** *respectively. A. Negative control of the H460 cell pellet, B-C staining using 1:200 concentration in the Scrambled control cell pellet D-E staining using 1:100 concentration in the si611 cell pellet. Standard comparative protocol using labelled 1:200 used steam retrieval with IMMPRESS® signal detection system and pH 6.1 citrate target retrieval solution. Antibody signal on stained cells was developed with DAB for 1 minute, and cells were counterstained with Gill's hematoxylin for 10 seconds (N=1). Scale bars represent 50 to 200µm. All slides were scanned using a panoramic 250 slide scanner using a 20x objective.*

This is the optimised protocol used, *AURKB* Abcam antibody (1:200). Antigen retrieval was conducted using hot steam from a rice steamer over 20 mins with the cells submerged in DAKO pH 6.1; the I*MMP*RESS® signal detection system was used. The antibody signal on stained cells was developed with DAB for 1 minute, and cells were counterstained with Gill's haematoxylin for 10 seconds.

5.2.5 *AURKB* did not demonstrate visible staining in lung tissue using LC241m lung microarray cores.

Having optimised *AURKB* staining in H460 cell pellets. We tested the same protocol on commercially available **l**ung cancer with a matched lung tissue **array (LC241m).** Tissues were provided information, including pathology grade, TNM and clinical stage. Six lung cancer cases with matched lung tissue microarrays containing 24 cores were provided on the array (Table 6-3, Figures 6-23 and 6-24). However, none of the cores exhibited significant *AURKB* staining compared to their regular tissue counterparts.

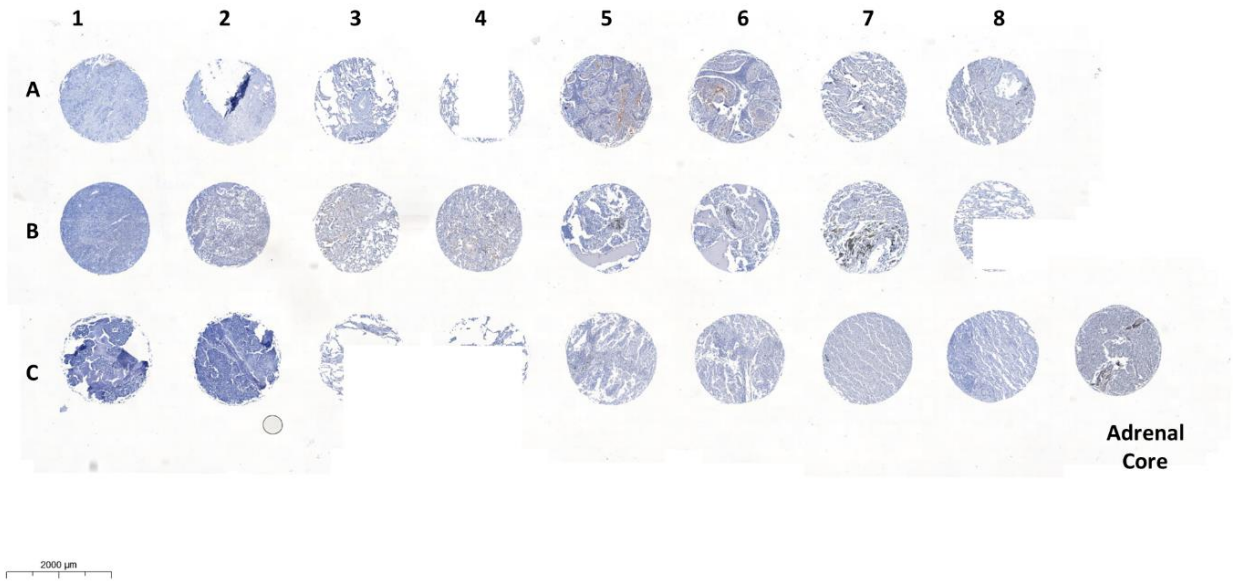
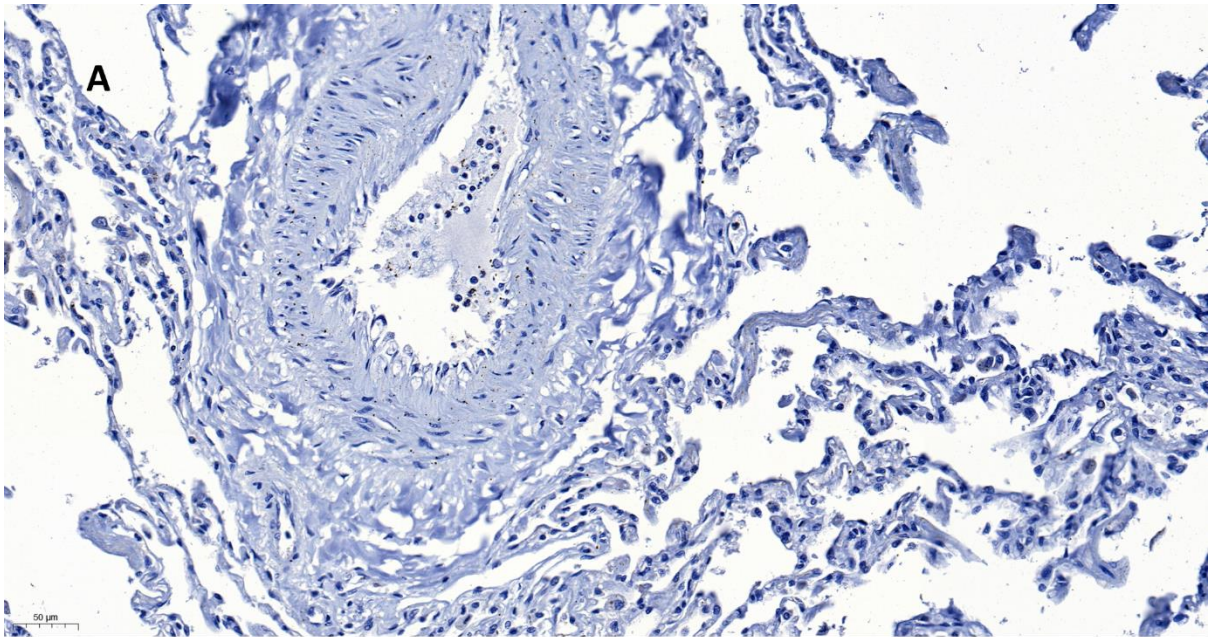


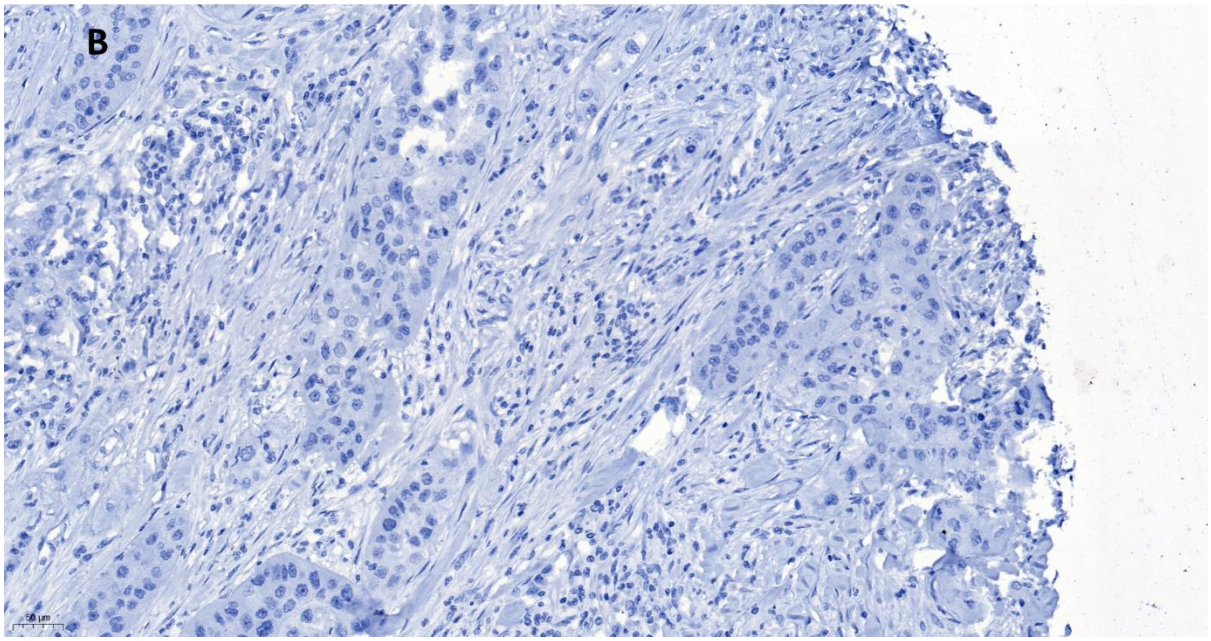
Figure 5-30 ***Representative images of (1:200) staining in*** **Lung cancer with matched lung tissue array (2015 WHO classification), including pathology grade, TNM and clinical stage (AJCC 7th edition), 6 cases/24 cores, replacing LC241l *using steam retrieval and DAKO***. *Standard comparative protocol using labelled 1:200 used steam retrieval with IMMPRESS® signal detection system and pH 6.1 citrate target retrieval solution. Antibody signal on stained cells was developed with DAB for 1 minute, and cells were counterstained with Gill's hematoxylin for 10 seconds (N=1). Scale bars represent 2000 µm. All slides were scanned using a panoramic 250 slide scanner using a 2000x objective.*

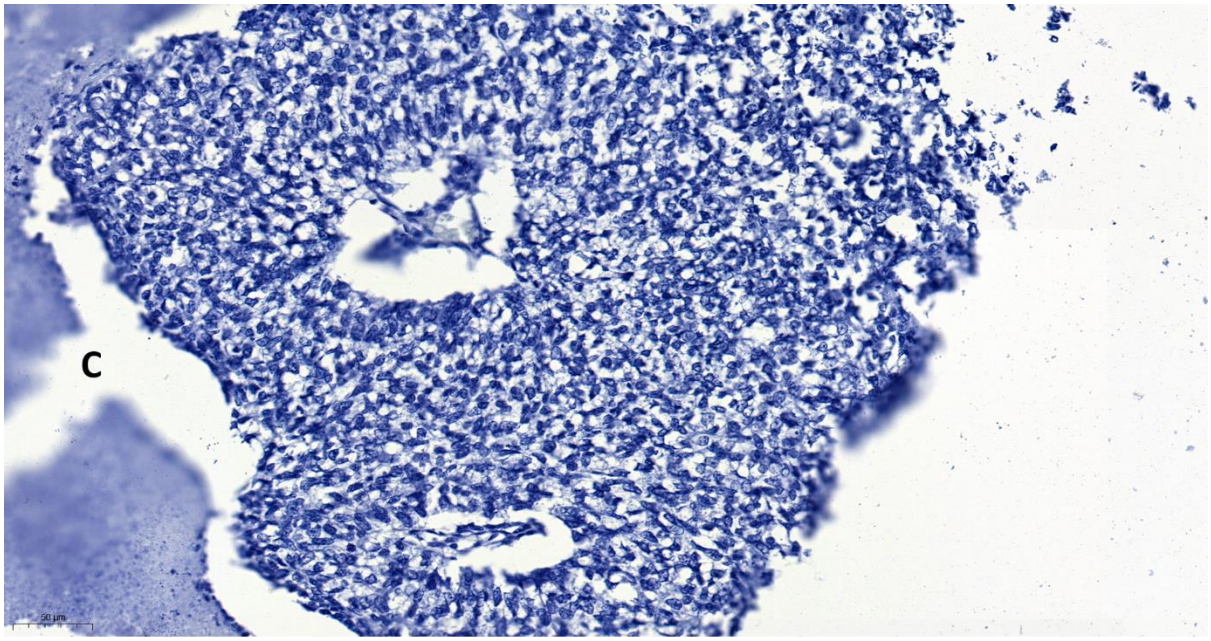
Position on the Grid	No.	Age	Sex	Organ/Anatomic Site	Pathology diagnosis	TNM	Grade	Stage	Type
A1	1	67	M	Lung	Keratinized squamous cell carcinoma	T2aN0M0	2	IB	Malignant
A2	2	67	M	Lung	Keratinized squamous cell carcinoma	T2aN0M0	2	IB	Malignant
A3	3	67	M	Lung	Adjacent normal lung tissue	-	-	-	NAT
A4	4	67	M	Lung	Adjacent normal lung tissue	-	-	-	NAT
A5	5	53	M	Lung	Keratinized squamous cell carcinoma	T2bN1M0	2	IIB	Malignant
A6	6	53	M	Lung	Keratinized squamous cell carcinoma	T2bN1M0	2	IIB	Malignant
A7	7	53	M	Lung	Adjacent normal lung tissue	-	-	-	NAT
A8	8	53	M	Lung	Adjacent normal lung tissue	-	-	-	NAT
B1	9	56	F	Lung	Keratinized squamous cell carcinoma (sparse)	T2bN1M0	3	IIB	Malignant
B2	10	56	F	Lung	Keratinized squamous cell carcinoma	T2bN1M0	3	IIB	Malignant
B3	11	56	F	Lung	Cancer adjacent lung tissue	-	-	-	AT
B4	12	56	F	Lung	Cancer adjacent lung tissue	-	-	-	AT
B5	13	35	F	Lung	Keratinized squamous cell carcinoma	T3N1M0	3	IIIA	Malignant
B6	14	35	F	Lung	Keratinized squamous cell carcinoma	T3N1M0	3	IIIA	Malignant
B7	15	35	F	Lung	Cancer adjacent lung tissue	-	-	-	AT
B8	16	35	F	Lung	Cancer adjacent lung tissue	-	-	-	AT

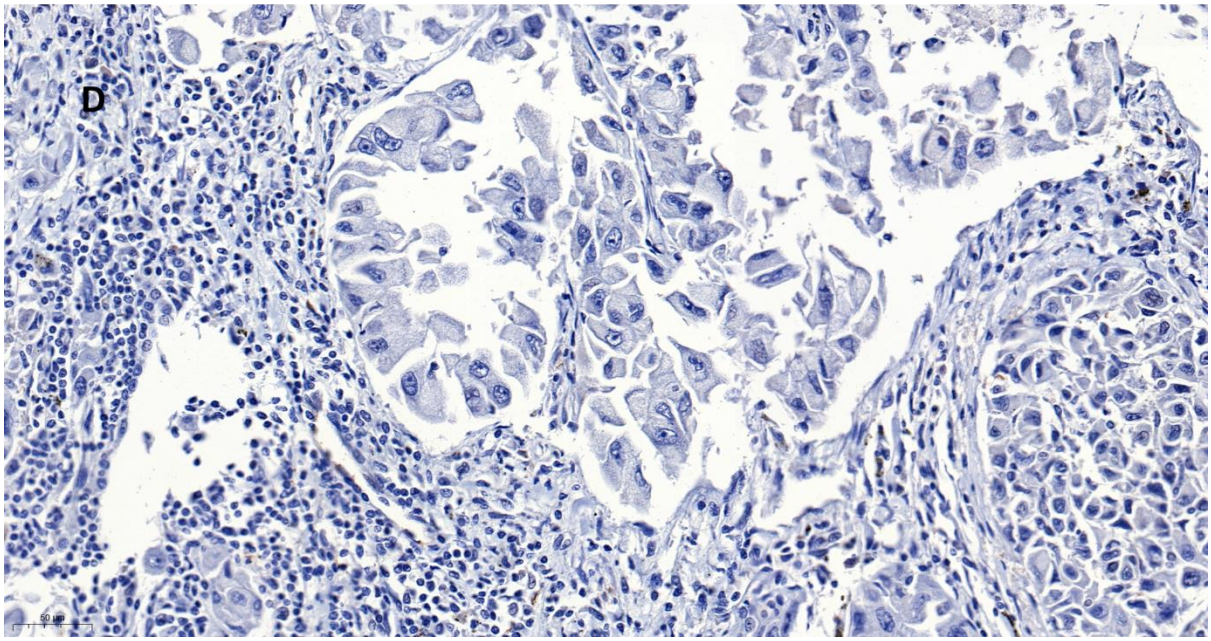
Position on the Grid	No.	Age	Sex	Organ/Anatomic Site	Pathology diagnosis	TNM	Grade	Stage	Type
C1	17	68	M	Lung	Basal squamous cell carcinoma	T1bN1M0	3	IIA	Malignant
C2	18	68	M	Lung	Basal squamous cell carcinoma	T1bN1M0	3	IIA	Malignant
C3	19	68	M	Lung	Adjacent normal lung tissue	-	-	-	NAT
C4	20	68	M	Lung	Adjacent normal lung tissue	-	-	-	NAT
C5	21	65	M	Lung	Acinar adenocarcinoma	T2aN2M0	2	IIIA	Malignant
C6	22	65	M	Lung	Acinar adenocarcinoma	T2aN2M0	2	IIIA	Malignant
C7	23	65	M	Lung	Adjacent normal lung tissue	-	-	-	NAT
C8	24	65	M	Lung	Adjacent normal lung tissue	-	-	-	NAT
-	0	42	M	Adrenal gland	Pheochromocytoma (tissue marker)		-		Malignant

Table 5-12 ***Table of*** **Lung cancer with matched lung tissue array (2015 WHO classification)**, including pathology grade, TNM and clinical stage (AJCC 7th edition), 6 cases/24 cores, replacing LC241l *using steam retrieval and DAKO as shown in Figure 6-21.*


A
50 µm


B
50 µm


C


D

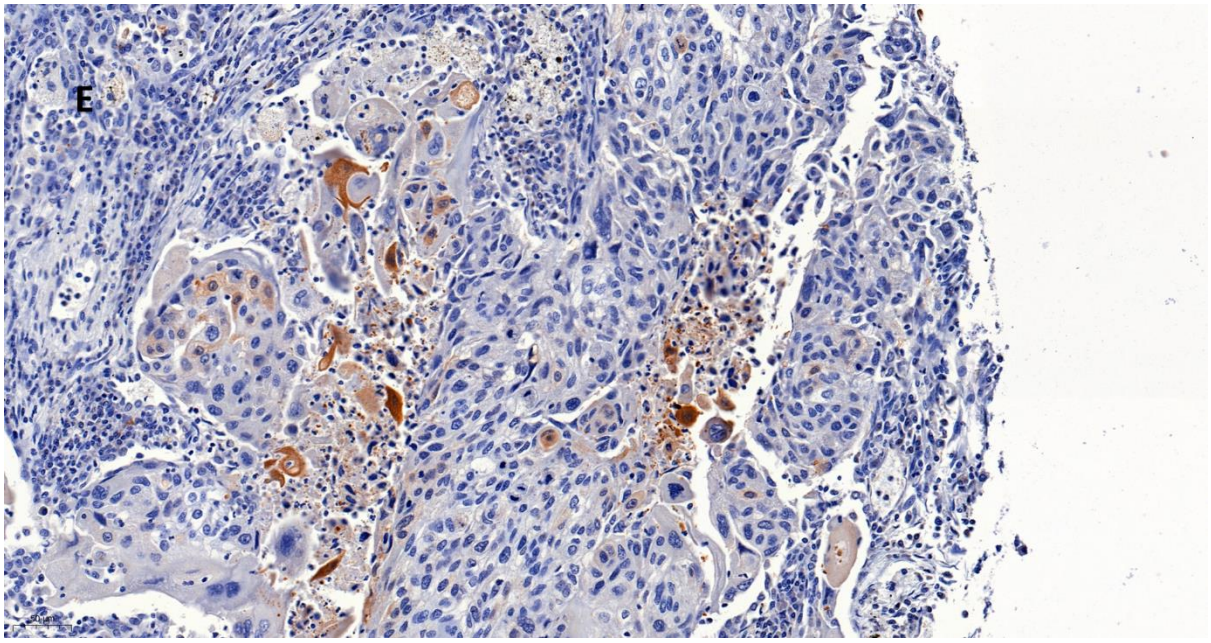


Figure 5-31 ***Representative images of (1:200) staining in selected cores (A-E) from the*** **Lung cancer with matched lung tissue array (2015 WHO classification), including pathology grade, TNM and clinical stage (AJCC 7th edition), 6 cases/24 cores, replacing LC241l *using steam retrieval and DAKO.*** *A represents normal lung tissue, B Keratinized Squamous Cell Cancer, C Basal Squamous Cell Cancer, D Acinar Adenocarcinoma E Slide of Squamous cell core showing early signs of stromal staining but non-specific nuclear cellular staining present in that slide. Standard comparative protocol using labelled 1:200 used steam retrieval with IMMPRESS® signal detection system and pH 6.1 citrate target retrieval solution. Antibody signal on stained cells was developed with DAB for 1 minute, and cells were counterstained with Gill's hematoxylin for 10 seconds (N=1). Scale bars represent 2000µm. All slides were scanned using a panoramic 250 slide scanner using a 2000x objective.*

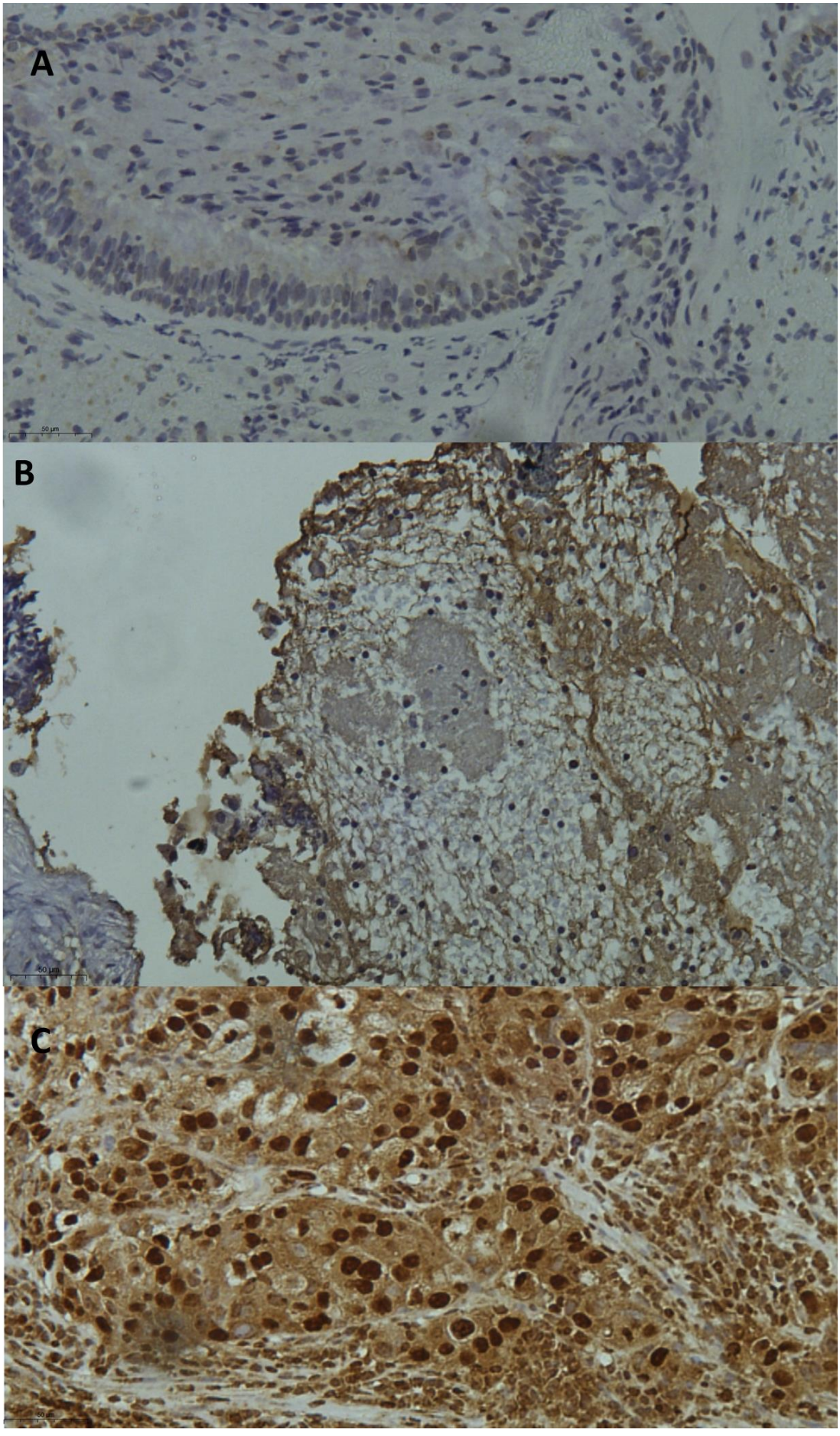
5.2.6 Use of the I*MMP*RESS Excel Amplified Polymer Staining Kit, Anti-Rabbit IgG, increased stromal staining and generally did not improve *AURKB* staining on tissue samples.

As minimal staining was seen in patient tissue using the microarray cores, we used the I*MMP*RESS Excel Amplified Polymer Staining Kit to investigate whether this could improve the sensitivity of the *AURKB* antibody.

Using an enhancement kit did not improve the nuclear staining in patient tissue (Figure 6-25). Most slides displayed weak cy*top*lasmic or inconsistent nuclear staining, making analysis difficult. Only one slide had consistent nuclear staining that was easily readable without heavy stromal background interference (Figure 6-26). Therefore, the enhancement kit resulted in dirty stromal and heavy background staining, ultimately leading to inconsistent results and no improvement over not using the kit.

Slide number	Antibody concentration	Pathologist review
1	1 in 10	Dirty
2	1 in 10	Dirty
3	1 in 10	Dirty
4	1 in 25	Weak
5	1 in 25	Dirty and weak
6	1 in 25	Dirty cyto + nuclear but maybe some
7	1 in 50	Dirty
8	1 in 50	Positve
9	1 in 50	Dirty
10	1 in 100	Weak
11	1 in 100	Weak
12	1 in 100	Cytoplasmic staining
13	1 in 200	Nil
14	1 in 200	Nil
15	1 in 200	Nil
16	1 in 400	Mixed, some nuclei
17	1 in 400	Nil
18	1 in 400	Nil

Table 5-13 ***Results of the optimisation of antibody using the IMMPRESS® Excel Amplified Polymer Staining Kit:*** *Standard comparative protocol using labelled 1:10, 1:25, 1:50, 1:100, 1:400 and 1:200 used microwave retrieval with IMMPRESS® Excel Amplified Polymer Staining Kit and pH 6.1 citrate target retrieval solution. Antibody signal on stained cells was developed with DAB for 3 minutes 30 seconds, and cells were counterstained with Gill's hematoxylin for 10 seconds (N=1).*


A
B
C

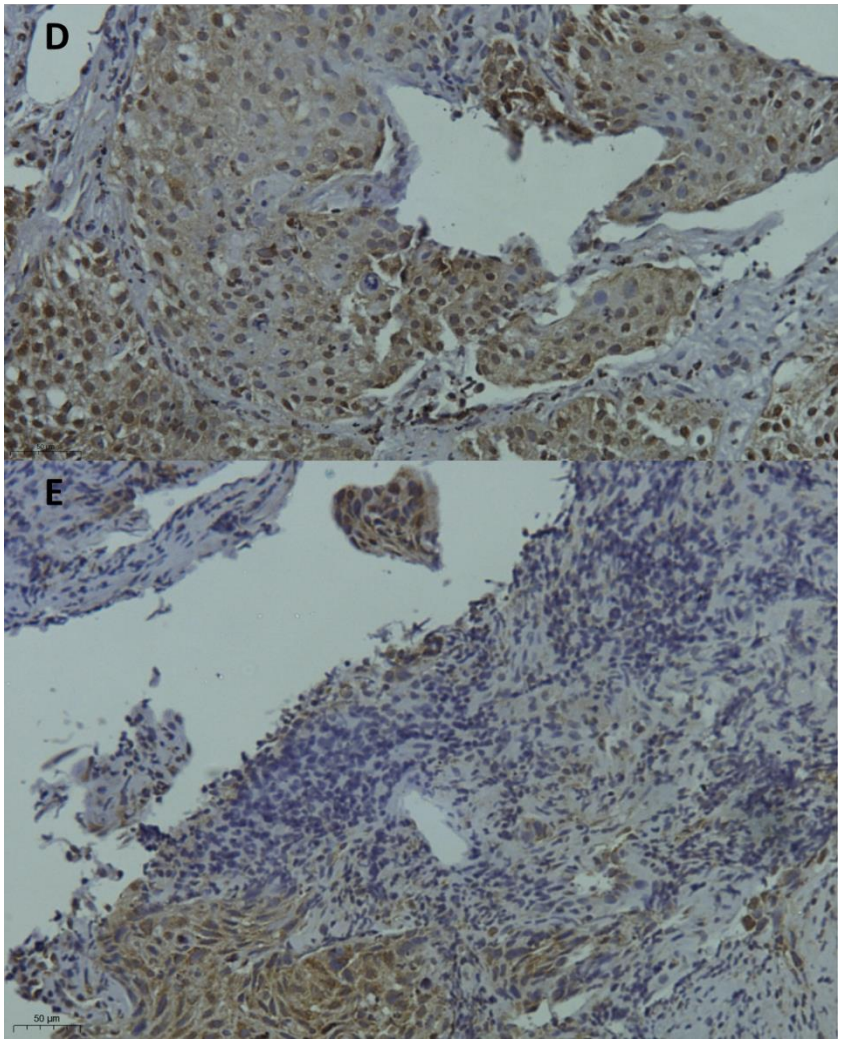


Figure 5-32 ***Results of the optimisation of antibody using the IMMPRESS® Excel Amplified Polymer Staining Kit:*** *Standard comparative protocol using labelled 1:10, 1:25, 1:50, 1:100, 1:400 and 1:200 A. Weak staining of the nuclei with some stromal staining using antibody concentration of 1:200, B. Dirty staining of the stroma with no noticeable nuclear staining using antibody concentration of 1:10, C. Heavy stromal staining with dirty staining of the nuclei using antibody concentration of 1:10, D. Half stained nuclei with moderate to heavy stromal staining using antibody concentration of 1:25, E. Half stained nuclei, dirty nuclear staining and moderate stromal staining using antibody concentration of 1:50. used microwave retrieval with IMMPRESS® Excel Amplified Polymer Staining Kit and pH 6.1 citrate target retrieval solution. Antibody signal on stained cells was developed with DAB for 3 minutes 30 seconds, and cells were counterstained with Gill's hematoxylin for 10 seconds (N=1).*

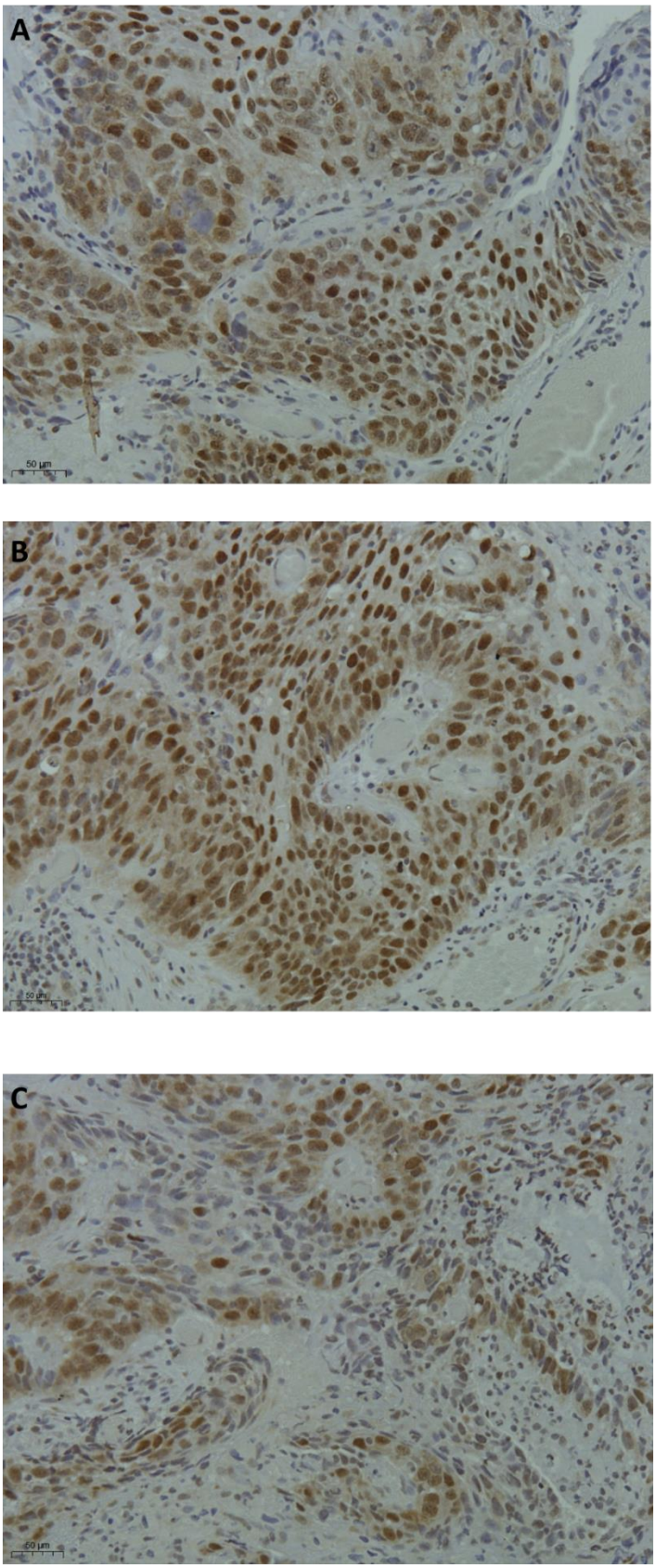


Figure 5-33 *Antibody signal on stained cells was developed with DAB for 1 minute, and cells were counterstained with Gill's hematoxylin for 10 seconds (N=1).*

Thus, further optimisation is needed before we stain the patient tissue collected in the study above. The difference between the cell pellets and the tissue sections is the presence of stroma; therefore, antigen retrieval is the most reasonable step that needs altering. Preliminary testing on some tissue without using the I*MMP*RESS Excel Amplified Polymer Staining Kit confirmed this suspicion (Figure 6-26).

5.3 Discussion

Multiple studies have identified *AURKA* and *AURKB* as hub genes in NSCLC (Gao et al., 2020; Selvaraj et al., 2018) and *AURKA* as a hub gene in oropharyngeal (Xu et al., 2022; Yang et al., 2021), laryngeal, and nasopharyngeal tissue.

We performed bioinformatic analyses on existing data sets to investigate the expression of *AURKA* and *AURKB* in NSCLC and H&N patients. Our work demonstrated that *AURKA* and *AURKB* had increased differential expression in tumour vs. normal tissue in three of five NSCLC datasets. *AURKA* and *AURKB* were determined to be hub genes in NSCLC; however, their expression had no greater prognostic value than any of the other hub genes in the dataset.

In Head and Neck Cancer, *AURKA* but not *AURKB* was differentially expressed in oropharyngeal tumours compared to normal, while neither *AURKA* nor *AURKB* was differentially expressed in nasopharyngeal datasets. Neither *AURKA* nor *AURKB* was a hub gene in oropharyngeal or nasopharyngeal cancer.

In our study, *AURKB* was not shown to be a potential hub gene in either oropharyngeal or nasopharyngeal tissues in keeping with published literature.

The approach was to use only the [HG-U133_Plus_2] Affymetrix Human Genome U133 Plus 2.0 arrays; our approach differed from most studies, for example, *Chen and Liu* where they aimed to get as many patients as possible, therefore not limiting themselves to one singular platform. Using the bioinformatic pathway, we developed led to small sample sizes due to the strict inclusion and cut-off criteria; this could have increased the false negative rate and thus excluded our desired genes. We feel

the relative lack of patient samples in the nasopharyngeal datasets could have led to the findings of Neither *AURKA* nor *AURKB* being differentially expressed nor a hub gene.

5.3.1 Pros and Cons of different data sources.

Gene Expression Omnibus (GEO)

GEO, a repository for a wide range of gene expression datasets, encompasses a broad spectrum of biological research. Researchers can access data from various organisms and experimental conditions, making it a valuable resource for diverse research interests. However, the data quality and annotation in GEO can vary widely, which may require additional effort to curate and analyse effectively**.**

GEO is not limited to human data; it includes information from many species of interest. Researchers can access data from a wide range of studies, including those related to developmental biology, disease research, pharmacology, and more. This breadth makes GEO a valuable resource for scientists with diverse research interests and allows for cross-disciplinary exploration. The data hosted on GEO come from a wide range of sources, and the quality of the data can differ significantly. Some datasets may be meticulously curated with detailed annotations, while others may lack essential metadata or quality control. This variability can make it challenging for researchers to identify high-quality datasets for their analyses. Researchers using GEO often need to invest additional effort in data curation and pre-processing. Such tasks can be time-consuming and require expertise in data analysis and bioinformatics.

The Cancer Genome Atlas (TCGA)

The Cancer Genome Atlas (TCGA) is a resource that provides extensive genomic and clinical data across multiple cancer types. Its major advantage is the depth and breadth of the data it offers. TCGA encompasses various types of genomic information, including DNA sequencing, RNA sequencing, DNA methylation, and more, along with corresponding clinical data such as patient demographics, treatment history, and survival outcomes.

However, one limitation of TCGA is its primary focus on cancer research. While this focus is essential for advancing our understanding of cancer and developing targeted therapies, it does limit its applicability to other research areas. Researchers studying non-cancer-related biology or diseases may find TCGA less useful because the majority of the data available is specific to cancer.

Gene Expression Barcode (*GEB*)

GEB, on the other hand, is a specialised resource for barcode-based gene expression analysis. It offers a straightforward approach to gene expression profiling, focusing on simplicity and cost-efficiency. This can be advantageous for small-scale experiments or studies with limited resources. Nevertheless, *GEB* may lack the depth and complexity of data provided by TCGA or GEO.

It employs barcode-based methods to measure gene expression levels, which can be less expensive and less complex compared to some other gene expression profiling methods, such as RNA sequencing. This simplicity can be particularly

advantageous for researchers working with limited resources or those conducting small-scale experiments. It allows for the rapid generation of gene expression data without the need for extensive sample preparation or specialised equipment.

While *GEB* is efficient and cost-effective, it may not provide the same level of depth and complexity as other methods like RNA sequencing. Barcode-based approaches may capture a subset of gene expression information, potentially missing nuances and alternative splicing events that can be important in some research contexts.

GEB's specialisation means it is most useful for projects requiring barcode-based gene expression analysis. Researchers with broader research questions or those interested in investigating other aspects of genomics (e.g., DNA sequencing, epigenetics) may find *GEB* less versatile compared to more comprehensive resources like TCGA or Gene Expression Omnibus (GEO).

5.3.2 Differential gene expression and Biomarker activity.

Differential gene expression refers to the differences in gene expression levels between different conditions or groups, such as healthy versus diseased individuals or treated versus untreated samples. It involves measuring the expression of genes across the genome and identifying genes that are differentially expressed in one condition compared to another (Liang and Pardee, 2003).

Biomarkers, conversely, are measurable indicators that can be used to assess various biological processes or conditions. They can be molecules, such as RNA, proteins, metabolites, or even genetic variations. Biomarkers often diagnose

diseases, monitor disease progression, evaluate treatment responses, or predict patient outcomes.

The relationship between differential gene expression and biomarkers lies in the fact that differential gene expression analysis can help identify potential mRNA biomarkers. Researchers can identify significantly upregulated or downregulated genes in a particular condition by comparing gene expression profiles between different groups. These differentially expressed genes are candidates that can be further investigated to determine if they have diagnostic, prognostic, or therapeutic value as biomarkers.

Once potential biomarkers are identified through differential gene expression analysis, further validation and characterisation are required to establish their utility as biomarkers. This may involve using protein expression analysis or clinical validation studies to determine if the identified biomarkers are consistently associated with the condition of interest and exhibit the necessary sensitivity and specificity to be helpful in a clinical setting (Han et al., 2018).

5.3.3 The difference between differential expression and a hub gene.

Hub genes have many connections or interactions with other genes in the network, indicating their importance in coordinating gene expression and regulating biological processes. While differential gene expression analysis can provide valuable

information about individual genes that are differentially expressed in a specific condition, it does not directly determine the hub status of a gene in a co-expression network.

Analysing the functional annotations associated with hub genes provides valuable insights into the dysregulated biological processes within tumours. This analysis aids in identifying specific cellular functions, signalling pathways, or altered biological networks implicated in tumour cells, leading to an enhanced comprehension of tumour biology.

Differential expression analysis can identify candidate genes for further investigation, including their potential role as hub genes within a co-expression network. Integrating both approaches can provide a more comprehensive understanding of gene regulatory networks and their association with biological states or diseases (Ding, K, 2015).

Gene co-expression networks are constructed by analysing gene expression data across multiple samples or conditions to identify genes that exhibit similar expression patterns. These networks provide insights into the relationships and interactions between genes, allowing researchers to uncover modules or clusters of genes that work together in specific biological processes (Saelens et al., 2018).

Hub genes within a co-expression network have high connectivity or interaction with other genes. They serve as central regulators or coordinators of gene expression within the network. Hub genes often occupy critical positions in the network, linking multiple genes or modules together and influencing the overall behaviour of the network; in our work, degree centrality was used to identify the potential hub genes (Wang et al., 2015).

Degree centrality measures the number of connections (edges) a node (gene) has in a network. Degree centrality can be calculated for all nodes in the network, and those with the highest degree of centrality are typically identified as hub genes. These hub genes are potential targets for further investigation as they may be dysregulated in cancer or play essential roles in cancer development and progression (Azuaje, 2014).

Characteristics and roles of hub genes in gene co-expression networks:

One of the primary functions of hub genes is their role in regulating the expression of other genes within the network. These genes act as key players, such as transcription factors or signalling molecules that control downstream genes and influence cellular processes. By modulating the activity of target genes, hub genes serve as critical regulators, ensuring proper functioning and coordination of cellular activities.

Regarding diseases and disorders, hub genes within co-expression networks have garnered considerable attention. Changes in the expression or regulation of hub genes can disrupt the network's functioning and contribute to disease progression (Wang et al., 2019; Z. Zhou et al., 2018).

Their strong associations with disease-related processes make hub genes valuable candidates for further investigation as potential biomarkers for disease diagnosis, prognosis, and treatment response (L. Zhang et al., 2019).

Role of *AURKA* and *AURKB* as hub genes in various studies

AURKA is overexpressed in various cancer types and is strongly associated with poor prognosis (Marampon et al., 2014). *AURKB*, a key regulator of malignant mitosis involved in chromosome segregation and cytokinesis, has been associated with bladder cancer development. (Bufo et al. 2010). Aurora kinase B (*AURKB*) and ubiquitin-conjugating enzyme E2 C (*UBE*2C) have been implicated in the tumorigenesis of gliomas and various malignancies, with their elevated expression strongly linked to poor prognosis and therapy resistance in glioma (Alafate et al. 2019). Interactions between aurora kinase A (*AURKA*) and *AURKB* stabilise and protect *AURKA*/B from degradation, with *AURKB* closely associated with chemoresistance and radioresistance (Alafate et al. 2019).

AURKA and *AURKB* exhibit high expression levels in tumour-derived mesenchymal stem cells (TMSCs). These highly conserved serine/threonine kinases regulate chromosome alignment and segregation during mitosis and meiosis, as well as the cell cycle and growth.

AURKA overexpression accelerates wound healing and reduces apoptosis in adipose-derived mesenchymal stem cells (AMSCs), while *AURKA* depletion affects pluripotency and elevates *p53* levels, maintaining multipotency by suppressing *p53*-driven differentiation.

5.3.4 Prospective Patient Study.

The study design was a prospective study looking at 101 patients with NSCLC treated with radiotherapy correlating their survival with *AURKA* expression in their biopsy samples.

Despite a considerable amount of research being done in radiotherapy, there are no known radiotherapy biomarkers at the time of writing. A biomarker is any measurable characteristic or molecular feature that provides information about a biological process, disease state, or treatment response. Identifying a biomarker through IHC associated with patient survival after treatment in radiotherapy can have important clinical implications. It can help identify patients with a higher or lower likelihood of responding to radiotherapy and predict their overall survival or treatment outcomes.

Even if the biopsy was performed before treatment, the expression level of a specific protein detected through IHC could still be evaluated as a potential biomarker for predicting patient survival after radiotherapy. The rationale is that the expression level of the biomarker detected in the pre-treatment biopsy may provide insights into the biological characteristics of the tumour, which can influence its response to radiotherapy and subsequent patient survival.

Some problems with this approach are that tumours are highly heterogeneous, both inter and intra-patient, in terms of their genetic makeup, molecular profiles, and treatment response. The expression of a single protein detected by IHC may not capture the full complexity of tumour biology and response to radiotherapy. It is crucial to consider the potential influence of tumour heterogeneity on biomarker identification and interpretation. Various factors, such as age, tumour stage, treatment regimen, comorbidities, and genetic variations, can influence patient survival after radiotherapy. The expression levels of biomarkers on pre-treatment biopsies may not necessarily reflect their expression during or after radiotherapy. The dynamic changes in biomarker expression throughout treatment and their impact on patient survival must be considered. Longitudinal studies with multiple time points may be necessary to capture these temporal dynamics. The robustness

and reproducibility of the observed associations between biomarker expression and patient survival must be validated in independent patient cohorts. Replicating the findings across different populations and treatment settings is crucial to establish the clinical utility of the biomarker.

Our work demonstrated that *AURKA* did not correlate with overall nor progression-free survival in our cohort of patient tumour samples. However, very high staining (*TOP* 25 %) significantly reduced survival compared to the lowest expression.

A Meta-analysis of studies looking at *AURKA* expression in tumour tissue demonstrated that increased *AURKA* expression can be associated with increased OS, PFS DFS and cancer-specific survival (CSS) in NSCLC (Zhang et al., 2015). There was a high amount of variation across studies and tumour types, but a high *AURKA* expression level was related to poor prognosis in lung cancer, ovarian cancer, colorectal cancer and nasopharyngeal carcinoma, and pooled HR was not statistically significant in breast cancer (HR, 1.68; 95% CI, 0.73–3.89) and oesophageal cancer (HR, 1.35; 95% CI, 0.64–2.85).

In line with our observations, previous studies by In-Ho Choi (2012) and Lo Iacono et al. (2011) have reported significant increases in *AURKA* expression in squamous cell carcinoma (SCC) compared to adenocarcinoma (ADC) tissue. However, contrary to our findings, a study by Ogawa et al. (2008) demonstrated higher *AURKA* expression in SCC tissue compared to ADC and correlated it with a poor prognosis. The clinical implications of elevated *AURKA* expression in SCC remain unclear due to conflicting information regarding its expression in different tumour types (SCC vs

ADC) and its correlation with tumour behaviour, overall survival, and progression-free survival.

For instance, Tanaka et al. (2005) argue that high *AURKA* expression in oesophageal cancer leads to increased tumour aggressiveness and a poor prognosis, while Zhang et al. (2015) showed no correlation between *AURKA* expression in oesophageal cancer and survival in a meta-analysis. This inconsistency is a common finding when analysing clinical study data on *AURKA* staining in various tumour types, indicating that further research is necessary before drawing definitive conclusions on the clinical significance of *AURKA* expression in SCC based on staining results.

IHC *AURKB* is overexpressed in hepatocellular and bladder cancers compared to normal tissue. We showed that the *AURKB* antibody is specific to *AURKB* in the lung cancer cell line H460 using IHC, but further work is needed to improve antigen retrieval in patient tissue before analysis can be carried out. The presence of normal tissue stroma is likely limiting antigen retrieval. Using steam instead of boiling in the microwave may reduce high background staining, allowing us to use a lower antibody dilution. However, increasing the time the tissue is exposed to the steam or possibly using a lower setting on the microwave for a more extended period could improve antigen retrieval. Once optimisation is done, further work will be done staining the patient slides to test the correlation between the resulting H-scores, OS and PFS.

We could not translate the differential staining in the cell pellets to NSCLC tissue, possibly due to prolonged fixation in the patient samples. While cell pellets are a commonly used method of optimising the staining protocol due to the unlimited

amount of slides that can be *mad*e, it does not match the lung tissue architecture, leading to differences in staining (Gedda et al., 2010).

5.4 Future Work

5.4.1 Strengthening the Case for *AURKA* and *AURKB* as Biomarkers

While *AURKA* and *AURKB* show promise as biomarkers in NSCLC and HNSCC, more work is needed to confirm their reliability. We need validation studies with larger, more homogenous datasets, especially in prospective clinical settings, to clarify their roles. Understanding how these genes contribute to tumour progression could further solidify their importance in cancer biology.

5.4.2 Exploring Other Key Genes

Beyond *AURKA* and *AURKB*, other genes like *CD276*, *TPX2*, and *CDKN2A* have emerged as significant hub genes in NSCLC and HNSCC. These genes could be explored further, not only as potential therapeutic targets but also for their role in patient stratification, especially given their strong link to survival outcomes.

5.4.3 Personalized Biomarker Strategies for Different Cancers

The variation in *AURKA* and *AURKB* expression between NSCLC subtypes (like adenocarcinoma and squamous cell carcinoma) and their absence in nasopharyngeal carcinomas highlights the need for cancer-specific biomarker strategies. Future research should dive deeper into the tissue-specific mechanisms

driving gene expression and explore how these markers can be combined with others to create more personalized diagnostic and treatment approaches.

5.4.4 Addressing Technical Hurdles and Improving Data Integration

Differences in dataset quality and platform technology can lead to inconsistent bioinformatic results. Future work should focus on refining data integration methods and standardizing bioinformatic pipelines to ensure more reliable gene expression analysis. Utilizing next-generation sequencing (NGS) alongside traditional microarray datasets could also strengthen the validity of these findings.

5.4.5 Understanding the Functional Role of Key Genes

To truly understand how *AURKA* and *AURKB* influence cancer progression, metastasis, and treatment resistance we would need to do functional studies. Experiments involving gene knockdowns, overexpression, and investigations into the signalling pathways and how they regulate in different cancers could shed light on their role in tumour biology and the relationship with Aurora Kinases.

5.4.6 Finding Stronger Biomarkers

The lack of a strong correlation between *AURKA* expression and survival in the general NSCLC cohort signals an urgent need for more reliable biomarkers. Identifying these biomarkers is crucial for better patient stratification, allowing more personalized treatments. Future research should also look at other Aurora kinase

family members *AURKC* and explore alternative molecular pathways in lung cancer progression to discover new, robust prognostic and predictive markers.

5.4.7 Overcoming Challenges in Immunohistochemistry (IHC)

This study highlights the technical challenges in immunohistochemistry (IHC), particularly the variability in staining intensity and background interference, which can affect the reliability of *AURKA* and *AURKB* as biomarkers. Future efforts should focus on optimizing antigen retrieval methods for *AURKA* and *AURKB*.

5.4.8 Personalized Treatments for NSCLC Subtypes

The promising results seen in adenocarcinoma patients suggest that *AURKA* could be a valuable therapeutic target for this NSCLC subtype. Future research should validate these findings in larger cohorts and investigate the efficacy of *AURKA* inhibitors like alisertib. On the other hand, *AURKB's* limited presence in NSCLC tissues suggests it may not be a viable treatment target for lung cancer, although its role in other cancers should still be explored.

5.4.9 Refining IHC Protocols

To reliably detect *AURKA* and *AURKB* in clinical samples, further optimization of IHC protocols is required. This involves testing alternative staining kits, retrieval solutions, and antibody concentrations to improve specificity and sensitivity. Additionally, validating these findings in larger, independent cohorts will be crucial to confirming their clinical value and integrating them into diagnostic workflows.

5.4.10 Targeting *AURKA* in Therapy

AURKA plays a key role in cancer progression, particularly in mitotic entry and spindle assembly (Nikonova et al., 2013). Its overexpression in adenocarcinoma supports further exploration of *AURKA*-targeted therapies, like alisertib, in future NSCLC clinical trials. Understanding *AURKA's* role in cancer stem cell regulation and chemotherapy resistance could also open up new treatment strategies and improve outcomes for adenocarcinoma patients.

5.5 Conclusion

This chapter presents a bioinformatic analysis of *AURKA* and *AURKB* in NSCLC and HNSCC, highlighting their differential expression and involvement in cancer biology. While both genes emerged as potential biomarkers in specific NSCLC subtypes, their prognostic significance did not surpass that of other hub genes identified in the PPI network. *AURKA* demonstrated some utility as a biomarker in HNSCC, though its expression was inconsistent across datasets. The findings emphasize the complexity of using *AURKA* and *AURKB* as universal biomarkers, underscoring the need for further validation and functional studies to clarify their roles in cancer progression and patient outcomes. Additionally, the identification of other key hub genes warrants exploration as potential therapeutic targets, particularly in personalized treatment strategies for NSCLC and HNSCC.

We explored the expression of *AURKA* and *AURKB* in a cohort of NSCLC patients and highlighted the challenges in correlating these markers with clinical outcomes. While *AURKA* showed significant expression differences between adenocarcinoma and squamous cell carcinoma, it did not correlate with overall survival or progression-free survival across the entire patient population. However, subgroup analyses revealed potential significance in adenocarcinoma patients, suggesting a need for further investigation. The difficulties encountered with IHC staining, particularly with inconsistent results and background staining, underscore the importance of further technical optimisations. Despite the current limitations, this study lays the groundwork for future research into the prognostic and therapeutic relevance of *AURKA* in specific NSCLC subtypes, while also calling attention to the need for better biomarkers and more refined laboratory techniques in lung cancer research.

6 Discussion

This research provided novel insights into the cellular consequences of Aurora Kinase B (*AURKB*) inhibition by Barasertib in both non-small cell lung cancer (NSCLC) and head and neck squamous cell carcinoma (HNSCC) cell lines. The experiments presented compelling evidence that Barasertib effectively induced mitotic slippage and prolonged mitotic arrest, both of which are mechanisms thought to contribute to its anti-proliferative effects. This finding was consistent across NSCLC cell lines such as A549 and H520, as well as in HNSCC cell lines like UPCI-SCC72 and SCC89. The response to Barasertib, however, was heterogeneous across different cell lines, with variations in sensitivity, slippage, and cell death outcomes.

One of the most striking observations was the increased levels of mitotic slippage observed in the UPCI-SCC72 and SCC89 cell lines after treatment with Barasertib. This suggests a direct impact of *AURKB* inhibition on the fidelity of mitotic processes in these cancer types. Interestingly, although mitotic slippage increased, this phenomenon did not entirely account for the significant decrease in cell survival noted in clonogenic assays. This discrepancy suggests that while mitotic slippage is an important contributor to cell fate, other mechanisms, such as direct induction of apoptosis or necrosis, may play roles in Barasertib's anti-cancer effects.

6.1 Mitotic Slippage and Cellular Outcomes

Mitotic slippage, a key feature observed in this study, appears to play a central role in the cellular response to Barasertib treatment (Marxer et al., 2014). Slippage results from a failure to properly execute cell division due to prolonged mitotic arrest and misregulation of mitotic checkpoints (Lok et al., 2020). Cells escape mitosis without proper chromosome segregation, leading to aneuploidy, genomic instability, and eventually, cell death (Wurzenberger et al., 2012).

However, the cellular fate post-slippage varied depending on the cancer cell line and dose of Barasertib. In UPCI-SCC72 and SCC89 cells, slippage was frequently followed by cell death in mitosis, likely due to the accumulation of fatal genomic errors during the aberrant exit from mitosis (Cheng and Crasta, 2017). This suggests that in highly sensitive cell lines, Barasertib effectively drives cell death by pushing cells into an unsustainable state of genomic instability. This hypothesis aligns with findings from long-term live cell imaging over 72 hours, which demonstrated that even after multiple rounds of slippage, most cells eventually succumb to mitotic catastrophe or apoptosis.

Interestingly, in less sensitive cell lines such as BICR22 and FNB6, slippage was not as frequently followed by immediate cell death, indicating a possible resistance mechanism in which cells can tolerate the genomic abnormalities induced by slippage. Further investigation into the molecular players involved in this resistance

is warranted to explore potential combination therapies that might enhance Barasertib's efficacy in resistant cell lines.

6.2 Radiosensitisation Potential and Clinical Implications

A key translational aspect of this research is the exploration of Barasertib as a radiosensitizer in NSCLC and HNSCC. Radiosensitisation has been a major focus in overcoming resistance to conventional radiotherapy, especially in aggressive cancer subtypes. The results from this study demonstrated that while Barasertib induced radiosensitisation in NSCLC cells, particularly H460, its effects were variable across other cell lines. Specifically, in HNSCC lines, radiosensitisation was not observed, suggesting that the interplay between *AURKB* inhibition and radiation-induced DNA damage response might be more complex than initially thought.

These findings imply that the radiosensitising effects of Barasertib may depend on specific cellular contexts, such as *p53* status and the intrinsic DNA repair capacities of the cells. Further investigation into these mechanisms could help identify biomarkers predictive of radiosensitisation, allowing for more targeted therapeutic strategies. Additionally, future work should focus on optimizing the timing and dose of Barasertib when combined with radiotherapy, as the full potential of this combination may not have been realized in our experiments.

6.3 Mechanisms of Resistance and Future Directions

The resistance observed in certain cell lines, particularly BICR22 and FNB6, poses a significant challenge to the therapeutic potential of *AURKB* inhibition. The lack of effect on cell survival, mitotic duration, and cell death in these lines suggests that additional resistance mechanisms are at play. One hypothesis is that these cells may engage alternative pathways that bypass the need for *AURKB* during mitosis. Identifying these compensatory mechanisms will be important for developing combination therapies that could sensitize resistant cells/tumors to Barasertib.

Future research should focus on unraveling the molecular pathways which lead to this resistance. Proteomics, and functional assays could be employed to identify novel drug targets that, when inhibited, could possibly overcome resistance. Additionally, extending live cell imaging beyond the currently used 72-hour window we used may reveal longer-term cellular outcomes that could inform treatment schedules and improve therapeutic efficacy.

6.4 Conclusion

In conclusion, this research has shed light on the cellular mechanisms underlying *AURKB* inhibition by Barasertib in NSCLC and HNSCC cell lines. The study highlights Barasertib's ability to induce mitotic slippage and prolonged mitotic arrest, which are critical contributors to its anti-proliferative effects (Yamauchi et al., 2013). However, the varied response across different cell lines suggests that additional factors, such as genomic instability and direct apoptosis, may influence Barasertib's efficacy. The findings also reveal the potential of Barasertib as a radiosensitizer, although its effects are context-dependent, particularly in relation to cellular DNA repair mechanisms and p53 status. The resistance observed in certain cell lines points to the need for further investigation into alternative pathways that may confer survival advantages. Future studies focused on the molecular mechanisms of resistance and optimizing combination therapies will be crucial to enhancing the clinical potential of *AURKB* inhibitors like Barasertib.

7 Appendix

7.1 Source code for bioinformatics DGE pathway.

```
# libraries I need

library(affy)
library(GEOquery)
library(EnhancedVolcano)
library(ggplot2)
library(ggrepel)
library(wesanderson)
library(annotate)
library(enrichplot)
library(pheatmap)
library(dplyr)
library(EnhancedVolcano)
library(PCAtools)
library(limma)
library(ggpubr)

# may need in the future

library(oligo)
```

```
# testing if needed

library(BiocManager)
library(clusterProfiler)
library(DOSE)
library(DT)
library(genefilter)
library(hgu133plus2.db)
library(magrittr)
library(meshes)
library(MeSH.Hsa.eg.db)
library(pathview)
library(readr)
library(rWikiPathways)
library(survival)
library(survminer)
library(topGO)
library(vroom)
library(xtable)

# These are affy libraries

library(affyPLM)
library(affycoretools)
library(affyQCReport)
library(arrayQualityMetrics)
```

```
library(simpleaffy)



# 1. may have memory issues, so can check.

memory.size()
memory.limit()
memory.limit(size = 56000)


# Expression data from three datasets using GEO
omnibus

my_id =  "GSE74530"
my_data_1 = getGEO(my_id)

# analysis for my_id----
## Check how many platforms or array chips used

length(my_data_1)

my_data_1 = my_data_1[[1]]

# Gives a detailed description of the number of
samples, the PhenoData, featureData and
annotation
```

```
my_data_1

# Gives a histogram and box plot before normalisation

pData(my_data_1) ## print the sample information.
fData(my_data_1) ## print the gene annotation.
exprs(my_data_1) ## print the expression data.

## exprs get the expression levels as a data frame and get the distribution

summary(exprs(my_data_1))

# The values go beyond 16, so we must perform a log2 transformation and mark this.

# exprs(my_data_1) = log2(exprs(my_data_1))

# boxplot of the distributions should be similar

names(wes_palettes)

boxplot(exprs(my_data_1),outline=FALSE,
```

```
        col = wes_palette("Zissou1", 10, type =
"continuous"))


# This gives a table of the information from the
experiment similar to the GEO2R analysis

sampleInfo = pData(my_data_1)

View(sampleInfo)
write.csv(sampleInfo,"C:\\Users\\New\\Desktop\\Bioi
nformatics\\GSE74530.csv", row.names=FALSE)

## Here is where the analysis begins----
## I will be looking at tumour vs normal tissue in the
patients, so choose those columns

sampleInfo = dplyr::select(sampleInfo,
`source_name_ch1`)

## Optionally, rename to more convenient column
names

sampleInfo = dplyr::rename(sampleInfo,
sample_type = `source_name_ch1`)
```

```
###### use if needed
#sampleInfo <- na.omit(sampleInfo)
#sampleInfo

## argument use="c" stops an error if there are any
missing data points

corMatrix = cor(exprs(my_data_1),use="c")

## Print the row names of the sample informatrix.
and check that it matches the correlation matrix.

rownames(sampleInfo)
colnames(corMatrix)

rownames(sampleInfo) = colnames(corMatrix)

pheatmap(corMatrix,
         annotation_col=sampleInfo)

##########################################################
##########
## MAKE SURE TO TRANSPOSE THE
EXPRESSION MATRIX##----
##########################################################
#########
```

```
pca <- prcomp(t(exprs(my_data_1)))

## Join the PCs for the sample information


cbind(sampleInfo, pca$x) %>% ggplot(aes(x = PC1,
y=PC2, col=sample_type,

label=base::paste("Sample_type", sample_type))) +
  geom_point() + geom_text_repel()


##############################################################
#####
# Export the expression data to a CSV file.# ----
##############################################################
###

full_output =
cbind(fData(my_data_1),exprs(my_data_1))

write.csv(full_output, "Expression
data_GSE74530.csv")
```

```
# The features of the data, for example, gene symbol, etc.

features = fData(my_data_1)

### Look at the features data frame and decide the names of the columns you want to keep

features = dplyr::select(features, `Gene Symbol`, `ENTREZ_GENE_ID`)

full_output = cbind(features,exprs(my_data_1))

write.csv(full_output, "featuresdata_GSE74530.csv")

################################################
###### Differential Expression ###### -----
################################################

# Allocate the samples in our dataset to the sample groups of interest

design = model.matrix(~0+sampleInfo$sample_type)
```

```
dim(design)

colnames(design) = c("Control","Cancer")

design

## Filter lowly-expressed genes prior to performing the analysis ----
summary(exprs(my_data_1))

## Calculate median expression level
cutoff = median(exprs(my_data_1))

## TRUE or FALSE for whether each gene is "expressed" in each sample
is_expressed = exprs(my_data_1) > cutoff

## Identify genes expressed in more than two samples

keep = rowSums(is_expressed) > 2

## Check how many genes are removed/retained.
table(keep)

## subset to just those expressed genes
```

```
my_data_1 = my_data_1[keep,]

# Estimate the expression level in each of the
groups that we specified

fit = lmFit(exprs(my_data_1), design)

head(fit$coefficients)

contrasts = makeContrasts(Control-Cancer,
levels=design)

## can define multiple contrasts
## e.g., makeContrasts(Group1 - Group2, Group2 -
Group3....levels=design)

fit2 = contrasts.fit(fit, contrasts)

fit2

fit2 = eBayes(fit2)

topTable(fit2)

topTable(fit2, coef=1)
```

```
#########################################################
#########################################################
#########################################
# If we want to know how many genes are
differentially expressed overall, we can use the
decideTests function.#
#########################################################
#########################################################
#########################################

decideTests(fit2, coef=1)

table(decideTests(fit2, coef=1))

## Calculate relative array weights
aw = arrayWeights(exprs(my_data_1),design)

aw

fit = lmFit(exprs(my_data_1), design,
            weights = aw)

fit2 = contrasts.fit(fit, contrasts)

fit2 = eBayes(fit2)
```

```
anno <- fData(my_data_1)

anno <- dplyr::select(anno, `Gene Symbol`,
`ENTREZ_GENE_ID`)

fit2$genes <- anno

topTable(fit2, coef = 1)

# Remember there can be more than one contrasts

full_results_2 <- topTable(fit2, number=Inf)

full_results_2 <-
tibble::rownames_to_column(full_results_2,"ID_2")

## Change according to your needs

p_cutoff = 0.05
fc_cutoff = 1

full_results_2 %>%
  dplyr::mutate(Significant = adj.P.Val < p_cutoff,
abs(logFC) > fc_cutoff ) %>%
```

```
  ggplot(aes(x = logFC, y = B, col=Significant)) +
geom_point()

# Order your dataframe by gene id and pvalue and
remove duplicated values

full_results_2 =
 full_results_2[order(full_results_2$Gene.Symbol,ful
l_results_2$adj.P.Val),]

full_results_2 = full_results_2[
!duplicated(full_results_2$Gene.Symbol),]


EnhancedVolcano(full_results_2,
                lab = full_results_2$Gene.Symbol,
                x = 'logFC',
                y = 'P.Value',
                selectLab = c('AURKA', 'AURKB'),
                title = 'Volcano plot examining differential
gene
          expression of AURKA and AURKB',
                xlab = bquote(~Log[2]~ 'fold change'),
                pCutoff = 0.05,
                FCcutoff = 1,
                pointSize = 4.0,
```

```
                labSize = 4.0,
                # shape = c(4, 35, 17, 18),
                colAlpha = 1,
                legendPosition = 'right',
                legendLabSize = 14,
                legendIconSize = 5.0)


# labels top 20 genes
# The gene labels may be hard to plot if there are
too many
# overlaps

topN <- 20

options(ggrepel.max.overlaps = Inf)

full_results_2 %>%
  dplyr::mutate(Significant = adj.P.Val < p_cutoff,
abs(logFC) > fc_cutoff ) %>%
  dplyr::mutate(Rank = 1:n(), Label = ifelse(Rank <
topN, `Gene.Symbol`,"ID")) %>%
  ggplot(aes(x = logFC, y = B,
col=Significant,label=Label)) + geom_point() +
  geom_text_repel(col="black")
```

```
# up and down-regulated genes----

my_filter_2 = filter(full_results_2, adj.P.Val < 0.05,
abs(logFC) >2)


filter(my_filter_2, `Gene.Symbol` == "AURKA")
filter(my_filter_2, `Gene.Symbol` == "AURKB")
filter(my_filter_2, `Gene.Symbol` == "AURKC")

EnhancedVolcano(my_filter_2,
                lab = my_filter_2$Gene.Symbol,
                x = 'logFC',
                y = 'P.Value',
                selectLab = c('AURKA'),
                title = 'Volcano plot examining differential
gene expression for AURKA and AURKB',
                xlab = bquote(~Log[2]~ 'fold change'),
                pCutoff = 0.05,
                FCcutoff = 1,
                pointSize = 4.0,
                labSize = 4.0,
                # shape = c(4, 35, 17, 18),
                colAlpha = 1,
                legendPosition = 'right',
                legendLabSize = 14,
```

```
                legendIconSize = 5.0)

# filtered genes

dplyr::filter(full_results_2, adj.P.Val < 0.05,
abs(logFC) > 2) %>%

  write.csv("filtered_gene_resultsGSE74530.csv")

##############################################################
#########################################
##                      PHEATMAP
 ##
############################################################
#########################################


# Introduce a new column to the results, which
gives a row number to each gene
## Use the top 20 genes for illustration

topN = 25


##
```

```
ids_of_interest <- mutate(my_filter_2, Rank = 1:n())
%>%
  dplyr::filter(Rank < topN) %>%
  pull(ID_2)

gene_names <- mutate(my_filter_2, Rank = 1:n())
%>%
  dplyr::filter(Rank < topN) %>%
  dplyr::pull(Gene.Symbol)

gene_matrix <- exprs(my_data_1)[ids_of_interest,]


pheatmap(gene_matrix, annotation_col=sampleInfo,
         labels_row = gene_names, scale="row")


# Draw a heatmap with the Genes of interest

my_genes <- c("AURKA")

ids_of_interest =
 dplyr::filter(my_filter_2,Gene.Symbol %in%
my_genes) %>%
  dplyr::pull(ID_2)
```

```
gene_names <-
dplyr::filter(my_filter_2,Gene.Symbol %in%
my_genes) %>%
  dplyr::pull(Gene.Symbol)

gene_matrix <- exprs(my_data_1)[ids_of_interest,]

pheatmap(gene_matrix,
         labels_row = gene_names,
         scale="row")



##############################################################
############################
###              Then use cytoscape
 #######
##############################################################
############################

# Order the genes by the logfold change, then
export as CSV

cytoscape_filter =
my_filter_2[order(my_filter_2$logFC),]
```

```
write.csv(cytoscape_filter,"cytoscape_filter_2_GSE74530.csv",
          row.names = FALSE)


###############
####boxplot##
###############


df= read.csv("cytoscape_filter_GSE30784.csv")
tab<-topTable(fit2, number = 3e6, adjust.method = "BH", sort.by = "P")
pr<-row.names(tab)

# may need to alternate libraries
library(illuminaHumanv3.db)
library(hgu133plus2.db)

sy<-getSYMBOL(pr, data = "hgu133plus2.db")

df<-data.frame(Gene_Symbol = sy, tab)


###########
# AURKA##
###########
```

```
rn<-row.names(df)[which(sy=="AURKA")]

# can use an independent dataset here; name it
my_data_2

ex-<-exprs(my_data_1)[rn,]

if(!is.vector(ex)){
  varfilter<-apply(ex, 1, var)
  ex<-ex[which.max(varfilter),]
}

pl<-data.frame(Intensity = ex, Phenotype =
sampleInfo$sample_type)

a<-ggplot(pl, aes(y = Intensity, x = Phenotype, fill =
Phenotype))

a<-a+theme_classic(base_size = 16)

a<-a+scale_y_log10(breaks=c(1, 2, 4, 6, 8, 10, 12))

a<-a+ggtitle("AURKA Expression\n")

a<-a+ylab("Log2 Intensity")
```

```
a<-a+xlab('')

a<-a+scale_fill_manual(values =
wes_palette("Zissou1")[c(1,4,3)], guide=FALSE)

a<-a+scale_x_discrete(labels=c("Tumour",
"Normal"))

a <- a+geom_boxplot()

a

a + stat_compare_means()

a + stat_compare_means(method = "t.test")

a + stat_compare_means(paired = TRUE)

##############
#####AURKB##
##############
rn<-row.names(df)[which(sy=="AURKB")]

# can use an independent dataset here; name it
my_data_2
```

```
ex<-exprs(my_data_1)[rn,]

if(!is.vector(ex)){
  varfilter<-apply(ex, 1, var)
  ex<-ex[which.max(varfilter),]
}

pl<-data.frame(Intensity = ex, Phenotype =
sampleInfo$sample_type)

a<-ggplot(pl, aes(y = Intensity, x = Phenotype, fill =
Phenotype))

a<-a+theme_classic(base_size = 16)

a<-a+scale_y_log10(breaks=c(1, 2, 4, 6, 8, 10, 12))

a<-a+ggtitle("AURKB Expression\n")

a<-a+ylab("Log2 Intensity")

a<-a+xlab('')

a<-a+scale_fill_manual(values =
wes_palette("Zissou1")[c(1,4,3)], guide=FALSE)
```

```
a<-a+scale_x_discrete(labels=c("Tumour",
"Normal"))

a <- a+geom_boxplot()

a

a + stat_compare_means()

a + stat_compare_means(method = "t.test")

a + stat_compare_means(paired = TRUE)


#############
####AURKC##
#############
rn<-row.names(df)[which(sy=="AURKC")]

# can use an independent dataset here; name it
my_data_2

ex<-exprs(my_data_1)[rn,]

if(!is.vector(ex)){
```

```
  varfilter<-apply(ex, 1, var)
  ex<-ex[which.max(varfilter),]
}

pl<-data.frame(Intensity = ex, Phenotype =
sampleInfo$sample_type)

a<-ggplot(pl, aes(y = Intensity, x = Phenotype, fill =
Phenotype))

a<-a+theme_classic(base_size = 16)

a<-a+scale_y_log10(breaks=c(1, 2, 4, 6, 8, 10, 12))

a<-a+ggtitle("AURKC Expression\n")

a<-a+ylab("Log2 Intensity")

a<-a+xlab('')

a<-a+scale_fill_manual(values =
wes_palette("Zissou1")[c(1,4,3)], guide=FALSE)

a<-a+scale_x_discrete(labels=c("Tumour",
"Normal"))
```

```
a <- a+geom_boxplot()

a

a + stat_compare_means()

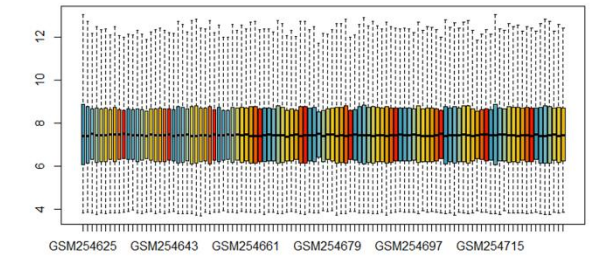
a + stat_compare_means(method = "t.test")

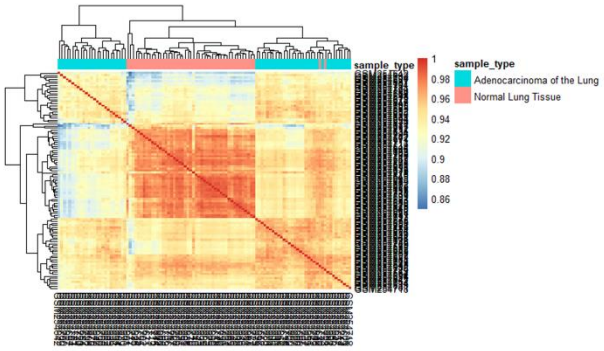
a + stat_compare_means(paired = TRUE)
```

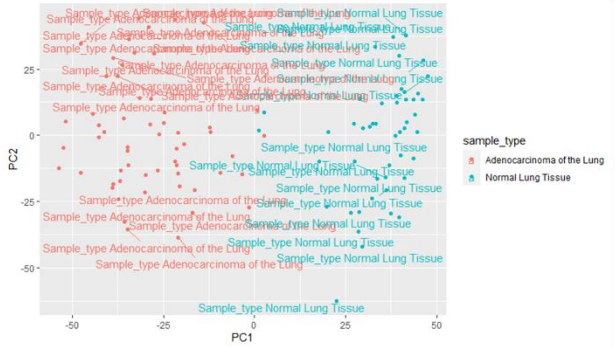
7.2 Volcano plots and DEG tables used in bioinformatics study.

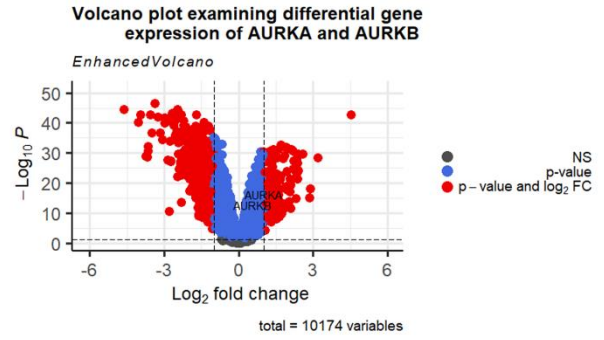
7.2.1 NCSLC plots

7.2.1.1 GSE10072

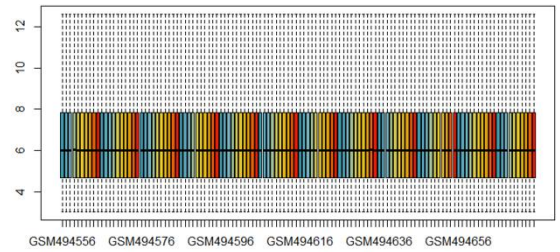


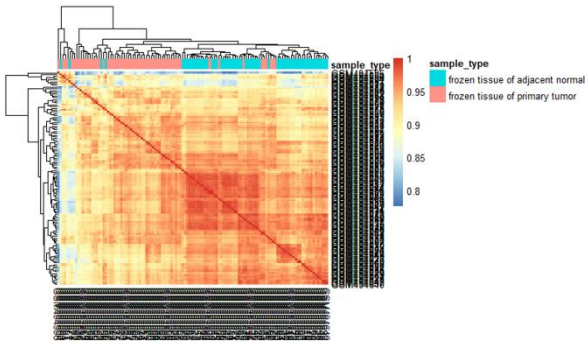


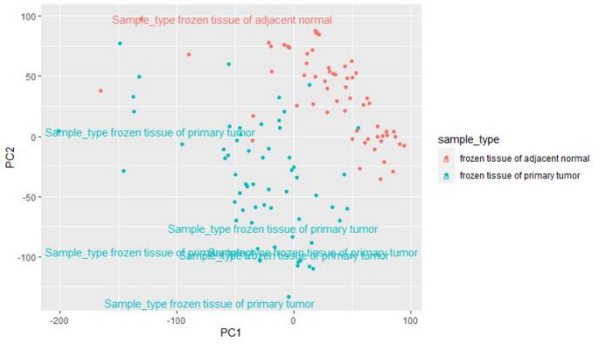


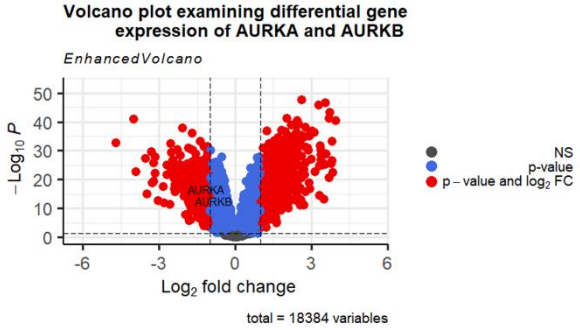


7.2.1.2 GSE19804

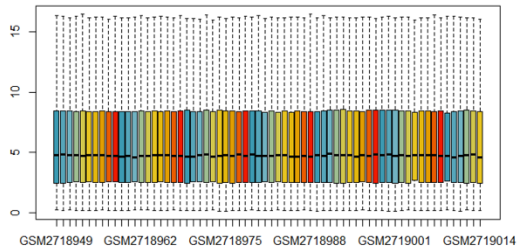


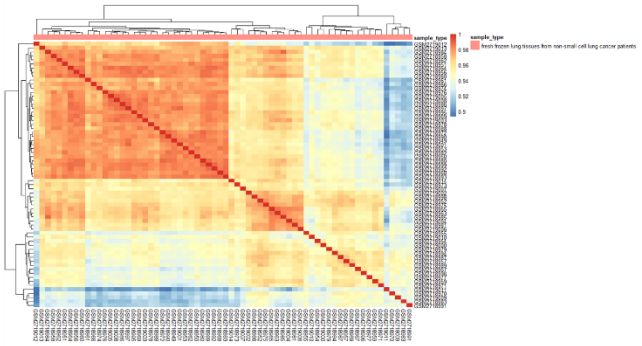


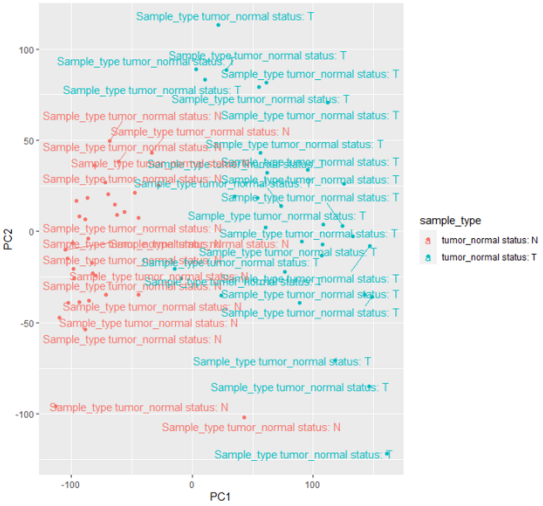


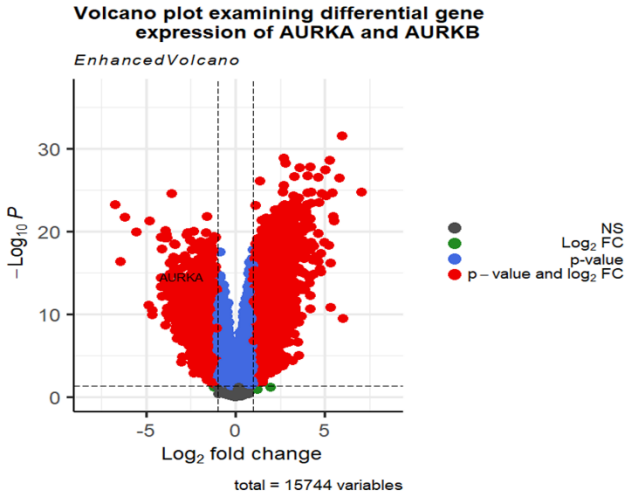


7.2.1.3 GSE101929

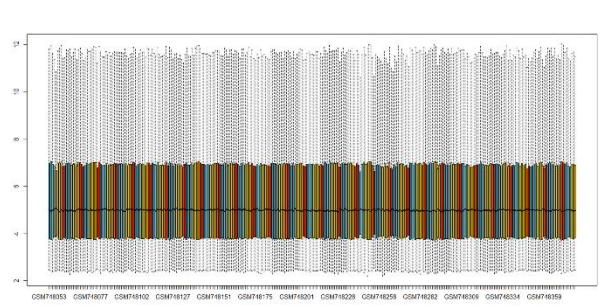


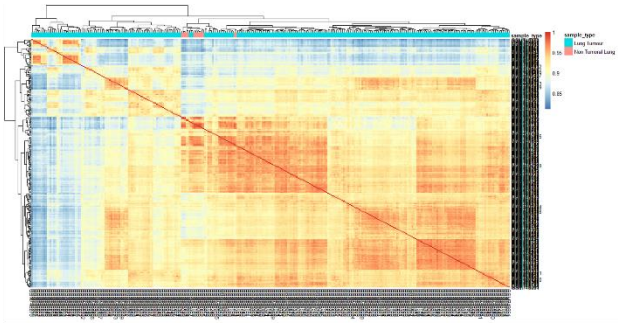




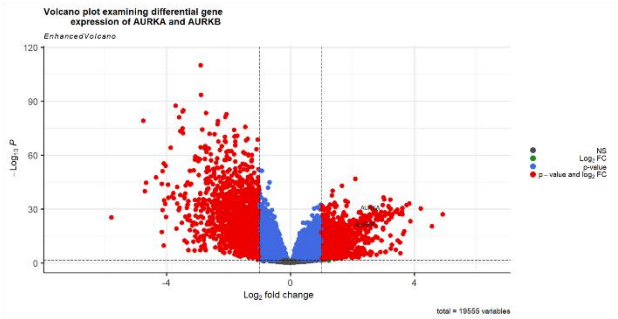


7.2.1.4 GSE30219

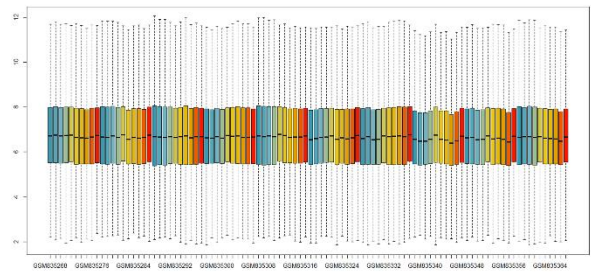


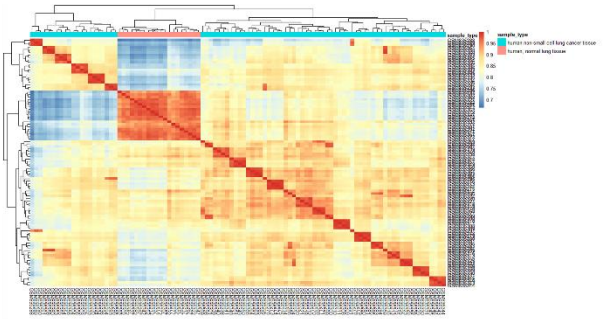


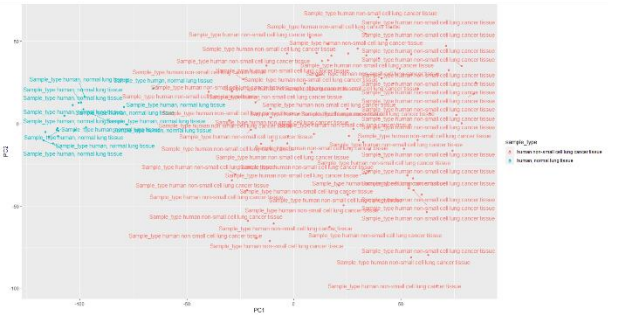


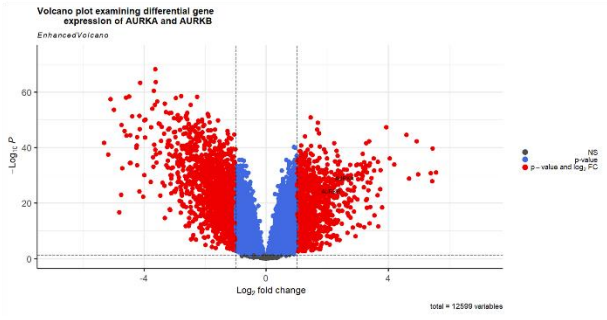


7.2.1.5 GSE33532



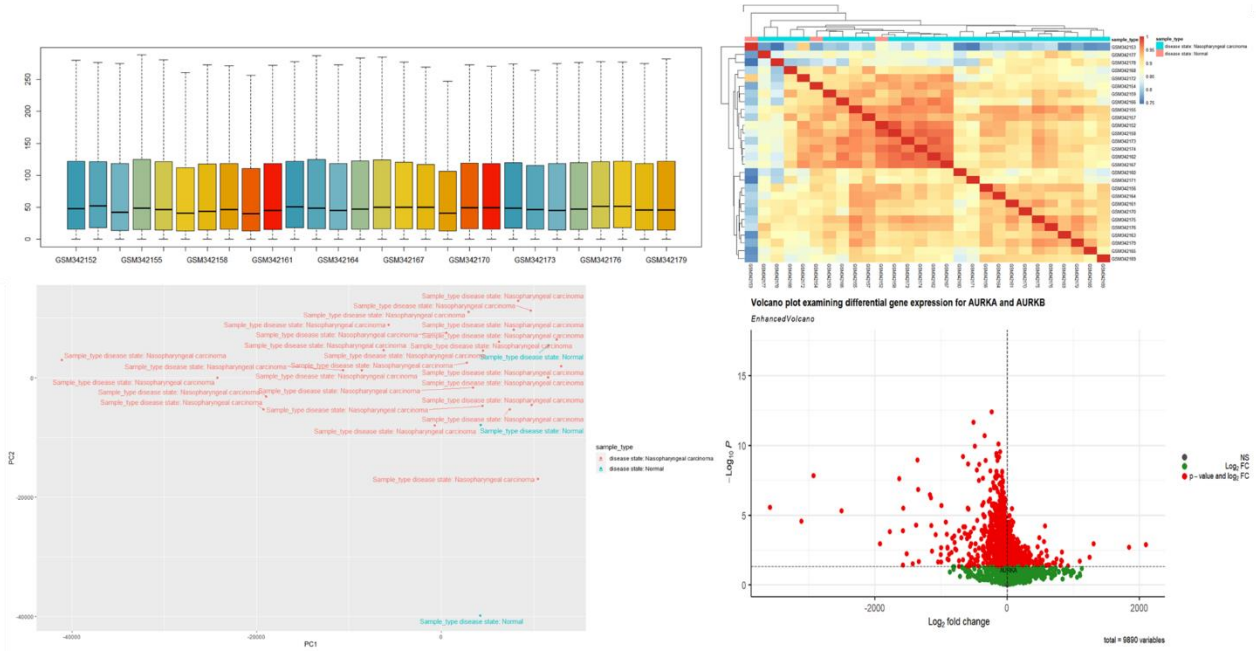




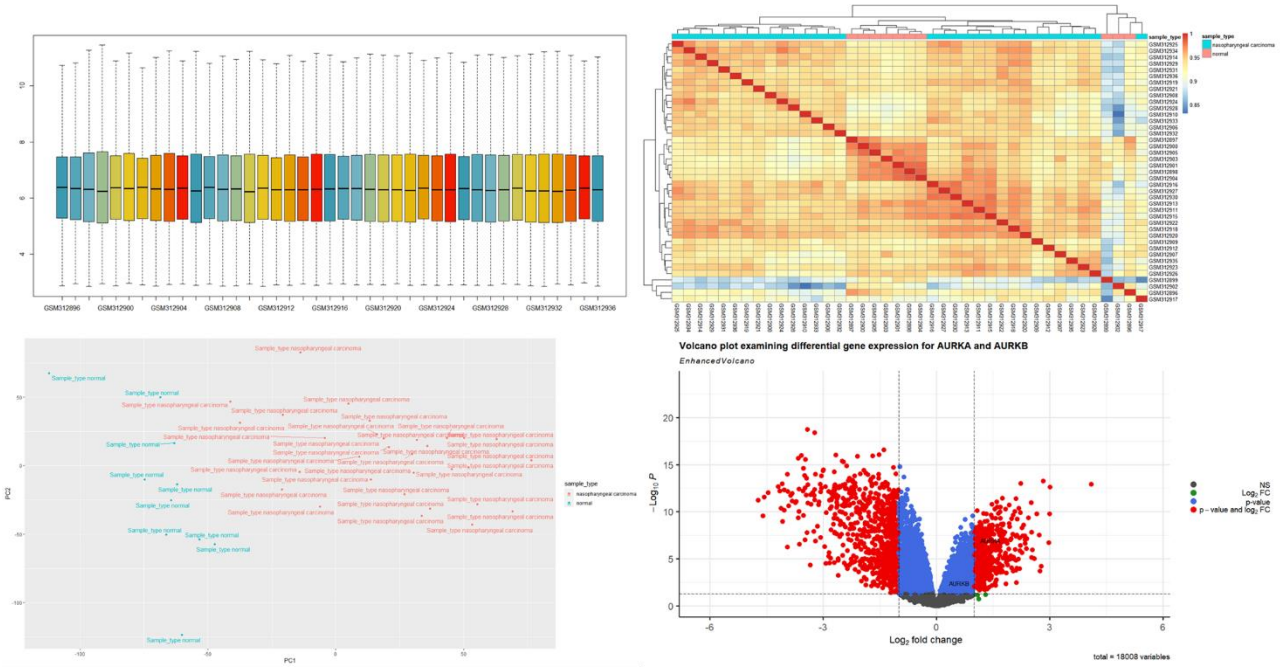


7.2.2 Nasopharyngeal plots

7.2.2.1 GSE13597

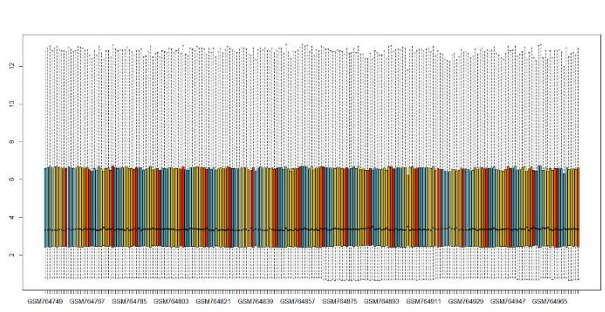


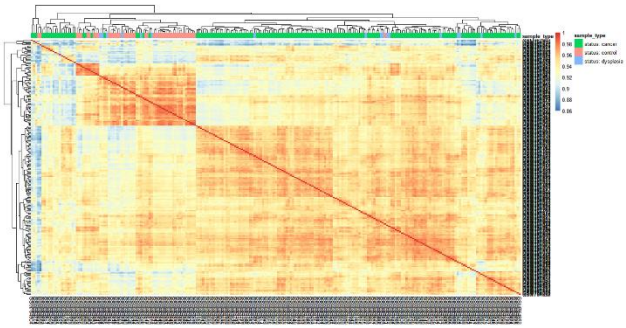
7.2.2.2 GSE12452

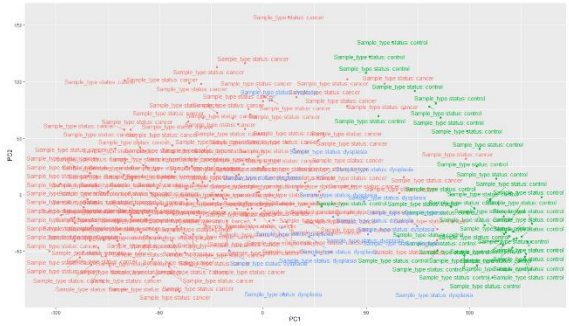


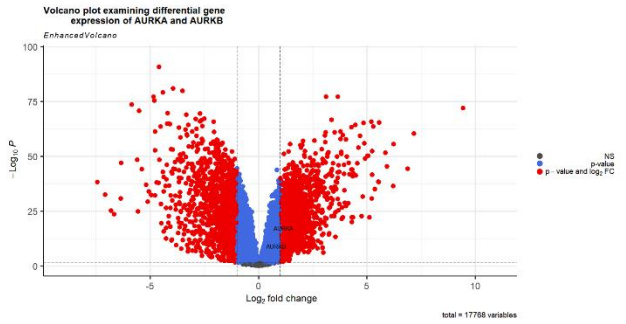
7.2.3 Oropharyngeal plots

7.2.3.1 GSE30784

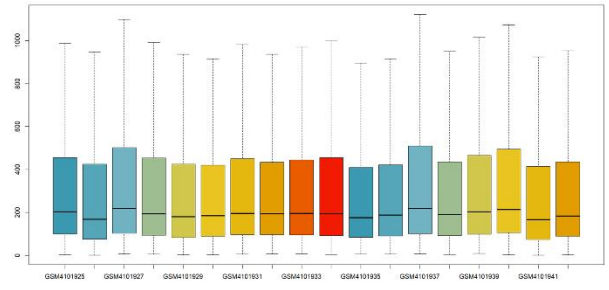


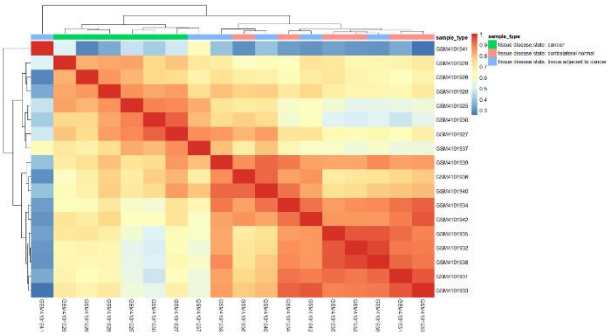


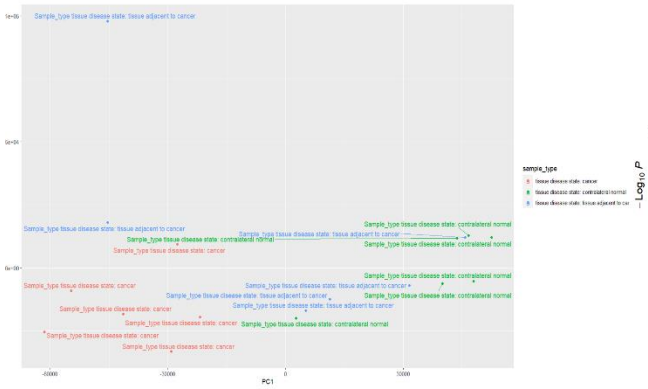


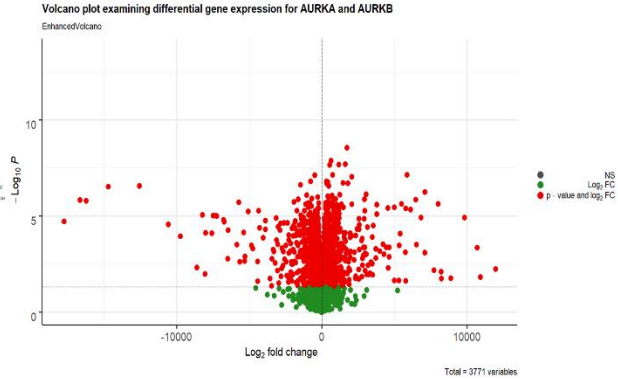


7.2.3.2 GSE138206

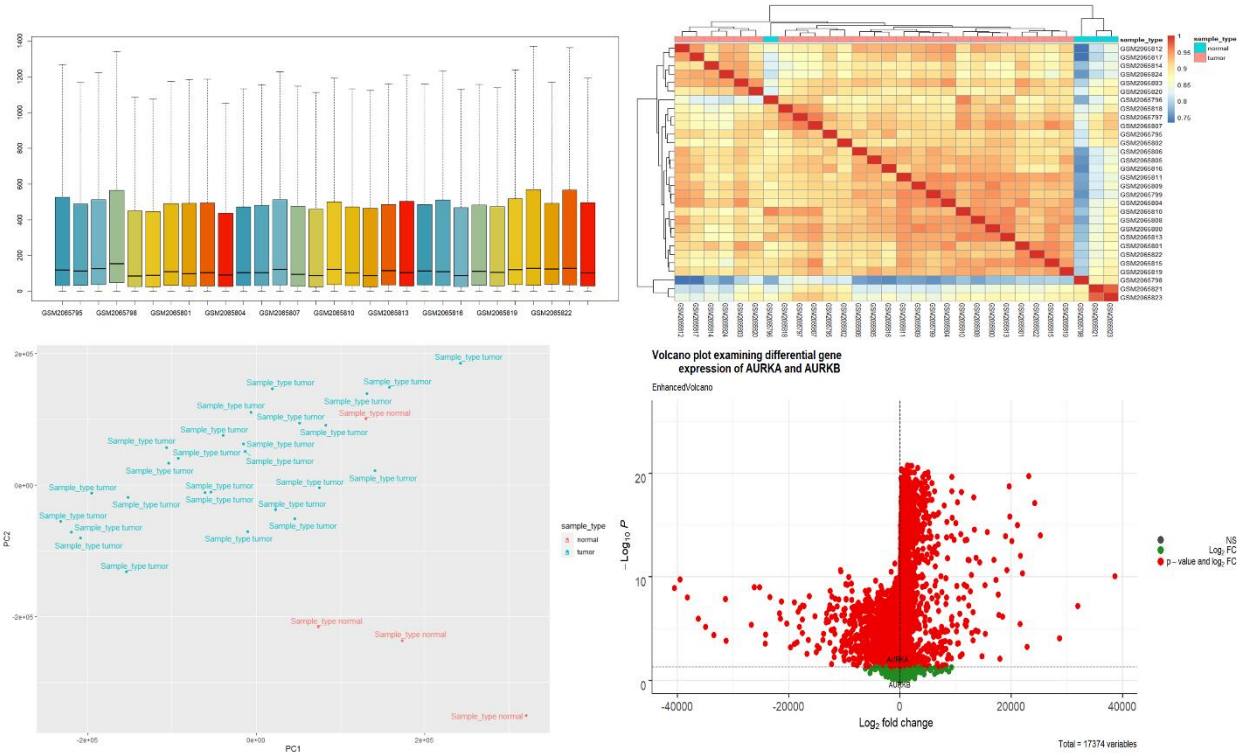




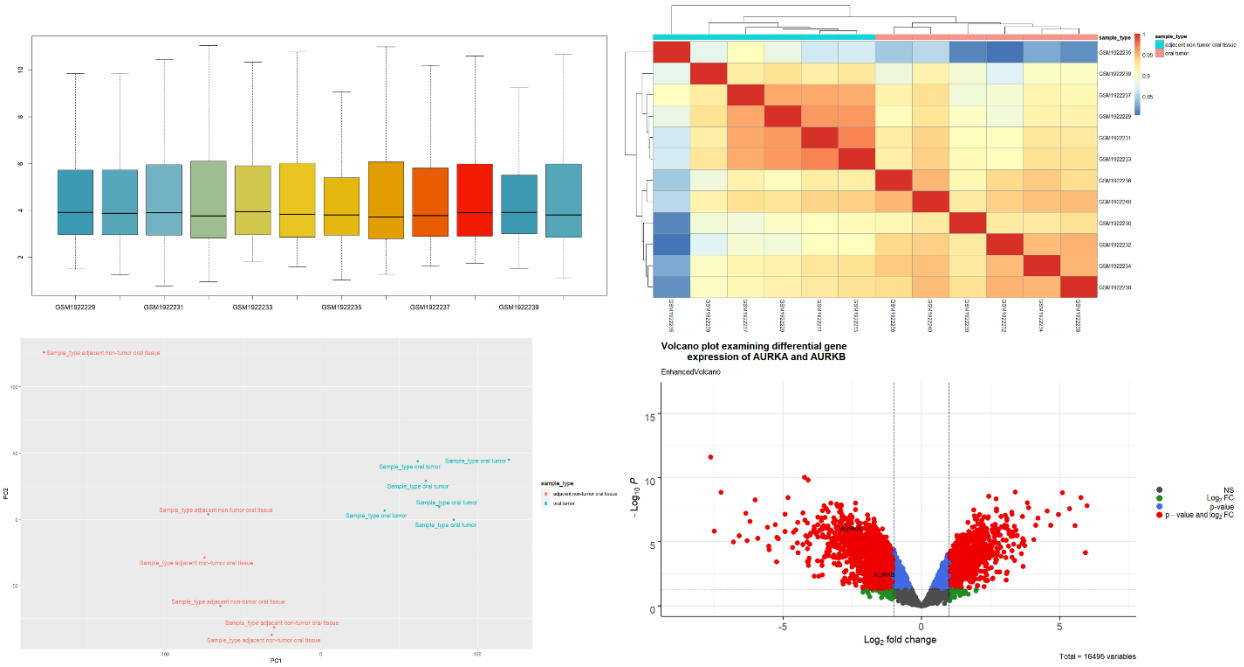




7.2.3.3 GSE78060



7.2.3.4 GSE74530



7.3 A SequeNtial Phase One stUdy of an Aurora Kinase inhibitor concurrent with radical fracTionated radiotherapy for Non-Small Cell Lung cancer.

NUTS: A sequential phase one study of an aurora kinase inhibitor concurrent with radical fractionated radiotherapy for non-small cell lung cancer.

Investigator:	Prof. Sarah Danson
Co-Principal Investigator(s):	Dr Helen Bryant Prof. Matthew Hatton
Sponsor:	Sheffield Teaching Hospitals NHS Foundation Trust
STH Project Reference:	-
EUDRACT Number:	-
CTA number:	-
The Phase of Trial:	Phase 1
STH Directorate Affiliation:	Specialised Cancer Services

Version:	Date:

1.0	3/3/2023

Confidentiality Statement:

This document contains confidential information that must not be disclosed to anyone other than the Sponsor, the Trials Office, the Investigator team, host NHS Trusts(s), regulatory authorities, and members of the Research Ethics Committee.

General Contact Information:

Trial Office

Level 10

Worsley Building

Clarendon Way

University of Leeds

Leeds

LS2 9NL

medctrur@leeds.ac.uk

Telephone: +44 (0) 113 343 1477

Chief Investigator

Professor Sarah Danson

Department of Oncology & Metabolism

Weston Park Hospital

Whitham Road

Sheffield

S10 2SJ

UK

Office: Room 227, WPH

Tel: +44 (0)114 226 5221/5704

Fax: +44 (0)114 226 5364

email: s.danson@sheffield.ac.uk

Other Investigators

Dr Helen Bryant

Senior Lecturer

Head of The DNA replication and repair group

Academic Unit of Molecular Oncology

Department of Oncology & Metabolism

The Medical School

Beech Hill Road

Sheffield

S10 2RX

United Kingdom

Telephone: +44 (0)114 215 9040

Email: h.bryant@sheffield.ac.uk

Twitter: @bryantlab1

Professor Matthew Hatton

Department of Oncology & Metabolism

Weston Park Hospital

Whitham Road

Sheffield

S10 2SJ

UK

Telephone: 0114 226 5071

Email: matthewhatton@nhs.net

Lead NHS Trust

Weston Park Hospital

Telephone: 0114 226 5000

Address: Whitham Road, Sheffield, South Yorkshire, S10 2SJ

Website: http://www.sth.nhs.uk

Trial Statistician

TBA

Patient Representative

TBA

Clinical queries and emergency contact details

TBA

During office hours: Clinical Queries should be directed to the Leeds Institute of Clinical Trials Research and contact the Clinical Trial Coordinator. The call will be passed on to the Chief Investigator, the Clinical Coordinator (medically qualified), or an appropriate member of the Trial Management Group.

Out of office hours: Call the Weston Park Cancer Centre switchboard at +44 (0) 0114 226 5000 and ask to call the **NUTS** Clinical Coordinator.

7.3.1 Study Summary:

Full Title of Study:	A Sequential Phase I study of an Aurora Kinase inhibitor concurrent with radical fractionated radiotherapy for Non-Small Cell Lung cancer.
Trial Acronym:	NUTS
Objectives:	This study aims to conduct a dose escalation phase I trial to evaluate the combination of an Aurora Kinase inhibitor and fractionated radiotherapy in patients with non-small cell lung cancer (NSCLC). **The primary objectives of the trial are twofold.** Firstly, to assess the safety and toxicity profile of the combined treatment using the National Cancer Institute Common Terminology Criteria for Adverse Events (NCI CTCAE) version 5.0. Secondly, to determine the maximum tolerated dose (MTD) of the combination therapy. **Secondary objectives include** establishing the recommended phase II (RPII) dose and schedule for the Aurora Kinase inhibitor and fractionated radiotherapy combination. Additionally, the trial aims to investigate the pharmacokinetics (PK) of the combined treatment, examine pharmacodynamic (PD) biomarkers in tumour samples (where feasible), and conduct a preliminary assessment of

	the efficacy of the RPII dose. A dose expansion cohort phase will be performed after the dose escalation phase. The primary objective of this phase is to investigate the response to treatment with the RPII dose of combination therapy. Secondary objectives include evaluating the efficacy of the RPII dose and further assessing the Aurora Kinase inhibitor's safety, toxicity profile, and tolerability and fractionated radiotherapy combination.
Protocol Number:	TBA
Phase	Phase I/II
Scientific rationale:	Non-Small Cell Lung Cancer (NSCLC) is a prevalent, aggressive malignancy with limited treatment options and poor overall survival rates. Despite advances in therapeutic strategies, developing resistance to targeted agents and radiotherapy remains a significant challenge. Therefore, there is a critical need to explore novel treatment approaches that can improve patient outcomes. Aurora Kinases are a family of serine/threonine kinases that play crucial roles in cell division and genomic stability. Overexpression and dysregulation of Aurora Kinases have been observed in various cancers, including NSCLC, making them attractive targets for anticancer therapy. Preclinical studies have demonstrated the

	potential of Aurora Kinase inhibitors to induce cell cycle arrest, inhibit tumour growth, and enhance the radiosensitivity of cancer cells. Fractionated radiotherapy is a widely used therapeutic modality in NSCLC, delivering radiation doses in multiple fractions over a prolonged treatment period. This approach maximises tumour control while minimising damage to surrounding healthy tissues. However, resistance to radiotherapy and local tumour recurrence remain significant obstacles. Combining Aurora Kinase inhibitors with fractionated radiotherapy holds promise for improving treatment outcomes in NSCLC. The rationale for this combination therapy is multifaceted. Firstly, Aurora Kinase inhibitors can potentiate the effects of radiotherapy by inhibiting DNA repair mechanisms and inducing cell cycle arrest, thereby enhancing the radiosensitivity of tumour cells. Additionally, Aurora Kinases regulate angiogenesis, a process critical for tumour growth and metastasis. By targeting these kinases, it is possible to inhibit angiogenesis and disrupt the tumour microenvironment, potentially augmenting the efficacy of radiotherapy. There is limited clinical evidence regarding the safety, tolerability, and efficacy of combining Aurora Kinase inhibitors with fractionated radiotherapy in NSCLC patients. Therefore, a sequential phase I study is warranted to investigate this combination therapy's feasibility and potential benefits. The primary objective of this study

	is to determine the maximum tolerated dose (MTD) of the Aurora Kinase inhibitor when administered concurrently with radical fractionated radiotherapy in NSCLC patients. Furthermore, the study aims to assess the safety and toxicity profile, establish the recommended phase II dose and schedule, explore pharmacokinetics and pharmacodynamic biomarkers, and provide a preliminary assessment of treatment efficacy.
Clinical Rationale:	Non-Small Cell Lung Cancer (NSCLC) is a complex disease with a high morbidity and mortality rate. Despite advancements in treatment options, the prognosis for many patients remains poor. The development of resistance to targeted therapies and radiotherapy further limits the effectiveness of current treatment approaches. Therefore, a clinical imperative exists to explore innovative therapeutic strategies to enhance treatment response and improve patient outcomes. Aurora Kinases are a family of proteins that play crucial roles in regulating cell division and genomic stability. Dysregulation of Aurora Kinases has been implicated in the pathogenesis of various cancers, including NSCLC. Preclinical studies have demonstrated that inhibition of Aurora Kinases can lead to cell cycle arrest, inhibition of tumour growth, and increased sensitivity to radiotherapy. Fractionated radiotherapy is a standard treatment modality for NSCLC, aiming to deliver radiation doses in multiple fractions over

	a prolonged treatment period. This approach allows optimal tumour control while minimising damage to healthy surrounding tissues. However, intrinsic and acquired resistance to radiotherapy remains a significant challenge, leading to local tumour recurrence and treatment failure. Combining an Aurora Kinase inhibitor with fractionated radiotherapy holds great potential in overcoming resistance mechanisms and improving treatment outcomes in NSCLC. The rationale for this combination therapy is supported by preclinical evidence demonstrating synergistic effects. Aurora Kinase inhibitors can enhance the radiosensitivity of cancer cells by impairing DNA repair mechanisms and inducing cell cycle arrest, leading to increased cell death upon radiation exposure. Furthermore, these inhibitors have also been shown to interfere with angiogenesis, a process critical for tumour growth and metastasis, thereby potentially augmenting the efficacy of radiotherapy. While preclinical data is promising, the clinical feasibility and efficacy of combining an Aurora Kinase inhibitor with fractionated radiotherapy in NSCLC patients remain largely unexplored. Thus, conducting a clinical trial to evaluate this combination therapy is justified. Such a study would provide critical insights into this novel

	treatment approach's safety, tolerability, and potential benefits. The trial's primary objective would be determining the Aurora Kinase inhibitor's maximum tolerated dose (MTD) when administered concurrently with radical fractionated radiotherapy in NSCLC patients. Secondary objectives would include assessing the safety and toxicity profile, establishing the recommended phase II dose and schedule, investigating pharmacokinetics and pharmacodynamic biomarkers, and providing an initial assessment of treatment efficacy.
Primary Endpoint:	**Dose Escalation Phase:** <u>Primary Endpoint: Safety and Toxicity Profile</u> The primary objective in the dose escalation phase is to assess the safety and toxicity profile of the combined treatment regimen. This endpoint focuses on monitoring and documenting any adverse events, treatment-related toxicities, and dose-limiting toxicities (DLTs) experienced by the patients. The evaluation of safety and toxicity will be conducted using established guidelines such as the National Cancer Institute Common Terminology Criteria for Adverse Events (NCI CTCAE) version 5.0. <u>Primary Endpoint: Maximum Tolerated Dose (MTD)</u> Another primary endpoint in the dose escalation phase is determining the Aurora Kinase inhibitor's maximum tolerated dose

	(MTD) in combination with fractionated radiotherapy. The MTD is the highest dose level at which the incidence of DLTs does not exceed a predefined threshold. The MTD is essential for further studies and informs the recommended phase II dose. **Dose Expansion Phase:** <u>Primary Endpoint: Treatment Response</u> The primary endpoint in the dose expansion phase would likely be the treatment response to the recommended phase II dose of the combination therapy. The treatment response can be assessed using various criteria, such as Response Evaluation Criteria in Solid Tumours (RECIST) or other relevant response assessment guidelines. This endpoint aims to evaluate the objective tumour response rate, including complete response (CR), partial response (PR), stable disease (SD), or progressive disease (PD), to determine the efficacy of the treatment. <u>Primary Endpoint: Safety and Tolerability</u> Safety and tolerability assessment would remain a primary endpoint in the dose expansion phase. Similar to the dose escalation phase, the focus would be monitoring and documenting any treatment-related adverse events and toxicities and evaluating the safety and tolerability of the recommended phase II dose.

	Dose Escalation Phase: Secondary Endpoint: Recommended Phase II (RPII) Dose and Schedule The trial may aim to define the recommended phase II (RPII) dose and schedule the combination therapy based on the safety and efficacy data obtained during the dose escalation phase. This endpoint would involve determining the dose level at which an acceptable safety profile is observed and encouraging preliminary efficacy signals. Secondary Endpoint: Pharmacokinetics (PK) Analysis The trial may include a secondary objective of investigating the pharmacokinetics (PK) of the Aurora Kinase inhibitor when administered in combination with fractionated radiotherapy. PK analysis would involve measuring drug concentrations in blood samples at specified time points to determine drug absorption, distribution, metabolism, and elimination characteristics. Secondary Endpoint: Pharmacodynamic (PD) Biomarkers The trial may aim to investigate pharmacodynamic (PD) biomarkers in tumour samples (where feasible) to assess the effect of the combination therapy on molecular pathways and cellular processes. This analysis could involve examining changes in gene expression, protein activation, or other relevant biomarkers associated with Aurora Kinase inhibition and radiotherapy

Secondary Endpoint:	response. <u>Secondary Endpoint: Preliminary Assessment of Efficacy</u> The trial may include a secondary objective of conducting a preliminary assessment of the efficacy of the recommended phase II dose. This could involve evaluating parameters such as overall response rate (ORR), progression-free survival (PFS), and overall survival (OS) to obtain initial insights into the treatment's efficacy. **Dose Expansion Phase:** <u>Secondary Endpoint: Efficacy Assessment</u> Similar to the dose escalation phase, a secondary endpoint in the dose expansion phase would be to assess the efficacy of the recommended phase II dose of the combination therapy. This may involve evaluating parameters such as ORR, PFS, and OS in a larger cohort of patients to provide a more comprehensive understanding of treatment effectiveness.

	Secondary Endpoint: Safety and Tolerability Continuation of the secondary endpoint from the dose escalation phase, the dose-expansion phase, would aim to investigate further the safety and tolerability of the recommended phase II dose of the combination therapy. This would involve monitoring and documenting any treatment-related adverse events and toxicities.
Exploratory and Tertiary Endpoints:	Biomarker Analysis: Exploration of additional biomarkers associated with response to the combination therapy can provide valuable insights into the underlying mechanisms of action and potential predictors of treatment response. This could involve analysing genetic mutations, gene expression profiles, protein markers, or other molecular characteristics in tumour samples to identify potential biomarkers that may correlate with treatment response or resistance. Quality of Life Assessment: Assessing the impact of combination therapy on patients' quality of life can provide valuable information on the treatment's overall benefit. This may involve using validated questionnaires or assessments to measure patient-reported outcomes such as symptom burden, physical functioning, emotional well-being, and treatment-related side effects.

	Radiomics Analysis: Radiomics analysis involves extracting and analysing quantitative imaging features from radiological images. This exploratory endpoint investigates whether specific radiomic features derived from pretreatment or post-treatment imaging scans can serve as predictive or prognostic markers of treatment response and survival outcomes. Pharmacokinetic-Pharmacodynamic (PK-PD) Analysis: An exploratory PK-PD analysis can provide insights into the relationship between drug exposure (pharmacokinetics) and combination therapy's biological response (pharmacodynamics). This analysis aims to explore potential correlations between drug concentrations, biomarker modulation, and treatment response. Immune Profiling: Immune profiling aims to evaluate the impact of combination therapy on the immune system and the tumour microenvironment. This could involve analysing immune cell subsets, immune checkpoint markers, cytokine levels, or other immune-related factors to explore the potential immunomodulatory effects of the

	treatment. Long-Term Follow-up and Survival Analysis: Long-term follow-up and survival analysis beyond the primary study period can provide insights into the durability of treatment response, long-term survival outcomes, and potential late toxicities associated with combination therapy.
Methodology/ Study Design:	1. Define the Target Toxicity and Dose Levels: Determine the specific toxicity endpoint that will guide the dose escalation process. This could be the maximum tolerated dose (MTD), dose-limiting toxicities (DLTs), or another relevant toxicity measure. Also, define the initial set of dose levels to be evaluated. 2. Select the Prior Distribution: Specify the prior distribution for the model parameters. This prior distribution reflects the initial beliefs or knowledge about the dose-toxicity relationship before any data from the study is collected. The prior choice should be based on existing information, previous studies, or expert opinion. 3. Determine the Starting Dose: Assign the first patient to the

	initial dose level. The starting dose can be based on preclinical data, early-phase trial results, or expert judgment. 4. Observe and Evaluate Dose-Limiting Toxicities: Monitor and record the toxicities experienced by each patient at their assigned dose level. Use predefined criteria to identify dose-limiting toxicities (DLTs) based on the target toxicity endpoint. DLTs typically influence the subsequent dose assignments. 5. Update the Model: After observing the toxicities from each patient, update the model parameters using the Bayesian approach. Incorporate the accumulating data to refine the estimates of the dose-toxicity relationship. 6. Dose Assignment: Based on the updated model, determine the next dose level to assign to the next patient. This decision is guided by the probabilities of toxicity associated with each dose level, aiming to balance efficacy and safety. 7. Continue Dose Escalation: Repeat steps 4 to 6 for subsequent patients, continuously updating the model and

	assigning doses according to the CRM framework. The number of patients treated at each dose level may vary, depending on the study design and the specific implementation of the CRM. 8. Assess the MTD: Analyse the data collected during the study to estimate the MTD or other relevant toxicity endpoint based on the CRM approach. This estimation is typically based on the posterior distribution of the model parameters. 9. Explore Additional Objectives: Depending on your study's specific research questions and objectives, you may incorporate additional design elements, such as exploring efficacy measures or investigating specific subgroups.
Patient numbers:	Up to 30 patients will be recruited
	Dose escalation phase: Adult patients with pathologically proven NSCLC tumours with a performance status of 0 - 2 and who are not fit for Platinum Chemotherapy. **Dose expansion phase:** Adult patients with pathologically proven NSCLC tumours with a

Target Population:	performance status of 0 - 2 and who are not fit for Platinum Chemotherapy.
Inclusion and Exclusion criteria	**Inclusion Criteria** <u>All Patients:</u> 1. Age 16 years or older 2. Eastern Cooperative Oncology Group (ECOG) performance status of 0-1 3. Adequate respiratory function assessed by FEV1 > 1L and/or DLCO > 40% 4. Left ventricular ejection fraction (LVEF) ≥ 50% determined by multigated acquisition (MUGA) scan or echocardiogram. 5. Capacity to provide informed consent and comply with the study protocol. 6. Haematological and biochemical indices within specified ranges: 7. Haemoglobin (Hb) ≥ 9g/dL (transfusion allowed to achieve this) a) Neutrophils ≥ 1,500/μL b) Platelet count ≥ 100,000/μL c) AST or ALT ≤ 2.5 x upper limit of normal (ULN) d) Alkaline phosphatase ≤ -5 x ULN

Inclusion and	e) Serum bilirubin ≤ 1.5 x ULN f) Creatinine clearance ≥ 50 mL/min (calculated by Cockcroft Gault equation or EDTA) 8. Ability to swallow oral medication. 9. Expected life expectancy of at least three months. **Dose Escalation Phase:** Patients eligible for the dose escalation phase must meet the following criteria: Histologically confirmed non-small cell lung cancer (NSCLC) Suitable for curative radical treatment but ineligible for Platinum chemotherapy. **Dose Expansion Phase:** The criteria for the dose expansion phase will be determined and provided at a later time. **Exclusion criteria** <u>All patients</u> 1. Unstable ischaemic heart disease, cardiac dysrhythmias, coronary/peripheral artery bypass graft or cerebrovascular

Exclusion Criteria:	accident within six months prior to starting treatment. 2. Uncontrolled arterial hypertension despite medical treatment. 3. Ongoing congestive heart failure or cardiac dysrhythmias of NCI CTCAE Grade ≥2 or uncontrolled atrial fibrillation. 4. History of extensive disseminated/bilateral or known presence of Grade 3 or 4 interstitial fibrosis or interstitial lung disease, including a history of pneumonitis, hypersensitivity pneumonitis, interstitial pneumonia, interstitial lung disease (ILD), obliterative bronchiolitis, and pulmonary fibrosis. A history of prior radiation pneumonitis is allowed. 5. Any active central nervous system (CNS) lesion (i.e., those with radiographically unstable, symptomatic lesions) or leptomeningeal metastases. However, patients treated with stereotactic radiotherapy or surgery are eligible if the patient remains without evidence of CNS disease progression ≥ 3 months. Patients must be off corticosteroid therapy for ≥ 3 weeks.

	6. Patients who have neuromuscular disorders that are associated with elevated CK. (e.g., inflammatory myopathies, muscular dystrophy, amyotrophic lateral sclerosis, spinal muscular atrophy) 7. Carcinomatous meningitis or leptomeningeal disease. 8. History of hypoalbuminemia, or patients with peritoneal disease or pleural disease, where there is a requirement for ascitic or pleural taps. 9. History of retinal vein occlusion, intraocular pressure > 21 mmHg or patient considered at risk of retinal vein thrombosis (e.g., history of hyper viscosity or hypercoagulability syndromes). 10. History of retinal degenerative disease. 11. History of Gilbert's syndrome.

	12. Active infections (including chronic hepatitis type B or C and HIV infection if status known), severe immunologic defect, compromised bone marrow function. 13. Other severe acute or chronic medical (including severe gastro-intestinal disorders, e.g., partial bowel obstruction, malabsorption, active inflammatory bowel disease) or psychiatric conditions or laboratory abnormalities that the investigator considers would make the patient a poor trial candidate would impart excess risk associated with the study participation or drug administration or could interfere with protocol compliance or the interpretation of trial results. 14. Patients who have undergone major surgery ≤ 3 weeks prior to starting the study drug or who have not recovered from side effects of such procedure. 15. Use drugs or foods known as potent CYP3A4 inhibitors or inhibitors or are CYP3A4 substrates with narrow therapeutic indices.

	16. Previous Thoracic radiotherapy (except for palliative reasons), endocrine therapy, immunotherapy, or chemotherapy during the previous four weeks (six weeks for nitrosoureas, Mitomycin-C) and four weeks for investigational medicinal products before treatment. Patients with prostate cancer may continue to receive endocrine therapy to maintain castrate levels of androgens. 17. Resting ECG with QTc > 480msec at two or more time points within 24 hours (using Fredericia correction). 18. Requirement for medication known to prolong QT interval. 19. History of other malignancy less than two years before the diagnosis of current cancer, EXCLUDING the following: non-melanoma skin cancer, in situ carcinoma of the cervix treated surgically with curative intent, other malignant tumours that have been treated curatively and the patient is deemed disease-free. 20. Women with the ability to become pregnant (or already pregnant or lactating). However, those female patients who

	have a negative serum pregnancy test before enrolment and agree to use one highly effective form of contraception (oral, injected or implanted hormonal contraception or intra-uterine device) in addition to condom plus spermicide for four weeks before entering the trial, during the trial and for six months afterwards are considered eligible. 21. Male patients with partners of child-bearing potential (unless they agree to take measures not to father children by using one form of highly effective contraception, including oral, injected, or implanted hormonal contraception or intra-uterine device) in addition to condom plus spermicide during the trial and for six months afterwards). Men with pregnant or lactating partners should be advised to use barrier method contraception (condom plus spermicidal gel) to prevent exposure to the foetus or neonate. 22. Prior exposure to any *AURKA* inhibitor. 23. Patients who cannot have IV medication
Trial Dose and Administration:	**Dose Escalation Phase:** This non-randomised study will enrol eligible patients diagnosed

	with non-small cell lung cancer (NSCLC) and planned for radical radiotherapy. Following completion of the screening process, patients will receive intravenous (IV) Barasertib at five escalating doses: 25 mg, 50 mg, 100 mg, 150 mg, and 225 mg, administered over 48 hours. **Dose Expansion Phase:** In the dose expansion cohort, patients with NSCLC tumours will be recruited. The recommended phase II (RPII) dose and schedule of Barasertib in combination with fractionated radiotherapy will be employed in this study. No randomization or dose escalation will occur during this phase; however, dose reduction or delay may be allowed in the event of toxicities. Computed tomography (CT) imaging will be conducted every eight weeks throughout the study until patients either withdraw from the study, cannot tolerate the therapy, or experience disease progression, as defined by Response Evaluation Criteria in Solid Tumours (RECIST) version 1.1 or clinical assessment.
Study Duration:	Patients will continue on the study (with appropriate dose delay and modification if necessary) until intolerable side effects or if they choose to withdraw.
Study Procedures and Frequency:	**Dose escalation phase:** Detailed adverse event monitoring will be conducted according to

	CTCAE v5.0. The dose-limiting toxicity (DLT) is defined as any adverse event or laboratory abnormality considered to be related to a combination of Aurora Kinase inhibitor and radiotherapy related to the treatment during radiotherapy. **Dose expansion phase:** TBA
Patient care post-trial:	<u>Follow-up Visits:</u> Scheduled follow-up visits will be arranged to assess the patient's condition and monitor potential long-term effects or outcomes. The frequency and duration of follow-up visits will be determined based on the specific requirements of the trial protocol and the individual patient's needs. <u>Monitoring of Adverse Events:</u> Ongoing monitoring of adverse events or treatment-related complications will be conducted during the post-trial period. Timely detection, assessment, and management of adverse events will be prioritized to ensure patient safety and well-being.

	Disease Monitoring: Continuation or implementation of disease monitoring procedures may be necessary to evaluate the patient's response to treatment and disease progression. Imaging tests, laboratory assessments, or other diagnostic procedures may be performed to monitor disease status and guide further management decisions. Supportive Care: The provision of supportive care measures may be recommended based on the patient's specific needs and treatment outcomes. This may include supportive therapies, rehabilitation programs, pain management, or psychological support to optimize the patient's quality of life and overall well-being. Referral to Specialists: If required, patients may be referred to appropriate specialists or healthcare providers for specialized care or further management of any treatment-related complications or long-term effects.
Criteria for evaluation:	See below
Efficacy	Disease status will be monitored according to RECIST version 1.1.

Safety	Safety and toxicity will be reported using NCI CTCAE (currently version 5.0.)
Pharmacokinetic Assays:	1. Sample Collection: Blood samples will be collected from enrolled patients at designated time points. The timing and frequency of sample collection will be determined based on the specific requirements of the study protocol. Samples may be collected before dosing, at various time intervals after dosing, and during the post-dose period. 2. Analytical Techniques: State-of-the-art analytical techniques will be employed to measure the concentrations of the Aurora Kinase inhibitor in the collected blood samples. These techniques may include high-performance liquid chromatography (HPLC), liquid chromatography-mass spectrometry (LC-MS), or other validated methods. The selected analytical method will ensure accurate and reliable quantification of the drug levels in the samples. 3. Pharmacokinetic Parameters:

	Pharmacokinetic parameters, such as maximum plasma concentration (Cmax), time to reach Cmax (Tmax), the area under the plasma concentration-time curve (AUC), and elimination half-life (t½), will be calculated from the measured drug concentrations. These parameters provide insights into the absorption, distribution, metabolism, and elimination characteristics of the Aurora Kinase inhibitor within the body. 4. Data Analysis: The obtained pharmacokinetic data will be analysed using appropriate statistical and pharmacokinetic modelling techniques. The analysis will help characterize the pharmacokinetic profile of the Aurora Kinase inhibitor, including its absorption, distribution, metabolism, and excretion properties. Correlations between pharmacokinetic parameters and clinical outcomes, safety, or efficacy endpoints may be explored. 5. Reporting and Interpretation: The results of the pharmacokinetic assays will be reported and interpreted in the context of the study objectives. The findings will contribute to understanding the drug's behaviour in the body and inform decisions regarding dosing, administration,

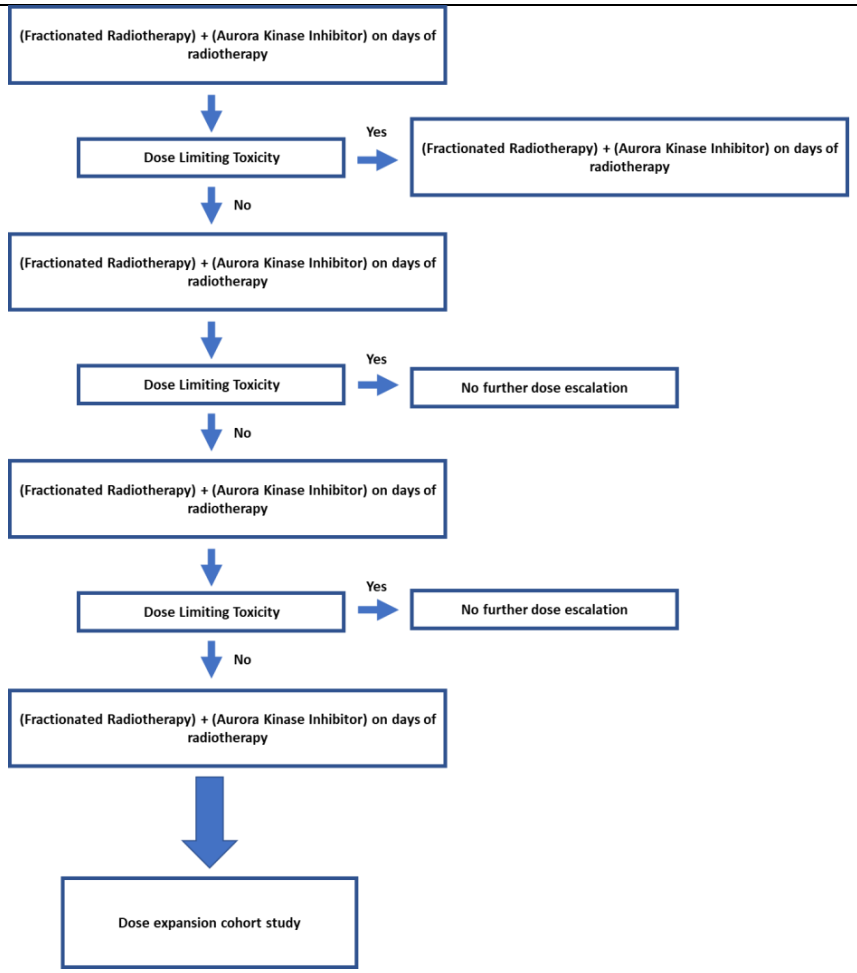
	and further clinical development.
Pharmacodynamic Assays:	1. Selection of Pharmacodynamic Biomarkers: Relevant pharmacodynamic biomarkers will be selected based on the mechanism of action of the Aurora Kinase inhibitor and the desired pharmacological effects. Biomarkers may include molecular markers, signalling pathway components, cellular markers, or other measurable indicators of drug activity or target engagement. Biomarkers will be selected based on their known or hypothesized correlation with drug response, treatment efficacy, or safety endpoints. 2. Sample Collection: Biological samples, such as tumour tissue, blood, or other relevant specimens, may be collected from enrolled patients for pharmacodynamic analysis. The timing and frequency of sample collection will be determined based on the study's specific objectives and the expected dynamics of the selected pharmacodynamic biomarkers. 3. Assay Techniques:

	State-of-the-art laboratory techniques will be employed to measure the pharmacodynamic biomarkers in the collected samples. These techniques may include immunohistochemistry (IHC), enzyme-linked immunosorbent assay (ELISA), polymerase chain reaction (PCR), Western blotting, flow cytometry, or other validated methods. The selected assay method will ensure accurate and reliable quantification or detection of the pharmacodynamic biomarkers. 4. <u>Data Analysis:</u> The pharmacodynamic data obtained from the assays will be analysed using appropriate statistical and analytical methods. Data analysis may involve comparisons between treatment groups, correlation analyses with clinical outcomes, or exploration of dose-response relationships. The goal is to gain insights into the drug's impact on the selected pharmacodynamic biomarkers and their relationship to therapeutic response or other relevant endpoints. 5. <u>Reporting and Interpretation:</u> The results of the pharmacodynamic assays will be reported and

	interpreted in the context of the study objectives. The findings will contribute to understanding the drug's mechanism of action, its effects on target pathways or cellular processes, and the potential correlation between pharmacodynamic biomarkers and clinical outcomes. Interpretation of the pharmacodynamic data will help inform decisions regarding dose selection, treatment response assessment, and potential biomarker-driven patient stratification.
Study Centre(s):	We plan to use at least four centre(s) for the dose escalation cohorts.
End of Study:	<u>Final Study Visit:</u> Participants will undergo a final study visit, which may include a comprehensive evaluation of their health status, clinical assessments, and data collection. This visit serves to gather any remaining study-related information and ensures the completion of all required study procedures. <u>Data Collection and Analysis:</u> All collected data will be compiled and analysed, including clinical, safety, efficacy, pharmacokinetic, and pharmacodynamic data. Statistical analyses and other appropriate methods will be applied to evaluate the study outcomes and address the research objectives.

	Study Report: A comprehensive study report will summarise the study's findings, outcomes, and conclusions. The report will include a detailed description of the study design, patient demographics, treatment outcomes, adverse events, pharmacokinetic and pharmacodynamic results, and any additional relevant data. The report will adhere to regulatory guidelines and scientific standards, providing a complete overview of the study's conduct and results. Ethical Considerations: Ethical considerations will be addressed, ensuring all applicable ethical guidelines and regulations are followed throughout the study. Study participants' rights, safety, and confidentiality will be respected and protected, and any necessary approvals or ethical clearances will be obtained. Dissemination of Results: The study findings may be disseminated through scientific

	publications, conference presentations, or other appropriate channels. The aim is to share the knowledge gained from the study with the scientific community, healthcare professionals, and the public, contributing to the advancement of medical knowledge and potential future treatment options. <u>Follow-up and Long-Term Monitoring:</u> Depending on the study outcomes and specific requirements, participants may be offered long-term follow-up or monitoring to assess any potential late effects or treatment-related sequelae. This follow-up may include periodic visits, diagnostic tests, or other assessments as deemed necessary to ensure ongoing patient care and safety.
Publication Policy:	The results of this study will be published in a peer-reviewed scientific journal and presented in an academic research meeting.
Trial Schema:	Aurora Kinase inhibitor in combination with radiotherapy


(Fractionated Radiotherapy) + (Aurora Kinase Inhibitor) on days of radiotherapy
Dose Limiting Toxicity
Yes
(Fractionated Radiotherapy) + (Aurora Kinase Inhibitor) on days of radiotherapy
No
(Fractionated Radiotherapy) + (Aurora Kinase Inhibitor) on days of radiotherapy
Dose Limiting Toxicity
Yes
No further dose escalation
No
(Fractionated Radiotherapy) + (Aurora Kinase Inhibitor) on days of radiotherapy
Dose Limiting Toxicity
Yes
No further dose escalation
No
(Fractionated Radiotherapy) + (Aurora Kinase Inhibitor) on days of radiotherapy
Dose expansion cohort study

7.3.2 Summary Schedule of events:

7.3.2.1 Dose escalation phase:

Visit Description	Screening	Aurora Kinase Inhibitor concurrent with radiotherapy 66 Gy in 33 fractions					End of treatment	Post end of treatment	Follow up
Visit No	1	2	3	4	5	6			
Day		D1	D8	D15	D21	D28		6 weeks after end of Radiotherapy	
Informed Consent	X								
Demographics and History	X								
Concomitant medication	X	X	X	X	X	X	X	X	
ECOG	X	X	X	X	X	X	X	X	
Physical examination	X	X		X		X	X	X	
Tumour assessment	X								
Vital signs	X	X	X	X	X	X	X	X	
Height and Weight	X	X	X	X				X	
Ophthalmic exam	X	X			X		X	X	
Haematology and Clinical chemistry bloods	X	X	X	X	X	X	X	X	
Urinalysis	X	X	X	X	X			X	
Pregnancy Tests	X	X						X	
12 Lead ECG	X	X	x	X	x	X	X	X	
ECHO/MUGA	X	X					x		
Inclusion/Exclusion criteria	X								
Tumour Marker	X								
PK 24 hour Profile									
PK trough									
PD PBMC/plasma									
AE review		X	X	X	X	X	x	x	x
Aurora Kinase Inhibitor administration	Continuous administration or Days 1-21								
Survival data (PFS and OS)									x
Biological studies									
Tumour AURKA expression	X								
Blood AURKA expression	X								
Mitotic index	X								
Spindle Alignment	X								
Angiogenisis Markers	X								

Table 7-1: Schedule demonstrating the timing of Barasertib use in the dose escalation phase between day 1 to day 28.

7.3.2.2 Dose Expansion phase:

Visit Description	Screening	Aurora Kinase Inhibitor concurrent with radiotherapy 66 Gy in 33 fractions					End of treatment	Post end of treatment	Follow up
Visit No	1	2	3	4	5	6			
Day		D1	D8	D15	D21	D28		6 weeks after end of Radiotherapy	
Informed Consent	X								
Demographics and History	X								
Concomitant medication	X	X	X	X	X	X	X	X	
ECOG	X	X	X	X	X	X	X	X	
Physical examination	X	X		X		X	X	X	
Tumour assessment	X								
Vital signs	X	X	X	X	X	X	X	X	
Height and Weight	X	X	X	X				X	
Ophthalmic exam	X	X			X		X	X	
Haematology and Clinical chemistry bloods	X	X	X	X	X	X	X	X	
Urinalysis	X	X	X	X	X			X	
Pregnancy Tests	X	X						X	
12 Lead ECG	X	X	x	X	x	X	X	X	
ECHO/MUGA	X	X							
Inclusion/Exclusion criteria	X								
Tumour Marker	X								
PK 24 hour Profile									
PK trough									
PD PBMC/plasma									
AE review		X	X	X	X	X	x	x	x
Aurora Kinase Inhibitor administration	Continuous administration or Days 1-21								
Survival data (PFS and OS)									
Biological studies									
Tumour AURKA expression	X								
Blood AURKA expression	X								
Mitotic index	X								
Spindle Alignment	X								
Angiogenisis Markers	X								

Table 7-2: The dose expansion phase

7.3.3 Introduction

7.3.3.1 Background:

Disease background:

Lung cancer is a global problem. It is the most common cancer diagnosed as well as the leading cause of cancer mortality worldwide. (Barta et al., 2019) In 2018, over 2 million new cancer cases were, making up just around eleven per cent of the most common cancers diagnosed globally. (Bray et al., 2018) The trend in incidence for both men and women are declining. Correspondingly, there were 1.7 million deaths from lung cancer; it is the most common cause of cancer death in men, while in women, it is second only to breast cancer in terms of mortality.

Treatment background:

In the United Kingdom, the decision to proceed with curative or palliative therapy is *mad*e in a Multidisciplinary Meeting (MDT). Patients will have had a Computed Tomography scan (CT), Positron Emitted Computed Tomography scan (PET CT), Lung Function testing, a CT-guided biopsy and, if indicated, an Endobronchial Ultrasound (EBUS).

Patients who are chosen to be treated with curative intent are usually offered radical surgery; these patients will need to have early-stage disease and should be clinically fit for radical treatment. Adjuvant radiotherapy is offered if there is margin positivity,

while adjuvant chemotherapy is given to patients with good performance status (WHO 0 or 1) and T1a–4, N1–2, M0 NSCLC. Adjuvant therapy can also be considered in patients with good performance status (WHO 0 or 1) and T2b–4, N0, M0 NSCLC with tumours greater than 4 cm in diameter.

The surgical options range from a wedge resection, segmentectomy or lobectomy to more extensive surgery (pneumonectomy) in patients where clear margins are needed. As most patients present with advanced disease, they are not fit for radical surgery; if they are deemed fit for curative treatment, the options would be radiotherapy alone or chemoradiotherapy.

Radiotherapy doses and fractionations vary across the UK and with general guidance from the Royal College of Radiology (RCR). Usually, the minimum dose offered to radical patients is 55 Gy in 20 fractions up to 66 Gy in 33 fractions given concurrently with chemotherapy (a platinum agent in addition to vinorelbine).

7.3.4 Investigational Medicinal Products (IMP) used in the study:

The investigational medicinal product (IMP) utilized in this study is Barasertib. Barasertib is an IV-administered small molecule inhibitor that explicitly targets Aurora Kinase enzymes, including Aurora Kinase A and B. It has demonstrated potential as an anticancer agent in preclinical and early clinical studies. The IMP will be provided in the form of a pharmaceutical formulation developed explicitly for this study. The formulation will be prepared and labelled according to Good Manufacturing Practice (GMP) guidelines to ensure quality, consistency, and traceability.

Dosage and administration instructions for Barasertib will be clearly specified in the study protocol. Participants will receive the IMP according to the assigned treatment regimen, as determined by the study design (e.g., dose escalation or dose expansion phase). The IMP administration will be supervised by qualified healthcare professionals to ensure compliance with the study protocol and to monitor any potential adverse reactions or interactions. Compliance with the scheduled IMP administration will be closely monitored throughout the study.

Storage and handling procedures for Barasertib will adhere to appropriate regulations and guidelines. The IMP will be stored under the recommended storage conditions, such as temperature, humidity, and light exposure, to maintain its stability and integrity. Documentation of IMP usage, including accountability, dispensing, and reconciliation, will be meticulously maintained in accordance with regulatory requirements. Proper recording of IMP administration, adherence, and any relevant deviations will be carried out to ensure accurate data collection and analysis.

An authorized sponsor or manufacturer will supply the IMP, and its provision will comply with applicable regulatory and ethical guidelines. Any necessary approvals or

permissions required for the use of Barasertib as an investigational medicinal product will be obtained prior to the initiation of the study.

7.3.5 The rationale for the study:

a. Non-Small Cell Lung Cancer (NSCLC) Treatment Challenges:

NSCLC is a prevalent form of lung cancer with significant morbidity and mortality rates.

Despite advances in treatment options, there remains a need for more effective therapeutic strategies.

The combination of Aurora Kinase inhibitors with fractionated radiotherapy has shown promise in preclinical studies, warranting further exploration in clinical trials.

b. Potential Synergistic Effects:

Aurora Kinases play crucial roles in cell division and are frequently overexpressed in cancer, including NSCLC.

Inhibition of Aurora Kinases has shown the potential to disrupt tumour growth and enhance sensitivity to radiotherapy.

Combining an Aurora Kinase inhibitor with fractionated radiotherapy may have synergistic effects, leading to improved treatment outcomes.

c. Safety and Toxicity Profile:

Assessing the safety and toxicity profile of the combined treatment is essential to determine its feasibility and tolerability.

Understanding the potential adverse effects and their management is critical for optimizing patient care and treatment decisions.

d. Maximum Tolerated Dose (MTD) and Recommended Phase II (RPII) Dose:

Identifying the combination therapy's maximum tolerated dose (MTD) is necessary to establish the optimal dose range for further investigation.

Determining the recommended phase II (RPII) dose and schedule is crucial for designing subsequent efficacy studies.

e. Pharmacokinetic and Pharmacodynamic Considerations:

Investigating the Aurora Kinase inhibitor's pharmacokinetic properties and its interaction with radiotherapy can provide insights into drug exposure, distribution, metabolism, and elimination.

Exploring pharmacodynamic biomarkers can help assess the combination therapy's target engagement and biological effects.

f. Preliminary Efficacy Assessment:

A preliminary evaluation of the efficacy of the RPII dose of the combined therapy will provide initial indications of its potential clinical benefits.

Assessing the response to treatment and disease control will guide future research and inform clinical decision-making.

By conducting this study, we aim to contribute to understanding the safety, tolerability, pharmacokinetics, and preliminary efficacy of the combined Aurora Kinase inhibitor and fractionated radiotherapy in patients with NSCLC. The results of this study may provide valuable insights for developing more effective treatment approaches and potentially improving patient outcomes.

7.3.6 The primary hypothesis of the trial:

The combination of an Aurora Kinase inhibitor with fractionated radiotherapy is safe and tolerable in patients with Non-Small Cell Lung Cancer (NSCLC) and will establish the maximum tolerated dose (MTD) of the combination therapy.

7.3.7 Trial Design:

7.3.7.1 Outline:

This phase one study will combine a novel agent, Barasertib, with standard fractionated radical radiotherapy. The study design for this non-randomized phase I trial involves a dose escalation phase followed by a dose expansion phase. The Continual Reassessment Method (CRM) will be employed as the dose-finding approach to efficiently determine the maximum tolerated dose (MTD) of the combination therapy while minimizing the exposure of patients to suboptimal or toxic doses.

There will be an initial dose escalation phase using patients with NSCLC fit for radical radiotherapy, combining it with Barasertib. This will be followed by a dose expansion phase, recruiting patients with the RPII dose determined from the phase one study and combining it with the standard radiotherapy dose.

7.3.7.2 Treatment Schedule and Duration:

Up to 30 patients will be recruited to determine the RP2D and to enable evaluation of clinical activity, assuming five dose levels to be investigated. Early stopping rules will be incorporated to stop early should a sufficient number of patients being treated at the MTD with no DLTs observed. The time-to-event methodology will be used to consider longer-term toxicities while enabling the trial to continue recruitment during DLT follow-up periods.

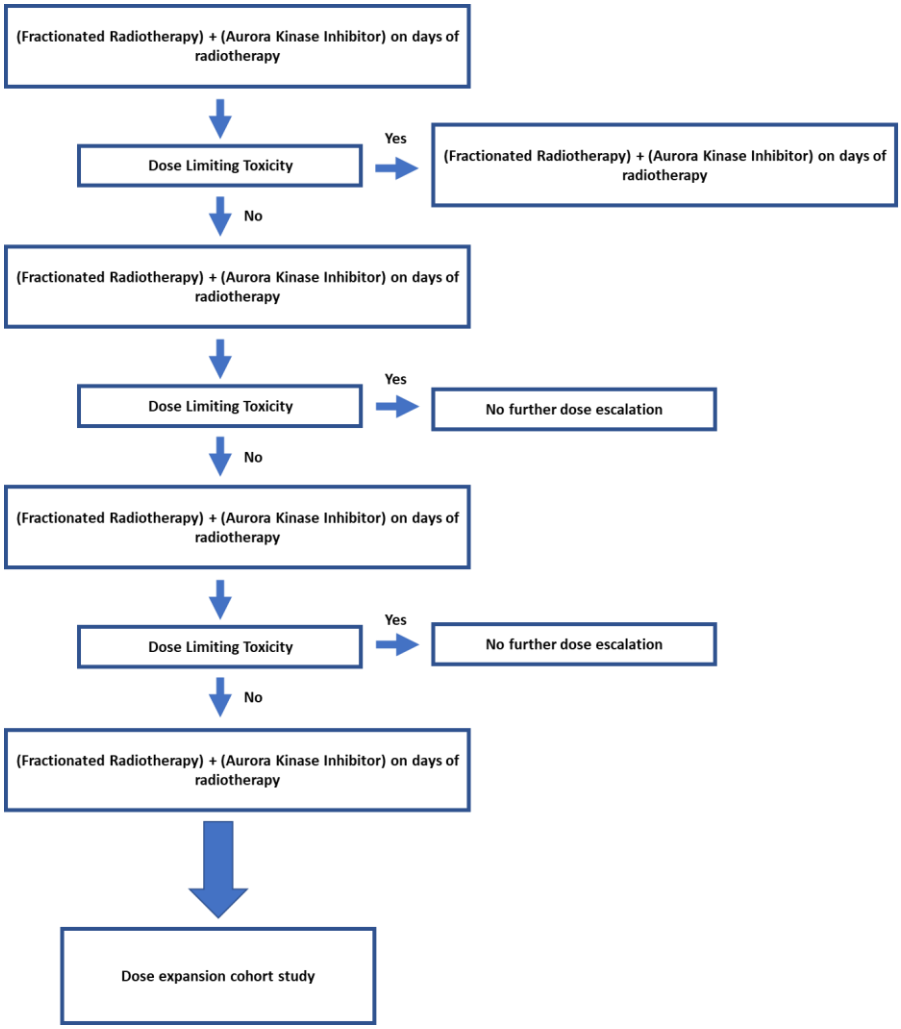


Figure 3: Schema of the combination trial examining Barasertib and fractionated radiotherapy

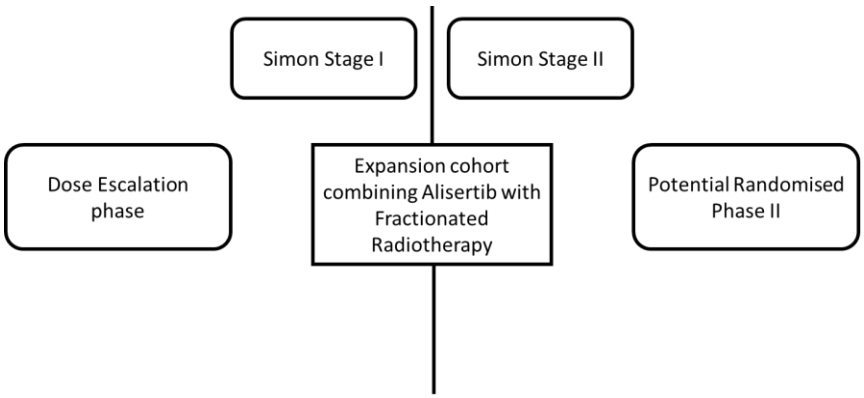
7.3.7.3 Dose levels:

Dose level	(Insert Aurora Kinase inhibitor)
1	25 mg OD
2	50 mg OD

3	100 mg OD
4	150 mg OD
5	225 mg OD

Dose level assignment will be based on the number of patients currently enrolled in the cohort, the number of dose-limiting toxicities observed, and the number of patients at risk for developing DLT. Once the MTD has been defined, dosing at a higher level must not occur.

7.3.7.4 The dose expansion phase of the study:



Following the completion of the dose escalation phase, a dose expansion cohort will be initiated to evaluate further the recommended phase II (RPII) dose and schedule of the combination therapy. Unlike the dose escalation phase, the dose expansion phase does not involve randomization or further dose escalation. Instead, it aims to

assess the treatment efficacy and safety at the RPII dose level. The dose expansion cohort will consist of a predefined number of patients with NSCLC tumours who meet the inclusion criteria for the study. These patients will be enrolled at the RPII dose determined from the dose escalation phase.

The primary objective of the dose expansion phase is to investigate the response to treatment with the RPII dose of the combination therapy. This will involve assessing the tumour response using appropriate imaging techniques, such as CT imaging, according to the RECIST v1.1 criteria. The objective is to determine the combination therapy's efficacy in tumour regression, stabilization, or progression.

In addition to assessing treatment response, the dose expansion phase will also aim to evaluate further the safety and tolerability profile of the combination therapy. Adverse events and treatment-related toxicities will be closely monitored, and dose reductions or delays may be allowed to manage any observed toxicities while maintaining treatment efficacy.

Regular follow-up visits will be scheduled throughout the dose-expansion phase to monitor the patient's overall health, disease progression, and treatment-related outcomes. The frequency and duration of these visits will be determined based on the study protocol and standard clinical practice.

The data collected during the dose expansion phase will provide valuable insights into the treatment efficacy, safety, and tolerability of the combination therapy at the RPII dose level. These findings will contribute to a comprehensive assessment of the potential benefits and risks associated with the therapy and inform future clinical decision-making.

7.3.8 Projected Number of Subjects:

The study will be conducted in at least four UK centres for the dose escalation phase, increasing to 30 for the dose expansion phase. It was anticipated that up to 30 patients would be required for the initial dose escalation.

For the dose expansion phase of the study, it is anticipated that 30 patients will be required, bringing the expected total patient number for the trial to between 50 and 70, not counting any replacements.

7.3.9 Replacement of Subjects:

In the event that a participant enrolled in the study withdraws their consent, is unable to comply with the study requirements, or experiences a significant protocol deviation, a process for subject replacement will be implemented. The replacement of subjects will be carried out following predefined guidelines and ethical considerations.

The decision to replace a subject will be *mad*e in consultation with the principal investigator and the study team, taking into account the specific circumstances and reasons for subject withdrawal or exclusion. Every effort will be *mad*e to maintain an appropriate sample size and ensure the integrity of the study results.

Subject replacement will be conducted systematically and transparently. Potential replacement subjects will be identified from the eligible patients who meet the inclusion and exclusion criteria. The replacement subjects will undergo the same screening and evaluation procedures as the original subjects to ensure they meet all the requirements for study participation.

It is important to note that the replacement of subjects will only occur when it is deemed necessary to maintain the statistical power, scientific validity, and generalizability of the study findings. The process will be carried out in accordance with applicable regulatory guidelines, institutional policies, and ethical considerations to safeguard the rights and well-being of all participants.

Efforts will be *mad*e to minimize any potential bias or confounding effects resulting from subject replacement. The replacement subjects will be enrolled and treated under similar conditions as the original subjects, and their data will be included in the final analysis to contribute to the overall study outcomes.

Regular monitoring and documentation of subject replacement will be conducted throughout the course of the study, ensuring transparency, accountability, and adherence to established protocols. Any replacement subjects will be clearly identified, and the reasons for their inclusion will be recorded and reported in the study documentation.

The process of subject replacement will be conducted with utmost care and consideration for ethical principles, scientific rigour, and patient safety. It is intended to ensure the completeness and validity of the study results and maintain the overall integrity of the research endeavour.

7.3.10 Post-trial care and follow-up:

Upon completion of the trial, appropriate post-trial care and follow-up will be provided to the study participants to ensure their well-being and continuity of care. The post-trial care plan will be designed in accordance with ethical guidelines, regulatory requirements, and standard clinical practice.

The post-trial care and follow-up will include the following components:

a. Transition of Care: Participants will be provided with a clear plan for their care transition to their primary healthcare providers or appropriate specialists. This will ensure that ongoing medical needs or follow-up requirements are promptly addressed.

b. Monitoring of Adverse Events: Any adverse events or treatment-related complications that arise after the completion of the trial will be carefully monitored and managed. Participants will be educated on the signs and symptoms to watch for and will be encouraged to report any concerns to their healthcare providers.

c. Long-Term Follow-up: A schedule for long-term follow-up visits may be established depending on the nature of the study intervention and the potential long-term effects. These visits will aim to assess the durability of treatment response, monitor late-onset adverse events, and evaluate the overall long-term outcomes of the study intervention.

d. Access to Investigational Medicinal Products (IMP): If the study intervention involves investigational medicinal products, provisions may be *mad*e for continued access to these products if deemed appropriate and permitted by regulatory authorities. This will be done in compliance with applicable regulations and guidelines to ensure patient safety and ethical considerations.

e. Supportive Care and Counselling: Participants may be provided with resources, information, and support services to address any physical, psychological, or emotional needs that may arise post-trial. This can include referrals to appropriate support groups, counselling services, or access to educational materials.

f. Data Analysis and Reporting: The collected data will be analysed, and the study findings will be summarized and reported to protect the participants' privacy and confidentiality. Participants may have the opportunity to receive

summary study results upon request, in line with applicable regulations and ethical considerations.

7.3.11 Objectives and Endpoints:

7.3.11.1 Primary Objectives:

1. To assess the safety and toxicity profile of the combination therapy using the National Cancer Institute's Common Terminology Criteria for Adverse Events (NCI CTCAE) version 5.0.

2. To determine the combination therapy's maximum tolerated dose (MTD) during the dose escalation phase.

7.3.11.2 Primary Endpoint:

1. Incidence and severity of treatment-related adverse events and toxicities.

2. Identification of the MTD based on the occurrence of dose-limiting toxicities (DLTs).

7.3.11.3 Secondary Objectives:

1. To define the recommended phase II (RPII) dose and schedule of the combination therapy for the dose expansion phase.

2. To investigate the pharmacokinetics (PK) of the combination therapy.

3. To investigate pharmacodynamic (PD) biomarkers of the combination therapy in tumour samples (where possible).

4. To preliminarily assess the efficacy of the RPII dose of the combination therapy.

1.1.1.1 Secondary Endpoint:

1. Identification of the RPII dose based on an acceptable balance between efficacy and safety.

2. Assessment of drug absorption, distribution, metabolism, and elimination profiles through plasma concentration measurements.

3. Analysis of molecular pathways, target inhibition, and downstream signalling pathways to assess the pharmacodynamic effects of the combination therapy.

4. Secondary Endpoint: Evaluation of tumour response, progression-free survival, and overall survival rates in patients receiving the RPII dose.

7.3.11.4 Exploratory Objectives:

1. To explore additional safety and tolerability parameters beyond the primary endpoints.
2. To explore potential biomarkers or predictive factors associated with treatment response or toxicity.

7.3.11.5 Exploratory Endpoint:

1. Evaluation of specific adverse events, laboratory abnormalities, and treatment-related complications.
2.
3. Identification of biomarkers or genetic markers that may correlate with treatment response or adverse reactions.

7.3.12 Inclusion Criteria:

All Patients:

1. Age 16 years or older

2. Eastern Cooperative Oncology Group (ECOG) performance status of 0-1

3. Adequate respiratory function assessed by FEV1 > 1L and/or DLCO > 40%

4. Left ventricular ejection fraction (LVEF) ≥ 50% determined by multigated acquisition (MUGA) scan or echocardiogram

5. Capacity to provide informed consent and comply with the study protocol

6. Haematological and biochemical indices within specified ranges:

7. Haemoglobin (Hb) ≥ 9g/dL (transfusion allowed to achieve this)

Neutrophils ≥ 1,500/μL

Platelet count ≥ 100,000/μL

AST or ALT ≤ 2.5 x upper limit of normal (ULN)

Alkaline phosphatase ≤ -5 x ULN

Serum bilirubin ≤ 1.5 x ULN

Creatinine clearance ≥ 50 mL/min (calculated by Cockcroft Gault equation or EDTA)

8. Ability to swallow oral medication

9. Expected life expectancy of at least three months

Dose Escalation Phase:

Patients eligible for the dose escalation phase must meet the following criteria:

1. Histologically confirmed non-small cell lung cancer (NSCLC)
2. Suitable for curative radical treatment but ineligible for Platinum chemotherapy.

Dose Expansion Phase:

The criteria for the dose expansion phase will be determined and provided at a later time.

7.3.13 Exclusion criteria:

All patients

1. Unstable ischaemic heart disease, cardiac dysrhythmias, coronary/peripheral artery bypass graft or cerebrovascular accident within six months prior to starting treatment.

2. Uncontrolled arterial hypertension despite medical treatment.

3. Ongoing congestive heart failure or cardiac dysrhythmias of NCI CTCAE Grade ≥2 or uncontrolled atrial fibrillation.

4. History of extensive disseminated/bilateral or known presence of Grade 3 or 4 interstitial fibrosis or interstitial lung disease, including a history of pneumonitis, hypersensitivity pneumonitis, interstitial pneumonia, interstitial lung disease (ILD), obliterative bronchiolitis, pulmonary fibrosis. A history of prior radiation pneumonitis is allowed.

5. Any active central nervous system (CNS) lesion (i.e., those with radiographically unstable, symptomatic lesions) and leptomeningeal metastases. However, patients treated with stereotactic radiotherapy or surgery are eligible if the patient remains without evidence of CNS disease progression ≥ 3 months. Patients must be off corticosteroid therapy for ≥ 3 weeks.

6. Patients who have neuromuscular disorders that are associated with elevated CK. (e.g., inflammatory myopathies, muscular dystrophy, amyotrophic lateral sclerosis, spinal muscular atrophy)

7. Carcinomatous meningitis or leptomeningeal disease.

8. History of hypoalbuminemia, or patients with peritoneal disease or pleural disease, where there is a requirement for ascitic or pleural taps.

9. History of retinal vein occlusion, intraocular pressure > 21 mmHg or patient considered at risk of retinal vein thrombosis (e.g., history of hyper viscosity or hypercoagulability syndromes).

10. History of retinal degenerative disease.

11. History of Gilbert's syndrome.

12. Active infections (including chronic hepatitis type B or C and HIV infection if status known), severe immunologic defect, compromised bone marrow function.

13. Other severe acute or chronic medical (including severe gastro-intestinal disorders, e.g., partial bowel obstruction, malabsorption, active inflammatory bowel disease) or psychiatric conditions or laboratory abnormalities that the investigator

considers would make the patient a poor trial candidate would impart excess risk associated with study participation or drug administration or could interfere with protocol compliance or the interpretation of trial results.

14. Patients who have undergone major surgery ≤ 3 weeks prior to starting the study drug or who have not recovered from side effects of such procedure.

15. Use drugs or foods known as potent CYP3A4 inhibitors or inhibitors or are CYP3A4 substrates with narrow therapeutic indices.

16. Previous Thoracic radiotherapy (except for palliative reasons), endocrine therapy, immunotherapy, or chemotherapy during the previous four weeks (six weeks for nitrosoureas, Mitomycin-C) and four weeks for investigational medicinal products before treatment. Patients with prostate cancer may continue to receive endocrine therapy to maintain castrate levels of androgens.

17. Resting ECG with QTc > 480msec at two or more time points within 24 hours (using Fredericia correction).

18. Requirement for medication known to prolong QT interval

19. History of other malignancy less than two years before the diagnosis of current cancer, EXCLUDING the following: non-melanoma skin cancer, in situ carcinoma of the cervix treated surgically with curative intent, other malignant tumours that have been treated curatively and the patient is deemed disease-free.

20. Women with the ability to become pregnant (or already pregnant or lactating). However, those female patients who have a negative serum pregnancy test before enrolment and agree to use one highly effective form of contraception (oral, injected or implanted hormonal contraception or intra-uterine device) in addition to condom plus spermicide for four weeks before entering the trial, during the trial and for six months afterwards are considered eligible.

21. Male patients with partners of child-bearing potential (unless they agree to take measures not to father children by using one form of highly effective contraception, including oral, injected, or implanted hormonal contraception or intra-uterine device) in addition to condom plus spermicide during the trial and for six months afterwards). Men with pregnant or lactating partners should be advised to use barrier method contraception (condom plus spermicidal gel) to prevent exposure to the foetus or neonate.

22. Prior exposure to any *AURKA* inhibitor.

24. Patients who cannot have IV medication.

7.3.14 Patient registration procedure:

Patients will be prospectively enrolled from the pool of individuals referred to oncology services at participating sites seeking management for their advanced solid cancers. A comprehensive screening log will be maintained to ensure thorough documentation and transparency, capturing all patients considered for study inclusion, including those subsequently excluded. The rationale for exclusion will be meticulously recorded on this form.

Upon consideration for study enrolment, the Principal Investigator or an authorized designee will verify each patient's eligibility, following a rigorous assessment process. Should any uncertainties arise regarding eligibility, the Chief Investigator will be consulted to ensure informed decisions are *mad*e. Details of any inquiries and the corresponding outcomes will be diligently documented on the registration/eligibility checklist.

After completing suitability checks and obtaining the necessary informed consent, both for trial participation and the collection of blood and tissue samples, site personnel will employ appropriate scanning procedures to electronically transmit the Registration Form, if applicable, to confirm the patient's eligibility officially. This procedural step ensures streamlined communication between the site and the trial office while maintaining patient confidentiality by excluding identifiable information.

7.3.15 Registration of patients:

Trial Office Registration by email to (email TBC) The patient will then be registered.

Once the Investigator/research nurse has a study number for the patient, they will be asked to provide the original Registration Form along with a copy of the histology report to the Trials office.

Trial Assessments and Procedures:

Pre-trial screening consent and procedure (dose-expansion phase only):

1. Written informed consent will be obtained to perform radical radiotherapy before seeking consent to the main study.

2. The patient must also have a biopsy confirmed NSCLC.

3. The Investigator must ensure that a copy of the relevant radiotherapy consent is obtained and held in the medical record.

4. Patients will only be eligible for the main study if they consent to undergo radical radiotherapy.

7.3.16 Informed consent for the main study:

Potential participants will be provided with an up-to-date and approved version of the patient information sheet, which contains comprehensive details about the study. In addition, they will receive explicit verbal explanations, ensuring a thorough understanding of the study's nature, protocol implications and constraints, known side effects, and potential risks associated with participation. It will be emphasized that participants have the autonomy to withdraw from the study at any time without prejudicing their future care and without the obligation to provide a reason for their decision. Adequate time, a minimum of 24 hours, will be granted for participants to consider the provided information carefully, and they will have the opportunity to seek clarification from the Investigator, their General Practitioner (GP), or other independent sources before making their participation decision.

To signify their voluntary participation, the participant and the Investigator (or a designated representative) will personally sign and date the currently approved version of the informed consent form in each other's presence. A copy of the information provided and the signed consent form will be provided to the participant, ensuring their access to the documented details. Moreover, a copy of the signed and dated consent form will be submitted to the trial office for central monitoring purposes, contributing to the overall oversight of the study.

7.3.17 Contraceptive/ Pregnancy counselling:

All participants must be advised on the need to use reliable methods of contraception during the study. The advice should include:

a. The acceptable methods include male or female sterilisation, implants, injectables, combined oral contraceptives, some intrauterine devices (IUDs), and abstinence.

b. Male patients with partners of child-bearing potential unless they agree to take measures not to father children by using one form of highly effective contraception (oral, injected or implanted hormonal contraception or intra-uterine device) in addition to condom plus spermicide during the trial and for six months afterwards).

c. Men with pregnant or lactating partners should be advised to use barrier method contraception (condom plus spermicidal gel) during the trial and for six months afterwards to prevent exposure to the foetus or neonate. A barrier method (condom with spermicide) should be used in addition to a highly effective form of contraception.

d. Males should continue to take these precautions for a minimum of (n) months after the last dose of the study drug.

e. Females should continue to take these precautions a minimum of (n) months after the last dose of the study drug.

f. That any pregnancy (also applies to females partners of male trial subjects) occurring within (n) months of the last administration of study drug / other trial intervention will be followed up, and the outcome of all pregnancies (spontaneous miscarriage, elective termination, normal birth or congenital abnormality) will be reported and followed up even if the participant is discontinued from the study.

7.3.18 Main screening: pre-dosing evaluations:

The following must be performed/obtained within 28 days before the patient receives the first administration of the study drug.

All patients:

a) Written informed consent
b) Demographic details

c) Medical history (including prior diagnosis, prior treatment, concomitant diseases, concomitant medications, therapies received by the patient within 28 days prior to cycle 1, day 1, and known ophthalmologic medical history).
d) ECOG Performance Status (PS)
e) Full physical examination
f) Clinical and radiological (CT chest, abdomen and pelvis) disease assessment
g) Vital signs (systolic/diastolic blood pressure, pulse, body temperature and respiratory rate), height and weight.
h) Ophthalmic assessment, including visual acuity, pressure, perimetry, slit lamp examination, fundoscopy with digital photography, and optical coherence tomography (OCT).
i) Blood for assessment of tumour markers (if appropriate)
j) Cardiac muscle/enzyme levels - CK and troponin
k) Urinalysis
l) Serum pregnancy test for women of childbearing potential.
m) 12-lead electrocardiogram
n) Echocardiography or MUGA
o) Review of inclusion and exclusion criteria
p) Safety blood laboratory examination
q) Haematology: haemoglobin, white blood cells (WBC) with differential count and platelets.
r) Clinical chemistry: sodium, potassium, calcium, phosphate, urea, creatinine, total protein, albumin, bilirubin, alkaline phosphatase (ALP), AST and ALT and LDH; Coagulation screen: APTT, PT)

Dose escalation phase:

a. Obtain archived tumour tissue for biomarker analysis.
b. Obtain fresh tumour biopsy for PD assessment, where additional consent has been given.

Dose expansion phase:

a. Obtain archived tumour tissue for biomarker analysis
b. Obtain baseline blood sample for circulating DNA

I. Evaluations during dosing:

Concurrent Treatment Day 1

All patients

a) ECOG PS
b) Record of concomitant medications
c) Full physical examination
d) Vital signs (systolic/diastolic blood pressure, pulse, body temperature) and weight.
e) Ophthalmic exam (fundoscopy)
f) ECG (12-lead)

g) Blood for assessment of haematology, clinical chemistry, cardiac/muscle enzymes - CK and troponin status and coagulation status.
h) Urinalysis
i) Serum or urine Human Chorionic Gonadotropin (HCG) pregnancy test for women of childbearing potential.
j) Plasma samples for biomarkers
k) Assessment of adverse events
l) Start dosing with Barasertib

Dose expansion phase only

TBA

Concurrent Treatment Day 8

a) ECOG PS
b) Record of concomitant medications
c) Vital signs (systolic/diastolic blood pressure, pulse, body temperature) and weight.
d) Blood for assessment of haematology, clinical chemistry, cardiac/muscle enzymes - CK and troponin status and coagulation status.
e) Urinalysis
f) 12 Lead ECG
g) Assessment of adverse events
h) Dosing with Barasertib

Concurrent Treatment Day 15

a) ECOG PS
b) Record of concomitant medications
c) Full physical examination
d) Vital signs (systolic/diastolic blood pressure, pulse, body temperature) and weight.
e) ECG (12-lead)
f) Blood for assessment of haematology, clinical chemistry, cardiac/muscle enzymes – CK and troponin status and coagulation status
g) Urinalysis
h) Assessment of adverse events
i) Dosing with Barasertib

Concurrent Treatment Day 21

a. ECOG PS
a) Record of concomitant medications
b) Full physical examination
c) Vital signs (systolic/diastolic blood pressure, pulse, body temperature) and weight.
d) Ophthalmologic exam (fundoscopy)
e) Blood for assessment of haematology, clinical chemistry, cardiac/muscle enzymes - CK and troponin status and coagulation status

f) 12 lead ECG

g) Assessment of adverse events

h) Dosing with Barasertib

Concurrent Treatment Day 28

a) ECOG PS

b) Record of concomitant medications

c) Full physical examination

d) Vital signs (systolic/diastolic blood pressure, pulse, body temperature) and weight.

e) ECG (12-lead)

f) Blood for assessment of haematology, clinical chemistry, cardiac/muscle enzymes – CK and troponin status and coagulation status

g) Assessment of adverse events

h) Dosing with Barasertib

II. End of treatment evaluations:

All patients

a) ECOG PS

b) Record of concomitant medications

c) Full physical examination

d) Assessment of adverse events

e) Vital signs (systolic/diastolic blood pressure, pulse, body temperature) and weight.

f) ECG (12-lead)

g) Urinalysis

h) Blood for cardiac/muscle enzymes - CK and troponin status

i) Blood for assessment of haematology, clinical chemistry, and coagulation status

j) Blood for assessment of tumour markers (if appropriate)

k) Tumour assessment: CT scan of chest/abdomen/pelvis using RECIST v1.1.

Dose expansion phase

TBA

III. Post-treatment follow-up – evaluations:

All patients

a) Assessment of adverse events

b) Record of post-trial therapy

c) Patients will be followed up for survival status (3 monthly x 4, 4 monthly x 4, 6 monthly x 4, then yearly) until death or study closure, whichever happens first.

Dose expansion phase

TBA

Evaluations on early withdrawal:

If the patient is withdrawn from treatment for any of the reasons indicated in the section below, a final off-study visit assessment should be performed 28 - 30 days after the last administration of Barasertib

The following assessments will be done:

a) ECOG PS
b) Record of concomitant medications
c) Full physical examination
d) Assessment of adverse events
e) Vital signs (systolic/diastolic blood pressure, pulse, body temperature) and weight.
f) ECG (12-lead)
g) Urinalysis
h) Blood for cardiac/muscle enzymes - CK and troponin status
i) Blood for assessment of haematology, clinical chemistry, and coagulation status

If the patient is withdrawn from the trial and declines attendance for a final off-study visit, then a withdrawal assessment should be performed, if possible, on the day the decision is *mad*e to take the patient off-study or as soon as possible. Telephone review is permitted in these circumstances. These patients will be followed up for progression and overall survival.

7.3.19 Early Patient Withdrawal:

Treatment Withdrawal:

During the course of the trial, a patient may withdraw early from treatment. This may happen for a number of reasons, including:

Unacceptable toxicity, including but not limited to:

1. Life-threatening grade 4 toxicity.
2. Repetition of non-life-threatening grade 4 toxicity despite per-protocol dose reduction.
3. Delay of a treatment cycle for more than three consecutive weeks beyond the due date.
4. A CT scan, X-ray, ultrasound, and clinical examination determine objective evidence of progressive disease.
5. A clinical decision by the investigator that continued participation in the trial is contrary to the patient's best interests.
6. The patient's decision to discontinue treatment (as opposed to participation in all aspects of the study)

When a patient stops treatment early, an 'End of Treatment' Form and any other relevant form (for example, an SAE form) should be completed.

The reason for withdrawing from treatment early should be clearly documented in the medical records.

An off study visit assessment should be performed, and the results of the evaluations and observations should be reported in the CRF.

7.3.20 Withdrawal of Consent:

Withdrawal of consent means that a patient wishes to withdraw from the study altogether. Under these circumstances, the site must document all relevant discussions in the patient notes and notify the Trials Office.

Under these conditions, ongoing SAEs require follow-up until resolution.

7.3.21 Patient evaluability and replacement:

Patients will not be replaced in the dose escalation phase if they come off treatment due to a DLT. If, however, a patient withdraws for reasons other than safety/toxicity prior to the end of the concurrent treatment, they will need to be replaced and will not

receive any further Barasertib; they may continue their radical radiotherapy as prescribed; this will need to be evaluated by the responsible clinician.

All withdrawn patients will no longer receive the study drug and will be followed up for progression-free and overall survival unless they withdraw their consent. In the dose expansion phase, non-evaluable patients for the primary endpoint of response to treatment will be replaced.

Samples for Laboratory Analysis:

1. Blood
2. Lung tissue

Investigational Medicinal Products:

Name of IMP(s): Barasertib

7.3.22 Treatment dose:

Dose escalation phase:

Following completion of the screening process, patients will receive intravenous (IV) Barasertib at five escalating doses: 25 mg, 50 mg, 100 mg, 150 mg, and 225 mg, administered over 48 hours.

Dose expansion phase:

Following completion of the screening process, patients will receive intravenous (IV) Barasertib at five escalating doses: 25 mg, 50 mg, 100 mg, 150 mg, and 225 mg, administered over 48 hours.

7.3.23 Duration of treatment:

Each participant's treatment duration will vary depending on their response, tolerability, and disease status. The treatment regimen consists of a combination of Barasertib and fractionated radiotherapy, administered according to the specified dose escalation and dose expansion phases. During the dose escalation phase, participants will receive the investigational medicinal product (IMP) Barasertib intravenously over 48 hours at five escalating doses (25 mg, 50 mg, 100 mg, 150 mg, and 225 mg). Each dose will be administered once, with a sufficient interval between dose levels to evaluate safety and tolerability.

In the dose expansion phase, participants will receive the recommended phase II (RPII) dose of Barasertib determined during the dose escalation phase. The specific treatment schedule and duration will be based on the established RPII dose and

individual participants' responses in accordance with the study protocol. The duration of treatment for each participant may continue until disease progression, unacceptable toxicity, withdrawal of consent, or completion of the planned treatment course as determined by the treating physician and as specified in the study protocol.

Regular assessments and monitoring will be conducted throughout treatment to evaluate safety, efficacy, and pharmacokinetic/pharmacodynamic parameters. The treatment duration for each participant will be carefully documented and recorded for analysis and reporting purposes.

7.3.24 Dose-limiting Toxicity (DLT):

Dose escalation and expansion phase:

The dose-limiting toxicity (DLT) and maximum tolerated dose (MTD) are defined using the National Cancer Institute (NCI) Common Terminology Criteria for Adverse Events (CTCAE) Version 50. DLTs identified during the first cycle will inform the decision to dose escalate through the increasing dose levels. A DLT is defined as an almost certainly or probably drug-related adverse event to Barasertib.

A dose-limiting toxicity (DLT) will be defined as follows:

All grade 3 or higher toxicities that occur during or within 30 days of completing radiation treatment will be considered “treatment-related”, with the exception of Symptoms that are related to cancer or other pathology (in the opinion of the treating physician)

1. Febrile neutropenia (even in the absence of hospitalisation)

2. Hematologic DLTs will be defined as either Grade 4 neutropenia lasting for ≥ 7 days in duration, any Grade 4 anaemia, any Grade 4 thrombocytopenia, or any Grade 5 hematologic toxicity. All patients will be evaluated for hematologic toxicity.

3. Any neurological toxicity of Grades 3, 4 or 5 will be considered a DLT, with the exception of 1) symptoms present prior to study enrolment and 2) expected sequelae of the neurosurgical procedure.

4. Grade 3 event of hypocalcaemia, hypophosphatemia, hypokalaemia, or hypomagnesemia lasting more than 24 hours without responding to medical therapy or responding to medical therapy and lasting more than 72 hours.

5. Grade 3 transaminase elevation is associated with ≥ grade 2 bilirubin elevation.

6. Non-hematologic dose-limiting toxicity will be defined as any Grade 3, 4 or 5 non-hematologic toxicity, with the specific exception of

7. Grade 3 nausea or Grade 3 vomiting that, in the opinion of the Investigator, occurs in the setting of inadequate compliance with supportive care measures and lasts for less than 48 hours.

8. Grade 3 diarrhoea, in the opinion of the Investigator, occurs in the setting of inadequate compliance with supportive care measures and lasts for less than 48 hours.

9. Grade 3 dehydration, in the opinion of the Investigator, occurs in the setting of inadequate compliance with supportive care measures and lasts for less than 48 hours.

10. Grade 3 acidosis or alkalosis responds to medical intervention by returning to ≤ Grade 2 within 48 hours.

11. Isolated Grade 3 elevation of liver function tests (LFTs) without associated clinical symptoms, lasting ≤ 14 days.

12. Grade 3 hypocalcaemia, hypokalaemia, hypomagnesemia, hyponatremia, or hypophosphatemia, which responds to medical intervention.

13. Grade 3 hypercholesterolemia

14. Grade 3 hypertriglyceridemia

15. Grade 3 alopecia

16. AE with a fatal outcome

7.3.25 Maximum Tolerated Dose (MTD)

Dose escalation phase:

The maximum tolerated dose (MTD) will be determined using the Continual Reassessment Method (CRM), a model-based dose-finding approach. The CRM is a

statistical algorithm that efficiently identifies the MTD by incorporating both safety and efficacy data from each participant, adapting the dose levels based on the observed toxicities. In the dose escalation phase, the CRM will guide the selection of dose levels for subsequent participants, considering the toxicity outcomes observed in previous participants. The initial dose level will be determined based on preclinical data and available clinical information. As each participant completes their treatment, their individual toxicity data will be analysed, and the next dose level for subsequent participants will be determined by the CRM, aiming to find the MTD with the fewest participants exposed to suboptimal or toxic doses.

The CRM adjusts the dose escalation or de-escalation probability based on the observed toxicities, ensuring a balance between safety and dose optimization. The escalation or de-escalation decisions are *mad*e based on predefined rules and statistical modelling, incorporating information from all participants enrolled in the study. This iterative process continues until the MTD is estimated with high confidence. Determining the MTD using the CRM method allows for identifying a dose level that maximizes the therapeutic effect while minimizing the risk of dose-limiting toxicities. The MTD will serve as a crucial reference point for subsequent phases of the study, including the dose-expansion phase, where the recommended phase II (RPII) dose will be administered to assess efficacy and further evaluate safety.

Throughout the trial, the CRM will be rigorously applied to ensure the optimal dose escalation and expansion strategies are employed, contributing to the safe and effective conduct of the study.

This dose will be determined after discussing all the relevant toxicity data between the trial's office and the trial management group. Once the MTD has been defined, dosing at a higher dose must not occur.

7.3.26 Dose modification

Barasertib in combination with fractionated radiotherapy:

Every effort should be *mad*e to administer trial treatment on the planned schedule—the toxicity of each concurrent Barasertib.

The radiotherapy schedule must be recorded and graded according to the current version of the Common Terminology Criteria for Adverse Events (CTCAE Version 5.0). If individual patients experience treatment-related toxicity, subsequent trial treatment may be delayed, omitted and dose modified according to the worst toxicity observed during the previous cycle, as described below.

Dose reductions are permanent (no intra-patient dose re-escalation is permitted).

The dose modification guidelines in this study will be based on the Continual Reassessment Method (CRM), a model-based dose-finding approach that allows for adaptive dose adjustments in response to observed toxicities and safety outcomes.

As participants progress through the dose escalation phase, dose modifications will be implemented according to the toxicity profile and the dose-toxicity relationship estimated by the CRM. The CRM algorithm considers the accumulated safety data from all participants, continuously updating the dose recommendations to achieve the desired balance between efficacy and tolerability.

Dose modifications may be warranted in cases where participants experience dose-limiting toxicities or severe adverse events. The specific dose modification criteria will be predefined in the study protocol, considering the nature and severity of adverse events observed in the trial. The CRM will guide the decision-making process, recommending dose adjustments, including dose reductions or delays, to manage and mitigate treatment-related toxicities while maintaining therapeutic efficacy.

The study investigators will implement the dose modification guidelines with the medical monitoring team. Any dose modification decisions will be *mad*e in accordance with the predefined rules and algorithms of the CRM, ensuring consistency and adherence to the dose-finding methodology. Regular safety assessments will be conducted to guide the dose modification process, including monitoring of adverse events and laboratory parameters. The CRM will continually evaluate the accumulating safety data and update the dose recommendations, providing a dynamic framework for dose adjustment decisions throughout the trial.

The use of the CRM-based dose modification strategy in this study enables the optimization of treatment efficacy while ensuring participant safety by promptly addressing and managing toxicities. This approach allows for a tailored and individualized treatment plan for each participant, optimizing the therapeutic benefits while minimizing the risks associated with the investigational treatment.

In that case, we need to explore the following:

Alternate schedules of Barasertib whereby a substantial amendment will be submitted to the MHRA prior to administering the proposed new dosing schedule.

For grade 3, grade 4 or intolerable grade 2 toxicities, the treatment will be interrupted until recovery to <grade 2 or baseline (in the investigator's judgment). If the patient fails to recover to this extent within three weeks, then trial treatment will be discontinued. Trial treatment will be discontinued if a patient cannot tolerate treatment after two successive dose reductions.

This trial investigates the use of combined Barasertib and fractionated radiotherapy; complete cessation of Barasertib may not necessarily lead to the patient discontinuing the radiotherapy treatment. In any of these circumstances, patients will then undergo end-of-treatment evaluation as per the section outlining end-of-treatment evaluations. Furthermore, it will be followed up at the end of the study visit on days 28-30 following the last treatment.

Patients will then be monitored for progression and survival per the **post-treatment follow-up evaluation** section.

7.3.27 Toxicities associated with Barasertib

Most Common (≥ 30%)

Nausea

Diarrhoea

Leukopenia

Mucositis

Anaemia

Weakness and fatigue

Hair loss

Very Common (10% and <30%)

Pain, including muscle pain, chest pain, and pain from cancer

Fever with or without decreased white blood cells

Sleepiness or Drowsiness

Bleeding events with or without a decreased number of blood platelets

Cough

Shortness of breath

Rash/skin eruption

Constipation

Vomiting

Decrease in weight or loss of appetite

Fluid retention and swelling (e.g., hands, feet, legs)

Headache

Dehydration (decreased body fluids)

Dizziness

Common (>1% and <10%)

Confusion and mental status changes

Imbalance, which can lead to falling

Anxiety or depression

Difficulty sleeping

High or low blood pressure

Itchy or dry skin

Bruises

Inflamed or dry eyes, blurred vision

Dry mouth

Difficulty or pain when swallowing, altered taste

Upset stomach, flatulence

Difficult or blocked bowel movements

Haemorrhoids

Runny nose, sinus or voice problems

Numbness or tingling in hands or feet

Abnormal heart rhythm

Ringing in the ears

Muscle spasms/weakness

Fluid around the lungs or abdomen

Increased sweating or chills

Abnormal kidney function

Abnormal liver function test

Abnormal levels of blood sugar, chemistry, protein or blood clotting time

Bacterial, fungal or viral infection

Increased blood bilirubin

Blood clot (usually in the legs)

Loss of bladder control

Uncommon (< 1%)

Serious and treatment-related adverse events include:

Rhabdomyolysis (muscle breakdown that can damage kidneys)

Bone fracture

Blistering skin reaction

Multiple organ failure

Deafness, shock

Hepatic veno-occlusive disease (also known as sinusoidal obstruction syndrome)

Heart problems

Agitation or irritability

Injury to one or more organs that may be life-threatening or fatal.

Other Treatments (Non-IMPS):

Supportive medication:

The use of supportive medication as per local hospital policy is allowed in this trial.

Concomitant medication and non-drug therapies:

Concomitant medication may be given as medically indicated. All patients will be asked to provide a complete list of prescription, over the counter and complementary and alternative medications taken within the previous four weeks before the first treatment visit. They must also inform the investigator about any new medication started during the trial. Details (including indication, doses, frequency, and start/stop dates) of concomitant medication taken during the trial until the completion of the off-study visit must be recorded in the medical record and the appropriate CRF.

Prohibited therapies:

Patients should not be prescribed any other anti-cancer or investigational therapies while participating in this study.

(Potential) Drug Interactions:

TBA

7.3.28 Patient data acquisition

A planning CT scan will be performed in the treatment position with contiguous 2.0 mm slices to include the entire lung volume. 4D-CT scanning is highly desirable and will become standard practice when 4DCT capacity allows.

Reconstruction of 4D scans is performed according to local guidelines. Intravenous contrast may be used at the request of the treating clinician to facilitate the contouring of mediastinal and nodal disease.

7.3.29 Treatment planning

IMRT planning for RapidArc delivery will be performed as standard. This will be planned according to ICRU 83 in a single phase using 6MV photons.

Isodose distributions must be provided at the reference point plane. Dose-volume histograms (DVH) for the PTV, CTV, GTV, normal lung tissue, spinal cord, heart, oesophagus, and brachial plexus must be calculated and printed.

<u>Target volume:</u>

Treatment will be planned using information from bronchoscopy, mediastinoscopy or thoracotomy, if performed, in addition to CT and PET findings.

Gross Tumour Volume (GTV) will be the primary tumour mass and involved nodes, defined by PET, or short axis > 10 mm.

Clinical Target Volume (CTV) is arrived at by expansion of GTV by 5 mm. In those patients responding to induction chemotherapy, the CTV should aim to encompass the initial tumour volume and the nodes which were initially involved.

Planning Tumour Volume (PTV) is arrived at by expansion of CTV by a 10 mm margin (15 mm margin in the craniocaudal direction). CT fusion techniques can be used in patients down staged by chemotherapy to check that the PTV encompasses the pre-chemotherapy tumour volume.

Normal tissues:

Critical normal structures to be contoured are the spinal cord, lung, heart, oesophagus, and brachial plexus.

OAR tolerances:

Absolute constraints	
Spinal Cord	Maximum dose < 44 Gy
Spinal Cord PRV (5mm)	Dose to 1 cc < 48 Gy (for 29+ #) or < 44 Gy (for 20 #)
Lungs GTV	V_{20Gy} < 35%
Non-mandatory constraints	
Heart	V_{30Gy} < 40% V_{40Gy} < 30%
Oesophagus	Mean dose < 34 Gy V_{55Gy} < 35%
Brachial Plexus	Dose to 1cc < 55Gy

Target verification:

Radical treatments are verified in the first three days using CBCT. Online soft tissue match with 5mm tolerance will be performed, and set-up shifts will be adjusted for subsequent fractions using averaged offset values if reproducible and consistent.

Dose prescription:

The prescription is to the median PTV dose.

IMRT

PTV	D_{min} (1cc) > 90%	(Mandatory: 80%)
	$D_{95\%}$ > 90%	
	D_{1cc} < 107%	
CTV	$D_{95\%}$ > 95%	
	99% < Mean dose < 101%	

Radiotherapy Quality Assurance:

Quality Assurance will be done as routine clinical practice.

7.3.30 Drug Management:

Drug supplies:

TBA

Drug ordering:

TBA

IMP Receipt:

Upon receipt of each drug delivery, the site must complete and return the scanned enclosed acknowledgement of receipt by email within 24 hours. If supplies are damaged on arrival, please contact the trial office promptly.

Handling and storage:

The investigator or an approved representative (e.g., pharmacist) will ensure that all study drugs are stored in a secured area, under recommended storage conditions, in accordance with applicable regulatory requirements.

Barasertib should be stored at (-20^{o}C), and there are no specific restrictions.

Labelling:

Barasertib will be supplied to participating sites appropriately labelled in accordance with all applicable regulatory requirements.

Dosing dispensing:

TBA

Drug returns from patients:

Patients will be asked to return all bottles, whether empty or not, to the hospital. Unused Barasertib must be returned to the pharmacy for counting and recording in

the patient's Drug Accountability Log. Returns must be retained until permission to destroy is given by the trial office at the end of the study.

Drug destruction:

TBA

Occupational safety:

The product is not expected to pose an occupational safety risk to site staff under normal conditions of use and administration.

7.3.31 Evaluation of Response:

Measurement of disease for solid tumour:

Objective disease response must be measured according to the RECIST version 1.1 criteria.

In the dose escalation and expansion phase, radiological tumour response with a CT scan of the chest/abdomen/pelvis will be evaluated prior to study entry, six weeks post-treatment and then every three months after that until intolerable toxicity or progressive disease.

Tumour assessment:

A clinical and CT-graphic evaluation of malignancy, as judged appropriate by the Investigator and in line with the protocol, must be performed before starting the study treatment.

The same methods that detect lesions at baseline will be used to follow these lesion(s) throughout the study. The radiological assessments used to assess response must be performed using identical techniques to ensure compatibility.

Baseline evaluations:

These will include radiological measurements of the extent of the disease by CT chest/abdomen/pelvis. All areas of disease present must be mentioned (even if specific lesions are not going to be followed for response), and the measurements of all measurable lesions must be recorded on the scan reports. Any non-measurable lesions must be stated as being present. All patients with at least one measurable lesion can be included in the trial.

Evaluations during treatment and at off-study:

Tumour assessment will be repeated as per the schedule of events given or more frequently if clinically indicated. All lesions measured at baseline must be measured at subsequent disease assessments and recorded on the scan reports. All non-measurable lesions noted at baseline must be reported as present or absent.

Tumour response:

All patients included in the study must be assessed for response to treatment, even if there is a major protocol treatment deviation or if they are ineligible or not followed/re-evaluated.

Each patient will be assigned one of the following categories:

1. Complete response
2. Partial response
3. Stable disease
4. Progressive disease
5. Early death from malignant disease
6. Early death from toxicity
7. Early death from other cause or unknown (not assessable, insufficient data)

Response duration will be measured from the time measurement criteria for CR/PR (whichever is first recorded) are first met until the first date that recurrent or progressive disease is objectively documented. The date of progression is defined as the first day when RECIST (version 1.1) PD is observed. Early death is defined as any death occurring before the first per protocol time point of tumour re-evaluation. Patients for whom the response is not confirmed will be classified as "unknown" unless they meet the criteria for stable disease (or the criteria for partial response in case of a complete unconfirmed response). Patients' responses will also be

classified as "unknown" if insufficient data were collected to allow evaluation per these criteria. Should rapid tumour progression occur before the completion of radiotherapy treatment, the patient will be classified as having early progression (EP). Tumour response should be classified as “not evaluable” (NE) only when it is not possible to classify it under another response category, e.g., when baseline and follow-up assessment is not performed or not performed appropriately. The appropriate overall response category for each visit that includes disease assessment must be recorded in the medical record for inclusion in the appropriate CRF in our named database.

Other definitions of outcome:

Toxic death: Any death to which drug toxicity is thought to have a major contribution.

Early death: Death during the first three weeks of treatment that is not a toxic death.

7.3.32 Assessment of Safety:

The Investigator will monitor each patient for clinical and laboratory evidence of adverse events on a routine basis throughout the study. Should an Investigator become aware of any study drug-related SAEs following this period, these must also be reported as stated below.

Adverse event monitoring starts from the time the patient consents to the study until they complete the trial. Any reportable AEs that are unresolved at the patient's last visit in the study are followed up by the Investigator for as long as medically indicated but without further recording in the CRF. All AEs reported to the trial office will be processed according to internal SOPs. The trial office may request additional information for any AE as judged necessary.

Adverse Event Definitions:

An Adverse Event or experience (AE) is any untoward medical occurrence in a study subject temporally associated with the administration of an investigational medicinal product (IMP) or a comparator product, whether or not considered related to the IMP or a comparator product.

An AE can, therefore, be any unfavourable and unintended sign, symptom, disease (new or exacerbated), and significant abnormal laboratory or physiological observation temporally associated with using a medicinal product.

A Serious Adverse Event (SAE) is any AE, regardless of dose, causality, or expectedness, that:

1. Results in death
2. Is life-threatening.
3. Requires in-patient hospitalisation or prolongs existing inpatient hospitalisation.

4. Results in persistent or significant incapacity or disability
5. Is a congenital anomaly or congenital disability.
6. Is any other medically important event.

An Adverse Drug Reaction (ADR) is a response to a medicinal product which is noxious and unintended. Response in this context means that a causal relationship between a medicinal product and an adverse event is at least a reasonable possibility.

An Unexpected Drug Reaction is an adverse drug reaction, the nature or severity of which is not consistent with the applicable reference safety information section (referring to SPC or IB).

A Suspected Unexpected Serious Adverse Drug Reaction (SUSAR) is a serious adverse drug reaction, the nature or severity of which is not consistent with the applicable product information (e.g., Investigator's Brochure for an unapproved investigational product or SPC for an approved product).

Clinical laboratory abnormalities and other abnormal assessments as AEs and SAEs

Abnormal laboratory findings (e.g., clinical chemistry, haematology, urinalysis) or other abnormal assessments (e.g., ECGs, X-rays, and scans) that the investigator judges as clinically significant will be recorded as AEs or SAEs if they meet the abovementioned definitions.

Suspected Unexpected Serious Adverse Drug Reactions (SUSARs)

All SUSARs must be reported to the responsible Authority and main REC within very tight deadlines depending on the outcome, so it is imperative that sites report potential SUSARs to the trial's office without delay.

Events exempt from being reported as AE/ SAEs:

1. Abnormal findings associated with the disease being studied.
2. Clinically significant abnormal laboratory findings or other abnormal assessments detected during the study or present at baseline and significantly worsening following the start of the study will be reported as AEs or SAEs.

However, clinically significant abnormal laboratory findings or other abnormal assessments that are associated with the disease being studied, unless judged by the investigator as more severe than expected for the patient's condition or that are present or detected at the start of the study and do not worsen, should not be reported as AEs or SAEs.

7.3.33 Death on study

Death due to the disease under study is to be recorded on the Death CRF form, providing the death is not unexpected or if a causal relationship is suspected.

The investigator must clearly state whether the death was expected or unexpected and whether a causal relationship to the study IMP or other protocol treatment intervention is suspected.

7.3.34 Elective admissions and supportive care

Elective admissions to the hospital for patient convenience, planned procedures, investigations, or treatment as specified in this protocol and standard supportive care are not SAEs and do not require SAE reporting.

Hospital admission for the following supportive care procedures is considered standard for this patient group and should not be reported as SAEs:

1. Admission for IV rehydration
2. Admission for blood or platelet transfusion
3. Admission for acute radiation chest toxicity
4. Admission for treatment-related fatigue
5. Admission for nutritional optimisation

7.3.35 Development Safety Update Reports (DUSRs)

DSURs will be coordinated by OCTO, prepared in collaboration with the CI, and submitted in parallel to the regulatory authority and responsible Research Ethics Committee within 60 days of the anniversary of the regulatory approval date. A copy of each report will be provided to (**insert study funder/pharmaceutical company**)

7.3.36 Pregnancy and Breast Feeding:

Pregnancies (in a participant or partner) occurring within (n) months of treatment dosing with Barasertib must be reported using the Pregnancy Notification Form, which should be scanned and emailed to the clinical trial coordinator within 24 hours of receipt of information.

If the pregnancy results in an abnormal outcome and meets the criteria for immediate classification as a serious adverse event (i.e., spontaneous abortion, stillbirth, neonatal death, or congenital anomaly), the investigator should follow the procedures for reporting serious adverse events.

Note: Pregnancy itself is only considered an AE/SAE if there is reason to believe it may be the result of an interaction between the study IMP and the contraceptive used.

Women who become pregnant should be withdrawn from treatment at the earliest opportunity. All reported pregnancies should be followed up until the outcome. Pregnancy outcomes must be recorded in the medical record and in the follow-up section of the Pregnancy Notification Form. Any abnormal outcome (other than elective abortion) for the mother or child should also be reported as an SAE.

(Insert the name of Funder here) should also be informed by the trial's office of any pregnancy arising in a study participant or his/her partner whilst taking part in the trial

or during a stage where the foetus could have been exposed to the medicinal product.

7.3.37 Defining the End of Trial:

For this study, the end of the trial is defined as the last visit of the last patient undergoing the trial (LPLV).

The study will be stopped when:

a. The stated number of patients to be recruited is reached.

AND

b. All patients have discontinued treatment with a combination of aurora kinase inhibitors with radical radiotherapy.

In consultation with the trial committee, the sponsor, the Chief Investigator, reserves the right to terminate the study earlier at any time.

In terminating the study, they must ensure adequate consideration for protecting the participant's best interests.

7.3.38 Statistical Considerations:

This will need to be discussed with the Statistician.

7.3.39 Trial Committees:

Trial Management Group (TMG)

The Chief Investigator will chair a TMG responsible for overseeing the successful conduct and publication of the trial per the protocol.

Members of the TMG will include:

1. Chief Investigator
2. Trial management staff from the trial office
3. Trial Statistician
4. Principal Investigators from participating sites

7.3.40 Data Management:

Data management will be performed via a trial database. The Chief Investigator will act as Data Custodian for the trial. A guide explaining how to use **(name of database)** will be provided to every site. Relevant Trial office staff will have an overview of all entered data.

Case report forms (CRFs)

The Investigator and study site staff will ensure that data collected on each subject is recorded in the CRFs within **(name of database)** as accurately and thoroughly as possible. The CRFs will not contain any source data.

All appropriate laboratory data, summary reports and Investigator observations will be transcribed into the CRFs from the relevant medical record(s). Please ensure that:

1. The relevant CRFs are completed.
2. All CRF data are verifiable in the source documentation, or the discrepancies must be explained.
3. CRF sections are completed promptly, i.e., within 7-14 days of the study visit or reported event.
4. Data queries are resolved and documented by authorised study staff, giving a reason for the change or correction where appropriate.

The above considerations also apply to patients who are withdrawn early. If a patient withdraws from the study, the reason must be noted on the appropriate form, and the patient must be followed up as per protocol.

Accounting for missing, unused, or spurious data. Missing data found will be chased up and supplemented where possible after consultation with the investigator. The control of the correctness of the data is performed with ranking tests, validity tests and consistency checks. Unused data will be retained as user data.

Clinical Study Report:

All clinical data will be presented as data listings at the end of the study. These will be checked to confirm that the lists accurately represent the data collected during the study. The trial data will then be locked, and a final listing will be produced. The

clinical study report will be based on the final data listings. The locked trial data may then be used for analysis and publication.

7.3.41 Study Site Management:

Study site responsibilities:

The Principal Investigator (the PI or lead clinician for the study site) has overall responsibility for the conduct of the study but may delegate responsibility where appropriate to suitably experienced and trained members of the study site team (e.g., drug supplies will be monitored by the on-site pharmacist, trial forms completed by the Data Manager, etc.).

All members of the study site team must complete the delegation log, or the Staff Contact Responsibility Sheet provided prior to undertaking any study duties. The PI must counter-sign and date each entry in a timely manner, authorising staff to take on the delegated responsibilities. The Principal Investigator must ensure that all staff involved in the study are adequately trained and that their duties have been logged on the forms provided. All Principal Investigators and Co-Investigators must have valid and up to date GCP training.

Study site set-up and activation:

A Principal Investigator should lead the study at each site, providing the local study office with all core documentation and attending a ‘Site Training Call’ organised by

the trial office or visit before the site becomes activated (usually carried out as a telephone conference call or personal visit).

The Trial Office will call to check that the site has all the required study information/documentation and is ready to recruit. The site will then be notified once they are activated on the MErCuRIC database and able to recruit.

Study documentation:

The trial office will provide an Investigator File and Pharmacy File (where applicable) to each investigational site, including contact details, study procedures and all other documents required for the completion of the study. Before use, the trial office must review and approve any local changes *mad*e to any study documentation, including patient information and consent forms. Additional documentation generated during the trial, including relevant communications, must be retained in the site files as necessary to reconstruct the conduct of the trial.

A screening log must be kept of all patients considered for the study and subsequently excluded; the reason for exclusion must be recorded on this form. A copy of the screening log without patient identifiers should be sent to the trial office on a **(monthly or yearly)** basis or as requested by the trial office. The original must be retained on-site.

7.3.42 Regulatory and Ethical Considerations:

The Sponsor and Investigators will ensure that this protocol will comply with the European Clinical Trials Regulations, the Principles of Good Clinical Practice (GCP) and the applicable policies of the sponsoring organisation.

These implement the ethical principles of the Declaration of Helsinki (1996) and the regulatory requirements for clinical trials of an investigational medicinal product under the European Union Clinical Trials Directive.

Ethical conduct of the trial and ethics approval

The protocol, patient information sheet, consent form and any other information that will be presented to potential trial patients (e.g., advertisements or information that supports or supplements the informed consent) will be reviewed and approved by an appropriately constituted, independent Research Ethics Committee (REC) or equivalent for non-UK countries (IRB etc.). The relevant national and local bodies will approve Principal Investigators.

Regulatory Authority approval

Approval to conduct the study will be obtained from the relevant Competent Authority in each participating country before initiating the study. The study will be conducted

in the UK under a Medicines and Healthcare Products Regulatory Agency (MHRA) Clinical Trial Authorisation (CTA).

Local Approvals

Investigators are responsible for ensuring they obtain appropriate local approvals to conduct the trial in accordance with local arrangements and policies.

7.3.43 Protocol amendments

Amendments are changes *mad*e to the research following initial approval. A 'substantial amendment' is an amendment to the terms of the Responsible Authority application (if applicable), the REC application, or to the protocol or any other supporting documentation that is likely to affect to a significant degree:

1. The safety or physical or mental integrity of the subjects of the trial
2. The scientific value of the trial
3. The conduct or management of the trial
4. The quality or safety of the investigational medicinal product(s) used in the trial.

Non-substantial amendments are those where the change(s) involve only minor logistical or administrative aspects of the study. All amendments will be generated

and managed according to the trial office's standard operating procedures to ensure compliance with applicable regulations and other requirements. Written confirmation of all applicable REC, regulatory and local approvals must be in place before implementation by Investigators.

Urgent safety measures:

The sponsor or Investigator may take appropriate urgent safety measures to protect trial participants from any immediate hazard to their health or safety. Urgent safety measures may be taken without prior authorisation. The trial may continue with the urgent safety measures in place. The Investigator must inform the trial team IMMEDIATELY if the study site initiates an urgent safety measure:

a) Tel: (insert telephone number)
b) Email: (insert email number)

The notification must include the following:

1. Date of the urgent safety measure
2. Who took the decision?
3. Why the action was taken.

The Investigator will provide any other information that may be required to enable the trial office to report and manage the urgent safety measures in accordance with the

current regulatory and ethical requirements for expedited reporting and closeout. The Trials office will follow written procedures to implement the changes accordingly.

Temporary halt:

The sponsor and Investigators reserve the right to place recruitment to this protocol on hold for short periods for administrative reasons or to declare a temporary halt. A temporary halt is defined as a formal decision to:

Interrupt the treatment of subjects already in the trial for safety reasons.

1. Stop recruitment on safety grounds **or**
2. Stop recruitment for any other reason(s) considered to meet the substantial amendment criteria, including the possible impact on the feasibility of completing the trial in a timely manner.

The trial office will report the temporary halt via an expedited substantial amendment procedure. The trial may not restart after a temporary halt until a further substantial amendment to re-open is in place. If it is decided not to restart the trial, this will be reported as an early termination.

Serious Breaches:

The Medicines for Human Use (Clinical Trials) Regulations require the Sponsor to notify the MHRA of any "serious breaches" to the MHRA within seven days of the sponsor becoming aware of the breach. A serious breach is defined as “A breach of GCP or the trial protocol which is likely to affect to a significant degree:

1. The safety or physical or mental integrity of the subjects of the trial
2. The scientific value of the trial
3. Investigators must immediately notify the trial's office if any serious breach of GCP is suspected.

Progress, Safety and End of Study Reports:

This protocol will comply with all current applicable Regulatory Authority, Research Ethics Committee and Sponsor requirements for the provision of periodic study safety and progress reports. Any additional reports will be provided on request. The trial’s office will manage reporting according to internal SOPs. Sites will be urged to return as much data as possible before each database lock point.

The trial office will determine which reports need to be circulated to Principal Investigators and other interested parties according to internal SOPs. Study sites are responsible for forwarding trial reports they receive to their local Institutions as required.

7.3.44 Expenses and Benefits:

Each participating centre will follow local regulations and policies on reimbursement of travel expenses.

7.3.45 Quality Assurance:

Risk assessment and monitoring:

The study will undergo a risk assessment before starting to determine the extent and nature of site monitoring. Risk assessments will be performed throughout the duration of the study on an ad hoc need basis and in line with any substantial amendments and any significant findings that might change the risk/benefit balance of the study. Monitoring plans will be amended accordingly. Monitoring (on-site and central) will be performed according to the plan and trial office SOPs.

On-Site Monitoring:

Data will be evaluated for compliance with the protocol and accuracy in relation to source documents. Monitoring visit reports will be sent to the site in a timely fashion.

Central Monitoring:

Study sites will be monitored centrally by both programmed validation within the data collection database and manual checking of incoming data for compliance with the protocol, data consistency, missing data, and timing. All changes to data that could influence the outcome will be queried with and approved by the study site in a timely manner. For all other data, where there is no doubt about the source of any errors, clear changes to data will be *mad*e internally by trial office staff without referring back to the study site. Study staff will regularly contact site personnel to check on progress and deal with any queries they may have, including those arising from queries raised by the trial office.

Audit and Regulatory Inspection:

All aspects of the study conduct may be subject to internal or external quality assurance audit to ensure compliance with the protocol, GCP requirements and other applicable regulations or standards. It may also be subject to a regulatory inspection.

Such audits or inspections may occur at any time during or after the completion of the study. Investigators and their host Institution(s) should understand that it is necessary to allow auditors/inspectors direct access to all relevant documents and study facilities and to allocate their time and the time of their staff to facilitate the audit or inspection visit.

Anyone receiving notification of a Regulatory Inspection that will (or is likely to) involve this trial must inform the trial office without delay.

Records Retention and Archiving:

During the clinical trial and after trial closure, the investigator must maintain adequate and accurate records to enable the conduct of a clinical trial and the quality of the research data to be evaluated and verified. These essential documents, detailed in the trial office SOP, must be stored to ensure that they are readily available, upon request, to the sponsor or the Regulatory Agency for the minimum period required by national legislation or for longer if needed.

The medical files of trial subjects shall be retained in accordance with national legislation and in accordance with the host institution's policy. Retention and storage of laboratory records for clinical trial samples will follow national guidelines. Retention and storage of central laboratory records supporting PK or PD endpoints, and the disposition of samples donated via the trial must also comply with applicable legislation and Sponsor requirements. It is the University of Sheffield’s policy to store data for a minimum of (n) years. Investigators may not archive or destroy study essential documents or samples without written instruction from the trial office.

Patient Confidentiality:

Personal data recorded on all documents will be regarded as confidential, and to preserve each patient's anonymity, only their patient study number, initials, and date of birth (or other identified as appropriate to country regulations and agreed with the Sponsor) will be recorded on the CRFs.

The Investigator site must maintain the patient's anonymity in all communications and reports related to the research. The Investigator site team must keep a separate log of enrolled patients' personal identification details as necessary to enable them to be tracked.

7.3.46 Study Funding:

The Leeds Clinical Trials Office is organising this trial at the University of Leeds and is being funded by **(Insert pharmaceutical company to be determined later).** Any additional NHS clinical service support costs of patient care while on the study should be met by the host study site.

Sponsorship and Indemnity:

<u>Sponsorship</u>

The Sponsor will provide written confirmation of Sponsorship and authorise the trial commencement once satisfied that all arrangements and approvals for the proper conduct of the trial are in place.

A separate study delegation agreement, setting out the responsibilities of the Chief Investigator and Sponsor, will be put in place between the parties.

Insurance

The University has a specialist insurance policy in place: - **TBA.**

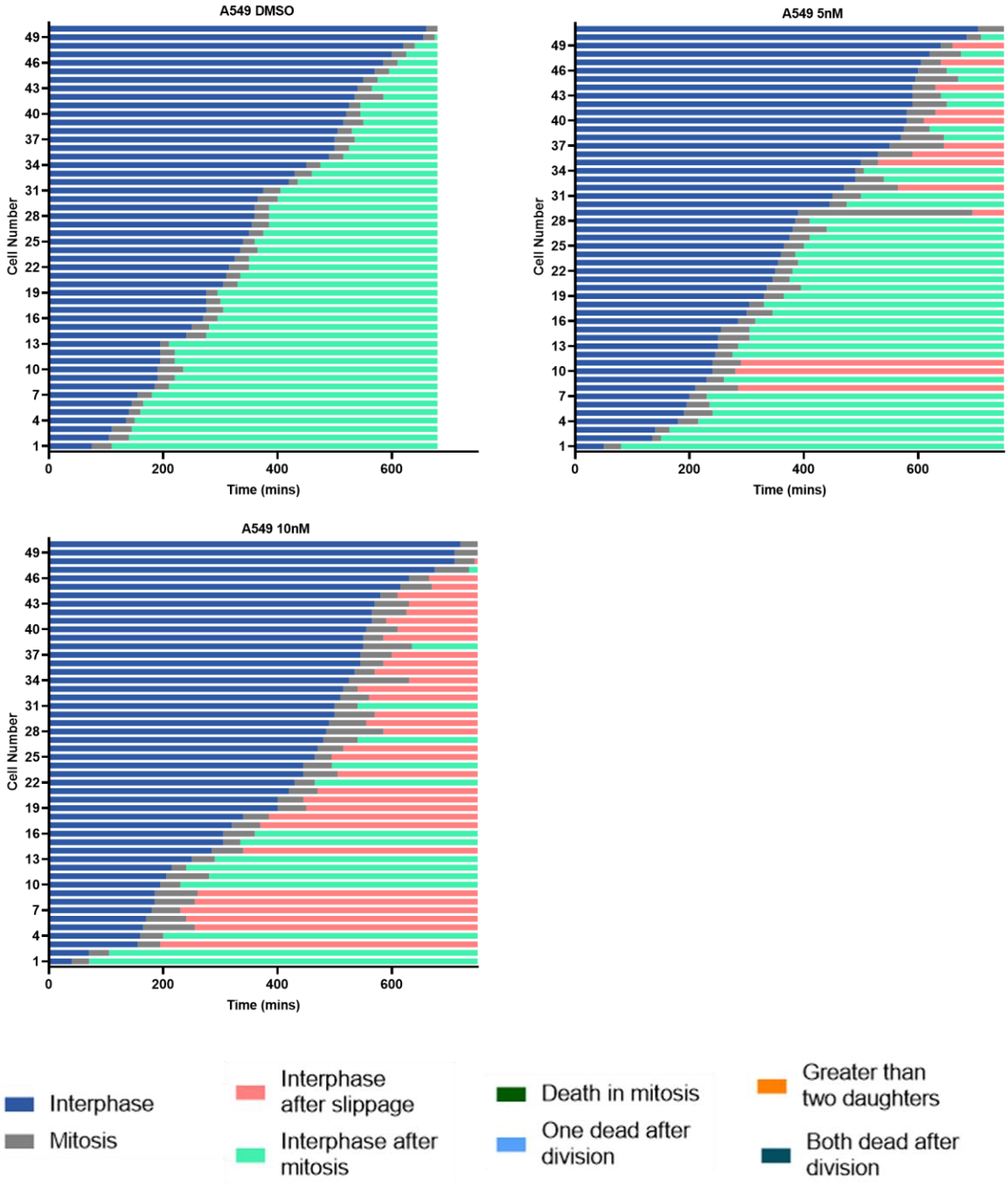
Publication Policy:

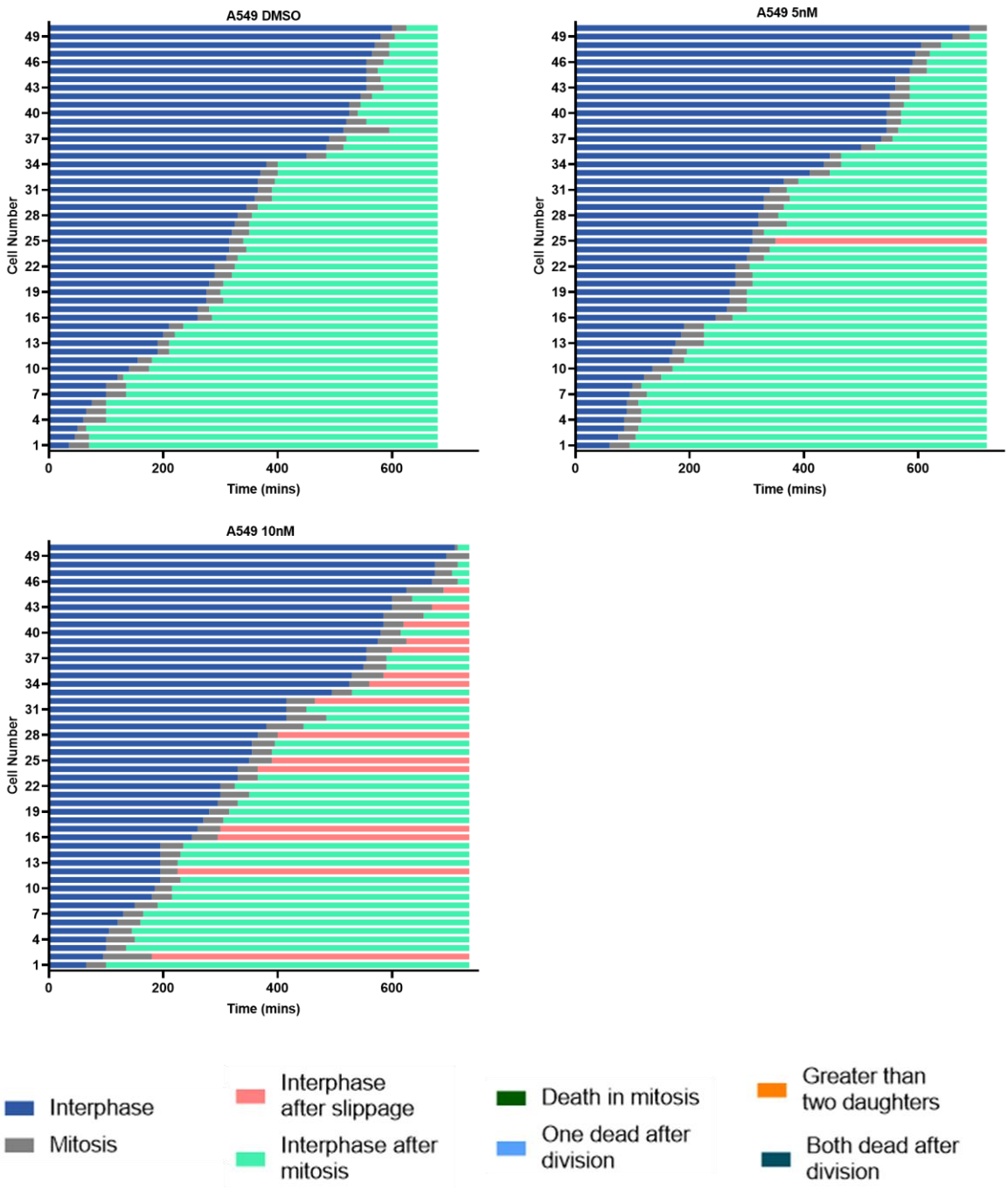
Ownership and publication policy will be per the trial group's agreement.

7.4 Stacked Bar graphs of Live cell data.

7.4.1 0–16-hour time frame

7.4.1.1 A549 plus Barasertib alone




A549 DMSO
A549 5nM
A549 10nM
Cell Number
Time (mins)
0
200
400
600
1
4
7
10
13
16
19
22
25
28
31
34
37
40
43
46
49
Interphase
Mitosis
Interphase after slippage
Interphase after mitosis
Death in mitosis
One dead after division
Greater than two daughters
Both dead after division

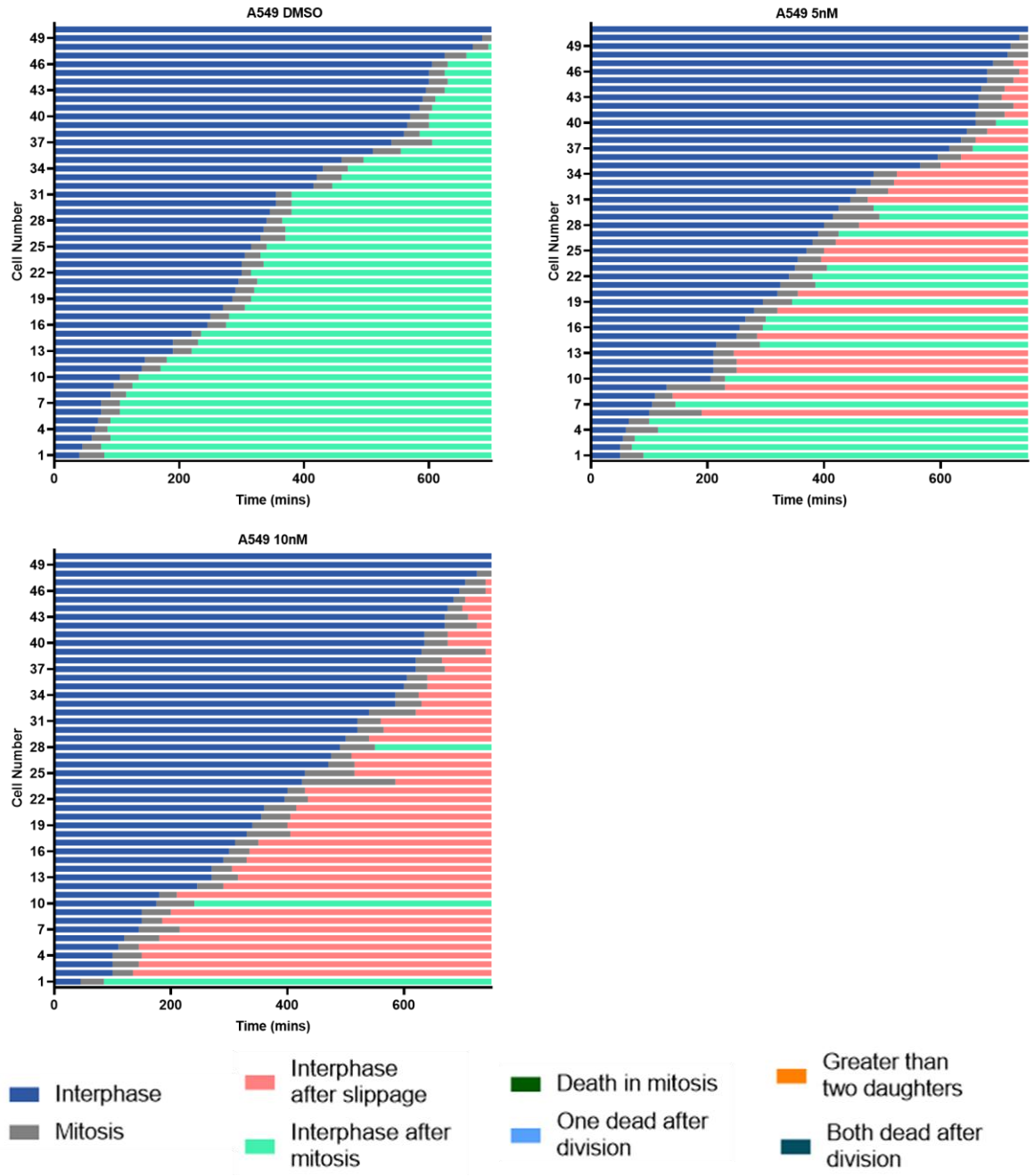
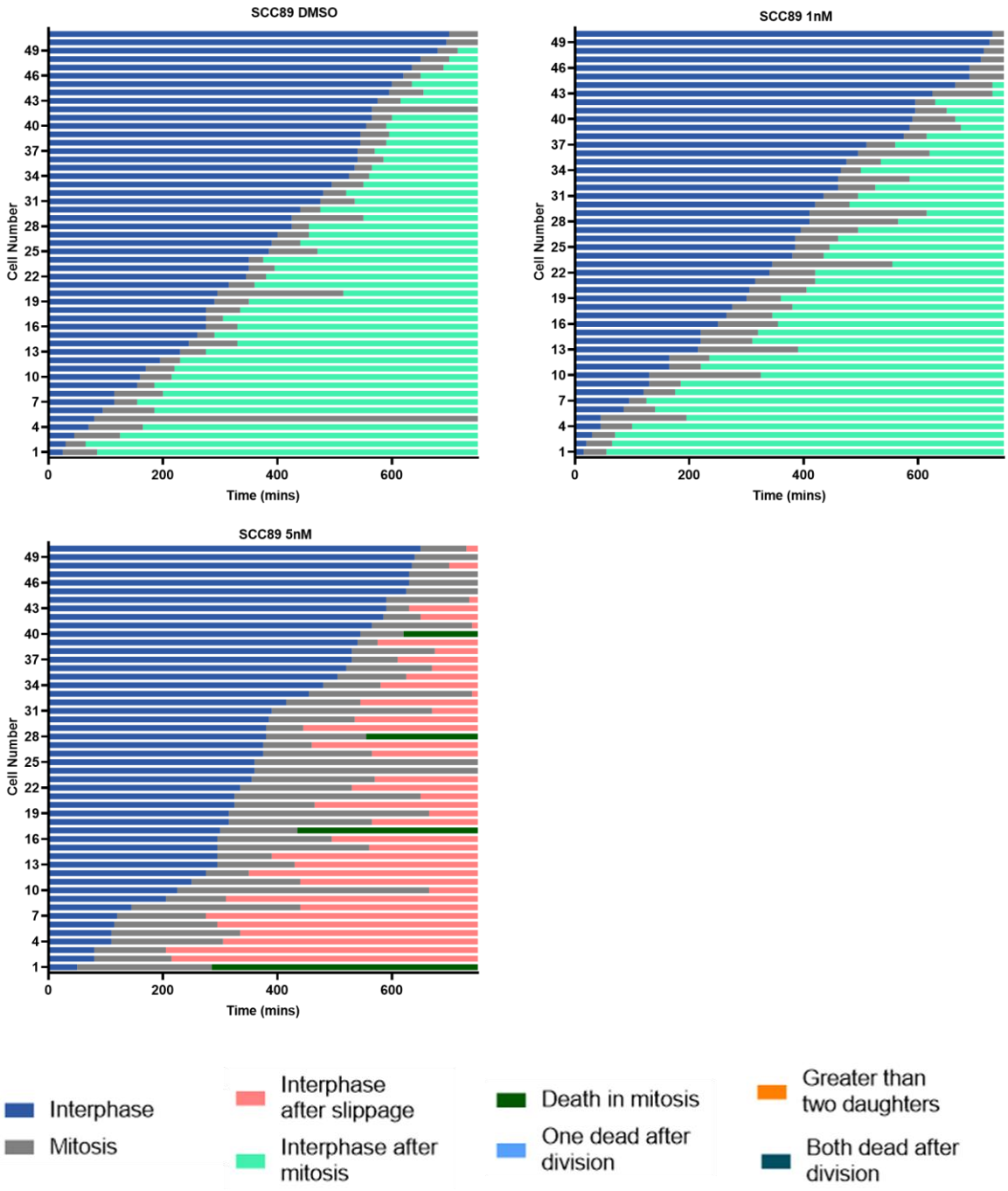
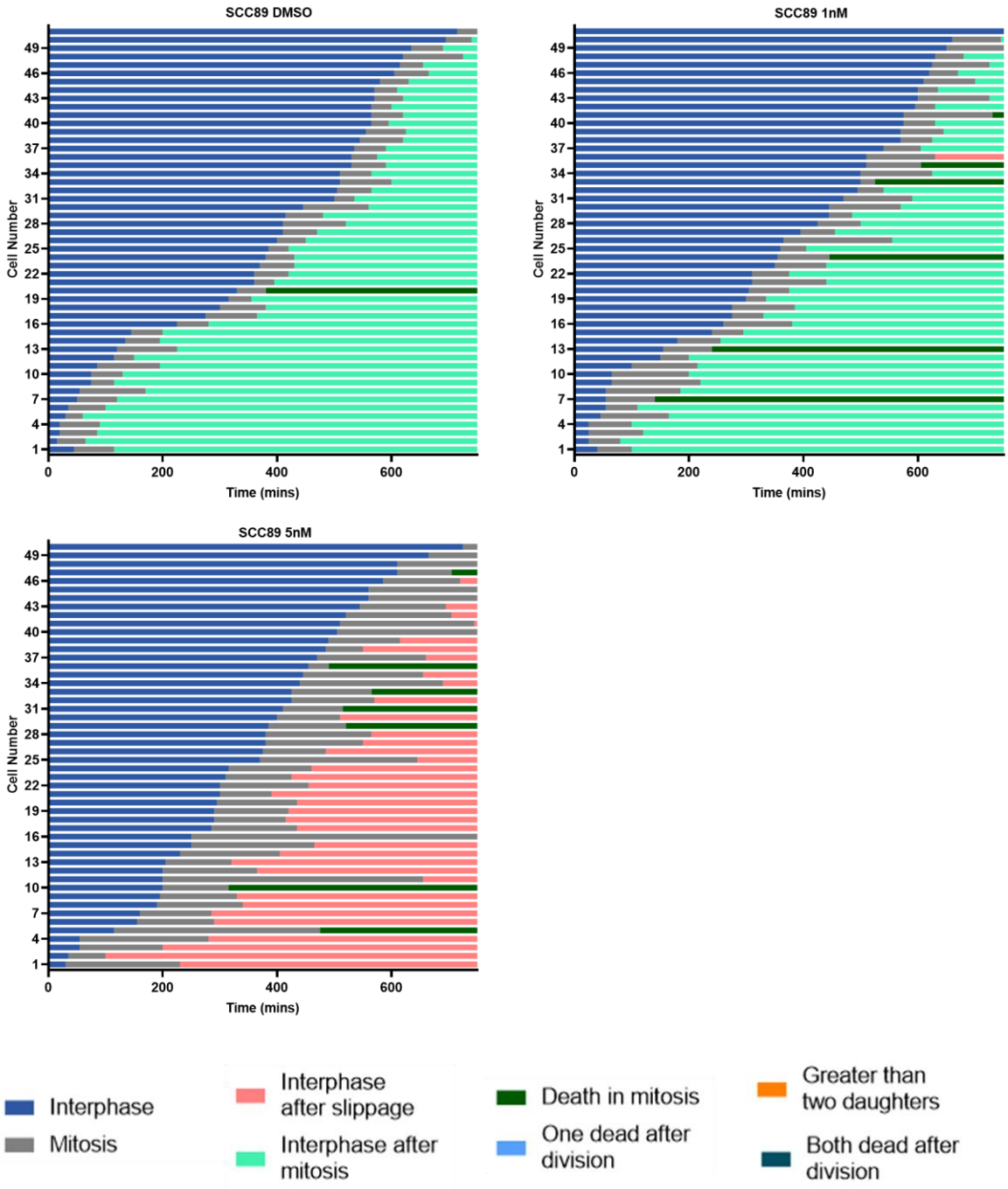


Figure 7-1: ***Stacked Bar charts showing the cellular outcomes of Barasertib*** *on live cell imaging using the conditions DMSO, 5nM and 10nM between 0-16 hours in A549 cells. Cells were treated with Barasertib for 2 hours before adding to IR and left for seven days. Dark blue indicates interphase before mitosis or slippage; Grey indicates mitosis; Pink indicates Interphase after slippage; Cyan indicates Interphase after mitosis; Green indicates Cell death in Mitosis; Sky blue indicates one cell died after division; Teal indicates both daughter cells died after division and orange indicates that the mother cell divided into more than two daughters.*

7.4.1.2 SCC89 plus Barasertib alone




SCC89 DMSO
SCC89 1nM
SCC89 5nM
Cell Number
Time (mins)
0
200
400
600
1
4
7
10
13
16
19
22
25
28
31
34
37
40
43
46
49
Interphase
Mitosis
Interphase after slippage
Interphase after mitosis
Death in mitosis
One dead after division
Greater than two daughters
Both dead after division

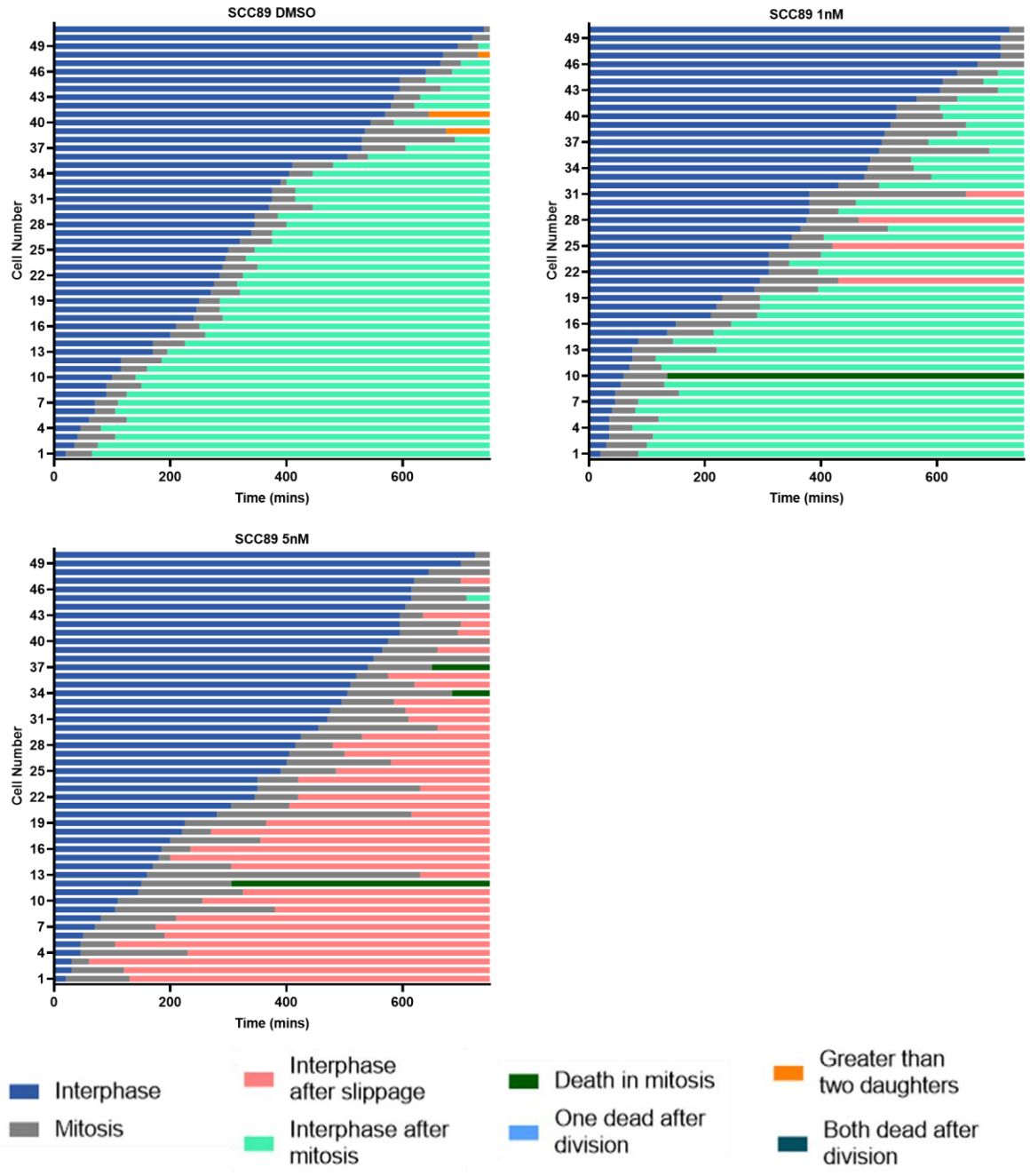
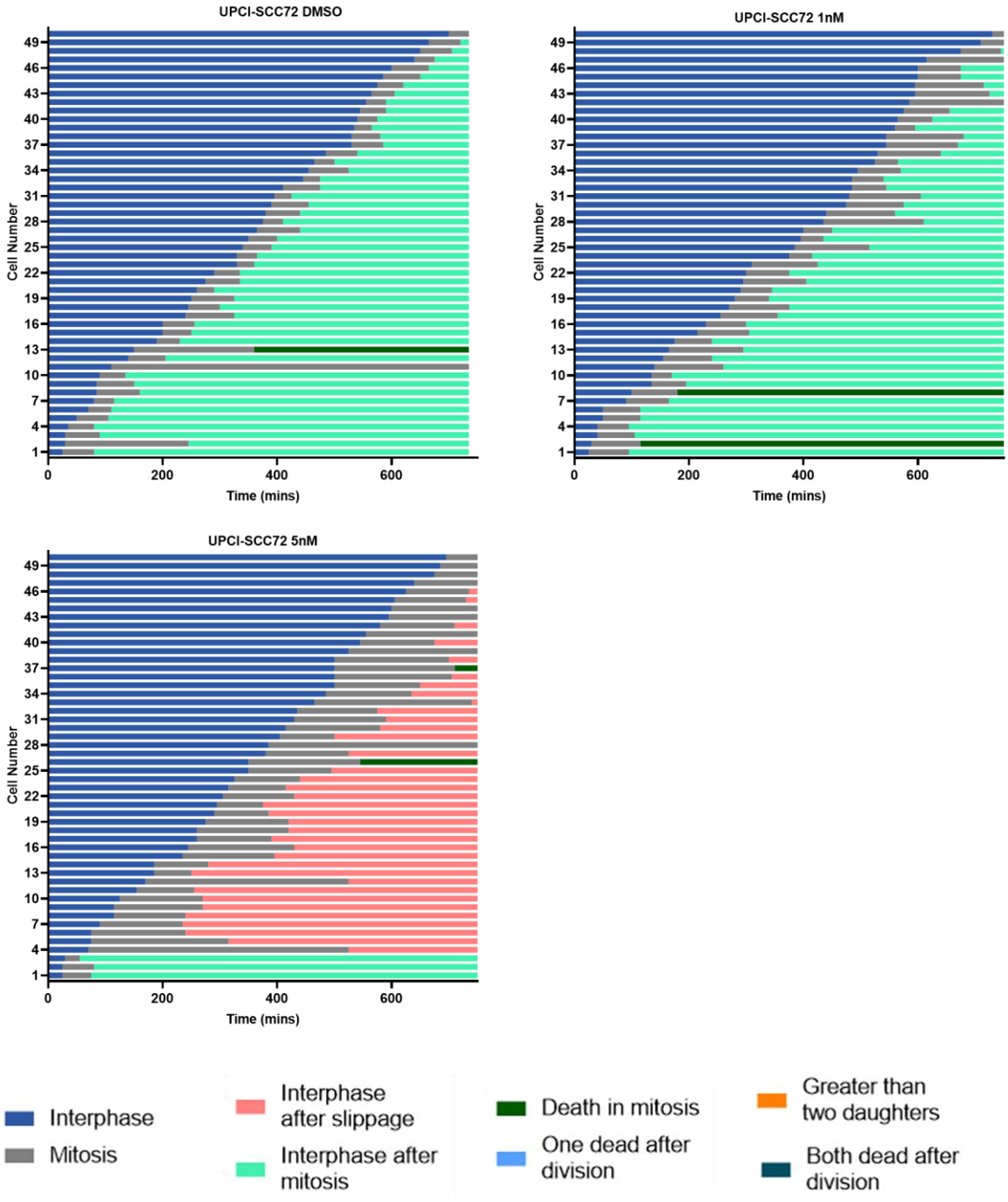
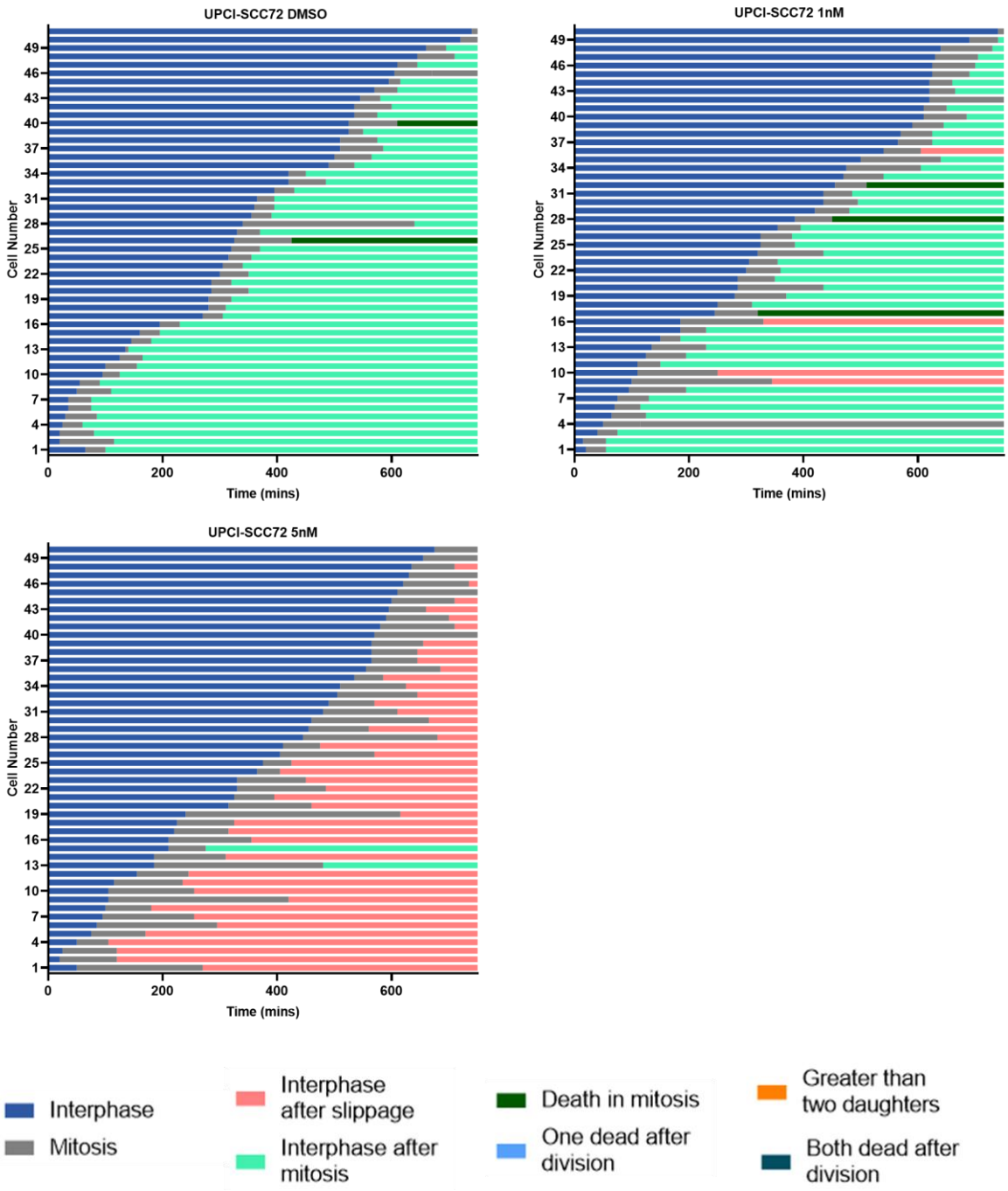


Figure 7-2: ***Stacked Bar charts showing the cellular outcomes of Barasertib*** *on live cell imaging using the conditions DMSO, 5nM and 10nM between 0-16 hours in SCC89 cells. Cells were treated with Barasertib for 2 hours before adding to IR and left for seven days. Dark blue indicates interphase before mitosis or slippage; Grey indicates mitosis; Pink indicates interphase after slippage; Cyan indicates interphase after mitosis; Green indicates Cell death in Mitosis; Sky blue indicates one cell died after division; Teal indicates both daughter cells died after division and orange indicates that the mother cell divided into more than two daughters.*

7.4.1.3 UPCI-SCC72 plus Barasertib alone




UPCI-SCC72 DMSO
UPCI-SCC72 1nM
UPCI-SCC72 5nM
Cell Number
Time (mins)
0
200
400
600
1
4
7
10
13
16
19
22
25
28
31
34
37
40
43
46
49
Interphase
Mitosis
Interphase after slippage
Interphase after mitosis
Death in mitosis
One dead after division
Greater than two daughters
Both dead after division

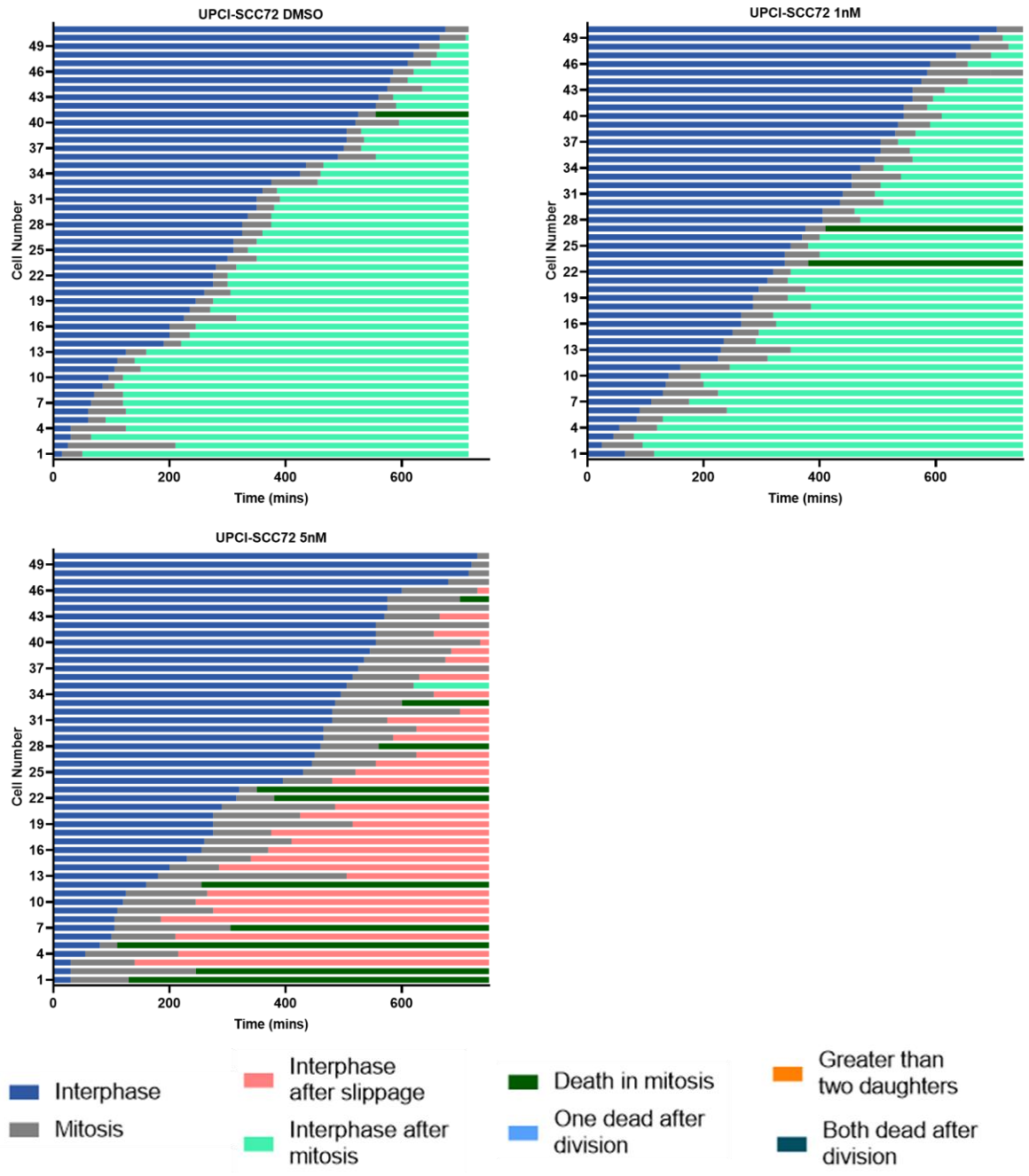
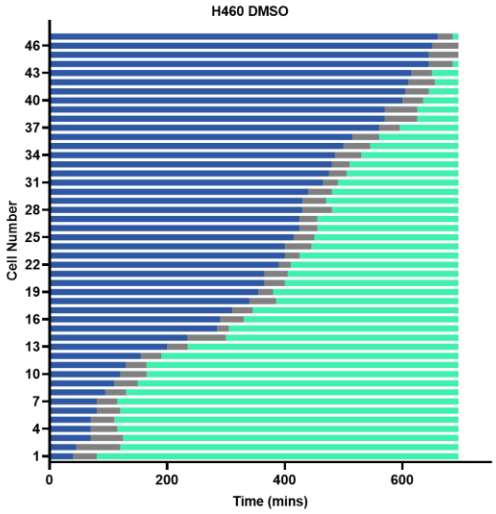
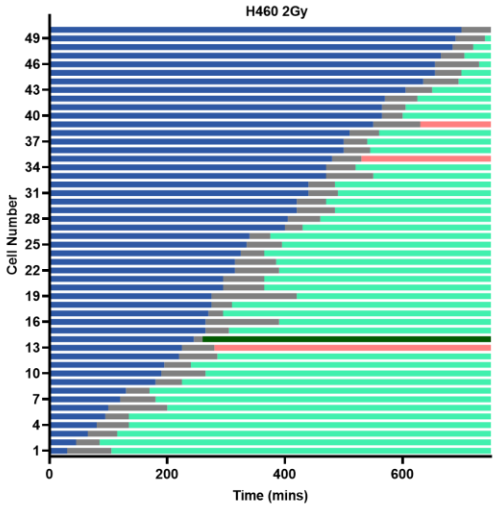


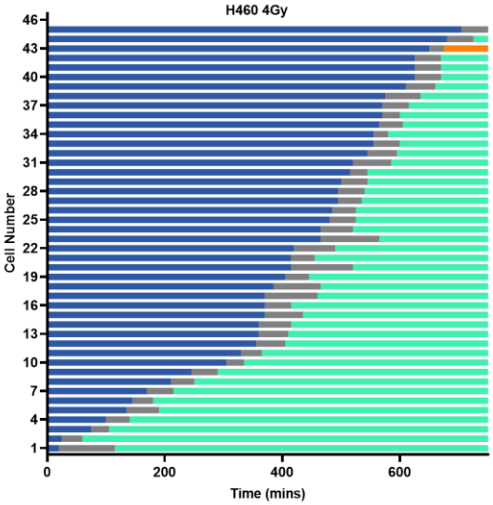
Figure 7-3: ***Stacked Bar charts showing the cellular outcomes of Barasertib*** *on live cell imaging using the conditions DMSO, 5nM and 10nM between 0-16 hours in UPCI-SCC72 cells. Cells were treated with Barasertib for 2 hours before adding to IR and left for seven days. Dark blue indicates interphase before mitosis or slippage; Grey indicates mitosis; Pink indicates Interphase after slippage; Cyan indicates Interphase after mitosis; Green indicates Cell death in Mitosis; Sky blue indicates one cell died after division; Teal indicates both daughter cells died after division and orange indicates that the mother cell divided into more than two daughters.*

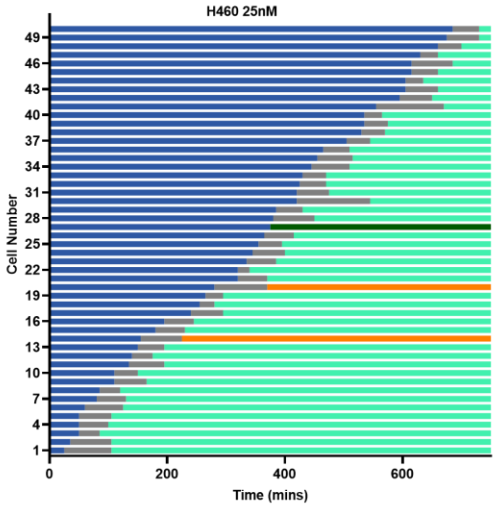
7.4.2 24–36-hour time frame

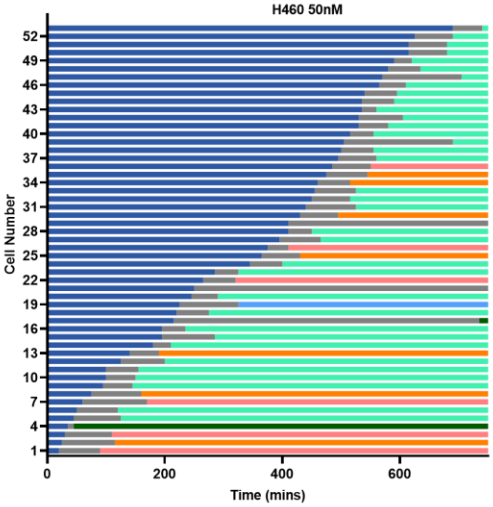
7.4.2.1 H460 +/- IR

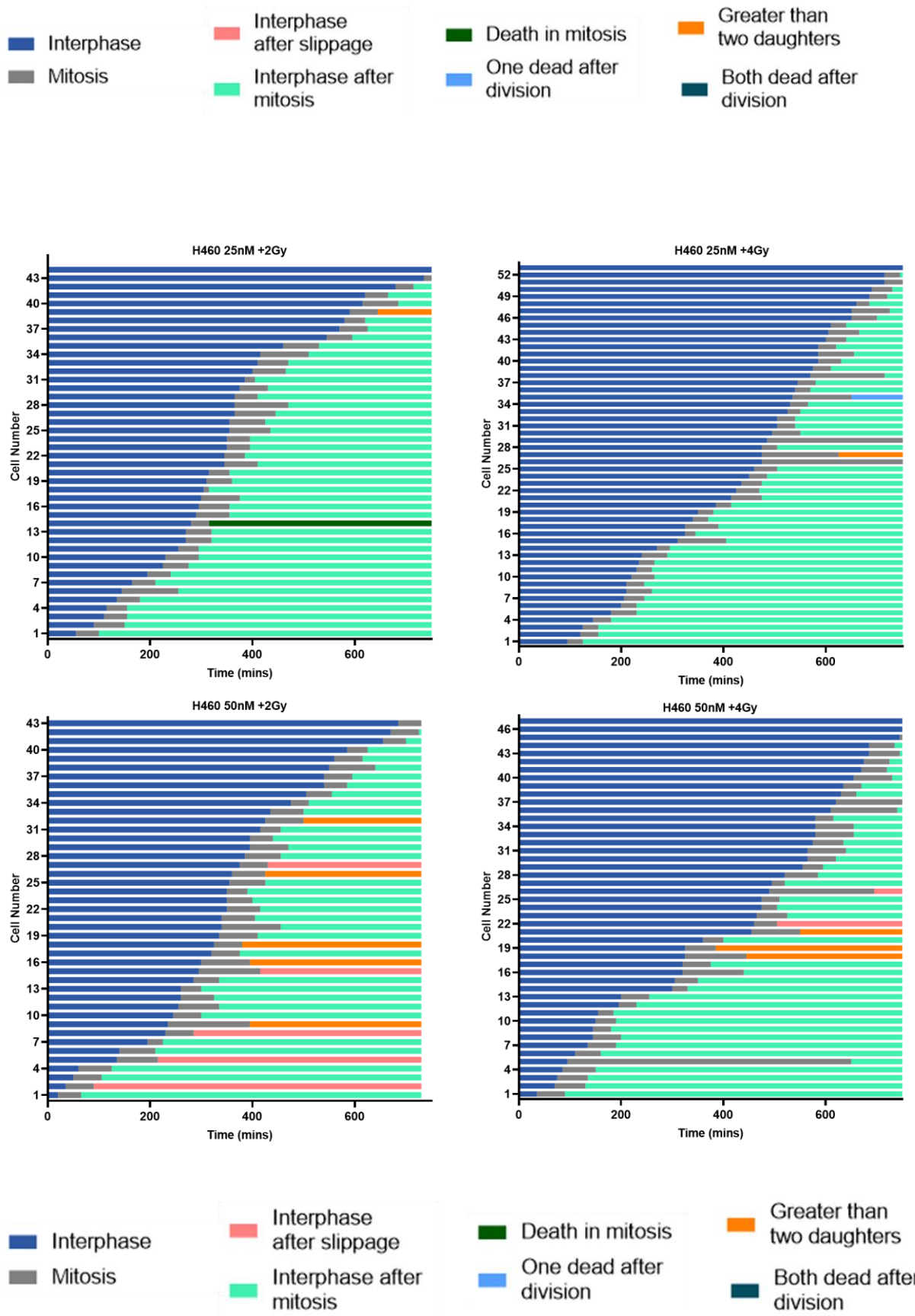


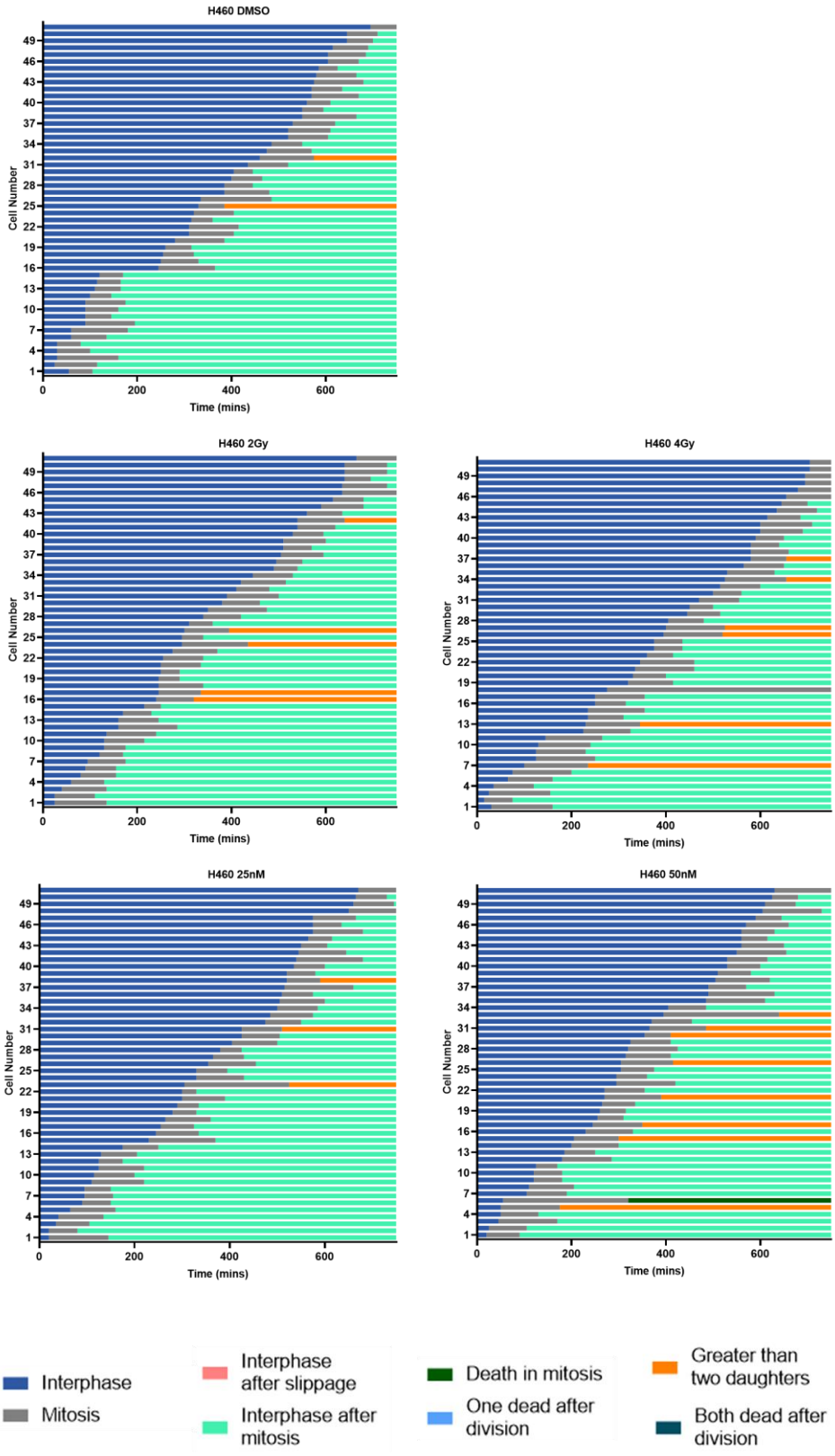


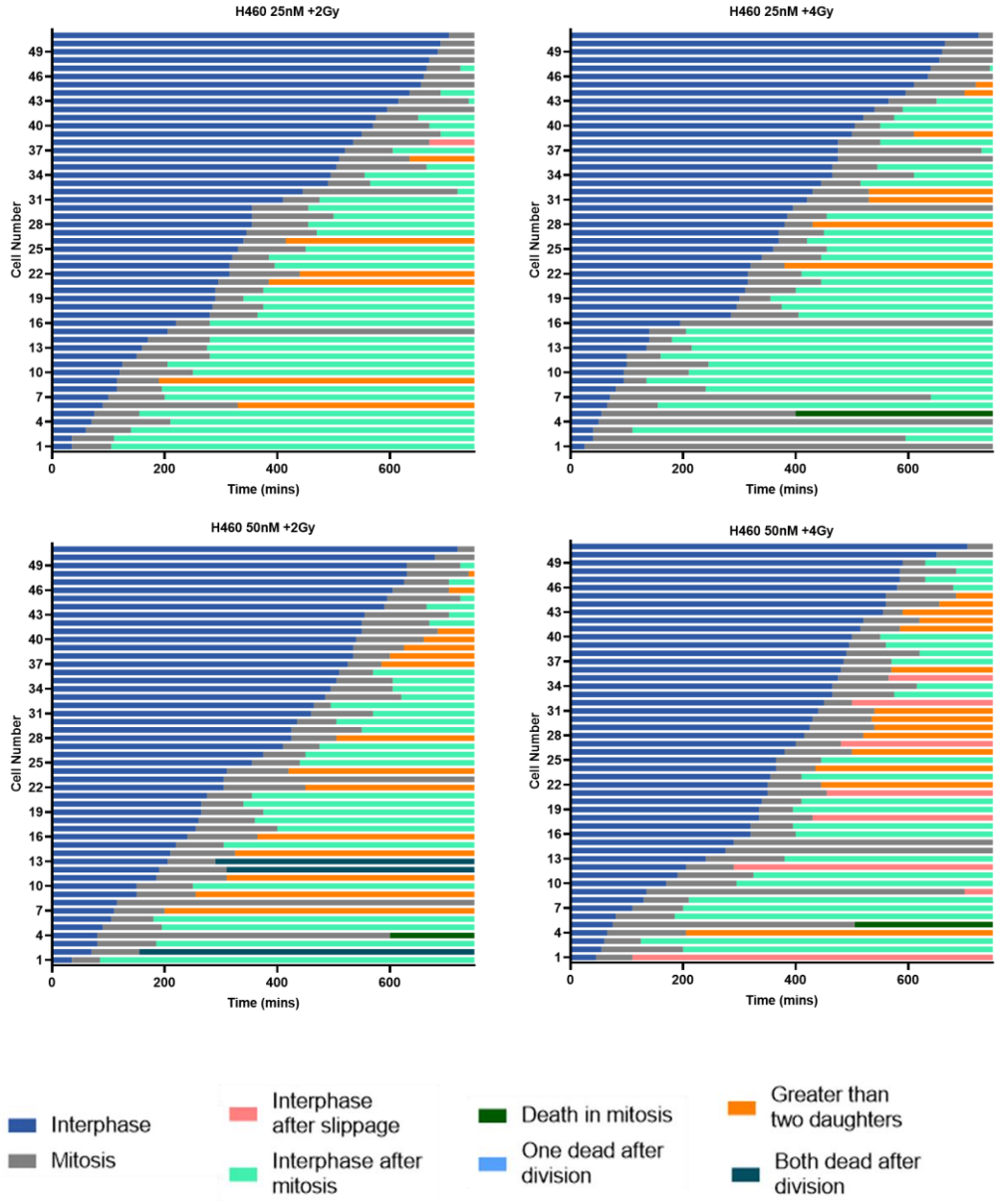


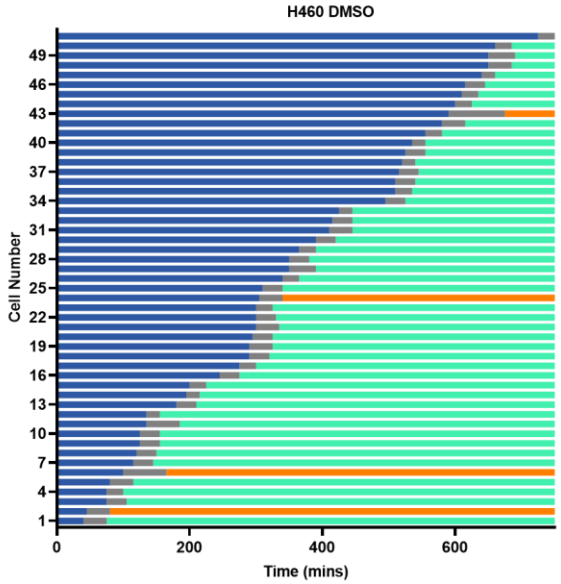


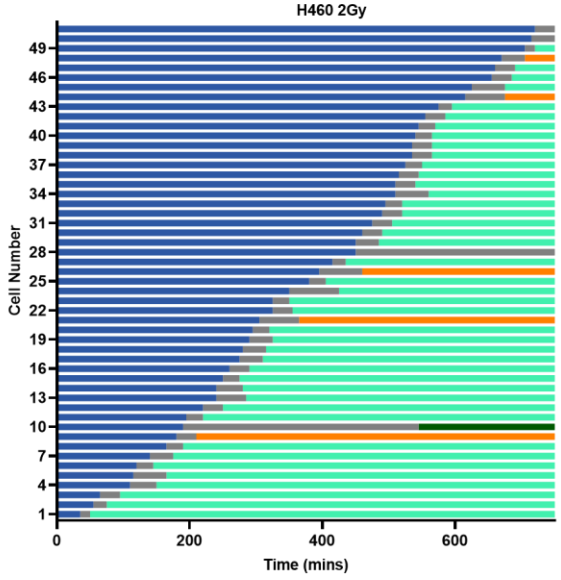


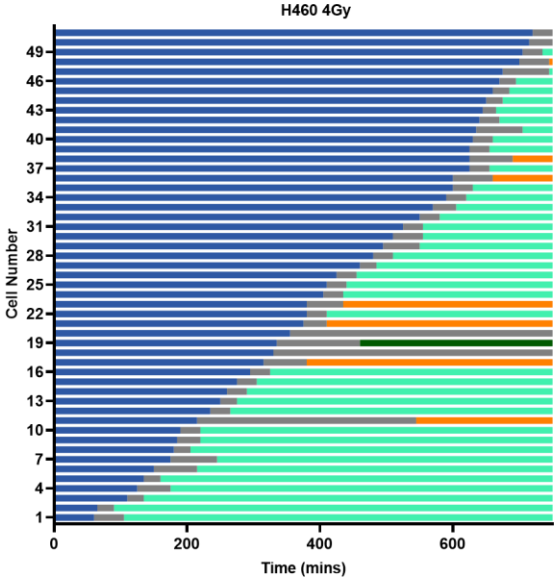

Interphase
Mitosis
Interphase after slippage
Interphase after mitosis
Death in mitosis
One dead after division
Greater than two daughters
Both dead after division
H460 25nM +2Gy
H460 25nM +4Gy
H460 50nM +2Gy
H460 50nM +4Gy
Cell Number
Time (mins)

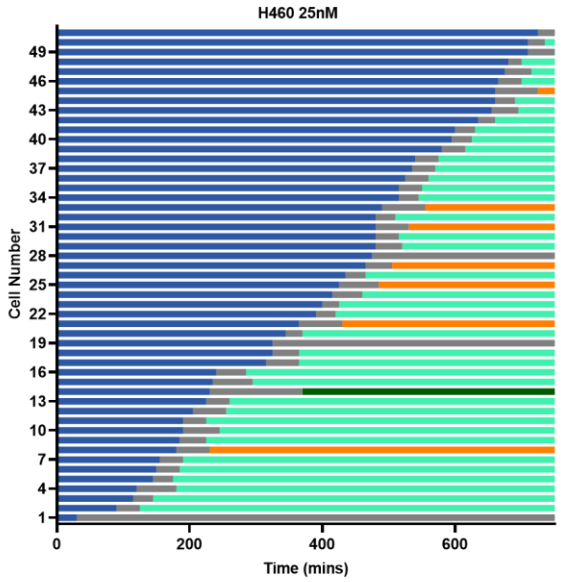

H460 DMSO
H460 2Gy
H460 4Gy
H460 25nM
H460 50nM
Cell Number
Time (mins)
0
200
400
600
1
4
7
10
13
16
19
22
25
28
31
34
37
40
43
46
49
Interphase
Mitosis
Interphase after slippage
Interphase after mitosis
Death in mitosis
One dead after division
Greater than two daughters
Both dead after division

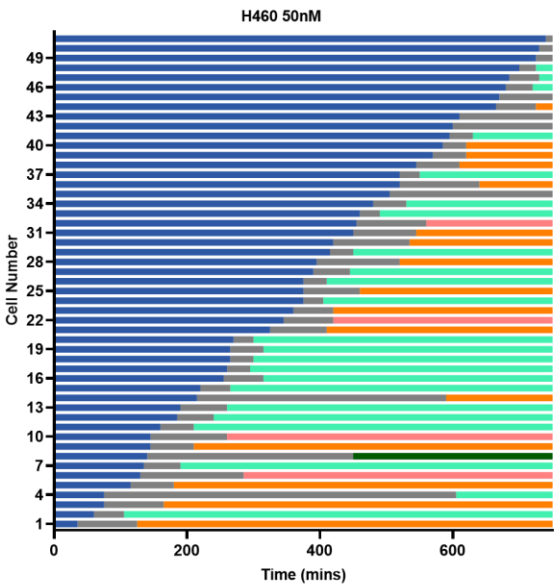

H460 25nM +2Gy
H460 25nM +4Gy
H460 50nM +2Gy
H460 50nM +4Gy
Cell Number
Time (mins)
0
200
400
600
Interphase
Mitosis
Interphase after slippage
Interphase after mitosis
Death in mitosis
One dead after division
Greater than two daughters
Both dead after division


H460 DMSO
Cell Number
Time (mins)


H460 2Gy
Cell Number
Time (mins)


H460 4Gy
Cell Number
Time (mins)


H460 25nM
Cell Number
Time (mins)


H460 50nM
Cell Number
Time (mins)

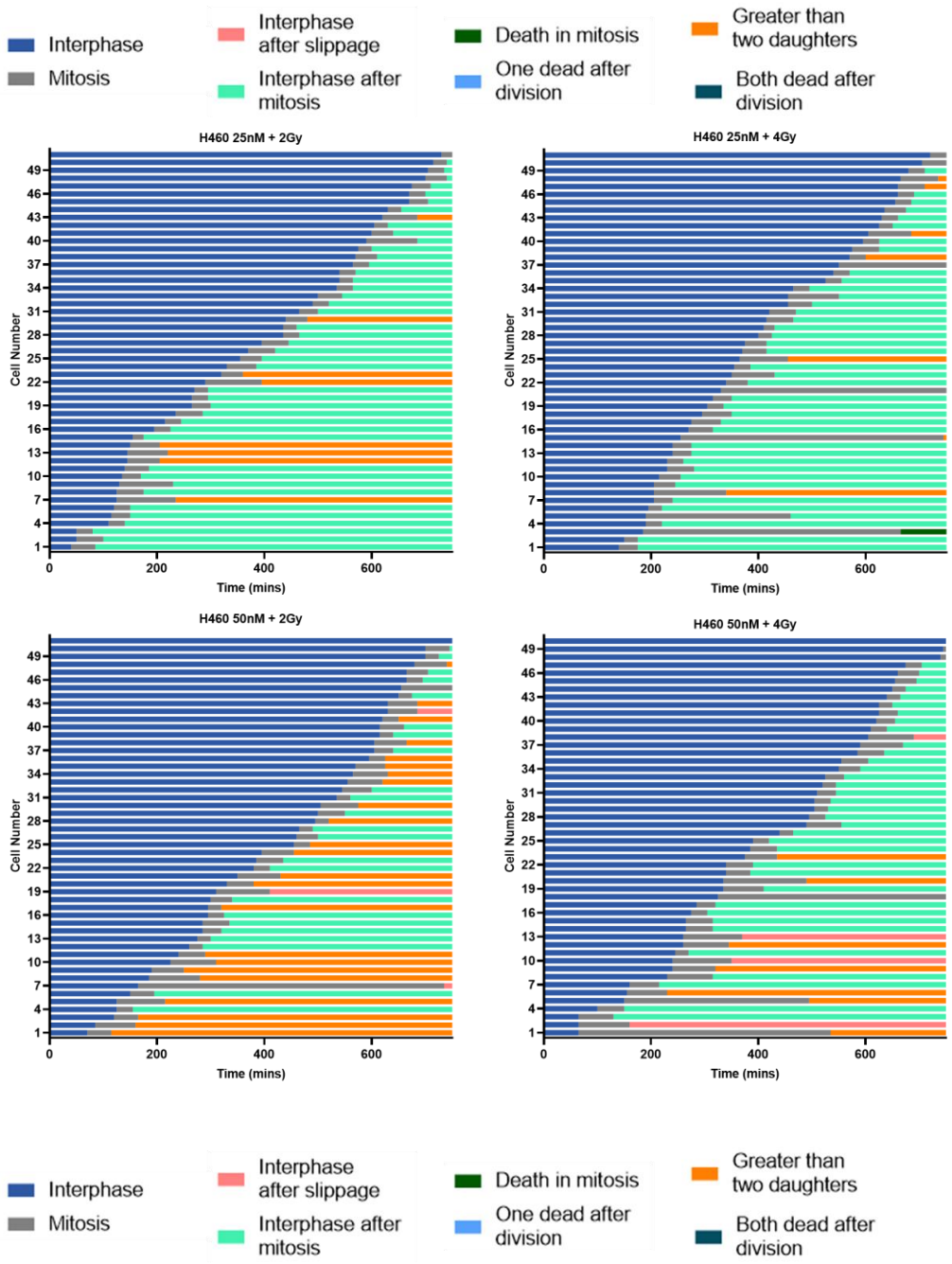
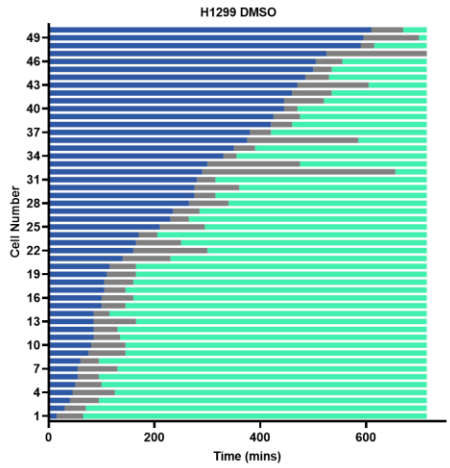
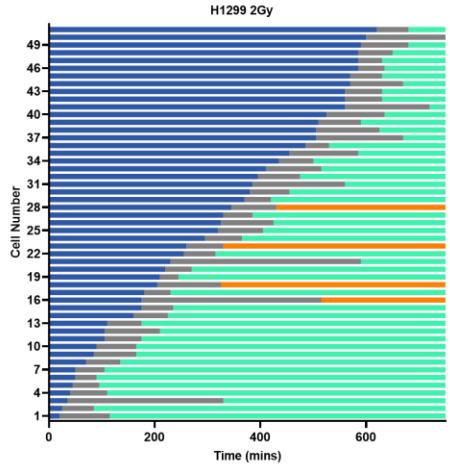
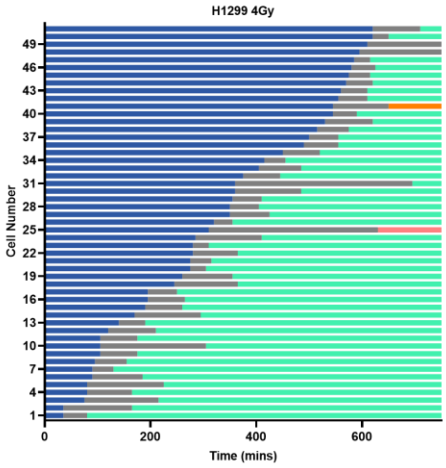


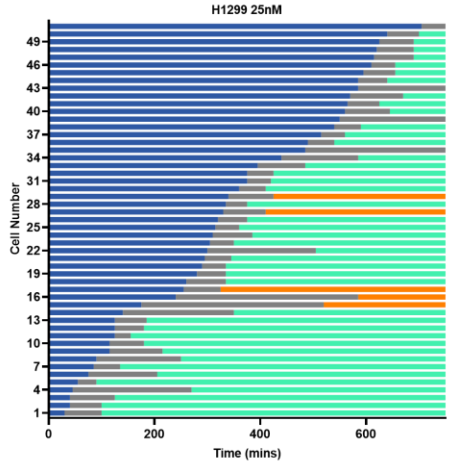
Figure 7-4: ***Stacked Bar charts showing the cellular outcomes of Barasertib +/-IR*** *on live cell imaging using the conditions DMSO, 2Gy, 4Gy, 25nM, 50nM, 25nM + 2Gy, 25 + 4Gy, 50nM + 2Gy, 50nM + 4Gy between 24-36 hours in H460 cells. Cells were treated with Barasertib for 2 hours before adding to IR and left for seven days. Dark blue indicates interphase before mitosis or slippage; Grey indicates mitosis; Pink indicates Interphase after slippage; Cyan indicates Interphase after mitosis; Green indicates Cell death in Mitosis; Sky blue indicates one cell died after division; Teal indicates both daughter cells died after division. Orange indicates that the mother cell is divided into more than two daughters.*

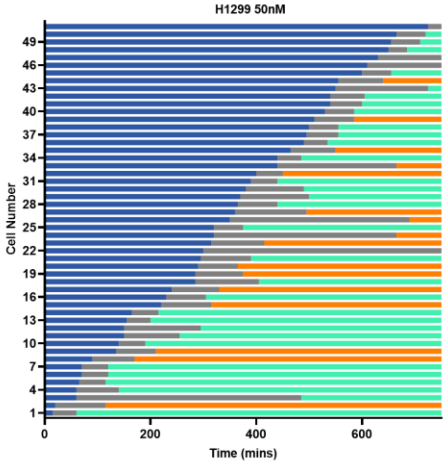
7.4.2.2 H1299 +/- IR

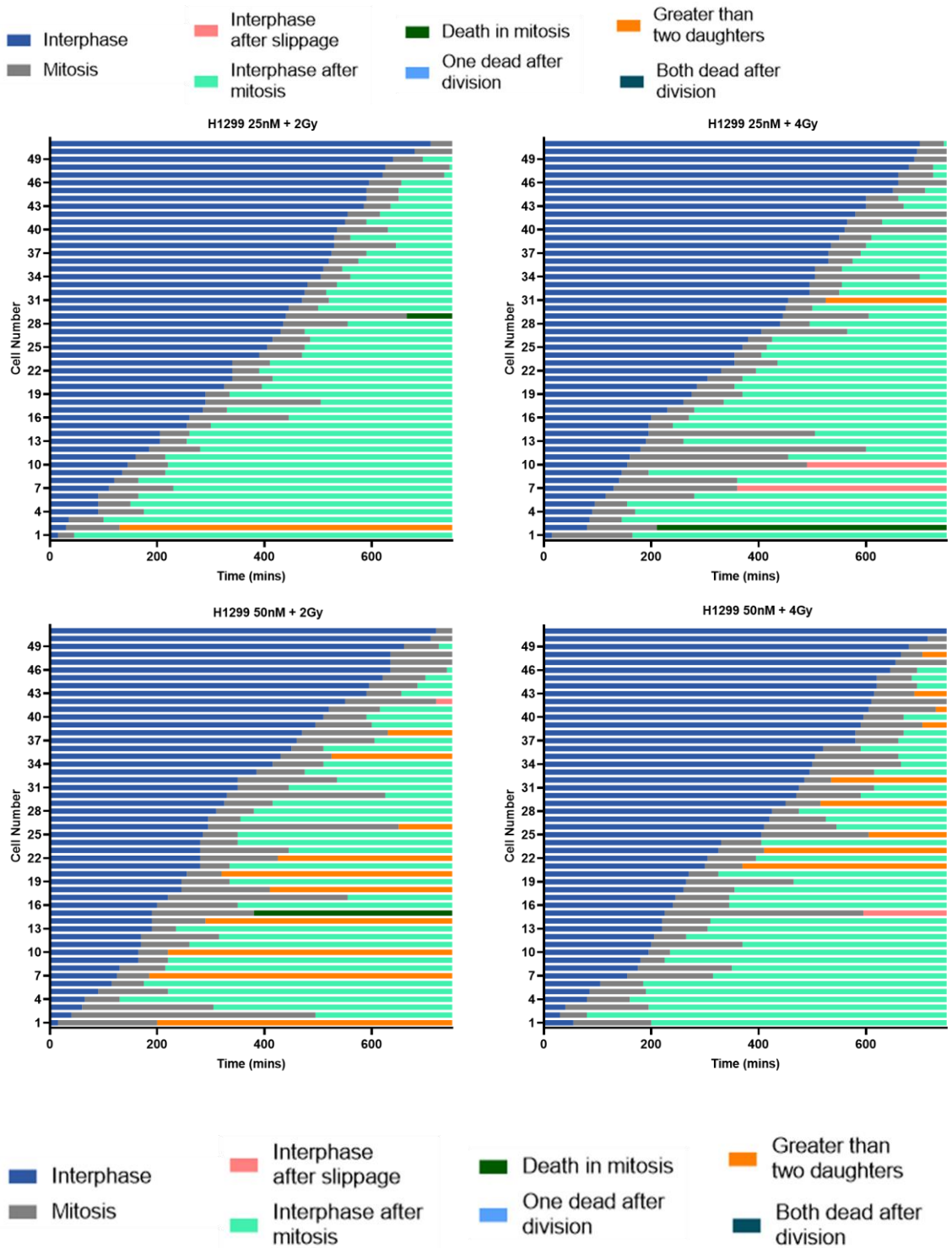


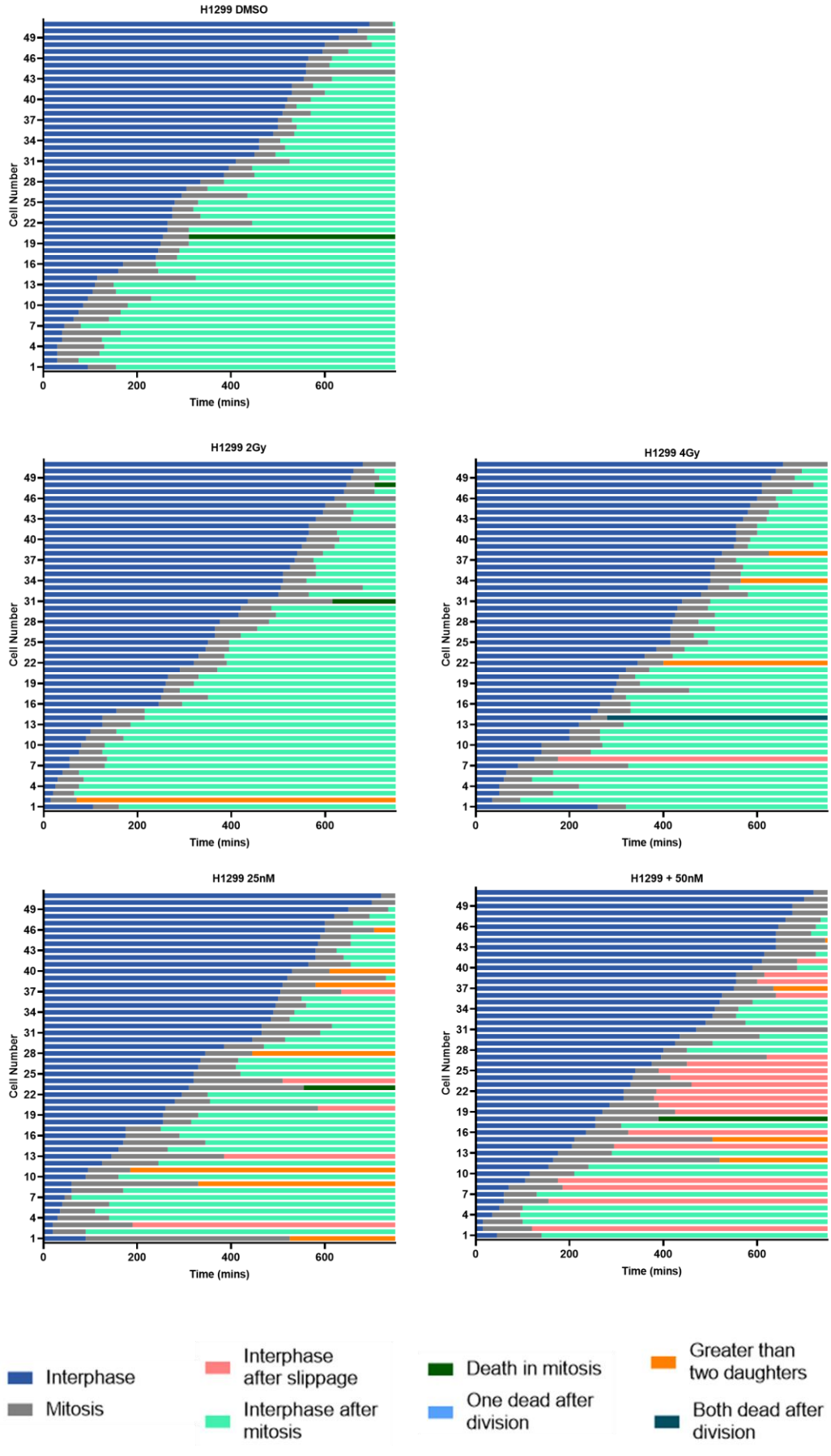


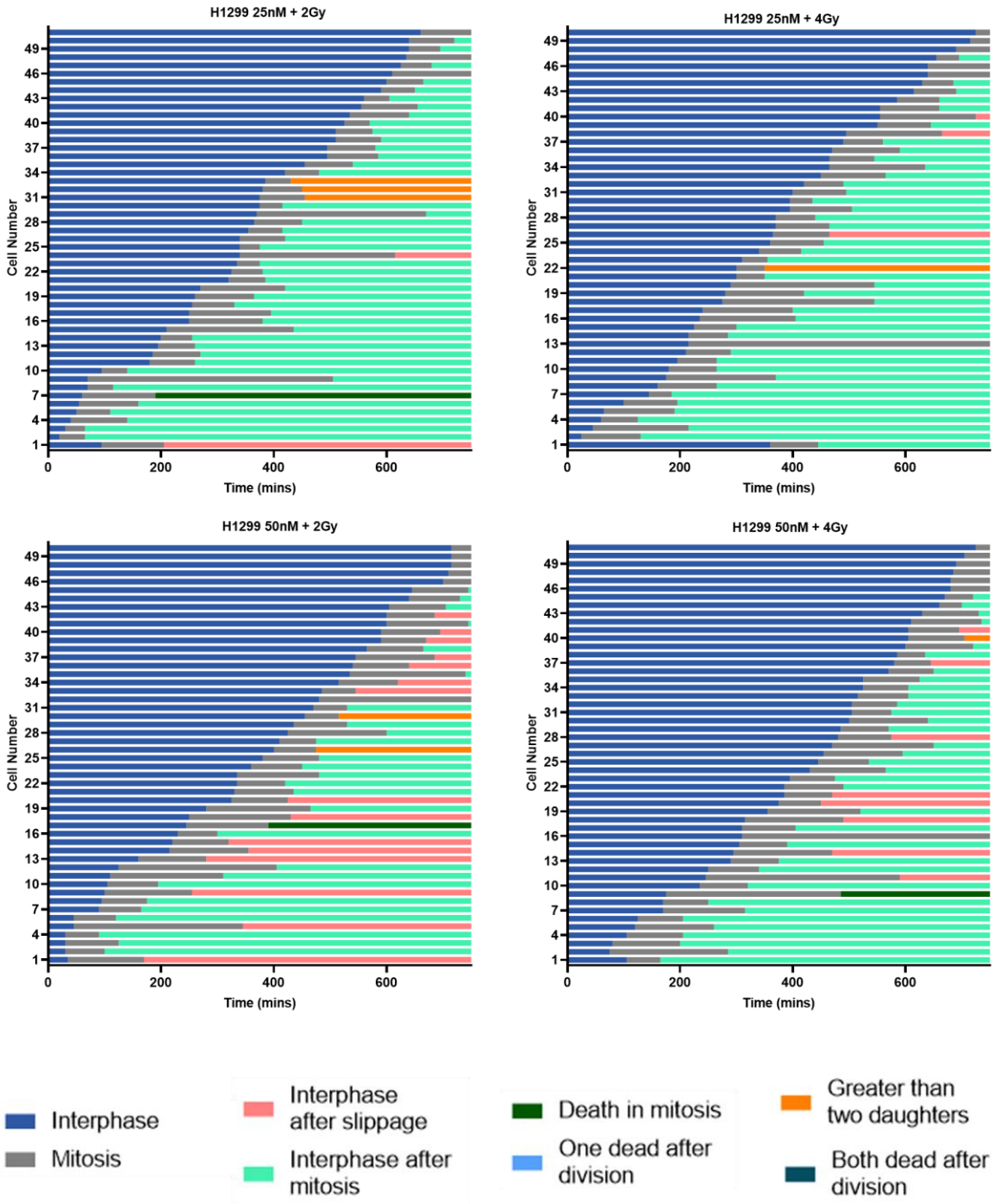


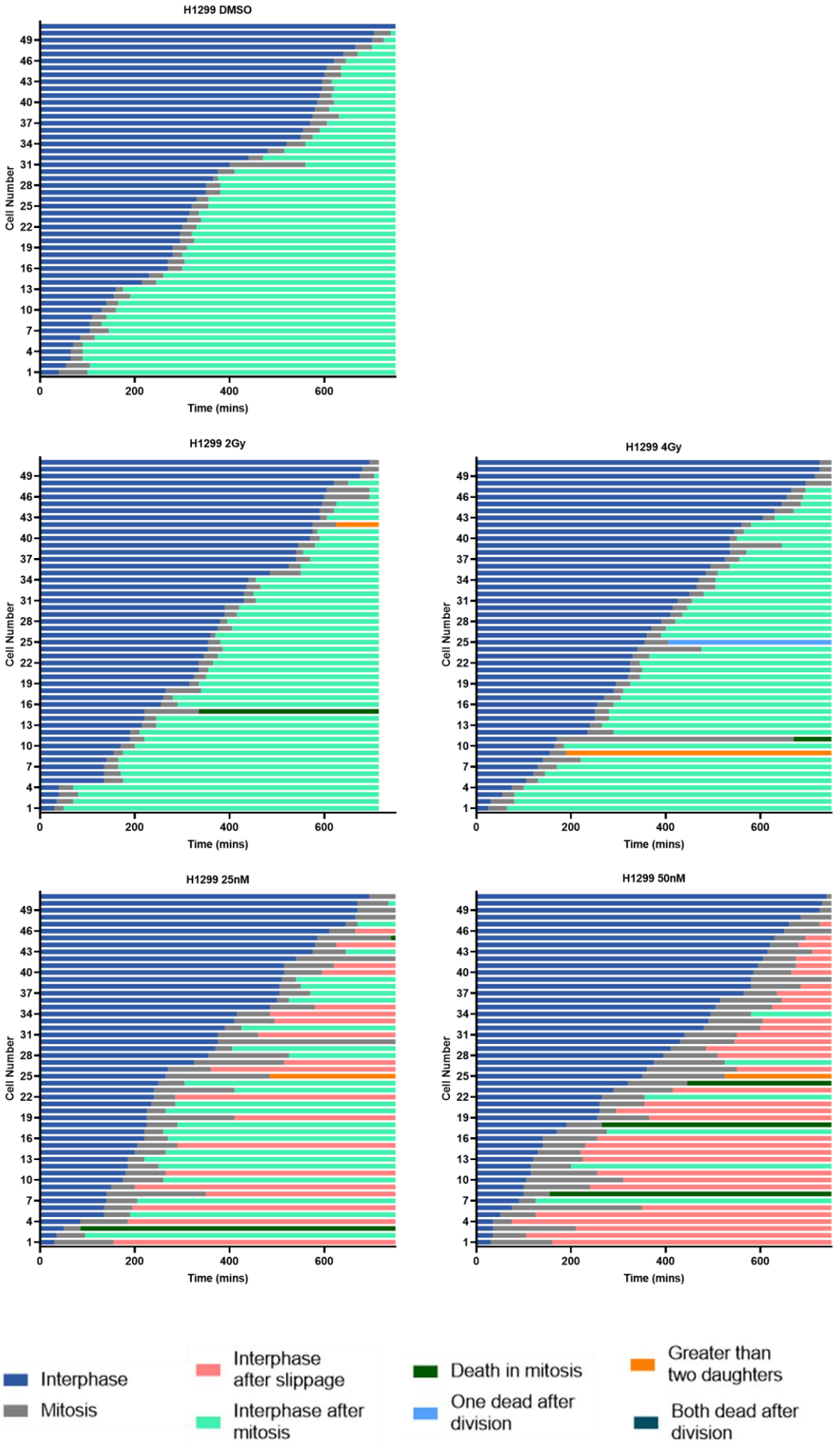





Interphase
Mitosis
Interphase after slippage
Interphase after mitosis
Death in mitosis
One dead after division
Greater than two daughters
Both dead after division
H1299 25nM + 2Gy
H1299 25nM + 4Gy
H1299 50nM + 2Gy
H1299 50nM + 4Gy
Cell Number
Time (mins)
0
200
400
600
1
4
7
10
13
16
19
22
25
28
31
34
37
40
43
46
49


H1299 DMSO
H1299 2Gy
H1299 4Gy
H1299 25nM
H1299 + 50nM
Cell Number
Time (mins)
0
200
400
600
1
4
7
10
13
16
19
22
25
28
31
34
37
40
43
46
49
Interphase
Mitosis
Interphase after slippage
Interphase after mitosis
Death in mitosis
One dead after division
Greater than two daughters
Both dead after division


H1299 25nM + 2Gy
H1299 25nM + 4Gy
H1299 50nM + 2Gy
H1299 50nM + 4Gy
Cell Number
Time (mins)
0
200
400
600
1
4
7
10
13
16
19
22
25
28
31
34
37
40
43
46
49
Interphase
Mitosis
Interphase after slippage
Interphase after mitosis
Death in mitosis
One dead after division
Greater than two daughters
Both dead after division


H1299 DMSO
H1299 2Gy
H1299 4Gy
H1299 25nM
H1299 50nM
Cell Number
Time (mins)
0
200
400
600
Interphase
Mitosis
Interphase after slippage
Interphase after mitosis
Death in mitosis
One dead after division
Greater than two daughters
Both dead after division

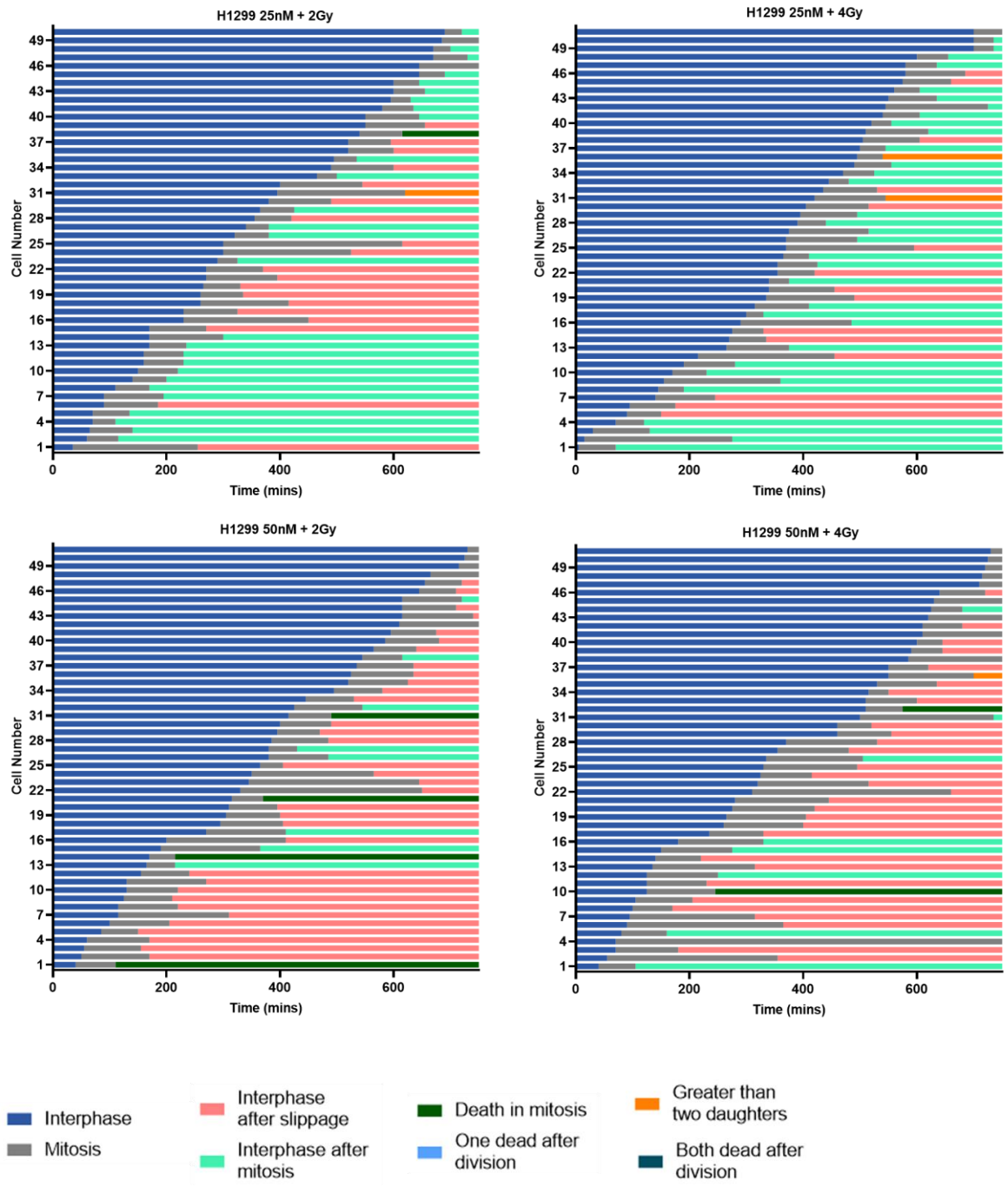
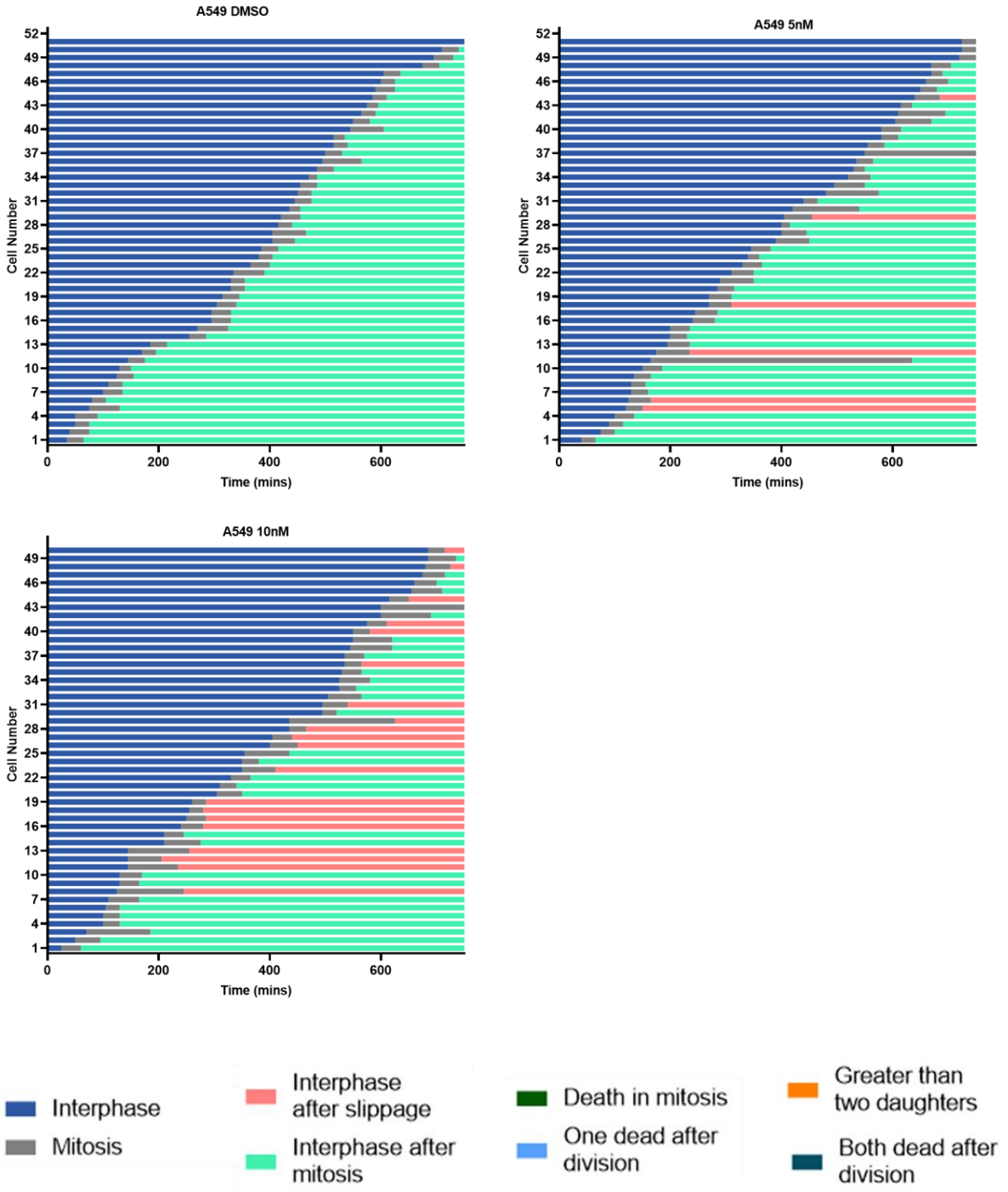
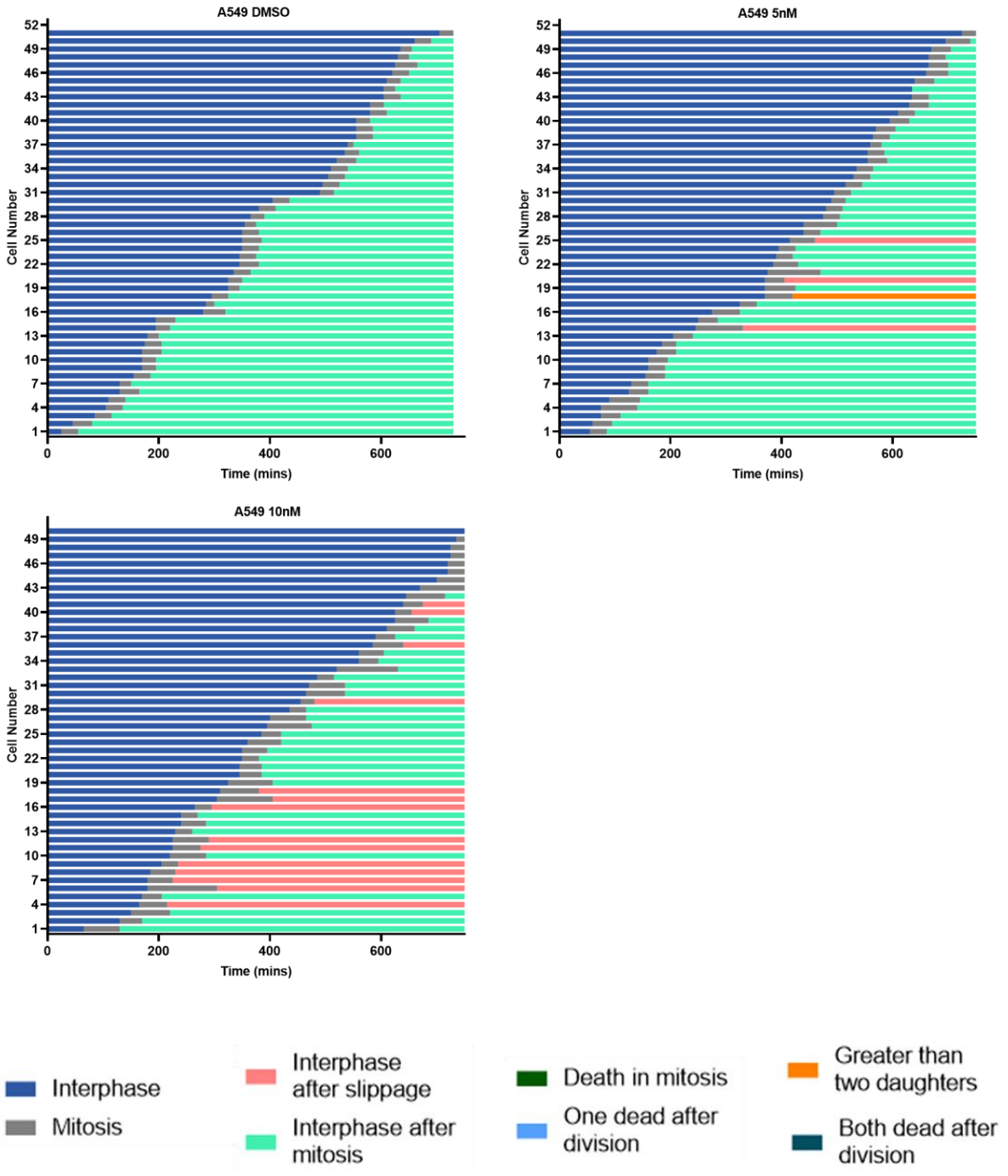


Figure 7-5: ***Stacked Bar charts showing the cellular outcomes of Barasertib +/-IR*** *on live cell imaging using the conditions DMSO, 2Gy, 4Gy, 25nM, 50nM, 25nM + 2Gy, 25 + 4Gy, 50nM + 2Gy, 50nM + 4Gy between 24-36 hours in H1299 cells. Cells were treated with Barasertib for 2 hours before adding to IR and left for seven days. Dark blue indicates interphase before mitosis or slippage; Grey indicates mitosis; Pink indicates Interphase after slippage; Cyan indicates Interphase after mitosis; Green indicates Cell death in Mitosis; Sky blue indicates one cell died after division, Teal*

indicates both daughter cells died after division, and orange indicates that the mother cell divided into more than two daughters.

7.4.2.3 A549 plus Barasertib alone




A549 DMSO
A549 5nM
A549 10nM
Cell Number
Time (mins)
0
200
400
600
Interphase
Mitosis
Interphase after slippage
Interphase after mitosis
Death in mitosis
One dead after division
Greater than two daughters
Both dead after division

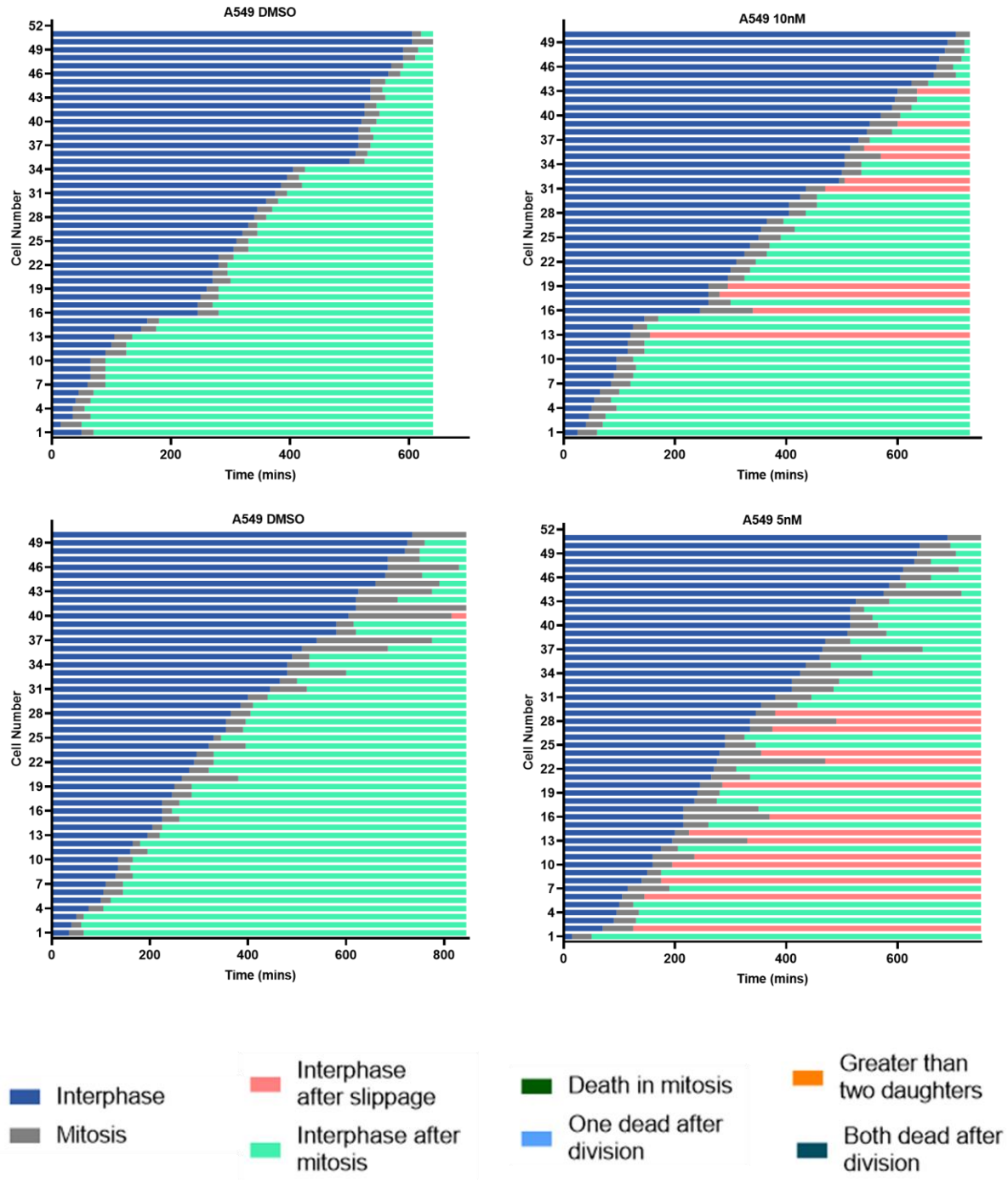
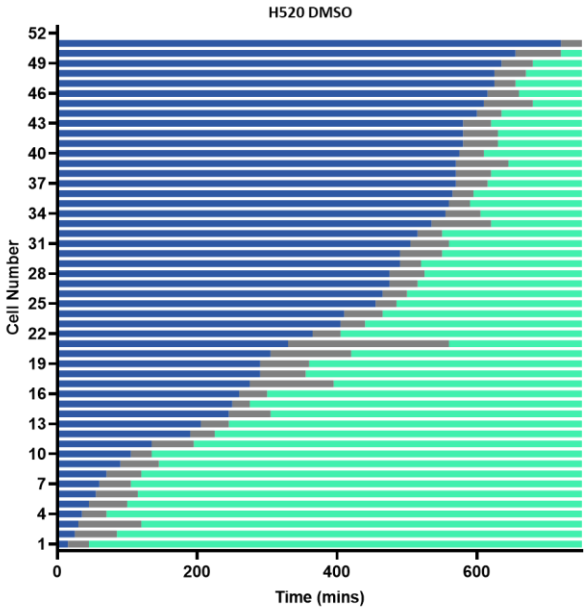
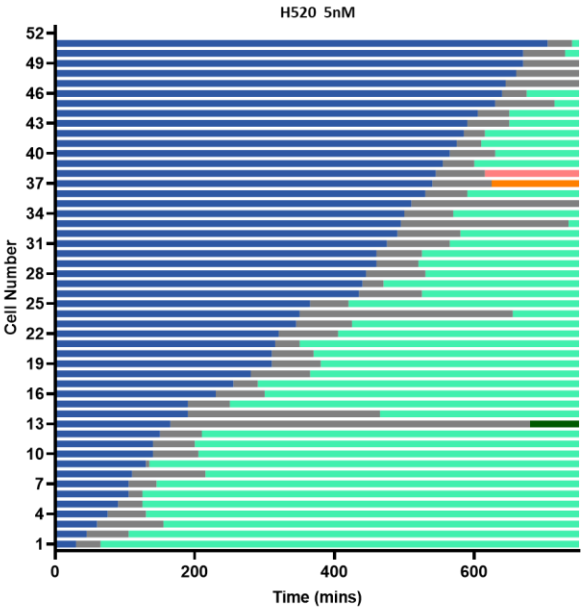


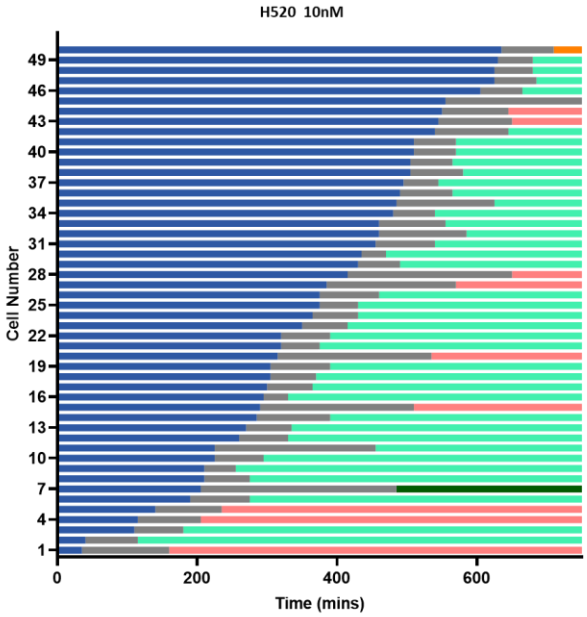
Figure 7-6: ***Stacked Bar charts showing the cellular outcomes of Barasertib*** *on live cell imaging using the conditions DMSO, 5nM and 10nM in 4Gy between 24-36 hours in A549 cells. Cells were treated with Barasertib for 2 hours before adding to IR and left for seven days. Dark blue indicates interphase before mitosis or slippage; Grey indicates mitosis; Pink indicates Interphase after slippage; Cyan indicates Interphase after mitosis; Green indicates Cell death in Mitosis; Sky blue indicates one*

cell died after division, Teal indicates both daughter cells died after division, and orange indicates that the mother cell divided into more than two daughters.

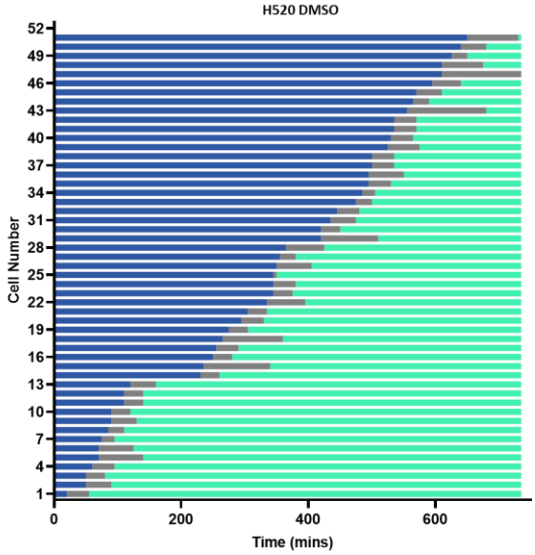
7.4.2.4 H520 plus Barasertib alone

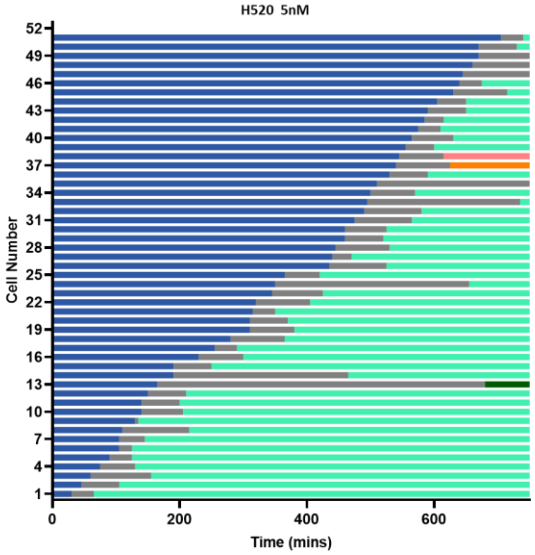


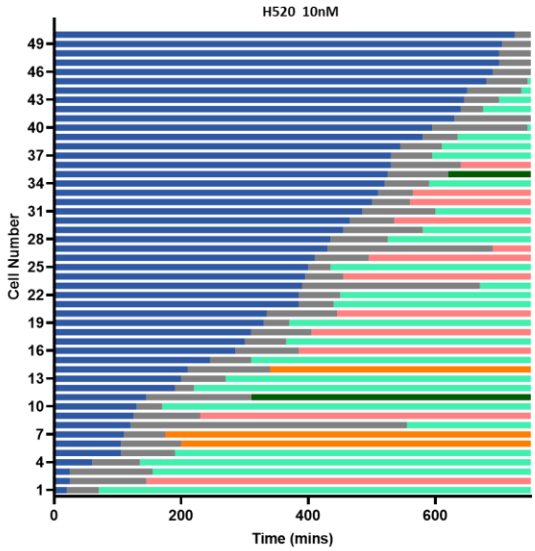





Interphase
Mitosis
Interphase after slippage
Interphase after mitosis
Death in mitosis
One dead after division
Greater than two daughters
Both dead after division


H520 DMSO
Cell Number
Time (mins)


H520 5nM
Cell Number
Time (mins)


H520 10nM
Cell Number
Time (mins)


Interphase
Mitosis
Interphase after slippage
Interphase after mitosis
Death in mitosis
One dead after division
Greater than two daughters
Both dead after division

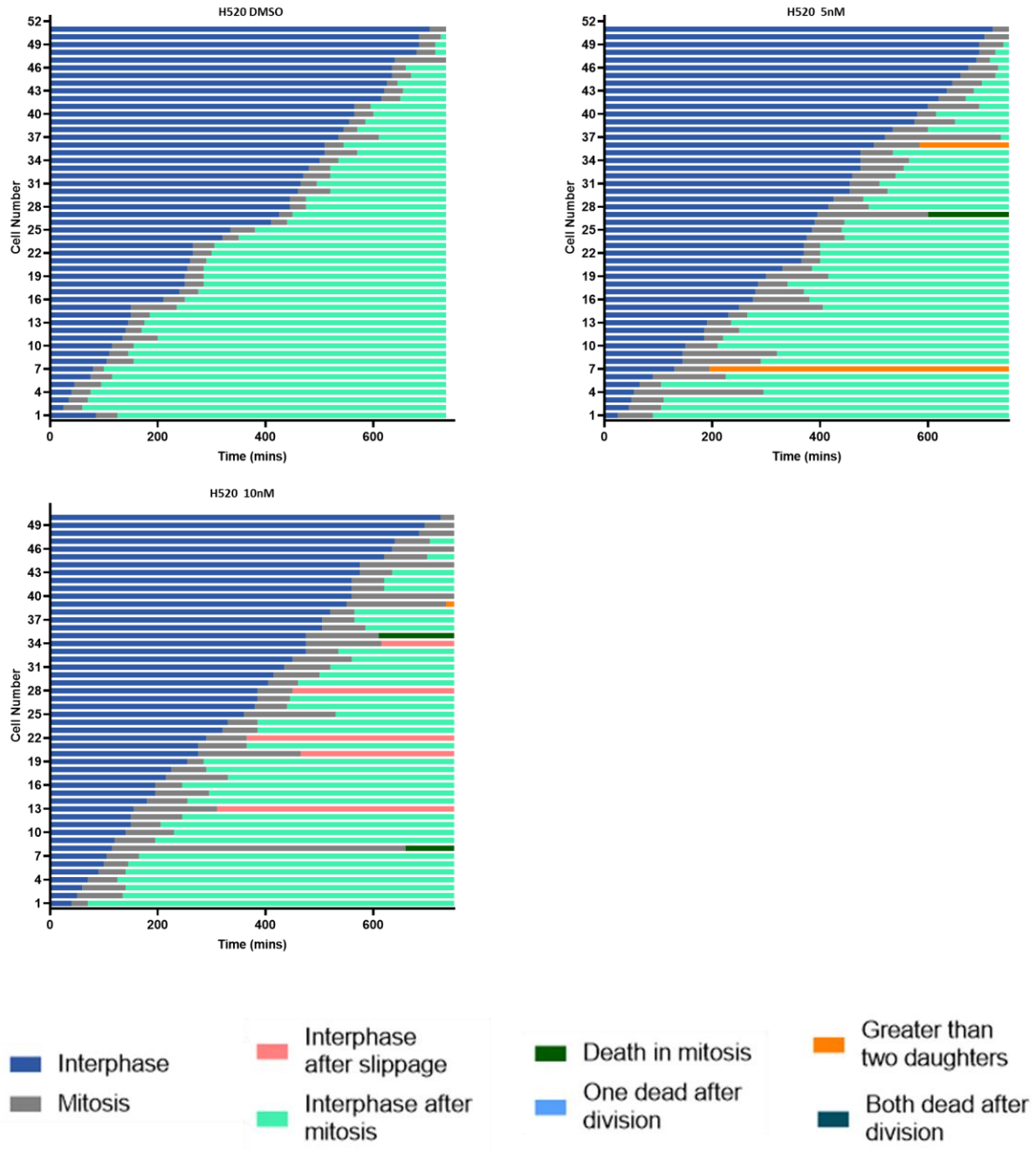
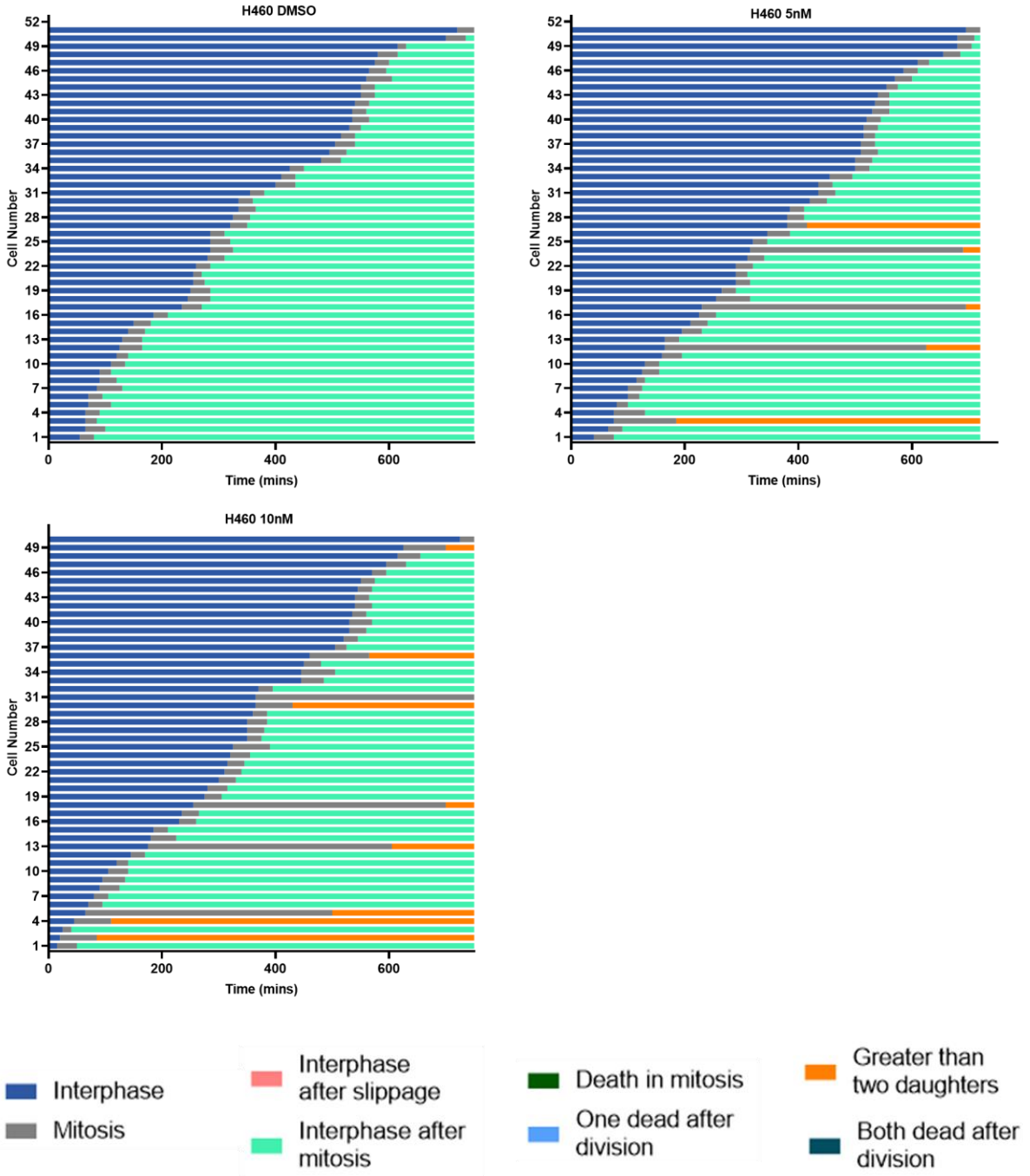
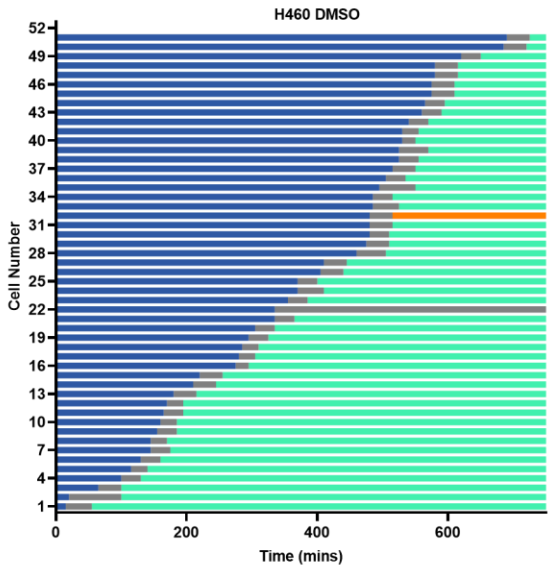
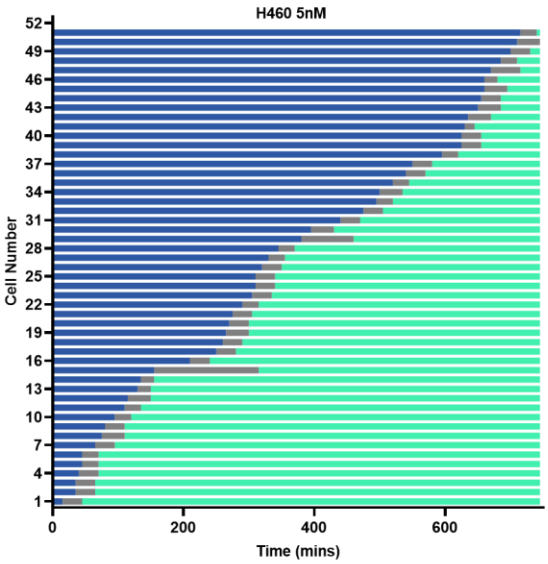


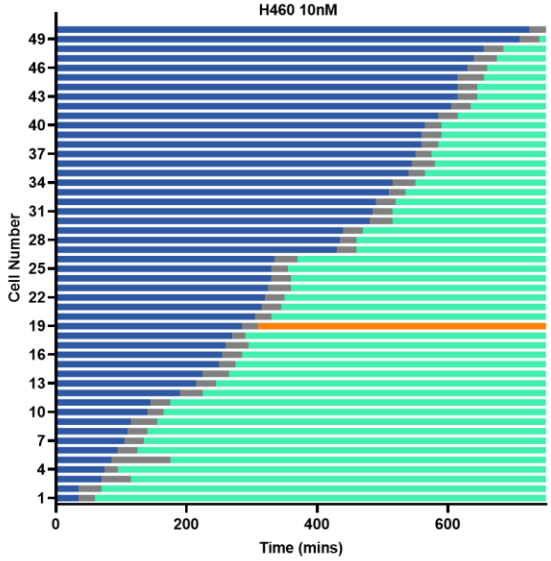
Figure 7-7: ***Stacked Bar charts showing the cellular outcomes of Barasertib*** *on live cell imaging using the conditions DMSO, 5nM and 10nM in 4Gy between 24-36 hours in H520 cells. Cells were treated with Barasertib for 2 hours before adding to IR and left for seven days. Dark blue indicates interphase before mitosis or slippage; Grey indicates mitosis; Pink indicates interphase after slippage; Cyan indicates interphase after mitosis; Green indicates Cell death in Mitosis; Sky blue indicates one cell died after division, Teal indicates both daughter cells died after division, and orange indicates that the mother cell divided into more than two daughters.*

7.4.2.5 H460 plus Barasertib alone




H460 DMSO
Cell Number
Time (mins)
0
200
400
600
1
4
7
10
13
16
19
22
25
28
31
34
37
40
43
46
49
52


H460 5nM
Cell Number
Time (mins)
0
200
400
600
1
4
7
10
13
16
19
22
25
28
31
34
37
40
43
46
49
52


H460 10nM
Cell Number
Time (mins)
0
200
400
600
1
4
7
10
13
16
19
22
25
28
31
34
37
40
43
46
49

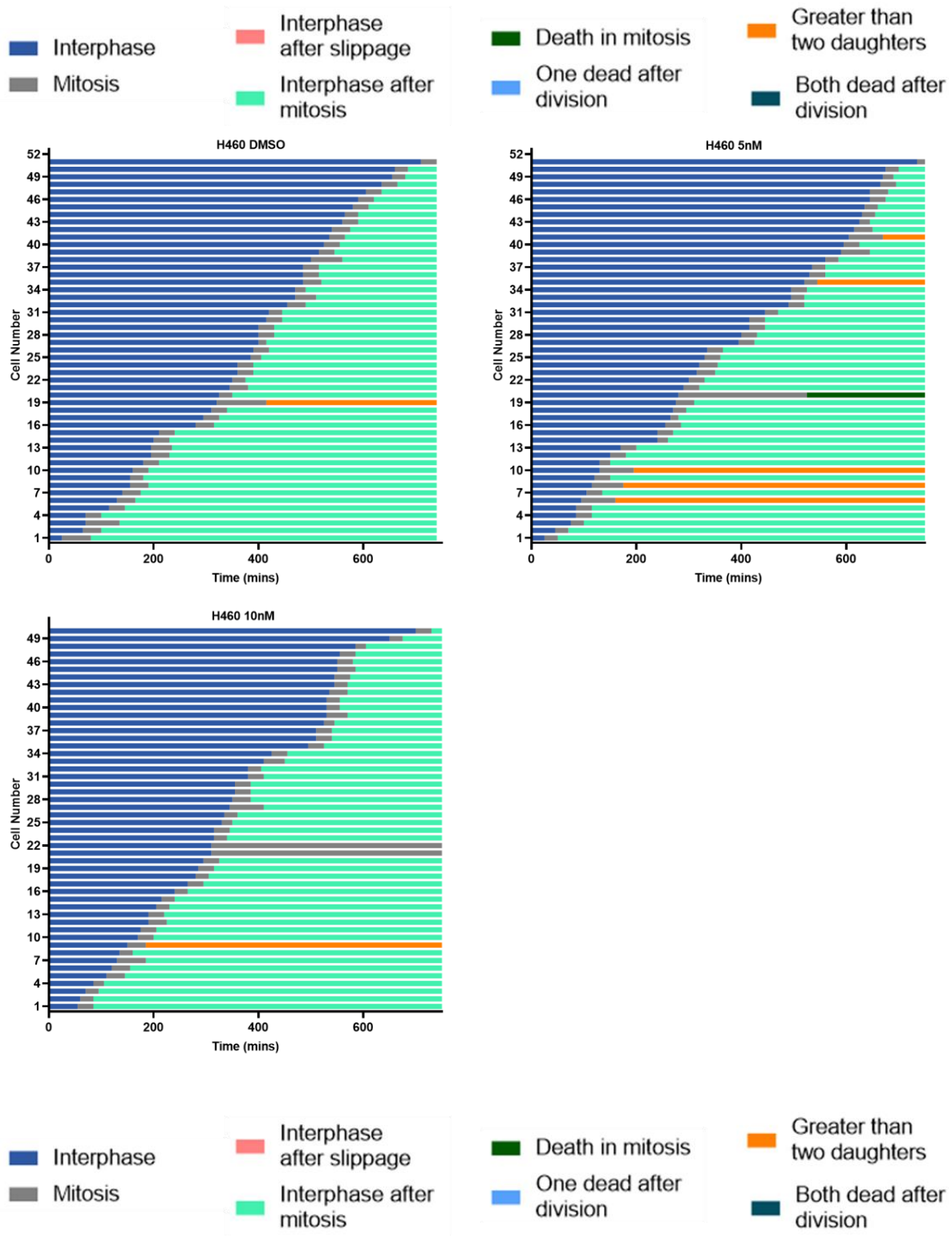
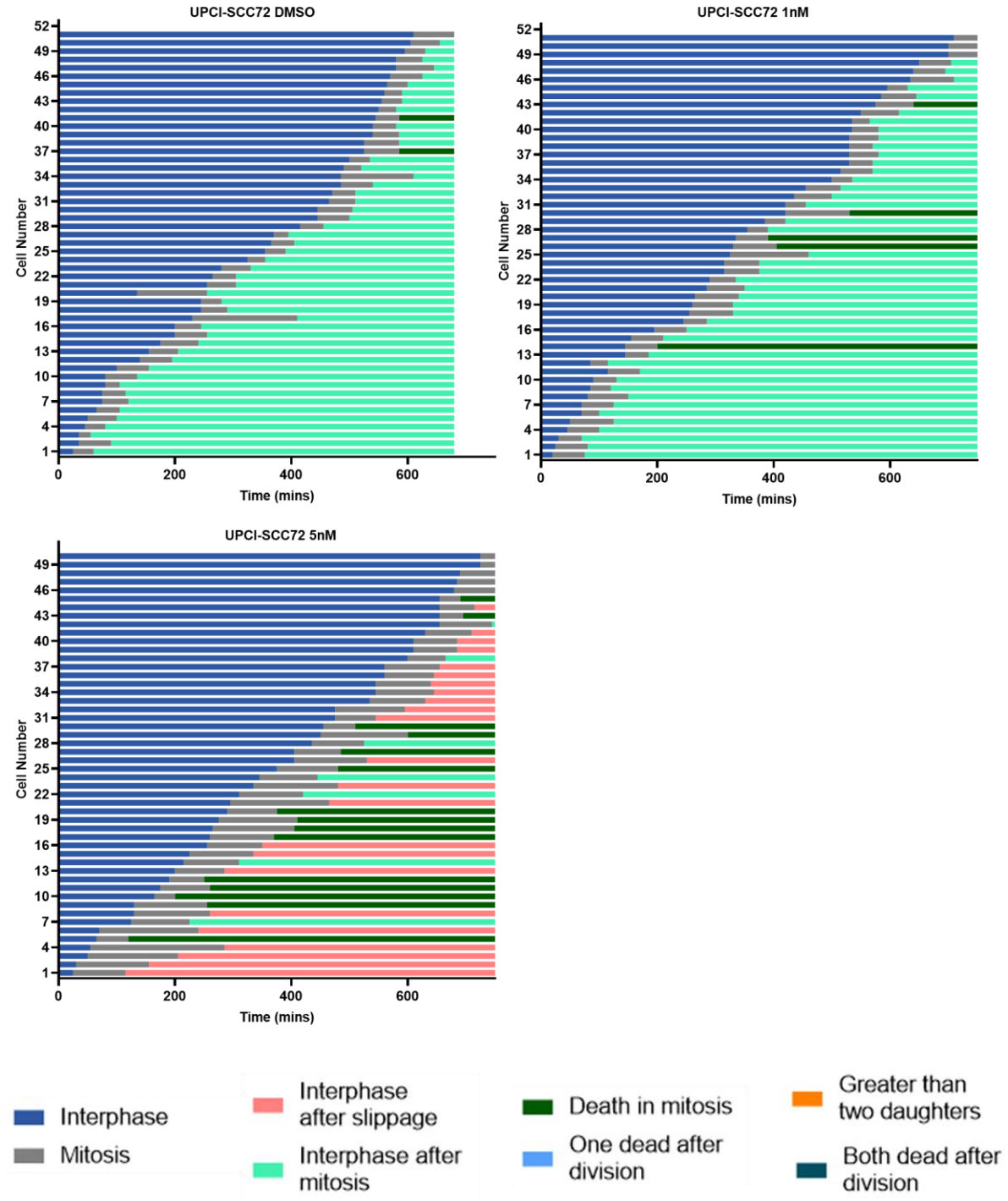
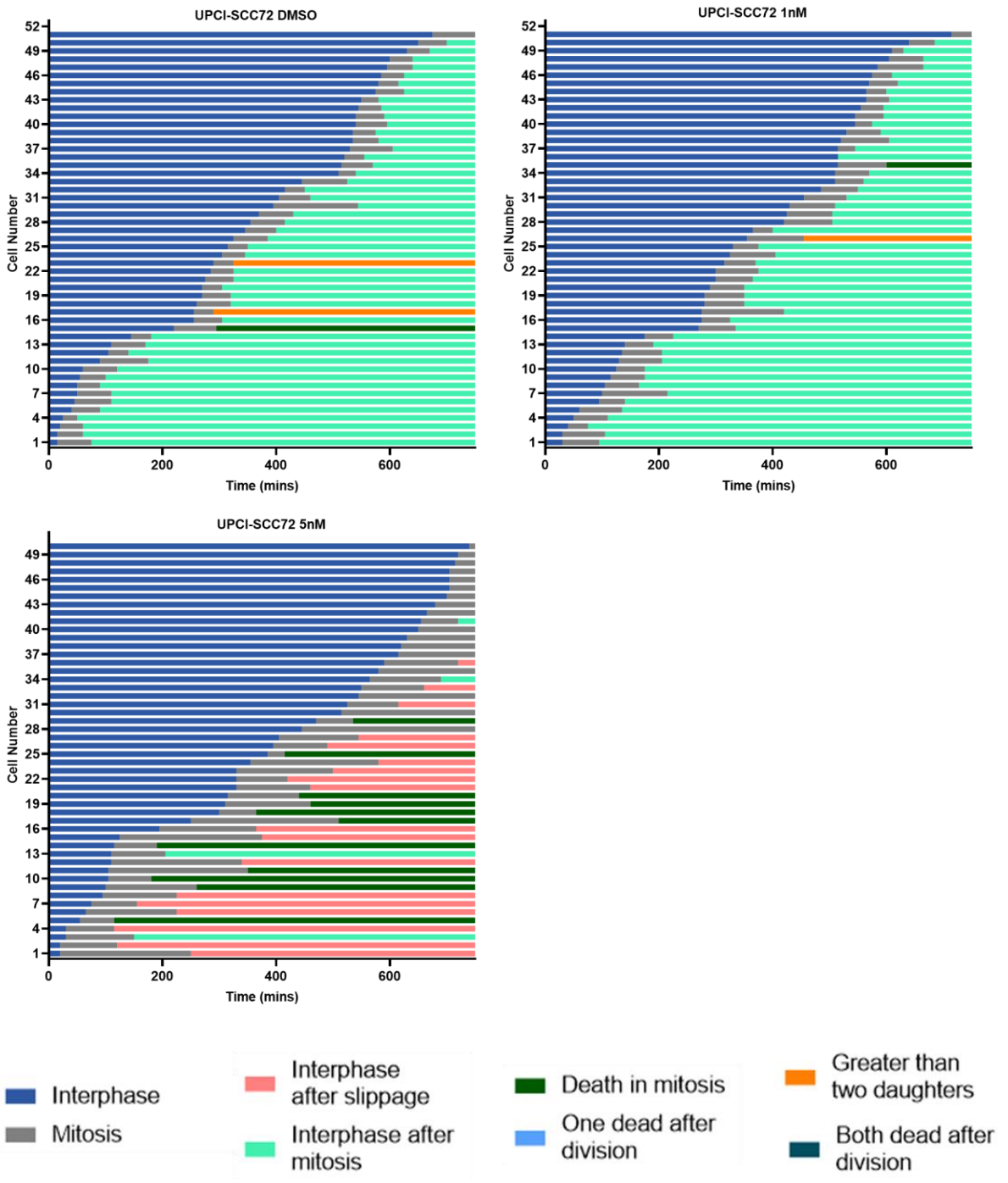


Figure 7-8: ***Stacked Bar charts showing the cellular outcomes of Barasertib*** *on live cell imaging using the conditions DMSO, 5nM and 10nM between 24-36 hours in H460 cells. Cells were treated with Barasertib for 2 hours before adding to IR and left for seven days. Dark blue indicates interphase before mitosis or slippage; Grey indicates mitosis; Pink indicates Interphase after slippage; Cyan*

indicates Interphase after mitosis; Green indicates Cell death in Mitosis; Sky blue indicates one cell died after division, Teal indicates both daughter cells died after division, and orange indicates that the mother cell divided into more than two daughters.

7.4.2.6 UPCI-SCC72 plus Barasertib alone




UPCI-SCC72 DMSO
UPCI-SCC72 1nM
UPCI-SCC72 5nM
Cell Number
Time (mins)
0
200
400
600
Interphase
Mitosis
Interphase after slippage
Interphase after mitosis
Death in mitosis
One dead after division
Greater than two daughters
Both dead after division

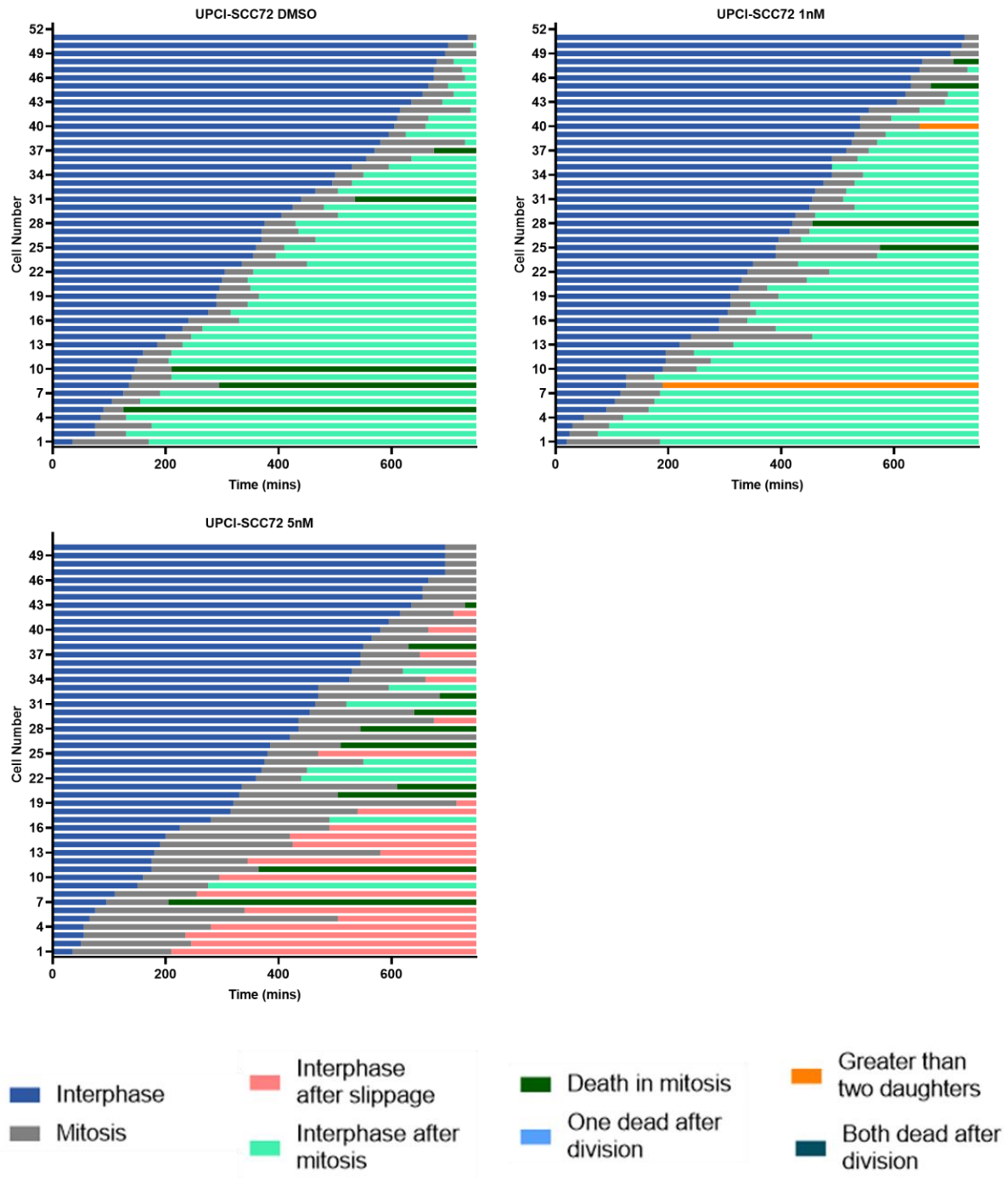
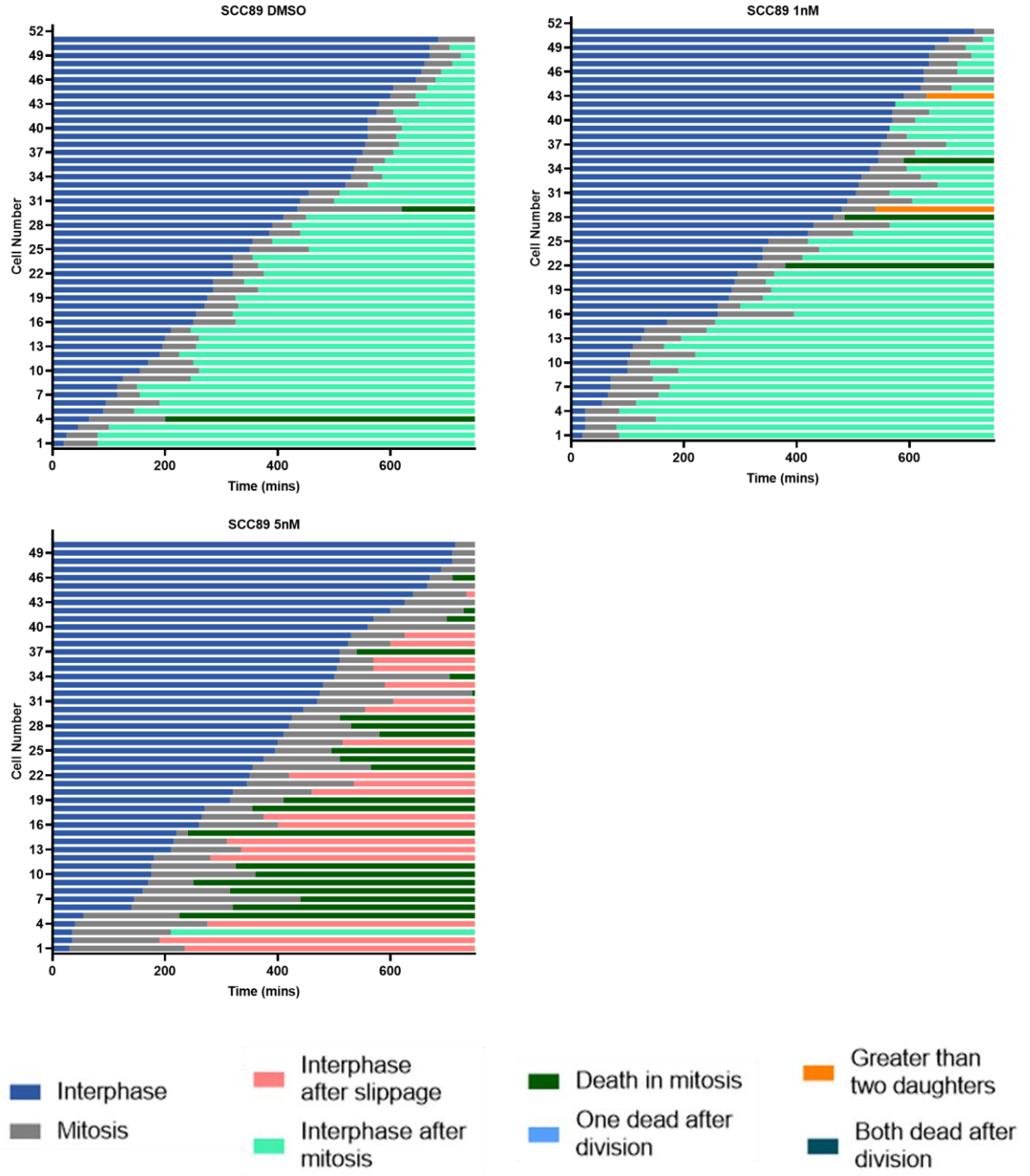
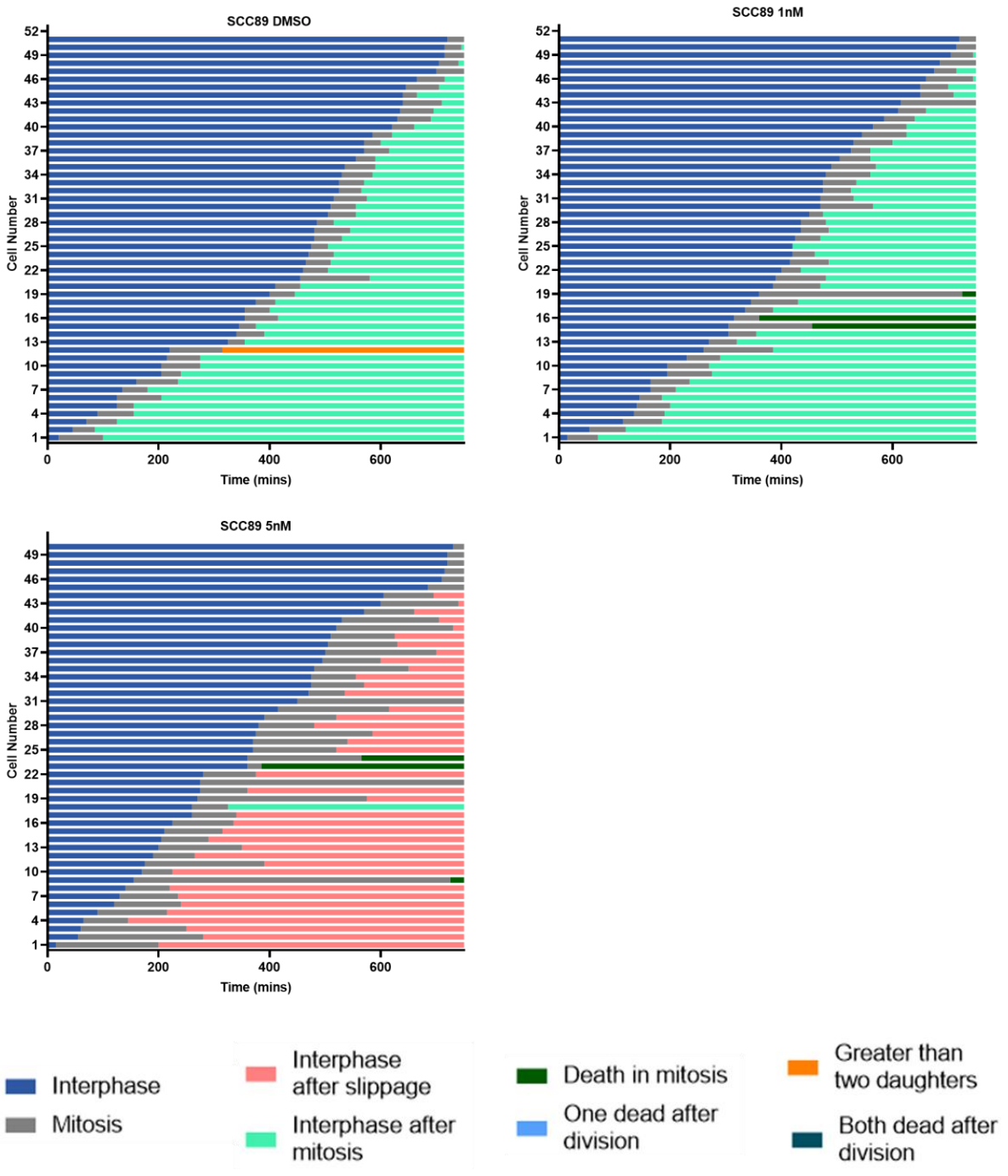


Figure 7-9: ***Stacked Bar charts showing the cellular outcomes of Barasertib*** *on live cell imaging using the conditions DMSO, 5nM and 10nM in 4Gy between 24-36 hours in UPCI-SCC72 cells. Cells were treated with Barasertib for 2 hours before adding to IR and left for seven days. Dark blue indicates interphase before mitosis or slippage; Grey indicates mitosis; Pink indicates Interphase after slippage; Cyan indicates Interphase after mitosis; Green indicates Cell death in Mitosis; Sky blue indicates one cell died after division, Teal indicates both daughter cells died after division, and orange indicates that the mother cell divided into more than two daughters.*

7.4.2.7 SCC89 plus Barasertib alone




SCC89 DMSO
SCC89 1nM
SCC89 5nM
Cell Number
Time (mins)
0
200
400
600
Interphase
Mitosis
Interphase after slippage
Interphase after mitosis
Death in mitosis
One dead after division
Greater than two daughters
Both dead after division

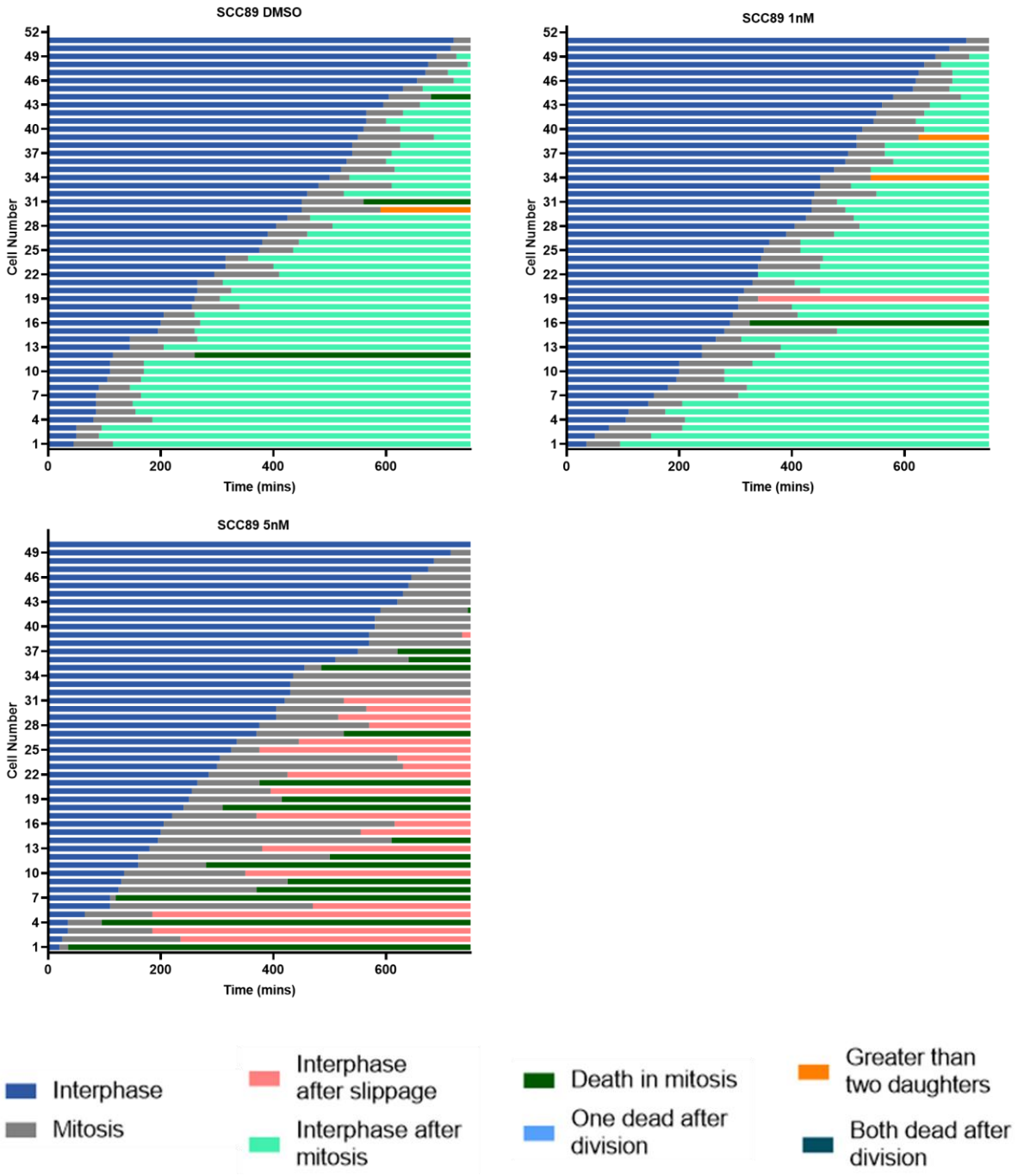
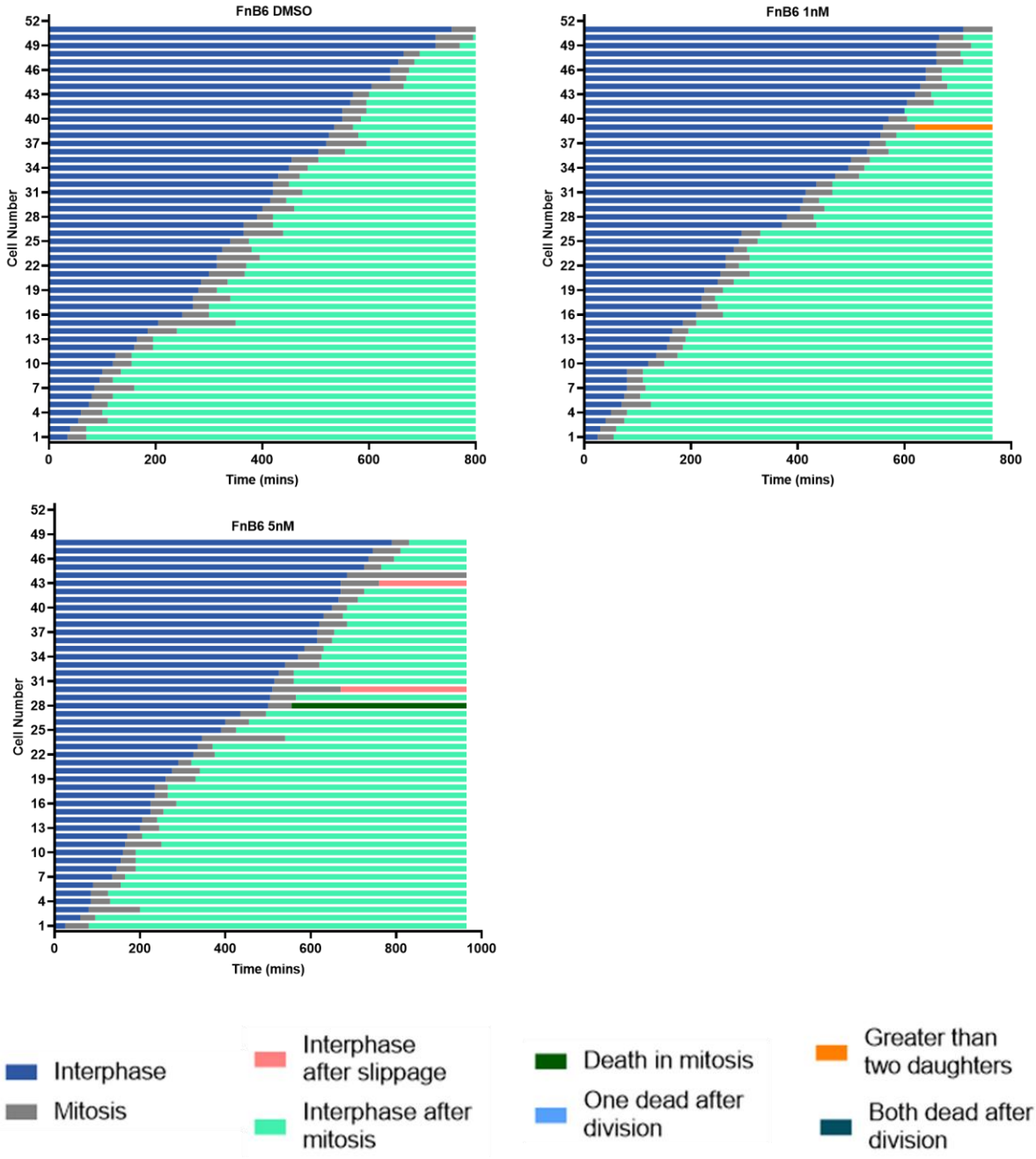
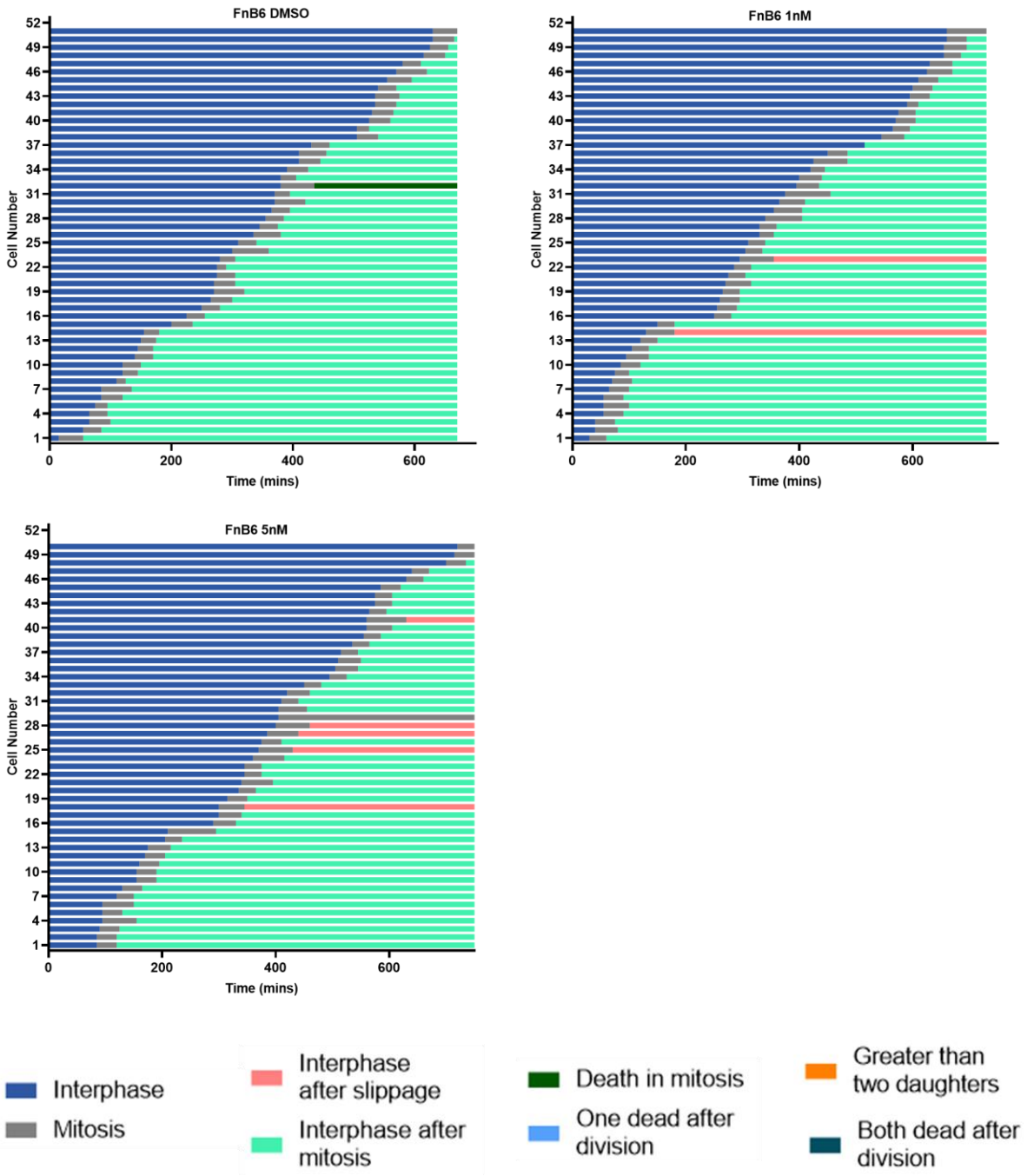


Figure 7-10: ***Stacked Bar charts showing the cellular outcomes of Barasertib*** *on live cell imaging using the conditions DMSO, 5nM and 10nM in 4Gy between 24-36 hours in SCC89 cells. Cells were treated with Barasertib for 2 hours before adding to IR and left for seven days. Dark blue indicates interphase before mitosis or slippage; Grey indicates mitosis; Pink indicates interphase after slippage; Cyan indicates interphase after mitosis; Green indicates Cell death in Mitosis; Sky blue indicates one cell died after division, Teal indicates both daughter cells died after division, and orange indicates that the mother cell divided into more than two daughters.*

7.4.2.8 FnB6 plus Barasertib alone




FnB6 DMSO
FnB6 1nM
FnB6 5nM
Cell Number
Time (mins)
0
200
400
600
1
4
7
10
13
16
19
22
25
28
31
34
37
40
43
46
49
52
Interphase
Mitosis
Interphase after slippage
Interphase after mitosis
Death in mitosis
One dead after division
Greater than two daughters
Both dead after division

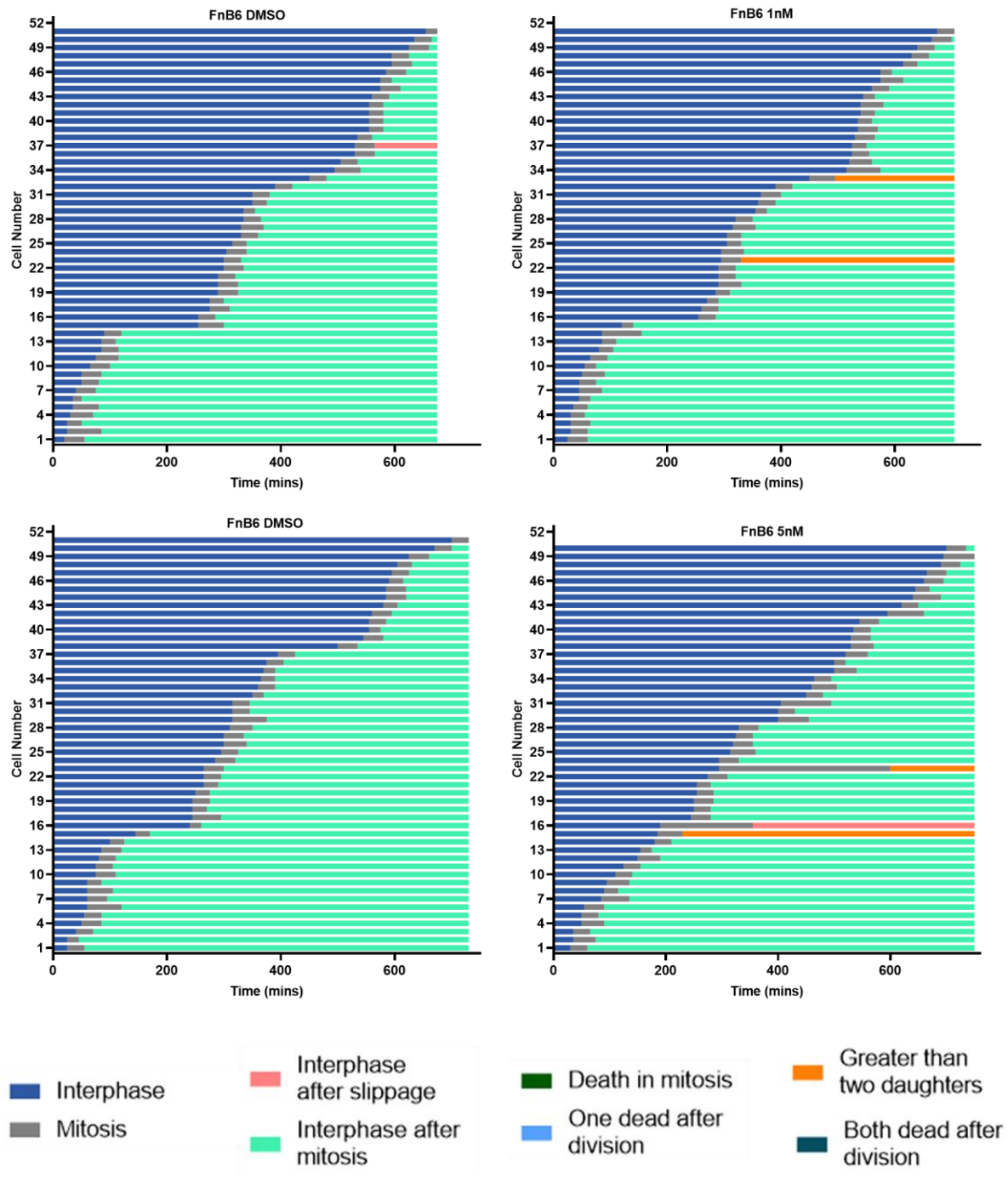
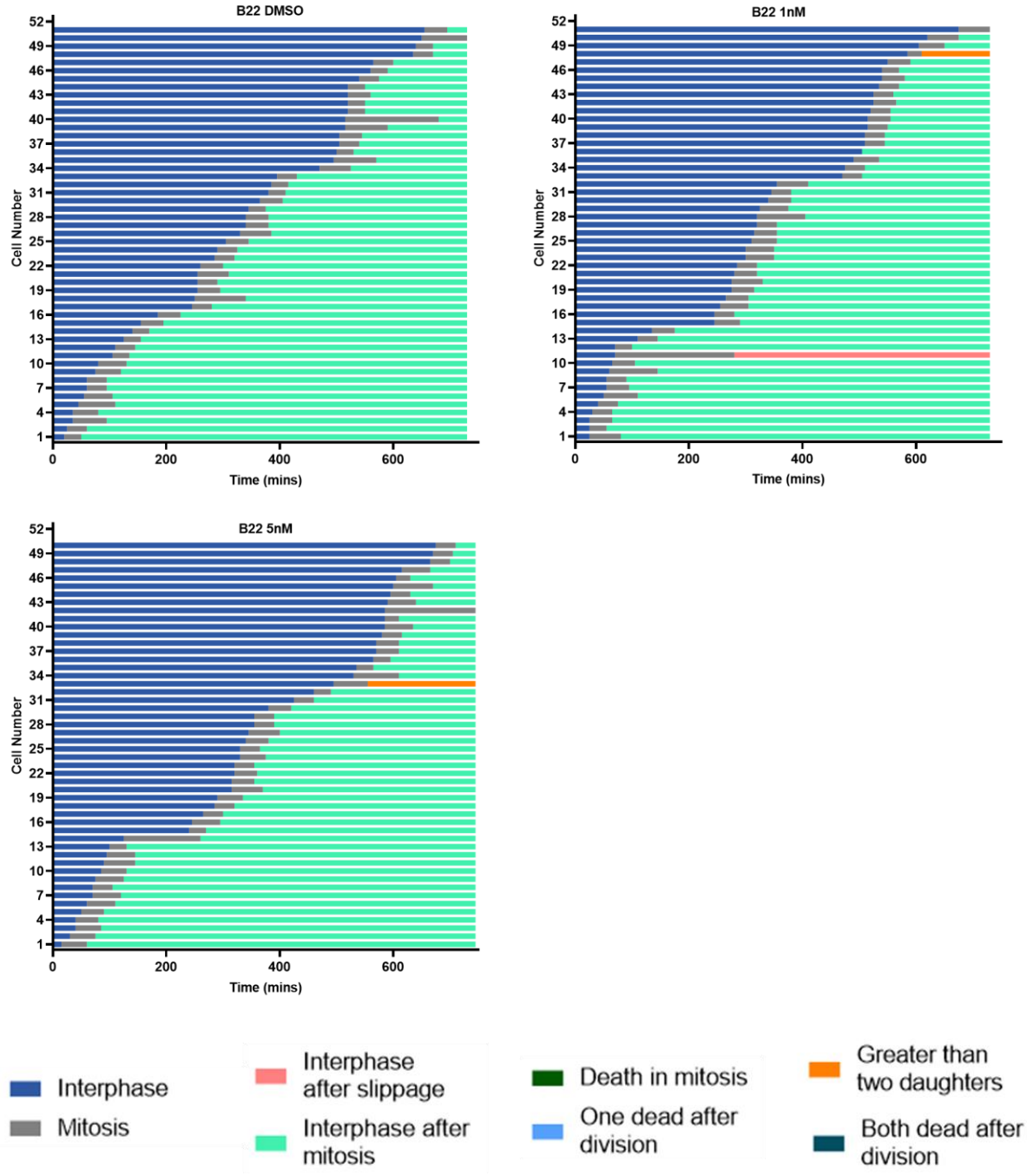
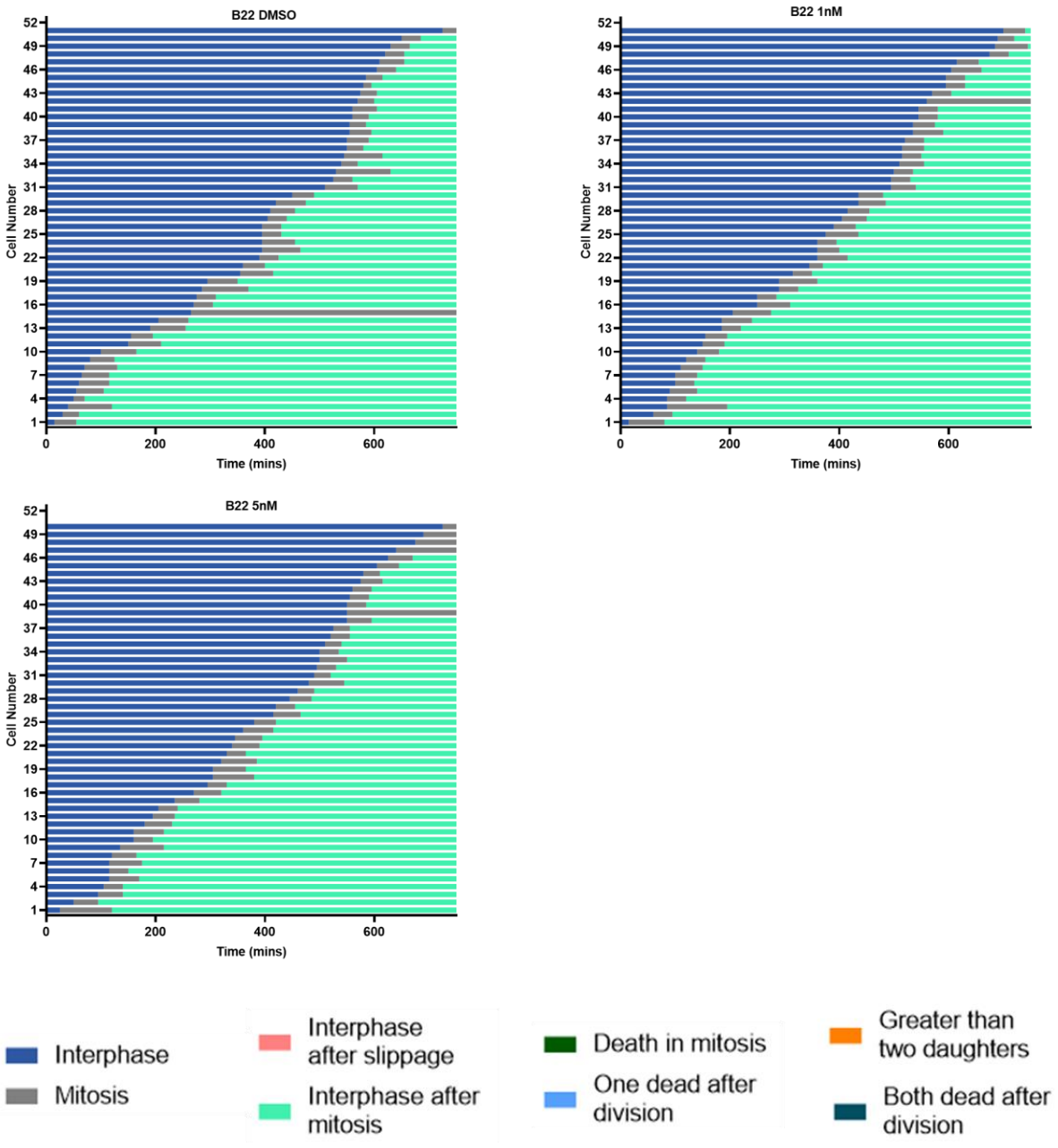


Figure 7-11: ***Stacked Bar charts showing the cellular outcomes of Barasertib*** *on live cell imaging using the conditions DMSO, 5nM and 10nM in 4Gy between 24-36 hours in FnB6 cells. Cells were treated with Barasertib for 2 hours before adding to IR and left for seven days. Dark blue indicates interphase before mitosis or slippage; Grey indicates mitosis; Pink indicates Interphase after slippage; Cyan indicates Interphase after mitosis; Green indicates Cell death in Mitosis; Sky blue indicates one cell died after division, Teal indicates both daughter cells died after division, and orange indicates that the mother cell divided into more than two daughters.*

7.4.2.9 BICR22 plus Barasertib alone




B22 DMSO
B22 1nM
B22 5nM
Cell Number
Time (mins)
0
200
400
600
Interphase
Mitosis
Interphase after slippage
Interphase after mitosis
Death in mitosis
One dead after division
Greater than two daughters
Both dead after division

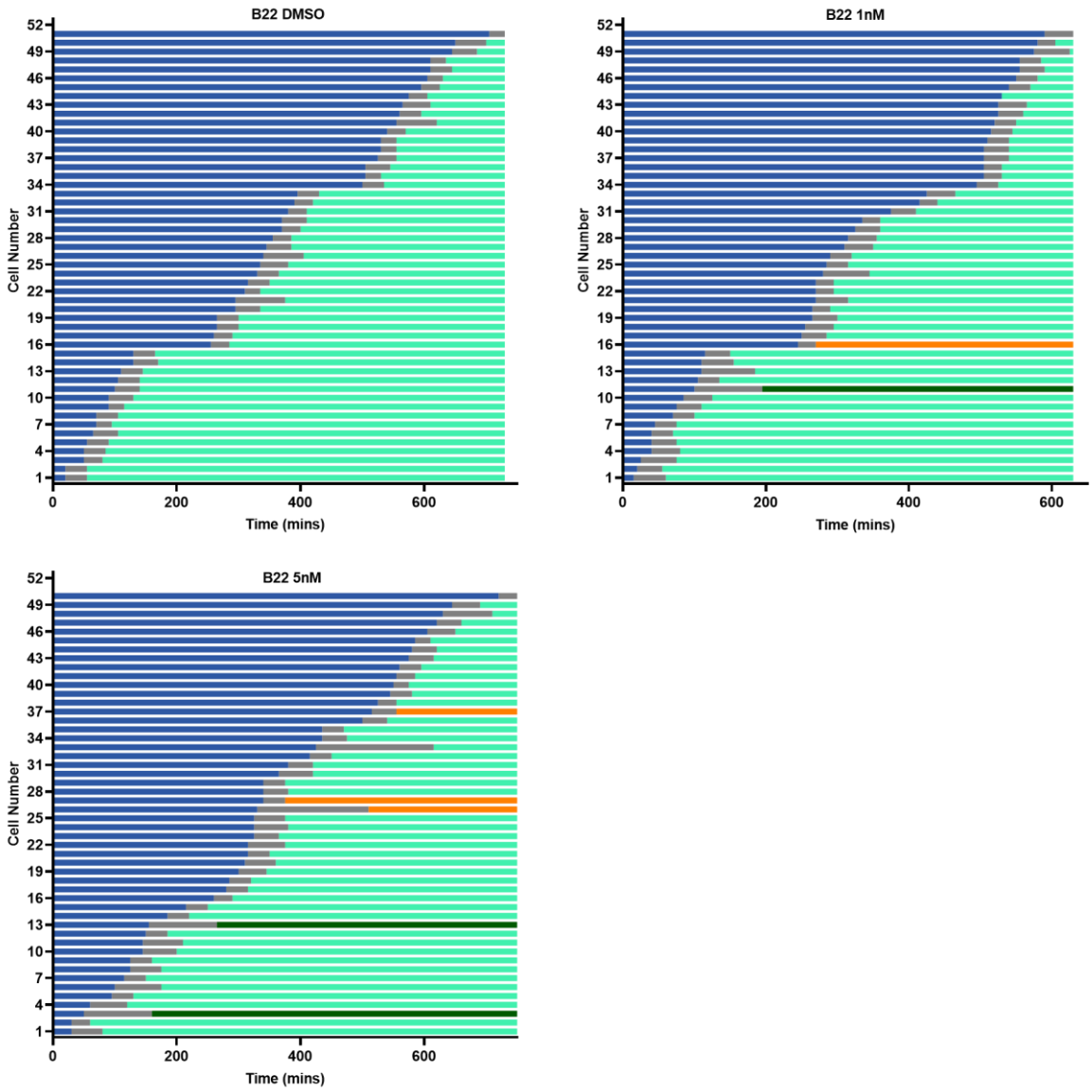
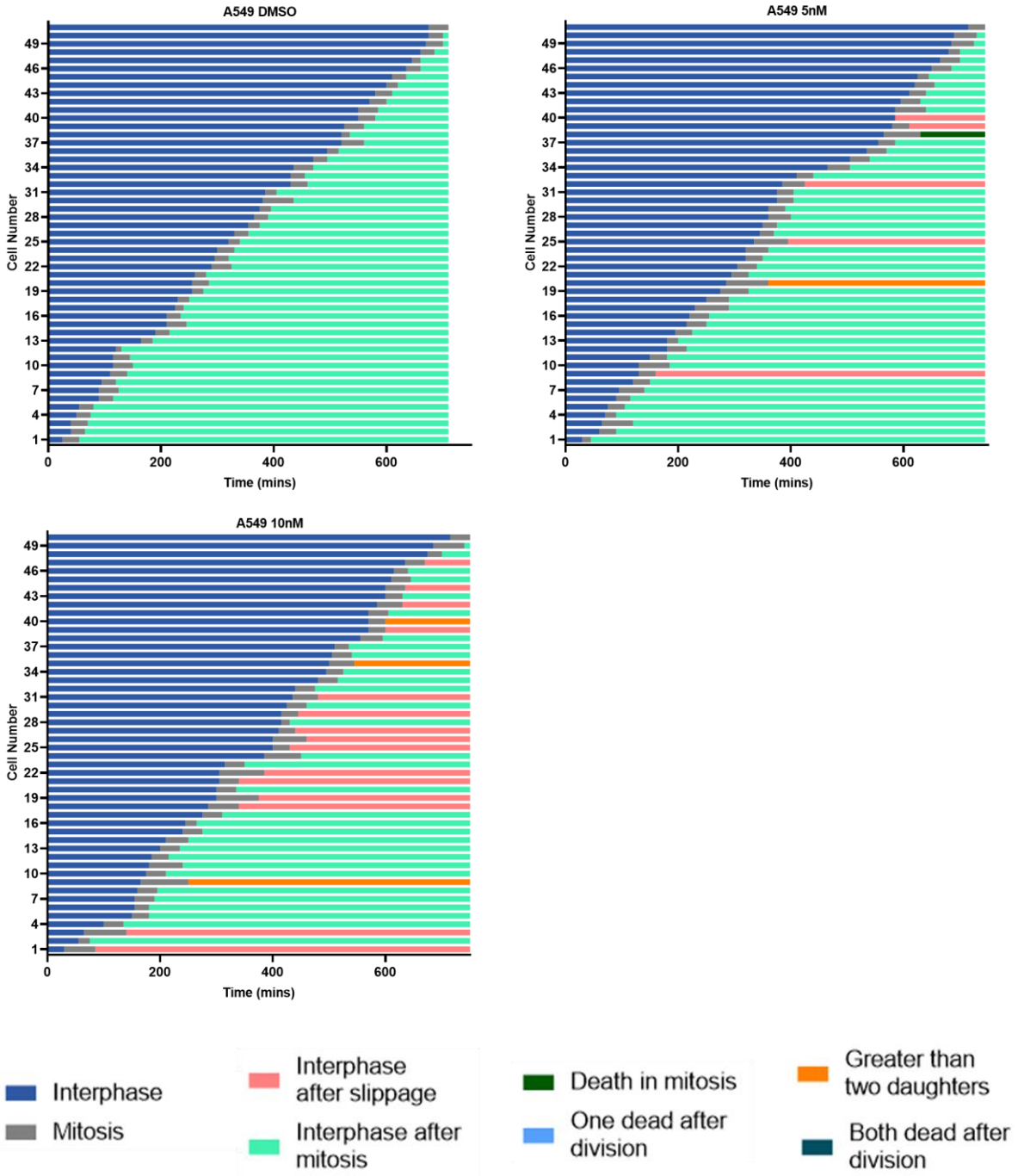
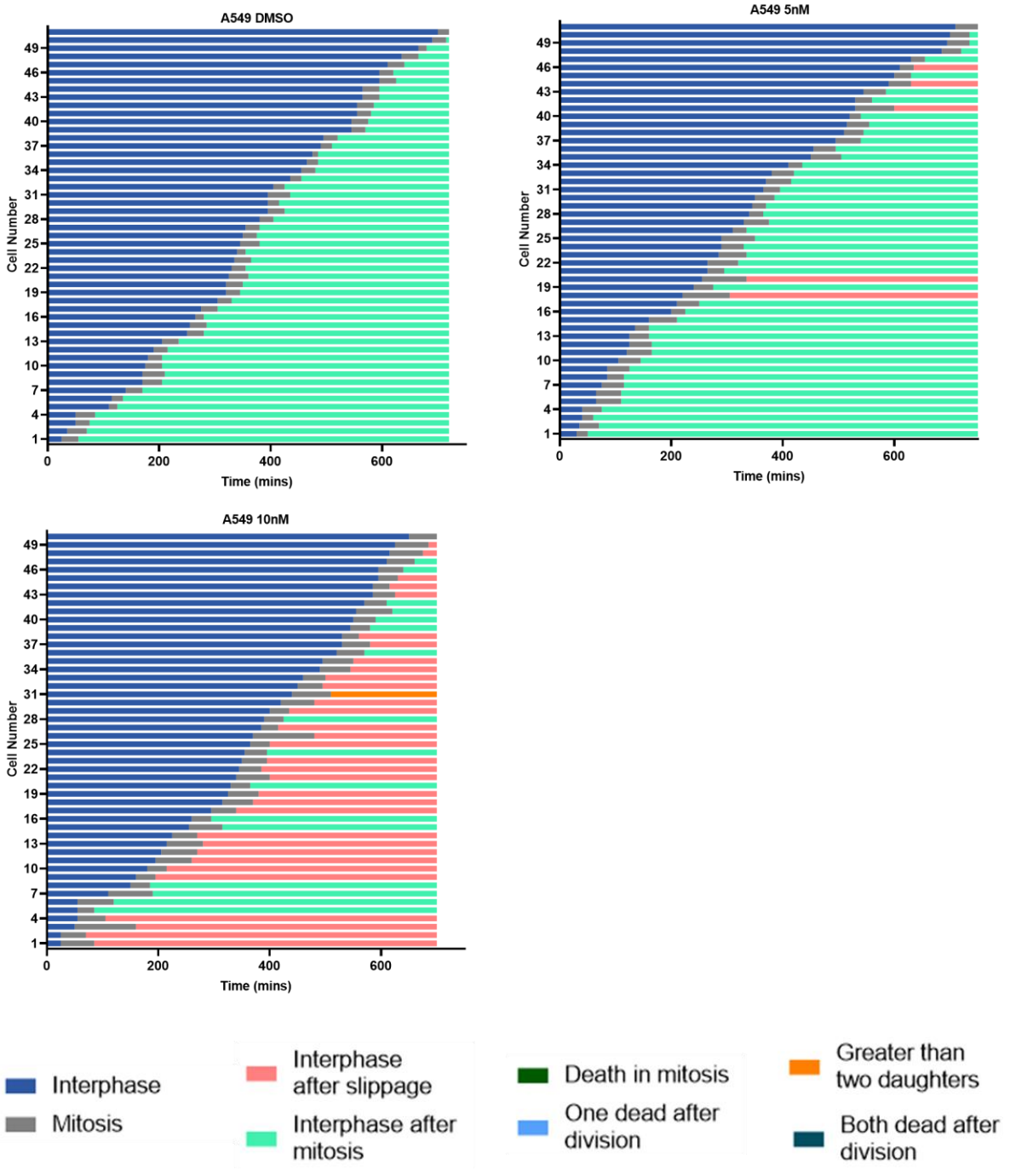


Figure 7-12: ***Stacked Bar charts showing the cellular outcomes of Barasertib*** *on live cell imaging using the conditions DMSO, 5nM and 10nM in 4Gy between 24-36 hours in BICR22 cells. Cells were treated with Barasertib for 2 hours before adding to IR and left for seven days. Dark blue indicates interphase before mitosis or slippage; Grey indicates mitosis; Pink indicates interphase after slippage; Cyan indicates interphase after mitosis; Green indicates Cell death in Mitosis; Sky blue indicates one cell died after division, Teal indicates both daughter cells died after division, and orange indicates that the mother cell divided into more than two daughters.*

7.4.3 36–48-hour time frame

7.4.3.1 A549 plus Barasertib alone




A549 DMSO
A549 5nM
A549 10nM
Cell Number
Time (mins)
0
200
400
600
1
4
7
10
13
16
19
22
25
28
31
34
37
40
43
46
49
Interphase
Mitosis
Interphase after slippage
Interphase after mitosis
Death in mitosis
One dead after division
Greater than two daughters
Both dead after division

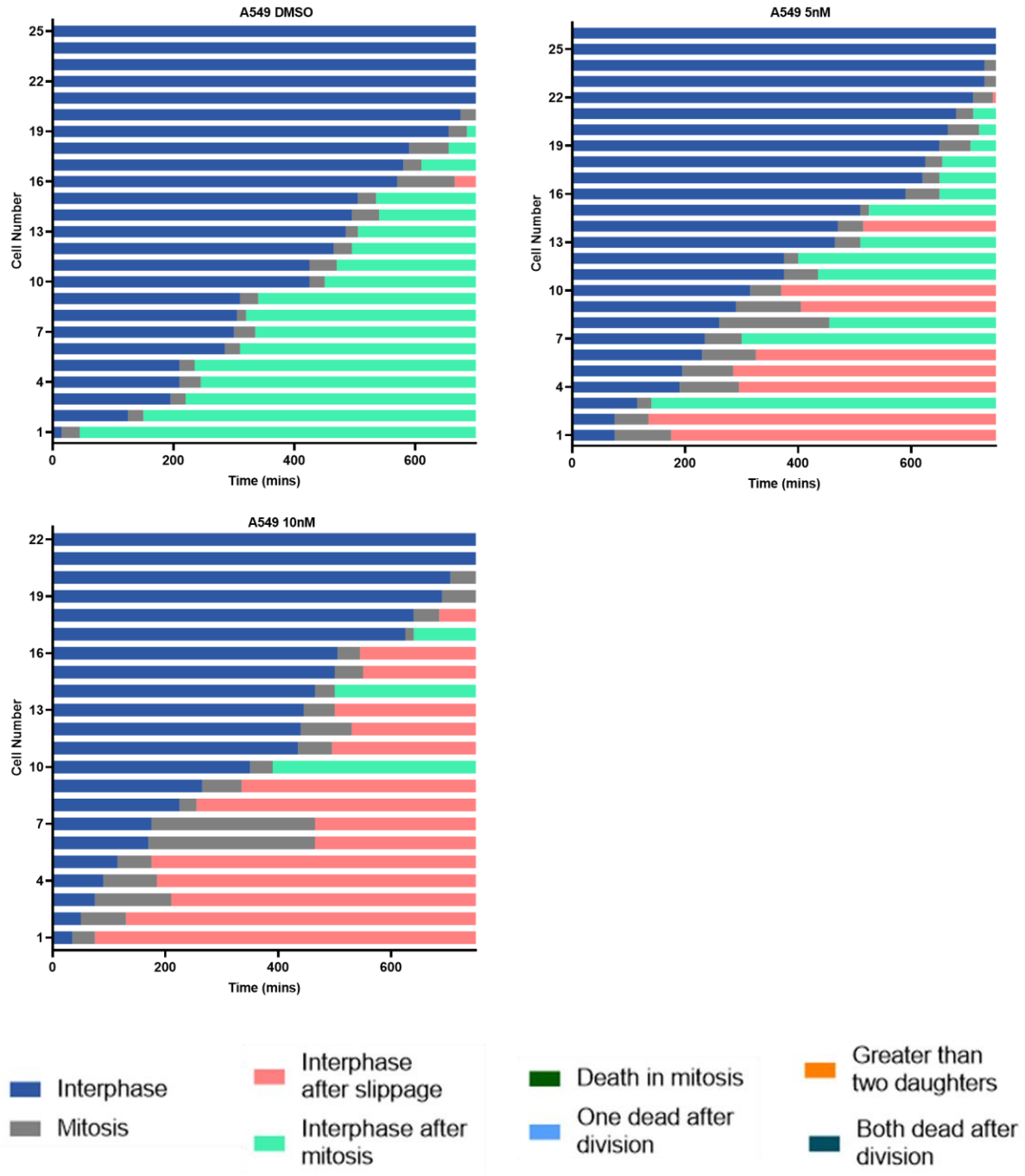
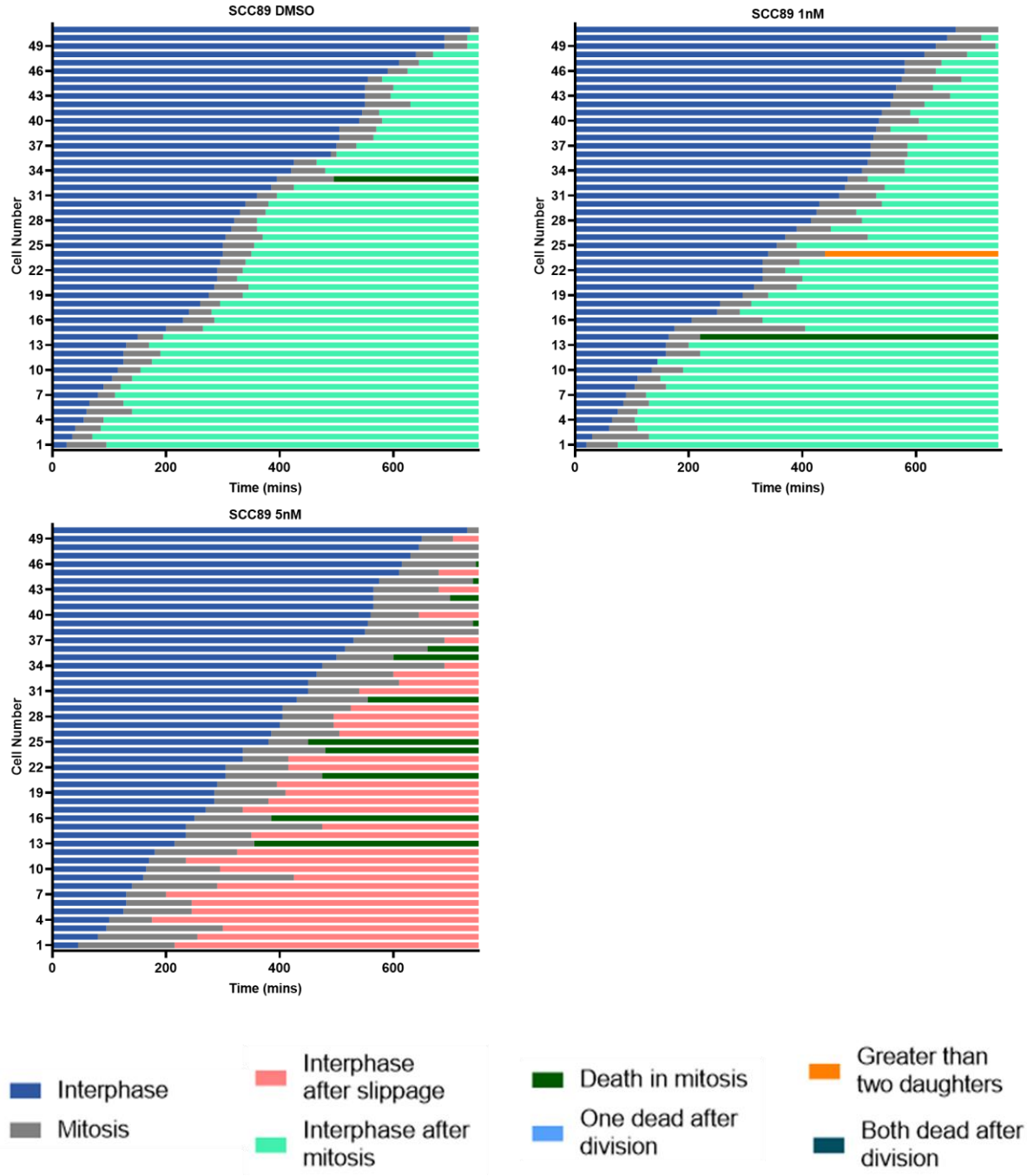
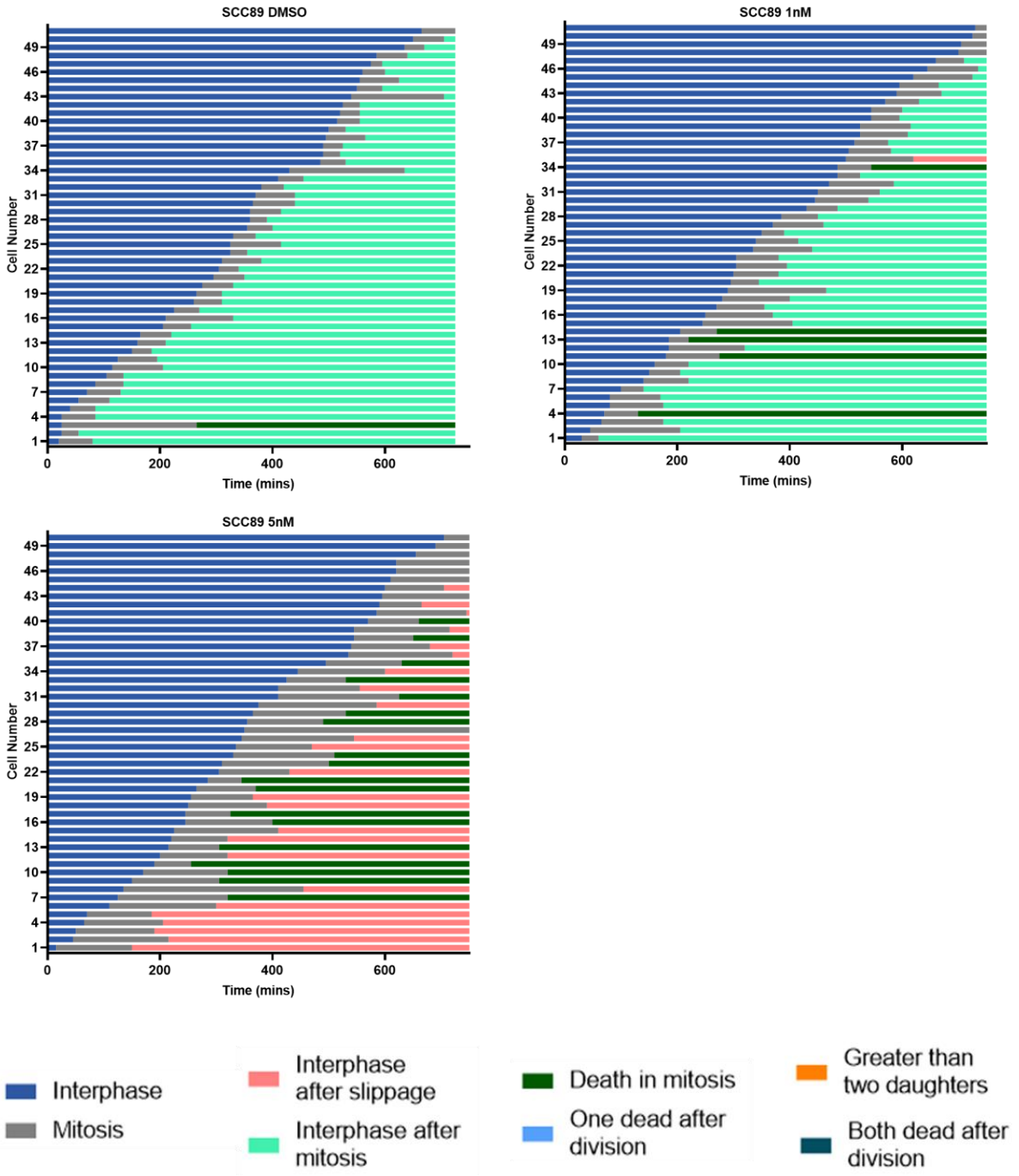


Figure 7-13: ***Stacked Bar charts showing the cellular outcomes of Barasertib*** *on live cell imaging using the conditions DMSO, 5nM and 10nM between 36-48 hours in A549 cells. Cells were treated with Barasertib for 2 hours before adding to IR and left for seven days. Dark blue indicates interphase before mitosis or slippage; Grey indicates mitosis; Pink indicates Interphase after slippage; Cyan indicates Interphase after mitosis; Green indicates Cell death in Mitosis; Sky blue indicates one cell died after division, Teal indicates both daughter cells died after division, and orange indicates that the mother cell divided into more than two daughters.*

7.4.3.2 SCC89 plus Barasertib alone




SCC89 DMSO
SCC89 1nM
SCC89 5nM
Cell Number
Time (mins)
0
200
400
600
1
4
7
10
13
16
19
22
25
28
31
34
37
40
43
46
49
Interphase
Mitosis
Interphase after slippage
Interphase after mitosis
Death in mitosis
One dead after division
Greater than two daughters
Both dead after division

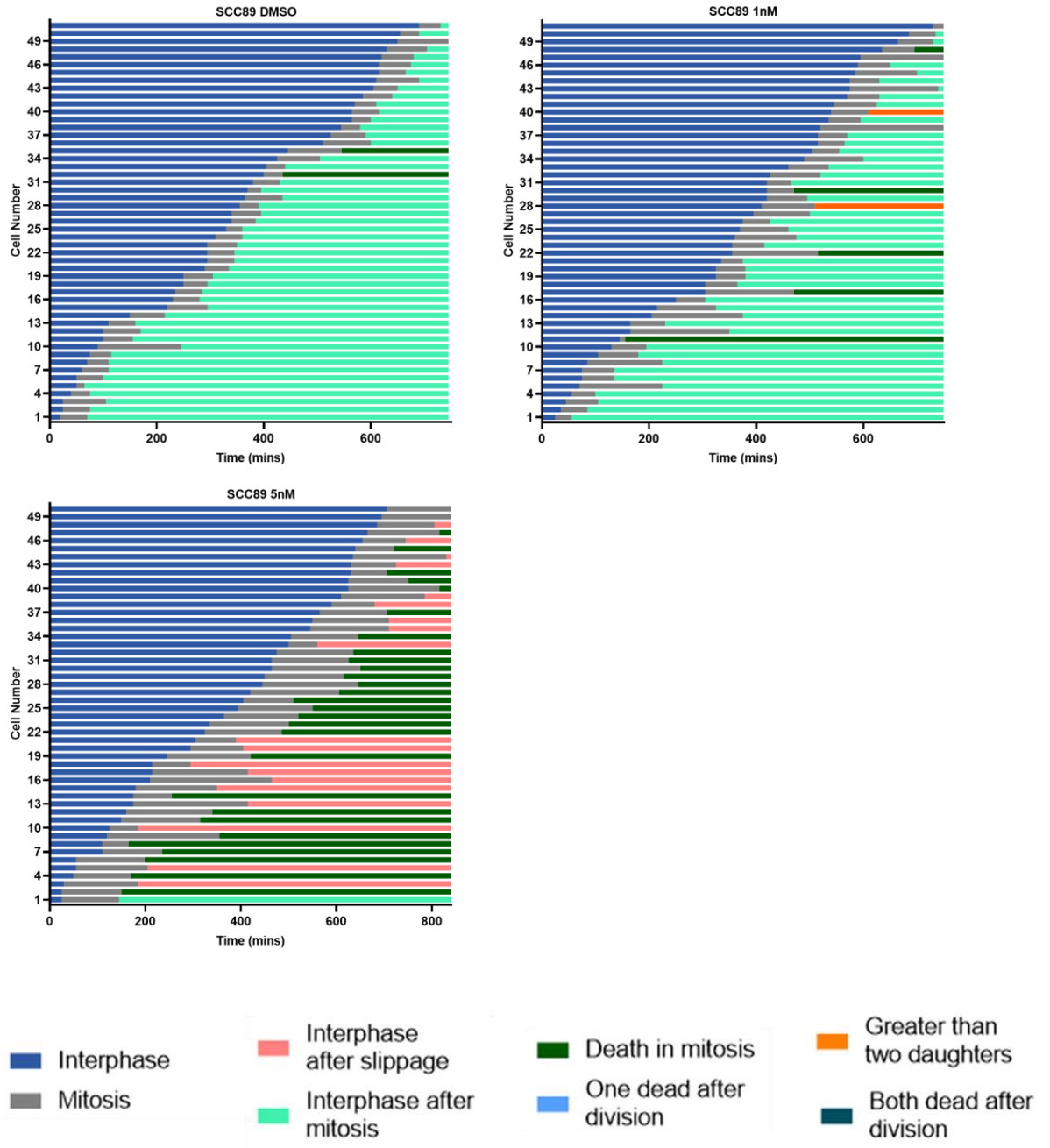
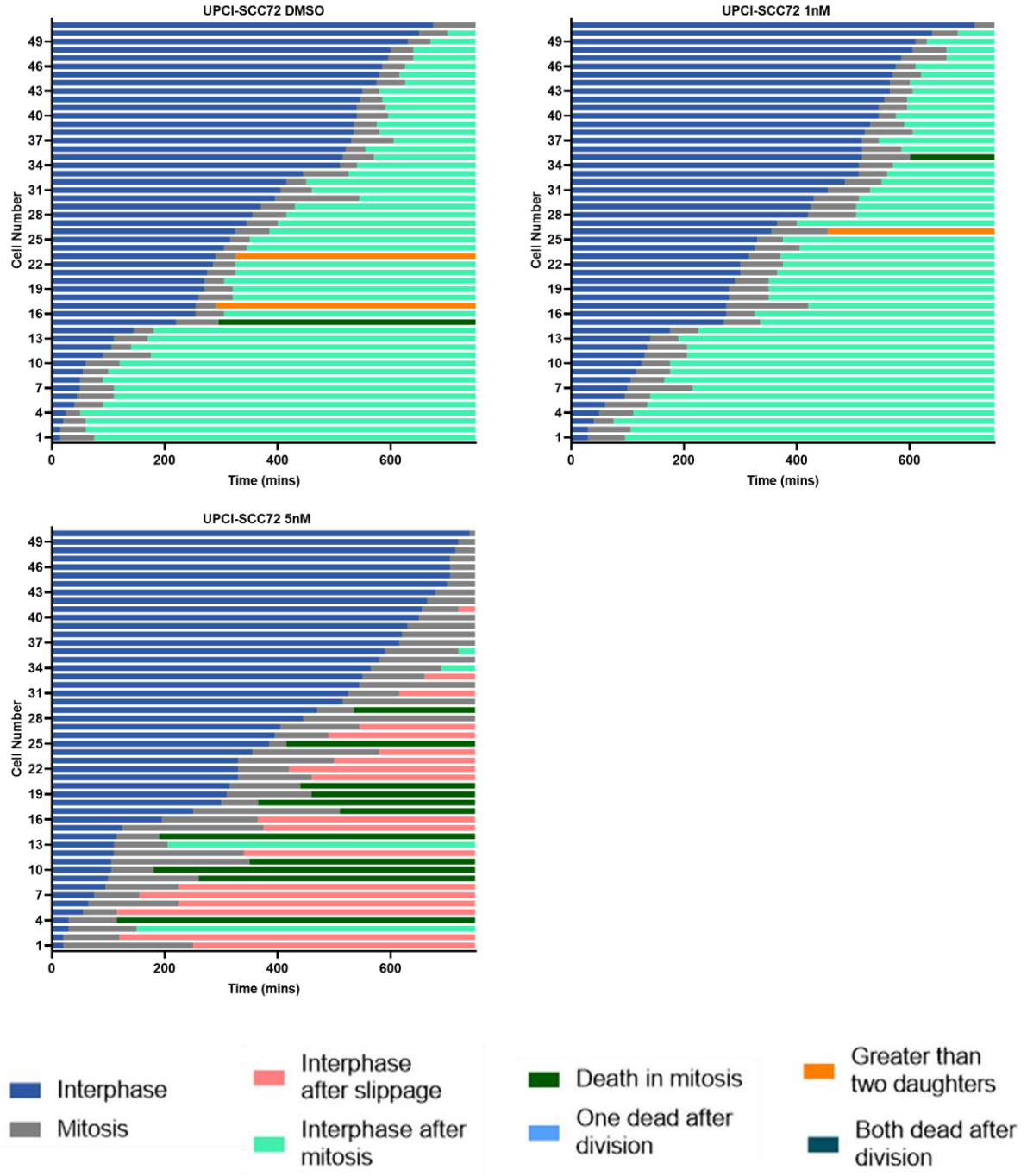
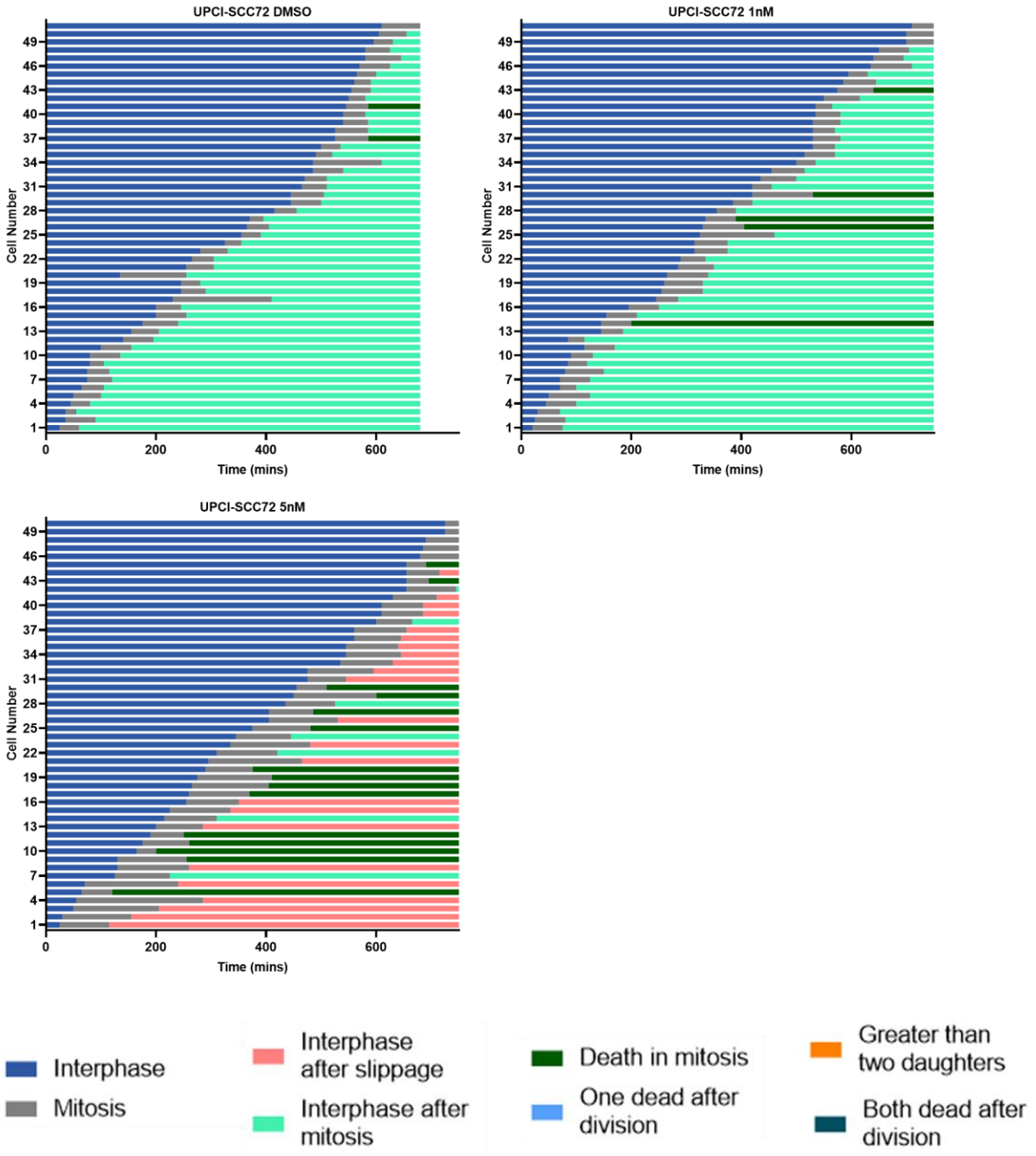


Figure 7-14: ***Stacked Bar charts showing the cellular outcomes of Barasertib*** *on live cell imaging using the conditions DMSO, 5nM and 10nM between 36-48 hours in SCC89 cells. Cells were treated with Barasertib for 2 hours before adding to IR and left for seven days. Dark blue indicates interphase before mitosis or slippage; Grey indicates mitosis; Pink indicates interphase after slippage; Cyan indicates interphase after mitosis; Green indicates Cell death in Mitosis; Sky blue indicates one cell died after division, Teal indicates both daughter cells died after division, and orange indicates that the mother cell divided into more than two daughters.*

7.4.3.3 UPCI-SCC72 plus Barasertib alone




UPCI-SCC72 DMSO
UPCI-SCC72 1nM
UPCI-SCC72 5nM
Cell Number
Time (mins)
0
200
400
600
1
4
7
10
13
16
19
22
25
28
31
34
37
40
43
46
49
Interphase
Mitosis
Interphase after slippage
Interphase after mitosis
Death in mitosis
One dead after division
Greater than two daughters
Both dead after division

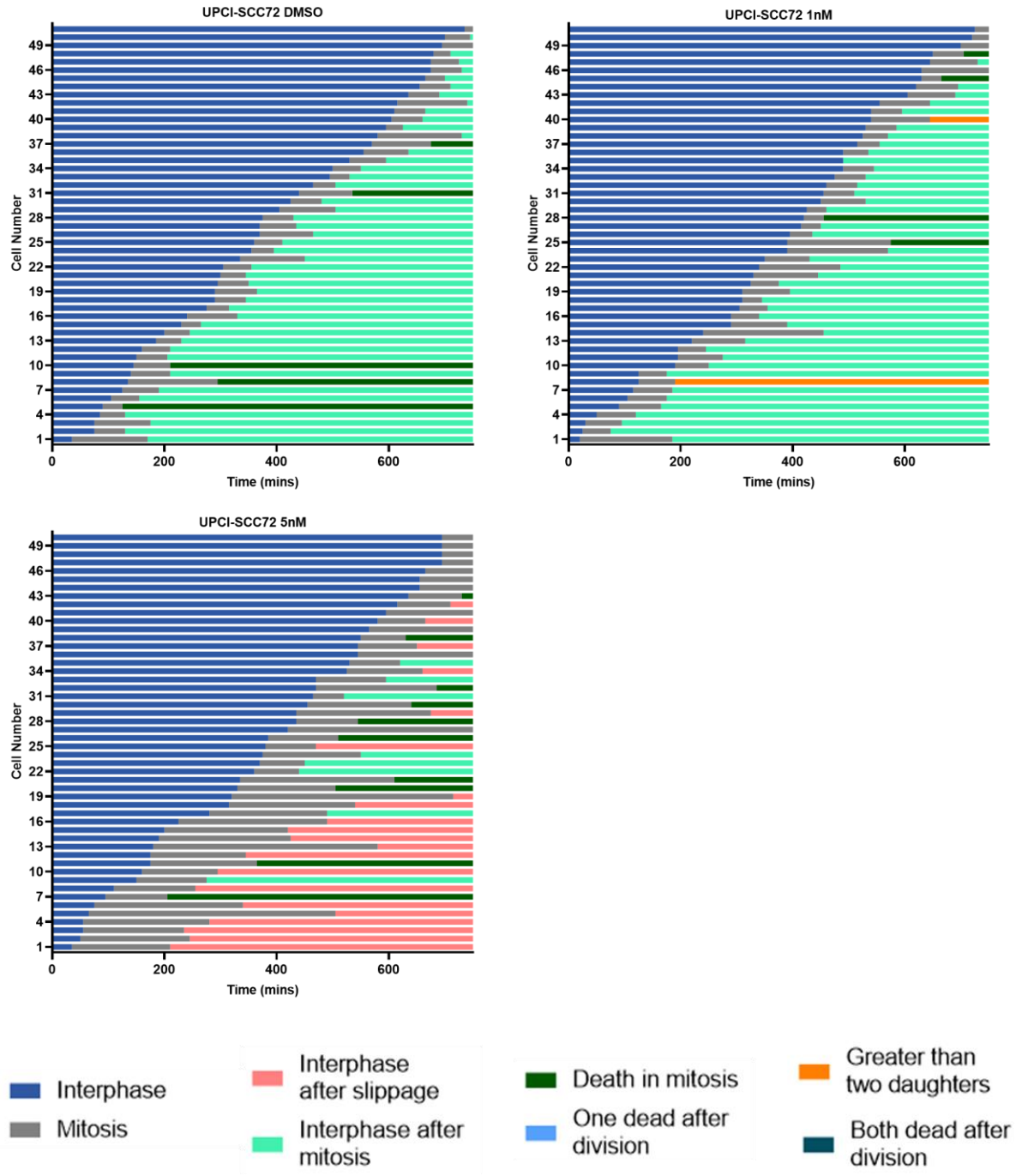
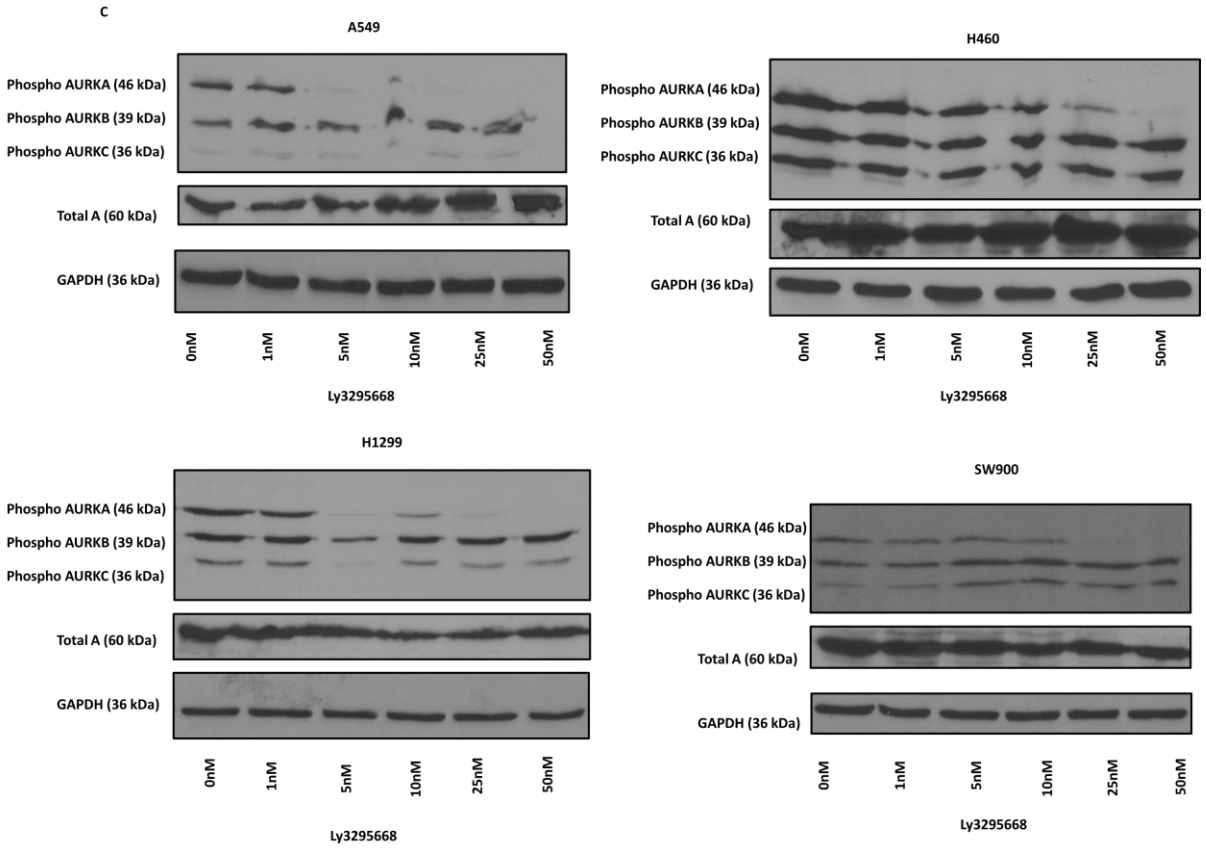
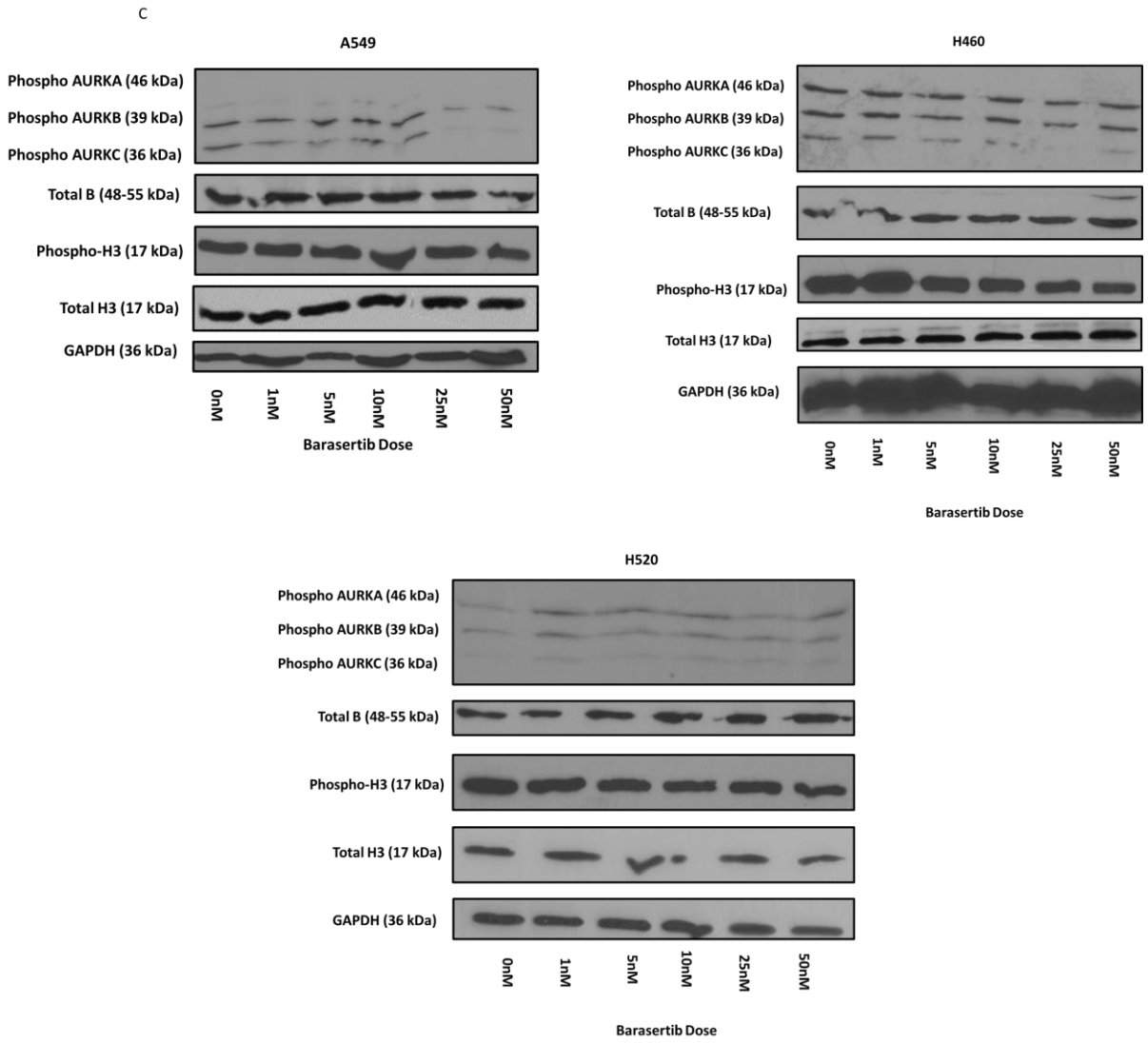


Figure 7-15: ***Stacked Bar charts showing the cellular outcomes of Barasertib*** *on live cell imaging using the conditions DMSO, 5nM and 10nM between 36-48 hours in UPCI-SCC72 cells. Cells were treated with Barasertib for 2 hours before adding to IR and left for seven days. Dark blue indicates interphase before mitosis or slippage; Grey indicates mitosis; Pink indicates interphase after slippage; Cyan indicates interphase after mitosis; Green indicates Cell death in Mitosis; Sky blue indicates one cell died after division, Teal indicates both daughter cells died after division, and orange indicates that the mother cell divided into more than two daughters.*

7.5 Ly3295668 western phospho-blots



7.6 Barasertib western phospho-blots



7.7 IHC optimization work done by Prior PhD student

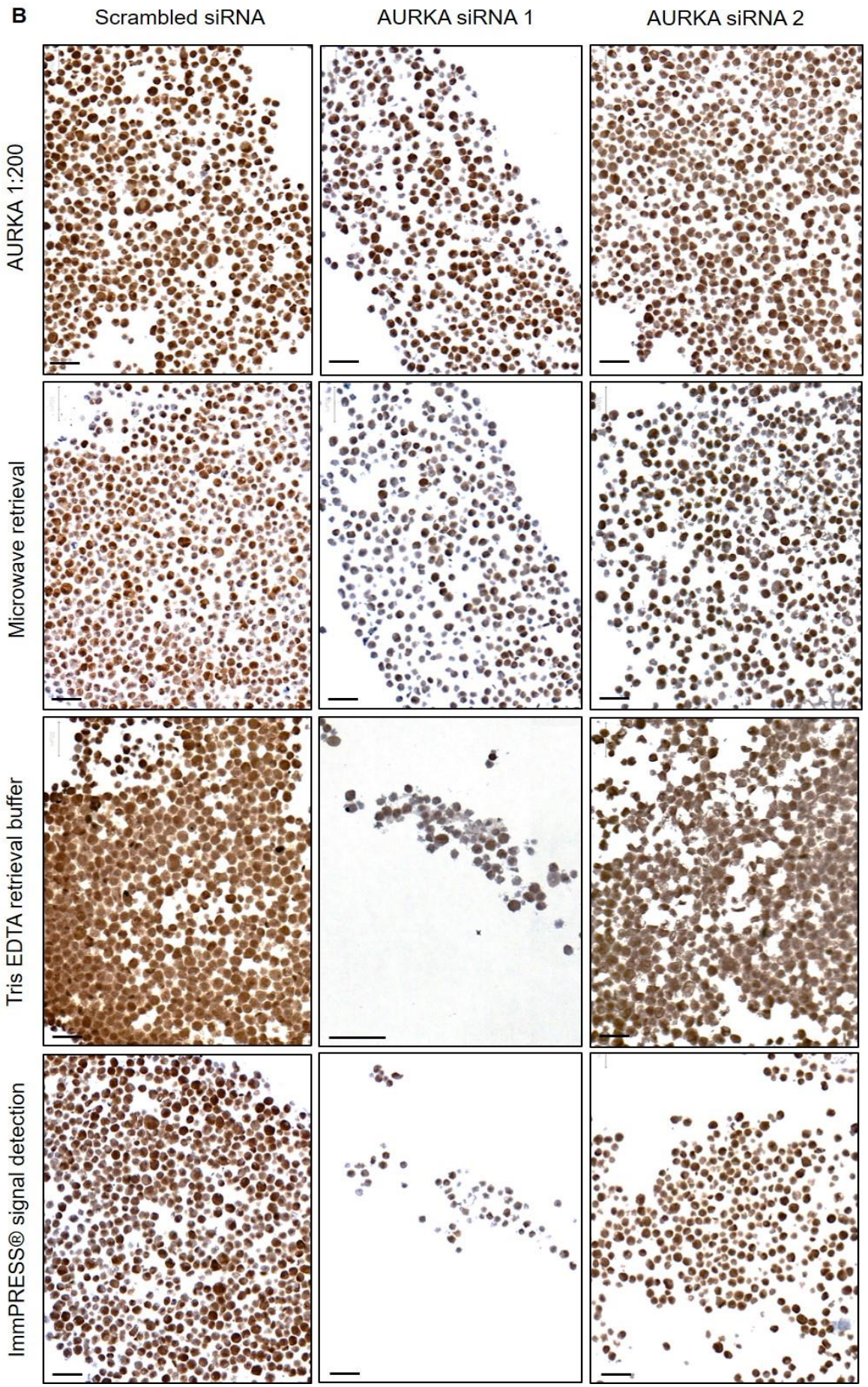
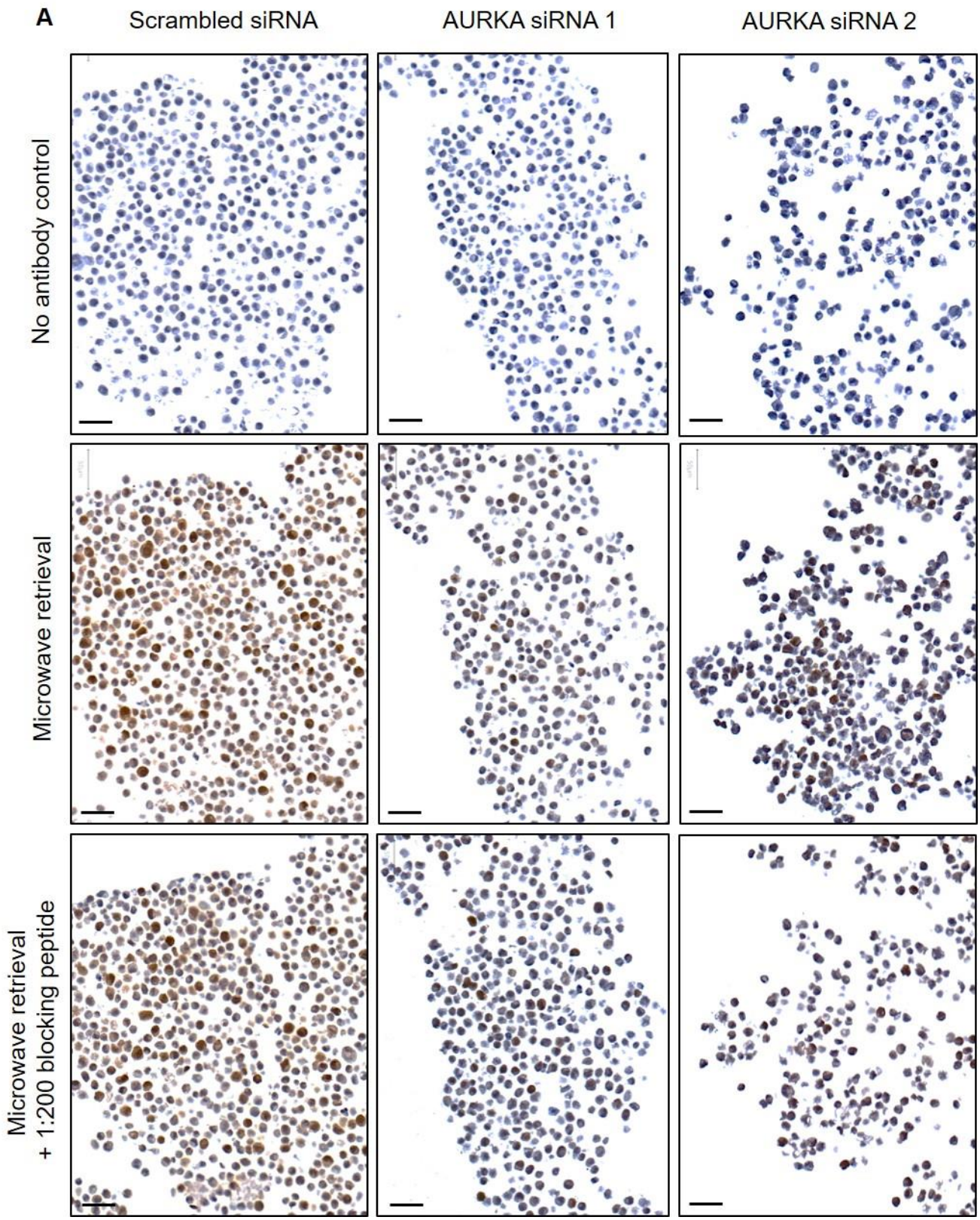
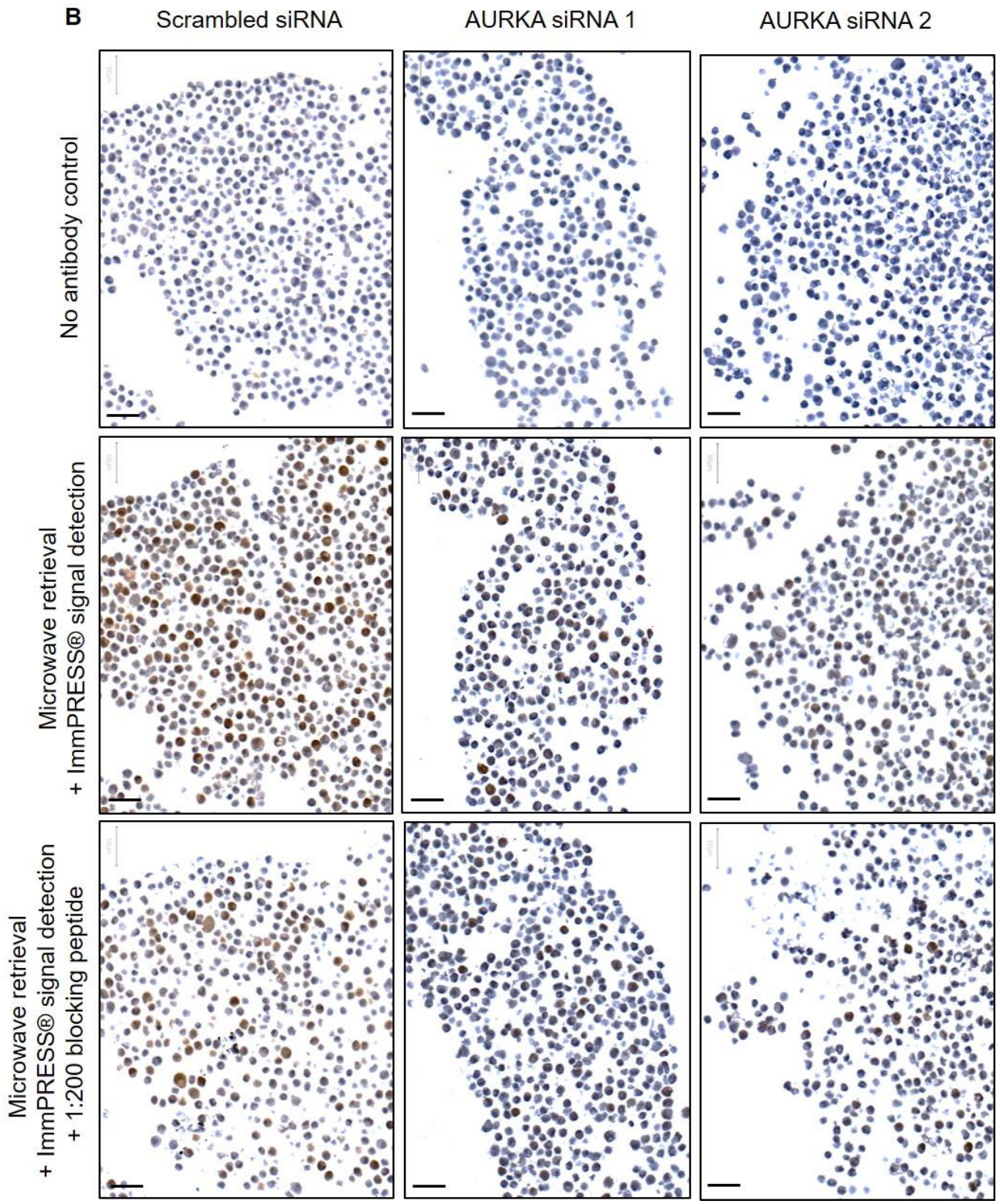
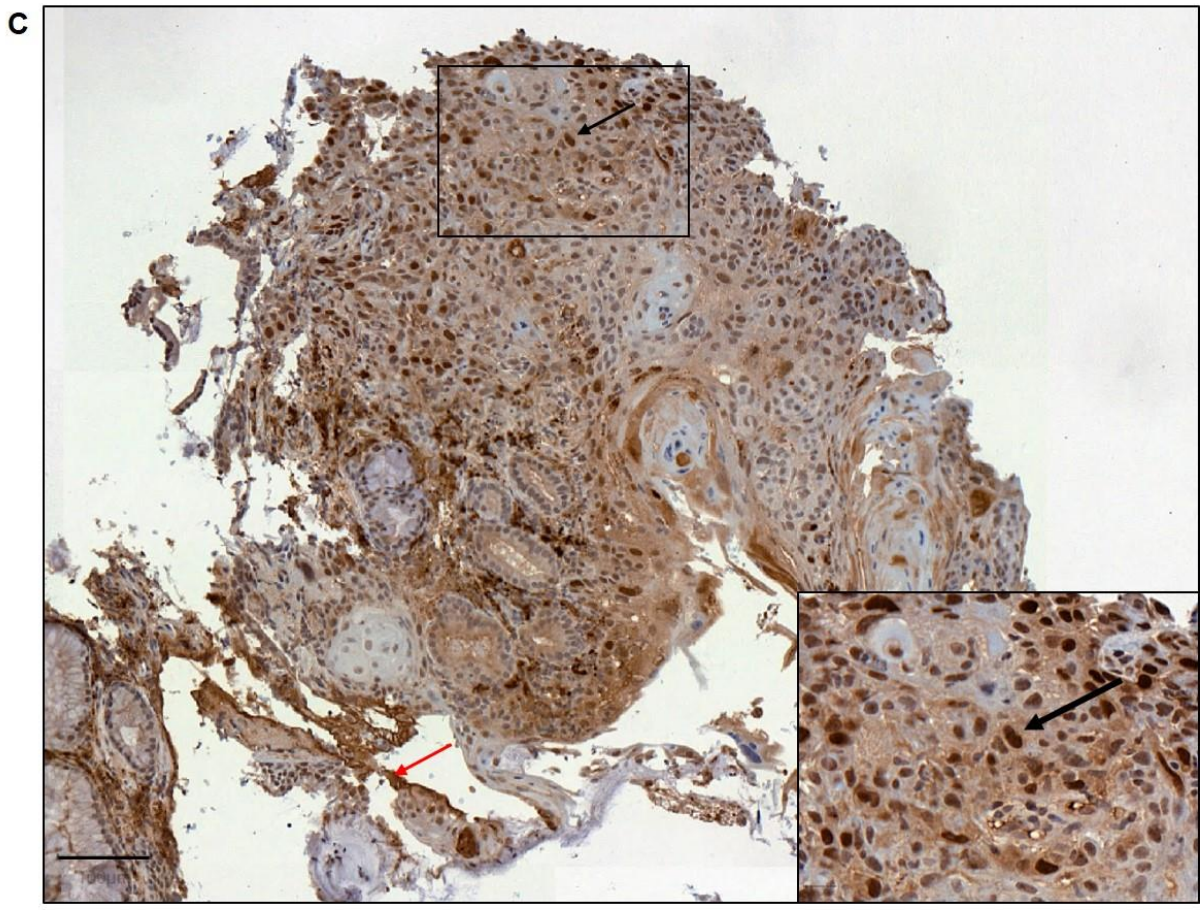

B
Scrambled siRNA
AURKA siRNA 1
AURKA siRNA 2
AURKA 1:200
Microwave retrieval
Tris EDTA retrieval buffer
ImmPRESS® signal detection

Figure 7-16: ***AURKA* IHC staining in H460 cell line pellets transfected with scrambled or *AURKA* siRNA after varying antigen retrieval method, antigen retrieval buffer and signal detection system.** Representative images of *AURKA* IHC staining in H460 cell line pellets after **A.** 1-hour primary antibody incubation and **B.** overnight primary antibody incubation. Standard comparative protocol using labelled 1:200 *AURKA* used pressure cooker retrieval, pH 6.1 citrate target retrieval solution and ABC detection system. Antibody signal on stained cells was developed with DAB for 3 minutes 30 seconds, and cells were counterstained with Gill's Haematoxylin (N=1). Scale bars represent 50 µm. All slides were scanned using a panoramic 250 slide scanner using a 20x objective.


A
Scrambled siRNA
AURKA siRNA 1
AURKA siRNA 2
No antibody control
Microwave retrieval
Microwave retrieval
+ 1:200 blocking peptide


B
Scrambled siRNA
AURKA siRNA 1
AURKA siRNA 2
No antibody control
Microwave retrieval
+ ImmPRESS® signal detection
Microwave retrieval
+ ImmPRESS® signal detection
+ 1:200 blocking peptide


C

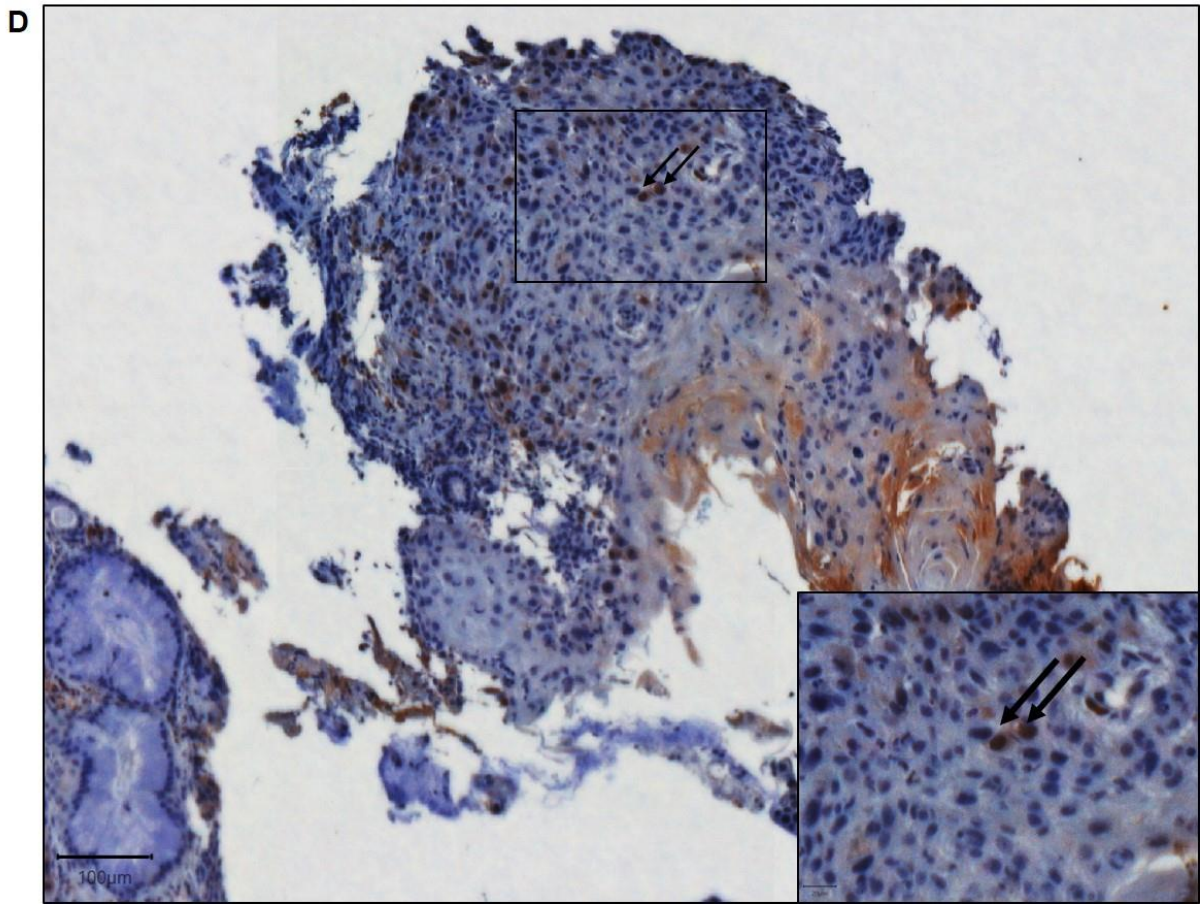
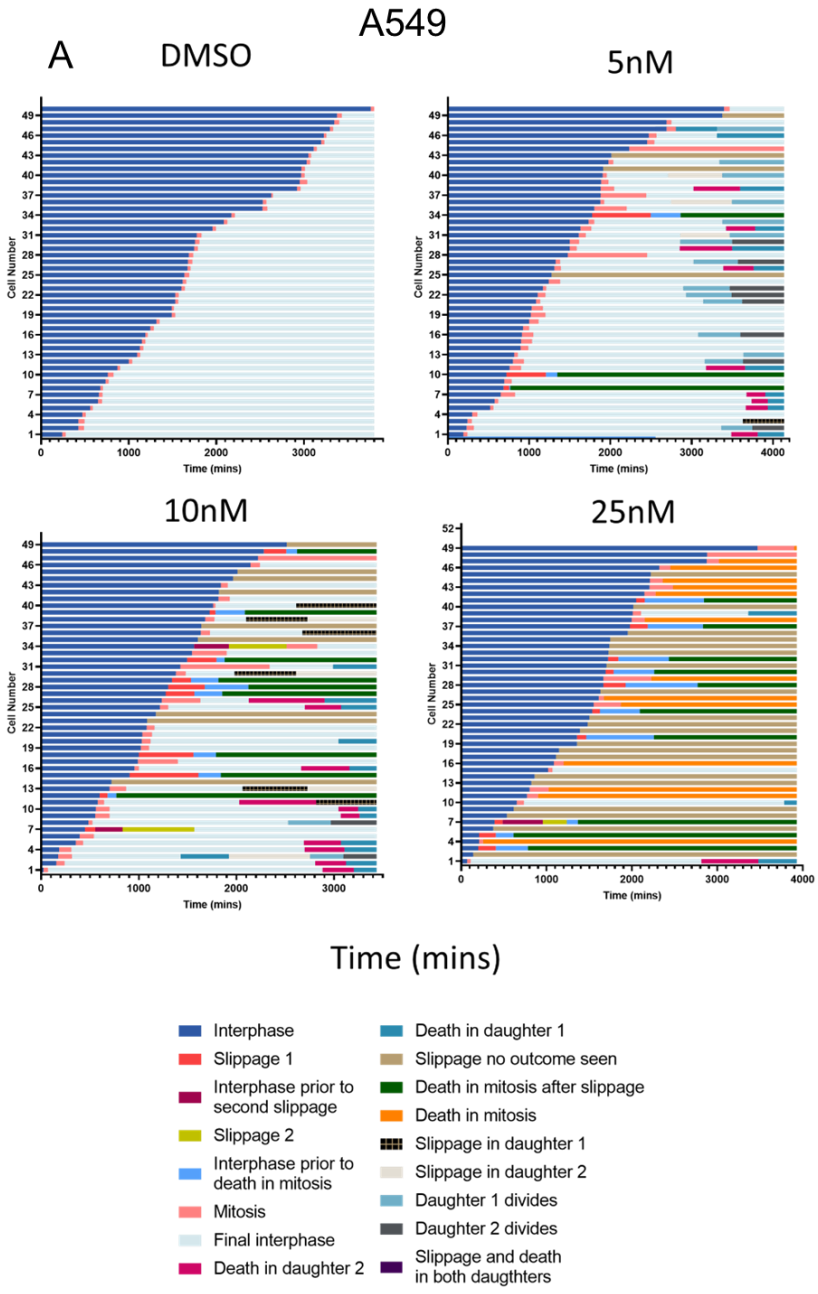

D
100µm

Figure 7-17: ***AURKA* IHC staining in H460 cell line pellets transfected with scrambled or *AURKA* siRNA and patient biopsy samples after microwave retrieval method and ImmPRESS® detection system.** Representative images of *AURKA* IHC staining using H460 cell line pellets after **A.** microwave retrieval with ABC signal detection system and **B.** microwave retrieval with ImmPRESS® signal detection system. Tissues stained with 1:200 *AURKA* primary antibody +/- blocking peptide. Antibody signal on stained cells was developed with DAB for 3 minutes 30 seconds, and cells were counterstained with Gill's haematoxylin (N=1). Scale bars represent 50 µm **C.** *AURKA* staining in the diagnostic biopsy of an SCC NSCLC patient using 1:1000 primary antibody with overnight incubation, pressure cooker retrieval and ABC signal detection system re-represented for comparative purposes. DAB exposure was for 3 minutes. **D.** *AURKA* staining in a section from the same diagnostic biopsy in C, using 1:200 primary antibody with 1-hour incubation, microwave antigen retrieval and ImmPRESS® signal detection system. DAB exposure was for 15 minutes. Cells were counterstained with haematoxylin. Scale bars represent 100 µm. The area within the small rectangle is re-represented in the image's bottom right corner, which is 5x larger. The black arrow indicates epithelial cancer cells with positive nuclear and cytoplasmic staining. All slides were scanned using a panoramic 250 slide scanner using a 20x objective.

7.8 Live cell analysis plots over 72 hours in NSCLC cell lines



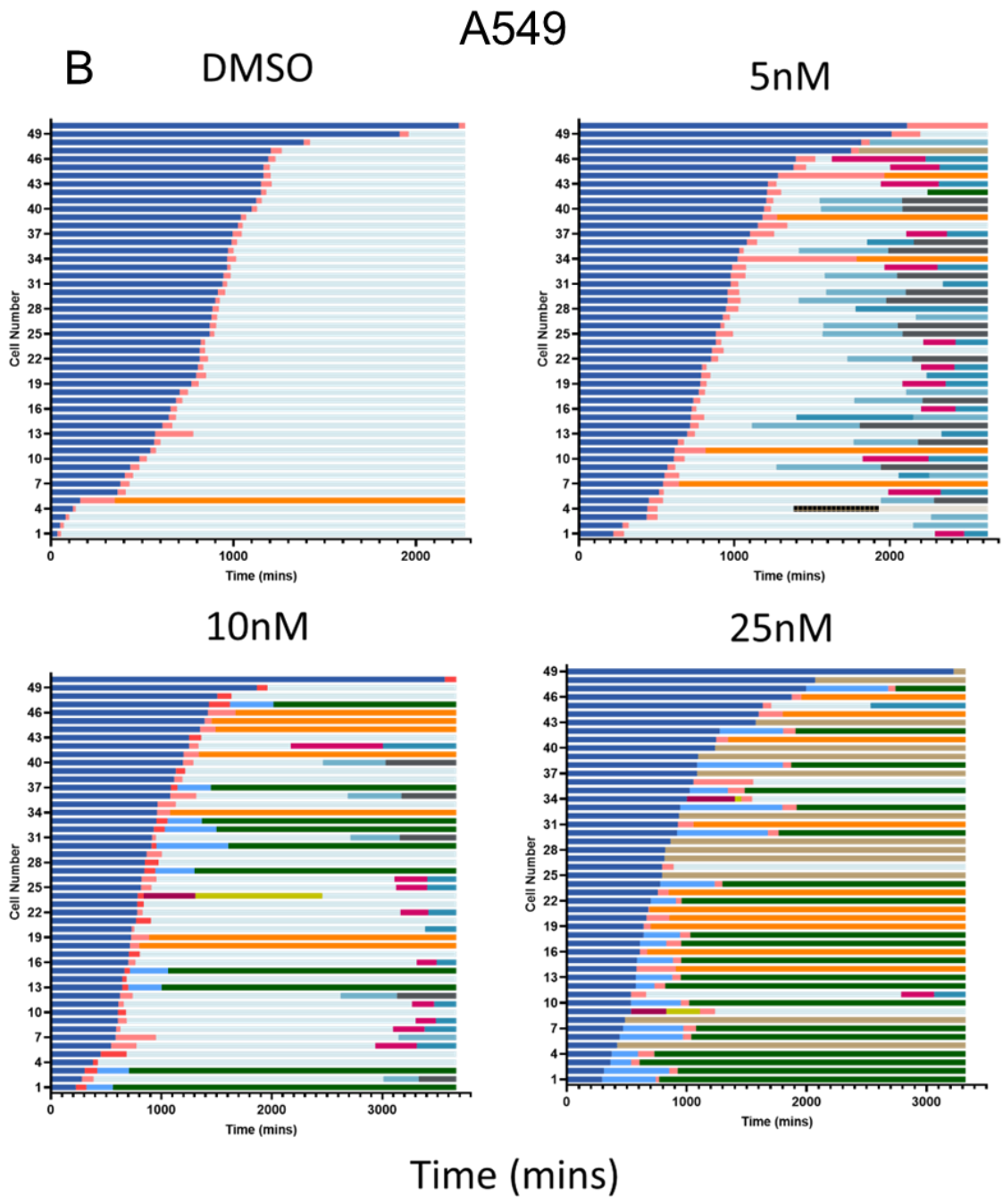
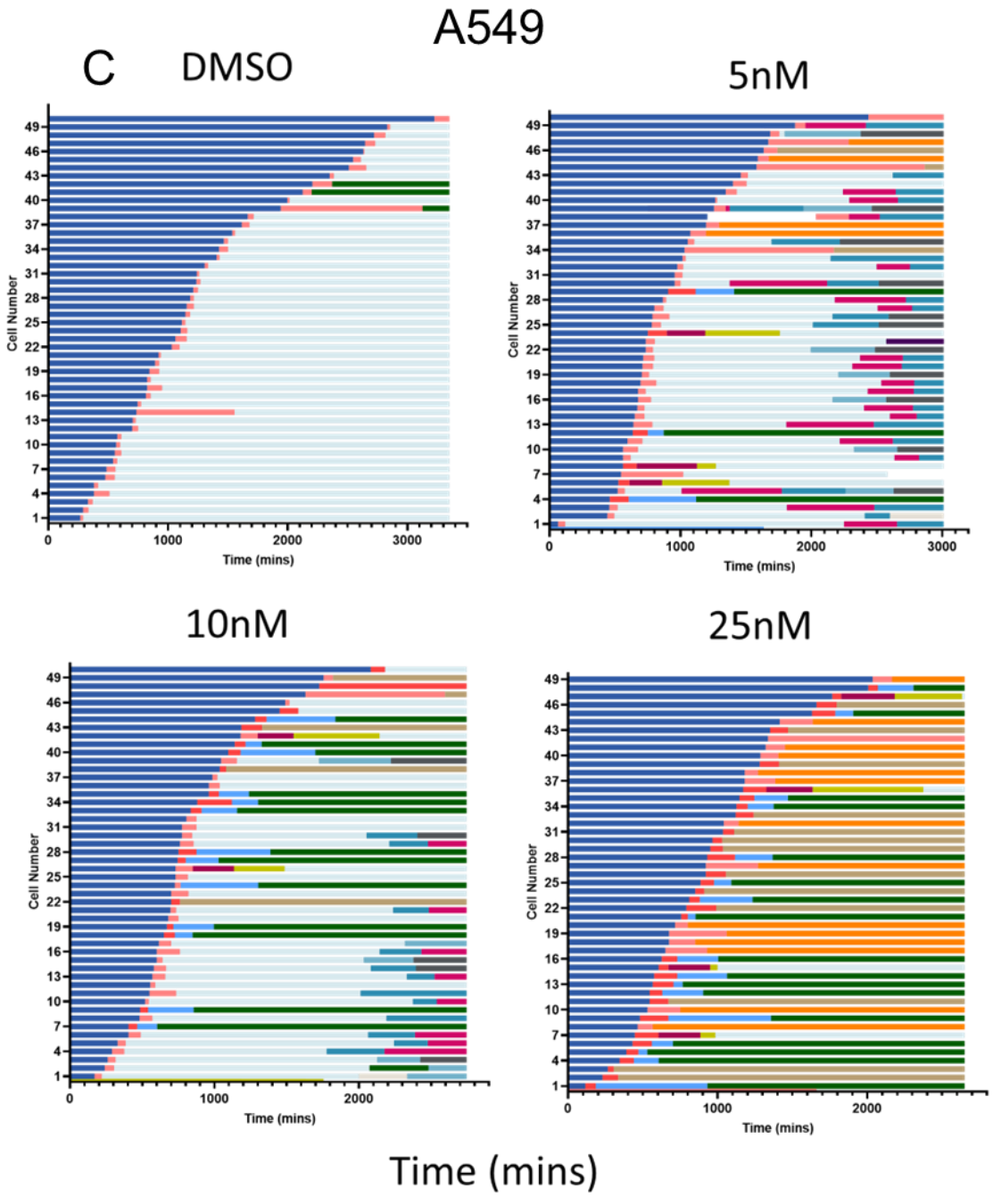
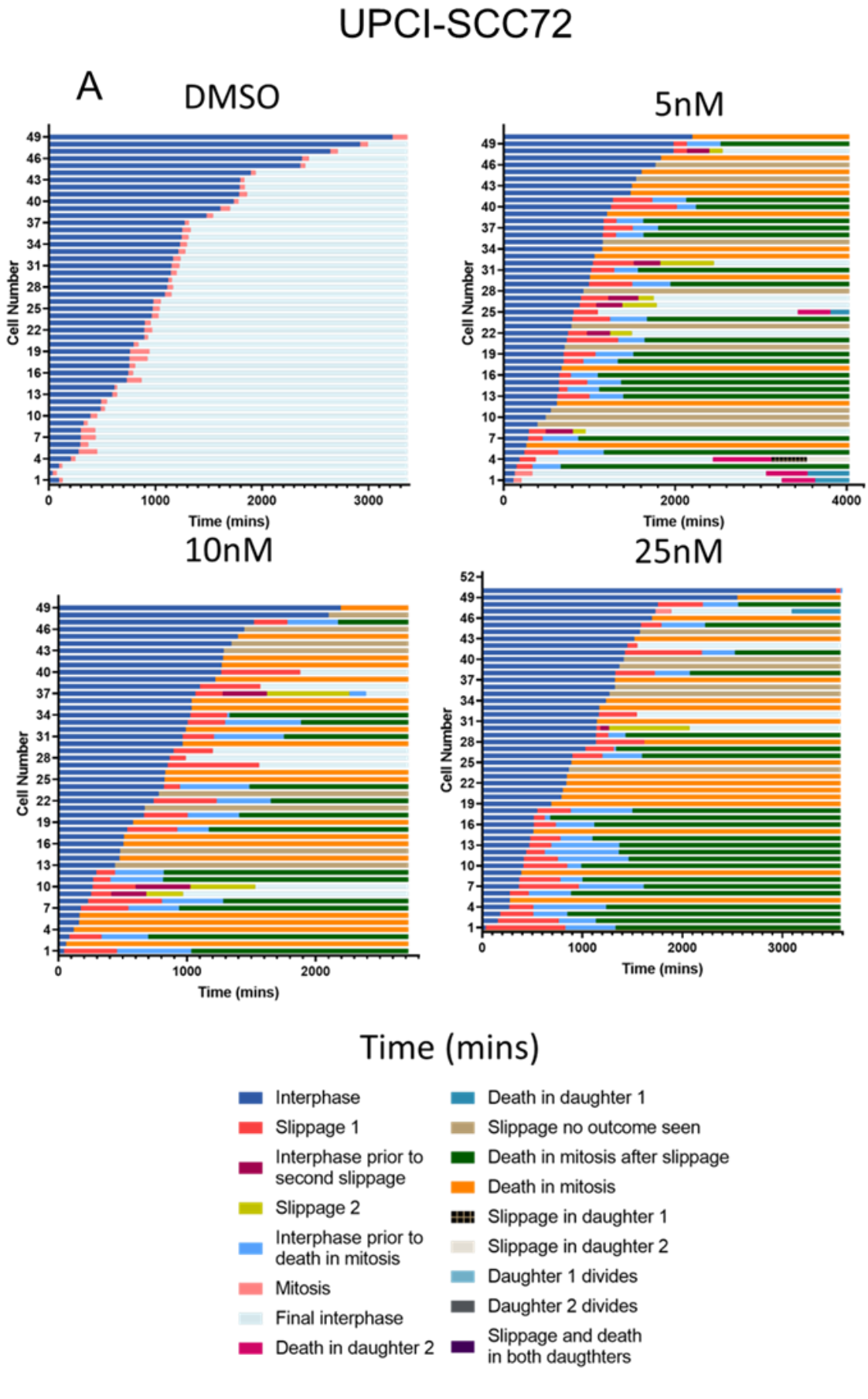
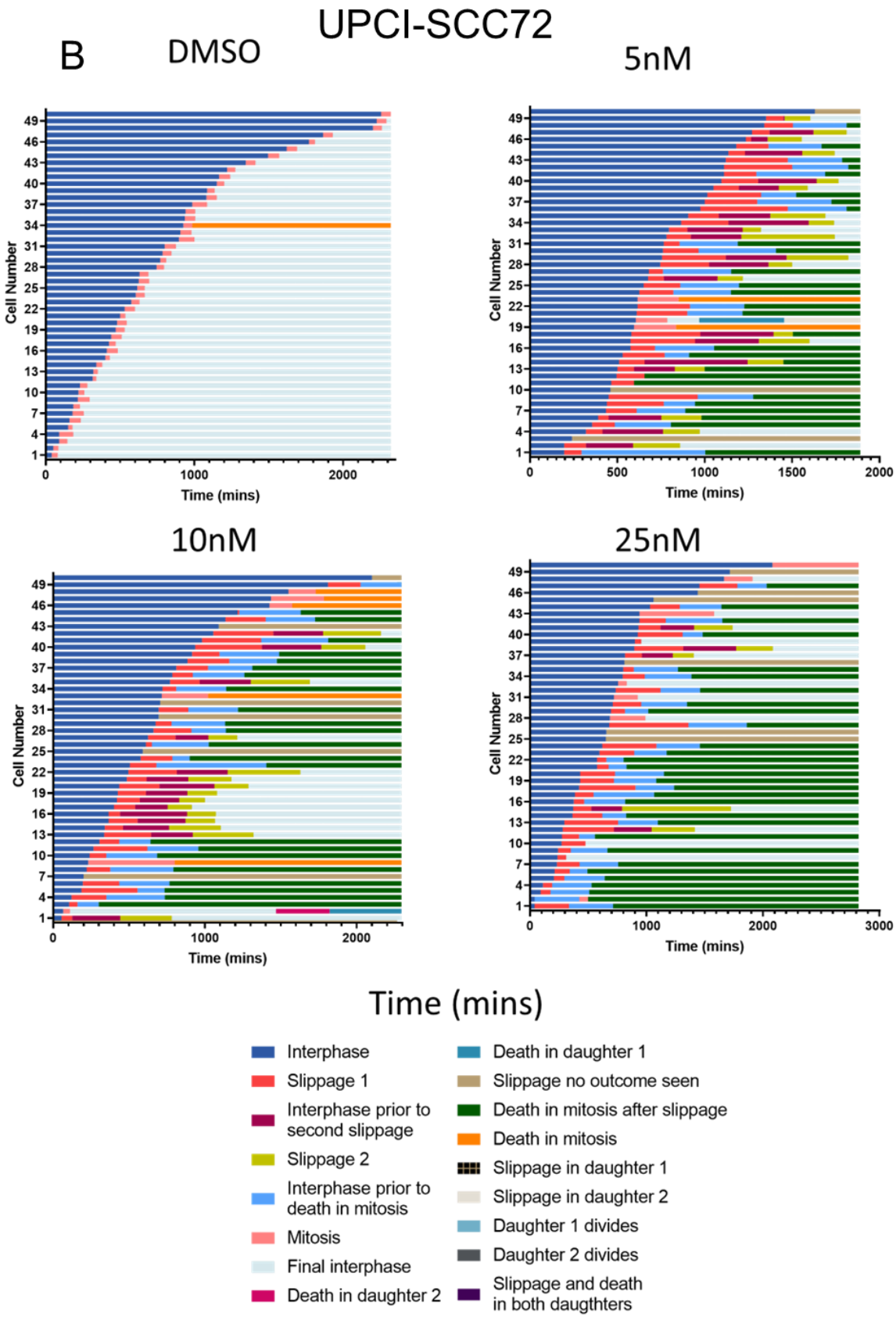

A549
B
DMSO
5nM
10nM
25nM
Cell Number
Time (mins)
Time (mins)
Interphase
Slippage 1
Interphase prior to second slippage
Slippage 2
Interphase prior to death in mitosis
Mitosis
Final interphase
Death in daughter 2
Death in daughter 1
Slippage no outcome seen
Death in mitosis after slippage
Death in mitosis
Slippage in daughter 1
Slippage in daughter 2
Daughter 1 divides
Daughter 2 divides
Slippage and death in both daugthters

Figure 7-18: ***Stacked Bar charts showing the cellular outcomes of Barasertib (3 repeats A-B respectively)*** *on live cell imaging using the conditions DMSO, 5nM, 10nM and 25nM between 0-72 hours in A549 cells. Cells were treated with Barasertib for 72 hours and left for 7-10 days. Dark blue indicates interphase before mitosis or slippage; Dark Pink indicates slippage; dark violet indicates interphase after second slippage; Yellow-Green indicates second slippage; Sky blue indicates interphase prior to death in Mitosis; Light pink indicates mitosis, Turquoise indicates the final interphase, Light violet indicates death in the second daughter cell, Olympic blue indicates death in daughter one, Dark Cream indicates no observable event after slippage, Green indicates death in mitosis after slippage, Orange indicates cell death in mitosis, Black and white stripes indicates slippage in one daughter cells, Light cream indicates slippage in the second daughter cell, Cyan indicates division in daughter one of two, Grey indicates division in daughter two of two and Purple indicates slippage* ***and*** *death in both daughter cells.*


A549
C
DMSO
5nM
10nM
25nM
Cell Number
Time (mins)
Interphase
Slippage 1
Interphase prior to second slippage
Slippage 2
Interphase prior to death in mitosis
Mitosis
Final interphase
Death in daughter 2
Death in daughter 1
Slippage no outcome seen
Death in mitosis after slippage
Death in mitosis
Slippage in daughter 1
Slippage in daughter 2
Daughter 1 divides
Daughter 2 divides
Slippage and death in both daugthters

7.9 Live cell analysis plots over 72 hours in HNSCC cell lines


UPCI-SCC72
A
DMSO
5nM
10nM
25nM
Cell Number
Time (mins)
Time (mins)
Interphase
Slippage 1
Interphase prior to second slippage
Slippage 2
Interphase prior to death in mitosis
Mitosis
Final interphase
Death in daughter 2
Death in daughter 1
Slippage no outcome seen
Death in mitosis after slippage
Death in mitosis
Slippage in daughter 1
Slippage in daughter 2
Daughter 1 divides
Daughter 2 divides
Slippage and death in both daugthters


UPCI-SCC72
B
DMSO
5nM
10nM
25nM
Cell Number
Time (mins)
Time (mins)
Interphase
Slippage 1
Interphase prior to second slippage
Slippage 2
Interphase prior to death in mitosis
Mitosis
Final interphase
Death in daughter 2
Death in daughter 1
Slippage no outcome seen
Death in mitosis after slippage
Death in mitosis
Slippage in daughter 1
Slippage in daughter 2
Daughter 1 divides
Daughter 2 divides
Slippage and death in both daugthters

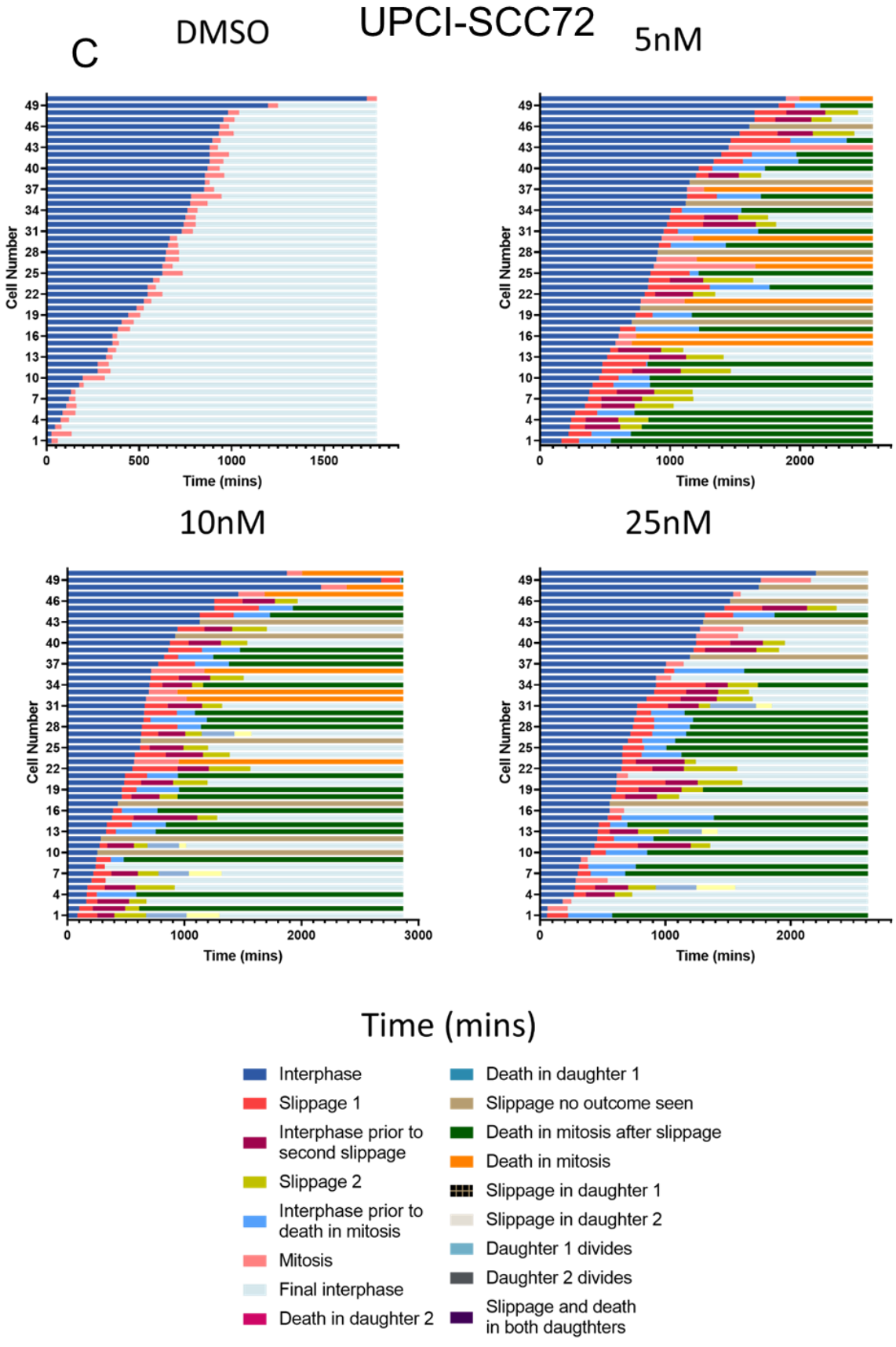
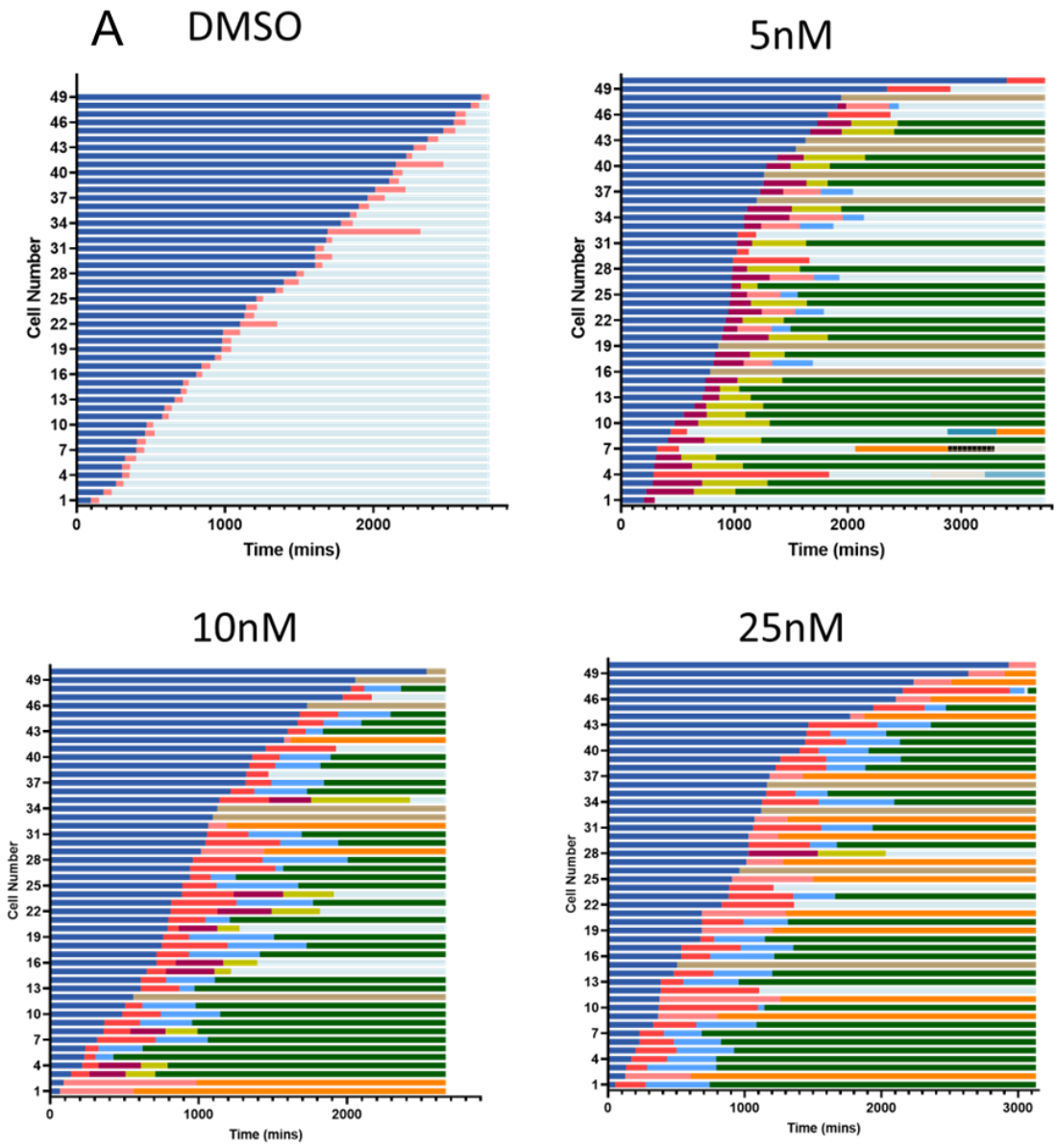

C
DMSO
UPCI-SCC72
5nM
10nM
25nM
Cell Number
Time (mins)
Time (mins)
Interphase
Slippage 1
Interphase prior to second slippage
Slippage 2
Interphase prior to death in mitosis
Mitosis
Final interphase
Death in daughter 2
Death in daughter 1
Slippage no outcome seen
Death in mitosis after slippage
Death in mitosis
Slippage in daughter 1
Slippage in daughter 2
Daughter 1 divides
Daughter 2 divides
Slippage and death in both daugthters

Figure 7-19: ***Stacked Bar charts showing the cellular outcomes of Barasertib (3 repeats A-B respectively)*** *on live cell imaging using the conditions DMSO, 5nM, 10nM and 25nM between 0-72 hours in UPCI-SCC72 cells. Cells were treated with Barasertib for 72 hours and left for 7-10 days. Dark blue indicates interphase before mitosis or slippage; Dark Pink indicates slippage; dark violet indicates Interphase after second slippage; Yellow-Green indicates second slippage; Sky blue indicates interphase prior to death in Mitosis; Light pink indicates mitosis, Turquoise indicates the final interphase, Light violet indicates death in the second daughter cell, Olympic blue indicates death in daughter one, Dark Cream indicates no observable event after slippage, Green indicates death in mitosis after slippage, Orange indicates cell death in mitosis, Black and white stripes indicates slippage in one daughter cells, Light cream indicates slippage in the second daughter cell, Cyan indicates division in daughter one of two, Grey indicates division in daughter two of two and Purple indicates slippage* ***and*** *death in both daughter cells.*

SCC89

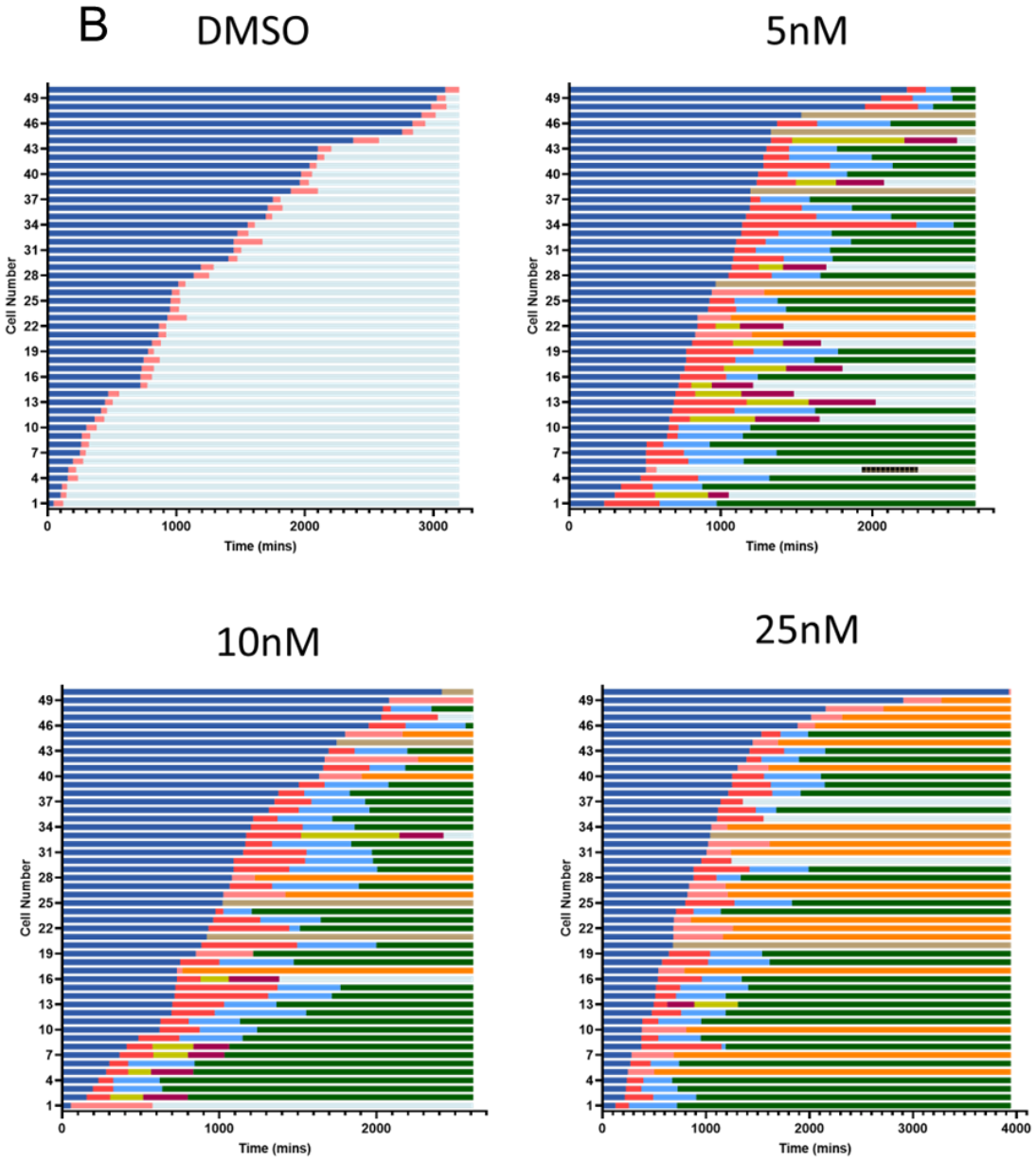


Time (mins)

- Interphase
- Slippage 1
- Interphase prior to second slippage
- Slippage 2
- Interphase prior to death in mitosis
- Mitosis
- Final interphase
- Death in daughter 2
- Death in daughter 1
- Slippage no outcome seen
- Death in mitosis after slippage
- Death in mitosis
- Slippage in daughter 1
- Slippage in daughter 2
- Daughter 1 divides
- Daughter 2 divides
- Slippage and death in both daugthters

SCC89

B


DMSO
5nM
10nM
25nM
Cell Number
Time (mins)
Time (mins)
Interphase
Slippage 1
Interphase prior to second slippage
Slippage 2
Interphase prior to death in mitosis
Mitosis
Final interphase
Death in daughter 2
Death in daughter 1
Slippage no outcome seen
Death in mitosis after slippage
Death in mitosis
Slippage in daughter 1
Slippage in daughter 2
Daughter 1 divides
Daughter 2 divides
Slippage and death in both daugthters

SCC89

C

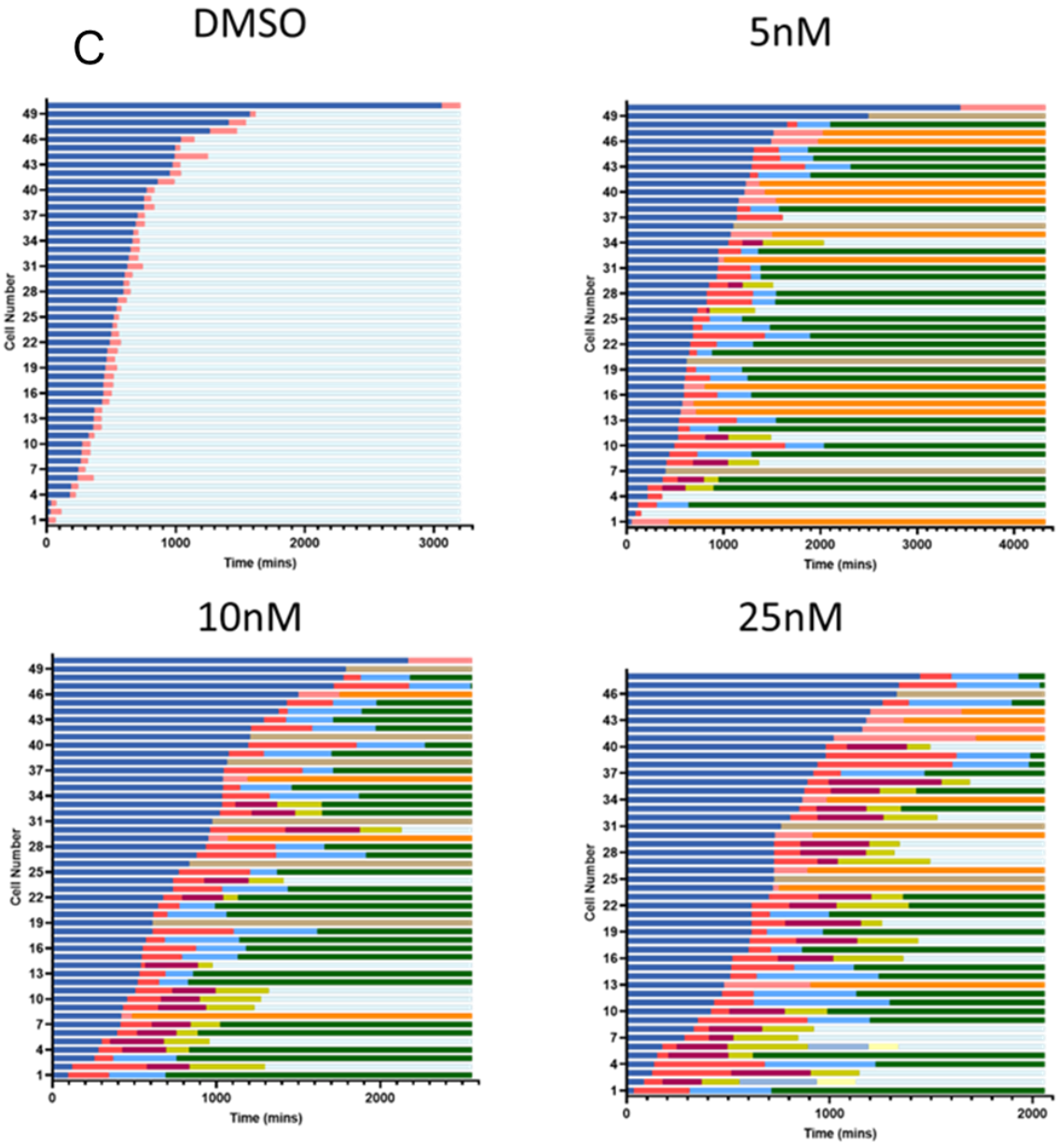
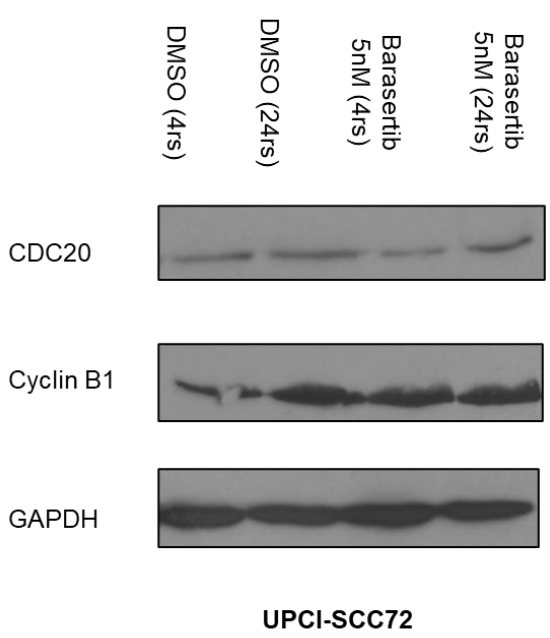
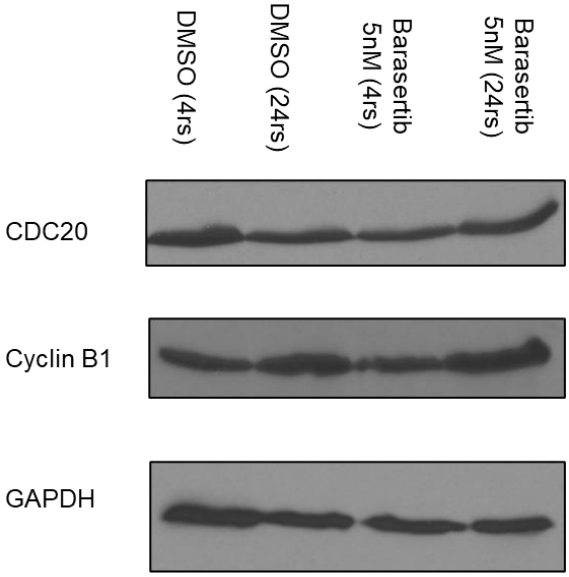

DMSO
5nM
10nM
25nM
Cell Number
Time (mins)
Interphase
Mitosis
Slippage 1
Interphase prior to second slippage
Slippage 2
Interphase prior to death in mitosis
Interphase before third slippage
Slippage 3
Final interphase
Slippage no outcome seen
Death in mitosis after slippage
Death in mitosis
Death in daughter 1
Death in daughter 2
Slippage in daughter 1
Slippage in daughter 2
Daughter 1 divides
Daughter 2 divides
Slippage and death in both daugthters

Figure 7-20: ***Stacked Bar charts showing the cellular outcomes of Barasertib (3 repeats A-B respectively)*** *on live cell imaging using the conditions DMSO, 5nM, 10nM and 25nM between 0-72 hours in SCC89 cells. Cells were treated with Barasertib for 72 hours and left for 7-10 days. Dark blue indicates interphase before mitosis or slippage; Dark Pink indicates slippage; dark violet indicates Interphase after second slippage; Yellow-Green indicates second slippage; Sky blue indicates interphase prior to death in Mitosis; Light pink indicates mitosis, Turquoise indicates the final interphase, Light violet indicates death in the second daughter cell, Olympic blue indicates death in daughter one, Dark Cream indicates no observable event after slippage, Green indicates death in mitosis after slippage, Orange indicates cell death in mitosis, Black and white stripes indicates slippage in one daughter cells, Light cream indicates slippage in the second daughter cell, Cyan indicates division in daughter one of two, Grey indicates division in daughter two of two and Purple indicates slippage* ***and*** *death in both daughter cells.*

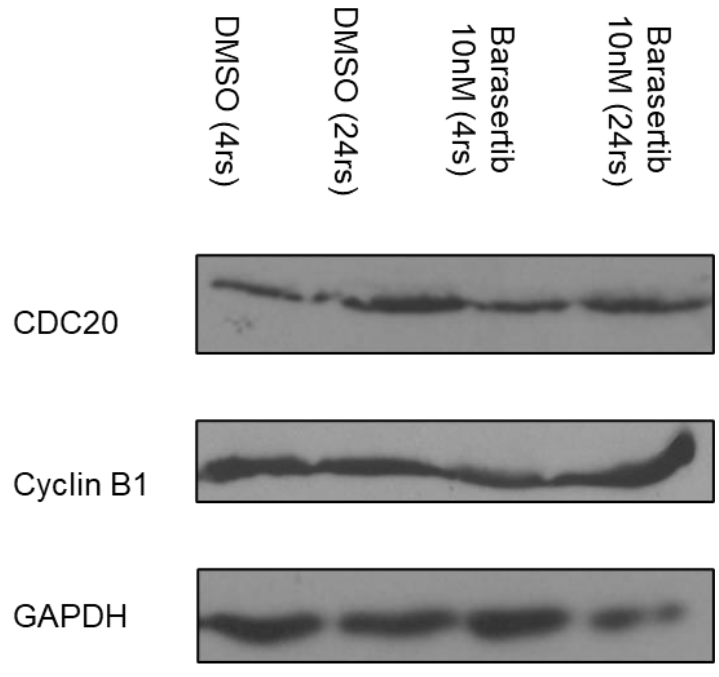
7.10 Western Blots CDC20, Cyclin B1 in HNSCC and NSCLC cell lines



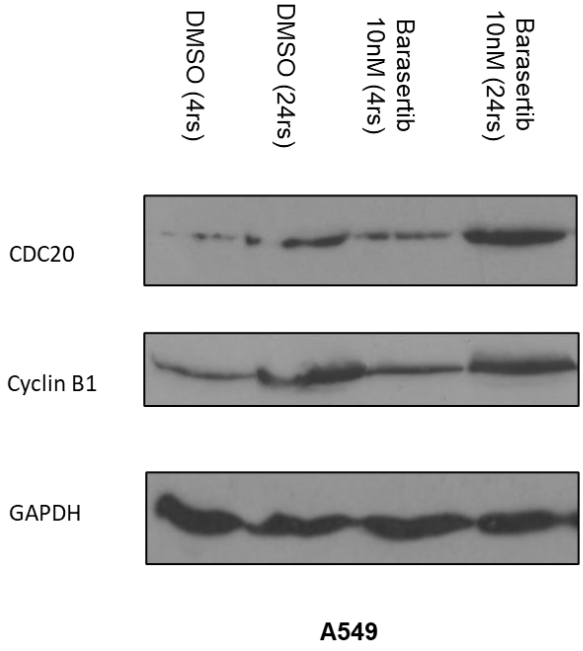
UPCI-SCC72



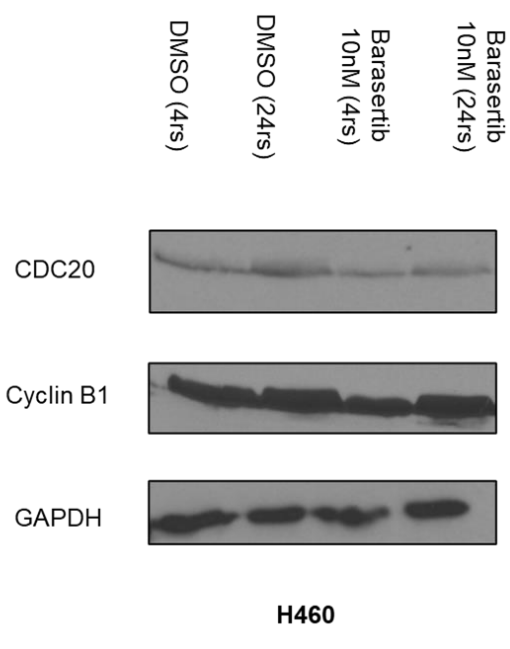
SCC89



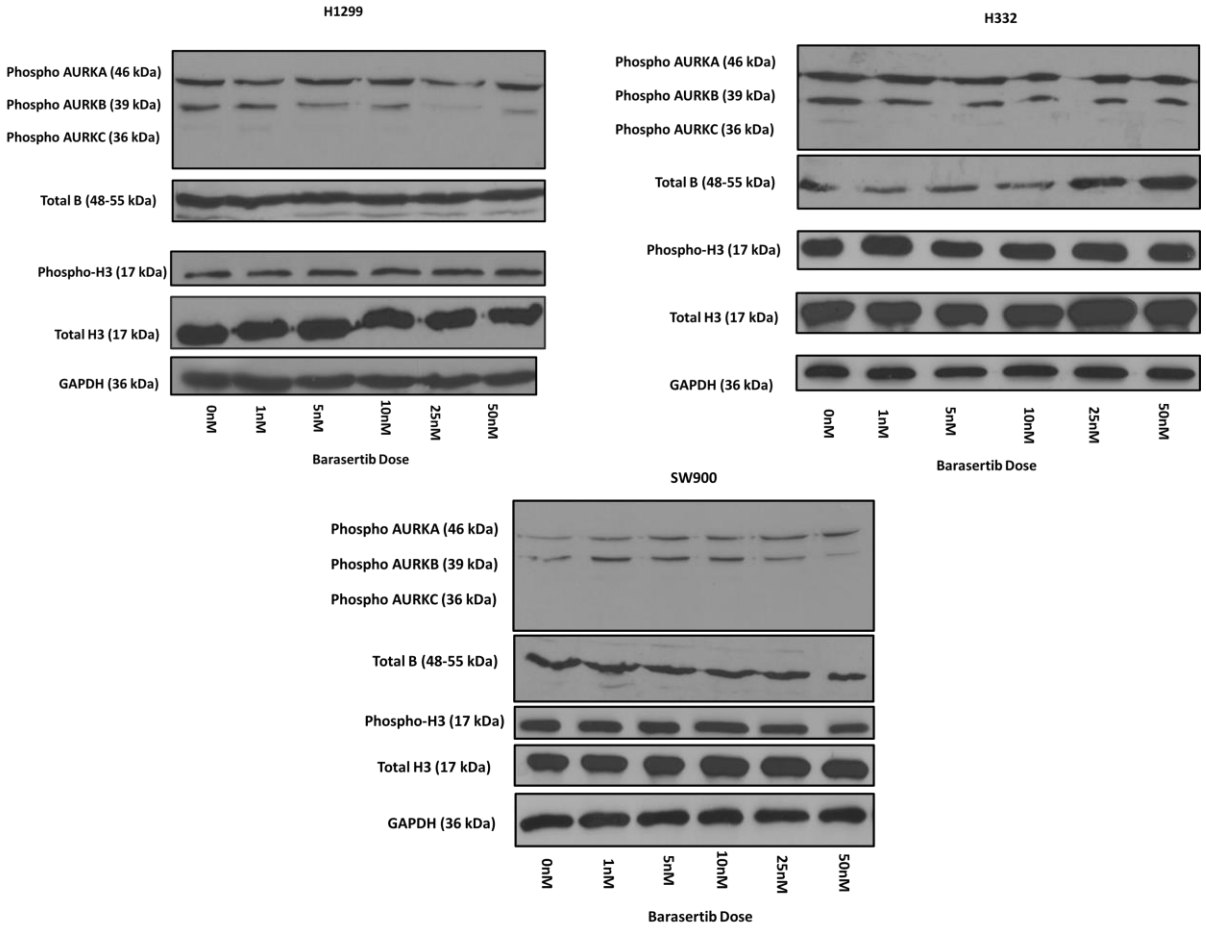
BICR22


DMSO (4rs)
DMSO (24rs)
Barasertib 10nM (4rs)
Barasertib 10nM (24rs)
CDC20
Cyclin B1
GAPDH

A549


DMSO (4rs)
DMSO (24rs)
Barasertib 10nM (4rs)
Barasertib 10nM (24rs)
CDC20
Cyclin B1
GAPDH

H460


H1299
Phospho AURKA (46 kDa)
Phospho AURKB (39 kDa)
Phospho AURKC (36 kDa)
Total B (48-55 kDa)
Phospho-H3 (17 kDa)
Total H3 (17 kDa)
GAPDH (36 kDa)
0nM
1nM
5nM
10nM
25nM
50nM
Barasertib Dose
H332
Phospho AURKA (46 kDa)
Phospho AURKB (39 kDa)
Phospho AURKC (36 kDa)
Total B (48-55 kDa)
Phospho-H3 (17 kDa)
Total H3 (17 kDa)
GAPDH (36 kDa)
0nM
1nM
5nM
10nM
25nM
50nM
Barasertib Dose
SW900
Phospho AURKA (46 kDa)
Phospho AURKB (39 kDa)
Phospho AURKC (36 kDa)
Total B (48-55 kDa)
Phospho-H3 (17 kDa)
Total H3 (17 kDa)
GAPDH (36 kDa)
0nM
1nM
5nM
10nM
25nM
50nM
Barasertib Dose

8 References

, Cathie Garnis, C.T.D.D., 2015. Molecular characterization of immortalized normal and dysplastic oral cell lines. Oral Pathology and Medicine 44, 329–336.

Abe, Y., Ohsugi, M., Haraguchi, K., Fujimoto, J., Yamamoto, T., 2006. LATS2-Ajuba complex regulates γ-tubulin recruitment to centrosomes and spindle organization during mitosis. FEBS Letters 580, 782–788. https://doi.org/10.1016/j.febslet.2005.12.096

Adams, R.R., Carmena, M., Earnshaw, W.C., 2001. Chromosomal passengers and the (aurora) ABCs of mitosis. Trends in Cell Biology 11, 49–54. https://doi.org/10.1016/S0962-8924(00)01880-8

Adderley, H., Blackhall, F.H., Lindsay, C.R., 2019. KRAS-mutant non-small cell lung cancer: Converging small molecules and immune checkpoint inhibition. EBioMedicine 41, 711–716. https://doi.org/10.1016/j.ebiom.2019.02.049

Adriaans, I.E., Basant, A., Ponsioen, B., Glotzer, M., Lens, S.M.A., 2019. PLK1 plays dual roles in centralspindlin regulation during cytokinesis. Journal of Cell Biology 218, 1250–1264. https://doi.org/10.1083/jcb.201805036

Afonso, O., Figueiredo, A.C., Maiato, H., 2017. Late mitotic functions of Aurora kinases. Chromosoma 126, 93–103. https://doi.org/10.1007/s00412-016-0594-5

Afonso, Olga, Matos, I., Maiato, H., 2014. Spatial control of the anaphase-telophase transition. Cell Cycle 13, 2985–2986. https://doi.org/10.4161/15384101.2014.959853

Afonso, O., Matos, I., Pereira, A.J., Aguiar, P., Lampson, M.A., Maiato, H., 2014. Feedback control of chromosome separation by a midzone Aurora B gradient. Science 345, 332–336. https://doi.org/10.1126/science.1251121

Ali, E.M., Abdelraheem, A.G., 2011. Concurrent radiotherapy and chemotherapy for locally advanced squamous cell carcinoma of the head and neck. Head Neck Oncol 3, 48. https://doi.org/10.1186/1758-3284-3-48

Arbour, K.C., Riely, G.J., 2017. Diagnosis and Treatment of Anaplastic Lymphoma Kinase–Positive Non–Small Cell Lung Cancer. Hematology/Oncology Clinics of North America 31, 101–111. https://doi.org/10.1016/j.hoc.2016.08.012

Asteriti, I.A., De Mattia, F., Guarguaglini, G., 2015. Cross-talk between AURKA and Plk1 in mitotic entry and spindle assembly. Frontiers in Oncology 5, 1–9. https://doi.org/10.3389/fonc.2015.00283

Aupérin, A., Le Péchoux, C., Rolland, E., Curran, W.J., Furuse, K., Fournel, P., Belderbos, J., Clamon, G., Ulutin, H.C., Paulus, R., Yamanaka, T., Bozonnat, M.-C., Uitterhoeve, A., Wang, X., Stewart, L., Arriagada, R., Burdett, S., Pignon, J.-P., 2010. Meta-Analysis of Concomitant Versus Sequential Radiochemotherapy in Locally Advanced Non–Small-Cell Lung Cancer. JCO 28, 2181–2190. https://doi.org/10.1200/JCO.2009.26.2543

Azuaje, F.J., 2014. Selecting biologically informative genes in co-expression networks with a centrality score. Biol Direct 9, 12. https://doi.org/10.1186/1745-6150-9-12

Azzariti, A., Porcelli, L., Quatrale, A., Sidella, L., Iacobazzi, R., Guida, G., Maida, I., Cocco, T., Ferretta, A., Strippoli, S., Giuda, S., Tommasi, S., Paradiso, A., Guida, M., 2014. Barasertib: a novel approach for the treatment of metastatic melanoma. J Transl Med 12, P7. https://doi.org/10.1186/1479-5876-12-S1-P7
Bader, G.D., Hogue, C.W., 2003. An automated method for finding molecular complexes in large protein interaction networks. BMC Bioinformatics.
Ban, R., Nishida, T., Urano, T., 2011. Mitotic kinase Aurora-B is regulated by SUMO-2/3 conjugation/deconjugation during mitosis: Mitotic regulation of Aurora-B by SUMO. Genes to Cells 16, 652–669. https://doi.org/10.1111/j.1365-2443.2011.01521.x
Banerjee, B., Kestner, C.A., Stukenberg, P.T., 2014. EB1 enables spindle microtubules to regulate centromeric recruitment of Aurora B. Journal of Cell Biology 204, 947–963. https://doi.org/10.1083/jcb.201307119
Barta, J.A., Powell, C.A., Wisnivesky, J.P., 2019. Global epidemiology of lung cancer. Annals of Global Health 85, 1–16. https://doi.org/10.5334/aogh.2419
Bastos, R.N., Cundell, M.J., Barr, F.A., 2014. KIF4A and PP2A–B56 form a spatially restricted feedback loop opposing Aurora B at the anaphase central spindle. Journal of Cell Biology 207, 683–693. https://doi.org/10.1083/jcb.201409129
Baumann, M., Zips, D., Appold, S., 2009. Radiotherapy of lung cancer: Technology meets biology meets multidisciplinarity. Radiotherapy and Oncology 91, 279–281. https://doi.org/10.1016/j.radonc.2009.05.001
Becker, M., Stolz, A., Ertych, N., Bastians, H., 2010. Centromere localization of INCENP-Aurora B is sufficient to support spindle checkpoint function. Cell Cycle 9, 1360–1372. https://doi.org/10.4161/cc.9.7.11177
Bertran-Alamillo, J., Cattan, V., Schoumacher, M., Codony-Servat, J., Giménez-Capitán, A., Cantero, F., Burbridge, M., Rodríguez, S., Teixidó, C., Roman, R., Castellví, J., García-Román, S., Codony-Servat, C., Viteri, S., Cardona, A.-F., Karachaliou, N., Rosell, R., Molina-Vila, M.-A., 2019a. AURKB as a target in non-small cell lung cancer with acquired resistance to anti-EGFR therapy. Nat Commun 10, 1812. https://doi.org/10.1038/s41467-019-09734-5
Bertran-Alamillo, J., Cattan, V., Schoumacher, M., Codony-Servat, J., Giménez-Capitán, A., Cantero, F., Burbridge, M., Rodríguez, S., Teixidó, C., Roman, R., Castellví, J., García-Román, S., Codony-Servat, C., Viteri, S., Cardona, A.-F., Karachaliou, N., Rosell, R., Molina-Vila, M.-A., 2019b. AURKB as a target in non-small cell lung cancer with acquired resistance to anti-EGFR therapy. Nat Commun 10, 1812. https://doi.org/10.1038/s41467-019-09734-5
Bevacizumab for the treatment of non-small-cell lung cancer (terminated appraisal), n.d. . Lung cancer.
Biggins, S., Murray, A.W., 2001. The budding yeast protein kinase Ipl1/Aurora allows the absence of tension to activate the spindle checkpoint. Genes Dev. 15, 3118–3129. https://doi.org/10.1101/gad.934801
Blackford, A.N., Jackson, S.P., 2017. ATM, ATR, and DNA-PK: The Trinity at the Heart of the DNA Damage Response. Molecular Cell 66, 801–817. https://doi.org/10.1016/j.molcel.2017.05.015
Bonner, J.A., Azarnia, N., Jones, C.U., Jassem, J., Baselga, J., Rowinsky, E.K., 2006. Radiotherapy plus Cetuximab for Squamous-Cell Carcinoma of the Head and Neck. The New England Journal of Medicine.
Borah, N.A., Reddy, M.M., 2021. Aurora Kinase B Inhibition: A Potential Therapeutic Strategy for Cancer. Molecules 26, 1981. https://doi.org/10.3390/molecules26071981

Bradley, J.D., Paulus, R., Komaki, R., Masters, G., Blumenschein, G., Schild, S., Bogart, J., Hu, C., Forster, K., Magliocco, A., Kavadi, V., Garces, Y.I., Narayan, S., Iyengar, P., Robinson, C., Wynn, R.B., Koprowski, C., Meng, J., Beitler, J., Gaur, R., Curran, W., Choy, H., 2015. Standard-dose versus high-dose conformal radiotherapy with concurrent and consolidation carboplatin plus paclitaxel with or without cetuximab for patients with stage IIIA or IIIB non-small-cell lung cancer (RTOG 0617): a randomised, two-by-two factorial phase 3 study. The Lancet Oncology 16, 187–199. https://doi.org/10.1016/S1470-2045(14)71207-0

Bradley, P.J., 2012. Multidisciplinary clinical approach to the management of head and neck cancer. Eur Arch Otorhinolaryngol 269, 2451–2454. https://doi.org/10.1007/s00405-012-2209-y

Bray, F., Ferlay, J., Soerjomataram, I., Siegel, R.L., Torre, L.A., Jemal, A., 2018. Global cancer statistics 2018: GLOBOCAN estimates of incidence and mortality worldwide for 36 cancers in 185 countries. CA: A Cancer Journal for Clinicians 68, 394–424. https://doi.org/10.3322/caac.21492

Brustugun, O.T., 2015. Hypoxia as a Cause of Treatment Failure in Non–Small Cell Carcinoma of the Lung. Seminars in Radiation Oncology 25, 87–92. https://doi.org/10.1016/j.semradonc.2014.11.006

Bukhari, A.B., Lewis, C.W., Pearce, J.J., Luong, D., Chan, G.K., Gamper, A.M., 2019. Inhibiting Wee1 and ATR kinases produces tumor-selective synthetic lethality and suppresses metastasis. Journal of Clinical Investigation 129, 1329–1344. https://doi.org/10.1172/JCI122622

Burgess, S.G., Mukherjee, M., Sabir, S., Joseph, N., Gutiérrez-Caballero, C., Richards, M.W., Huguenin-Dezot, N., Chin, J.W., Kennedy, E.J., Pfuhl, M., Royle, S.J., Gergely, F., Bayliss, R., 2018. Mitotic spindle association of TACC3 requires Aurora-A-dependent stabilization of a cryptic α-helix. The EMBO Journal 37, e97902. https://doi.org/10.15252/embj.201797902

Carlton, J.G., Caballe, A., Agromayor, M., Kloc, M., Martin-Serrano, J., 2012. ESCRT-III Governs the Aurora B-Mediated Abscission Checkpoint Through CHMP4C. Science 336, 220–225. https://doi.org/10.1126/science.1217180

Carmena, M., Wheelock, M., Funabiki, H., Earnshaw, W.C., 2012. The chromosomal passenger complex (CPC): from easy rider to the godfather of mitosis. Nat Rev Mol Cell Biol 13, 789–803. https://doi.org/10.1038/nrm3474

Carretero, M., Ruiz-Torres, M., Rodríguez-Corsino, M., Barthelemy, I., Losada, A., 2013. Pds5B is required for cohesion establishment and Aurora B accumulation at centromeres: Pds5B is required for cohesion establishment and Aurora B accumulation. The EMBO Journal 32, 2938–2949. https://doi.org/10.1038/emboj.2013.230

Chapman, A.M., Sun, K.Y., Ruestow, P., Cowan, D.M., Madl, A.K., 2016. Lung cancer mutation profile of EGFR, ALK, and KRAS: Meta-analysis and comparison of never and ever smokers. Lung Cancer 102, 122–134. https://doi.org/10.1016/j.lungcan.2016.10.010

Chen, B.B., Glasser, J.R., Coon, T.A., Mallampalli, R.K., 2013. Skp-cullin-F box E3 ligase component FBXL2 ubiquitinates Aurora B to inhibit tumorigenesis. Cell Death Dis 4, e759–e759. https://doi.org/10.1038/cddis.2013.271

Chen, W.S., Bindra, R.S., Mo, A., Hayman, T., Husain, Z., Contessa, J.N., Gaffney, S.G., Townsend, J.P., Yu, J.B., 2018. CDKN2A Copy Number Loss Is an Independent Prognostic Factor in HPV-Negative Head and Neck Squamous Cell Carcinoma. Front. Oncol. 8, 95. https://doi.org/10.3389/fonc.2018.00095

Cheng, B., Crasta, K., 2017. Consequences of mitotic slippage for antimicrotubule drug therapy. Endocrine-Related Cancer 24, T97–T106. https://doi.org/10.1530/ERC-17-0147
Cheng, L., Zhang, J., Ahmad, S., Rozier, L., Yu, H., Deng, H., Mao, Y., 2011. Aurora B Regulates Formin mDia3 in Achieving Metaphase Chromosome Alignment. Developmental Cell 20, 342–352. https://doi.org/10.1016/j.devcel.2011.01.008
Cheung, P., Faria, S., Ahmed, S., Chabot, P., Greenland, J., Kurien, E., Mohamed, I., Wright, J.R., Hollenhorst, H., De Metz, C., Campbell, H., Vu, T.T., Karvat, A., Wai, E.S., Ung, Y.C., Goss, G., Shepherd, F.A., O'Brien, P., Ding, K., O'Callaghan, C., 2014. Phase II Study of Accelerated Hypofractionated Three-Dimensional Conformal Radiotherapy for Stage T1-3 N0 M0 Non-Small Cell Lung Cancer: NCIC CTG BR.25. JNCI Journal of the National Cancer Institute 106, dju164–dju164. https://doi.org/10.1093/jnci/dju164
Chieffi, P., Cozzolino, L., Kisslinger, A., Libertini, S., Staibano, S., Mansueto, G., De Rosa, G., Villacci, A., Vitale, M., Linardopoulos, S., Portella, G., Tramontano, D., 2006. Aurora B expression directly correlates with prostate cancer malignancy and influence prostate cell proliferation. Prostate 66, 326–333. https://doi.org/10.1002/pros.20345
Chin, C.-H., Chen, S.-H., Wu, H.-H., Ho, C.-W., Ko, M.-T., Lin, C.-Y., 2014. cytoHubba: identifying hub objects and sub-networks from complex interactome. BMC Syst Biol 8, S11. https://doi.org/10.1186/1752-0509-8-S4-S11
Chu, Q.S., Bouganim, N., Fortier, C., Zaknoen, S., Stille, J.R., Kremer, J.D., Yuen, E., Hui, Y.-H., De La Peña, A., Lithio, A., Smith, P.S., Batist, G., 2021. Aurora kinase A inhibitor, LY3295668 erbumine: a phase 1 monotherapy safety study in patients with locally advanced or metastatic solid tumors. Invest New Drugs 39, 1001–1010. https://doi.org/10.1007/s10637-020-01049-3
Chu, Y., Yao, P.Y., Wang, W., Wang, D., Wang, Z., Zhang, L., Huang, Y., Ke, Y., Ding, X., Yao, X., 2011. Aurora B kinase activation requires survivin priming phosphorylation by PLK1. Journal of Molecular Cell Biology 3, 260–267. https://doi.org/10.1093/jmcb/mjq037
Cooper, W.A., Lam, D.C.L., O'Toole, S.A., Minna, J.D., 2013. Molecular biology of lung cancer. Journal of Thoracic Disease 5.
Cox, J.D., Azarnia, N., Byhardt, R.W., Shin, K.H., Emami, B., Pajak, T.F., 1990. A randomized phase I/II trial of hyperfractionated radiation therapy with total doses of 60.0 Gy to 79.2 Gy: possible survival benefit with greater than or equal to 69.6 Gy in favorable patients with Radiation Therapy Oncology Group stage III non-small-cell lung carcinoma: report of Radiation Therapy Oncology Group 83-11. JCO 8, 1543–1555. https://doi.org/10.1200/JCO.1990.8.9.1543
Curran, W.J., Paulus, R., Langer, C.J., Komaki, R., Lee, J.S., Hauser, S., Movsas, B., Wasserman, T., Rosenthal, S.A., Gore, E., Machtay, M., Sause, W., Cox, J.D., 2011. Sequential vs Concurrent Chemoradiation for Stage III Non-Small Cell Lung Cancer: Randomized Phase III Trial RTOG 9410. JNCI Journal of the National Cancer Institute 103, 1452–1460. https://doi.org/10.1093/jnci/djr325
Delaval, B., Ferrand, A., Conte, N., Larroque, C., Hernandez-Verdun, D., Prigent, C., Birnbaum, D., 2004. Aurora B -TACC1 protein complex in cytokinesis. Oncogene 23, 4516–4522. https://doi.org/10.1038/sj.onc.1207593

DeLuca, K.F., Meppelink, A., Broad, A.J., Mick, J.E., Peersen, O.B., Pektas, S., Lens, S.M.A., DeLuca, J.G., 2018. Aurora A kinase phosphorylates Hec1 to regulate metaphase kinetochore-microtubule dynamics. Journal of Cell Biology 217, 163–177. https://doi.org/10.1083/jcb.201707160

Deng, S., Vlatkovic, T., Li, M., Zhan, T., Veldwijk, M.R., Herskind, C., 2022. Targeting the DNA Damage Response and DNA Repair Pathways to Enhance Radiosensitivity in Colorectal Cancer. Cancers 14, 4874. https://doi.org/10.3390/cancers14194874

Din, O.S., Harden, S.V., Hudson, E., Mohammed, N., Pemberton, L.S., Lester, J.F., Biswas, D., Magee, L., Tufail, A., Carruthers, R., Sheikh, G., Gilligan, D., Hatton, M.Q.F., 2013. Accelerated hypo-fractionated radiotherapy for non small cell lung cancer: Results from 4 UK centres. Radiotherapy and Oncology 109, 8–12. https://doi.org/10.1016/j.radonc.2013.07.014

Ding, K, B., Ning, n.d. Gene expression patterns combined with network analysis identify hub genes associated with bladder cancer. Computational Biology and Chemistry., 56, 71–83.

Dische, S., Saunders, M.I., n.d. Continuous, hyperfractionated, accelerated radiotherapy (CHART).

Ditchfield, C., Johnson, V.L., Tighe, A., Ellston, R., Haworth, C., Johnson, T., Mortlock, A., Keen, N., Taylor, S.S., 2003a. Aurora B couples chromosome alignment with anaphase by targeting BubR1, Mad2, and Cenp-E to kinetochores. Journal of Cell Biology 161, 267–280. https://doi.org/10.1083/jcb.200208091

Ditchfield, C., Johnson, V.L., Tighe, A., Ellston, R., Haworth, C., Johnson, T., Mortlock, A., Keen, N., Taylor, S.S., 2003b. Aurora B couples chromosome alignment with anaphase by targeting BubR1, Mad2, and Cenp-E to kinetochores. Journal of Cell Biology 161, 267–280. https://doi.org/10.1083/jcb.200208091

Du, J., Yan, L., Torres, R., Gong, X., Bian, H., Marugán, C., Boehnke, K., Baquero, C., Hui, Y.-H., Chapman, S.C., Yang, Y., Zeng, Y., Bogner, S.M., Foreman, R.T., Capen, A., Donoho, G.P., Van Horn, R.D., Barnard, D.S., Dempsey, J.A., Beckmann, R.P., Marshall, M.S., Chio, L.-C., Qian, Y., Webster, Y.W., Aggarwal, A., Chu, S., Bhattachar, S., Stancato, L.F., Dowless, M.S., Iversen, P.W., Manro, J.R., Walgren, J.L., Halstead, B.W., Dieter, M.Z., Martinez, R., Bhagwat, S.V., Kreklau, E.L., Lallena, M.J., Ye, X.S., Patel, B.K.R., Reinhard, C., Plowman, G.D., Barda, D.A., Henry, J.R., Buchanan, S.G., Campbell, R.M., 2019. Aurora A–Selective Inhibitor LY3295668 Leads to Dominant Mitotic Arrest, Apoptosis in Cancer Cells, and Shows Potent Preclinical Antitumor Efficacy. Molecular Cancer Therapeutics 18, 2207–2219. https://doi.org/10.1158/1535-7163.MCT-18-0529

Eberhardt, W.E.E., De Ruysscher, D., Weder, W., Le Péchoux, C., De Leyn, P., Hoffmann, H., Westeel, V., Stahel, R., Felip, E., Peters, S., Stahel, Rolf, Felip, Enriqueta, Peters, Solange, Kerr, K., Besse, B., Vansteenkiste, J., Eberhardt, W., Edelman, M., Mok, T., O'Byrne, K., Novello, S., Bubendorf, L., Marchetti, A., Baas, P., Reck, M., Syrigos, K., Paz-Ares, L., Smit, E.F., Meldgaard, P., Adjei, A., Nicolson, M., Crinó, L., Van Schil, P., Senan, S., Faivre-Finn, C., Rocco, G., Veronesi, G., Douillard, J.-Y., Lim, E., Dooms, C., Weder, Walter, De Ruysscher, Dirk, Le Pechoux, C., De Leyn, Paul, Westeel, Virginie, 2015. 2nd ESMO Consensus Conference in Lung Cancer: locally advanced stage III

non-small-cell lung cancer. Annals of Oncology 26, 1573–1588. https://doi.org/10.1093/annonc/mdv187
Faitar, S.L., Sossey-Alaoui, K., Ranalli, T.A., Cowell, J.K., 2006. EVI5 protein associates with the INCENP-aurora B kinase-survivin chromosomal passenger complex and is involved in the completion of cytokinesis. EXPERIMENTAL CELL RESEARCH 11.
Fernandez-Miranda, G., de Castro, I.P., Carmena, M., Aguirre-Portoles, C., Ruchaud, S., Fant, X., Montoya, G., Earnshaw, W.C., Malumbres, M., 2010. SUMOylation modulates the function of Aurora-B kinase. Journal of Cell Science 123, 2823–2833. https://doi.org/10.1242/jcs.065565
Ferrand, A., Chevrier, V., Chauvin, J.-P., Birnbaum, D., 2009. Ajuba: a new microtubule-associated protein that interacts with BUBR1 and Aurora B at kinetochores in metaphase. Biology of the Cell 101, 221–240. https://doi.org/10.1042/BC20080060
Fischer, A.H., Cibas, E.S., Howell, L.P., Kurian, E.M., Laucirica, R., Moriarty, A.T., Renshaw, A.A., Zakowski, M.F., Young, N.A., 2011. Role of Cytology in the Management of Non–Small-Cell Lung Cancer. JCO 29, 3331–3332. https://doi.org/10.1200/JCO.2011.35.2534
Fu, K.K., Pajak, T.F., Trotti, A., Jones, C.U., Spencer, S.A., Phillips, T.L., Garden, A.S., Ridge, J.A., Cooper, J.S., Ang, K.K., 2000. A radiation therapy oncology group (RTOG) phase III randomized study to compare hyperfractionation and two variants of accelerated fractionation to standard fractionation radiotherapy for head and neck squamous cell carcinomas: first report of RTOG 9003. International Journal of Radiation Oncology*Biology*Physics 48, 7–16. https://doi.org/10.1016/S0360-3016(00)00663-5
Gan, Z., Han, K., Lin, S., Hu, H., Shen, Z., Min, D., 2017. Knockdown of ubiquitin-specific peptidase 39 inhibited the growth of osteosarcoma cells and induced apoptosis in vitro. Biol Res 50, 15. https://doi.org/10.1186/s40659-017-0121-z
Gao, M., Kong, W., Huang, Z., Xie, Z., 2020. Identification of Key Genes Related to Lung Squamous Cell Carcinoma Using Bioinformatics Analysis. IJMS 21, 2994. https://doi.org/10.3390/ijms21082994
Gedda, L., Björkelund, H., Andersson, K., 2010. Real-time immunohistochemistry analysis of embedded tissue. Applied Radiation and Isotopes 68, 2372–2376. https://doi.org/10.1016/j.apradiso.2010.06.003
Gendarme, S., Bylicki, O., Chouaid, C., Guisier, F., 2022. ROS-1 Fusions in Non-Small-Cell Lung Cancer: Evidence to Date. Current Oncology 29, 641–658. https://doi.org/10.3390/curroncol29020057
Girdler, F., Gascoigne, K.E., Eyers, P.A., Hartmuth, S., Crafter, C., Foote, K.M., Keen, N.J., Taylor, S.S., 2006. Validating Aurora B as an anti-cancer drug target. Journal of Cell Science 119, 3664–3675. https://doi.org/10.1242/jcs.03145
Glastonbury, C.M., 2020. Head and Neck Squamous Cell Cancer: Approach to Staging and Surveillance, in: Hodler, J., Kubik-Huch, R.A., Von Schulthess, G.K. (Eds.), Diseases of the Brain, Head and Neck, Spine 2020–2023, IDKD Springer Series. Springer International Publishing, Cham, pp. 215–222. https://doi.org/10.1007/978-3-030-38490-6_17
Gohard, F.H., St-Cyr, D.J., Tyers, M., Earnshaw, W.C., 2014. Targeting the INCENP IN-box–Aurora B interaction to inhibit CPC activity *in vivo*. Open Biol. 4, 140163. https://doi.org/10.1098/rsob.140163

Gully, Chris P., Velazquez-Torres, G., Shin, J.-H., Fuentes-Mattei, E., Wang, E., Carlock, C., Chen, J., Rothenberg, D., Adams, H.P., Choi, H.H., Guma, S., Phan, L., Chou, P.-C., Su, C.-H., Zhang, F., Chen, J.-S., Yang, T.-Y., Yeung, S.-C.J., Lee, M.-H., 2012. Aurora B kinase phosphorylates and instigates degradation of p53. Proc. Natl. Acad. Sci. U.S.A. 109. https://doi.org/10.1073/pnas.1110287109

Gully, C. P., Velazquez-Torres, G., Shin, J.-H., Fuentes-Mattei, E., Wang, E., Carlock, C., Chen, J., Rothenberg, D., Adams, H.P., Choi, H.H., Guma, S., Phan, L., Chou, P.-C., Su, C.-H., Zhang, F., Chen, J.-S., Yang, T.-Y., Yeung, S.-C.J., Lee, M.-H., 2012. Aurora B kinase phosphorylates and instigates degradation of p53. Proceedings of the National Academy of Sciences 109, E1513–E1522. https://doi.org/10.1073/pnas.1110287109

Guo, Y., Cheng, L., Ahmad, S., Mao, Y., 2011. Formin mDia3: A novel target for Aurora B kinase. BioArchitecture 1, 88–90. https://doi.org/10.4161/bioa.1.2.16240

Guo, Y., Kim, C., Ahmad, S., Zhang, J., Mao, Y., 2012. CENP-E–dependent BubR1 autophosphorylation enhances chromosome alignment and the mitotic checkpoint. Journal of Cell Biology 198, 205–217. https://doi.org/10.1083/jcb.201202152

Guse, A., Mishima, M., Glotzer, M., 2005. Phosphorylation of ZEN-4/MKLP1 by Aurora B Regulates Completion of Cytokinesis. Current Biology 15, 778–786. https://doi.org/10.1016/j.cub.2005.03.041

Győrffy, B., Surowiak, P., Budczies, J., Lánczky, A., 2013. Online Survival Analysis Software to Assess the Prognostic Value of Biomarkers Using Transcriptomic Data in Non-Small-Cell Lung Cancer. PLoS ONE 8, e82241. https://doi.org/10.1371/journal.pone.0082241

Han, J., Chen, M., Wang, Y., Gong, B., Zhuang, T., Liang, L., Qiao, H., 2018. Identification of Biomarkers Based on Differentially Expressed Genes in Papillary Thyroid Carcinoma. Sci Rep 8, 9912. https://doi.org/10.1038/s41598-018-28299-9

Haratake, N., Seto, T., 2021. NTRK Fusion-positive Non–small-cell Lung Cancer: The Diagnosis and Targeted Therapy. Clinical Lung Cancer 22, 1–5. https://doi.org/10.1016/j.cllc.2020.10.013

Hashibe, M., 2010. Risk Factors: Tobacco and Alcohol, in: Olshan, A.F. (Ed.), Epidemiology, Pathogenesis, and Prevention of Head and Neck Cancer. Springer New York, New York, NY, pp. 65–85. https://doi.org/10.1007/978-1-4419-1472-9_4

Hattori, A., Takamochi, K., Oh, S., Suzuki, K., 2019. New revisions and current issues in the eighth edition of the TNM classification for non-small cell lung cancer. Japanese Journal of Clinical Oncology 49, 3–11. https://doi.org/10.1093/jjco/hyy142

Hauf, S., Cole, R.W., LaTerra, S., Zimmer, C., Schnapp, G., Walter, R., Heckel, A., Van Meel, J., Rieder, C.L., Peters, J.-M., 2003. The small molecule Hesperadin reveals a role for Aurora B in correcting kinetochore–microtubule attachment and in maintaining the spindle assembly checkpoint. The Journal of Cell Biology 161, 281–294. https://doi.org/10.1083/jcb.200208092

Haughey, B.H., Von Hoff, D.D., Windle, B.E., Wahl, G.M., Mock, P.M., 1992. c-myc oncogene copy number in squamous carcinoma of the head and neck. American Journal of Otolaryngology 13, 168–171. https://doi.org/10.1016/0196-0709(92)90117-C

Hayama, S., Daigo, Y., Yamabuki, T., Hirata, D., Kato, T., Miyamoto, M., Ito, T., Tsuchiya, E., Kondo, S., Nakamura, Y., 2007. Phosphorylation and Activation of Cell Division Cycle Associated 8 by Aurora Kinase B Plays a Significant Role in Human Lung Carcinogenesis. Cancer Res 67, 4113–4122. https://doi.org/10.1158/0008-5472.CAN-06-4705

Head and Neck Cancer Study Group (HNCSG), Monden, N., Asakage, T., Kiyota, N., Homma, A., Matsuura, K., Hanai, N., Kodaira, T., Zenda, S., Fujii, H., Tahara, M., Yokota, T., Akimoto, T., Iwae, S., Onitsuka, T., Ogawa, T., Okano, S., Takahashi, S., Shimizu, Y., Yonezawa, K., Hayashi, R., 2019. A review of head and neck cancer staging system in the TNM classification of malignant tumors (eighth edition). Japanese Journal of Clinical Oncology 49, 589–595. https://doi.org/10.1093/jjco/hyz052

Hendriks, L.E., Kerr, K.M., Menis, J., Mok, T.S., Nestle, U., Passaro, A., Peters, S., Planchard, D., Smit, E.F., Solomon, B.J., Veronesi, G., Reck, M., 2023. Oncogene-addicted metastatic non-small-cell lung cancer: ESMO Clinical Practice Guideline for diagnosis, treatment and follow-up. Annals of Oncology 34, 339–357. https://doi.org/10.1016/j.annonc.2022.12.009

Hirota, T., Kunitoku, N., Sasayama, T., Marumoto, T., Zhang, D., Nitta, M., Hatakeyama, K., Saya, H., 2003. Aurora-A and an Interacting Activator, the LIM Protein Ajuba, Are Required for Mitotic Commitment in Human Cells. Cell 114, 585–598. https://doi.org/10.1016/S0092-8674(03)00642-1

Hirota, T., Lipp, J.J., Toh, B.-H., Peters, J.-M., 2005. Histone H3 serine 10 phosphorylation by Aurora B causes HP1 dissociation from heterochromatin. Nature 438, 1176–1180. https://doi.org/10.1038/nature04254

Hochegger, H., Hégarat, N., Pereira-Leal, J.B., 2013. Aurora at the pole and equator: Overlapping functions of Aurora kinases in the mitotic spindle. Open Biology 3. https://doi.org/10.1098/rsob.120185

Hoeijmakers, J.H.J., 2001. Genome maintenance mechanisms for preventing cancer. Nature 411, 366–374. https://doi.org/10.1038/35077232

Hong, D.S., Fakih, M.G., Strickler, J.H., Desai, J., Durm, G.A., Shapiro, G.I., Falchook, G.S., Price, T.J., Sacher, A., Denlinger, C.S., Bang, Y.-J., Dy, G.K., Krauss, J.C., Kuboki, Y., Kuo, J.C., Coveler, A.L., Park, K., Kim, T.W., Barlesi, F., Munster, P.N., Ramalingam, S.S., Burns, T.F., Meric-Bernstam, F., Henary, H., Ngang, J., Ngarmchamnanrith, G., Kim, J., Houk, B.E., Canon, J., Lipford, J.R., Friberg, G., Lito, P., Govindan, R., Li, B.T., 2020. KRAS ^{G12C} Inhibition with Sotorasib in Advanced Solid Tumors. N Engl J Med 383, 1207–1217. https://doi.org/10.1056/NEJMoa1917239

Horst, K.C., Giaccia, A.J. (2010). Basic Principles of Radiobiology. In: Dirbas, F., Scott-Conner, C. (eds) Breast Surgical Techniques and Interdisciplinary Management. Springer, New York, NY. https://doi.org/10.1007/978-1-4419-6076-4_66, n.d.

Hu, C., Liu, X., Zeng, Y., Liu, J., Wu, F., 2021. DNA methyltransferase inhibitors combination therapy for the treatment of solid tumor: mechanism and clinical application. Clin Epigenet 13, 166. https://doi.org/10.1186/s13148-021-01154-x

Hu, S., Liao, Y., Chen, L., 2018. Identification of Key Pathways and Genes in Anaplastic Thyroid Carcinoma via Integrated Bioinformatics Analysis. Med Sci Monit 24, 6438–6448. https://doi.org/10.12659/MSM.910088

Huang, P.-Y., Li, Y., Luo, D.-H., Hou, X., Zeng, T.-T., Li, M.-Q., Mai, H.-Q., Zhang, L., 2015. Expression of Aurora-B and FOXM1 predict poor survival in patients

with nasopharyngeal carcinoma. Strahlenther Onkol 191, 649–655. https://doi.org/10.1007/s00066-015-0840-4
Hubaux, R., Becker-Santos, D.D., Enfield, K.S., Lam, S., Lam, W.L., Martinez, V.D., 2012. Arsenic, asbestos and radon: emerging players in lung tumorigenesis. Environ Health 11, 89. https://doi.org/10.1186/1476-069X-11-89
Iimori, M., Watanabe, S., Kiyonari, S., Matsuoka, K., Sakasai, R., Saeki, H., Oki, E., Kitao, H., Maehara, Y., 2016. Phosphorylation of EB2 by Aurora B and CDK1 ensures mitotic progression and genome stability. Nat Commun 7, 11117. https://doi.org/10.1038/ncomms11117
Imai, H., Kaira, K., Minato, K., 2017. Clinical significance of post-progression survival in lung cancer: Post-progression survival in lung cancer. Thorac Cancer 8, 379–386. https://doi.org/10.1111/1759-7714.12463
Imai, H., Kaira, K., Mori, K., Watase, N., Hisada, T., Yamada, M., Minato, K., 2020. Post-progression survival is strongly linked to overall survival in refractory small-cell lung cancer patients who received amrubicin. J Can Res Ther 16, 764. https://doi.org/10.4103/jcrt.JCRT_1170_16
Imai, H., Mori, K., Watase, N., Fujimoto, S., Kaira, K., Yamada, M., Minato, K., 2016. Clinical Significance of the Relationship between Progression-Free Survival or Postprogression Survival and Overall Survival in Patients with Extensive Disease-Small-Cell Lung Cancer Treated with Carboplatin plus Etoposide. Canadian Respiratory Journal 2016, 1–8. https://doi.org/10.1155/2016/5405810
Jang, S.H., Kim, A.-R., Park, N.-H., Park, J.W., Han, I.-S., 2016. DRG2 Regulates G2/M Progression via the Cyclin B1-Cdk1 Complex. Molecules and Cells 39, 699–704. https://doi.org/10.14348/molcells.2016.0149
Jin, C., Jin, Y., Gisselsson, D., Wennerberg, J., Wah, T.S., Strömbäck, B., Kwong, Y.-L., Mertens, F., 2006. Molecular cytogenetic characterization of the 11q13 amplicon in head and neck squamous cell carcinoma. Cytogenet Genome Res 115, 99–106. https://doi.org/10.1159/000095228
Jin, X., Mo, Q., Zhang, Y., Gao, Y., Wu, Y., Li, J., Hao, X., Ma, D., Gao, Q., Chen, P., 2016. The p38 MAPK inhibitor BIRB796 enhances the antitumor effects of VX680 in cervical cancer. Cancer Biology & Therapy 17, 566–576. https://doi.org/10.1080/15384047.2016.1177676
Jin, Y., Li, Jingwen, Li, Jieyun, Zhang, N., Guo, K., Zhang, Q., Wang, X., Yang, K., 2021. Visualized Analysis of Heavy Ion Radiotherapy: Development, Barriers and Future Directions. Front. Oncol. 11, 634913. https://doi.org/10.3389/fonc.2021.634913
Jonuscheit, S., Jost, T., Gajdošová, F., Wrobel, M., Hecht, M., Fietkau, R., Distel, L., 2021. PARP Inhibitors Talazoparib and Niraparib Sensitize Melanoma Cells to Ionizing Radiation. Genes 12, 849. https://doi.org/10.3390/genes12060849
Jung, K., Kang, H., Mehra, R., 2018. Targeting phosphoinositide 3-kinase (PI3K) in head and neck squamous cell carcinoma (HNSCC). Cancers Head Neck 3, 3. https://doi.org/10.1186/s41199-018-0030-z
Kantarjian, H.M., Martinelli, G., Jabbour, E.J., Quintás-Cardama, A., Ando, K., Bay, J., Wei, A., Gröpper, S., Papayannidis, C., Owen, K., Pike, L., Schmitt, N., Stockman, P.K., Giagounidis, A., SPARK-AML1 Investigators, 2013. Stage I of a phase 2 study assessing the efficacy, safety, and tolerability of barasertib (AZD1152) versus low-dose cytosine arabinoside in elderly patients with acute myeloid leukemia. Cancer 119, 2611–2619. https://doi.org/10.1002/cncr.28113

Khodjakov, A., Rieder, C.L., 1999. <J Cell Biol 1999 Khodjakov A.pdf> 146, 585–596.
Kim, H.-S., Kim, S.-H., Park, H.-Y., Lee, J., Yoon, J.H., Choi, S., Ryu, S.H., Lee, H., Cho, H.-S., Lee, C.-W., 2013. Functional interplay between Aurora B kinase and Ssu72 phosphatase regulates sister chromatid cohesion. Nat Commun 4, 2631. https://doi.org/10.1038/ncomms3631
Kitagawa, M., Fung, S.Y.S., Onishi, N., Saya, H., Lee, S.H., 2013. Targeting Aurora B to the Equatorial Cortex by MKlp2 Is Required for Cytokinesis. PLoS ONE 8, e64826. https://doi.org/10.1371/journal.pone.0064826
Krewski, D., Lubin, J.H., Zielinski, J.M., Alavanja, M., Catalan, V.S., Field, R.W., Klotz, J.B., L??tourneau, E.G., Lynch, C.F., Lyon, J.I., Sandler, D.P., Schoenberg, J.B., Steck, D.J., Stolwijk, J.A., Weinberg, C., Wilcox, H.B., 2005. Residential Radon and Risk of Lung Cancer: A Combined Analysis of 7 North American Case-Control Studies. Epidemiology 16, 137–145. https://doi.org/10.1097/01.ede.0000152522.80261.e3
Kumari, G., Ulrich, T., Gaubatz, S., 2013. A role for p38 in transcriptional elongation of p21 ^{CIP1} in response to Aurora B inhibition. Cell Cycle 12, 2051–2060. https://doi.org/10.4161/cc.25100
Kumari, G., Ulrich, T., Krause, M., Finkernagel, F., Gaubatz, S., 2014. Induction of p21CIP1 Protein and Cell Cycle Arrest after Inhibition of Aurora B Kinase Is Attributed to Aneuploidy and Reactive Oxygen Species. Journal of Biological Chemistry 289, 16072–16084. https://doi.org/10.1074/jbc.M114.555060
Kunitoku, N., Sasayama, T., Marumoto, T., Zhang, D., Honda, S., Kobayashi, O., Hatakeyama, K., Ushio, Y., Saya, H., Hirota, T., 2003. CENP-A Phosphorylation by Aurora-A in Prophase Is Required for Enrichment of Aurora-B at Inner Centromeres and for Kinetochore Function. Developmental Cell 5, 853–864. https://doi.org/10.1016/S1534-5807(03)00364-2
Lewin, F., Norell, S.E., Johansson, H., Gustavsson, P., Wennerberg, J., Bi□rklund, A., Rutqvist, L.E., 1998. Smoking tobacco, oral snuff, and alcohol in the etiology of squamous cell carcinoma of the head and neck: A population-based case-referent study in Sweden. Cancer 82, 1367–1375. https://doi.org/10.1002/(SICI)1097-0142(19980401)82:7<1367::AID-CNCR21>3.0.CO;2-3
Li, M., Dong, Q., Zhu, B., 2017. Aurora Kinase B Phosphorylates Histone H3.3 at Serine 31 during Mitosis in Mammalian Cells. Journal of Molecular Biology 429, 2042–2045. https://doi.org/10.1016/j.jmb.2017.01.016
Li, X., Zhang, Y., Ye, Y., Tian, S., Hu, T., Chai, H., Zhang, T., Wen, F., 2024. Carbon-ion radiotherapy alone vs. standard dose photon radiation with carbon-ion radiotherapy boost for high-grade gliomas: a retrospective study. BMC Cancer 24, 837. https://doi.org/10.1186/s12885-024-12606-x
Liang, P., Pardee, A.B., 2003. Analysing differential gene expression in cancer. Nat Rev Cancer 3, 869–876. https://doi.org/10.1038/nrc1214
Libertini, S., Abagnale, A., Passaro, C., Botta, G., Portella, G., 2010. Aurora A and B Kinases - Targets of Novel Anticancer Drugs. Recent Patents on Anti-Cancer Drug Discovery 5, 219–241. https://doi.org/10.2174/157489210791760517
Lindblom, E., Antonovic, L., Dasu, A., Lax, I., Wersäll, P., Toma-Dasu, I., 2014. Treatment fractionation for stereotactic radiotherapy of lung tumours: a modelling study of the influence of chronic and acute hypoxia on tumour control probability. Radiat Oncol 9, 149. https://doi.org/10.1186/1748-717X-9-149

Lipp, J.J., Hirota, T., Poser, I., Peters, J.-M., 2007. Aurora B controls the association of condensin I but not condensin II with mitotic chromosomes. Journal of Cell Science 120, 1245–1255. https://doi.org/10.1242/jcs.03425
Liu, F., Wei, Y., Zhang, H., Jiang, J., Zhang, P., Chu, Q., 2022. NTRK Fusion in Non-Small Cell Lung Cancer: Diagnosis, Therapy, and TRK Inhibitor Resistance. Front. Oncol. 12, 864666. https://doi.org/10.3389/fonc.2022.864666
Liu, S., Qin, Z., Mao, Y., Zhang, W., Wang, Y., Jia, L., Peng, X., 2022. Therapeutic Targeting of MYC in Head and Neck Squamous Cell Carcinoma. OncoImmunology 11, 2130583. https://doi.org/10.1080/2162402X.2022.2130583
Lo Iacono, M., Monica, V., Saviozzi, S., Ceppi, P., Bracco, E., Papotti, M., Scagliotti, G.V., 2011. Aurora Kinase A expression is associated with lung cancer histological-subtypes and with tumor de-differentiation. J Transl Med 9, 100. https://doi.org/10.1186/1479-5876-9-100
Lok, T.M., Wang, Y., Xu, W.K., Xie, S., Ma, H.T., Poon, R.Y.C., 2020. Mitotic slippage is determined by p31comet and the weakening of the spindle-assembly checkpoint. Oncogene 39, 2819–2834. https://doi.org/10.1038/s41388-020-1187-6
Lung cancer statistics, Cancer Research UK, 2023.
Luo, Y., Barrios-Rodiles, M., Gupta, G.D., Zhang, Y.Y., Ogunjimi, A.A., Bashkurov, M., Tkach, J.M., Underhill, A.Q., Zhang, L., Bourmoum, M., Wrana, J.L., Pelletier, L., 2019. Atypical function of a centrosomal module in WNT signalling drives contextual cancer cell motility. Nature Communications 10. https://doi.org/10.1038/s41467-019-10241-w
Mackay, D.R., Ullman, K.S., 2015. ATR and a Chk1-Aurora B pathway coordinate postmitotic genome surveillance with cytokinetic abscission. MBoC 26, 2217–2226. https://doi.org/10.1091/mbc.E14-11-1563
Maerki, S., Olma, M.H., Staubli, T., Steigemann, P., Gerlich, D.W., Quadroni, M., Sumara, I., Peter, M., 2009. The Cul3–KLHL21 E3 ubiquitin ligase targets Aurora B to midzone microtubules in anaphase and is required for cytokinesis. Journal of Cell Biology 187, 791–800. https://doi.org/10.1083/jcb.200906117
Maguire, J., Khan, I., McMenemin, R., O'Rourke, N., McNee, S., Kelly, V., Peedell, C., Snee, M., 2014. SOCCAR: A randomised phase II trial comparing sequential versus concurrent chemotherapy and radical hypofractionated radiotherapy in patients with inoperable stage III Non-Small Cell Lung Cancer and good performance status. European Journal of Cancer 50, 2939–2949. https://doi.org/10.1016/j.ejca.2014.07.009
Mahankali, M., Henkels, K.M., Speranza, F., Gomez-Cambronero, J., 2015. A non-mitotic role for Aurora kinase A as a direct activator of cell migration upon interaction with PLD, FAK and Src. Journal of Cell Science 128, 516–526. https://doi.org/10.1242/jcs.157339
Maia, A.F., Feijão, T., Vromans, M.J.M., Sunkel, C.E., Lens, S.M.A., 2010a. Aurora B kinase cooperates with CENP-E to promote timely anaphase onset. Chromosoma 119, 405–413. https://doi.org/10.1007/s00412-010-0265-x
Maia, A.F., Feijão, T., Vromans, M.J.M., Sunkel, C.E., Lens, S.M.A., 2010b. Aurora B kinase cooperates with CENP-E to promote timely anaphase onset. Chromosoma 119, 405–413. https://doi.org/10.1007/s00412-010-0265-x
Maiato, H., Afonso, O., Matos, I., 2015. A chromosome separation checkpoint: A midzone Aurora B gradient mediates a chromosome separation checkpoint

that regulates the anaphase-telophase transition. BioEssays 37, 257–266. https://doi.org/10.1002/bies.201400140
Mallampalli, R.K., Glasser, J.R., Coon, T.A., Chen, B.B., 2013. Calmodulin protects Aurora B on the midbody to regulate the fidelity of cytokinesis. Cell Cycle 12, 663–673. https://doi.org/10.4161/cc.23586
Manisalidis, I., Stavropoulou, E., Stavropoulos, A., Bezirtzoglou, E., 2020. Environmental and Health Impacts of Air Pollution: A Review. Front. Public Health 8, 14. https://doi.org/10.3389/fpubh.2020.00014
Marabelle, A., Cassier, P.A., Fakih, M., Kao, S., Nielsen, D., Italiano, A., Guren, T.K., Van Dongen, M.G.J., Spencer, K., Bariani, G.M., Ascierto, P.A., Santoro, A., Shah, M., Asselah, J., Iqbal, S., Takahashi, S., Piha-Paul, S.A., Ott, P.A., Chatterjee, A., Jin, F., Norwood, K., Delord, J.-P., 2022. Pembrolizumab for previously treated advanced anal squamous cell carcinoma: results from the non-randomised, multicohort, multicentre, phase 2 KEYNOTE-158 study. The Lancet Gastroenterology & Hepatology 7, 446–454. https://doi.org/10.1016/S2468-1253(21)00382-4
Marima, R., Hull, R., Penny, C., Dlamini, Z., 2021. Mitotic syndicates Aurora Kinase B (AURKB) and mitotic arrest deficient 2 like 2 (MAD2L2) in cohorts of DNA damage response (DDR) and tumorigenesis. Mutation Research/Reviews in Mutation Research 787, 108376. https://doi.org/10.1016/j.mrrev.2021.108376
Martel, M., 1999. Estimation of tumor control probability model parameters from 3-D dose distributions of non-small cell lung cancer patients. Lung Cancer 24, 31–37. https://doi.org/10.1016/S0169-5002(99)00019-7
Marxer, M., Ma, H.T., Man, W.Y., Poon, R.Y.C., 2014. p53 deficiency enhances mitotic arrest and slippage induced by pharmacological inhibition of Aurora kinases. Oncogene 33, 3550–3560. https://doi.org/10.1038/onc.2013.325
Mathiot, L., Herbreteau, G., Robin, S., Fenat, C., Bennouna, J., Blanquart, C., Denis, M., Pons-Tostivint, E., 2022. HRAS Q61L Mutation as a Possible Target for Non-Small Cell Lung Cancer: Case Series and Review of Literature. Current Oncology 29, 3748–3758. https://doi.org/10.3390/curroncol29050300
Mazzone, R., Zwergel, C., Mai, A., Valente, S., 2017. Epi-drugs in combination with immunotherapy: a new avenue to improve anticancer efficacy. Clin Epigenet 9, 59. https://doi.org/10.1186/s13148-017-0358-y
Mentzel, J., Hildebrand, L.S., Kuhlmann, L., Fietkau, R., Distel, L.V., 2024. Effective Radiosensitization of HNSCC Cell Lines by DNA-PKcs Inhibitor AZD7648 and PARP Inhibitors Talazoparib and Niraparib. IJMS 25, 5629. https://doi.org/10.3390/ijms25115629
Minoshima, Y., Kawashima, T., Hirose, K., Tonozuka, Y., Kawajiri, A., Bao, Y.C., Deng, X., Tatsuka, M., Narumiya, S., May, W.S., Nosaka, T., Semba, K., Inoue, T., Satoh, T., Inagaki, M., Kitamura, T., 2003. Phosphorylation by Aurora B Converts MgcRacGAP to a RhoGAP during Cytokinesis. Developmental Cell 4, 549–560. https://doi.org/10.1016/S1534-5807(03)00089-3
Mo, Q.Q., Chen, P.B., Jin, X., Chen, Q., Tang, L., Wang, B.B., Li, K.Z., Wu, P., Fang, Y., Wang, S.X., Zhou, J.F., Ma, D., Chen, G., 2013. Inhibition of Hec1 expression enhances the sensitivity of human ovarian cancer cells to paclitaxel. Acta Pharmacologica Sinica 34, 541–548. https://doi.org/10.1038/aps.2012.197

Moghe, S., Jiang, F., Miura, Y., Cerny, R.L., Tsai, M.-Y., Furukawa, M., 2012. The CUL3-KLHL18 ligase regulates mitotic entry and ubiquitylates Aurora-A. Biology Open 1, 82–91. https://doi.org/10.1242/bio.2011018
Mogi, A., Kuwano, H., 2011. TP53 Mutations in Nonsmall Cell Lung Cancer. Journal of Biomedicine and Biotechnology 2011, 1–9. https://doi.org/10.1155/2011/583929
Monteonofrio, L., Valente, D., Ferrara, M., Camerini, S., Miscione, R., Crescenzi, M., Rinaldo, C., Soddu, S., 2018. HIPK2 and extrachromosomal histone H2B are separately recruited by Aurora-B for cytokinesis. Oncogene 37, 3562–3574. https://doi.org/10.1038/s41388-018-0191-6
Mou, P.K., Yang, E.J., Shi, C., Ren, G., Tao, S., Shim, J.S., 2021. Aurora kinase A, a synthetic lethal target for precision cancer medicine. Exp Mol Med 53, 835–847. https://doi.org/10.1038/s12276-021-00635-6
Nair, S., Bonner, J.A., Bredel, M., 2022. EGFR Mutations in Head and Neck Squamous Cell Carcinoma. IJMS 23, 3818. https://doi.org/10.3390/ijms23073818
NCI Staff, 2020. Ret Alerations Spur cancer growth.
Nehlig, A., Molina, A., Rodrigues-Ferreira, S., Honoré, S., Nahmias, C., 2017. Regulation of end-binding protein EB1 in the control of microtubule dynamics. Cell. Mol. Life Sci. 74, 2381–2393. https://doi.org/10.1007/s00018-017-2476-2
Neppl, C., Keller, M.D., Scherz, A., Dorn, P., Schmid, R.A., Zlobec, I., Berezowska, S., 2019. Comparison of the 7th and 8th Edition of the UICC/AJCC TNM Staging System in Primary Resected Squamous Cell Carcinomas of the Lung—A Single Center Analysis of 354 Cases. Front. Med. 6, 196. https://doi.org/10.3389/fmed.2019.00196
Nicholson, A.G., Tsao, M.S., Beasley, M.B., Borczuk, A.C., Brambilla, E., Cooper, W.A., Dacic, S., Jain, D., Kerr, K.M., Lantuejoul, S., Noguchi, M., Papotti, M., Rekhtman, N., Scagliotti, G., Van Schil, P., Sholl, L., Yatabe, Y., Yoshida, A., Travis, W.D., 2022. The 2021 WHO Classification of Lung Tumors: Impact of Advances Since 2015. Journal of Thoracic Oncology 17, 362–387. https://doi.org/10.1016/j.jtho.2021.11.003
Niermann, K.J., Moretti, L., Giacalone, N.J., Sun, Y., Schleicher, S.M., Kopsombut, P., Mitchell, L.R., Kim, K.W., Lu, B., 2011. Enhanced Radiosensitivity of Androgen-Resistant Prostate Cancer: AZD1152-Mediated Aurora Kinase B Inhibition. Radiation Research 175, 444–451. https://doi.org/10.1667/RR2317.1
Nikonova, A.S., Astsaturov, I., Serebriiskii, I.G., Dunbrack, R.L., Golemis, E.A., 2013. Aurora A kinase (AURKA) in normal and pathological cell division. Cell. Mol. Life Sci. 70, 661–687. https://doi.org/10.1007/s00018-012-1073-7
Overgaard, J., Hansen, H.S., Specht, L., Overgaard, M., Grau, C., Andersen, E., Bentzen, J., Bastholt, L., Hansen, O., Johansen, J., Andersen, L., Evensen, J.F., 2003. Five compared with six fractions per week of conventional radiotherapy of squamous-cell carcinoma of head and neck: DAHANCA 6&7 randomised controlled trial. The Lancet 362, 933–940. https://doi.org/10.1016/S0140-6736(03)14361-9
Paik, P.K., Felip, E., Veillon, R., Sakai, H., Cortot, A.B., Garassino, M.C., Mazieres, J., Viteri, S., Senellart, H., Van Meerbeeck, J., Raskin, J., Reinmuth, N., Conte, P., Kowalski, D., Cho, B.C., Patel, J.D., Horn, L., Griesinger, F., Han, J.-Y., Kim, Y.-C., Chang, G.-C., Tsai, C.-L., Yang, J.C.-H., Chen, Y.-M., Smit, E.F., Van Der Wekken, A.J., Kato, T., Juraeva, D., Stroh, C., Bruns, R.,

Straub, J., Johne, A., Scheele, J., Heymach, J.V., Le, X., 2020. Tepotinib in Non–Small-Cell Lung Cancer with *MET* Exon 14 Skipping Mutations. N Engl J Med 383, 931–943. https://doi.org/10.1056/NEJMoa2004407

Pajonk, F., Vlashi, E., McBride, W.H., 2010. Radiation Resistance of Cancer Stem Cells: The 4 R's of Radiobiology Revisited. Stem Cells 28, 639–648. https://doi.org/10.1002/stem.318

Parrilla, A., Cirillo, L., Thomas, Y., Gotta, M., Pintard, L., Santamaria, A., 2016. Mitotic entry: The interplay between Cdk1, Plk1 and Bora. Cell Cycle 15, 3177–3182. https://doi.org/10.1080/15384101.2016.1249544

Pignon, J.-P., Tribodet, H., Scagliotti, G.V., Douillard, J.-Y., Shepherd, F.A., Stephens, R.J., Dunant, A., Torri, V., Rosell, R., Seymour, L., Spiro, S.G., Rolland, E., Fossati, R., Aubert, D., Ding, K., Waller, D., Le Chevalier, T., 2008. Lung Adjuvant Cisplatin Evaluation: A Pooled Analysis by the LACE Collaborative Group. JCO 26, 3552–3559. https://doi.org/10.1200/JCO.2007.13.9030

Pinkiewicz, M., Dorobisz, K., Zatoński, T., 2022. Human Papillomavirus-Associated Head and Neck Cancers. Where are We Now? A Systematic Review. CMAR Volume 14, 3313–3324. https://doi.org/10.2147/CMAR.S379173

Pollock, N.I., Grandis, J.R., 2015. HER2 as a Therapeutic Target in Head and Neck Squamous Cell Carcinoma. Clinical Cancer Research 21, 526–533. https://doi.org/10.1158/1078-0432.CCR-14-1432

Posch, M., Khoudoli, G.A., Swift, S., King, E.M., DeLuca, J.G., Swedlow, J.R., 2010. Sds22 regulates aurora B activity and microtubule–kinetochore interactions at mitosis. Journal of Cell Biology 191, 61–74. https://doi.org/10.1083/jcb.200912046

Qi, M., Yu, W., Liu, S., Jia, H., Tang, L., Shen, M., Yan, X., Saiyin, H., Lang, Q., Wan, B., Zhao, S., Yu, L., 2005. Septin1, a new interaction partner for human serine/threonine kinase aurora-B. Biochemical and Biophysical Research Communications 336, 994–1000. https://doi.org/10.1016/j.bbrc.2005.06.212

Qiu, B., Aili, A., Xue, L., Jiang, P., Wang, J., 2020. Advances in Radiobiology of Stereotactic Ablative Radiotherapy. Front. Oncol. 10, 1165. https://doi.org/10.3389/fonc.2020.01165

Rakotomalala, A., Escande, A., Furlan, A., Meignan, S., Lartigau, E., 2021. Hypoxia in Solid Tumors: How Low Oxygenation Impacts the "Six Rs" of Radiotherapy. Front. Endocrinol. 12, 742215. https://doi.org/10.3389/fendo.2021.742215

Rassamegevanon, T., Feindt, L., Koi, L., Müller, J., Freudenberg, R., Löck, S., Sihver, W., Çevik, E., Kühn, A.C., Von Neubeck, C., Linge, A., Pietzsch, H.-J., Kotzerke, J., Baumann, M., Krause, M., Dietrich, A., 2021. Molecular Response to Combined Molecular- and External Radiotherapy in Head and Neck Squamous Cell Carcinoma (HNSCC). Cancers 13, 5595. https://doi.org/10.3390/cancers13225595

Reck, M., Rodríguez-Abreu, D., Robinson, A.G., Hui, R., Csőszi, T., Fülöp, A., Gottfried, M., Peled, N., Tafreshi, A., Cuffe, S., O'Brien, M., Rao, S., Hotta, K., Leiby, M.A., Lubiniecki, G.M., Shentu, Y., Rangwala, R., Brahmer, J.R., 2016. Pembrolizumab versus Chemotherapy for PD-L1–Positive Non–Small-Cell Lung Cancer. N Engl J Med 375, 1823–1833. https://doi.org/10.1056/NEJMoa1606774

Rehmani, H.S., Issaeva, N., 2020. EGFR in head and neck squamous cell carcinoma: exploring possibilities of novel drug combinations. Ann Transl Med 8, 813–813. https://doi.org/10.21037/atm.2020.04.07

Roy, S., Salerno, K.E., Citrin, D.E., 2021. Biology of Radiation-Induced Lung Injury. Seminars in Radiation Oncology 31, 155–161. https://doi.org/10.1016/j.semradonc.2020.11.006
Ryser, S., Dizin, E., Jefford, C.E., Delaval, B., Gagos, S., Christodoulidou, A., Krause, K.-H., Birnbaum, D., Irminger-Finger, I., 2009. Distinct Roles of BARD1 Isoforms in Mitosis: Full-Length BARD1 Mediates Aurora B Degradation, Cancer-Associated BARD1β Scaffolds Aurora B and BRCA2. Cancer Res 69, 1125–1134. https://doi.org/10.1158/0008-5472.CAN-08-2134
Saddawi-Konefka, R., Schokrpur, S., Lui, A.J., Gutkind, J.S., 2022. HER2 and HER3 as Therapeutic Targets in Head and Neck Cancer. Cancer J 28, 339–345. https://doi.org/10.1097/PPO.0000000000000622
Saelens, W., Cannoodt, R., Saeys, Y., 2018. A comprehensive evaluation of module detection methods for gene expression data. Nat Commun 9, 1090. https://doi.org/10.1038/s41467-018-03424-4
Sak, A., Stuschke, M., Groneberg, M., Kübler, D., Pöttgen, C., Eberhardt, W.E.E., 2012. Inhibiting the Aurora B Kinase Potently Suppresses Repopulation During Fractionated Irradiation of Human Lung Cancer Cell Lines. International Journal of Radiation Oncology*Biology*Physics 84, 492–499. https://doi.org/10.1016/j.ijrobp.2011.12.021
Sasai, K., Katayama, H., Stenoien, D.L., Fujii, S., Honda, R., Kimura, M., Okano, Y., Tatsuka, M., Suzuki, F., Nigg, E.A., Earnshaw, W.C., Brinkley, W.R., Sen, S., 2004. Aurora-C kinase is a novel chromosomal passenger protein that can complement Aurora-B kinase function in mitotic cells. Cell Motility and the Cytoskeleton 59, 249–263. https://doi.org/10.1002/cm.20039
Sathyan, K.M., Sailasree, R., Jayasurya, R., Lakshminarayanan, K., Abraham, T., Nalinakumari, K.R., Abraham, E.K., Kannan, S., 2006. Carcinoma of tongue and the buccal mucosa represent different biological subentities of the oral carcinoma. J Cancer Res Clin Oncol 132, 601–609. https://doi.org/10.1007/s00432-006-0111-y
Saurin, A.T., Van Der Waal, M.S., Medema, R.H., Lens, S.M.A., Kops, G.J.P.L., 2011. Aurora B potentiates Mps1 activation to ensure rapid checkpoint establishment at the onset of mitosis. Nat Commun 2, 316. https://doi.org/10.1038/ncomms1319
Schecher, S., Walter, B., Falkenstein, M., Macher-Goeppinger, S., Stenzel, P., Krümpelmann, K., Hadaschik, B., Perner, S., Kristiansen, G., Duensing, S., Roth, W., Tagscherer, K.E., 2017. Cyclin K dependent regulation of Aurora B affects apoptosis and proliferation by induction of mitotic catastrophe in prostate cancer. Intl Journal of Cancer 141, 1643–1653. https://doi.org/10.1002/ijc.30864
Schwartz, G.K., Carvajal, R.D., Midgley, R., Rodig, S.J., Stockman, P.K., Ataman, O., Wilson, D., Das, S., Shapiro, G.I., 2013. Phase I study of barasertib (AZD1152), a selective inhibitor of Aurora B kinase, in patients with advanced solid tumors. Invest New Drugs 31, 370–380. https://doi.org/10.1007/s10637-012-9825-7
Selvaraj, G., Kaliamurthi, S., Kaushik, A.C., Khan, A., Wei, Y.-K., Cho, W.C., Gu, K., Wei, D.-Q., 2018. Identification of target gene and prognostic evaluation for lung adenocarcinoma using gene expression meta-analysis, network analysis and neural network algorithms. Journal of Biomedical Informatics 86, 120–134. https://doi.org/10.1016/j.jbi.2018.09.004

Shaalan, A.K., Teshima, T.H.N., Tucker, A.S., Proctor, G.B., 2021. Inhibition of Aurora Kinase B activity disrupts development and differentiation of salivary glands. Cell Death Discov. 7, 16. https://doi.org/10.1038/s41420-020-00393-w
Shandilya, J., Senapati, P., Dhanasekaran, K., Bangalore, S.S., Kumar, M., Hari Kishore, A., Bhat, A., Kodaganur, G.S., Kundu, T.K., 2014. Phosphorylation of multifunctional nucleolar protein nucleophosmin (NPM1) by aurora kinase B is critical for mitotic progression. FEBS Letters 588, 2198–2205. https://doi.org/10.1016/j.febslet.2014.05.014
Shaw, A.T., Kim, D.-W., Mehra, R., Tan, D.S.W., Felip, E., Chow, L.Q.M., Camidge, D.R., Vansteenkiste, J., Sharma, S., De Pas, T., Riely, G.J., Solomon, B.J., Wolf, J., Thomas, M., Schuler, M., Liu, G., Santoro, A., Lau, Y.Y., Goldwasser, M., Boral, A.L., Engelman, J.A., 2014. Ceritinib in *ALK* -Rearranged Non–Small-Cell Lung Cancer. N Engl J Med 370, 1189–1197. https://doi.org/10.1056/NEJMoa1311107
Shi, M.-Q., Xu, Y., Fu, X., Pan, D.-S., Lu, X.-P., Xiao, Y., Jiang, Y.-Z., 2024. Advances in targeting histone deacetylase for treatment of solid tumors. J Hematol Oncol 17, 37. https://doi.org/10.1186/s13045-024-01551-8
Shiloh, Y., Ziv, Y., 2013. The ATM protein kinase: regulating the cellular response to genotoxic stress, and more. Nat Rev Mol Cell Biol 14, 197–210. https://doi.org/10.1038/nrm3546
Shuda, K., Schindler, K., Ma, J., Schultz, R.M., Donovan, P.J., 2009. Aurora kinase B modulates chromosome alignment in mouse oocytes: AURKB AND MOUSE OOCYTES. Mol. Reprod. Dev. 76, 1094–1105. https://doi.org/10.1002/mrd.21075
Skálová, A., Bradová, M., Michal, M., Mosaieby, E., Klubíčková, N., Vaněček, T., Leivo, I., 2024. Molecular pathology in diagnosis and prognostication of head and neck tumors. Virchows Arch 484, 215–231. https://doi.org/10.1007/s00428-023-03731-2
Slattery, S.D., Mancini, M.A., Brinkley, B.R., Hall, R.M., 2009. Aurora-C kinase supports mitotic progression in the absence of Aurora-B. Cell Cycle 8, 2986–2997. https://doi.org/10.4161/cc.8.18.9591
Slattery, S.D., Moore, R.V., Brinkley, B.R., Hall, R.M., n.d. Aurora-C and Aurora-B share phosphorylation and regulation of cenp-A and borealin during mitosis. Cell Cycle 7, 10.
Soeda, S., Nakayama, Y., Honda, T., Aoki, A., Tamura, N., Abe, K., Fukumoto, Y., Yamaguchi, N., 2013. v-Src causes delocalization of Mklp1, Aurora B, and INCENP from the spindle midzone during cytokinesis failure. Experimental Cell Research 319, 1382–1397. https://doi.org/10.1016/j.yexcr.2013.02.023
Solomon, B.J., Mok, T., Kim, D.-W., Wu, Y.-L., Nakagawa, K., Mekhail, T., Felip, E., Cappuzzo, F., Paolini, J., Usari, T., Iyer, S., Reisman, A., Wilner, K.D., Tursi, J., Blackhall, F., 2014. First-Line Crizotinib versus Chemotherapy in *ALK* -Positive Lung Cancer. N Engl J Med 371, 2167–2177. https://doi.org/10.1056/NEJMoa1408440
Song, H., Wan, Y., Xu, Y.-Y., 2015. Betel Quid Chewing Without Tobacco: A Meta-analysis of Carcinogenic and Precarcinogenic Effects. Asia Pac J Public Health 27, NP47–NP57. https://doi.org/10.1177/1010539513486921
Song, S.J., Kim, S.J., Song, M.S., Lim, D.-S., 2009. Aurora B-Mediated Phosphorylation of RASSF1A Maintains Proper Cytokinesis by Recruiting Syntaxin16 to the Midzone and Midbody. Cancer Research 69, 8540–8544. https://doi.org/10.1158/0008-5472.CAN-09-1554

Sorrentino, R., Libertini, S., Pallante, P.L., Troncone, G., Palombini, L., Bavetsias, V., Spalletti-Cernia, D., Laccetti, P., Linardopoulos, S., Chieffi, P., Fusco, A., Portella, G., 2005. Aurora B Overexpression Associates with the Thyroid Carcinoma Undifferentiated Phenotype and Is Required for Thyroid Carcinoma Cell Proliferation. The Journal of Clinical Endocrinology & Metabolism 90, 928–935. https://doi.org/10.1210/jc.2004-1518

Takeshita, M., Koga, T., Takayama, K., Ijichi, K., Yano, T., Maehara, Y., Nakanishi, Y., Sueishi, K., 2013. Aurora-B overexpression is correlated with aneuploidy and poor prognosis in non-small cell lung cancer. Lung Cancer 80, 85–90. https://doi.org/10.1016/j.lungcan.2012.12.018

Tammemagi, M.C., McLaughlin, J.R., Bull, S.B., n.d. Meta-Analyses of p53 Tumor Suppressor Gene Alterations and Clinicopathological Features in Resected Lung Cancers.

Tang, A., Gao, K., Chu, L., Zhang, R., Yang, J., Zheng, J., 2017. Aurora kinases: Novel therapy targets in cancers. Oncotarget 8, 23937–23954. https://doi.org/10.18632/oncotarget.14893

Tao, Y., Leteur, C., Calderaro, J., Girdler, F., Zhang, P., Frascogna, V., Varna, M., Opolon, P., Castedo, M., Bourhis, J., Kroemer, G., Deutsch, E., 2009. The Aurora B kinase inhibitor AZD1152 sensitizes cancer cells to fractionated irradiation and induces mitotic catastrophe. Cell Cycle 8, 3172–3181. https://doi.org/10.4161/cc.8.19.9729

Tao, Y., Zhang, P., Girdler, F., Frascogna, V., Castedo, M., Bourhis, J., Kroemer, G., Deutsch, E., 2008a. Enhancement of radiation response in p53-deficient cancer cells by the Aurora-B kinase inhibitor AZD1152. Oncogene 27, 3244–3255. https://doi.org/10.1038/sj.onc.1210990

Tao, Y., Zhang, P., Girdler, F., Frascogna, V., Castedo, M., Bourhis, J., Kroemer, G., Deutsch, E., 2008b. Enhancement of radiation response in p53-deficient cancer cells by the Aurora-B kinase inhibitor AZD1152. Oncogene 27, 3244–3255. https://doi.org/10.1038/sj.onc.1210990

Tcherniuk, S., Skoufias, D.A., Labriere, C., Rath, O., Gueritte, F., Guillou, C., Kozielski, F., 2010. Relocation of Aurora B and Survivin from Centromeres to the Central Spindle Impaired by a Kinesin-Specific MKLP-2 Inhibitor. Angewandte Chemie International Edition 49, 8228–8231. https://doi.org/10.1002/anie.201003254

Teng, C.-L., Hsieh, Y.-C., Phan, L., Shin, J., Gully, C., Velazquez-Torres, G., Skerl, S., Yeung, S.-C.J., Hsu, S.-L., Lee, M.-H., 2012a. FBXW7 is involved in Aurora B degradation. Cell Cycle 11, 4059–4068. https://doi.org/10.4161/cc.22381

Teng, C.-L., Hsieh, Y.-C., Phan, L., Shin, J., Gully, C., Velazquez-Torres, G., Skerl, S., Yeung, S.-C.J., Hsu, S.-L., Lee, M.-H., 2012b. FBXW7 is involved in Aurora B degradation. Cell Cycle 11, 4059–4068. https://doi.org/10.4161/cc.22381

Tian, J., Tian, C., Ding, Y., Li, Z., Geng, Q., Xiahou, Z., Wang, J., Hou, W., Liao, J., Dong, M.-Q., Xu, X., Li, J., 2015. Aurora B-dependent phosphorylation of Ataxin-10 promotes the interaction between Ataxin-10 and Plk1 in cytokinesis. Sci Rep 5, 8360. https://doi.org/10.1038/srep08360

Tinhofer, I., Braunholz, D., Klinghammer, K., 2020. Preclinical models of head and neck squamous cell carcinoma for a basic understanding of cancer biology and its translation into efficient therapies. Cancers Head Neck 5, 9. https://doi.org/10.1186/s41199-020-00056-4

Tsuboi, K., Yokozawa, T., Sakura, T., Watanabe, T., Fujisawa, S., Yamauchi, T., Uike, N., Ando, K., Kihara, R., Tobinai, K., Asou, H., Hotta, T., Miyawaki, S., 2011. A Phase I study to assess the safety, pharmacokinetics and efficacy of barasertib (AZD1152), an Aurora B kinase inhibitor, in Japanese patients with advanced acute myeloid leukemia. Leukemia Research 35, 1384–1389. https://doi.org/10.1016/j.leukres.2011.04.008

Ulisse, S., Baldini, E., Toller, M., Delcros, J.-G., Guého, A., Curcio, F., De Antoni, E., Giacomelli, L., Ambesi-Impiombato, F.S., Bocchini, S., D'Armiento, M., Arlot-Bonnemains, Y., 2007. Transforming acidic coiled-coil 3 and Aurora-A interact in human thyrocytes and their expression is deregulated in thyroid cancer tissues. Endocr Relat Cancer 14, 827–837. https://doi.org/10.1677/ERC-07-0053

Van Gijn, S.E., Wierenga, E., Van Den Tempel, N., Kok, Y.P., Heijink, A.M., Spierings, D.C.J., Foijer, F., Van Vugt, M.A.T.M., Fehrmann, R.S.N., 2019. TPX2/Aurora kinase A signaling as a potential therapeutic target in genomically unstable cancer cells. Oncogene 38, 852–867. https://doi.org/10.1038/s41388-018-0470-2

van Leuken, R.J., Luna-Vargas, M.P., Sixma, T.K., Wolthuis, R.M.F., Medema, R.H., 2008. Usp39 is essential for mitotic spindle checkpoint integrity and controls mRNA-levels of Aurora B. Cell Cycle 7, 2710–2719. https://doi.org/10.4161/cc.7.17.6553

Vidhyadharan, S., Thankappan, K., Subramaniam, N., Ramu, J., Ajith, A., Balasubramanian, D., Iyer, S., 2019. Robot-Assisted Surgery Avoids Mandibulotomy in a Case of Adenoid Cystic Carcinoma of Base of the Tongue. Craniomaxillofacial Trauma & Reconstruction 12, 163–166. https://doi.org/10.1055/s-0039-1683410

Vischioni, B., Oudejans, J.J., Vos, W., Rodriguez, J.A., Giaccone, G., 2006. Frequent overexpression of aurora B kinase, a novel drug target, in non–small cell lung carcinoma patients. Mol Cancer Ther 5, 2905–2913. https://doi.org/10.1158/1535-7163.MCT-06-0301

Wang, C., Chen, J., Cao, W., Sun, L., Sun, H., Liu, Y., 2016. Aurora-B and HDAC synergistically regulate survival and proliferation of lymphoma cell via AKT, mTOR and Notch pathways. European Journal of Pharmacology 779, 1–7. https://doi.org/10.1016/j.ejphar.2015.11.049

Wang, Q.L., Chen, X., Zhang, M.H., Shen, Q.H., Qin, Z.M., 2015. Identification of hub genes and pathways associated with retinoblastoma based on co-expression network analysis. Genet. Mol. Res. 14, 16151–16161. https://doi.org/10.4238/2015.December.8.4

Wang, Y., Chen, L., Wang, G., Cheng, S., Qian, K., Liu, X., Wu, C., Xiao, Y., Wang, X., 2019. Fifteen hub genes associated with progression and prognosis of clear cell renal cell carcinoma identified by coexpression analysis. Journal Cellular Physiology 234, 10225–10237. https://doi.org/10.1002/jcp.27692

Willems, E., Dedobbeleer, M., Digregorio, M., Lombard, A., Lumapat, P.N., Rogister, B., 2018. The functional diversity of Aurora kinases: a comprehensive review. Cell Div 13, 7. https://doi.org/10.1186/s13008-018-0040-6

Wolf, J., Seto, T., Han, J.-Y., Reguart, N., Garon, E.B., Groen, H.J.M., Tan, D.S.W., Hida, T., De Jonge, M., Orlov, S.V., Smit, E.F., Souquet, P.-J., Vansteenkiste, J., Hochmair, M., Felip, E., Nishio, M., Thomas, M., Ohashi, K., Toyozawa, R., Overbeck, T.R., De Marinis, F., Kim, T.-M., Laack, E., Robeva, A., Le Mouhaer, S., Waldron-Lynch, M., Sankaran, B., Balbin, O.A., Cui, X.,

Giovannini, M., Akimov, M., Heist, R.S., 2020. Capmatinib in *MET* Exon 14–Mutated or *MET* -Amplified Non–Small-Cell Lung Cancer. N Engl J Med 383, 944–957. https://doi.org/10.1056/NEJMoa2002787
Wrona, A., Mornex, F., 2021. Hypofractionation in Early Stage Non-Small Cell Lung Cancer. Seminars in Radiation Oncology 31, 97–104. https://doi.org/10.1016/j.semradonc.2020.11.003
Wu, L., Ma, C.A., Jain, A., 2011a. When Aurora B met p53: Newly revealed regulatory phosphorylation in an old protein. Cell Cycle 10, 171–172. https://doi.org/10.4161/cc.10.2.14349
Wu, L., Ma, C.A., Zhao, Y., Jain, A., 2011b. Aurora B Interacts with NIR-p53, Leading to p53 Phosphorylation in Its DNA-binding Domain and Subsequent Functional Suppression. J. Biol. Chem. 286, 2236–2244. https://doi.org/10.1074/jbc.M110.174755
Wu, L., Ma, C.A., Zhao, Y., Jain, A., 2011c. Aurora B Interacts with NIR-p53, Leading to p53 Phosphorylation in Its DNA-binding Domain and Subsequent Functional Suppression. Journal of Biological Chemistry 286, 2236–2244. https://doi.org/10.1074/jbc.M110.174755
Wurzenberger, C., Held, M., Lampson, M.A., Poser, I., Hyman, A.A., Gerlich, D.W., 2012. Sds22 and Repo-Man stabilize chromosome segregation by counteracting Aurora B on anaphase kinetochores. Journal of Cell Biology 198, 173–183. https://doi.org/10.1083/jcb.201112112
Xu, M., Hou, Y., Li, N., Yu, W., Chen, L., 2024. Targeting histone deacetylases in head and neck squamous cell carcinoma: molecular mechanisms and therapeutic targets. J Transl Med 22, 418. https://doi.org/10.1186/s12967-024-05169-9
Yabuta, N., Mukai, S., Okada, N., Aylon, Y., Nojima, H., 2011. The tumor suppressor Lats2 is pivotal in Aurora A and Aurora B signaling during mitosis. Cell Cycle 10, 2724–2736. https://doi.org/10.4161/cc.10.16.16873
Yamauchi, T., Uzui, K., Shigemi, H., Negoro, E., Yoshida, A., Ueda, T., 2013. Aurora B inhibitor barasertib and cytarabine exert a greater-than-additive cytotoxicity in acute myeloid leukemia cells. Cancer Sci 104, 926–933. https://doi.org/10.1111/cas.12164
Yan, J., Jin, S., Li, J., Zhan, Q., 2010. Aurora B Interaction of Centrosomal Nlp Regulates Cytokinesis. J. Biol. Chem. 285, 40230–40239. https://doi.org/10.1074/jbc.M110.140541
Yan, M., 2009. Aurora A Kinase: A potent Oncogene and Target for Cancer Therapy. Medicinal Research Reviews 30, 1–22. https://doi.org/10.1002/med
Yan, N., Guo, S., Zhang, H., Zhang, Z., Shen, S., Li, X., 2022. BRAF-Mutated Non-Small Cell Lung Cancer: Current Treatment Status and Future Perspective. Front. Oncol. 12, 863043. https://doi.org/10.3389/fonc.2022.863043
Yang, H., Burke, T., Dempsey, J., Diaz, B., Collins, E., Toth, J., Beckmann, R., Ye, X., 2005. Mitotic requirement for aurora A kinase is bypassed in the absence of aurora B kinase. FEBS Letters 579, 3385–3391. https://doi.org/10.1016/j.febslet.2005.04.080
Yokoyama, T., Goto, H., Izawa, I., Mizutani, H., Inagaki, M., 2005. Aurora-B and Rho-kinase/ROCK, the two cleavage furrow kinases, independently regulate the progression of cytokinesis: possible existence of a novel cleavage furrow kinase phosphorylates ezrin/radixin/moesin (ERM): Aurora-B and Rho-kinase/ROCK. Genes to Cells 10, 127–137. https://doi.org/10.1111/j.1365-2443.2005.00824.x

You, J., Li, Q., Wu, C., Kim, J., Ottinger, M., Howley, P.M., 2009. Regulation of Aurora B Expression by the Bromodomain Protein Brd4. MCB 29, 5094–5103. https://doi.org/10.1128/MCB.00299-09
Yu, J., Zhou, J., Xu, F., Bai, W., Zhang, W., 2018. High expression of Aurora-B is correlated with poor prognosis and drug resistance in non-small cell lung cancer. Int J Biol Markers 33, 215–221. https://doi.org/10.1177/1724600817753098
Yu, K., Zhong, N., Xiao, Y., She, Z., 2019. Mechanisms of kinesin-7 CENP-E in kinetochore–microtubule capture and chromosome alignment during cell division. Biol. Cell 111, 143–160. https://doi.org/10.1111/boc.201800082
Yu, X., Liang, Q., Liu, W., Zhou, L., Li, W., Liu, H., 2017. Deguelin, an Aurora B Kinase Inhibitor, Exhibits Potent Anti-Tumor Effect in Human Esophageal Squamous Cell Carcinoma. EBioMedicine 26, 100–111. https://doi.org/10.1016/j.ebiom.2017.10.030
Yuan, K., Li, N., Huo, Y., Yan, F., Yang, Y., Ward, T., Jin, C., Yao, X., 2009a. Recruitment of separase to mitotic chromosomes is regulated by Aurora B. Cell Cycle 8, 1433–1443. https://doi.org/10.4161/cc.8.9.8331
Yuan, K., Li, N., Huo, Y., Yan, F., Yang, Y., Ward, T., Jin, C., Yao, X., 2009b. Recruitment of separase to mitotic chromosomes is regulated by Aurora B. Cell Cycle 8, 1433–1443. https://doi.org/10.4161/cc.8.9.8331
Zanoni, D.K., Patel, S.G., Shah, J.P., 2019. Changes in the 8th Edition of the American Joint Committee on Cancer (AJCC) Staging of Head and Neck Cancer: Rationale and Implications. Curr Oncol Rep 21, 52. https://doi.org/10.1007/s11912-019-0799-x
Zeitlin, S.G., Shelby, R.D., Sullivan, K.F., 2001. CENP-A is phosphorylated by Aurora B kinase and plays an unexpected role in completion of cytokinesis. Journal of Cell Biology 155, 1147–1158. https://doi.org/10.1083/jcb.200108125
Zhang, J., Li, B., Yang, Q., Zhang, P., Wang, H., 2015. Prognostic value of Aurora kinase A (AURKA) expression among solid tumor patients: a systematic review and meta-analysis. Japanese Journal of Clinical Oncology 45, 629–636. https://doi.org/10.1093/jjco/hyv058
Zhang, L., Zhang, X., Fan, S., Zhang, Z., 2019. Identification of modules and hub genes associated with platinum-based chemotherapy resistance and treatment response in ovarian cancer by weighted gene co-expression network analysis. Medicine 98, e17803. https://doi.org/10.1097/MD.0000000000017803
Zhang, Q., Lu, D., Liu, W., Ye, S., Guo, H., Liao, T., Chen, C., 2019. Effects of KIF2A on the prognosis of nasopharyngeal carcinoma and nasopharyngeal carcinoma cells. Oncol Lett. https://doi.org/10.3892/ol.2019.10597
Zhao, S., An, L., Yang, X., Wei, Z., Zhang, H., Wang, Y., 2022. Identification and validation of the role of c-Myc in head and neck squamous cell carcinoma. Front. Oncol. 12, 820587. https://doi.org/10.3389/fonc.2022.820587
Zhou, C., Shen, Z., Ye, D., Li, Q., Deng, H., Liu, H., Li, J., 2018. The Association and Clinical Significance of CDKN2A Promoter Methylation in Head and Neck Squamous Cell Carcinoma: a Meta-Analysis. Cell Physiol Biochem 50, 868–882. https://doi.org/10.1159/000494473
Zhou, G., Liu, Z., Myers, J.N., 2016. *TP53* Mutations in Head and Neck Squamous Cell Carcinoma and Their Impact on Disease Progression and Treatment

Response: *TP53* M UTATIONS IN H EAD AND N ECK C ANCER. J. Cell. Biochem. 117, 2682–2692. https://doi.org/10.1002/jcb.25592
Zhou, Z., Cheng, Y., Jiang, Y., Liu, S., Zhang, M., Liu, J., Zhao, Q., 2018. Ten hub genes associated with progression and prognosis of pancreatic carcinoma identified by co-expression analysis. Int. J. Biol. Sci. 14, 124–136. https://doi.org/10.7150/ijbs.22619